

Hepatitis B Virus Infection of Hepatoma Cells Differentiated in Human Serum Culture

by

Connie Le

A thesis submitted in partial fulfillment of the requirements for the degree of

Doctor of Philosophy

in

Virology

Department of Medical Microbiology and Immunology

University of Alberta

© Connie Le, 2022

Abstract

Hepatitis B virus (HBV) has infected two billion people worldwide, culminating in approximately 250 million chronic carriers. Chronic HBV carriers are at high risk of developing severe liver diseases, such as cirrhosis and cancer, resulting in an estimated 600,000 HBV-associated deaths annually. A major obstacle to studies of HBV has been the lack of a biologically relevant and easily infectable cell culture model. Immortalized cell lines have low infection efficiency, while primary liver cells are difficult to acquire and maintain in culture. To overcome this problem, a human hepatoma cell culture system was developed for studying HBV infection.

Overexpression of the HBV entry receptor, sodium taurocholate cotransporting polypeptide (NTCP), in Huh7.5 hepatoma cells rendered them susceptible to HBV infection. The Huh7.5-NTCP hepatoma cells were differentiated in Dulbecco's modified Eagle's medium (DMEM) supplemented with 4% human serum (HS). This was compared to the conventional culture system using DMEM supplemented with fetal bovine serum (FBS) and requiring high concentrations (2–2.5%) of dimethyl sulfoxide (DMSO) to promote HBV infection. This new HS culture system produced robust HBV infection in Huh7.5-NTCP hepatoma cells in the absence of DMSO. HBV pregenomic RNA (pgRNA) levels in the HS cultures were increased by as much as 200-fold in comparison with FBS cultures and 19-fold in comparison with FBS+DMSO cultures. The HS culture increased levels of albumin secretion, a hepatocyte differentiation marker, in Huh7.5-NTCP cells to similar levels found in primary human hepatocytes. N-glycosylation of NTCP induced by HS-culture may contribute to viral entry.

Single-cell RNA sequencing (scRNA-seq) analysis of Huh7.5-NTCP cells differentiated in HS cultures revealed that most of the cells had similar transcriptome profiles to those of primary hepatocytes from human liver. This transcriptomic characterization shows that the HS-cultured

Huh7.5-NTCP cell model is a useful alternative to primary human hepatocytes. scRNA-seq analysis also revealed the presence of cholangiocyte-like cells in the HS-cultured Huh7.5 and Huh7.5-NTCP cell lines. The cholangiocyte-like cells in the hepatoma cell population had similar gene expression profiles and regulatory pathways to cholangiocytes from human liver tissue.

scRNA-seq analyses were conducted to determine whether HBV infection alters interferon (IFN)-stimulated gene expression in Huh7.5 and Huh7.5-NTCP cells. Much higher amounts of the host cell RNA relative to low levels of HBV transcripts made the detection of HBV transcripts difficult. To overcome this problem, a CRISPR technique was developed to deplete highly abundant off-target transcripts and preferentially enrich the HBV transcripts. With CRISPR-mediated enrichment, scRNA-seq successfully detected HBV transcripts in more than 74% of the cells. This is compared to only 0.6% of the cells having detectable HBV transcripts when they were not enriched. The improved detection of HBV transcripts facilitated a scRNA-seq study of HBV infection and IFN treatment of Huh7.5-NTCP cells. Cells in the mock infection and HBV infection samples had the same transcriptome profiles. IFN treatment of Huh7.5-NTCP cells increased levels of IFN-stimulated genes. But HBV infection of the IFN-treated Huh7.5-NTCP cells did not alter the patterns or expression levels of IFN-stimulated genes. These results at the single-cell resolution support the idea that HBV is a “stealth virus”; it neither stimulates nor suppresses the interferon response. In contrast, hepatitis C virus (HCV) infection significantly changed transcriptome profiles of the host cells. HCV infection also altered expression patterns of IFN-stimulated genes, with upregulation of most and downregulation of a few IFN-stimulated genes.

This study established an *in vitro* HBV infection model of Huh7.5-NTCP cells without using DMSO. scRNA-seq analysis of the cell model showed similar transcriptome profiles to those of

primary human hepatocytes. scRNA-seq results also supported the hypothesis that HBV is a “stealth virus”. The discovery of cholangiocyte-like cells in HS-cultured Huh7.5-NTCP suggests a useful approach of cell differentiation. The tools and results described in this thesis contribute to an improved understanding of HBV infection.

Preface

This thesis is an original work I am responsible for. Components of Chapter 2 have been published (Le, C.; Sirajee, R.; Steenbergen, R.; Joyce, M.A.; Addison, W.R.; Tyrrell, D.L. *In vitro* infection with hepatitis B virus using differentiated human serum culture of Huh7.5-NTCP cells without requiring dimethyl sulfoxide. *Viruses*, **2021**, *13*, 97). As the first author, I contributed to all aspects of research reported in this paper, including conceptualization, conducting the experiments, analyzing data, generating figures, and writing and editing the manuscript for publication. Sirajee, R. helped me with repeating some experiments on HBV infection of the cells when the summer student worked with me for three months. Contributions of Steenbergen, R. (postdoctoral fellow), Joyce, M.A. (Research Associate), and Addison, W.R. (Research Associate) included editing the manuscript and providing suggestions and resources. Tyrrell, D.L. is my PhD supervisor who contributed to all aspects of the research, including conceptualization, funding acquisition, project administration, manuscript editing, and supervision. Permission for adaptation and reproduction of this paper was granted under a Creative Commons Attribution 4.0 International License.

The contents of Chapter 3 have been published (Le, C.; Liu, Y.; Lopez-Orozco, J.; Joyce, M.A.; Le, X.C.; Tyrrell, D.L. CRISPR technique incorporated with single-cell RNA sequencing for studying hepatitis B infection. *Analytical Chemistry*, **2021**, *93*, 10756–10761). As the first author, I contributed to all aspects of research reported in this paper, including conceptualization, conducting most experiments, analyzing data, generating figures, and writing and editing the manuscript for publication. Liu, Y. (collaborating postdoctoral fellow) conducted the PCR experiments. Lopez-Orozco, J. in the Faculty of Medicine and Dentistry Core Facilities prepared the scRNA-seq libraries. Joyce, M.A. provided suggestions and resources. Le, X.C. and Tyrrell, D.L. contributed to funding acquisition, project administration, manuscript editing, and supervision. Permission for reproduction of this paper in this thesis was granted by the American Chemical Society (ACS) Publications Support.

A method for detecting HBeAg was published (Liu, Y.;[#] Le, C.;[#] Tyrrell, D.L.; Le, X.C.; Li, X.-F. Aptamer binding assay for the E antigen of hepatitis B using modified aptamers with G-quadruplex structures. *Analytical Chemistry*, **2020**, *92*, 6495–6501). This method was used for research in Chapter 2. The full contents of this paper are not included in this thesis. As the joint first authors,[#] Liu, Y. contributed to the aptamer aspect and I contributed to the HBeAg aspect of

the research. We collaboratively developed and applied the assay to HBeAg analysis. Tyrrell, D.L.; Le, X.C. and Li, X.-F. contributed to funding acquisition, project administration, manuscript editing, and supervision.

The following three publications which I co-authored during my PhD program are not included in this thesis. These publications are results of interdisciplinary collaborations.

I spent some time at the University of Washington (Seattle) and collaborated on CRISPR/Cas9 gene editing of hepatitis B virus (Stone, D.; Long, K.R.; Loprieno, M.A.; De Silva Feelixge, H.S.; Kenkel, E.J.; Liley, R.M.; Rapp, S.; Roychoudhury, P.; Nguyen, T.; Stensland, L.; Colón-Thillet, R.; Klouser, L.M.; Weber, N.D.; **Le, C.**; Wagoner, J.; Goecker, E.A.; Li, A.Z.; Eichholz, K.; Corey, L.; Tyrrell, D.L.; Greninger, A.L.; Huang, M.-L.; Polyak, S.L.; Aubert, M.; Sagartz, J.E.; Jerome, K.R. CRISPR/Cas9 gene editing of hepatitis B virus in chronically infected humanized mice. *Molecular Therapy - Methods & Clinical Development*, **2021**, *20*, 258–275).

Another collaboration was initiated in the summer of 2017 after my seminar on CRISPR, presented to the Analytical and Environmental Toxicology (AET) Division at the University of Alberta. This successful and on-going collaboration has resulted in two recent review papers involving CRISPR. As one of the joint first authors,[#] I wrote the “fundamental features of CRISPR-Cas system” section of the critical review paper (Feng, W.,[#] Newbigging, A.M.,[#] Tao, J.,[#] Cao, Y.,[#] Peng, H.,[#] **Le, C.**,[#] Wu, J.; Li, J.; Pang, B.; Tyrrell, D. L.; Zhang, H.; Le, X. C. CRISPR technology incorporating amplification strategies: Molecular assays for nucleic acids, proteins, and small molecules. *Chemical Science*, **2021**, *12*, 4683–4698).

As a joint first author,[#] I wrote the “life cycle and genome organization of SARS-CoV-2” section of this review paper (Feng, W.,[#] Newbigging, A.M.,[#] **Le, C.**,[#] Pang, B.,[#] Peng, H.,[#] Cao, Y.,[#] Wu, J.; Abbas, G.; Song, J.; Wang, D.-B.; Cui, M.; Tao, J.; Tyrrell, D. L.; Zhang, X.-E.; Zhang, H.; Le, X. C. Molecular diagnosis of COVID-19: Challenges and research needs. *Analytical Chemistry*, **2020**, *92*, 10196–10209). This paper was written during the first wave of COVID-19 when the access to research laboratories was limited. Subsequently other members of the Tyrrell group continued collaboration with the AET Division on developing assays for detecting SARS-CoV-2. This work is not included in this thesis.

Dedication

This thesis is dedicated to my parents, Xiaochun Chris Le and Xing-Fang Li. I owe my love and appreciation for education, academic accolades, and completion of this thesis entirely to your unwavering support. Any of my professional achievements to date and to come are by virtue of your immeasurable sacrifices. With all my love, thank you.

Acknowledgements

I am exceptionally grateful to Dr. Lorne Tyrrell for your inspiration, encouragement, guidance, and support throughout my MD/PhD program. An exemplary clinician, educator, researcher, and innovator, you consistently excel in patient care, teaching, research, and health advocacy. You always share your wealth of expertise, encourage innovation, promote excellence, create opportunities, and foster my growth. Thank you for encouraging me to establish new collaboration and explore new tools for my thesis research. Your example and mentorship in discovery research, clinical medicine, and health advocacy inspire me to become a clinician-scientist contributing to medical research and patient care.

I am indebted to my PhD supervisory committee, Drs. David Evans, Maya Shmulevitz, and James Smiley, for your advice, constructive suggestions, guidance, and support. Well-respected academic leaders in your respective areas, you contribute a wealth of knowledge and perspectives to my PhD program. Your diverse expertise, profound insights, and dedication to science set an example of excellence. Thank you for your time, patience, and enthusiastic energy.

I am grateful to all colleagues and friends in Dr. Tyrrell's team and in the Li Ka Shing Institute of Virology and the Department of Medical Microbiology and Immunology. A special thank you to Dr. William Addison, Karyn Berry-Wynne, Bonnie Bock, Tiing Tiing Chua, Dr. Carla Craveiro Salvado, Karl Fischer, Dr. Michael Joyce, Gerald Lachance, Suellen Lamb, Dr. Aviad Levin, Darci Loewen-Dobler, Holly Saffran, Justin Shields, Reshma Sirajee, Dr. Rineke Steenbergen, and Wilson Tat for your help, collaboration, suggestions, technical resources, and friendship. Thank you to Dr. Addison for kindly reviewing my thesis and providing constructive suggestions and comments.

My research experience is enriched by collaborations. I would like to thank all my collaborators for your contribution to the teamwork. It is a privilege to work with you, learn from you, and publish with you. Thank you to the members of the Houghton group, including Daren Hockman, Janelle Johnson, Dr. John Law, Dr. Michael Logan, and Gillian Minty, for your continued collaboration and help.

I would like to thank Bonnie Bock and other members in the Department of Medical Microbiology and Immunology for your assistance and support on many aspects of my graduate studies and research. Your professionalism and care for students' wellness are truly appreciated.

I am grateful to Drs. Sarah Forgie, Mel Lewis, and Alan Underhill for your guidance to succeed in a demanding MD/PhD program and for your advice on developing a career in research and clinical medicine.

A special thank you to my dear friends in the department: Farah Elawar, Laura Henao, Ninad Mehta, Kathryn Mitran, Ryan Noyce, Mira Shenouda, and Brittany Umer. I am endlessly grateful for the steadfast support scientifically and through your generous friendship. I am incredibly thankful to Jared Jacobson, David Kramer, Marissa Ledger, Qaasim Mian, Owen Scheirer, Scott Stewart, Sameera Zia, Kathryn Chevalier, Oksana Dacko, Lucy Ford, Luanne Lerner, Conor Ruzycski, and Rose Wang for your friendship and support during the MD/PhD program.

I am eternally indebted to my family for your unwavering love and support. Thank you to my brother Andy, I am so incredibly fortunate to have such an empathetic and kind sibling. I will never be able to fully recompense the guidance you have provided in recent years. You will always be my longest friendship, a gift I cherish most in life. My utmost thanks to Grandma Sharon. To have been so lucky to be graced with chosen family as loving and generous as you will forever be a blessing in our family. I am grateful to Matthew Kingston for your limitless encouragement and uncanny talent of brightening my day. My greatest fortune is the nurturing love and guidance I have been so fortuitous to be gifted from my parents. In many ways, this thesis would not have been possible without your supernatural work ethic and value of educational pursuits. My reverence for your extraordinary endeavors and dedication to continued growth is my humble offering to honor the immeasurable privileges you have endowed. Thank you for sharing this MD/PhD journey with me.

This research was supported by the Canadian Institutes of Health Research, the Li Ka Shing Institute of Virology, Alberta Innovates, and the University of Alberta. I am incredibly grateful to generous support of a Vanier Canada Graduate Scholarship, an Alberta Innovates MD–PhD Studentship, the John Thibault Good Citizen Award, and the Canadian Medical Hall of Fame Medical Student Award.

Table of Contents

Chapter 1. Introduction	1
1.1. Global Health Burden of the Hepatitis B Virus	1
1.2. Disease Progression	3
1.3. Hepatitis B Virus (HBV)	5
1.3.1. <i>Hepadnaviridae</i> Family	5
1.3.2. Virion Structure	5
1.3.3. Genome Characteristics	6
1.3.4. HBV Proteins	9
1.3.5. HBV Life Cycle	12
1.4. HBV Cell Culture Models	24
1.4.1. Primary Human Hepatocytes	25
1.4.2. Hepatoma Cell Lines	27
1.4.3. Hepatocyte-like Induced Pluripotent and Embryonic Stem Cells	31
1.5. Innate Immunity and HBV	32
1.6. Single-Cell RNA Sequencing (scRNA-seq) in Studies of HBV	33
1.7. Rationale, Objectives, and Scope of this Thesis	35
1.8. References	38
Chapter 2. <i>In Vitro</i> Infection with Hepatitis B Virus Using Huh7.5-NTCP Cells	
Differentiated in Human Serum Culture without Requiring Dimethyl Sulfoxide	72
2.1. Introduction	72
2.2. Materials and Methods	73
2.2.1. Production of Lentiviral Vectors Expressing NTCP	73
2.2.2. Establishment of Stable NTCP-Expressing Huh7.5 Cell Line	74
2.2.3. Conventional Culture of Huh7.5 and Huh7.5-NTCP Cells	75
2.2.4. Differentiation of Huh7.5 and Huh7.5-NTCP Cells in Human Serum (HS)	75
2.2.5. Infection of Cells with HBV	76
2.2.6. Culture of PXB Cells	76
2.2.7. Analysis of Pregenomic RNA (pgRNA)	77
2.2.8. Analysis of Covalently Closed Circular DNA (cccDNA)	78

2.2.9. Enzyme-Linked Immunosorbent Assays (ELISAs)	79
2.2.10. Aptamer-Binding Assay for the E Antigen (HBeAg)	80
2.2.11. Immunofluorescence Staining of Huh7.5 Cells Overexpressing NTCP	82
2.2.12. Flow Cytometry Analysis of NTCP Expression	83
2.2.13. Western Blotting	83
2.2.14. Nanoluciferase Reporter Luminescence Assay	84
2.2.15. Statistical Analysis	87
2.3. Results	87
2.3.1. Huh7.5 Cells Overexpressing NTCP (Huh7.5-NTCP Cells)	87
2.3.2. Human Serum Culture Enhanced HBV Infection in Huh7.5-NTCP Cells	89
2.3.3. Huh7.5-NTCP Cells in HS Culture as a Model for Long-Term HBV Infection	94
2.3.4. Human Serum Alters Hepatocyte Differentiation Markers in Huh7.5-NTCP	95
2.3.5. Involvement of NTCP and Possible Effect of its N-Glycosylation on Viral Entry	98
2.4. Discussion	104
2.5. Conclusion	107
2.6. References	108
Chapter 3. A CRISPR Technique Incorporated with Single-Cell RNA Sequencing for Studying Hepatitis B Infection	114
3.1. Introduction	114
3.2. Materials and Methods	116
3.2.1. Cell Culture and HBV Infection	116
3.2.2. Preparation of Single-Cell RNA Sequencing Libraries	116
3.2.3. Single-Cell RNA Sequencing (scRNA-seq)	118
3.2.4. Data Analysis	119
3.2.5. PCR Technique for the Enrichment of HBV Transcripts	119
3.2.6. CRISPR-Cas9 Technique for the Enrichment of HBV Transcripts	124
3.3. Results and Discussion	130
3.4. Conclusions	138
3.5. References	139

Chapter 4. Single-Cell RNA Sequencing Reveals Heterogeneity and Cell Subtypes	
in Huh7.5 and Huh7.5-NTCP Cells Differentiated in Human Serum Culture	144
4.1. Introduction	144
4.2. Materials and Methods	145
4.2.1. Huh7.5 and Huh7.5-NTCP Cells Cultured in HS Medium	145
4.2.2. scRNA-seq of Huh7.5 and Huh7.5-NTCP Cells Cultured in HS Medium	145
4.2.3. scRNA-seq of Human Liver Cells	146
4.2.4. Data Analysis	146
4.2.5. Data Storage and Availability	147
4.3. Results and Discussion	148
4.3.1. scRNA-seq Analysis of Human Liver, Huh7.5, and Huh7.5-NTCP Cells	148
4.3.2. Expression Levels of NTCP in Huh7.5-NTCP Cells Confirmed by scRNA-seq	149
4.3.3. Clustering Analysis of Representative Genes for Delineating Cell Types in Clusters	149
4.3.4. Delineation of Cell Types within the Hepatocyte Cluster	151
4.3.5. Clustering Analysis of Genes Related to Cell Cycle	152
4.3.6. Clustering Analysis of Cholangiocyte-associated Genes	153
4.3.7. Cell Types Present in Human Liver and Huh7.5 and Huh7.5-NTCP Cultures	153
4.3.8. Hepatocyte and Cholangiocyte Cell Types Present in Liver and Cell Population	154
4.3.9. Analysis of Differential Gene Expression	154
4.3.10. Analysis of Gene Ontology (GO) Term Enrichment	155
4.3.11. Regulon Analysis of Cell Clusters	155
4.4. Conclusions	156
4.5. References	158
Chapter 5. Single-Cell RNA Sequencing of Huh7.5-NTCP Cells Infected with	
Hepatitis B Virus and Huh7.5 Cells Infected with Hepatitis C Virus	206
5.1. Introduction	206
5.2. Materials and Methods	207
5.2.1. Huh7.5-NTCP Cells Cultured in HS-Supplemented Medium	207
5.2.2. Infection of Huh7.5-NTCP Cells with HBV and Treatment with Interferon (IFN)	208
5.2.3. scRNA-seq of Huh7.5-NTCP Cells Infected with HBV and Treated with IFN	208

5.2.4. scRNA-seq Analysis of Huh7.5 Cells Infected with HCV and Treated with IFN	209
5.2.5. Data Analysis	209
5.3. Results and Discussion	210
5.3.1. scRNA-seq Analysis of Huh7.5-NTCP Cells with or without HBV Infection and IFN Treatment	210
5.3.2. HBV Transcripts in Huh7.5-NTCP Cells after HBV Infection and IFN Treatment	212
5.3.3. Differentially Expressed Genes in Huh7.5-NTCP Cells with or without HBV Infection and IFN Treatment	213
5.3.4. Interferon-Stimulated Gene Expression in Huh7.5-NTCP Cells after IFN Treatment and HBV Infection	213
5.3.5. scRNA-seq Analysis of Huh7.5 Cells with or without HCV Infection and IFN Treatment	214
5.3.6. Expression of Interferon-Stimulated Genes in Huh7.5 Cells after IFN Treatment and HCV Infection	215
5.3.7. Comparison of Interferon-Stimulated Gene Expression in HBV-infected Huh7.5-NTCP Cells and HCV-infected Huh7.5 Cells	217
5.4. Conclusion	217
5.5. References	218
Chapter 6. Conclusions and Perspectives on Further Research	237
6.1. Conclusions	237
6.2. Perspectives and Future Research	240
6.3. References	243
Bibliography	247
Appendix A. Example script (Seurat code) used for scRNA-seq data analysis	290
Appendix B. Peptide Array Enabling Studies of Nuclear Localization and Export Signals of Hepatitis B Virus	300

List of Tables

Table 3.1. Sequences used for the preparation of 10X Genomics library	118
Table 3.2. Primers used for the PCR enrichment of the HBV transcripts	124
Table 3.3. sgRNA sequences used for the CRISPR-Cas9 technique	127
Table 3.4. Percent of Huh7.5-NTCP cells determined to contain HBV RNA	136

List of Figures

Figure 1.1. HBV genome organization, viral transcripts and protein products	7
Figure 1.2. Schematic depicting multiple steps involved in the HBV life cycle	14
Figure 1.3. Overall processes and steps involved in the formation of cccDNA from rcDNA	15
Figure 2.1. Timeline for culturing and infecting Huh7.5-NTCP cells	77
Figure 2.2. Aptamer-binding assay for HBeAg	81
Figure 2.3. pgRNA and ORFs derived from HBV, the plasmids HBV/NL, and HBV-D	86
Figure 2.4. Overexpression of NTCP in Huh7.5 cells	88
Figure 2.5. Enhancement of HBV replication by human serum culture	90
Figure 2.6. pgRNA levels in Huh7.5 NTCP cells infected with MOI of 100 GE per cell	92
Figure 2.7. pgRNA levels in infected Huh7.5 NTCP cells	93
Figure 2.8. Sustained infection by HBV in Huh7.5-NTCP cells cultured in HS	95
Figure 2.9. HBV replication and expression of hepatocyte markers in Huh7.5-NTCP	97
Figure 2.10. Reduction of HBV infection by MyrB, an entry inhibitor	99
Figure 2.11. Changes in NTCP mRNA levels and surface NTCP protein expression	101
Figure 2.12. NTCP glycosylation and inhibition by tunicamycin	103
Figure 2.13. HBV pgRNA levels in infected HepG2-NTCP cells	107
Figure 3.1. Processes for the preparation of a scRNA-seq library	117
Figure 3.2. PCR technique for the enrichment of the HBV transcripts	123
Figure 3.3. CRISPR-Cas9 and PCR for the enrichment of the HBV transcripts	126
Figure 3.4. CRISPR-Cas9 technique used to cleave MT-ATP6, SLC38A7 and MT-ND2	128
Figure 3.5. Gel images showing products from PCR and CRISPR treatment	130
Figure 3.6. scRNAseq analysis of Huh7.5-NTCP cells without enrichment	132
Figure 3.7. scRNAseq analysis of Huh7.5-NTCP cells after PCR enrichment	133
Figure 3.8. scRNAseq analysis of Huh7.5-NTCP cells after CRISPR enrichment	135
Figure 3.9. Clustering analysis of scRNAseq data from the Huh7.5 NTCP cells	137
Figure 4.1. UMAP visualization of scRNA-seq data obtained from primary liver, Huh7.5, and Huh7.5-NTCP cells	159
Figure 4.2. Number of cells and contribution of cells to each scRNA-seq cluster	161
Figure 4.3. Expression level of NTCP	162
Figure 4.4. Expression level of 20 representative hepatocyte genes	163

Figure 4.5. Expression level of 11 LSEC genes	165
Figure 4.6. Expression level of 12 monocyte and macrophage genes	167
Figure 4.7. Expression level of 20 lymphocyte-associated genes	169
Figure 4.8. Expression level of 16 B cell genes	171
Figure 4.9. Expression level of 16 T and NK cell genes	174
Figure 4.10. Expression level of 4 erythroid cell genes	177
Figure 4.11. Expression level of 6 stellate cell genes	180
Figure 4.12. Expression level of 10 pericentral hepatocyte genes in primary liver	181
Figure 4.13. Expression level of 16 midcentral hepatocyte genes in primary liver	183
Figure 4.14. Expression level of 8 midportal hepatocyte genes in primary liver	185
Figure 4.15. Expression level of 13 periportal hepatocyte genes in primary liver	187
Figure 4.16. Cell-cycle phase prediction of human liver, Huh7.5 and Huh7.5-NTCP	189
Figure 4.17. Expression level of 8 cholangiocyte-associated genes	190
Figure 4.18. Cell types in primary liver Huh7.5 and Huh7.5-NTCP	193
Figure 4.19. Hepatocyte and cholangiocyte celltypes	194
Figure 4.20. Differentially expressed genes among all 14 clusters	195
Figure 4.21. Differentially expressed genes in 12 celltypes	197
Figure 4.22. Dot plot illustrating differential expression of cholangiocyte-associated genes	199
Figure 4.23. Gene ontology (GO) term enrichment in the various cell types	200
Figure 4.24. pySCENIC regulon analysis of cell clusters	202
Figure 4.25. Enlarged area showing active regulons in clusters 6 and 11	203
Figure 4.26. Comparison of regulon and gene expression levels of transcription factors	204
Figure 4.27. Resident liver cell types and Huh7.5 cells cultured in FBS or HS	205
Figure 5.1. UMAP visualization of scRNA-seq data of four Huh7.5-NTCP samples	222
Figure 5.2. Number of cells contributing to each cluster of 4 culture samples	223
Figure 5.3. HBV transcripts in Huh7.5-NTCP cells after HBV infection and IFN treatment	224
Figure 5.4. Heat maps illustrating differentially expressed genes in Huh7.5-NTCP cells	225
Figure 5.5. Expression levels of 44 interferon-stimulating genes in Huh7.5-NTCP	226
Figure 5.6. UMAP visualization of scRNA-seq data of four Huh7.5 samples	228
Figure 5.7. Number of cells contributing to each cluster of the four Huh7.5 samples.	229
Figure 5.8. Expression level of 44 interferon-stimulating genes in Huh7.5 culture	230

Figure 5.9. Interferon scores of Huh7.5 treated with IFN or IFN+HCV	233
Figure 5.10. Interferon-stimulated gene expression in HCV and IFN treated cells	234
Figure 5.11. Interferon-stimulated gene expression in HBV- or HCV-infected cells	236

List of Abbreviations

ARM	arginine rich motif
cccDNA	covalent closed circular DNA
Cas9	CRISPR-associated protein 9
CRISPR	clustered regularly interspaced short palindromic repeats
DDB1	DNA-binding protein 1
DMSO	dimethyl sulfoxide
dsIDNA	double-stranded linear DNA
EGFR	epidermal growth factor receptor
ESC	embryonic stem cell
FBS	fetal bovine serum
GE	genome equivalents
HBeAg	HBV e antigen
HBsAg	HBV surface antigen
HBV	hepatitis B virus
HBV/NL	HBV containing a nanoluciferase reporter
HBx	HBV X protein
HCC	hepatocellular carcinoma
HCV	hepatitis C virus
HIV	human immunodeficiency virus
HLC	hepatocyte-like cells
HS	human serum
HSPG	heparin sulfate proteoglycans
Hsp90	heat shock protein 90
IFN	interferon (α , β , γ)
iPSC	induced pluripotent stem cells
kb	kilobase
kDa	kiloDalton
MOI	multiplicity of infection
MVB	multivesicular body
NES	nuclear export signal

NGS	next-generation sequencing
NHEJ	nonhomologous end joining
NLS	nuclear localization signal
NTCP	sodium taurocholate cotransporting polypeptide
ORF	open reading frame
pgRNA	pregenomic RNA
PKC	protein kinase C
PNES	putative nuclear export signal in HBV polymerase
rcDNA	relaxed circular DNA
RIG-I	retinoic acid inducible protein I
PCNA	proliferating cell nuclear antigen
PCR	polymerase chain reaction
PEG	polyethylene glycol
PHH	primary human hepatocyte
Pol	polymerase
RT	reverse transcriptase
scRNA-seq	single-cell RNA sequencing
sgRNA	single-guide RNA
Smc5/6	structural maintenance of chromosome 5/6 complex
STING	viral DNA sensing by stimulator of IFN genes
TP	terminal protein
UMAP	Uniform Manifold Approximation and Projection
VLDL	very low-density lipoprotein

Chapter 1. Introduction

1.1. Global Health Burden of the Hepatitis B Virus

Hepatitis B virus (HBV) is an enormous public health burden. An estimated 2 billion individuals worldwide have been infected with the virus, resulting in approximately 250 million people chronically carrying the infection [1]. The population of chronic HBV carriers is about 7 times greater than the number of individuals chronically infected with human immunodeficiency virus (HIV) [2]. HBV chronic carriers are at high risk for developing liver diseases, culminating in an estimated 600,000 HBV-associated deaths annually. Due to its immense prevalence, HBV is the leading cause of cirrhosis, liver cancer, and liver-disease induced mortality globally [3, 4]. Current HBV therapies have limited efficacy. Suppressive therapies effectively inhibit viral replication; however, these treatments usually require lifelong adherence to avoid viral rebound. The treatments decrease, but fail to completely prevent the lethal sequelae of chronic HBV [5]. Furthermore, economic barriers constrain adequate diagnostic and treatment accessibility in resource-limited areas where the disease burden is the highest. This resource scarcity in high prevalence regions and sparse awareness surrounding the impact of this illness contributes to only 27 million individuals (10.5% of the estimated total number of people chronically infected with HBV) having received an HBV diagnosis and only 4.5 million (16.7%) of these HBV chronic carriers receiving treatment [6].

HBV is an extraordinarily infectious virus *in vivo*, with an infectivity that is approximately 100 times and 10 times more infectious than HIV and HCV, respectively. It has been estimated that nearly everyone exposed to HBV without vaccination becomes acutely infected. However, the frequency of development to chronic infection depends on the age at infection. For instance, 90% of neonates exposed perinatally and 30% of children infected between 1 to 6 years of age

become chronic carriers of HBV [7]. In contrast, only 3-5% of acutely infected adults establish chronic infections. Transmission to infants typically occurs through vertical transmission from the mother and infection in children occurs within the household. Infection of adults with HBV generally arises through environmental exposure to HBV-containing bodily fluids, including sexual transmission or blood-to-blood contact, such as blood transfusions or intravenous drug use.

Global prevalence of chronic HBV is estimated to be 3.9% [8]. The regions of highest HBV endemicity is the West Pacific and Africa, with estimated prevalence of 5.3% and 8.8%, respectively. Within these regions, some countries have especially high levels of infection, for instance 22.7% in Kiribati and 22.4% in South Sudan. Europe and North America have lower rates of HBV, at an estimated 2.1% and 0.8%, respectively.

The United Nations (UN) included viral hepatitis in its 2030 Agenda for Sustainable Development. In 2016, the World Health Organization (WHO) outlined strategies to eliminate all viral hepatitis infections. The WHO aims to reduce new infection incidence by 90% and infection-associated mortality by 65% by 2030 [9-11]. Concerted research efforts, such as the International Coalition to Eliminate HBV (ICE-HBV)), aim to discover novel therapeutics that cure chronic HBV [12, 13]. However, a lack of curative therapy, worldwide prevalence, high infectivity, insufficient public health awareness and response have contributed to the continuous global health burden of HBV. Universal vaccination at birth is now being implemented or advocated in more than 200 countries and this will decrease the chronic carrier rate in the long term.

1.2. Disease Progression

Liver cirrhosis and hepatocellular carcinoma (HCC) are major liver diseases that can develop as a consequence of repeated and consistent inflammation and liver damage caused by chronic HBV infection. HCC is the primary cause of death among patients with cirrhotic livers [14]. The Lancet Global Burden of Disease studies estimate that liver cancer is the fifteenth most common cancer globally, and is the fourth most deadly kind of malignancy [3, 4]. Furthermore, these estimates suggest that HBV is the leading cause of cirrhosis and liver cancer worldwide. Two studies on “Risk Evaluation of Viral Load and Associated Liver Disease/Cancer” conducted in Taiwan reported that for individuals with greater than 10^6 copies of HBV DNA per mL of serum, incidence of liver cirrhosis and HCC were 2,498 and 1,152 per 100,000 patients per year, respectively. Conversely, patients with less than 300 copies of HBV DNA per mL of serum developed cirrhosis and HCC at lower rates of 338.8 and 108 per 100,000 person-years, respectively. These data illustrate a relationship between HBV DNA level and occurrence of cirrhosis and HCC, and reinforce the prognostic benefit of administering suppressive therapy in individuals with high viral load to repress HBV DNA levels [15, 16]. Without treatment, the relative risk of developing HCC among chronic HBV carriers is 100 times greater than uninfected individuals. In Europe and North America, HBV causes 10-15% of HCC occurrences, whereas in Asia and Africa, HBV is responsible for 70% of HCC cases [17], reflecting the relevant prevalence of chronic HBV. Globally, HBV is the strongest risk factor for developing HCC, besides cirrhosis, which contributes to the high HBV-related mortality worldwide.

Infection with HBV can progress in four ways: acute, occult, fulminant, or chronic hepatitis. Acute infection with HBV describes initial infection that can last up to 6 months and range in presentation from asymptomatic to self-limiting hepatic inflammation [18]. Occult HBV

infection is classified as having persistent detectable HBV DNA levels but no detectable HBV surface antigen (HBsAg) in serum [19]. The vast majority of individuals with occult infection do not develop HBV-related complications. However, occult HBV is concerning because undiagnosed individuals potentially transmit HBV through transfusions or liver donations or receiving immunosuppressive therapies that can reactivate HBV replication. Fulminant hepatitis is a condition characterized by rapid deterioration and liver failure leading to encephalopathy and a mortality of approximately 70% [20]. HBV-associated fulminant hepatitis occurs in less than 1% of acute infections or during reactivation of chronic infection [21].

Patients continuing to have HBV positive serology for over 6 months are diagnosed as having chronic infection. The disease course of chronic HBV has been described in three phases: immune tolerant, immune clearance, and inactive carrier phases [22]. The natural history of HBV is dynamic and does not necessarily follow these phases consecutively. These phases are delineated by serum levels of HBV antigens and alanine transaminase (ALT, a liver enzyme that is released from lysed liver tissue and is indicative of hepatic inflammation). The immune tolerant phase displays high HBV DNA and HBsAg but normal ALT levels. During the immune clearance phase, patients experience fluctuating ALT levels and ultimately acquire anti-HBe antibodies and lose HBeAg. In the inactive carrier state, also called the HBeAg-negative chronic infection phase, ALT levels remain normal and HBV DNA gradually declines. Some patients who undergo the inactive carrier state can eventually achieve spontaneous HBsAg seroclearance, which characterizes a 'functional cure' of HBV and is the target for chronic HBV treatment [23].

1.3. Hepatitis B Virus

1.3.1. *Hepadnaviridae* Family

HBV belongs to the *Hepadnaviridae* family, which includes five genera: *Orthohepadnaviruses*, *Avihepadnaviruses*, *Herpatohepadnaviruses*, *Metahepadnaviruses*, and *Parahepadnaviruses*. *Orthohepadnaviruses* infect mammals with narrow host and tissue tropism and include the prototypic human HBV. *Avihepadnaviruses* also have narrow liver tropism in specific bird species and includes the heavily studied duck HBV. *Herpatohepadnaviruses* infect reptiles and frogs while *Metahepadnaviruses* and *Parahepadnaviruses* infect fish [24, 25]. These three newer *Hepadnaviridae* genera were identified through genomic analyses of environmental samples showing overlapping open reading frames (ORFs) with sequences resembling *Hepadnaviridae* reverse transcriptase (RT) domains and surface antigen-like genes. Therefore, many of these fish, amphibian, and reptile virus species have been inferred solely from genetic sequencing and have not been confirmed to cause bona fide infections. Common characteristics of this family of viruses include the expression of core, surface, and polymerase proteins and replication of the partially double-stranded DNA genome by reverse transcription. This virus family has the smallest of double-stranded DNA viral genomes, ranging from 3 to 3.5 kilobases (kb).

1.3.2. Virion Structure

The first electron micrographs obtained of HBV virions were acquired by Dr. Dane, leading to the designation of these infectious virions as Dane particles [26]. These Dane particles are lipid bilayer enveloped virions 42 to 47 nanometers (nm) in diameter, containing an icosahedral nucleocapsid with a diameter of 36 nm [27, 28]. The capsid is composed of 120 dimers of core protein, with a triangulation number of T=4 [29]. The viral envelope contains

small, medium, and large surface proteins [30]. Within the capsid is the partially double-stranded, relaxed circular DNA (rcDNA) genome covalently attached to the HBV polymerase [31-33]. Host proteins, such as heat shock protein 90 (Hsp90) and protein kinase C (PKC), have been shown to be packaged within the Dane particle and implicated in mediating infection [34, 35].

Non-infectious viral particles that lack nucleic acid sequences are also secreted from infected cells. Genome-free or empty virions are composed of enveloped capsids devoid of any nucleic acid [36]. Filamentous and spherical subviral particles are 22 nm to 25 nm in diameter and only composed of lipid bilayers and surface antigen [37].

1.3.3. Genome Characteristics

HBV has a compact, partially double-stranded, 3.2 kb relaxed circular DNA (rcDNA) genome (**Figure 1.1**) comprised of a complete minus strand and approximately two thirds of the plus strand, missing from the 3' end of the plus strand [38]. Slight variations in genome length and sequence exist between the 10 HBV genotypes, A to J [39]. Within the virion, the 5' end of the minus strand is covalently attached to the viral polymerase [40]. Upon release of this partially double-stranded genome species into host cell nuclei, the partially double-stranded DNA becomes a completely double-stranded covalent closed circular DNA (cccDNA) that serves as a template for transcription (**Figure 1.1**).

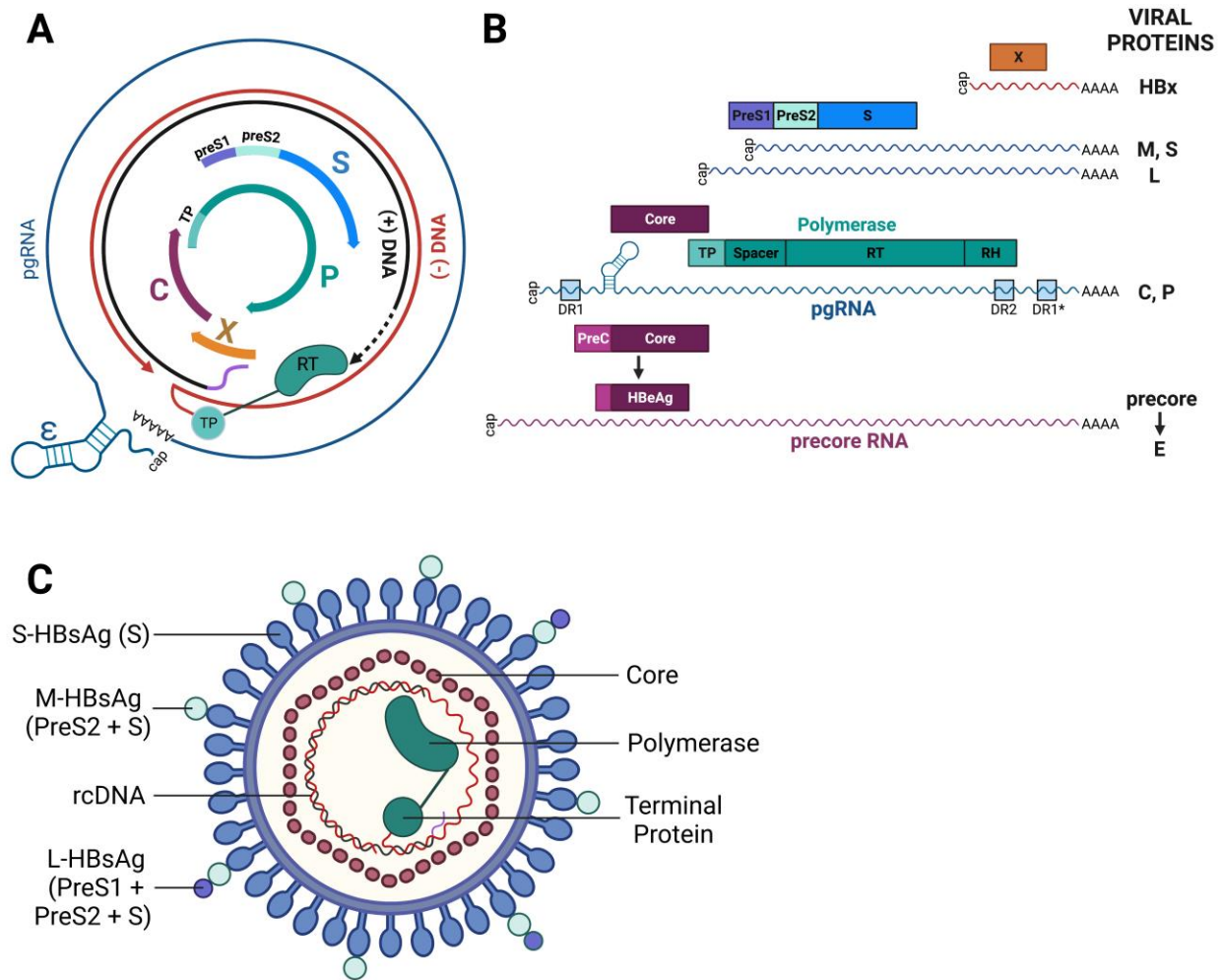


Figure 1.1. HBV genome organization (A) and viral transcripts and protein products (B). The blue and red lines in (A) depict partially double-stranded, relaxed circular DNA (rcDNA). On the minus-strand (red), the 5' end is linked to terminal protein (TP) domain of P protein. On the plus-strand (black), the purple oligo at the 5' end depicts the RNA primer and the dashed black line denotes the incompletely synthesized 3' end. The thicker arrows inside the rcDNA represent the ORFs for X protein (X), core (C), surface (S), and polymerase (P). The outer blue line represents pgRNA with the 5' proximal ϵ signal. Viral transcripts and protein products are shown in (B). Subgenomic RNAs and greater-than-genome length RNA are shown with linear representation of the ORFs. DR1, DR2, and DR1* are direct repeat sequences involved in the formation of rcDNA. Virion components are illustrated in (C). Adapted from [41] with permission under a Creative Commons Attribution 4.0 International License and created using tools from BioRender.com.

The entirety of the HBV genome encodes proteins with overlapping ORFs in different reading frames with regulatory elements embedded within these coding sequences. This extensive genomic overlap of sequences necessary for viral replication explain the inability to create viable reporter viruses, since a deletion or insertion in virtually any part of the HBV genome would disrupt crucial components. The genome has four major unidirectional, overlapped and frame-shifted ORFs: the precore/core (preC/C), polymerase (P), surface antigens (S), and X protein genes. Transcription is driven from 4 promoters (preC/pregenomic, preS1, preS2, and X) with further regulation from two enhancers (I and II). These regulatory elements coordinate variable transcription of different RNA species and their interaction with liver-specific transcription factors confer narrow host tropism [43]. Enhancer I promotes transcription from the preC/pregenomic and X promoters, whereas enhancer II upregulates transcription from the preS1, preS2, and X promoters.

Five unique RNA species are transcribed (**Figure 1.1**). They are unspliced, 5' capped, and co-terminal with a common 3' end and polyadenylation signal (An). They include two 3.5 kb greater-than-genome-length transcripts with terminal redundancies (precore and pregenomic RNA) and three subgenomic transcripts that are 2.4 kb, 2.1 kb, and 0.7 kb. These RNAs encode seven proteins. The pregenomic RNA (pgRNA) serves as a bicistronic mRNA for the production of core and polymerase proteins and is the template for reverse transcription of nascent DNA genomes. The precore RNA encodes precore protein, which is the precursor for e antigen (HBeAg). The 2.4 kb subgenomic RNA encodes large surface antigen (L-HBsAg) while the 2.1 kb subgenomic RNA encodes medium (M-HBsAg) and small surface antigen (S-HBsAg). The 0.7 kb transcript directs translation of X protein.

1.3.4. HBV Proteins

Precore proteins

Precore protein is the precursor for HBV e antigen (HBeAg) which is translated from a start codon 90 nucleotides in-frame with and upstream from the core protein start codon. Within these additional N-terminal amino acids (aa), called the preC region, is a 19-aa signal peptide that mediates translocation of the precore protein to the endoplasmic reticulum (ER). There, proteolytic cleavage removes the signal peptide at the N-terminus and an arginine rich motif (ARM) at the C-terminus [44]. The resultant 15 kDa HBeAg is secreted from infected cells. HBeAg is dispensable for viral replication and may play a role as a tolerogen in infected neonates and during chronic HBV [45, 46]. Because secreted HBeAg can be detected in serology, this viral antigen serves as a useful diagnostic and prognostic marker for monitoring patients with chronic HBV, and serves as a surrogate marker for active HBV replication. Development of antibodies against HBeAg (anti-HBe) and consequent loss of HBeAg on serology is associated with an approximate 2 log reduction in HBV DNA titers and improved clinical prognoses [47-49]. Therefore, HBeAg seroconversion is an important milestone in disease progression and one of the therapeutic goals of antiviral therapy.

Core Protein

The core protein is 21 kDa in size and is the unit that make up the nucleocapsid. The N-terminus facilitates dimerization and subsequent spontaneous capsid assembly, while the C-terminal domain binds nucleic acid and is essential for pgRNA encapsidation [50-52]. The C-terminus contains 16 arginine residues making up four arginine-rich motifs (ARMs) (I to IV). ARM I binds RNA and likely engages pgRNA to facilitate capsid formation. ARMs II, III, and IV bind DNA and are involved with reverse transcription and DNA synthesis within capsids

[53]. Core protein interactions with surface antigen and polymerase have also been demonstrated with likely roles in virion formation and viral replication [54, 55].

Polymerase

The HBV polymerase is the largest protein produced by the HBV virus, with an ORF spanning almost three quarters of the entire HBV genome, and the only protein with enzymatic activity. This 90 kDa enzyme is a DNA- and RNA- dependent DNA polymerase composed of 4 domains: the terminal protein (TP) at the N-terminus, a spacer region, a reverse transcriptase (RT) domain, and a C-terminal RNaseH domain [56]. The TP spans residues 1 to 177 and has a tyrosine residue at position 63 (Y63) that is essential for protein priming and initiation of DNA synthesis. The hydroxyl group on this tyrosine binds the 5' phosphate of the first guanosine for template driven DNA synthesis, thereby serving as the primer. This covalent bond between TP and this newly synthesized minus strand of HBV DNA remains throughout DNA synthesis until the TP is removed during cccDNA formation. In addition, the T3 motif in the TP is involved with RNA binding and packaging [57]. The TP domain is unique to *Hepadnaviridae* and has no homology with other reverse transcriptases. The spacer region serves as a linker, which may allow the TP and RT domains to form a conformation within a single protein to perform their respective functions. This 158-residue spacer region overlaps with the preS1 surface protein ORF, which is responsible for receptor binding and viral entry. Therefore, although the spacer region is dispensable to viral replication, mutations in the spacer region can affect virus viability if preS1 is altered into a non-functional protein. On the other hand, because the spacer is likely nonessential, selective pressure can influence preS1 to mutate and potentially benefit HBV infection without affecting the enzymatic activity of the polymerase. The RT domain possesses DNA dependent DNA polymerization and reverse transcriptase activities. No crystal structure

for any domains of the HBV polymerase has been identified. However, the RT and RNase H domains of HBV polymerase have homology to the HIV RT/RNase H. The homology of the HBV RT domain to the HIV RT have facilitated modelling studies based on HIV RT crystal structures [58]. The C-terminal 153 residues make up the RNase H domain, which removes all but the 5' end of the pgRNA template during reverse transcription. The RNase H domains of HBV and HIV are homologous, with HBV RNase H showing sensitivity to drugs originally designed to inhibit the HIV ribonuclease [59].

Surface Protein

HBV was discovered in 1965 by Blumberg *et al.* in serum of Australian Aborigines, with the identification of the Australia antigen, which was later named the surface antigen [60]. HBV surface antigen (HBsAg) proteins comes in three co-terminal forms that decorate virions and subviral particles and are distinguished by their size: small (24 kDa), medium (preS2, 30 kDa), or large (or preS1, 39 kDa) [61]. All three of these proteins share the same 24 kDa C-terminal end but have different in-frame translation start sites [62]. Therefore, the preS1 protein sequence exists in large HBsAg and the preS2 sequence exists in large and medium HBsAg. Large and small HBsAg are necessary for envelopment whereas medium HBsAg is nonessential but may enhance viral secretion [62-64]. The small HBsAg is the most abundant of the three surface proteins on viral envelopes [65]. These surface proteins are co-translationally inserted into the ER, where they are all glycosylated, and preS1 is additionally myristoylated on its N-terminus [66]. The 48 N-terminal myristoylated amino acids of preS1 is responsible for HBV binding and is essential for infection [67, 68]. Furthermore, this myristoyl group is required for viral entry.

X Protein

Unique to the *Orthohepadnavirus* genus is the expression of X protein (HBx). This 17 kDa protein is required for replication and promiscuously interacts with a variety of host proteins, far more than any other HBV protein [69]. These varied interactions with diverse proteins are implicated in cell signal transduction, transactivation, DNA repair, epigenetic modulation, apoptosis, cell cycling dysregulation, hepatocarcinogenesis, and protein degradation [70-79]. Elucidation of HBx interaction uncovered a novel host cell mechanism for silencing foreign DNA in the nucleus [78]. Structural maintenance of chromosome 5/6 complex (Smc5/6) was shown to bind and inhibit transcription from HBV cccDNA but not from the chromosomal genome. To combat this host defense mechanism, HBx recruits damage-specific DNA-binding protein 1 (DDB1), a component of a E3 ubiquitin ligase, which targets Smc5/6 for degradation and lifts the Smc5/6 induced transcription repression. In addition, integrated fragments of the HBx gene in infected host genome is expressed more frequently in malignant tissue in patients with chronic infection. In short, the diverse interactions of HBx with host proteins confer a multitude of potential functions that may contribute to HBV-induced disease.

1.3.5. HBV Life Cycle

The HBV life cycle involves multiple steps, including viral entry, cccDNA biogenesis, progeny nucleocapsid production, virion formation, and egress (**Figure 1.2**) [80, 90]. Viral entry is mediated by sodium taurocholate co-transporting polypeptide (NTCP), heparin sulfate proteoglycans (HSPG), and epidermal growth factor receptor (EGFR) on the surface of hepatocytes [81, 82]. cccDNA biogenesis consists of three distinct steps: nuclear transport of rcDNA and uncoating, repair of rcDNA to form cccDNA, and cccDNA chromatinization [90].

cccDNA can serve as the template for multiple sub-genomic mRNAs, pre-genomic and precore mRNAs, which are translated to several viral proteins, including capsid (core antigen), Pol (polymerase), HBx (X protein), and surface antigens. Progeny nucleocapsid production is initiated by the binding of the HBV polymerase to pre-genomic mRNA, which triggers the encapsidation (packaging) and synthesis of rcDNA. The resultant nucleocapsids can either be reimported into the nucleus or it can be enveloped in the multivesicular body (MVB) to complete virion formation. Subsequent virion egress completes the HBV life cycle.

Viral entry and translocation to the nucleus

The HBV lifecycle begins with reversible attachment to heparin sulfate proteoglycans (HSPG) and high affinity binding of preS1 to an entry receptor, sodium taurocholate co-transporting polypeptide (NTCP) [81, 82]. Through interactions between epidermal growth factor receptor (EGFR) and NTCP at the cell surface, the EGFR-NTCP-virion complex is translocated from the plasma membrane into intracellular vesicles [83]. Therefore, HBV internalization is facilitated through EGFR-mediated endocytosis [84]. EGFR activation and relocalization to early and late endosomes are required for HBV internalization, whereas EGFR downstream signal cascade is not essential to HBV infection. HBV becomes unenveloped and the nucleocapsid traffics to the nucleus through mechanisms that are not understood. Electron microscopy has shown the capsid stalls in and appears to dock in the nuclear basket of the nuclear pore complex [85]. It is speculated that interactions between core protein and the nuclear basket facilitate destabilization and potentially disassembly of the HBV capsid and release of the rcDNA genome into the nucleus [86, 87].

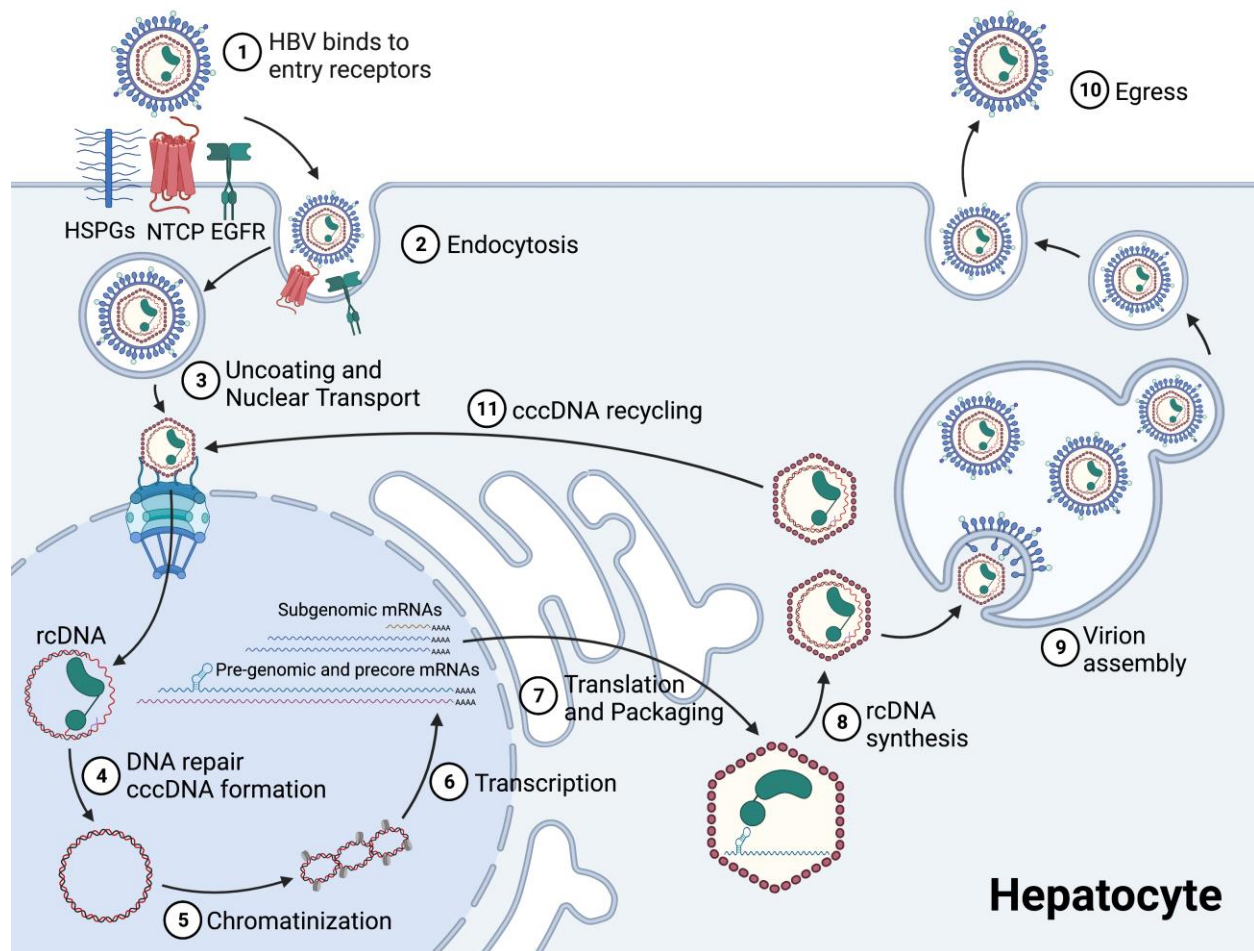


Figure 1.2. Schematic depicting multiple steps involved in the HBV life cycle, including viral entry, nuclear transport and capsid uncoating, cccDNA formation, transcription, translation, nucleocapsid production, virion assembly, and virion egress. Adapted from [90] with permission under a Creative Commons Attribution 4.0 International License and created using tools from BioRender.com.

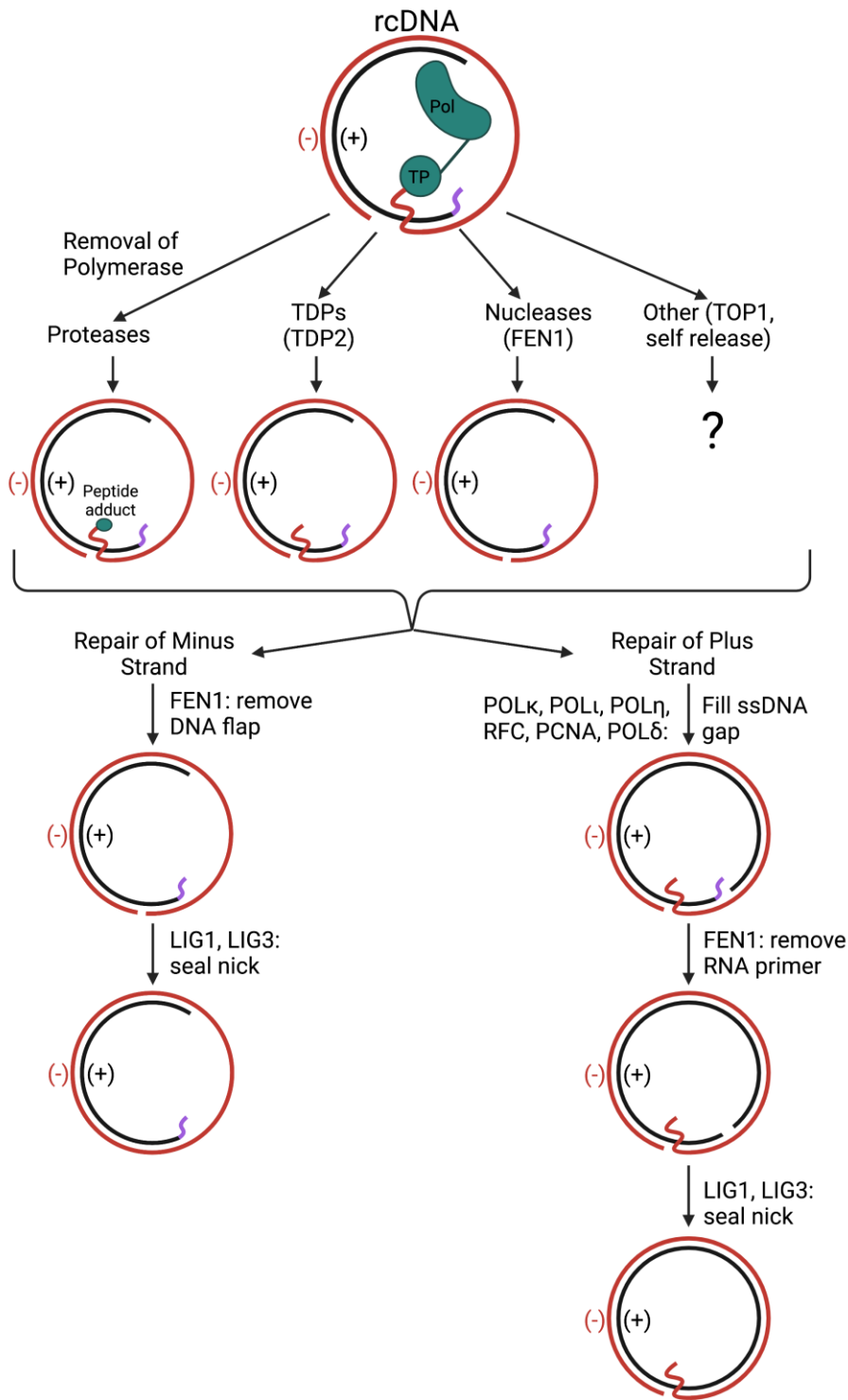


Figure 1.3. Schematic showing the overall processes and specific steps involved in the formation of cccDNA from rcDNA. Adapted from [89, 90] with permission under the Creative Commons Attribution 4.0 International License and created using tools from BioRender.com.

Formation of cccDNA

Within the nucleoplasm, the rcDNA is converted into cccDNA by the HBV polymerase and various host proteins [88-91]. The conversion of rcDNA to cccDNA involves DNA synthesis to complete the plus strand; removal of the polymerase covalently attached to the 5' end of the minus strand, removal of the short 5' terminal redundancy on the minus strand, and removal of the RNA primer used to initiate plus strand synthesis; as well as ligation of the plus and minus strands (**Figure 1.3**) [88-90]. The plus strand continues to be synthesized by the HBV polymerase upon release into the nucleus until the covalently bound protein is removed from the minus strand. Host DNA repair enzymes are presumed to be involved in cccDNA formation since the processes required to augment rcDNA to cccDNA closely resemble functions performed by host DNA repair machinery and cannot be executed by the HBV polymerase alone [91].

Recent investigations generated recombinant HBV rcDNA and biochemical assays, which suggested that proliferating cell nuclear antigen (PCNA), the replication factor C (RFC) complex, DNA polymerase δ (POL δ), flap endonuclease 1 (FEN1), and DNA ligase 1 (LIG1) were sufficient host factors for forming cccDNA [89, 92]. Removal of the polymerase covalently bound to the minus strand via a tyrosylphosphodiester bond can be accomplished with the tyrosyl-DNA phosphodiesterase 2 (TDP2), a cellular enzyme that cleaves tyrosyl-DNA linkages formed between topoisomerase II and host DNA [93, 94]. However, the requirement of TDP2 for cccDNA formation is debated with evidence that TDP2 is functional in biochemical assays but nonessential during HBV infection [94]. FEN1 is implicated in the removal of the 5' redundant overhang on the minus strand either while the polymerase remains covalently attached or following polymerase removal [89, 95]. However, FEN1 endonuclease activity was reduced if a

protein adduct was present on the minus strand overhang. POL δ complexed with PCNA and RFC may play a role in plus strand DNA synthesis and removal of the plus strand RNA primer, generating a flap that is subsequently removed by FEN1 [89, 92, 96]. Polymerase alpha and topoisomerase 1 may be involved in repairing the nick in the minus strand [96, 97], whereas polymerase kappa is implicated in filling the gap in the plus strand [98]. There is some evidence that topoisomerase 2 is required for circularization of both viral DNA strands [97]. There is evidence that LIG1 and DNA ligase 3 are involved with the ligation of the minus and plus strands [99]. Double-stranded linear DNA (dslDNA) are a minor form of HBV genomes that can also form cccDNA through nonhomologous end joining (NHEJ) [100]. Host proteins involved with NHEJ, such as Lu80 and DNA ligase 4, may be required for NHEJ mediated cccDNA formation [99, 101]. Although *in vitro* and biochemical investigations have revealed several potential host proteins involved in cccDNA synthesis, several redundancies exist in host DNA repair and may likewise occur in the formation of cccDNA.

Upon formation of the cccDNA, this fully double-stranded HBV genome becomes associated with host histones into a chromatin-like episome [102, 103]. The cccDNA is therefore stable and has a long half-life, making this episome the reservoir for chronic HBV infection [104-106]. This minichromosome serves as the template for transcription by host machinery. The cccDNA is associated with histones enriched in posttranslational modifications linked to active transcription and low levels of transcriptionally repressive histone modifications [107]. This leads to the production of the aforementioned viral transcript species and proteins by host machinery [108]. The steps from HBV entry to cccDNA formation are considered to be early steps of the viral life cycle, whereas transcription to viral secretion are denoted as late steps of the HBV life cycle.

Pregenomic RNA and polymerase encapsidation

Following transcription from cccDNA and subsequent translation of HBV proteins, pgRNA is packaged with polymerase inside viral capsids [109]. For efficient viral replication, pgRNA must be packaged preferentially to host RNAs. The epsilon sequence (ϵ), HBV polymerase, and core protein are all involved with this specific pgRNA packaging [53, 109-111]. The ϵ near the 5' end of pgRNA is required and sufficient for mediating this selective encapsidation [110, 112]. The additional 30 nt at the 5' end of the precore RNA results in ϵ being farther from the 5' end compared to in pgRNA. This is what discriminates packaging of pgRNA instead of precore RNA despite their similar size and sequence [112]. The ϵ is within the terminal repeated sequences and therefore exists on the 5' and 3' ends of pgRNA. The ϵ is a stem loop structure containing a lower stem, an internal 6 nt bulge, an upper stem containing a single unpaired U bulge, and an apical 3 nt loop. The ϵ bulge, RNA immediately surrounding the bulge, single unpaired U bulge in the upper stem, and apical loop are essential to pgRNA packaging [110, 113]. The two 5' nucleotides of the bulge sequence as well as the apical loop sequence are required for polymerase binding whereas the other nucleotides in the bulge can be altered and the bulge remains functional [114]. The lower stem can also be mutated and still facilitate pgRNA packaging as long as the sequences are complementary.

Binding of the polymerase to the ϵ requires portions of the TP, spacer region, and RT. These portions of the polymerase do not include the C-terminus of the RT domain nor the RNase H domain, suggesting enzymatic activity is not required for HBV polymerase binding to the ϵ . However, ϵ binding is required to poise the polymerase for downstream processes including protein-primed initiation of reverse transcription [115]. Furthermore, although only portions of the polymerase are required for binding the ϵ , the entire polymerase has been shown to be

required for packaging of pgRNA [116]. Once the polymerase binds the ϵ , nucleocapsid assembly is triggered thereby selectively encapsidating the polymerase and pgRNA inside viral capsids [117]. Core interacts with at least three sites on polymerase, one each in the TP, RT, and RNase H domains [54]. The C-terminal ARDs of core also binds pgRNA to facilitate capsid assembly [50]. This shields replicative intermediates from detection by innate immune system.

Reverse transcription and rcDNA synthesis

Reverse transcription and DNA synthesis occurs within viral capsids within the cytoplasm of infected cells. These processes involve the translocation of the polymerase on and between template strands mediated by transferring between direct repeat sequences (**Figure 1.1**). Direct repeats (DR1 and DR2) are 11 to 16 bp sequences that are identical to each other in all sequenced *Hepadnaviridae* [118]. Because DR1 and DR2 flank the gap in the minus strand, these direct repeats thereby mediate the circular shape of the rcDNA genome despite both DNA strands being incomplete. Therefore, in pgRNA DR1 exists twice, upstream of each ϵ , and DR2 occurs once, upstream of the 3' DR1.

The minus DNA strand is synthesized by the HBV polymerase with the Y63 residue in TP for protein priming and reverse transcription using the pgRNA as a template [119]. The bulge of the 5' ϵ serves as the origin of replication, with the Y63 forming a phosphodiester bond with a dGTP, which is complementary to a cytosine in the ϵ bulge and the first nucleotide of the DNA minus strand [120]. This covalent bond between dGTP and the polymerase remains until the rcDNA can be deposited into a nucleus and conversion to cccDNA occurs. The dGTP is extended by an addition 2 or 3 nucleotides, creating a short DNA primer. This primer then translocates from the 5' ϵ to the 3' terminal direct repeat 1 (DR1*) of pgRNA and proceeds with minus strand reverse transcription in a 5' to 3' direction (**Figure 1.1**) [121]. As reverse

transcription occurs, the RNase H concurrently degrades the pgRNA template, leaving only a short portion of the 5' capped end [122]. This 11–16 nt RNA contains the pgRNA DR1, which serves as a primer for plus strand elongation either through translocation or *in situ* priming [118].

Plus strand synthesis typically begins when the RNA primer translocates and binds with complementarity to the DR2 site on the newly synthesized DNA minus strand. In approximately 10% of cases, the RNA primer translocation does not occur, resulting in *in situ* priming and subsequent formation of dsIDNA instead of rcDNA [100]. RNA primer translocation leads to DNA synthesis progressing to the 5' end of the minus strand template. Because of the terminally redundant regions in the minus strand, template switching can then occur to use the DR1 on the 3' end of the minus strand as a template [123]. This template switching results in genome circularization, plus strand synthesis, and rcDNA maturation [124]. Varying lengths of plus strand synthesis is completed within the viral capsid, resulting in heterologous 3' ends of the plus strand [33, 38, 125]. This plus strand gap can be attributed to volume and concentration constraints as well as reduced substrates once the capsid is enveloped [126]. Mature capsids formed with plus strand synthesis can now undergo egress or intracellular recycling processes.

Nucleocapsid envelopment and viral egress

Empty nucleocapsids and capsids containing mature rcDNA can be enveloped and secreted from infected cells. In contrast, immature capsids containing pgRNA or single stranded minus DNA are largely excluded from envelopment. The vast majority (over 90%) of enveloped capsids are empty lacking any nucleic acid [36, 127]. Virion envelopment for the creation of Dane particles is linked to the state of the viral genome, as evidenced by varying stages of genome replication in capsids within infected cells as opposed to serum derived virions predominantly containing mature partially double-stranded rcDNA [128, 129]. The signals and

processes that favors secretion of empty capsids and mature capsids, but not RNA or single stranded DNA containing capsids, remain unknown [130]. Regions of large and small HBsAg have been implicated in interacting with the nucleocapsid and facilitating secretion [131-133]. Capsids become enveloped by budding into the ER containing co-translationally inserted surface proteins [62]. In addition to Dane particles, empty capsids and subviral particles are secreted 100 and 100 to 100,000 fold excess, respectively [36, 37, 134]. Some evidence suggests the pathways for formation of virions and subviral particles are distinct, indicating there may be a mechanism causing the higher levels of subviral particles [64]. Although not fully elucidated, the immense secretion of non-infectious enveloped particles has been proposed to sequester HBs antibodies and promote immune tolerance to facilitate persistent infection [135-137]. Whereas subviral particles are excreted through the constitutive secretory pathway [138], some investigations demonstrate the involvement of endosomal sorting complex required for transport (ESCRT) machinery in virion secretion [139, 140]. The HBV life cycle and viral budding tends to culminate in a noncytopathic and nonlytic infection.

cccDNA amplification

Over the course of initial and persistent HBV infection, cccDNA copies in the nucleus can increase. Because earlier studies into HBV biology relied heavily on cell culture models that used transient transfection of overlength HBV constructs or could only be infected by initial HBV inoculum but not by subsequent secreted viral progeny, it was observed that cccDNA was amplified through an intracellular recycling process [141]. Intracellular recycling describes a process whereby mature intracellular capsids containing relaxed circular DNA are transported to the nucleus to un-coat and form more cccDNA as opposed to being enveloped and secreted. With the development of HBV research tools such as effective entry inhibitors and *in vitro* systems

that can propagate secondary infections, recent observations suggested that the major route of cccDNA amplification is an extracellular recycling pathway [142-144]. This pathway describes nascently secreted enveloped viral progeny re-entering the same cell from which it had just egressed and proceeding to cccDNA formation similar to initial exogenous infection. Viral and host mechanisms for regulating cccDNA amplification are generally poorly understood. Some studies have demonstrated an inverse correlation between the level of large HBsAg and cccDNA, with increased large HBsAg leading to more HBV secretion and less cccDNA [88, 145-147]. However, other investigations show no cccDNA amplification with ablation of envelope protein expression [148, 149]. Therefore, the involvement of surface antigen in regulating cccDNA amplification remains to be clarified.

Integration of HBV genome

Integration of HBV genome into host chromosomal DNA is frequently observed in patients experiencing chronic HBV infection [150-152]. Integration of HBV DNA occurs when double-stranded linear DNA (dslDNA) enters the host nucleus and, rather than being converted to cccDNA, is instead integrated into sites of double-stranded host genome breaks by NHEJ [153, 154]. Since pgRNA is greater than genome length due to transcription from a circular genome, dslDNA is 18nt longer than genome length, and the core promoter is separated from its ORF in dslDNA, integrated HBV genomes alone cannot support the production of virions. However, gene products with intact promoters can be expressed, such as surface antigen and X protein [71, 155, 156]. HBV genome integration occurs randomly with no reported hot-spots; however, integration of HBV in tumor tissues are enriched at sites linked to carcinogenesis [157]. Indeed, approximately 90% of HBV-associated tumors have integrated HBV DNA [158]. These HBV integrations have been reported to be oncogenic by causing chromosomal instability, *cis*

activation of host genes, insertion into tumor suppressor genes, inducing cellular stress from expression of viral proteins, and mediating chromosomal rearrangements [159-163]. In addition, the number of integration events is reported to be higher in HBV-induced tumor tissue compared to matched adjacent healthy tissue [164].

The process of HBV genome integration has long been considered a chance occurrence that happens over the course of chronic infection. Recently developed models for reliable detection of HBV integration events have demonstrated that integration can occur early in the viral life cycle during *in vitro* infection [165]. In primary human hepatocytes and a variety of infectable hepatoma cell lines, integration occurred at least once per cell which persisted up to 9 days post infection. The integration sites were distributed across the host cell genome. Integration was blocked by an HBV entry inhibitor, but not by nucleoside analogues, suggesting *de novo* genome replication is not required for integration in this model. However, *in vitro* infection requires a very high HBV titer of up to 1000 genomes per cell, which would consist of at least one virion-containing dsDNA per cell. Therefore, the kinetics of HBV integration *in vivo* where lower viral titers inoculate hepatocytes could be different. However, integration has been observed to occur early on during chronic infection in patients [152]. The surprisingly prompt integration of HBV genomes has incited speculation that integration may in fact play a role in the viral life cycle. Although its association with cancer development and being a potential reservoir for the production of large quantities of immunomodulatory HBsAg [166], it is unknown whether HBV integration is required for HBV infection. Due to challenges surrounding serial biopsies from livers of chronic HBV carriers, it is unclear how integrated HBV levels change in infected individuals. Hypothetical models speculate that cccDNA containing hepatocytes die and are replaced by division of nearby hepatocytes, over time resulting in clonal expansion of

hepatocytes containing integrated HBV DNA [152, 167, 168]. However, further investigations are required to characterize the dynamics of HBV integration over the course of chronic infection.

1.4. HBV Cell Culture Models

Cell culture models are crucial and invaluable to HBV research. However, the strict species and tissue tropism of the virus has frustrated the search for HBV *in vivo* models. The slow development of biologically representative and feasible *in vitro* models for HBV studies has been a major challenge in the pursuit of understanding HBV virology and expanding HBV treatment modalities.

HBV chronically infects chimpanzees and, to a lesser extent, tree shrews from the genus *Tupaia* [169, 170]. Chimpanzees are the only nonhuman primate fully susceptible to HBV and experiences disease progression and immune profile mimicking that seen in humans [171]. Like in humans, HBV is exceptionally infectious in chimpanzees with as little as one virion capable of inciting productive infection [171]. Because these chimpanzees are immunocompetent, their use as an HBV model was critically important to the development of a safe and effective HBV vaccine [173]. Chimpanzee models have also contributed a vast understanding of the pathogenesis of HBV. In 2013, the National Institute of Health (NIH) limited the use of great apes for the purpose of medical research due to ethical concerns. Therefore, current chimpanzee HBV work in North America can only be done on archived samples collected prior to the NIH restriction.

Tupaia are mammals with greater genetic similarity to primates than to rodents, despite what their appearance may suggest [174]. When infected with HBV, mature tree shrews develop

mild symptoms and low viremia, whereas neonatal tree shrews can progress to chronic infections with moderate levels of viral replication and liver sequelae like fibrosis or hepatocellular carcinoma [175]. Although these tupaia findings are compelling, the low infection efficiency, lack of inbred tupaia strains and tupaia research colonies, and the absence of available reagents limit their suitability for HBV *in vivo* studies. Due to their close phylogenetic relationship with humans, Tupaia primary hepatocytes can also be infected *in vitro* with HBV [176]. Because these cells do not proliferate *in vitro* they share the same challenges with *in vivo* tupaia studies, primary tupaia hepatocytes are infrequently utilized. However, the unique HBV tropism of tupaia hepatocytes led to the revelation of the HBV entry receptor NTCP in 2012, almost 50 years after the discovery of the virus [82]. The finding of the HBV entry receptor has considerably expanded the availability of cell culture models for studying HBV, which will be further discussed in section 1.5.2.

1.4.1. Primary Human Hepatocytes

The gold standard for *in vitro* cell culture studies of HBV infection are *ex vivo* primary human hepatocytes (PHHs), which for a long time were the only culture model that could support the full HBV lifecycle [177]. PHHs are the most physiologically relevant *in vitro* system, given that the human liver is the exclusive natural host for HBV. Despite their undeniable utility, PHHs are expensive, difficult to maintain, vary among donors, do not expand *in vitro*, are difficult to genetically modify, and can only survive for a few weeks in culture. When removed from its natural tissue organization, PHHs rapidly de-differentiate and lose hepatocyte characteristics, including xenobiotic metabolism and susceptibility to HBV infection and spread. In fact, no matter how fresh the isolated PHHs, plated monolayers of *ex vivo* hepatocytes cannot be infected at low multiplicity, whereas a single virion is sufficient for *in vivo* HBV chimpanzee

infection. The current approach for sustaining PHH differentiation *in vitro* is through addition of dimethyl sulfoxide (DMSO) to culture media [177]. Although the mechanism of DMSO mediated maintenance of PHHs in culture is not fully understood, DMSO is thought to increase virus adsorption and membrane fusion, promote PHH differentiation, and impede cell cycling.

Conventional HBV infection of plated PHHs also requires the addition of polyethylene glycol 8000 (PEG8000) [178] during inoculation and DMSO throughout the culture duration [177]. The added PEG8000 increases the effective concentration of the virus and possesses fusogenic properties, leading to sedimentation of the HBV onto the cell culture surface and facilitates HSPG binding, membrane fusion, and viral entry [81].

Given the longstanding problem of *in vitro* PHH maintenance and their considerable use in drug toxicity screening, a recent study outlined the use of small molecules to prolong PHH survival and function [179]. Due to the discriminating tropism of HBV for healthy, well-differentiated hepatocytes, Xiang *et al.* used HBV infectability as a proof-of-principle measure to test preservation of primary cell phenotype. By comparing freshly isolated PHHs with those that had been plated for 24 hours, they identified changes in cellular pathways due to culturing. They subsequently tested five small molecule drugs (forskolin, SB431542, DAPT, IWP2, and LDN193189) to counteract these cellular processes altered by culture. When these five drugs were administered throughout culture, the PHHs maintained liver functions as well as infectability with HBV for extended durations compared to conventional culture methods. This was the first PHH culture protocol developed that did not require the addition of DMSO to prevent de-differentiation [179].

The difference of *in vivo* environments versus two-dimensional culture in perpetuating PHH health and functional diversity is substantiated by a variety of approaches to simulate the

liver *in vitro*. Co-culturing PHHs with nonparenchymal cells is another classic technique that can help prevent immediate loss of function and susceptibility to HBV, likely by providing an organization resembling structured liver microenvironments [180, 181]. Further simulation of tissue arrangement can be achieved through micropatterned co-culture (MPCC) systems, which seed PHHs in equally spaced microscopic islands that are then surrounded by feeder fibroblasts [182]. This patterned culture technique prolongs PHH survival and promotes HBV infection. Another method for mimicking three-dimensional organization on a two-dimensional platform is by culturing 3-D PHH organoids rather than 2-D monolayers [183]. Recently, Ortega-Prieto *et al.* showed they could further recapitulate liver infrastructure using a microfluidic system composed of a microscopic filter and pump [184]. PHHs were seeded in the circular apertures in the filter with culture media circulated through that scaffold using the pump. This replication of the highly structured physiological conditions in the liver not only maintained PHH phenotypes, but also supported infection with a single HBV virion. These studies suggest a correlation between the extent of liver likeness and amenability to HBV infection.

1.4.2. Hepatoma Cell Lines

Although PHHs are the most biologically relevant *in vitro* culture model, immortalized liver cell lines have helped drive substantial progress in understanding HBV. Compared to primary tissue cultures, these proliferative cell lines present numerous benefits to feasibility of experiments since they are easily grown and cultured. Huh7 and HepG2 cells are immortalized hepatoma cell lines commonly used as surrogate for hepatocytes in research settings. Huh7 cells originated in 1982 from a 57-year-old Japanese male who was diagnosed with hepatocellular carcinoma induced by hepatitis C virus (HCV). Huh7.5 cells, a derivative of Huh7 cells, were generated by transfected HCV expression plasmids, selecting HCV positive cells, and then

eliminating the HCV by prolonged treatment with interferon alpha. HepG2 cells were generated in 1979 from liver resections obtained from a 15-year-old Caucasian male who was initially diagnosed with HCC [185]. More recent analysis has revealed the cell line is in fact derived from a primary hepatoblastoma [186]. If unmodified, these hepatoma cell lines are unable to support the full viral lifecycle of HBV. However, when these cell lines are transfected with greater-than-genome-length HBV expression plasmids, the plasmid mimics HBV cccDNA and the cells recapitulate HBV infection starting from the cccDNA transcription step [187]. For instance, through intracellular recycling pathways these transiently transfected plasmids can also produce legitimate HBV cccDNA [188]. In addition to challenges involving HBV infection, these hepatoma cell lines display differences in liver function as compared to PHHs. For example, xenobiotic metabolism varies greatly between hepatoma cells and PHHs [189]. Despite differences from PHHs and only modelling later steps in HBV infection, the reproducibility, available supply, and ease of *in vitro* maintenance and modification of these hepatoma cell lines warranted their use for 30 years and contributions to various discoveries in HBV biology.

Because these hepatoma cell lines are inefficiently transiently transfected, stably transfected hepatoma cell lines, such as HepG2.2.15 cells, have also been selected with integrated overlenght HBV genomes to constitutively secrete HBV [190]. HBV integrated cell lines have also been established with promoters for inducible expression of HBV. For instance, rather than using the native viral core promoter, HepAD38 and HepDE19 cells express HBV under control of a tetracycline-repressible promoter [191, 192]. Consequently, when these cell lines are maintained in tetracycline or doxycycline, transcription from integrated HBV genomes ceases and instead exclusively occurs from the pool of cccDNA established through intracellular cccDNA amplification. These cell culture systems have been very useful for producing

reproducible viral stocks, studying later steps in the HBV life cycle, and elucidating facets of cccDNA formation and molecular biology.

Differentiated HepaRG cells are the only unmodified immortalized hepatoma cell line that can be infected with HBV, yet these cells require involved differentiation procedures and have a low percentage of successful infection. HepaRG cells are a bi-potent liver cell line isolated from a female patient with HCV-induced HCC [193]. Following culture in corticoids and DMSO for 4 weeks, the HepaRG cell line differentiates into hepatocyte-like and bile duct epithelium-like cell types. Without this extended culture, the HepaRG cells are not permissive to HBV infection. As previously discussed in the context of cultured PHHs, HepaRG cells are an example in hepatoma cells where a more differentiated phenotype correlates with and possibly predicates increased HBV infection efficiency [194]. For several years, HepaRG cells were the only proliferative culture model that were permissive to HBV infection; therefore, this cell line has been helpful in elucidating earlier steps in the HBV lifecycle that could not be recapitulated with transfected HBV plasmids. Differentiated HepaRG cells were used to demonstrate the requirement of HSPG to initiate HBV entry [81]. NTCP was confirmed as a HBV entry receptor by comparing its expression in undifferentiated and differentiated HepaRG cells [195]. Compared to other hepatoma cell lines, differentiated HepaRG cells seem to mount innate immune responses similar to PHHs that are capable of suppressing HBV replication [196, 197]. In addition, the drug metabolizing enzyme activity of HepaRG cells more closely resembles those of PHHs, when compared to HepG2 cells, suggesting that HepaRG cells may be more appropriate for assessing efficacy of potential HBV therapies [198]. Although HepaRG cells present several advantages for *in vitro* HBV investigations, their widespread use is hampered by their low infection

efficiency and month-long differentiation, which can be cumbersome and affect experimental reproducibility.

In 2012, Yan *et al.* [82] demonstrated high affinity binding between the HBV pre-S1 envelope protein and the NTCP bile acid transporter which is exclusively expressed on the basolateral surface of hepatocytes. Undifferentiated hepatoma cell lines lack NTCP expression. The rapid loss or lack of NTCP in cultured PHHs and hepatoma cell lines, respectively, help explain the baffling low HBV infectivity in these *in vitro* systems. Overexpression of NTCP renders otherwise unsusceptible hepatoma cells permissive to HBV infection. These NTCP overexpressing cell lines are typically denoted as Huh7-NTCP, HepG2-NTCP, etc. This discovery of an HBV entry receptor has benefitted the decades-long search for an easy to maintain cell culture system that reproduces the entire HBV lifecycle. Cells overexpressing NTCP are now widely used to study HBV. However, high titers of inoculating virus are required, with high multiplicity of infections (MOIs) of greater than 1000 HBV genome equivalents (GE) per cell, 4% PEG 8000 in the inoculum, and a minimum overnight inoculation [199]. Even at these high MOIs, only about 30% of cells are infected. Recently, a HepG2-NTCP clone, has been shown to support HBV cell-to-cell spread *in vitro* and elevated secretion of infectious HBV above the levels of incoming inocula titers. This HepG2-NTCP^{sec+} cell line therefore represents the first hepatoma cell line capable of HBV spread and amplification [144]. König *et al.* [144] suggest that factors contributing to differences in HBV spread and amplification between these HepG2-NTCP^{sec+} cells and the background cell line are the clone's slower proliferation, increased secretion of enveloped capsids rather than naked HBV capsids, upregulated expression of some host genes associated with viral egress, upregulated expression of host factors involved with HBV transcription (including *CEBPA*, *FXR*, *PPARA*, *PPARGC1A/B*, and *PPARG*), and

downregulated expression of HBV inhibitory host factors (*DDX3X* and *DDX3Y*). Although promising for a variety of HBV research areas, HepG2-NTCPsec+ cells are deficient in the sophisticated functions and enzymatic activity of PHHs and therefore lack some biological relevance. Therefore, although progress has been made, existing hepatoma culture systems have deficits that continue to impede HBV studies.

1.4.3. Hepatocyte-like Induced Pluripotent and Embryonic Stem Cells

Recent advancements in stem cell manipulation and reprogramming in cell culture have dramatically expanded options for *in vitro* investigations [200, 201]. Specific culture protocols can induce differentiation of induced pluripotent stem cells (iPSCs) or embryonic stem cells (ESCs) into hepatocyte-like cells (HLCs), which closely resemble mature hepatocytes [202]. iPSCs can be generated from somatic cells isolated non-invasively from any donor. This has the benefit of a virtually unlimited supply of cells derived from a single donor, as well as the advantage of assessing influences from genetic variability by using iPSCs from different donors. ESCs are derived from human blastocysts and are thus more difficult to acquire than iPSCs. Following differentiation, these HLCs have more physiologic phenotypes of hepatocytes than hepatoma cells. HLCs are permissive to long-term HBV infection, support limited viral spread, and display some of the innate immune response observed in infected PHHs [182, 202]. Unlike PHHs, iPSCs have the advantage of amenability to genetic manipulation. HLCs have several benefits compared to other HBV *in vitro* models; however, involved differentiation protocols that require technical expertise, numerous reagents and differentiation factors, and frequent assays to assess the differentiation process make it inconvenient and difficult to establish this culture system.

1.5. Innate Immunity and HBV

A controversy revolves around whether an innate immune response is mounted against HBV. Transcriptional analyses reveal that no cellular genes correlate with HBV DNA levels, suggesting that HBV does not perturb host gene expression [203-207]. HBV may be inert to the innate immune system due to its concealed viral lifecycle including chromatinized cccDNA confined to the nucleus, viral RNA that is capped and polyadenylated, and reverse transcription with viral DNA synthesis occurring within capsids in the cytoplasm. Hence, HBV is often considered as a stealth virus: it neither stimulates nor inhibits the innate immune machinery, allowing for undetected spread until the adaptive immune response several weeks after initial infection [203]. Although HBV may not stimulate the innate immune response during infection, induction of interferon (IFN) α , β , or γ can inhibit HBV replication [208-213]. It is hypothesized that the virus has not evolved with mechanisms to evade IFN response, which explains the effective clearance of HBV with exogenous IFN exposure.

In contrast, several investigations have reported IFN activation by HBV [214, 215]. Suggested mechanisms of innate immune recognition of HBV infection include viral RNA sensing by retinoic acid inducible protein I (RIG-I) [215], melanoma differentiation-associated protein 5 (MDA5) [216], and toll-like receptor 3 [217], toll-like receptor 2 [218], as well as viral DNA sensing by stimulator of IFN genes (STING) [219]. Several reports show HBV evasion of innate immunity and disruption of IFN activity mediated by the polymerase [220, 221], X protein [222, 223], surface antigen [224, 225], capsid [217], and regulation of host factors [226, 227]. Altogether, whether HBV is stealthy or actively stimulates and inhibits the innate immune system continues to be a debated subject.

HBV produces low levels of genomes and antigen for several weeks following infection, resulting in delayed viral amplification and spread through the liver [228, 229]. Once infection is established, HBV produces high levels of core and surface antigen, which is thought to contribute to the recognition and clearance of the infection mediated by the adaptive immune system, particularly cellular immunity [230, 231]. The importance of the adaptive immune system in HBV clearance is further supported by the many strategies that the virus uses to evade the adaptive immune response [232-237]. Indeed, it is accepted that adaptive immunity is largely implicated in the potential elimination of HBV, unlike the contested role of innate immunity in this process.

1.6. Single-Cell RNA Sequencing in Studies of HBV

Single-cell RNA sequencing (scRNA-seq) is a novel and powerful technique that has been increasingly employed to characterize cell population with a single cell resolution. Fundamentally, scRNA-seq technologies allow for transcriptomic analysis of a single cell or multiple single cells. scRNA-seq involves separation of single cells, reverse transcription and amplification of cDNA, sequencing of cDNA libraries, and data analysis. Following the advent of scRNA-seq methodology in 2009 [238], there have been several advancements, including barcode labelling [239, 240] and automation of library preparation [241, 242]. Generally, single cells are separated using cell sorting into multi-well plates [243-245] or microfluidic systems [242, 246-248] prior to reverse-transcription and amplification into cDNA libraries. The libraries are sequenced using a next-generation sequencing (NGS) platform. Analyses of the rich transcriptomic data are enabled by computational bioinformatic methods, such as dimensionality reduction approaches for visualizing complex multivariate data [249], tools for combining

different datasets [250-252], and techniques for comparing spliced and unspliced transcripts [253], predicting transcription factor and regulatory network activity [254], and modeling differentiation pathways [255-257].

scRNA-seq has recently been applied to various areas of virology [258-265]. A few studies have explored HBV [262, 266] and liver tissue cell types [267-274] using scRNA-seq technologies. Bost *et al.* [262] developed a computational tool, Viral-Track, which enabled an unsupervised analysis to identify viral transcripts in scRNA-seq data [262]. Although this study focused on SARS-CoV-2, the authors also performed a proof-of-concept study with additional samples of cells infected with influenza A, lymphocytic choriomeningitis virus, vesicular stomatitis virus, herpes simplex virus 1, HIV, and HBV. Their *in silico* analysis successfully identified HBV transcripts in the hepatocytes of a clinical biopsy, as well as low viral levels in macrophages, endothelial, and epithelial cells. They used these results as validation of their technique, but did not perform further investigation of the HBV sample. Juhling *et al.* [266] applied scRNA-seq analysis to resected HCC tumor samples from two patients and discovered unique diversity among tumor cells. They demonstrated that HBV RNA levels were positively correlated with the level of tumor differentiation and the expression of host factors that mediate HBV replication [266]. Their analysis identified possible pathways involved in HBV-related oncogenesis, such as downregulation of tumor suppressing gene RFWD3, which could be perturbed even with low levels of HBV.

Other studies have examined the transcriptomes of HBV-associated HCC cells [276-278] or myeloid dendritic cells to HBV vaccination [279]. However, these studies did not analyze HBV transcripts. Single cell techniques have also been used to sequence the genome, rather than transcriptome, of HBV-infected cells, demonstrating variability in HBV integration sites [276]

and the decrease in HBV pgRNA, rcDNA, and cccDNA in single cells following NA treatment [280, 281].

Application of scRNA-seq and analyses of multi-dimensional data enable the delineation of known cell types and identification of new cell types in a variety of tissues [282]. Hence, several studies have explored novel cell types and heterogeneity in liver and HCC tissues using scRNA-seq [267-274].

1.7. Rationale, Objectives, and Scope of this Thesis

A major obstacle to studies of HBV has been the lack of an easily infectable cell culture model. Immortalized cell lines have low infection efficiency, while primary liver tissue (or cells) is difficult to acquire and maintain in culture. The first objective of my thesis research is to establish a human hepatoma cell culture system that produces robust HBV infection for studies of HBV infection.

Our group has previously shown that culturing the human hepatoma cell line Huh7 or Huh7.5 in a medium supplemented with human serum (HS) increased production of hepatitis C virus (HCV) [283]. Cells cultured in an HS-supplemented medium underwent growth arrest and developed characteristics similar to primary human hepatocytes, including a cuboid morphology, formation of bile canalicular surfaces, restored lipid metabolism, contact inhibition, differentiation marker expression, reversal of the Warburg effect, very low-density lipoprotein (VLDL) secretion, and increased expression of cytochrome P450 [189, 284, 285]. This method of producing hepatocyte-like cells enhanced production of HCV 1000-fold and resulted in a virus that more closely resembled the HCV present in the serum of infected patients.

Previous studies by others showed that overexpression of NTCP in hepatoma cells only moderately improved infection efficiency and, following infection, these cultures must be maintained in high concentrations (2–2.5%) of DMSO for infection [82, 195, 286–294]. However, DMSO is known to cause a variety of adverse effects on cells, such as significant alterations in viability and protein expression [295–299]. Therefore, an HBV infection model that eliminates the requirement of DMSO treatment would be desirable to more closely mimic physiological conditions [179].

Chapter 2 of this thesis focuses on the development of a Huh7.5-NTCP cell culture system for HBV studies. Huh7.5-NTCP hepatoma cells are allowed to differentiate in a medium supplemented with human serum (HS) instead of fetal bovine serum (FBS). This culture system permits robust HBV infection in the absence of DMSO.

The second objective of my research is to characterize the HS-cultured Huh7.5-NTCP cells and their HBV infection. Standard approaches include analysis of gene and protein expressions, hepatocyte differentiation markers, and specific HBV molecules, such as cccDNA, pgRNA, HBeAg, and HBsAg. Further scRNA-seq analysis can provide transcriptomic information at the single-cell resolution and reveal heterogeneity in the cultured cell population.

Although scRNA-seq can provide rich transcriptomic information for studying cell populations at the single-cell level, it is difficult to obtain scRNA-seq information from rare or low-abundance transcripts in the presence of other highly abundant transcripts. Highly abundant sequences in the scRNA-seq library are sequenced more frequently, and the rare transcripts are masked. This is a problem in scRNA-seq studies of HBV because of its low infectivity *in vitro*. The much higher amounts of the host cell RNA relative to the low abundance of HBV transcripts make scRNA-seq studies of the HBV infection challenging. Research described in Chapter 3 is

designed to confront this challenge. This chapter describes a CRISPR-Cas9 technique, which depletes high-abundance off-target transcripts, facilitating preferential enrichment of HBV transcripts and successful detection of HBV gene expression in the HBV-infected cells.

Research in Chapter 4 is designed to perform scRNA-seq analysis of the transcriptomic profiles of Huh7.5-NTCP cells in the HS-supplemented culture. This study provides further characterization of this hepatoma cell culture model, complementing investigations described in Chapter 2. By comparing gene expression profiles with those of primary cells from human liver, the scRNA-seq study enables the discovery of cell heterogeneity and identification of cell types in the cultured cell population.

On the basis of the established hepatoma cell model (Chapter 2) and techniques of CRISPR-Cas9 (Chapter 3) and scRNA-seq (Chapter 4), Chapter 5 illustrates a scRNA-seq study of Huh7.5-NTCP and Huh7.5 hepatoma cells infected with HBV or HCV and with or without interferon treatment. By comparing HBV and HCV infection and examining the effects of interferon treatment, this scRNA-seq study is designed to determine whether HBV is a “stealth virus”, it neither stimulating nor suppressing the interferon response.

This thesis research summarized the background and relevant knowledge of HBV (Chapter 1), created a human hepatoma cell culture system that produced robust HBV infection (Chapter 2), developed a CRISPR technique enabling scRNA-seq studies of HBV-infected cells (Chapter 3), characterized transcriptomic profiles and identified cell types in the human hepatoma cell culture (Chapter 4), and applied the CRISPR and scRNA-seq techniques to studying the effect of HBV and HCV infection on interferon responses (Chapter 5). This thesis research has contributed to tools and techniques for studying HBV infection. Studies using these new tools

have revealed new insights into HBV infection of hepatoma cells on the transcriptomic and single-cell levels.

1.8. References

1. Ott, J.J.; Stevens, G.A.; Groeger, J.; Wiersma, S.T. Global epidemiology of hepatitis B virus infection: new estimates of age-specific HBsAg seroprevalence and endemicity. *Vaccine* **2012**, *30*, 2212-2219. doi:10.1016/j.vaccine.2011.12.116.
2. World Health Organization (WHO). *HIV/AIDS Fact Sheets*. November 30, **2021**. <https://www.who.int/news-room/fact-sheets/detail/hiv-aids> (Accessed February 10, 2022).
3. GBD 2017 Disease Injury and Prevalence Collaborators (James, S.L. *et al.*). Global, regional, and national incidence, prevalence, and years lived with disability for 354 diseases and injuries for 195 countries and territories, 1990-2017: a systematic analysis for the Global Burden of Disease Study 2017. *Lancet* **2018**, *392*, 1789-1858. doi:10.1016/S0140-6736(18)32279-7.
4. GBD 2017 Causes of Death Collaborators (Roth, G.A. *et al.*). Global, regional, and national age-sex-specific mortality for 282 causes of death in 195 countries and territories, 1980-2017: A systematic analysis for the Global Burden of Disease Study 2017. *Lancet* **2018**, *392*, 1736-1788. doi:10.1016/S0140-6736(18)32203-7.
5. Dusheiko, G. Treatment of HBeAg positive chronic hepatitis B: interferon or nucleoside analogues. *Liver Int.* **2013**, *33 Suppl 1*, 137-150. doi:10.1111/liv.12078.
6. World Health Organization (WHO). *Hepatitis B Fact Sheets*. July 27, **2021**. [https://www.who.int/news-room/fact-sheets/detail/hepatitis-b#:~:text=WHO%20estimates%20that%20296%20million,carcinoma%20\(primary%20liver%20cancer\)](https://www.who.int/news-room/fact-sheets/detail/hepatitis-b#:~:text=WHO%20estimates%20that%20296%20million,carcinoma%20(primary%20liver%20cancer)). (Accessed February 10, 2022).
7. Te, H.S.; Jensen, D.M. Epidemiology of hepatitis B and C viruses: a global overview. *Clin. Liver Dis.* **2010**, *14*, 1-21, vii. doi:10.1016/j.cld.2009.11.009.
8. Polaris Observatory Collaborators (Razavi-Shearer, D. *et al.*). Global prevalence, treatment, and prevention of hepatitis B virus infection in 2016: a modelling study. *Lancet Gastroenterol. Hepatol.* **2018**, *3*, 383-403. doi:10.1016/S2468-1253(18)30056-6.

9. World Health Organization (WHO). *Combating Hepatitis B and C to reach elimination by 2030: Advocacy brief*. **2016**. <https://apps.who.int/iris/handle/10665/206453>
10. World Health Organization (WHO). Global Health Sector Strategy on Viral Hepatitis 2016-2021, Towards ending viral hepatitis. **2016**. <https://apps.who.int/iris/handle/10665/246177>
11. Nayagam, S.; Thursz, M.; Sicuri, E.; Conteh, L.; Wiktor, S.; Low-Beer, D.; Hallett, T.B. Requirements for global elimination of hepatitis B: a modelling study. *Lancet Infect. Dis.* **2016**, *16*, 1399-1408. doi:10.1016/S1473-3099(16)30204-3.
12. Revill, P.; Testoni, B.; Locarnini, S.; Zoulim, F. Global strategies are required to cure and eliminate HBV infection. *Nat. Rev. Gastroenterol. Hepatol.* **2016**, *13*, 239-248. doi:10.1038/nrgastro.2016.7.
13. Alter, H.; Block, T.; Brown, N.; Brownstein, A.; Brosgart, C.; Chang, K.M.; Chen, P.J.; Chisari, F.V.; Cohen, C.; El-Serag, H.; Feld, J.; Gish, R.; Glenn, J.; Greten, T.; Guo, H.; Guo, J.T.; Hoshida, Y.; Hu, J.; Kowdley, K.V.; Li, W.; Liang, J.; Locarnini, S.; Lok, A.S.; Mason, W.; McMahon, B.; Mehta, A.; Perrillo, R.; Revill, P.; Rice, C.M.; Rinaudo, J.; Schinazi, R.; Seeger, C.; Shetty, K.; Tavis, J.; Zoulim, F. A research agenda for curing chronic hepatitis B virus infection. *Hepatology* **2018**, *67*, 1127-1131. doi:10.1002/hep.29509.
14. Ferlay, J.; Shin, H.R.; Bray, F.; Forman, D.; Mathers, C.; Parkin, D.M. Estimates of worldwide burden of cancer in 2008: GLOBOCAN 2008. *Int. J. Cancer* **2010**, *127*, 2893-2917. doi:10.1002/ijc.25516.
15. Chen, C.J.; Yang, H.I.; Su, J.; Jen, C.L.; You, S.L.; Lu, S.N.; Huang, G.T.; Iloeje, U.H.; Group, R.-H.S. Risk of hepatocellular carcinoma across a biological gradient of serum hepatitis B virus DNA level. *JAMA* **2006**, *295*, 65-73. doi:10.1001/jama.295.1.65.
16. Iloeje, U.H.; Yang, H.I.; Su, J.; Jen, C.L.; You, S.L.; Chen, C.J.; Risk Evaluation of Viral Load, E., Associated Liver Disease/Cancer-In, H.B.V.S.G. Predicting cirrhosis risk based on the level of circulating hepatitis B viral load. *Gastroenterology* **2006**, *130*, 678-686. doi:10.1053/j.gastro.2005.11.016.
17. Venook, A.P.; Papandreou, C.; Furuse, J.; de Guevara, L.L. The incidence and epidemiology of hepatocellular carcinoma: a global and regional perspective. *Oncologist* **2010**, *15 Suppl 4*, 5-13. doi:10.1634/theoncologist.2010-S4-05.

18. Terrault, N.A.; Lok, A.S.F.; McMahon, B.J.; Chang, K.M.; Hwang, J.P.; Jonas, M.M.; Brown, R.S., Jr.; Bzowej, N.H.; Wong, J.B. Update on prevention, diagnosis, and treatment of chronic hepatitis B: AASLD 2018 hepatitis B guidance. *Hepatology* **2018**, *67*, 1560-1599. doi:10.1002/hep.29800.
19. Raimondo, G.; Locarnini, S.; Pollicino, T.; Levrero, M.; Zoulim, F.; Lok, A.S., Taormina Workshop on Occult HBV Infection Faculty Members. Update of the statements on biology and clinical impact of occult hepatitis B virus infection. *J. Hepatol.* **2019**, *71*, 397-408. doi:10.1016/j.jhep.2019.03.034.
20. Liaw, Y.F.; Chu, C.M. Hepatitis B virus infection. *Lancet* **2009**, *373*, 582-592. doi:10.1016/S0140-6736(09)60207-5.
21. Ichai, P.; Samuel, D. Management of Fulminant Hepatitis B. *Curr. Infect. Dis. Rep.* **2019**, *21*, 25. doi:10.1007/s11908-019-0682-9.
22. Seto, W.K.; Lo, Y.R.; Pawlotsky, J.M.; Yuen, M.F. Chronic hepatitis B virus infection. *Lancet* **2018**, *392*, 2313-2324. doi:10.1016/S0140-6736(18)31865-8.
23. Fanning, G.C.; Zoulim, F.; Hou, J.; Bertolotti, A. Therapeutic strategies for hepatitis B virus infection: towards a cure. *Nat. Rev. Drug Discov.* **2019**, *18*, 827-844. doi:10.1038/s41573-019-0037-0.
24. Hahn, C.M.; Iwanowicz, L.R.; Cornman, R.S.; Conway, C.M.; Winton, J.R.; Blazer, V.S. Characterization of a Novel Hepadnavirus in the White Sucker (*Catostomus commersonii*) from the Great Lakes Region of the United States. *J. Virol.* **2015**, *89*, 11801-11811. doi:10.1128/JVI.01278-15.
25. Dill, J.A.; Camus, A.C.; Leary, J.H.; Di Giallonardo, F.; Holmes, E.C.; Ng, T.F. Distinct Viral Lineages from Fish and Amphibians Reveal the Complex Evolutionary History of Hepadnaviruses. *J. Virol.* **2016**, *90*, 7920-7933. doi:10.1128/JVI.00832-16.
26. Dane, D.S.; Cameron, C.H.; Briggs, M. Virus-like particles in serum of patients with Australia-antigen-associated hepatitis. *Lancet* **1970**, *1*, 695-698. doi:10.1016/s0140-6736(70)90926-8.
27. Hirschman, S.Z.; Gerber, M.; Garfinkel, E. Purification of naked intranuclear particles from human liver infected by hepatitis B virus. *Proc. Natl. Acad. Sci. U. S. A.* **1974**, *71*, 3345-3349. doi:10.1073/pnas.71.9.3345.

28. Crowther, R.A.; Kiselev, N.A.; Bottcher, B.; Berriman, J.A.; Borisova, G.P.; Ose, V.; Pumpens, P. Three-dimensional structure of hepatitis B virus core particles determined by electron cryomicroscopy. *Cell* **1994**, *77*, 943-50. doi:10.1016/0092-8674(94)90142-2.
29. Wynne, S.A.; Crowther, R.A.; Leslie, A.G. The crystal structure of the human hepatitis B virus capsid. *Mol. Cell* **1999**, *3*, 771-780. doi:10.1016/s1097-2765(01)80009-5.
30. Shih, J.W.; Gerin, J.L. Immunochemistry of hepatitis B surface antigen (HBsAg): preparation and characterization of antibodies to the constituent polypeptides. *J. Immunol.* **1975**, *115*, 634-639.
31. Robinson, W.S.; Clayton, D.A.; Greenman, R.L. DNA of a human hepatitis B virus candidate. *J. Virol.* **1974**, *14*, 384-91.
32. Robinson, W.S. Greenman, R.L. DNA polymerase in the core of the human hepatitis B virus candidate. *J. Virol.* **1974**, *14*, 1231-1236.
33. Summers, J.; O'Connell, A.; Millman, I. Genome of hepatitis B virus: restriction enzyme cleavage and structure of DNA extracted from Dane particles. *Proc. Natl. Acad. Sci. U. S. A.* **1975**, *72*, 4597-4601. doi:10.1073/pnas.72.11.4597.
34. Hu, J.; Flores, D.; Toft, D.; Wang, X.; Nguyen, D. Requirement of heat shock protein 90 for human hepatitis B virus reverse transcriptase function. *J. Virol.* **2004**, *78*, 13122-31. doi:10.1128/JVI.78.23.13122-13131.2004.
35. Wittkop, L.; Schwarz, A.; Cassany, A.; Grun-Bernhard, S.; Delaleau, M.; Rabe, B.; Cazenave, C.; Gerlich, W.; Glebe, D.; Kann, M. Inhibition of protein kinase C phosphorylation of hepatitis B virus capsids inhibits virion formation and causes intracellular capsid accumulation. *Cell Microbiol.* **2010**, *12*, 962-975. doi:10.1111/j.1462-5822.2010.01444.x.
36. Ning, X.; Nguyen, D.; Mentzer, L.; Adams, C.; Lee, H.; Ashley, R.; Hafenstein, S.; Hu, J. Secretion of genome-free hepatitis B virus--single strand blocking model for virion morphogenesis of para-retrovirus. *PLoS Pathog.* **2011**, *7*, e1002255. doi:10.1371/journal.ppat.1002255.
37. Gavilanes, F.; Gonzalez-Ros, J.M.; Peterson, D.L. Structure of hepatitis B surface antigen. Characterization of the lipid components and their association with the viral proteins. *J. Biol. Chem.* **1982**, *257*, 7770-7777.

38. Nassal, M. Hepatitis B viruses: reverse transcription a different way. *Virus Res*, **2008**, *134*, 235-249. doi:10.1016/j.virusres.2007.12.024.
39. Tian, Q.; Jia, J. Hepatitis B virus genotypes: epidemiological and clinical relevance in Asia. *Hepatol. Int.* **2016**, *10*, 854-860. doi:10.1007/s12072-016-9745-2.
40. Gerlich, W.H.; Robinson, W.S. Hepatitis B virus contains protein attached to the 5' terminus of its complete DNA strand. *Cell* **1980**, *21*, 801-809. doi:10.1016/0092-8674(80)90443-2.
41. Niklasch, M.; Zimmermann, P.; Nassal, M. The hepatitis B virus nucleocapsid-dynamic compartment for infectious virus production and new antiviral target. *Biomedicines* **2021**, *9*. doi:10.3390/biomedicines9111577.
42. Karayiannis, P. Hepatitis B virus: virology, molecular biology, life cycle and intrahepatic spread. *Hepatol. Int.* **2017**, *11*, 500-508. doi:10.1007/s12072-017-9829-7.
43. Moolla, N.; Kew, M.; Arbuthnot, P. Regulatory elements of hepatitis B virus transcription. *J. Viral. Hepat.* **2002**, *9*, 323-331. doi:10.1046/j.1365-2893.2002.00381.x.
44. Messageot, F.; Salhi, S.; Eon, P.; Rossignol, J.M. Proteolytic processing of the hepatitis B virus e antigen precursor. Cleavage at two furin consensus sequences. *J. Biol. Chem.* **2003**, *278*, 891-895. doi:10.1074/jbc.M207634200.
45. Milich, D.R.; Jones, J.E.; Hughes, J.L.; Price, J.; Raney, A.K.; McLachlan, A. Is a function of the secreted hepatitis B e antigen to induce immunologic tolerance in utero? *Proc. Natl. Acad. Sci. U. S. A.* **1990**, *87*, 6599-6603. doi:10.1073/pnas.87.17.6599.
46. Milich, D.; Liang, T.J. Exploring the biological basis of hepatitis B e antigen in hepatitis B virus infection. *Hepatology* **2003**, *38*, 1075-1086. doi:10.1053/jhep.2003.50453.
47. Hsu, Y.S.; Chien, R.N.; Yeh, C.T.; Sheen, I.S.; Chiou, H.Y.; Chu, C.M.; Liaw, Y.F. Long-term outcome after spontaneous HBeAg seroconversion in patients with chronic hepatitis B. *Hepatology* **2002**, *35*, 1522-1527. doi:10.1053/jhep.2002.33638.
48. Parekh, S.; Zoulim, F.; Ahn, S.H.; Tsai, A.; Li, J.; Kawai, S.; Khan, N.; Trepo, C.; Wands, J.; Tong, S. Genome replication, virion secretion, and e antigen expression of naturally occurring hepatitis B virus core promoter mutants. *J. Virol.* **2003**, *77*, 6601-12. doi:10.1128/jvi.77.12.6601-6612.2003.

49. Chu, C.M.; Liaw, Y.F. Chronic hepatitis B virus infection acquired in childhood: special emphasis on prognostic and therapeutic implication of delayed HBeAg seroconversion. *J. Viral. Hepat.* **2007**, *14*, 147-52. doi:10.1111/j.1365-2893.2006.00810.x.
50. Birnbaum, F.; Nassal, M. Hepatitis B virus nucleocapsid assembly: primary structure requirements in the core protein. *J. Virol.* **1990**, *64*, 3319-30.
51. Zhou, S.; Standring, D.N. Hepatitis B virus capsid particles are assembled from core-protein dimer precursors. *Proc. Natl. Acad. Sci. U. S. A.* **1992**, *89*, 10046-10050. doi:10.1073/pnas.89.21.10046.
52. Hatton, T.; Zhou, S.; Standring, D.N. RNA- and DNA-binding activities in hepatitis B virus capsid protein: a model for their roles in viral replication. *J. Virol.* **1992**, *66*, 5232-5241.
53. Nassal, M. The arginine-rich domain of the hepatitis B virus core protein is required for pregenome encapsidation and productive viral positive-strand DNA synthesis but not for virus assembly. *J. Virol.* **1992**, *66*, 4107-4116.
54. Lott, L.; Beames, B.; Notvall, L.; Lanford, R.E. Interaction between hepatitis B virus core protein and reverse transcriptase. *J. Virol.* **2000**, *74*, 11479-11489. doi:10.1128/jvi.74.24.11479-11489.2000.
55. Pastor, F.; Herrscher, C.; Patient, R.; Eymieux, S.; Moreau, A.; Burlaud-Gaillard, J.; Seigneuret, F.; de Rocquigny, H.; Roingeard, P.; Hourieux, C. Direct interaction between the hepatitis B virus core and envelope proteins analyzed in a cellular context. *Sci. Rep.* **2019**, *9*, 16178. doi:10.1038/s41598-019-52824-z.
56. Clark, D.N.; Hu, J. Unveiling the roles of HBV polymerase for new antiviral strategies. *Future Virol.* **2015**, *10*, 283-295. doi:10.2217/fvl.14.113.
57. Jones, S.A.; Clark, D.N.; Cao, F.; Tavis, J.E.; Hu, J. Comparative analysis of hepatitis B virus polymerase sequences required for viral RNA binding, RNA packaging, and protein priming. *J. Virol.* **2014**, *88*, 1564-1572. doi:10.1128/JVI.02852-13.
58. Das, K.; Xiong, X.; Yang, H.; Westland, C.E.; Gibbs, C.S.; Sarafianos, S.G.; Arnold, E. Molecular modeling and biochemical characterization reveal the mechanism of hepatitis B virus polymerase resistance to lamivudine (3TC) and emtricitabine (FTC). *J. Virol.* **2001**, *75*, 4771-4779. doi:10.1128/JVI.75.10.4771-4779.2001.

59. Tavis, J.E.; Cheng, X.; Hu, Y.; Totten, M.; Cao, F.; Michailidis, E.; Aurora, R.; Meyers, M.J.; Jacobsen, E.J.; Parniak, M.A.; Sarafianos, S.G. The hepatitis B virus ribonuclease H is sensitive to inhibitors of the human immunodeficiency virus ribonuclease H and integrase enzymes. *PLoS Pathog.* **2013**, *9*, e1003125. doi:10.1371/journal.ppat.1003125.
60. Blumberg, B.S.; Alter, H.J.; Visnich, S. A "new" antigen in leukemia sera. *JAMA*, **1965**, *191*, 541-546. doi:10.1001/jama.1965.03080070025007.
61. Stibbe, W.; Gerlich, W.H. Structural relationships between minor and major proteins of hepatitis B surface antigen. *J. Virol.* **1983**, *46*, 626-628.
62. Bruss, V.; Ganem, D. The role of envelope proteins in hepatitis B virus assembly. *Proc. Natl. Acad. Sci. U. S. A.* **1991**, *88*, 1059-1063. doi:10.1073/pnas.88.3.1059.
63. Ueda, K.; Tsurimoto, T.; Matsubara, K. Three envelope proteins of hepatitis B virus: large S, middle S, and major S proteins needed for the formation of Dane particles. *J. Virol.* **1991**, *65*, 3521-3529.
64. Garcia, T.; Li, J.; Sureau, C.; Ito, K.; Qin, Y.; Wands, J.; Tong, S. Drastic reduction in the production of subviral particles does not impair hepatitis B virus virion secretion. *J. Virol.* **2009**, *83*, 11152-11165. doi:10.1128/JVI.00905-09.
65. Eble, B.E.; MacRae, D.R.; Lingappa, V.R.; Ganem, D. Multiple topogenic sequences determine the transmembrane orientation of the hepatitis B surface antigen. *Mol. Cell Biol.* **1987**, *7*, 3591-3601. doi:10.1128/mcb.7.10.3591.
66. Eble, B.E.; Lingappa, V.R.; Ganem, D. The N-terminal (pre-S2) domain of a hepatitis B virus surface glycoprotein is translocated across membranes by downstream signal sequences. *J. Virol.* **1990**, *64*, 1414-1419.
67. Gripon, P.; Le Seyec, J.; Rumin, S. Guguen-Guillouzo, C. Myristylation of the hepatitis B virus large surface protein is essential for viral infectivity. *Virology* **1995**, *213*, 292-299. doi:10.1006/viro.1995.0002.
68. Gripon, P.; Cannie, I.; Urban, S. Efficient inhibition of hepatitis B virus infection by acylated peptides derived from the large viral surface protein. *J. Virol.* **2005**, *79*, 1613-1622. doi:10.1128/JVI.79.3.1613-1622.2005.
69. Wu, Z.J.; Zhu, Y.; Huang, D.R.; Wang, Z.Q. Constructing the HBV-human protein interaction network to understand the relationship between HBV and hepatocellular carcinoma. *J. Exp. Clin. Cancer Res.* **2010**, *29*, 146. doi:10.1186/1756-9966-29-146.

70. Lin, Y.; Nomura, T.; Cheong, J.; Dorjsuren, D.; Iida, K.; Murakami, S. Hepatitis B virus X protein is a transcriptional modulator that communicates with transcription factor IIB and the RNA polymerase II subunit 5. *J. Biol. Chem.* **1997**, *272*, 7132-7139. doi:10.1074/jbc.272.11.7132.
71. Peng, Z.; Zhang, Y.; Gu, W.; Wang, Z.; Li, D.; Zhang, F.; Qiu, G.; Xie, K. Integration of the hepatitis B virus X fragment in hepatocellular carcinoma and its effects on the expression of multiple molecules: a key to the cell cycle and apoptosis. *Int. J. Oncol.* **2005**, *26*, 467-473.
72. Fabregat, I. Dysregulation of apoptosis in hepatocellular carcinoma cells. *World J. Gastroenterol.* **2009**, *15*, 513-520. doi:10.3748/wjg.15.513.
73. Belloni, L.; Pollicino, T.; De Nicola, F.; Guerrieri, F.; Raffa, G.; Fanciulli, M.; Raimondo, G.; Levrero, M. Nuclear HBx binds the HBV minichromosome and modifies the epigenetic regulation of cccDNA function. *Proc. Natl. Acad. Sci. U. S. A.* **2009**, *106*, 19975-19979. doi:10.1073/pnas.0908365106.
74. Wei, X.; Xiang, T.; Ren, G.; Tan, C.; Liu, R.; Xu, X.; Wu, Z. miR-101 is down-regulated by the hepatitis B virus x protein and induces aberrant DNA methylation by targeting DNA methyltransferase 3A. *Cell Signal* **2013**, *25*, 439-446. doi:10.1016/j.cellsig.2012.10.013.
75. Geng, M.; Xin, X.; Bi, L.Q.; Zhou, L.T.; Liu, X.H. Molecular mechanism of hepatitis B virus X protein function in hepatocarcinogenesis. *World J. Gastroenterol.* **2015**, *21*, 10732-10738. doi:10.3748/wjg.v21.i38.10732.
76. Wu, S.; Kanda, T.; Nakamoto, S.; Jiang, X.; Nakamura, M.; Sasaki, R.; Haga, Y.; Shirasawa, H.; Yokosuka, O. Cooperative effects of hepatitis B virus and TNF may play important roles in the activation of metabolic pathways through the activation of NF-kappaB. *Int. J. Mol. Med.* **2016**, *38*, 475-481. doi:10.3892/ijmm.2016.2643.
77. Jiang, T.; Liu, M.; Wu, J.; Shi, Y. Structural and biochemical analysis of Bcl-2 interaction with the hepatitis B virus protein HBx. *Proc. Natl. Acad. Sci. U. S. A.* **2016**, *113*, 2074-2079. doi:10.1073/pnas.1525616113.
78. Decorsiere, A.; Mueller, H.; van Breugel, P.C.; Abdul, F.; Gerossier, L.; Beran, R.K.; Livingston, C.M.; Niu, C.; Fletcher, S.P.; Hantz, O.; Strubin, M. Hepatitis B virus X protein identifies the Smc5/6 complex as a host restriction factor. *Nature* **2016**, *531*, 386-389. doi:10.1038/nature17170.

79. Xu, Y.; Qi, Y.; Luo, J.; Yang, J.; Xie, Q.; Deng, C.; Su, N.; Wei, W.; Shi, D.; Xu, F.; Li, X.; Xu, P. Hepatitis B virus X protein stimulates proliferation, wound closure and inhibits apoptosis of Huh-7 cells via CDC42. *Int. J. Mol. Sci.* **2017**, *18*. doi:10.3390/ijms18030586.
80. Urban, S.; Schulze, A.; Dandri, M.; Petersen, J. The replication cycle of hepatitis B virus. *J. Hepatol.* **2010**, *52*, 282-284. doi:10.1016/j.jhep.2009.10.031.
81. Schulze, A.; Gripon, P.; Urban, S. Hepatitis B virus infection initiates with a large surface protein-dependent binding to heparan sulfate proteoglycans. *Hepatology* **2007**, *46*, 1759-1768. doi:10.1002/hep.21896.
82. Yan, H.; Zhong, G.; Xu, G.; He, W.; Jing, Z.; Gao, Z.; Huang, Y.; Qi, Y.; Peng, B.; Wang, H.; Fu, L.; Song, M.; Chen, P.; Gao, W.; Ren, B.; Sun, Y.; Cai, T.; Feng, X.; Sui, J.; Li, W. Sodium taurocholate cotransporting polypeptide is a functional receptor for human hepatitis B and D virus. *Elife* **2012**, *1*, e00049. doi:10.7554/eLife.00049.
83. Iwamoto, M.; Saso, W.; Sugiyama, R.; Ishii, K.; Ohki, M.; Nagamori, S.; Suzuki, R.; Aizaki, H.; Ryo, A.; Yun, J.H.; Park, S.Y.; Ohtani, N.; Muramatsu, M.; Iwami, S.; Tanaka, Y.; Sureau, C.; Wakita, T.; Watashi, K. Epidermal growth factor receptor is a host-entry cofactor triggering hepatitis B virus internalization. *Proc. Natl. Acad. Sci. U. S. A.* **2019**, *116*, 8487-8492. doi:10.1073/pnas.1811064116.
84. Iwamoto, M.; Saso, W.; Nishioka, K.; Ohashi, H.; Sugiyama, R.; Ryo, A.; Ohki, M.; Yun, J.H.; Park, S.Y.; Ohshima, T.; Suzuki, R.; Aizaki, H.; Muramatsu, M.; Matano, T.; Iwami, S.; Sureau, C.; Wakita, T.; Watashi, K. The machinery for endocytosis of epidermal growth factor receptor coordinates the transport of incoming hepatitis B virus to the endosomal network. *J. Biol. Chem.* **2020**, *295*, 800-807. doi:10.1074/jbc.AC119.010366.
85. Schmitz, A.; Schwarz, A.; Foss, M.; Zhou, L.; Rabe, B.; Hoellenriegel, J.; Stoeber, M.; Pante, N.; Kann, M. Nucleoporin 153 arrests the nuclear import of hepatitis B virus capsids in the nuclear basket. *PLoS Pathog.* **2010**, *6*, e1000741. doi:10.1371/journal.ppat.1000741.
86. Rabe, B.; Vlachou, A.; Pante, N.; Helenius, A.; Kann, M. Nuclear import of hepatitis B virus capsids and release of the viral genome. *Proc. Natl. Acad. Sci. U. S. A.* **2003**, *100*, 9849-9854. doi:10.1073/pnas.1730940100.
87. Rabe, B.; Delaleau, M.; Bischof, A.; Foss, M.; Sominskaya, I.; Pumpens, P.; Cazenave, C.; Castroviejo, M.; Kann, M. Nuclear entry of hepatitis B virus capsids involves

- disintegration to protein dimers followed by nuclear reassociation to capsids. *PLoS Pathog.* **2009**, *5*, e1000563. doi:10.1371/journal.ppat.1000563.
88. Gao, W.; Hu, J. Formation of hepatitis B virus covalently closed circular DNA: removal of genome-linked protein. *J. Virol.* **2007**, *81*, 6164-6174. doi:10.1128/JVI.02721-06.
89. Wei, L.; Ploss, A. Hepatitis B virus cccDNA is formed through distinct repair processes of each strand. *Nat. Commun.* **2021**, *12*, 1591. doi:10.1038/s41467-021-21850-9.
90. Wei, L.; Ploss, A. Mechanism of Hepatitis B Virus cccDNA Formation. *Viruses* **2021**, *13*. doi:10.3390/v13081463.
91. Kock, J.; Schlicht, H.J. Analysis of the earliest steps of hepadnavirus replication: genome repair after infectious entry into hepatocytes does not depend on viral polymerase activity. *J. Virol.* **1993**, *67*, 4867-4874. doi:10.1128/JVI.67.8.4867-4874.1993.
92. Wei, L.; Ploss, A. Core components of DNA lagging strand synthesis machinery are essential for hepatitis B virus cccDNA formation. *Nat. Microbiol.* **2020**, doi:10.1038/s41564-020-0678-0.
93. Koniger, C.; Wingert, I.; Marsmann, M.; Rosler, C.; Beck, J.; Nassal, M. Involvement of the host DNA-repair enzyme TDP2 in formation of the covalently closed circular DNA persistence reservoir of hepatitis B viruses. *Proc. Natl. Acad. Sci. U. S. A.* **2014**, *111*, E4244-53. doi:10.1073/pnas.1409986111.
94. Cui, X.; McAllister, R.; Boregowda, R.; Sohn, J.A.; Cortes Ledesma, F.; Caldecott, K.W.; Seeger, C.; Hu, J. Does Tyrosyl DNA Phosphodiesterase-2 Play a Role in Hepatitis B Virus Genome Repair? *PLoS One* **2015**, *10*, e0128401. doi:10.1371/journal.pone.0128401.
95. Kitamura, K.; Que, L.; Shimadu, M.; Koura, M.; Ishihara, Y.; Wakae, K.; Nakamura, T.; Watashi, K.; Wakita, T.; Muramatsu, M. Flap endonuclease 1 is involved in cccDNA formation in the hepatitis B virus. *PLoS Pathog.* **2018**, *14*, e1007124. doi:10.1371/journal.ppat.1007124.
96. Tang, L.; Sheraz, M.; McGrane, M.; Chang, J.; Guo, J.T. DNA Polymerase alpha is essential for intracellular amplification of hepatitis B virus covalently closed circular DNA. *PLoS Pathog.* **2019**, *15*, e1007742. doi:10.1371/journal.ppat.1007742.
97. Sheraz, M.; Cheng, J.; Tang, L.; Chang, J.; Guo, J.T. Cellular DNA Topoisomerases Are Required for the Synthesis of Hepatitis B Virus Covalently Closed Circular DNA. *J. Virol.* **2019**, *93*. doi:10.1128/JVI.02230-18.

98. Qi, Y.; Gao, Z.; Xu, G.; Peng, B.; Liu, C.; Yan, H.; Yao, Q.; Sun, G.; Liu, Y.; Tang, D.; Song, Z.; He, W.; Sun, Y.; Guo, J.T.; Li, W. DNA Polymerase kappa Is a Key Cellular Factor for the Formation of Covalently Closed Circular DNA of Hepatitis B Virus. *PLoS Pathog.* **2016**, *12*, e1005893. doi:10.1371/journal.ppat.1005893.
99. Long, Q.; Yan, R.; Hu, J.; Cai, D.; Mitra, B.; Kim, E.S.; Marchetti, A.; Zhang, H.; Wang, S.; Liu, Y.; Huang, A.; Guo, H. The role of host DNA ligases in hepadnavirus covalently closed circular DNA formation. *PLoS Pathog.* **2017**, *13*, e1006784. doi:10.1371/journal.ppat.1006784.
100. Staprans, S.; Loeb, D.D.; Ganem, D. Mutations affecting hepadnavirus plus-strand DNA synthesis dissociate primer cleavage from translocation and reveal the origin of linear viral DNA. *J. Virol.* **1991**, *65*, 1255-1262.
101. Guo, H.; Xu, C.; Zhou, T.; Block, T.M.; Guo, J.T. Characterization of the host factors required for hepadnavirus covalently closed circular (ccc) DNA formation. *PLoS One* **2012**, *7*, e43270. doi:10.1371/journal.pone.0043270.
102. Bock, C.T.; Schranz, P.; Schroder, C.H.; Zentgraf, H. Hepatitis B virus genome is organized into nucleosomes in the nucleus of the infected cell. *Virus Genes* **1994**, *8*, 215-29. doi:10.1007/BF01703079.
103. Bock, C.T.; Schwinn, S.; Locarnini, S.; Fyfe, J.; Manns, M.P.; Trautwein, C.; Zentgraf, H. Structural organization of the hepatitis B virus minichromosome. *J. Mol. Biol.* **2001**, *307*, 183-96. doi:10.1006/jmbi.2000.4481.
104. Addison, W.R.; Walters, K.A.; Wong, W.W.; Wilson, J.S.; Madej, D.; Jewell, L.D.; Tyrrell, D.L. Half-life of the duck hepatitis B virus covalently closed circular DNA pool in vivo following inhibition of viral replication. *J. Virol.* **2002**, *76*, 6356-6363. doi:10.1128/jvi.76.12.6356-6363.2002.
105. Lythgoe, K.A.; Lumley, S.F.; Pellis, L.; McKeating, J.A.; Matthews, P.C. Estimating hepatitis B virus cccDNA persistence in chronic infection. *Virus Evol.* **2021**, *7*, veaa063. doi:10.1093/ve/veaa063.
106. Tu, T.; Zehnder, B.; Qu, B.; Urban, S. De novo synthesis of hepatitis B virus nucleocapsids is dispensable for the maintenance and transcriptional regulation of cccDNA. *JHEP Rep.* **2021**, *3*, 100195. doi:10.1016/j.jhepr.2020.100195.

107. Tropberger, P.; Mercier, A.; Robinson, M.; Zhong, W.; Ganem, D.E.; Holdorf, M. Mapping of histone modifications in episomal HBV cccDNA uncovers an unusual chromatin organization amenable to epigenetic manipulation. *Proc. Natl. Acad. Sci. U. S. A.* **2015**, *112*, E5715-24. doi:10.1073/pnas.1518090112.
108. Rall, L.B.; Standring, D.N.; Laub, O.; Rutter, W.J. Transcription of hepatitis B virus by RNA polymerase II. *Mol. Cell Biol.* **1983**, *3*, 1766-1773. doi:10.1128/mcb.3.10.1766.
109. Hirsch, R.C.; Lavine, J.E.; Chang, L.J.; Varmus, H.E.; Ganem, D. Polymerase gene products of hepatitis B viruses are required for genomic RNA packaging as well as for reverse transcription. *Nature* **1990**, *344*, 552-555. doi:10.1038/344552a0.
110. Knaus, T.; Nassal, M. The encapsidation signal on the hepatitis B virus RNA pregenome forms a stem-loop structure that is critical for its function. *Nucleic Acids Res.* **1993**, *21*, 3967-3975. doi:10.1093/nar/21.17.3967.
111. Porterfield, J.Z.; Dhasan, M.S.; Loeb, D.D.; Nassal, M.; Stray, S.J.; Zlotnick, A. Full-length hepatitis B virus core protein packages viral and heterologous RNA with similarly high levels of cooperativity. *J. Virol.* **2010**, *84*, 7174-84. doi:10.1128/JVI.00586-10.
112. Junker-Niepmann, M.; Bartenschlager, R.; Schaller, H. A short cis-acting sequence is required for hepatitis B virus pregenome encapsidation and sufficient for packaging of foreign RNA. *EMBO J.* **1990**, *9*, 3389-96.
113. Hu, J.; Boyer, M. Hepatitis B virus reverse transcriptase and epsilon RNA sequences required for specific interaction in vitro. *J. Virol.* **2006**, *80*, 2141-2150. doi:10.1128/JVI.80.5.2141-2150.2006.
114. Pollack, J.R.; Ganem, D. An RNA stem-loop structure directs hepatitis B virus genomic RNA encapsidation. *J. Virol.* **1993**, *67*, 3254-3263.
115. Pollack, J.R.; Ganem, D. Site-specific RNA binding by a hepatitis B virus reverse transcriptase initiates two distinct reactions: RNA packaging and DNA synthesis. *J. Virol.* **1994**, *68*, 5579-5587.
116. Bartenschlager, R.; Junker-Niepmann, M.; Schaller, H. The P gene product of hepatitis B virus is required as a structural component for genomic RNA encapsidation. *J. Virol.* **1990**, *64*, 5324-5332.
117. Bartenschlager, R.; Schaller, H. Hepadnaviral assembly is initiated by polymerase binding to the encapsidation signal in the viral RNA genome. *EMBO J.* **1992**, *11*, 3413-3420.

118. Haines, K.M.; Loeb, D.D. The sequence of the RNA primer and the DNA template influence the initiation of plus-strand DNA synthesis in hepatitis B virus. *J. Mol. Biol.* **2007**, *370*, 471-480. doi:10.1016/j.jmb.2007.04.057.
119. Zoulim, F.; Seeger, C. Reverse transcription in hepatitis B viruses is primed by a tyrosine residue of the polymerase. *J. Virol.* **1994**, *68*, 6-13.
120. Nassal, M.; Rieger, A. A bulged region of the hepatitis B virus RNA encapsidation signal contains the replication origin for discontinuous first-strand DNA synthesis. *J. Virol.* **1996**, *70*, 2764-2773.
121. Rieger, A.; Nassal, M. Specific hepatitis B virus minus-strand DNA synthesis requires only the 5' encapsidation signal and the 3'-proximal direct repeat DR1. *J. Virol.* **1996**, *70*, 585-589.
122. Loeb, D.D.; Hirsch, R.C.; Ganem, D. Sequence-independent RNA cleavages generate the primers for plus strand DNA synthesis in hepatitis B viruses: implications for other reverse transcribing elements. *EMBO J.* **1991**, *10*, 3533-3540.
123. Lewellyn, E.B.; Loeb, D.D. Base pairing between cis-acting sequences contributes to template switching during plus-strand DNA synthesis in human hepatitis B virus. *J. Virol.* **2007**, *81*, 6207-6215. doi:10.1128/JVI.00210-07.
124. Sattler, F.; Robinson, W.S. Hepatitis B viral DNA molecules have cohesive ends. *J. Virol.* **1979**, *32*, 226-233.
125. Scotto, J.; Hadchouel, M.; Wain-Hobson, S.; Sonigo, P.; Courouce, A.M.; Tiollais, P.; Brechot, C. Hepatitis B virus DNA in Dane particles: evidence for the presence of replicative intermediates. *J. Infect. Dis.* **1985**, *151*, 610-617. doi:10.1093/infdis/151.4.610.
126. Urban, S.; Urban, S.; Fischer, K.P.; Tyrrell, D.L. Efficient pyrophosphorolysis by a hepatitis B virus polymerase may be a primer-unblocking mechanism. *Proc. Natl. Acad. Sci. U. S. A.* **2001**, *98*, 4984-4989. doi:10.1073/pnas.091324398.
127. Ning, X.; Basagoudanavar, S.H.; Liu, K.; Luckenbaugh, L.; Wei, D.; Wang, C.; Wei, B.; Zhao, Y.; Yan, T.; Delaney, W.; Hu, J. Capsid Phosphorylation State and Hepadnavirus Virion Secretion. *J. Virol.* **2017**, *91*. doi:10.1128/JVI.00092-17.
128. Gerelsaikhan, T.; Tavis, J.E.; Bruss, V. Hepatitis B virus nucleocapsid envelopment does not occur without genomic DNA synthesis. *J. Virol.* **1996**, *70*, 4269-4274.

129. Wei, Y.; Tavis, J.E.; Ganem, D. Relationship between viral DNA synthesis and virion envelopment in hepatitis B viruses. *J. Virol.* **1996**, *70*, 6455-6458.
130. Ning, X.; Luckenbaugh, L.; Liu, K.; Bruss, V.; Sureau, C.; Hu, J. Common and Distinct Capsid and Surface Protein Requirements for Secretion of Complete and Genome-Free Hepatitis B Virions. *J. Virol.* **2018**, *92*. doi:10.1128/JVI.00272-18.
131. Bruss, V.; Thomssen, R. Mapping a region of the large envelope protein required for hepatitis B virion maturation. *J. Virol.* **1994**, *68*, 1643-1650.
132. Bruss, V. A short linear sequence in the pre-S domain of the large hepatitis B virus envelope protein required for virion formation. *J. Virol.* **1997**, *71*, 9350-9357.
133. Loffler-Mary, H.; Dumortier, J.; Klentsch-Zimmer, C.; Prange, R. Hepatitis B virus assembly is sensitive to changes in the cytosolic S loop of the envelope proteins. *Virology*, **2000**. *270*, 358-67. doi:10.1006/viro.2000.0268.
134. Bruss, V. Hepatitis B virus morphogenesis. *World J. Gastroenterol.* **2007**, *13*, 65-73. doi:10.3748/wjg.v13.i1.65.
135. Ganem, D. Assembly of hepadnaviral virions and subviral particles. *Curr. Top. Microbiol. Immunol.* **1991**, *168*, 61-83. doi:10.1007/978-3-642-76015-0_4.
136. Chai, N.; Chang, H.E.; Nicolas, E.; Han, Z.; Jarnik, M.; Taylor, J. Properties of subviral particles of hepatitis B virus. *J. Virol.* **2008**, *82*, 7812-7817. doi:10.1128/JVI.00561-08.
137. Fiscicaro, P.; Barili, V.; Montanini, B.; Acerbi, G.; Ferracin, M.; Guerrieri, F.; Salerno, D.; Boni, C.; Massari, M.; Cavallo, M.C.; Grossi, G.; Giuberti, T.; Lampertico, P.; Missale, G.; Levrero, M.; Ottonello, S. Ferrari, C. Targeting mitochondrial dysfunction can restore antiviral activity of exhausted HBV-specific CD8 T cells in chronic hepatitis B. *Nat. Med.* **2017**, *23*, 327-336. doi:10.1038/nm.4275.
138. Patient, R.; Hourieux, C.; Sizaret, P.Y.; Trassard, S.; Sureau, C.; Roingeard, P. Hepatitis B virus subviral envelope particle morphogenesis and intracellular trafficking. *J. Virol.* **2007**, *81*, 3842-3851. doi:10.1128/JVI.02741-06.
139. Rost, M.; Mann, S.; Lambert, C.; Doring, T.; Thome, N.; Prange, R. Gamma-adaptin, a novel ubiquitin-interacting adaptor, and Nedd4 ubiquitin ligase control hepatitis B virus maturation. *J. Biol. Chem.* **2006**, *281*, 29297-29308. doi:10.1074/jbc.M603517200.

140. Lambert, C.; Doring, T. Prange, R. Hepatitis B virus maturation is sensitive to functional inhibition of ESCRT-III, Vps4, and gamma 2-adaptin. *J. Virol.* **2007**, *81*, 9050-9060. doi:10.1128/JVI.00479-07.
141. Tuttleman, J.S.; Pourcel, C.; Summers, J. Formation of the pool of covalently closed circular viral DNA in hepadnavirus-infected cells. *Cell* **1986**, *47*, 451-460. doi:10.1016/0092-8674(86)90602-1.
142. Volz, T.; Allweiss, L.; Ben, M.M.; Warlich, M.; Lohse, A.W.; Pollok, J.M.; Alexandrov, A.; Urban, S.; Petersen, J.; Lutgehetmann, M. Dandri, M. The entry inhibitor Myrcludex-B efficiently blocks intrahepatic virus spreading in humanized mice previously infected with hepatitis B virus. *J. Hepatol.* **2013**, *58*, 861-867. doi:10.1016/j.jhep.2012.12.008.
143. Ko, C.; Chakraborty, A.; Chou, W.M.; Hasreiter, J.; Wettengel, J.M.; Stadler, D.; Bester, R.; Asen, T.; Zhang, K.; Wisskirchen, K.; McKeating, J.A.; Ryu, W.S.; Protzer, U. Hepatitis B virus genome recycling and de novo secondary infection events maintain stable cccDNA levels. *J. Hepatol.* **2018**, *69*, 1231-1241. doi:10.1016/j.jhep.2018.08.012.
144. Konig, A.; Yang, J.; Jo, E.; Park, K.H.P.; Kim, H.; Than, T.T.; Song, X.; Qi, X.; Dai, X.; Park, S.; Shum, D.; Ryu, W.S.; Kim, J.H.; Yoon, S.K.; Park, J.Y.; Ahn, S.H.; Han, K.H.; Gerlich, W.H.; Windisch, M.P. Efficient long-term amplification of hepatitis B virus isolates after infection of slow proliferating HepG2-NTCP cells. *J. Hepatol.* **2019**, *71*, 289-300. doi:10.1016/j.jhep.2019.04.010.
145. Summers, J.; Smith, P.M.; Horwich, A.L. Hepadnavirus envelope proteins regulate covalently closed circular DNA amplification. *J. Virol.* **1990**, *64*, 2819-2824. doi:10.1128/JVI.64.6.2819-2824.1990.
146. Walters, K.A.; Joyce, M.A.; Addison, W.R.; Fischer, K.P.; Tyrrell, D.L. Superinfection exclusion in duck hepatitis B virus infection is mediated by the large surface antigen. *J. Virol.* **2004**, *78*, 7925-7937. doi:10.1128/JVI.78.15.7925-7937.2004.
147. Lentz, T.B.; Loeb, D.D. Roles of the envelope proteins in the amplification of covalently closed circular DNA and completion of synthesis of the plus-strand DNA in hepatitis B virus. *J. Virol.* **2011**, *85*, 11916-11927. doi:10.1128/JVI.05373-11.
148. Ling, R.; Harrison, T.J. Production of hepatitis B virus covalently closed circular DNA in transfected cells is independent of surface antigen synthesis. *J. Gen. Virol.* **1997**, *78 (Pt 6)*, 1463-1467. doi:10.1099/0022-1317-78-6-1463.

149. Sprinzl, M.F.; Oberwinkler, H.; Schaller, H.; Protzer, U. Transfer of hepatitis B virus genome by adenovirus vectors into cultured cells and mice: crossing the species barrier. *J. Virol.* **2001**, *75*, 5108-5118. doi:10.1128/JVI.75.11.5108-5118.2001.
150. Chakraborty, P.R.; Ruiz-Opazo, N.; Shouval, D.; Shafritz, D.A. Identification of integrated hepatitis B virus DNA and expression of viral RNA in an HBsAg-producing human hepatocellular carcinoma cell line. *Nature* **1980**, *286*, 531-533. doi:10.1038/286531a0.
151. Brechot, C.; Pourcel, C.; Louise, A.; Rain, B.; Tiollais, P. Presence of integrated hepatitis B virus DNA sequences in cellular DNA of human hepatocellular carcinoma. *Nature* **1980**, *286*, 533-535. doi:10.1038/286533a0.
152. Mason, W.S.; Gill, U.S.; Litwin, S.; Zhou, Y.; Peri, S.; Pop, O.; Hong, M.L.; Naik, S.; Quaglia, A.; Bertolotti, A.; Kennedy, P.T. HBV DNA Integration and Clonal Hepatocyte Expansion in Chronic Hepatitis B Patients Considered Immune Tolerant. *Gastroenterology* **2016**, *151*, 986-998 e4. doi:10.1053/j.gastro.2016.07.012.
153. Yang, W.; Summers, J. Integration of hepadnavirus DNA in infected liver: evidence for a linear precursor. *J. Virol.* **1999**, *73*, 9710-9717. doi:10.1128/JVI.73.12.9710-9717.1999.
154. Bill, C.A.; Summers, J. Genomic DNA double-strand breaks are targets for hepadnaviral DNA integration. *Proc. Natl. Acad. Sci. U. S. A.* **2004**, *101*, 11135-11140. doi:10.1073/pnas.0403925101.
155. Hai, H.; Tamori, A.; Kawada, N. Role of hepatitis B virus DNA integration in human hepatocarcinogenesis. *World J Gastroenterol*, **2014**, *20*, 6236-43. doi:10.3748/wjg.v20.i20.6236.
156. Wooddell, C.I.; Yuen, M.F.; Chan, H.L.; Gish, R.G.; Locarnini, S.A.; Chavez, D.; Ferrari, C.; Given, B.D.; Hamilton, J.; Kanner, S.B.; Lai, C.L.; Lau, J.Y.N.; Schlupe, T.; Xu, Z.; Lanford, R.E.; Lewis, D.L. RNAi-based treatment of chronically infected patients and chimpanzees reveals that integrated hepatitis B virus DNA is a source of HBsAg. *Sci. Transl. Med.* **2017**, *9*. doi:10.1126/scitranslmed.aan0241.
157. Sung, W.K.; Zheng, H.; Li, S.; Chen, R.; Liu, X.; Li, Y.; Lee, N.P.; Lee, W.H.; Ariyaratne, P.N.; Tennakoon, C.; Mulawadi, F.H.; Wong, K.F.; Liu, A.M.; Poon, R.T.; Fan, S.T.; Chan, K.L.; Gong, Z.; Hu, Y.; Lin, Z.; Wang, G.; Zhang, Q.; Barber, T.D.; Chou, W.C.; Aggarwal, A.; Hao, K.; Zhou, W.; Zhang, C.; Hardwick, J.; Buser, C.; Xu, J.; Kan, Z.; Dai, H.; Mao, M.; Reinhard, C.; Wang, J.; Luk, J.M. Genome-wide survey of recurrent HBV

- integration in hepatocellular carcinoma. *Nat. Genet.* **2012**, *44*, 765-769.
doi:10.1038/ng.2295.
158. Brechot, C.; Gozuacik, D.; Murakami, Y.; Paterlini-Brechot, P. Molecular bases for the development of hepatitis B virus (HBV)-related hepatocellular carcinoma (HCC). *Semin. Cancer Biol.* **2000**, *10*, 211-231. doi:10.1006/scbi.2000.0321.
159. Paterlini-Brechot, P.; Saigo, K.; Murakami, Y.; Chami, M.; Gozuacik, D.; Mugnier, C.; Lagorce, D.; Brechot, C. Hepatitis B virus-related insertional mutagenesis occurs frequently in human liver cancers and recurrently targets human telomerase gene. *Oncogene* **2003**, *22*, 3911-3916. doi:10.1038/sj.onc.1206492.
160. Wang, H.C.; Huang, W.; Lai, M.D.; Su, I.J. Hepatitis B virus pre-S mutants, endoplasmic reticulum stress and hepatocarcinogenesis. *Cancer Sci.* **2006**, *97*, 683-688.
doi:10.1111/j.1349-7006.2006.00235.x.
161. Ding, D.; Lou, X.; Hua, D.; Yu, W.; Li, L.; Wang, J.; Gao, F.; Zhao, N.; Ren, G.; Li, L.; Lin, B. Recurrent targeted genes of hepatitis B virus in the liver cancer genomes identified by a next-generation sequencing-based approach. *PLoS Genet.* **2012**, *8*, e1003065.
doi:10.1371/journal.pgen.1003065.
162. Yan, H.; Yang, Y.; Zhang, L.; Tang, G.; Wang, Y.; Xue, G.; Zhou, W.; Sun, S. Characterization of the genotype and integration patterns of hepatitis B virus in early- and late-onset hepatocellular carcinoma. *Hepatology* **2015**, *61*, 1821-1831.
doi:10.1002/hep.27722.
163. Alvarez, E.G.; Demeulemeester, J.; Otero, P.; Jolly, C.; Garcia-Souto, D.; Pequeno-Valtierra, A.; Zamora, J.; Tojo, M.; Temes, J.; Baez-Ortega, A.; Rodriguez-Martin, B.; Oitaben, A.; Bruzos, A.L.; Martinez-Fernandez, M.; Haase, K.; Zumalave, S.; Abal, R.; Rodriguez-Castro, J.; Rodriguez-Casanova, A.; Diaz-Lagares, A.; Li, Y.; Raine, K.M.; Butler, A.P.; Otero, I.; Ono, A.; Aikata, H.; Chayama, K.; Ueno, M.; Hayami, S.; Yamaue, H.; Maejima, K.; Blanco, M.G.; Forns, X.; Rivas, C.; Ruiz-Banobre, J.; Perez-Del-Pulgar, S.; Torres-Ruiz, R.; Rodriguez-Perales, S.; Garaigorta, U.; Campbell, P.J.; Nakagawa, H.; Van Loo, P.; Tubio, J.M.C. Aberrant integration of Hepatitis B virus DNA promotes major restructuring of human hepatocellular carcinoma genome architecture. *Nat. Commun.* **2021**, *12*, 6910. doi:10.1038/s41467-021-26805-8.

164. Zhao, L.H.; Liu, X.; Yan, H.X.; Li, W.Y.; Zeng, X.; Yang, Y.; Zhao, J.; Liu, S.P.; Zhuang, X.H.; Lin, C.; Qin, C.J.; Zhao, Y.; Pan, Z.Y.; Huang, G.; Liu, H.; Zhang, J.; Wang, R.Y.; Yang, Y.; Wen, W.; Lv, G.S.; Zhang, H.L.; Wu, H.; Huang, S.; Wang, M.D.; Tang, L.; Cao, H.Z.; Wang, L.; Lee, T.L.; Jiang, H.; Tan, Y.X.; Yuan, S.X.; Hou, G.J.; Tao, Q.F.; Xu, Q.G.; Zhang, X.Q.; Wu, M.C.; Xu, X.; Wang, J.; Yang, H.M.; Zhou, W.P.; Wang, H.Y. Genomic and oncogenic preference of HBV integration in hepatocellular carcinoma. *Nat. Commun.* **2016**, *7*, 12992. doi:10.1038/ncomms12992.
165. Tu, T.; Budzinska, M.A.; Vondran, F.W.R.; Shackel, N.A.; Urban, S. Hepatitis B Virus DNA Integration Occurs Early in the Viral Life Cycle in an In Vitro Infection Model via Sodium Taurocholate Cotransporting Polypeptide-Dependent Uptake of Enveloped Virus Particles. *J. Virol.* **2018**, *92*. doi:10.1128/JVI.02007-17.
166. Prakash, K.; Larsson, S.B.; Rydell, G.E.; Andersson, M.E.; Ringlander, J.; Norkrans, G.; Norder, H.; Lindh, M. Hepatitis B Virus RNA Profiles in Liver Biopsies by Digital Polymerase Chain Reaction. *Hepatol. Commun.* **2020**, *4*, 973-982. doi:10.1002/hep4.1507.
167. Tu, T.; Mason, W.S.; Clouston, A.D.; Shackel, N.A.; McCaughan, G.W.; Yeh, M.M.; Schiff, E.R.; Ruszkiewicz, A.R.; Chen, J.W.; Harley, H.A.; Stroehrer, U.H.; Jilbert, A.R. Clonal expansion of hepatocytes with a selective advantage occurs during all stages of chronic hepatitis B virus infection. *J. Viral. Hepat.* **2015**, *22*, 737-753. doi:10.1111/jvh.12380.
168. Peneau, C.; Imbeaud, S.; La Bella, T.; Hirsch, T.Z.; Caruso, S.; Calderaro, J.; Paradis, V.; Blanc, J.F.; Letouze, E.; Nault, J.C.; Amaddeo, G.; Zucman-Rossi, J. Hepatitis B virus integrations promote local and distant oncogenic driver alterations in hepatocellular carcinoma. *Gut* **2022**, *71*, 616-626. doi:10.1136/gutjnl-2020-323153.
169. Lichter, E.A. Chimpanzee antibodies to Australia antigen. *Nature* **1969**, *224*, 810-811. doi:10.1038/224810a0.
170. Walter, E.; Keist, R.; Niederost, B.; Pult, I.; Blum, H.E. Hepatitis B virus infection of tupaia hepatocytes in vitro and in vivo. *Hepatology* **1996**, *24*, 1-5. doi:10.1002/hep.510240101.
171. Shikata, T.; Karasawa, T. Abe, K. Two distinct types of hepatitis in experimental hepatitis B virus infection. *Am. J. Pathol.* **1980**, *99*, 353-368.

172. Asabe, S.; Wieland, S.F.; Chattopadhyay, P.K.; Roederer, M.; Engle, R.E.; Purcell, R.H.; Chisari, F.V. The size of the viral inoculum contributes to the outcome of hepatitis B virus infection. *J. Virol.* **2009**, *83*, 9652-9662. doi:10.1128/JVI.00867-09.
173. Prince, A.M.; Brotman, B.; Purcell, R.H.; Gerin, J.L. A final report on safety and immunogenicity of a bivalent aqueous subunit HBV vaccine. *J. Med. Virol.* **1985**, *15*, 399-419. doi:10.1002/jmv.1890150410.
174. Sanada, T.; Tsukiyama-Kohara, K.; Shin, I.T.; Yamamoto, N.; Kayesh, M.E.H.; Yamane, D.; Takano, J.I.; Shioyama, Y.; Yasutomi, Y.; Ikeo, K.; Gojobori, T.; Mizokami, M. Kohara, M. Construction of complete *Tupaia belangeri* transcriptome database by whole-genome and comprehensive RNA sequencing. *Sci. Rep.* **2019**, *9*, 12372. doi:10.1038/s41598-019-48867-x.
175. Yang, C.; Ruan, P.; Ou, C.; Su, J.; Cao, J.; Luo, C.; Tang, Y.; Wang, Q.; Qin, H.; Sun, W.; Li, Y. Chronic hepatitis B virus infection and occurrence of hepatocellular carcinoma in tree shrews (*Tupaia belangeri chinensis*). *Virol. J.* **2015**, *12*, 26. doi:10.1186/s12985-015-0256-x.
176. Kock, J.; Nassal, M.; MacNelly, S.; Baumert, T.F.; Blum, H.E.; von Weizsacker, F. Efficient infection of primary tupaia hepatocytes with purified human and woolly monkey hepatitis B virus. *J. Virol.* **2001**, *75*, 5084-5089. doi:10.1128/JVI.75.11.5084-5089.2001.
177. Gripon, P.; Diot, C.; Theze, N.; Fourel, I.; Loreal, O.; Brechot, C.; Guguen-Guillouzo, C. Hepatitis B virus infection of adult human hepatocytes cultured in the presence of dimethyl sulfoxide. *J. Virol.* **1988**, *62*, 4136-4143.
178. Gripon, P.; Diot, C.; Guguen-Guillouzo, C. Reproducible high level infection of cultured adult human hepatocytes by hepatitis B virus: effect of polyethylene glycol on adsorption and penetration. *Virology* **1993**, *192*, 534-540. doi:10.1006/viro.1993.1069.
179. Xiang, C.; Du, Y.; Meng, G.; Yi, L.S.; Sun, S.; Song, N.; Zhang, X.; Xiao, Y.; Wang, J.; Yi, Z.; Liu, Y.; Xie, B.; Wu, M.; Shu, J.; Sun, D.; Jia, J.; Liang, Z.; Sun, D.; Huang, Y.; Shi, Y.; Xu, J.; Lu, F.; Li, C.; Xiang, K.; Yuan, Z.; Lu, S.; Deng, H. Long-term functional maintenance of primary human hepatocytes in vitro. *Science* **2019**, *364*, 399-402. doi:10.1126/science.aau7307.
180. Clement, B.; Guguen-Guillouzo, C.; Campion, J.P.; Glaise, D.; Bourel, M.; Guillouzo, A. Long-term co-cultures of adult human hepatocytes with rat liver epithelial cells:

- modulation of albumin secretion and accumulation of extracellular material. *Hepatology* **1984**, *4*, 373-380. doi:10.1002/hep.1840040305.
181. Winer, B.Y.; Huang, T.S.; Pludwinski, E.; Heller, B.; Wojcik, F.; Lipkowitz, G.E.; Parekh, A.; Cho, C.; Shirao, A.; Muir, T.W.; Novik, E.; Ploss, A. Long-term hepatitis B infection in a scalable hepatic co-culture system. *Nat. Commun.* **2017**, *8*, 125. doi:10.1038/s41467-017-00200-8.
 182. Shlomai, A.; Schwartz, R.E.; Ramanan, V.; Bhatta, A.; de Jong, Y.P.; Bhatia, S.N.; Rice, C.M. Modeling host interactions with hepatitis B virus using primary and induced pluripotent stem cell-derived hepatocellular systems. *Proc. Natl. Acad. Sci. U. S. A.* **2014**, *111*, 12193-12198. doi:10.1073/pnas.1412631111.
 183. Sivaraman, A.; Leach, J.K.; Townsend, S.; Iida, T.; Hogan, B.J.; Stolz, D.B.; Fry, R.; Samson, L.D.; Tannenbaum, S.R.; Griffith, L.G. A microscale in vitro physiological model of the liver: predictive screens for drug metabolism and enzyme induction. *Curr. Drug Metab.* **2005**, *6*, 569-591. doi:10.2174/138920005774832632.
 184. Ortega-Prieto, A.M.; Skelton, J.K.; Wai, S.N.; Large, E.; Lussignol, M.; Vizcay-Barrena, G.; Hughes, D.; Fleck, R.A.; Thursz, M.; Catanese, M.T.; Dorner, M. 3D microfluidic liver cultures as a physiological preclinical tool for hepatitis B virus infection. *Nat. Commun.* **2018**, *9*, 682. doi:10.1038/s41467-018-02969-8.
 185. Aden, D.P.; Fogel, A.; Plotkin, S.; Damjanov, I.; Knowles, B.B. Controlled synthesis of HBsAg in a differentiated human liver carcinoma-derived cell line. *Nature* **1979**, *282*, 615-616. doi:10.1038/282615a0.
 186. Lopez-Terrada, D.; Cheung, S.W.; Finegold, M.J.; Knowles, B.B. Hep G2 is a hepatoblastoma-derived cell line. *Hum. Pathol.* **2009**, *40*, 1512-1515. doi:10.1016/j.humpath.2009.07.003.
 187. Sureau, C.; Romet-Lemonne, J.L.; Mullins, J.I.; Essex, M. Production of hepatitis B virus by a differentiated human hepatoma cell line after transfection with cloned circular HBV DNA. *Cell* **1986**, *47*, 37-47. doi:10.1016/0092-8674(86)90364-8.
 188. Gripon, P.; Diot, C.; Corlu, A.; Guguen-Guillouzo, C. Regulation by dimethylsulfoxide, insulin, and corticosteroids of hepatitis B virus replication in a transfected human hepatoma cell line. *J. Med. Virol.* **1989**, *28*, 193-199. doi:10.1002/jmv.1890280316.

189. Guo, L.; Dial, S.; Shi, L.; Branham, W.; Liu, J.; Fang, J.L.; Green, B.; Deng, H.; Kaput, J.; Ning, B. Similarities and differences in the expression of drug-metabolizing enzymes between human hepatic cell lines and primary human hepatocytes. *Drug Metab. Dispos.* **2011**, *39*, 528-538. doi:10.1124/dmd.110.035873.
190. Sells, M.A.; Chen, M.L.; Acs, G. Production of hepatitis B virus particles in Hep G2 cells transfected with cloned hepatitis B virus DNA. *Proc. Natl. Acad. Sci. U. S. A.* **1987**, *84*, 1005-1009. doi:10.1073/pnas.84.4.1005.
191. Ladner, S.K.; Otto, M.J.; Barker, C.S.; Zaifert, K.; Wang, G.H.; Guo, J.T.; Seeger, C.; King, R.W. Inducible expression of human hepatitis B virus (HBV) in stably transfected hepatoblastoma cells: a novel system for screening potential inhibitors of HBV replication. *Antimicrob. Agents Chemother.* **1997**, *41*, 1715-1720.
192. Guo, H.; Jiang, D.; Zhou, T.; Cuconati, A.; Block, T.M.; Guo, J.T. Characterization of the intracellular deproteinized relaxed circular DNA of hepatitis B virus: an intermediate of covalently closed circular DNA formation. *J. Virol.* **2007**, *81*, 12472-12484. doi:10.1128/JVI.01123-07.
193. Gripon, P.; Rumin, S.; Urban, S.; Le Seyec, J.; Glaise, D.; Cannie, I.; Guyomard, C.; Lucas, J.; Trepo, C.; Guguen-Guillouzo, C. Infection of a human hepatoma cell line by hepatitis B virus. *Proc. Natl. Acad. Sci. U. S. A.* **2002**, *99*, 15655-15660. doi:10.1073/pnas.232137699.
194. Quasdorff, M.; Hosel, M.; Odenthal, M.; Zedler, U.; Bohne, F.; Gripon, P.; Dienes, H.P.; Drebber, U.; Stippel, D.; Goeser, T.; Protzer, U. A concerted action of HNF4alpha and HNF1alpha links hepatitis B virus replication to hepatocyte differentiation. *Cell Microbiol.* **2008**, *10*, 1478-1490. doi:10.1111/j.1462-5822.2008.01141.x.
195. Ni, Y.; Lempp, F.A.; Mehrle, S.; Nkongolo, S.; Kaufman, C.; Falth, M.; Stindt, J.; Koniger, C.; Nassal, M.; Kubitz, R.; Sultmann, H.; Urban, S. Hepatitis B and D viruses exploit sodium taurocholate co-transporting polypeptide for species-specific entry into hepatocytes. *Gastroenterology* **2014**, *146*, 1070-1083. doi:10.1053/j.gastro.2013.12.024.
196. Lucifora, J.; Durantel, D.; Testoni, B.; Hantz, O.; Levrero, M.; Zoulim, F. Control of hepatitis B virus replication by innate response of HepaRG cells. *Hepatology* **2010**, *51*, 63-72. doi:10.1002/hep.23230.

197. Shen, F.; Li, Y.; Wang, Y.; Sozzi, V.; Revall, P.A.; Liu, J.; Gao, L.; Yang, G.; Lu, M.; Sutter, K.; Dittmer, U.; Chen, J.; Yuan, Z. Hepatitis B virus sensitivity to interferon-alpha in hepatocytes is more associated with cellular interferon response than with viral genotype. *Hepatology* **2018**, *67*, 1237-1252. doi:10.1002/hep.29609.
198. Gerets, H.H.; Tilmant, K.; Gerin, B.; Chanteux, H.; Depelchin, B.O.; Dhalluin, S.; Atienzar, F.A. Characterization of primary human hepatocytes, HepG2 cells, and HepaRG cells at the mRNA level and CYP activity in response to inducers and their predictivity for the detection of human hepatotoxins. *Cell Biol. Toxicol.* **2012**, *28*, 69-87. doi:10.1007/s10565-011-9208-4.
199. Verrier, E.R.; Colpitts, C.C.; Schuster, C.; Zeisel, M.B.; Baumert, T.F. Cell Culture Models for the Investigation of Hepatitis B and D Virus Infection. *Viruses* **2016**, *8*. doi:10.3390/v8090261.
200. Thomson, J.A.; Itskovitz-Eldor, J.; Shapiro, S.S.; Waknitz, M.A.; Swiergiel, J.J.; Marshall, V.S.; Jones, J.M. Embryonic stem cell lines derived from human blastocysts. *Science* **1998**, *282*, 1145-1147. doi:10.1126/science.282.5391.1145.
201. Takahashi, K.; Yamanaka, S. Induction of pluripotent stem cells from mouse embryonic and adult fibroblast cultures by defined factors. *Cell* **2006**, *126*, 663-676. doi:10.1016/j.cell.2006.07.024.
202. Xia, Y.; Carpentier, A.; Cheng, X.; Block, P.D.; Zhao, Y.; Zhang, Z.; Protzer, U.; Liang, T.J. Human stem cell-derived hepatocytes as a model for hepatitis B virus infection, spreading and virus-host interactions. *J. Hepatol.* **2017**, *66*, 494-503. doi:10.1016/j.jhep.2016.10.009.
203. Wieland, S.; Thimme, R.; Purcell, R.H.; Chisari, F.V. Genomic analysis of the host response to hepatitis B virus infection. *Proc. Natl. Acad. Sci. U. S. A.* **2004**, *101*, 6669-6674. doi:10.1073/pnas.0401771101.
204. Cheng, X.; Xia, Y.; Serti, E.; Block, P.D.; Chung, M.; Chayama, K.; Rehmann, B.; Liang, T.J. Hepatitis B virus evades innate immunity of hepatocytes but activates cytokine production by macrophages. *Hepatology* **2017**, *66*, 1779-1793. doi:10.1002/hep.29348.
205. Suslov, A.; Boldanova, T.; Wang, X.; Wieland, S.; Heim, M.H. Hepatitis B virus does not interfere with innate immune responses in the human liver. *Gastroenterology* **2018**, *154*, 1778-1790. doi:10.1053/j.gastro.2018.01.034.

206. Mutz, P.; Metz, P.; Lempp, F.A.; Bender, S.; Qu, B.; Schoneweis, K.; Seitz, S.; Tu, T.; Restuccia, A.; Frankish, J.; Dachert, C.; Schusser, B.; Koschny, R.; Polychronidis, G.; Schemmer, P.; Hoffmann, K.; Baumert, T.F.; Binder, M.; Urban, S.; Bartenschlager, R. HBV bypasses the innate immune response and does not protect HCV from antiviral activity of interferon. *Gastroenterology* **2018**, *154*, 1791-1804 e22. doi:10.1053/j.gastro.2018.01.044.
207. Winer, B.Y.; Gaska, J.M.; Lipkowitz, G.; Bram, Y.; Parekh, A.; Parsons, L.; Leach, R.; Jindal, R.; Cho, C.H.; Shrirao, A.; Novik, E.; Schwartz, R.E.; Ploss, A. Analysis of host responses to hepatitis B and Delta viral infections in a micro-scalable hepatic co-culture system. *Hepatology* **2020**, *71*, 14-30. doi:10.1002/hep.30815.
208. Franco, A.; Guidotti, L.G.; Hobbs, M.V.; Pasquetto, V.; Chisari, F.V. Pathogenetic effector function of CD4-positive T helper 1 cells in hepatitis B virus transgenic mice. *J. Immunol.* **1997**, *159*, 2001-2008.
209. Kakimi, K.; Guidotti, L.G.; Koezuka, Y.; Chisari, F.V. Natural killer T cell activation inhibits hepatitis B virus replication *in vivo*. *J. Exp. Med.* **2000**, *192*, 921-930. doi:10.1084/jem.192.7.921.
210. Cavanaugh, V.J.; Guidotti, L.G.; Chisari, F.V. Inhibition of hepatitis B virus replication during adenovirus and cytomegalovirus infections in transgenic mice. *J. Virol.* **1998**, *72*, 2630-2637. doi:10.1128/JVI.72.4.2630-2637.1998.
211. Pasquetto, V.; Guidotti, L.G.; Kakimi, K.; Tsuji, M.; Chisari, F.V. Host-virus interactions during malaria infection in hepatitis B virus transgenic mice. *J. Exp. Med.* **2000**, *192*, 529-536. doi:10.1084/jem.192.4.529.
212. McClary, H.; Koch, R.; Chisari, F.V.; Guidotti, L.G. Inhibition of hepatitis B virus replication during schistosoma mansoni infection in transgenic mice. *J. Exp. Med.* **2000**, *192*, 289-294. doi:10.1084/jem.192.2.289.
213. Isogawa, M.; Robek, M.D.; Furuichi, Y.; Chisari, F.V. Toll-like receptor signaling inhibits hepatitis B virus replication *in vivo*. *J. Virol.* **2005**, *79*, 7269-7272. doi:10.1128/JVI.79.11.7269-7272.2005.
214. Shlomai, A.; Schwartz, R.E.; Ramanan, V.; Bhatta, A.; de Jong, Y.P.; Bhatia, S.N.; Rice, C.M. Modeling host interactions with hepatitis B virus using primary and induced

- pluripotent stem cell-derived hepatocellular systems. *Proc. Natl. Acad. Sci. U. S. A.* **2014**, *111*, 12193-12198. doi:10.1073/pnas.1412631111.
215. Sato, S.; Li, K.; Kameyama, T.; Hayashi, T.; Ishida, Y.; Murakami, S.; Watanabe, T.; Iijima, S.; Sakurai, Y.; Watashi, K.; Tsutsumi, S.; Sato, Y.; Akita, H.; Wakita, T.; Rice, C.M.; Harashima, H.; Kohara, M.; Tanaka, Y., Takaoka, A. The RNA sensor RIG-I dually functions as an innate sensor and direct antiviral factor for hepatitis B virus. *Immunity* **2015**, *42*, 123-132. doi:10.1016/j.immuni.2014.12.016.
216. Lu, H.L. Liao, F. Melanoma differentiation-associated gene 5 senses hepatitis B virus and activates innate immune signaling to suppress virus replication. *J. Immunol.* **2013**, *191*, 3264-3276. doi:10.4049/jimmunol.1300512.
217. Luangsay, S.; Gruffaz, M.; Isorce, N.; Testoni, B.; Michelet, M.; Faure-Dupuy, S.; Maadadi, S.; Ait-Goughoulte, M.; Parent, R.; Rivoire, M.; Javanbakht, H.; Lucifora, J.; Durantel, D.; Zoulim, F. Early inhibition of hepatocyte innate responses by hepatitis B virus. *J. Hepatol.* **2015**, *63*, 1314-1322. doi:10.1016/j.jhep.2015.07.014.
218. Zhang, Z.; Trippler, M.; Real, C.I.; Werner, M.; Luo, X.; Schefczyk, S.; Kemper, T.; Anastasiou, O.E.; Ladiges, Y.; Treckmann, J.; Paul, A.; Baba, H.A.; Allweiss, L.; Dandri, M.; Gerken, G.; Wedemeyer, H.; Schlaak, J.F.; Lu, M.; Broering, R. Hepatitis B virus particles activate toll-like receptor 2 signaling initial upon infection of primary human hepatocytes. *Hepatology* **2020**, *72* (3), 829-244. doi:10.1002/hep.31112.
219. Dansako, H.; Ueda, Y.; Okumura, N.; Satoh, S.; Sugiyama, M.; Mizokami, M.; Ikeda, M.; Kato, N. The cyclic GMP-AMP synthetase-STING signaling pathway is required for both the innate immune response against HBV and the suppression of HBV assembly. *FEBS J.* **2016**, *283*, 144-156. doi:10.1111/febs.13563.
220. Liu, Y.; Li, J.; Chen, J.; Li, Y.; Wang, W.; Du, X.; Song, W.; Zhang, W.; Lin, L.; Yuan, Z. Hepatitis B virus polymerase disrupts K63-linked ubiquitination of STING to block innate cytosolic DNA-sensing pathways. *J. Virol.* **2015**, *89*, 2287-2300. doi:10.1128/JVI.02760-14.
221. Wang, H.; Ryu, W.S. Hepatitis B virus polymerase blocks pattern recognition receptor signaling via interaction with DDX3: implications for immune evasion. *PLoS Pathog.* **2010**, *6*, e1000986. doi:10.1371/journal.ppat.1000986.

222. Kumar, M.; Jung, S.Y.; Hodgson, A.J.; Madden, C.R.; Qin, J.; Slagle, B.L. Hepatitis B virus regulatory HBx protein binds to adaptor protein IPS-1 and inhibits the activation of beta interferon. *J. Virol.* **2011**, *85*, 987-995. doi:10.1128/JVI.01825-10.
223. Wang, X.; Li, Y.; Mao, A.; Li, C.; Li, Y.; Tien, P. Hepatitis B virus X protein suppresses virus-triggered IRF3 activation and IFN-beta induction by disrupting the VISA-associated complex. *Cell Mol. Immunol.* **2010**, *7*, 341-348. doi:10.1038/cmi.2010.36.
224. Wu, J.; Meng, Z.; Jiang, M.; Pei, R.; Trippler, M.; Broering, R.; Bucchi, A.; Sowa, J.P.; Dittmer, U.; Yang, D.; Roggendorf, M.; Gerken, G.; Lu, M.; Schlaak, J.F. Hepatitis B virus suppresses toll-like receptor-mediated innate immune responses in murine parenchymal and nonparenchymal liver cells. *Hepatology* **2009**, *49*, 1132-1140. doi:10.1002/hep.22751.
225. Deng, F.; Xu, G.; Cheng, Z.; Huang, Y.; Ma, C.; Luo, C.; Yu, C.; Wang, J.; Xu, X.; Liu, S.; Zhu, Y. Hepatitis B surface antigen suppresses the activation of nuclear factor Kappa B pathway via interaction with the TAK1-TAB2 complex. *Front. Immunol.* **2021**, *12*, 618196. doi:10.3389/fimmu.2021.618196.
226. Khan, M.; Syed, G.H.; Kim, S.J.; Siddiqui, A. Hepatitis B Virus-Induced Parkin-Dependent recruitment of Linear Ubiquitin Assembly Complex (LUBAC) to mitochondria and attenuation of innate immunity. *PLoS Pathog.* **2016**, *12*, e1005693. doi:10.1371/journal.ppat.1005693.
227. Zhou, L.; He, R.; Fang, P.; Li, M.; Yu, H.; Wang, Q.; Yu, Y.; Wang, F.; Zhang, Y.; Chen, A.; Peng, N.; Lin, Y.; Zhang, R.; Trilling, M.; Broering, R.; Lu, M.; Zhu, Y.; Liu, S. Hepatitis B virus rigs the cellular metabolome to avoid innate immune recognition. *Nat. Commun.* **2021**, *12*, 98. doi:10.1038/s41467-020-20316-8.
228. Guidotti, L.G.; Rochford, R.; Chung, J.; Shapiro, M.; Purcell, R.; Chisari, F.V. Viral clearance without destruction of infected cells during acute HBV infection. *Science* **1999**, *284*, 825-829. doi:10.1126/science.284.5415.825.
229. Dunn, C.; Peppas, D.; Khanna, P.; Nebbia, G.; Jones, M.; Brendish, N.; Lascar, R.M.; Brown, D.; Gilson, R.J.; Tedder, R.J.; Dusheiko, G.M.; Jacobs, M.; Klenerman, P.; Maini, M.K. Temporal analysis of early immune responses in patients with acute hepatitis B virus infection. *Gastroenterology* **2009**, *137*, 1289-1300. doi:10.1053/j.gastro.2009.06.054.

230. Thimme, R.; Wieland, S.; Steiger, C.; Ghayeb, J.; Reimann, K.A.; Purcell, R.H., Chisari, F.V. CD8(+) T cells mediate viral clearance and disease pathogenesis during acute hepatitis B virus infection. *J. Virol.* **2003**, *77*, 68-76. doi:10.1128/jvi.77.1.68-76.2003.
231. Guidotti, L.G.; Ishikawa, T.; Hobbs, M.V.; Matzke, B.; Schreiber, R., Chisari, F.V. Intracellular inactivation of the hepatitis B virus by cytotoxic T lymphocytes. *Immunity* **1996**, *4*, 25-36. doi:10.1016/s1074-7613(00)80295-2.
232. Maini, M.K.; Boni, C.; Ogg, G.S.; King, A.S.; Reignat, S.; Lee, C.K.; Larrubia, J.R.; Webster, G.J.; McMichael, A.J.; Ferrari, C.; Williams, R.; Vergani, D., Bertolotti, A. Direct ex vivo analysis of hepatitis B virus-specific CD8(+) T cells associated with the control of infection. *Gastroenterology* **1999**, *117*, 1386-1396. doi:10.1016/s0016-5085(99)70289-1.
233. Rehermann, B. Intrahepatic T cells in hepatitis B: viral control versus liver cell injury. *J. Exp. Med.* **2000**, *191*, 1263-1268. doi:10.1084/jem.191.8.1263.
234. Rehermann, B.; Fowler, P.; Sidney, J.; Person, J.; Redeker, A.; Brown, M.; Moss, B.; Sette, A.; Chisari, F.V. The cytotoxic T lymphocyte response to multiple hepatitis B virus polymerase epitopes during and after acute viral hepatitis. *J. Exp. Med.* **1995**, *181*, 1047-1058. doi:10.1084/jem.181.3.1047.
235. Bertolotti, A.; Sette, A.; Chisari, F.V.; Penna, A.; Levrero, M.; De Carli, M.; Fiaccadori, F.; Ferrari, C. Natural variants of cytotoxic epitopes are T-cell receptor antagonists for antiviral cytotoxic T cells. *Nature* **1994**, *369*, 407-410. doi:10.1038/369407a0.
236. Chen, M.T.; Billaud, J.N.; Sallberg, M.; Guidotti, L.G.; Chisari, F.V.; Jones, J.; Hughes, J.; Milich, D.R. A function of the hepatitis B virus precore protein is to regulate the immune response to the core antigen. *Proc. Natl. Acad. Sci. U. S. A.* **2004**, *101*, 14913-14918. doi:10.1073/pnas.0406282101.
237. Reignat, S.; Webster, G.J.; Brown, D.; Ogg, G.S.; King, A.; Seneviratne, S.L.; Dusheiko, G.; Williams, R.; Maini, M.K.; Bertolotti, A. Escaping high viral load exhaustion: CD8 cells with altered tetramer binding in chronic hepatitis B virus infection. *J. Exp. Med.* **2002**, *195*, 1089-1101. doi:10.1084/jem.20011723.
238. Tang, F.; Barbacioru, C.; Wang, Y.; Nordman, E.; Lee, C.; Xu, N.; Wang, X.; Bodeau, J.; Tuch, B.B.; Siddiqui, A.; Lao, K.; Surani, M.A. mRNA-Seq whole-transcriptome analysis of a single cell. *Nat. Methods* **2009**, *6*, 377-382. doi:10.1038/nmeth.1315.

239. Islam, S.; Kjallquist, U.; Moliner, A.; Zajac, P.; Fan, J.B.; Lonnerberg, P.; Linnarsson, S. Characterization of the single-cell transcriptional landscape by highly multiplex RNA-seq. *Genome Res.* **2011**, *21*, 1160-1167. doi:10.1101/gr.110882.110.
240. Islam, S.; Zeisel, A.; Joost, S.; La Manno, G.; Zajac, P.; Kasper, M.; Lonnerberg, P.; Linnarsson, S. Quantitative single-cell RNA-seq with unique molecular identifiers. *Nat. Methods* **2014**, *11*, 163-166. doi:10.1038/nmeth.2772.
241. Fan, H.C.; Fu, G.K.; Fodor, S.P. Expression profiling. Combinatorial labeling of single cells for gene expression cytometry. *Science* **2015**, *347*, 1258367. doi:10.1126/science.1258367.
242. Zheng, G.X.; Terry, J.M.; Belgrader, P.; Ryvkin, P.; Bent, Z.W.; Wilson, R.; Ziraldo, S.B.; Wheeler, T.D.; McDermott, G.P.; Zhu, J.; Gregory, M.T.; Shuga, J.; Montesclaros, L.; Underwood, J.G.; Masquelier, D.A.; Nishimura, S.Y.; Schnall-Levin, M.; Wyatt, P.W.; Hindson, C.M.; Bharadwaj, R.; Wong, A.; Ness, K.D.; Beppu, L.W.; Deeg, H.J.; McFarland, C.; Loeb, K.R.; Valente, W.J.; Ericson, N.G.; Stevens, E.A.; Radich, J.P.; Mikkelsen, T.S.; Hindson, B.J.; Bielas, J.H. Massively parallel digital transcriptional profiling of single cells. *Nat. Commun.* **2017** *8*, 14049. doi:10.1038/ncomms14049.
243. Hashimshony, T.; Wagner, F.; Sher, N.; Yanai, I. CEL-Seq: single-cell RNA-Seq by multiplexed linear amplification. *Cell Rep.* **2012**, *2*, 666-673. doi:10.1016/j.celrep.2012.08.003.
244. Papalexli, E.; Satija, R. Single-cell RNA sequencing to explore immune cell heterogeneity. *Nat. Rev. Immunol.* **2018**, *18*, 35-45. doi:10.1038/nri.2017.76.
245. Keren-Shaul, H.; Kenigsberg, E.; Jaitin, D.A.; David, E.; Paul, F.; Tanay, A.; Amit, I. MARS-seq2.0: an experimental and analytical pipeline for indexed sorting combined with single-cell RNA sequencing. *Nat. Protoc.* **2019**, *14*, 1841-1862. doi:10.1038/s41596-019-0164-4.
246. Klein, A.M.; Mazutis, L.; Akartuna, I.; Tallapragada, N.; Veres, A.; Li, V.; Peshkin, L.; Weitz, D.A.; Kirschner, M.W. Droplet barcoding for single-cell transcriptomics applied to embryonic stem cells. *Cell* **2015**, *161*, 1187-1201. doi:10.1016/j.cell.2015.04.044.
247. Macosko, E.Z.; Basu, A.; Satija, R.; Nemesh, J.; Shekhar, K.; Goldman, M.; Tirosh, I.; Bialas, A.R.; Kamitaki, N.; Martersteck, E.M.; Trombetta, J.J.; Weitz, D.A.; Sanes, J.R.; Shalek, A.K.; Regev, A.; McCarroll, S.A. Highly parallel genome-wide expression

- profiling of individual cells using nanoliter droplets. *Cell* **2015**, *161*, 1202-1214.
doi:10.1016/j.cell.2015.05.002.
248. Hashimshony, T.; Senderovich, N.; Avital, G.; Klochendler, A.; de Leeuw, Y.; Anavy, L.; Gennert, D.; Li, S.; Livak, K.J.; Rozenblatt-Rosen, O.; Dor, Y.; Regev, A.; Yanai, I. CEL-Seq2: sensitive highly-multiplexed single-cell RNA-Seq. *Genome Biol.* **2016**, *17*, 77.
doi:10.1186/s13059-016-0938-8.
249. Becht, E.; McInnes, L.; Healy, J.; Dutertre, C.A.; Kwok, I.W.H.; Ng, L.G.; Ginhoux, F.; Newell, E.W. Dimensionality reduction for visualizing single-cell data using UMAP. *Nat. Biotechnol.* **2018**, doi:10.1038/nbt.4314.
250. Satija, R.; Farrell, J.A.; Gennert, D.; Schier, A.F.; Regev, A. Spatial reconstruction of single-cell gene expression data. *Nat. Biotechnol.* **2015**, *33*, 495-502.
doi:10.1038/nbt.3192.
251. Butler, A.; Hoffman, P.; Smibert, P.; Papalexi, E.; Satija, R. Integrating single-cell transcriptomic data across different conditions, technologies, and species. *Nat. Biotechnol.* **2018**, *36*, 411-420. doi:10.1038/nbt.4096.
252. Stuart, T.; Butler, A.; Hoffman, P.; Hafemeister, C.; Papalexi, E.; Mauck, W.M., 3rd; Hao, Y.; Stoeckius, M.; Smibert, P.; Satija, R. Comprehensive integration of single-cell data. *Cell* **2019**, *177*, 1888-1902 e21. doi:10.1016/j.cell.2019.05.031.
253. La Manno, G.; Soldatov, R.; Zeisel, A.; Braun, E.; Hochgerner, H.; Petukhov, V.; Lidschreiber, K.; Kastrioti, M.E.; Lonnerberg, P.; Furlan, A.; Fan, J.; Borm, L.E.; Liu, Z.; van Bruggen, D.; Guo, J.; He, X.; Barker, R.; Sundstrom, E.; Castelo-Branco, G.; Cramer, P.; Adameyko, I.; Linnarsson, S.; Kharchenko, P.V. RNA velocity of single cells. *Nature* **2018**, *560*, 494-498. doi:10.1038/s41586-018-0414-6.
254. Aibar, S.; Gonzalez-Blas, C.B.; Moerman, T.; Huynh-Thu, V.A.; Imrichova, H.; Hulselmans, G.; Rambow, F.; Marine, J.C.; Geurts, P.; Aerts, J.; van den Oord, J.; Atak, Z.K.; Wouters, J.; Aerts, S. SCENIC: single-cell regulatory network inference and clustering. *Nat. Methods* **2017**, *14*, 1083-1086. doi:10.1038/nmeth.4463.
255. Trapnell, C.; Cacchiarelli, D.; Grimsby, J.; Pokharel, P.; Li, S.; Morse, M.; Lennon, N.J.; Livak, K.J.; Mikkelsen, T.S.; Rinn, J.L. The dynamics and regulators of cell fate decisions are revealed by pseudotemporal ordering of single cells. *Nat Biotechnol.* **2014**, *32*, 381-386. doi:10.1038/nbt.2859.

256. Street, K.; Risso, D.; Fletcher, R.B.; Das, D.; Ngai, J.; Yosef, N.; Purdom, E.; Dudoit, S. Slingshot: cell lineage and pseudotime inference for single-cell transcriptomics. *BMC Genomics* **2018**, *19*, 477. doi:10.1186/s12864-018-4772-0.
257. Van den Berge, K.; Roux de Bezieux, H.; Street, K.; Saelens, W.; Cannoodt, R.; Saeys, Y.; Dudoit, S.; Clement, L. Trajectory-based differential expression analysis for single-cell sequencing data. *Nat. Commun.* **2020**, *11*, 1201. doi:10.1038/s41467-020-14766-3.
258. Steurman, Y.; Cohen, M.; Peshes-Yaloz, N.; Valadarsky, L.; Cohn, O.; David, E.; Frishberg, A.; Mayo, L.; Bacharach, E.; Amit, I.; Gat-Viks, I. Dissection of influenza infection *in vivo* by single-cell RNA sequencing. *Cell Syst.* **2018**, *6*, 679-691 e4. doi:10.1016/j.cels.2018.05.008.
259. Zanini, F.; Pu, S.Y.; Bekerman, E.; Einav, S.; Quake, S.R. Single-cell transcriptional dynamics of flavivirus infection. *Elife* **2018**, *7*. doi:10.7554/eLife.32942.
260. O'Neal, J.T.; Upadhyay, A.A.; Wolabaugh, A.; Patel, N.B.; Bosinger, S.E.; Suthar, M.S. West Nile virus-inclusive single-cell RNA sequencing reveals heterogeneity in the type I interferon response within single cells. *J. Virol.* **2019**, *93*. doi:10.1128/JVI.01778-18.
261. Drayman, N.; Patel, P.; Vistain, L.; Tay, S. HSV-1 single-cell analysis reveals the activation of anti-viral and developmental programs in distinct sub-populations. *Elife* **2019**, *8*. doi:10.7554/eLife.46339.
262. Bost, P.; Giladi, A.; Liu, Y.; Bendjelal, Y.; Xu, G.; David, E.; Blecher-Gonen, R.; Cohen, M.; Medaglia, C.; Li, H.; Deczkowska, A.; Zhang, S.; Schwikowski, B.; Zhang, Z.; Amit, I. Host-viral infection maps reveal signatures of severe COVID-19 patients. *Cell* **2020**, *181*, 1475-1488 e12. doi:10.1016/j.cell.2020.05.006.
263. Shnayder, M.; Nachshon, A.; Rozman, B.; Bernshtein, B.; Lavi, M.; Fein, N.; Poole, E.; Avdic, S.; Blyth, E.; Gottlieb, D.; Abendroth, A.; Slobedman, B.; Sinclair, J.; Stern-Ginossar, N.; Schwartz, M. Single cell analysis reveals human cytomegalovirus drives latently infected cells towards an anergic-like monocyte state. *Elife* **2020**, *9*. doi:10.7554/eLife.52168.
264. O'Neill, M.B.; Quach, H.; Pothlichet, J.; Aquino, Y.; Bisiaux, A.; Zidane, N.; Deschamps, M.; Libri, V.; Hasan, M.; Zhang, S.Y.; Zhang, Q.; Matuozzo, D.; Cobat, A.; Abel, L.; Casanova, J.L.; Naffakh, N.; Rotival, M.; Quintana-Murci, L. Single-cell and bulk RNA-sequencing reveal differences in monocyte susceptibility to influenza A virus infection

- between Africans and Europeans. *Front. Immunol.* **2021**, *12*, 768189.
doi:10.3389/fimmu.2021.768189.
265. Speranza, E.; Williamson, B.N.; Feldmann, F.; Sturdevant, G.L.; Perez-Perez, L.; Meade-White, K.; Smith, B.J.; Lovaglio, J.; Martens, C.; Munster, V.J.; Okumura, A.; Shaia, C.; Feldmann, H.; Best, S.M.; de Wit, E. Single-cell RNA sequencing reveals SARS-CoV-2 infection dynamics in lungs of African green monkeys. *Sci. Transl. Med.* **2021**, *13*.
doi:10.1126/scitranslmed.abe8146.
266. Juhling, F.; Saviano, A.; Ponsolles, C.; Heydmann, L.; Crouchet, E.; Durand, S.C.; El Saghire, H.; Felli, E.; Lindner, V.; Pessaux, P.; Pochet, N.; Schuster, C.; Verrier, E.R.; Baumert, T.F. Hepatitis B virus compartmentalization and single-cell differentiation in hepatocellular carcinoma. *Life Sci. Alliance* **2021**, *4*. doi:10.26508/lsa.202101036.
267. MacParland, S.A.; Liu, J.C.; Ma, X.Z.; Innes, B.T.; Bartczak, A.M.; Gage, B.K.; Manuel, J.; Khuu, N.; Echeverri, J.; Linares, I.; Gupta, R.; Cheng, M.L.; Liu, L.Y.; Camat, D.; Chung, S.W.; Seliga, R.K.; Shao, Z.; Lee, E.; Ogawa, S.; Ogawa, M.; Wilson, M.D.; Fish, J.E.; Selzner, M.; Ghanekar, A.; Grant, D.; Greig, P.; Sapisochin, G.; Selzner, N.; Winegarten, N.; Adeyi, O.; Keller, G.; Bader, G.D.; McGilvray, I.D. Single cell RNA sequencing of human liver reveals distinct intrahepatic macrophage populations. *Nat. Commun.* **2018**, *9*, 4383. doi:10.1038/s41467-018-06318-7.
268. Aizarani, N.; Saviano, A.; Sagar, M.; Maily, L.; Durand, S.; Herman, J.S.; Pessaux, P.; Baumert, T.F.; Grun, D. A human liver cell atlas reveals heterogeneity and epithelial progenitors. *Nature* **2019**, *572*, 199-204. doi:10.1038/s41586-019-1373-2.
269. Segal, J.M.; Kent, D.; Wesche, D.J.; Ng, S.S.; Serra, M.; Oules, B.; Kar, G.; Emerton, G.; Blackford, S.J.I.; Darmanis, S.; Miquel, R.; Luong, T.V.; Yamamoto, R.; Bonham, A.; Jassem, W.; Heaton, N.; Vigilante, A.; King, A.; Sancho, R.; Teichmann, S.; Quake, S.R.; Nakauchi, H.; Rashid, S.T. Single cell analysis of human foetal liver captures the transcriptional profile of hepatobiliary hybrid progenitors. *Nat. Commun.* **2019**, *10*, 3350. doi:10.1038/s41467-019-11266-x.
270. Massalha, H.; Bahar Halpern, K.; Abu-Gazala, S.; Jana, T.; Massasa, E.E.; Moor, A.E.; Buchauer, L.; Rozenberg, M.; Pikarsky, E.; Amit, I.; Zamir, G.; Itzkovitz, S. A single cell atlas of the human liver tumor microenvironment. *Mol. Syst. Biol.* **2020**, *16*, e9682. doi:10.15252/msb.20209682.

271. Losic, B.; Craig, A.J.; Villacorta-Martin, C.; Martins-Filho, S.N.; Akers, N.; Chen, X.; Ahsen, M.E.; von Felden, J.; Labgaa, I.; D'Avola, D.; Allette, K.; Lira, S.A.; Furtado, G.C.; Garcia-Lezana, T.; Restrepo, P.; Stueck, A.; Ward, S.C.; Fiel, M.I.; Hiotis, S.P.; Gunasekaran, G.; Sia, D.; Schadt, E.E.; Sebra, R.; Schwartz, M.; Llovet, J.M.; Thung, S.; Stolovitzky, G.; Villanueva, A. Intratumoral heterogeneity and clonal evolution in liver cancer. *Nat. Commun.* **2020**, *11*, 291. doi:10.1038/s41467-019-14050-z.
272. Sharma, A.; Seow, J.J.W.; Dutertre, C.A.; Pai, R.; Bleriot, C.; Mishra, A.; Wong, R.M.M.; Singh, G.S.N.; Sudhagar, S.; Khalilnezhad, S.; Erdal, S.; Teo, H.M.; Khalilnezhad, A.; Chakarov, S.; Lim, T.K.H.; Fui, A.C.Y.; Chieh, A.K.W.; Chung, C.P.; Bonney, G.K.; Goh, B.K.; Chan, J.K.Y.; Chow, P.K.H.; Ginhoux, F.; DasGupta, R. Onco-fetal Reprogramming of Endothelial Cells Drives Immunosuppressive Macrophages in Hepatocellular Carcinoma. *Cell* **2020**, *183*, 377-394 e21. doi:10.1016/j.cell.2020.08.040.
273. Zhang, S.; Liu, Z.; Wu, D.; Chen, L.; Xie, L. Single-Cell RNA-Seq Analysis Reveals Microenvironmental Infiltration of Plasma Cells and Hepatocytic Prognostic Markers in HCC With Cirrhosis. *Front. Oncol.* **2020**, *10*, 596318. doi:10.3389/fonc.2020.596318.
274. Ma, L.; Wang, L.; Khatib, S.A.; Chang, C.W.; Heinrich, S.; Dominguez, D.A.; Forgues, M.; Candia, J.; Hernandez, M.O.; Kelly, M.; Zhao, Y.; Tran, B.; Hernandez, J.M.; Davis, J.L.; Kleiner, D.E.; Wood, B.J.; Greten, T.F.; Wang, X.W. Single-cell atlas of tumor cell evolution in response to therapy in hepatocellular carcinoma and intrahepatic cholangiocarcinoma. *J. Hepatol.* **2021**, *75*, 1397-1408. doi:10.1016/j.jhep.2021.06.028.
275. Le, C.; Liu, Y.; Lopez-Orozco, J.; Joyce, M.A.; Le, X.C.; Tyrrell, D.L. CRISPR technique incorporated with single-cell RNA sequencing for studying hepatitis B infection. *Anal. Chem.* **2021**, *93*, 10756-10761. doi:10.1021/acs.analchem.1c02227.
276. Duan, M.; Hao, J.; Cui, S.; Worthley, D.L.; Zhang, S.; Wang, Z.; Shi, J.; Liu, L.; Wang, X.; Ke, A.; Cao, Y.; Xi, R.; Zhang, X.; Zhou, J.; Fan, J.; Li, C.; Gao, Q. Diverse modes of clonal evolution in HBV-related hepatocellular carcinoma revealed by single-cell genome sequencing. *Cell Res.* **2018**, *28*, 359-373. doi:10.1038/cr.2018.11.
277. Ho, D.W.; Tsui, Y.M.; Chan, L.K.; Sze, K.M.; Zhang, X.; Cheu, J.W.; Chiu, Y.T.; Lee, J.M.; Chan, A.C.; Cheung, E.T.; Yau, D.T.; Chia, N.H.; Lo, I.L.; Sham, P.C.; Cheung, T.T.; Wong, C.C.; Ng, I.O. Single-cell RNA sequencing shows the immunosuppressive

- landscape and tumor heterogeneity of HBV-associated hepatocellular carcinoma. *Nat. Commun.* **2021**, *12*, 3684. doi:10.1038/s41467-021-24010-1.
278. Vong, J.S.L.; Ji, L.; Heung, M.M.S.; Cheng, S.H.; Wong, J.; Lai, P.B.S.; Wong, V.W.S.; Chan, S.L.; Chan, H.L.Y.; Jiang, P.; Chan, K.C.A.; Chiu, R.W.K.; Lo, Y.M.D. Single cell and plasma RNA sequencing for RNA liquid biopsy for hepatocellular carcinoma. *Clin. Chem.* **2021**, *67*, 1492-1502. doi:10.1093/clinchem/hvab116.
279. Aevermann, B.D.; Shannon, C.P.; Novotny, M.; Ben-Othman, R.; Cai, B.; Zhang, Y.; Ye, J.C.; Kobor, M.S.; Gladish, N.; Lee, A.H.; Blimkie, T.M.; Hancock, R.E.; Llibre, A.; Duffy, D.; Koff, W.C.; Sadarangani, M.; Tebbutt, S.J.; Kollmann, T.R.; Scheuermann, R.H. Machine learning-based single cell and integrative analysis reveals that baseline mDC predisposition correlates with hepatitis B vaccine antibody response. *Front. Immunol.* **2021**, *12*, 690470. doi:10.3389/fimmu.2021.690470.
280. Balagopal, A.; Hwang, H.S.; Grudde, T.; Quinn, J.; Sterling, R.K.; Sulkowski, M.S., Thio, C.L. Single Hepatocyte Hepatitis B Virus Transcriptional Landscape in HIV Coinfection. *J. Infect. Dis.* **2020**, *221*, 1462-1469. doi:10.1093/infdis/jiz607.
281. Balagopal, A.; Grudde, T.; Ribeiro, R.M.; Saad, Y.S.; Hwang, H.S.; Quinn, J.; Murphy, M.; Ward, K.; Sterling, R.K.; Zhang, Y.; Perelson, A.S.; Sulkowski, M.S.; Osburn, W.O.; Thio, C.L. Single hepatocytes show persistence and transcriptional inactivity of hepatitis B. *JCI Insight* **2020**, *5*. doi:10.1172/jci.insight.140584.
282. Regev, A.; Teichmann, S.A.; Lander, E.S.; Amit, I.; Benoist, C.; Birney, E.; Bodenmiller, B.; Campbell, P.; Carninci, P.; Clatworthy, M.; Clevers, H.; Deplancke, B.; Dunham, I.; Eberwine, J.; Eils, R.; Enard, W.; Farmer, A.; Fugger, L.; Gottgens, B.; Hacohen, N.; Haniffa, M.; Hemberg, M.; Kim, S.; Klenerman, P.; Kriegstein, A.; Lein, E.; Linnarsson, S.; Lundberg, E.; Lundeberg, J.; Majumder, P.; Marioni, J.C.; Merad, M.; Mhlanga, M.; Nawijn, M.; Netea, M.; Nolan, G.; Pe'er, D.; Phillipakis, A.; Ponting, C.P.; Quake, S.; Reik, W.; Rozenblatt-Rosen, O.; Sanes, J.; Satija, R.; Schumacher, T.N.; Shalek, A.; Shapiro, E.; Sharma, P.; Shin, J.W.; Stegle, O.; Stratton, M.; Stubbington, M.J.T.; Theis, F.J.; Uhlen, M.; van Oudenaarden, A.; Wagner, A.; Watt, F.; Weissman, J.; Wold, B.; Xavier, R.; Yosef, N., Human Cell Atlas Meeting Participants. The human cell atlas. *Elife* **2017**, *6*. doi:10.7554/eLife.27041.

283. Steenbergen, R.H.; Joyce, M. A.; Thomas, B.; Jones, D.; Law, J.; Russell, R.; Houghton, M.; Tyrrell, D. L. Human serum leads to differentiation of human hepatoma cells, restoration of very-low-density lipoprotein secretion, and a 1000-fold increase in HCV Japanese fulminant hepatitis type 1 titers. *Hepatology* **2013**, *58*, 1907–1917. doi:10.1002/hep.26566.
284. Steenbergen, R.; Oti, M.; ter Horst, R.; Tat, W.; Neufeldt, C.; Belovodskiy, A.; Chua, T. T.; Cho, W. J.; Joyce, M.; Dutilh, B. E.; Tyrrell, D. L. Establishing normal metabolism and differentiation in hepatocellular carcinoma cells by culturing in adult human serum. *Sci. Rep.* **2018**, *8*, 11685, doi:10.1038/s41598-018-29763-2.
285. Hart, S.N.; Li, Y.; Nakamoto, K.; Subileau, E.-A.; Steen, D.; Zhong, X.-B. A comparison of whole genome gene expression profiles of HepaRG cells and HepG2 cells to primary human hepatocytes and human liver tissues. *Drug Metab. Dispos.* **2010**, *38*, 988–994. doi:10.1124/dmd.109.031831.
286. Iwamoto, M.; Watashi, K.; Tsukuda, S.; Aly, H.H.; Fukasawa, M.; Fujimoto, A.; Suzuki, R.; Aizaki, H.; Ito, T.; Koiwai, O.; Kusuhara, H.; Wakita, T. Evaluation and identification of hepatitis B virus entry inhibitors using HepG2 cells overexpressing a membrane transporter NTCP. *Biochem. Biophys. Res. Commun.* **2014**, *443*, 808–813. doi:10.1016/j.bbrc.2013.12.052.
287. Seeger, C.; Sohn, J.A. Targeting hepatitis B virus with CRISPR/Cas9. *Mol. Ther.-Nucleic Acids* **2014**, *3*, e216. doi:10.1038/mtna.2014.68.
288. Yan, R.; Zhang, Y.; Cai, D.; Liu, Y.; Cuconati, A.; Guo, H. Spinoculation enhances HBV infection in NTCP-reconstituted hepatocytes. *PLoS One* **2015**, *10*, e0129889. doi:10.1371/journal.pone.0129889.
289. Li, W. The hepatitis B virus receptor. *Annu. Rev. Cell Dev. Biol.* **2015**, *31*, 125–147. doi:10.1146/annurev-cellbio-100814-125241.
290. Lempp, F.A.; Qu, B.; Wang, Y.X.; Urban, S. Hepatitis B virus infection of a mouse hepatic cell line reconstituted with human sodium taurocholate cotransporting polypeptide. *J. Virol.* **2016**, *90*, 4827–4831. doi:10.1128/jvi.02832-15.
291. Li, J.; Zong, L.; Sureau, C.; Barker, L.; Wands, J.R.; Tong, S. Unusual features of sodium taurocholate cotransporting polypeptide as a hepatitis B virus receptor. *J. Virol.* **2016**, *90*, 8302–8313. doi:10.1128/jvi.01153-16.

292. Michailidis, E.; Pabon, J.; Xiang, K.; Park, P.; Ramanan, V.; Hoffmann, H.H.; Schneider, W.M.; Bhatia, S.N.; De Jong, Y.P.; Shlomai, A.; et al. A robust cell culture system supporting the complete life cycle of hepatitis B virus. *Sci. Rep.* **2017**, *7*, 16616. doi:10.1038/s41598-017-16882-5.
293. Zhou, M.; Zhao, K.; Yao, Y.; Yuan, Y.; Pei, R.; Wang, Y.; Chen, J.; Hu, X.; Zhou, Y.; Chen, X.; et al. Productive HBV infection of well-differentiated, hNTCP-expressing human hepatoma-derived (Huh7) cells. *Virol. Sin.* **2017**, *32*, 465–475. doi:10.1007/s12250-017-3983-x.
294. Qiao, L.; Sui, J.; Luo, G. Robust human and murine hepatocyte culture models of hepatitis B virus infection and replication. *J. Virol.* **2018**, *92*, e01255–18. doi:10.1128/jvi.01255-18.
295. Vondráček, J.; Souček, K.; Sheard, M.A.; Chramostová, K.; Andryšik, Z.; Hofmanová, J.; Kozubík, A. Dimethyl sulfoxide potentiates death receptor-mediated apoptosis in the human myeloid leukemia U937 cell line through enhancement of mitochondrial membrane depolarization. *Leuk. Res.* **2006**, *30*, 81–89. doi:10.1016/j.leukres.2005.05.016.
296. Song, Y.M.; Song, S.O.; Jung, Y.K.; Kang, E.S.; Cha, B.S.; Lee, H.C.; Lee, B. Dimethyl sulfoxide reduces hepatocellular lipid accumulation through autophagy induction. *Autophagy* **2012**, *8*, 1085–1097. doi:10.4161/auto.20260.
297. Galvao, J.; Davis, B.; Tilley, M.; Normando, E.; Duchon, M.R.; Cordeiro, M.F. Unexpected low-dose toxicity of the universal solvent DMSO. *FASEB J.* **2014**, *28*, 1317–1330. doi:10.1096/fj.13-235440.
298. Pal, R.; Mamidi, M.K.; Das, A.; Bhonde, R. Diverse effects of dimethyl sulfoxide (DMSO) on the differentiation potential of human embryonic stem cells. *Arch. Toxicol.* **2012**, *86*, 651–661. doi:10.1007/s00204-011-0782-2.
299. Verheijen, M.; Lienhard, M.; Schrooders, Y.; Clayton, O.; Nudischer, R.; Boerno, S.; Timmermann, B.; Selevsek, N.; Schlapbach, R.; Gmuender, H.; et al. DMSO induces drastic changes in human cellular processes and epigenetic landscape *in vitro*. *Sci. Rep.* **2019**, *9*, 4641. doi:10.1038/s41598-019-40660-0.

Chapter 2

***In Vitro* Infection with Hepatitis B Virus Using Huh7.5-NTCP Cells Differentiated in Human Serum Culture without Requiring Dimethyl Sulfoxide**

2.1. Introduction

HBV infection in immortalized liver cells is generally inefficient compared to HBV infection in the liver [1–4]. A major obstacle to studies of HBV has been the lack of an easily infectable cell culture system [2–7]. HBV-infectable primary human hepatocytes are expensive, difficult to obtain, rapidly de-differentiate *ex vivo*, and can only survive for a few weeks in culture [8–10]. Until recently, HepaRG cells were the only immortalized hepatoma cell line that could be infected with HBV, but had a low percentage of successful infection [11, 12]. Other hepatoma cell lines cannot be infected with HBV, but can be transfected with HBV expression plasmids and, having bypassed cell entry, proceed with HBV infection from the genome transcription step [13, 14]. Some cell lines, such as HepAD38 and HepG2.2.15, have integrated HBV genomes, which also recapitulate infection from the point of genome transcription to the release of infectious virus [15, 16]. These systems permit investigations into post-transcriptional stages of infection.

Yan *et al.* demonstrated high-affinity binding between the HBV pre-S1 envelope protein and the NTCP bile acid transporter [17]. Furthermore, overexpression of NTCP renders otherwise unsusceptible hepatoma cells permissive to HBV infection. This discovery of a HBV entry receptor has benefitted the decades-long search for an easy-to-maintain cell culture system that supports the entire HBV lifecycle. This culture system, requiring the use of 2–2.5% dimethyl sulfoxide (DMSO) to promote infection, is now widely used to study HBV [17–28].

Our group has shown that culturing the human hepatoma cell line Huh7 or Huh7.5 in a medium supplemented with human serum (HS) increased production of hepatitis C virus (HCV) [29]. Cells cultured in an HS-supplemented medium underwent growth arrest and developed characteristics similar to primary human hepatocytes, including increased expression of cytochrome P450, restored lipid metabolism, differentiation marker expression, a cuboid morphology, and formation of bile canalicular surfaces [30–32].

Previous studies showed that overexpression of NTCP in hepatoma cells only moderately improved infection efficiency and, following infection, these cultures must be maintained in high concentrations (2–2.5%) of DMSO for infection [17–27]. However, DMSO is known to cause a variety of adverse effects on cells, such as significant alterations in viability and protein expression [33–37]. Therefore, an HBV infection model that eliminates the requirement of DMSO treatment would be desirable to more closely mimic physiological conditions [38].

The primary objective of this research was to explore alternative cell culture models for HBV infection. We hypothesized that overexpression of NTCP in Huh7.5 cells and differentiation of these hepatoma cells in HS-containing media would enhance HBV infection. We report here that culture of Huh7.5-NTCP cells in human serum permitted robust HBV infection in the absence of DMSO.

2.2. Materials and Methods

2.2.1. Production of Lentiviral Vectors Expressing NTCP

NTCP-expressing lentiviral expression plasmid with a puromycin selectable marker was purchased from GeneCopoeia (Rockville, MD). Lentiviral particles were generated in HEK-293T cells according to a previously reported method [39]. HEK-293T cells from American Type Culture Collection (ATCC, Manassas, VA) were seeded at 50% confluence on poly-L-lysine-

coated T150 flasks. Transfection was performed with Lipofectamine 2000 (Invitrogen, Carlsbad, CA) according to manufacturer's protocols.

2.2.2. Establishment of Stable NTCP-Expressing Huh7.5 Cell Line (Huh7.5-NTCP)

Huh7.5 cells, a kind gift from Dr C. Rice (Rockefeller University, New York, NY, USA), were maintained in Dulbecco's modified Eagle's medium (DMEM) (Sigma Aldrich, St. Louis, MO. D5796, high-glucose, with L-glutamine and sodium bicarbonate, without sodium pyruvate) supplemented with 10% fetal bovine serum (FBS) and penicillin/streptomycin. Briefly, low-passage Huh7.5 cells were seeded at 4×10^5 cells per well of a 6-well plate. To the lentiviral stock, polybrene was added to 4 $\mu\text{g}/\text{mL}$ and HEPES (pH 7.0) to 20 mM. The lentivirus inoculum (1 mL) was added to each well intended for transduction. The 6-well plate was then centrifuged at $150 \times g$ for 1 h at 37 °C. Following centrifugation, the lentivirus was further incubated with the cells for 6 h at 37 °C in 5% CO₂. The medium for the transduced cells was then changed to DMEM containing 10% FBS. After 48 h of incubation at 37 °C, the medium was changed to DMEM containing 10% FBS and 0.1 $\mu\text{g}/\text{mL}$ puromycin to select for cells that were successfully transduced. Transduced cells were cultured and selected in puromycin for one week prior to use in subsequent assays.

Overexpression of NTCP in transduced Huh7.5-NTCP cells was assessed and confirmed by RT-qPCR analysis of total RNA, flow cytometry analysis, and immunofluorescence staining of NTCP using an anti-NTCP antibody (Abcam, Cambridge, UK. ab175289). RT-qPCR was performed with the forward primer (5'-GGAGGGAACCTGTCCAATGTC-3'), reverse primer (5'-CATGCCAAGGGCACAGAAG-3'), and probe (5'-[6FAM]ACATGAACC/ZEN/TCAGCATTGTGATGACCACC-[IABk]-3'), all purchased from Integrated DNA Technologies (IDT, Coralville, IA). $\Delta\Delta\text{CT}$ values were calculated to determine fold change in NTCP mRNA expression. RT-qPCR for hypoxanthine-guanine

phosphoribosyltransferase (HPRT) mRNA was performed using the Taqman primer probe mix from Applied Biosystems (Foster City, CA. cat No. 4326321E).

2.2.3. Conventional Culture of Huh7.5 Cells and Huh7.5-NTCP Cells

Huh7.5 and Huh7.5-NTCP cells were maintained in a DMEM medium supplemented with 10% FBS. These cells reached confluence within 3–4 days in culture and were re-seeded twice a week at 25% seeding density. When reseeding confluent cultures, cell monolayers were washed once with filter-sterilized PBS (136.9 mM NaCl, 2.68 mM KCl, 6.48 mM Na₂HPO₄, and 0.866 mM KH₂PO₄, pH 7.4). Subsequently, adherent cells were detached by adding ATV solution (107.3 mM KCl, 6.84 mM NaCl, 11.9 mM NaHCO₃, 3.2 mM dextrose, 0.5 g/L trypsin, and 0.5 mM disodium EDTA) and incubating at 37 °C for 3 min. The flask was then gently percussed and the trypsin was inactivated by the addition of DMEM containing 10% FBS. Figure S1 shows the timeline for culturing and infecting cells in the different media.

2.2.4. Differentiation of Huh7.5 and Huh7.5-NTCP Cells in Human Serum

Confluent Huh7.5 and Huh7.5-NTCP cells, at passage 30 or fewer, were trypsinized with ATV solution and subsequently the trypsin was inactivated by the addition of DMEM supplemented with 4% pooled adult human serum (HS) (Valley Biomedical, Winchester, VA). The cells were then plated in a DMEM containing 4% HS at a density of 30%. After 4 days, the cells were again trypsinized as described and plated at 50% density in a DMEM containing 4% HS. Culture medium was then changed twice a week for an additional 17 days for a total of 21 days. During this time, the cells underwent contact inhibition and differentiation.

2.2.5. Infection of Cells with HBV

HBV inoculum was prepared using HepAD38 cells, a hepatoma cell line with an integrated greater than genome length copy of HBV genotype D subtype ayw [16]. Huh7.5 and Huh7.5-NTCP cells were infected with HBV at a multiplicity of infection (MOI) of 500 genome equivalents, unless otherwise stated, in the presence of 4% PEG 8000 for 18 h at 37 °C. Four culture media were compared in this study. DMEM medium was supplemented with: 10% FBS; 10% FBS and 2% DMSO; 4% HS; and 4% HS and 2% DMSO. After HBV infection, cells were washed three times with 1 × PBS and then maintained in one of these four media. The medium was changed twice a week following infection (see **Figure 2.1** for the timelines of culturing and infection).

2.2.6. Culture of PXB Cells

PXB cells were purchased from PhoenixBio (Hiroshima, Japan) and seeded at 1×10^7 cells per 24-well plate as per the manufacturer's recommendation. PXB cells are human hepatocytes isolated from chimeric humanized liver mice for the purposes of use for *in vitro* culture experiments [40]. The cells were cultured for seven days in a DMSO-supplemented hepatocyte clonal growth medium (dHCGM) purchased from PhoenixBio. These human hepatocytes were then subjected to the same protocol as the Huh7.5-NTCP cells for assaying albumin secretion.

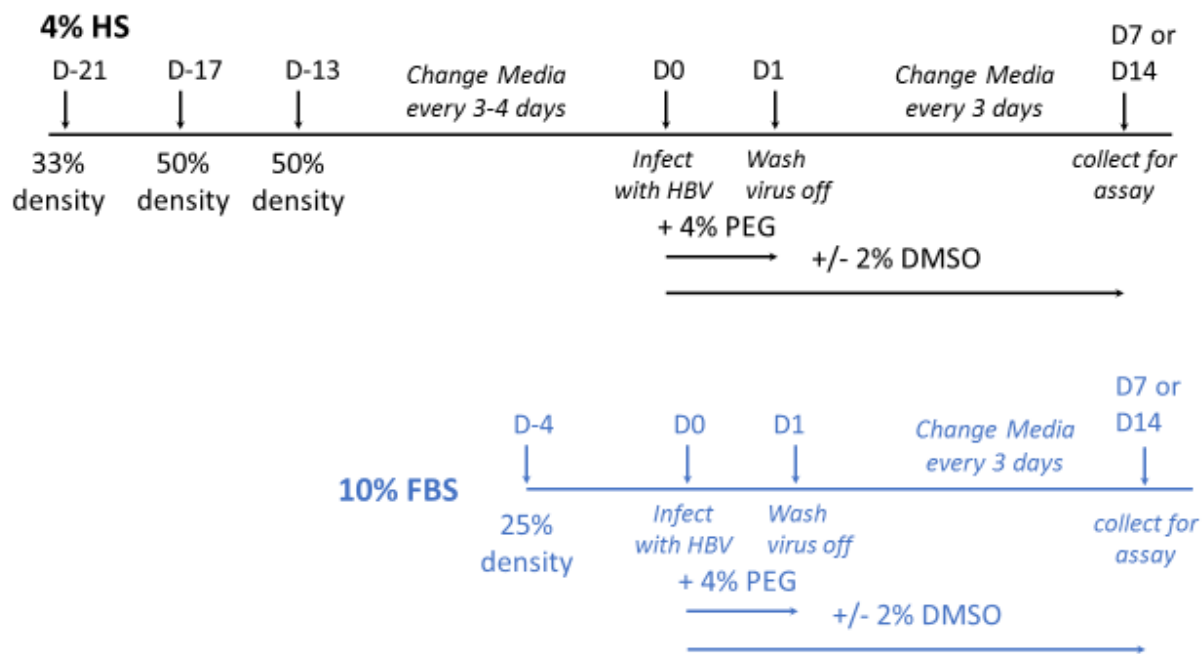


Figure 2.1. Schematic illustrating the timeline for culturing and infecting Huh7.5 NTCP cells. The day of inoculation with HBV is denoted as day 0 (D0). Days prior to infection are labelled with negative numbers (e.g., 21 days prior to infection is D-21). The percent density describes the cell seeding density onto new flasks or plates on the indicated day. Infection was done by HBV inoculation overnight along with 4% polyethylene glycol (PEG) 8000 and with or without 2% DMSO supplementation. The PEG was removed from cultures after infection. The infected cells were maintained in DMEM medium supplemented with FBS or HS and with or without 2% DMSO supplementation.

2.2.7. Analysis of Pregenomic RNA (pgRNA)

RNA was isolated from cell monolayers using either QIAzol reagent (Qiagen, Hilden, Germany) or Nucleospin RNA spin columns (Macherey Nagel, Duren, Germany) following the manufactures' procedures. Pregenomic RNA was measured using qPCR using the forward primer (5'-GGAGTGTGGATTTCGCACTCCT-3'), reverse primer (5'-AGATTGAGATCTTCTGCGAC-

3'), and Taqman probe (5'-[6FAM]-AGGCAGGTCCCCTAGAAGAAGAAGAACTCC-[BHQ1]-3'). The qPCR cycling conditions were 95 °C for 20 s, followed by 45 cycles of 95 °C for 1 s and then 60 °C for 20 s. The ramp speed between cycling steps was 4.14 °C per second. The results were expressed as pgRNA gene equivalents per 10 ng of total RNA.

2.2.8. Analysis of Covalently Closed Circular DNA (cccDNA)

Genomic DNA (gDNA) was isolated using a DNeasy Blood and Tissue kit (Qiagen) according to the manufacturer's protocol. The culture supernatant was removed and cell monolayers were rinsed once with PBS. For cccDNA isolation, the other viral DNA species that contain gaps in the DNA and are not completely circular were digested by mixing 1 µg of cellular DNA with 25 units of exonuclease III (New England Biolabs, NEB, Ipswich, MA) and 1× final concentration of NEB buffer 1 (New England Biolabs). This mixture was then incubated at 37 °C for 1 h and then heat inactivated at 70 °C for 30 min.

HBV cccDNA was measured using qPCR using the forward primer (5'-CTCCCCGTCTGTGCCTTCT-3'), reverse primer (5'-GCCCCAAAGCCACCCAAG-3'), and Taqman probe (5'-[6FAM]-AGCGAAGTGCACACGGACCGGCAGA-[BHQ1]-3'). Quantitative PCR was performed using TaqMan Fast Advanced Master Mix, but the cycling protocol was modified to have longer incubations at cycling steps and slower ramp speeds to accommodate the large amplicon size and low amounts of cccDNA. The cccDNA samples were held at 95 °C for 10 min, followed by 50 cycles of 95 °C for 10 s, 62 °C for 10 s, and 72 °C for 20 s. The ramp speed between qPCR steps was 1.6 °C per second. The qPCR analysis was conducted on MicroAmp Fast Optical 96-well reaction plates (Applied Biosystems) and the QuantStudio 3 Real-Time PCR system (Applied Biosystems) [41]. Covalently closed circular DNA levels were expressed as cccDNA copies per 10 ng total gDNA. PCR analysis of mtDNA use the forward primer (5'-

ACACTCATCGCCCTTACCAC-3'), reverse primer (5'-GTTGATGCAGAGTGGGGTTT-3'), and the SYBR Green probe.

2.2.9. Enzyme-Linked Immunosorbent Assays (ELISAs)

HBsAg was quantified using the QuickTiter Hepatitis B surface antigen (HBsAg) ELISA kit (Cell Biolabs Inc., San Diego, CA) according to the manufacturer's protocol. Briefly, HBV virions in culture medium samples were inactivated by the addition of Triton X-100 to a final concentration of 0.5% and heating at 56 °C for 30 min. Recombinant HBsAg standards and samples were loaded onto the anti-HBsAg antibody-coated wells. The plate was covered and incubated at 37 °C for 2 h. The wells were washed 5 times with 1× buffer. The wells were then incubated with the FITC-conjugated anti-HBsAg monoclonal antibody (diluted 1:250 in the assay diluent) for 1 h at room temperature. The wells were once again washed 5 times with 1× wash buffer. The HRP-conjugated anti-FITC monoclonal antibody (diluted 1:1000 in the assay diluent) was added and incubated for 1 h at room temperature. After washing the wells 5 times, 100 µL of the substrate solution were added and incubated at room temperature for 15 min. After that, 100 µL of the stop solution were added to each well and absorbance at 450 nm was measured immediately using a spectrophotometer.

Secreted albumin was measured using sandwich ELISA as described previously [29]. Briefly, cells were washed extensively with serum-free DMEM and then once with serum-free OptiMEM. The last wash with OptiMEM was collected to assess background levels of albumin. Fresh serum-free OptiMEM was added to each well with samples collected 6 and 24 h afterwards. ELISA plates were coated with 100 µL of 0.625 µg/mL goat anti-human albumin antibody (Bethyl Laboratories, Montgomery, TX. A80229A) diluted in the coating buffer (50 mM NaHCO₃, 51.9 mM Na₂CO₃) overnight at 4 °C. The next day, wells were washed three times with Tris-buffered

saline + 0.1% Tween-20 (TBST) and incubated in the blocking buffer (TBST and 1% gelatin; Bio-Rad, Hercules, CA. 1706537) for 30 min at room temperature. Samples were incubated on the antibody-coated plate for 1 h at room temperature. The wells were then washed three times with TBST and incubated with 100 μ L of 0.625 μ g/mL goat anti-human albumin HRP-conjugated antibody (Bethyl, A80229P) diluted in TBST for 1 h at room temperature. The plate was washed three times with TBST and the wells were incubated with 100 μ L of the TMB (3,3',5,5'-tetramethylbenzidine) substrate for 15 min. Absorbance at 450 nm was measured with a Perkin Elmer Enspire 2300 plate reader after adding 100 μ L of 1 M phosphoric acid.

2.2.10. Aptamer-Binding Assay for the E Antigen (HBeAg)

HBeAg was determined using a sandwich aptamer-binding assay (**Figure 2.2**) as reported recently [42]. Briefly, the NH₂-A-9S aptamer (10 pmol) in 1 \times PBS buffer (10 mM sodium phosphate, 137 mM NaCl, and 4.5 mM KCl, pH 7.4) was heated to 95 $^{\circ}$ C for 10 min and then cooled to 0 $^{\circ}$ C for 10 min before the addition of MgCl₂ to a final concentration of 7 mM. The aptamer solution was then incubated at room temperature for 10 min. The refolded NH₂-A-9S aptamer solution was added to an Immobilizer Amino 96-well plate. Incubation at room temperature for 6 h allowed for the conjugation of the NH₂-A-9S aptamer to the surface of the 96-well plate. A binding buffer (1 \times BB) containing 50 mM Tris-HCl (pH 7.4), 5 mM KCl, 50 mM NaCl, 7 mM MgCl₂, and 0.05% Tween 20 was added to the plate and incubated at room temperature for 30 min. The 96-well plate was ready for use after removal of the excess aptamer solution and buffer solution.

For the determination of HBeAg in each sample, triplicate aliquots of 100 μ L pretreated sample were added into three wells. The 96-well plate was incubated at 37 $^{\circ}$ C for 2 h. The plate was washed five times with the washing buffer that contained 1 \times binding buffer and 0.1% casein.

To each well, we added 100 μL of biotinylated eAg3-Py aptamer (1 μM) in $1\times$ binding buffer supplemented with 0.5% BSA and 5 μM blocker sequence (TGGGC). The plate was incubated at 37 $^{\circ}\text{C}$ for 30 min and washed three times with the washing buffer. To each well, we added 100 μL of $50\times$ diluted horseradish peroxidase (HRP)-conjugated streptavidin. The plate was incubated at room temperature for 30 min and each well was washed three times with the washing buffer. Finally, 100 μL of the substrate solution (Invitrogen) were added into each well and incubated for 30 min before the addition of 2 M phosphoric acid to stop the reaction of HRP. Absorbance at 450 nm was measured using a plate reader (Beckman, Indianapolis, IN).

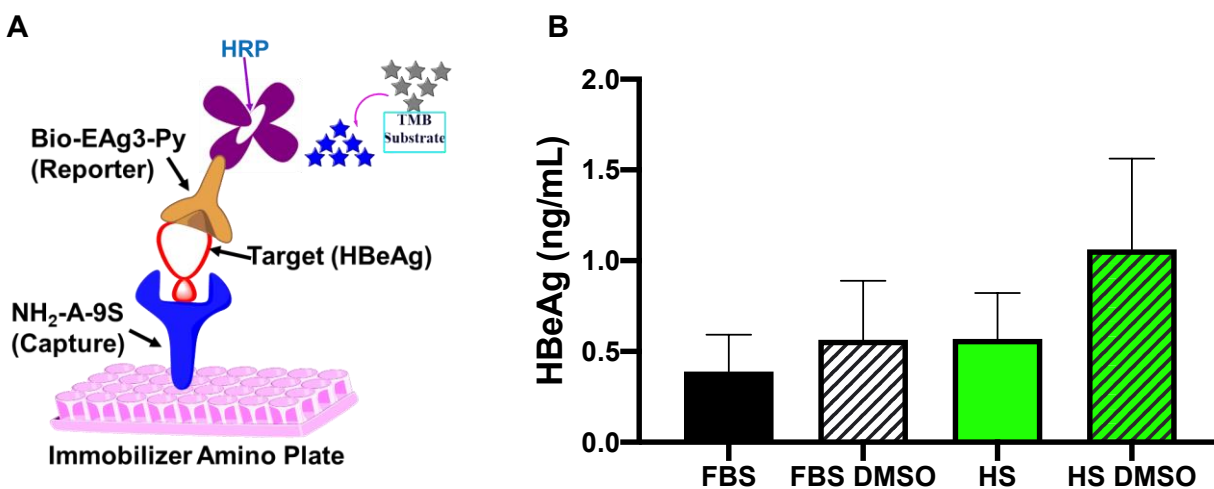


Figure 2.2. (A) Schematic showing the aptamer binding assay for HBeAg [42]. (B) Secreted HBeAg in HBV infected Huh7.5-NTCP cells. Huh7.5-NTCP cells were cultured in DMEM medium supplemented with FBS or HS. Cells were infected with multiplicity of infections (MOI) of 500 genome equivalents per cell. In a parallel set of experiments, 2% dimethyl sulfoxide (DMSO) was added during and after HBV infection. Culture supernatant was collected on day 7 post infection for the quantification of HBeAg using the aptamer binding assay. Average values with error bars ($\pm\text{SD}$) derived from three experiments are plotted. Adapted from [42] with permission from the American Chemical Society (ACS) Publications Support.

2.2.11. Immunofluorescence Staining of Huh7.5 Cells Overexpressing NTCP

For immunofluorescence staining of NTCP, Huh7.5 or Huh7.5-NTCP cells were seeded at 25% confluence onto glass coverslips placed in culture wells. The next day, cell monolayers were washed with PBS and then fixed with 4% formaldehyde in 1× PBS for 10 min at 37 °C. The formaldehyde solution was removed and coverslips were washed three times with PBS. Cells were permeabilized for 5 min with 0.1% Triton-X100 in PBS, then coverslips were washed with PBS. A block solution (1× PBS containing 5% BSA) was added and incubated for 1 h at room temperature. The cells were then incubated with rabbit anti-NTCP antibody (Abcam, ab175289; diluted 1:200 to a final concentration of 2.5 µg/mL in the block solution) at 4 °C overnight in a moist chamber. The coverslips were then washed three times with 1× PBS. Alexa568-labeled goat anti-rabbit secondary antibody (Invitrogen, A11036; diluted 1:400 (final concentration of 5 µg/mL) in 1× PBS with 5% BSA) was added and incubated for 1 h at room temperature. The coverslips were washed three times with 1× PBS before the addition of Hoechst 33,342 (Invitrogen) (diluted 1:5000 in 1× PBS). After a final PBS wash, Vectashield mounting medium for fluorescence (Vector Laboratories, Burlingame, CA. H-1000) was added. The cells were imaged with a Quorum Wave FX-2 spinning disk confocal microscope using 20×/0.85 NA oil immersion lenses and Velocity v. 6.2.1 software (Perkin Elmer, Waltham, MA).

Immunofluorescence staining of HBV-infected Huh7.5-NTCP cells was performed using procedures similar to those previously described [22]. After 14 days of infection, cells were fixed with formaldehyde and permeabilized with 0.1% Triton X-100 in PBS for 1 min at room temperature. Cell monolayers were washed three times with PBS after permeabilization and the plate was blocked with 1× PBS containing 5% BSA. The cells were then stained using rabbit anti-HBV core (Invitrogen, PA5-16368; diluted 1:200 in 1× PBS with 5% BSA) and Alexa568-

conjugated goat anti-rabbit secondary antibody (Invitrogen, A11036; diluted 1:400 in 1× PBS with 5% BSA).

2.2.12. Flow Cytometry Analysis of NTCP Expression

Adherent cells were dissociated with Accutase (Gibco, Dublin, Ireland. A1105-01), washed, and resuspended cells were blocked in 10% filtered human serum with 5% BSA in PBS. The cells were then analyzed using rabbit anti-NTCP primary antibody (Abcam, ab175289; diluted 1:100 (final concentration of 5 µg/mL) in the block solution) and the Alexa647-labeled anti-rabbit secondary antibody (Invitrogen, A31573; diluted 1:2000 (final concentration of 1 µg/mL) in the block solution). Flow cytometry was conducted on a BD LSR Fortessa X-20 instrument with BD FACSDIVA software (version 8.0.1) (BD Biosciences, San Jose, CA).

2.2.13. Western Blotting

Cell monolayers were washed twice with PBS and then lysed on ice for 10 min using a radioimmunoprecipitation assay (RIPA) buffer (50 mM Tris-HCl, pH 8.0, 150 mM NaCl, 0.1% SDS, 1% Triton X-100, 0.5% deoxycholic acid in Milli-Q water) with the addition of EDTA-free protease inhibitor (Roche, Basel, Switzerland). This whole cell lysate was centrifuged at 18,000× g for 15 min and the supernatant was collected. The protein concentration in cell lysates was quantified with the micro bicinchoninic acid (BCA) protein assay using the manufacturer's protocol (Pierce, Rockford, IL).

A 10% SDS-polyacrylamide gel of 1.5 mm thickness was used for gel electrophoresis separation. The denatured protein samples as well as the pre-stained protein standard ladder (Fisher Scientific, Waltham, MA) were run at an initial electrophoretic voltage of 80 V for 30 min, and then 160 V for approximately 1 h. The separated proteins were transferred onto a nitrocellulose

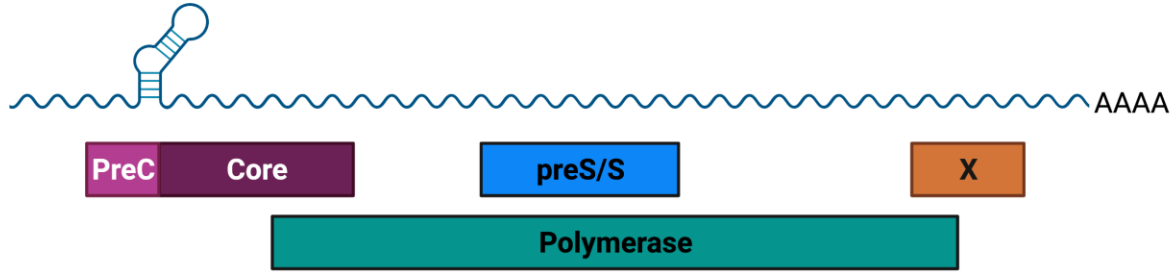
membrane (Amersham Hybond-ECL, GE, Marlborough, MA). The membrane was blocked, washed, and incubated with the rabbit anti-NTCP antibody (Abcam, ab175289; diluted 1:1000) and mouse anti-tubulin antibody (diluted 1:3000). Licor IRDye goat anti-rabbit 680 and goat anti-mouse 800 secondary antibodies (Licor, Lincoln, NE. cat. No. 926-32221 and cat. No. 926-32210, respectively) were used to detect the proteins. The membrane was scanned using a Licor Odyssey CLx imaging system and the images were analyzed using Image Studio software (Licor, Lincoln, NE).

2.2.14. Nanoluciferase Reporter Luminescence Assay

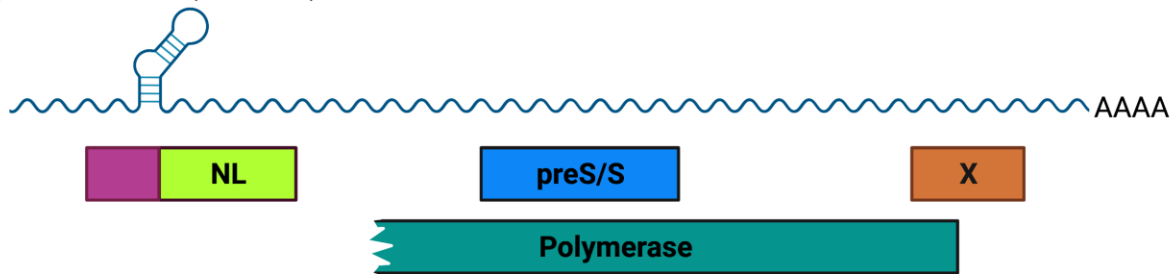
Constructs for producing HBV virus containing the nanoluciferase (NL) reporter were a kind gift from Dr. K. Shimotohno (Research Center for Hepatitis and Immunology, National Center for Global Health and Medicine, Tokyo, Japan) [43]. The HBV/NL plasmid, depicted in Figure 2.3, encodes the HBV genome with the nanoluciferase (NL) gene in frame with the viral pre-core/core open reading frame. This insertion of NL disrupts the pre-core/core and polymerase open reading frames, preventing expression of these proteins. The epsilon sequence, a stem loop secondary structure in pgRNA required for its encapsidation, remains intact in pgRNA from the HBV/NL plasmid. In contrast, the HBV-D plasmid encodes all of the HBV proteins; however, it contains sense mutations that disrupt the epsilon sequence secondary structure. Therefore, when the HBV/NL plasmid is co-transfected with the packaging-deficient HBV-D helper plasmid, the pgRNA generated by the HBV/NL plasmid is encapsidated with the core and polymerase proteins generated from the HBV-D plasmid. This creates non-replicative HBV/NL virions that express NL upon infection. Therefore, infection with recombinant HBV/NL virions generates NL activity, which is a surrogate marker for translation from viral RNA. Hence, the HBV/NL virus is a useful tool for assaying early steps in HBV infection, from entry to transcription.

Huh7.5-NTCP cells were infected with HBV/NL in the same manner as described for HBV infection. The Nano-Glo Luciferase Assay System (Promega, Madison, WI) was used according to the manufacturer's protocol to assess nanoluciferase reporter activity. Briefly, for a 96-well plate with 100 μ L medium per well, 50 μ L of the medium were removed, leaving 50 μ L in each well. Subsequently, 50 μ L of the Nano-Glo reagent (a 1:50 solution of substrate/buffer) was added to each well and incubated for 2 min at room temperature. The contents of the wells were thoroughly mixed to lyse the cell monolayers and then the luminescence of 50 μ L of the mixture was measured on a Perkin Elmer Enspire 2300 plate reader.

HBV genome (3.2kb)



pHBV/NL (3.3kb)



pHBV-D

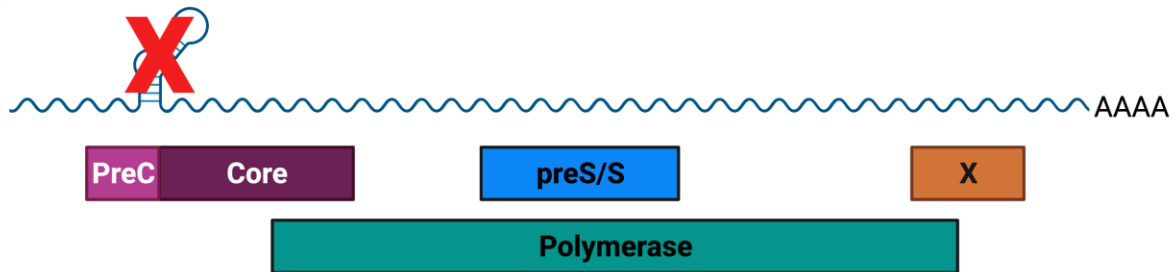


Figure 2.3. Depiction of pgRNA and ORFs derived from HBV, the plasmids HBV/NL, and HBV-D. Schematics show precore/core (PreC/C), polymerase (Pol), pre-surface/surface antigen (PreS/S), X protein, nanoluciferase (NL), and poly A tails (AAA) at the 3'-end. The stem loop labelled with “E” denotes the epsilon sequence required for packaging of the pgRNA. The HBV-D “E” stem loop filled with “x” represents mutations leading to a defect in secondary structure formation and encapsidation of the HBV-D pregenome. Modified from Nishitsuji *et al.* [43] and created using tools from BioRender.com.

2.2.15. Statistical Analysis

Statistical analysis was performed using Prism software for Mac OS version 8 (GraphPad, San Diego, CA). All data are represented as mean values \pm standard deviation. Experiments comparing two groups were analyzed using unpaired Student's *t*-tests. One-way analysis of variance (ANOVA) with the Bonferroni correction for multiple comparisons was used to evaluate experiments with more than two groups. Two-way ANOVA with the Bonferroni correction for multiple comparisons was used to assess experiments with two independent variables. *P*-values less than 0.05 were considered statistically significant.

2.3. Results

2.3.1. Huh7.5 Cell Line Overexpressing NTCP (Huh7.5-NTCP Cells)

To establish an *in vitro* HBV infection model, we first subjected Huh7.5 cells to transduction with lentiviral NTCP expression constructs followed by puromycin selection. The resulting Huh.7.5-NTCP cell line had more than a 3500-fold increase in NTCP mRNA when compared with the parental Huh.7.5 cell line using real-time quantitative polymerase chain reaction (RT-qPCR) (**Figure 2.4A**). Flow cytometry analysis revealed increased cell surface expression of NTCP (**Figure 2.4B**) and immunofluorescent staining followed by confocal microscopy (**Figure 2.4C**) also showed increased expression of cell surface NTCP protein in Huh7.5-NTCP cells compared to the parental cell line.

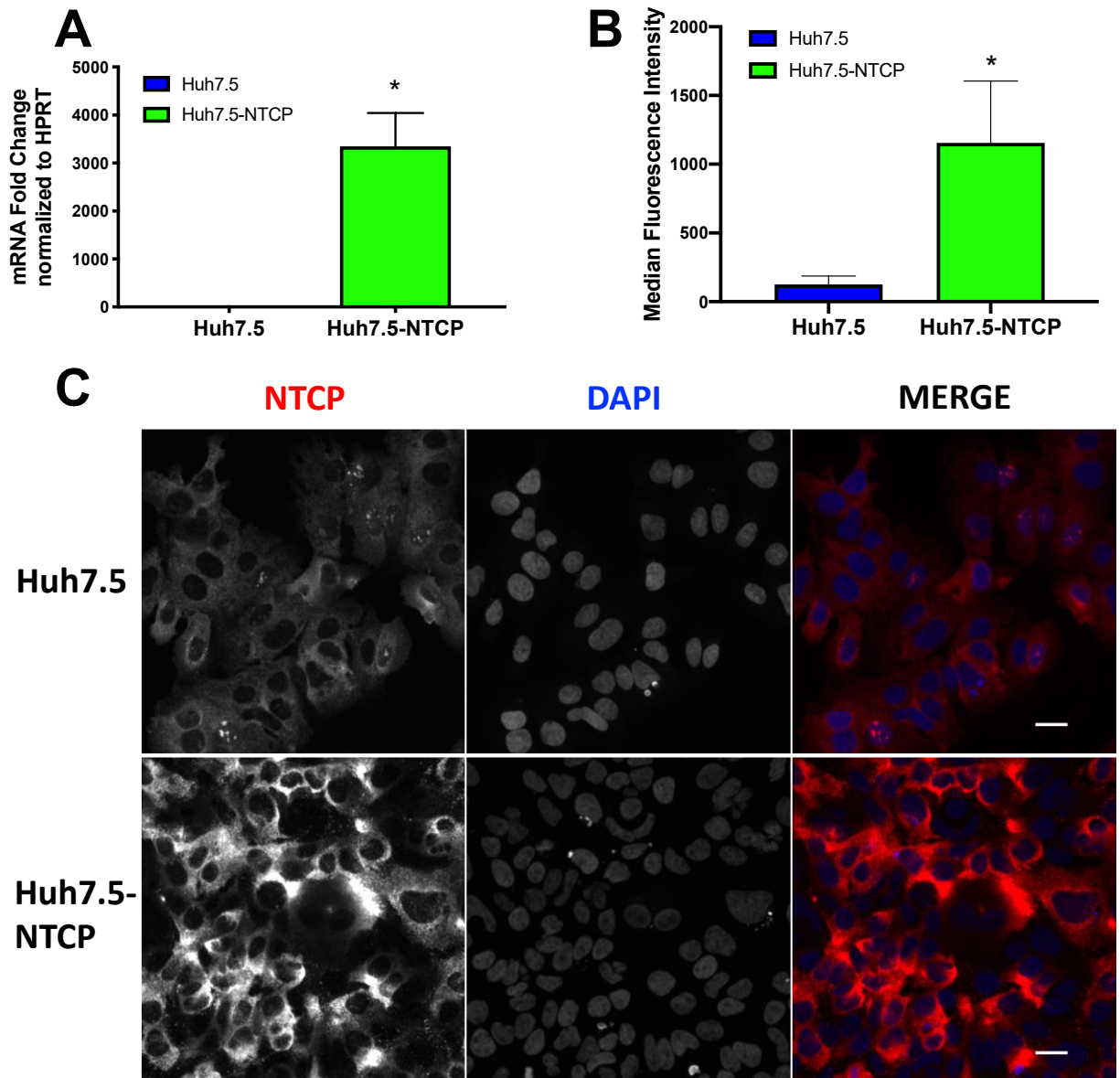


Figure 2.4. Overexpression of NTCP in Huh7.5 cells. (A) Lentiviral-transduced puromycin-selected Huh7.5-NTCP cell line expressed more NTCP mRNA than the parental Huh7.5 cell line. RT-qPCR was used to measure NTCP and hypoxanthine-guanine phosphoribosyltransferase (HPRT) mRNA levels. Huh7.5-NTCP cells expressed more cell surface NTCP than parental Huh7.5 cells as illustrated with (B) flow cytometry and (C) immunofluorescence (IF) microscopy. Immunofluorescent staining of NTCP is shown in red, and the DAPI (4',6-diamidino-2-phenylindole) stain of nuclei is shown in blue. Images show a single plane/z-stack. The scale bars are 10 μ m. (A, B) Average values with error bars (\pm SD) derived from three experiments ($n = 3$) are plotted. Unpaired Student's *t*-test was used for statistical analysis. * $p < 0.05$ compared to Huh7.5 cells.

2.3.2. Human Serum Culture Enhanced Productive HBV Infection in Huh7.5-NTCP Cells

We tested the susceptibility of Huh7.5-NTCP cells in human serum culture to HBV infection. Previous studies reported that NTCP-expressing HepG2 and AML12 cells were permissive to HBV infection and that treatment with DMSO significantly promoted HBV replication and production [27]. Cell culture protocols for HBV infection commonly use Dulbecco's modified Eagle's medium (DMEM) supplemented with 10% fetal bovine serum (FBS) and require 2–2.5% DMSO throughout. We compared HBV infection of Huh7.5-NTCP cells cultured in DMEM and supplemented either with FBS or human serum (HS) with or without the addition of DMSO.

We assayed HBV pregenomic RNA (pgRNA), covalently closed circular DNA (cccDNA), surface antigen (HBsAg), and E antigen (HBeAg) as markers of infection. Analysis of HBV pgRNA by RT-qPCR 14 days after infection showed that Huh7.5-NTCP cells cultured in the HS-supplemented DMEM medium produced 12-fold more copies of pgRNA than the cells cultured in the standard FBS-supplemented DMEM medium (**Figure 2.5A**). The FBS-supplemented culture required DMSO (2%) during HBV infection, and the pgRNA level was 10-fold lower than that in the HS-supplemented cultures if DMSO was also added during HBV infection (**Figure 2.5A**). The earliest biochemical step in HBV infection is the generation of HBV cccDNA from which pgRNA is transcribed. Measured using qPCR, the cccDNA levels in the HBV-infected Huh7.5-NTCP cells were higher when cultured in the medium supplemented with HS than in the FBS culture conditions (**Figure 2.5B**).

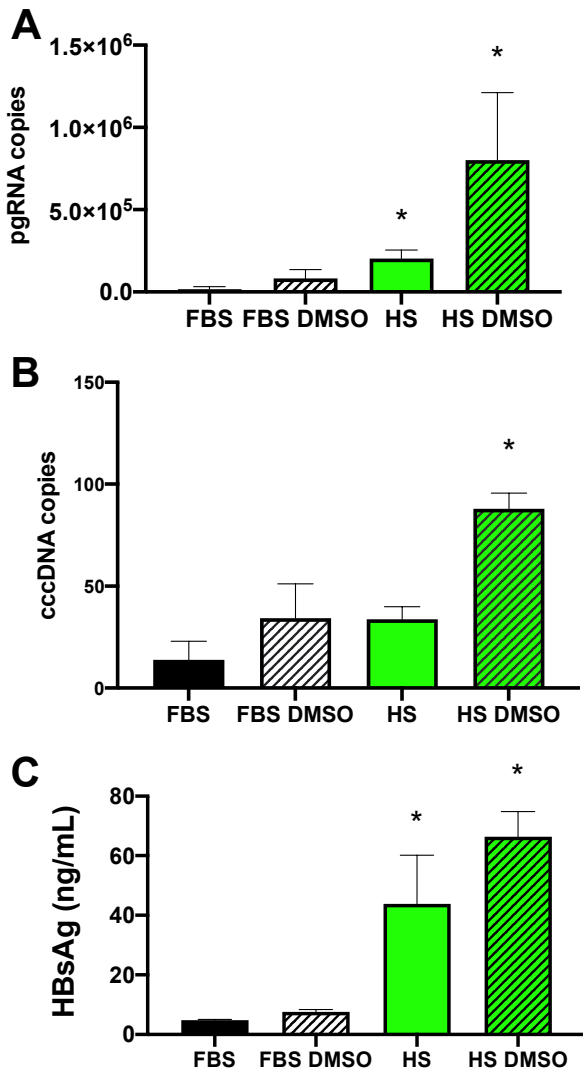


Figure 2.5. Enhancement of HBV replication by human serum culture. Human serum culture increased HBV (A) pgRNA (per 10 ng of total RNA), (B) cccDNA (10 ng of gDNA), and (C) HBV surface antigen (HBsAg) levels from Huh7.5-NTCP cells. Huh7.5-NTCP cells were cultured in the media supplemented with FBS or HS and with or without the addition of DMSO during HBV infection. Samples were collected on day 14 (A, B) or day 7 (C) post-infection. pgRNA was measured using RT-qPCR from 10 ng of total RNA. dddDNA was quantified using q-PCR from 10 ng of gDNA. HBsAg was measured in a culture supernatant using enzyme-linked immunosorbent assay (ELISA). Average values with error bars (\pm SD) derived from three experiments are plotted. One-way analysis of variance (ANOVA) was used with the Bonferroni correction for multiple comparison test. * $p < 0.05$ compared to FBS condition.

HBsAg released into the supernatant of infected cells was measured using enzyme-linked immunosorbent assay (ELISA). The supernatants of HS-supplemented cultures had significantly higher levels of HBsAg than did the FBS-supplemented cultures with or without further supplementation of DMSO during infection (**Figure 2.5C**). Additional analysis of the secreted HBeAg (Figure 2.2) showed higher levels of this protein in supernatants of the HS-supplemented cultures than in the FBS-supplemented cultures. Together, these results of pgRNA, cccDNA, and HBV proteins all support the conclusion that Huh7.5-NTCP cells in cultures supplemented with human serum enhance HBV infection.

We also examined whether the effect of HS-supplemented culture on HBV infection of Huh7.5-NTCP cells was consistent at a lower multiplicity of infection (MOI). The levels of HBV pgRNA from cells infected with 100 genome equivalents per cell (**Figure 2.6**) showed similar trends, but at about 1/3 the level, to results from cells infected with 500 genome equivalents per cell (Figure 2.5A), with pgRNA levels increasing with HS supplementation compared to FBS-supplemented cultures. This shows that the enhancement of HBV infection of Huh7.5-NTCP cells using the HS-supplemented cultures is sustained at a lower MOI (Figure 2.6). Since the HS culture contains lower serum concentrations than the FBS culture, we tested culture conditions containing 10% FBS, 4% FBS, and 4% HS (**Figure 2.7**). While cells supplemented with 4% FBS contained higher levels of HBV pgRNA, they did not reach the levels in the cultures that were HS-supplemented (Figure 2.7). Thus, the observed enhancement of HBV infection is not due to a difference in the concentrations of serum in the culture medium.

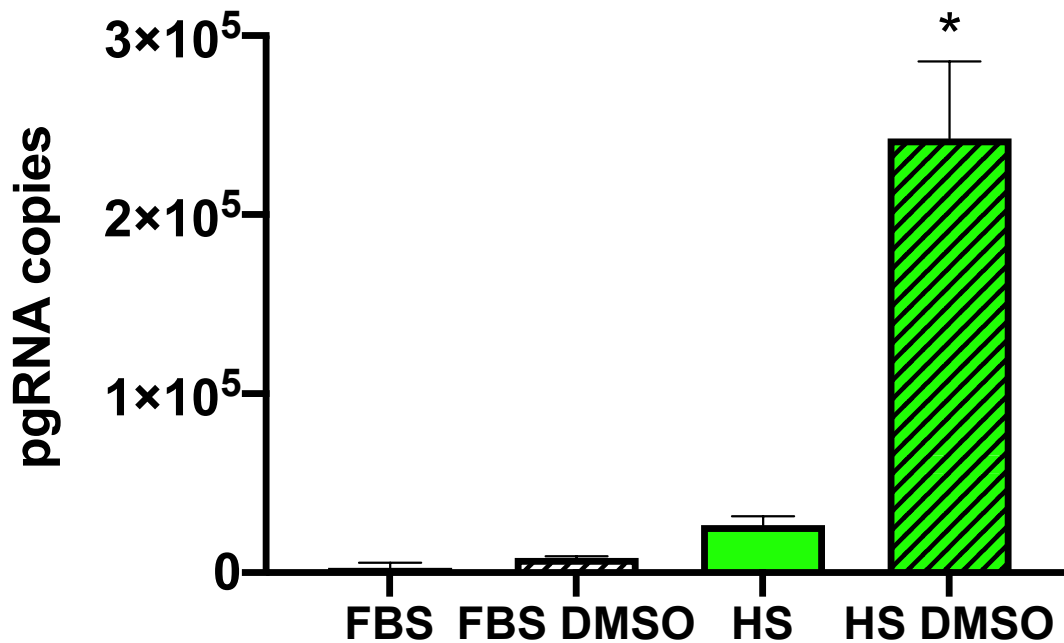


Figure 2.6. HBV pgRNA levels (per 10 ng total RNA) in Huh7.5 NTCP cells infected with a multiplicity of infections (MOI) of 100 genome equivalents per cell. Huh7.5-NTCP cells were cultured in DMEM medium supplemented with FBS or HS. In a parallel set of experiments, 2% DMSO was added during and after HBV infection. Samples were collected on day 14 post infection for RT-qPCR analysis of HBV pgRNA from 10 ng total RNA. One-way analysis of variance (ANOVA) was used with Bonferroni's correction for multiple-comparison test. * $p < 0.05$ compared to the FBS culture condition. The error bars indicate standard deviation (n=3).

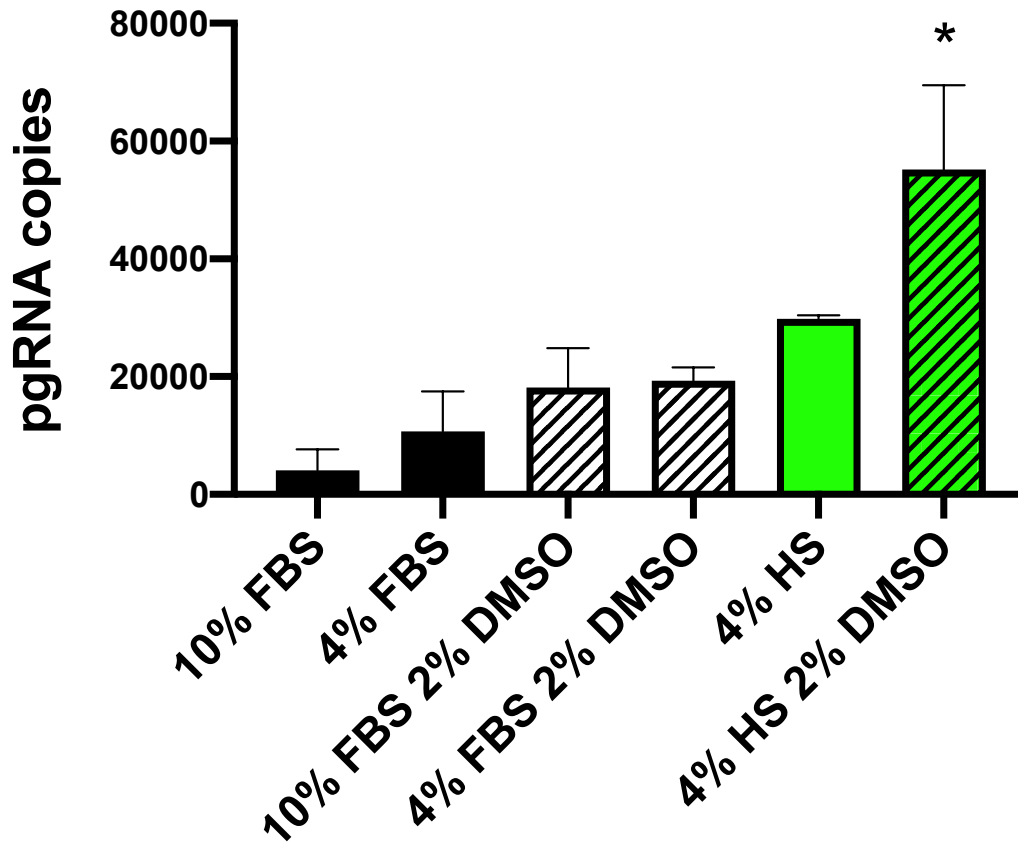


Figure 2.7. HBV pgRNA levels (per 10 ng total RNA) in infected Huh7.5 NTCP cells that were cultured under different conditions. Huh7.5-NTCP cells were cultured in DMEM medium supplemented with 10% FBS, 4% FBS, or 4% HS. In a parallel set of experiments, 2% DMSO was added during and after HBV infection. Cells were infected with multiplicity of infections (MOI) of 500 genome equivalents per cell. Samples were collected on day 14 post infection for RT-qPCR analysis of pgRNA from 10 ng total RNA. One-way analysis of variance (ANOVA) was used with Bonferroni's correction for multiple-comparison test. * $p < 0.05$ compared to the 10% FBS 2% DMSO condition. The error bars indicate standard deviation (n=3).

This is the first hepatoma cell culture HBV infection system that does not require DMSO to promote or maintain HBV infection. The differentiation of Huh7.5-NTCP hepatoma cells in human serum culture offers an alternative *in vitro* tool for studying HBV infection. It complements primary human hepatocytes (PHHs), which are difficult to acquire. The only other *in vitro* model where DMSO is not required for HBV infection used PHHs [38].

2.3.3. Huh7.5-NTCP Cells in a Human Serum Culture Serve as a Model for Long-Term HBV Infection

To investigate whether Huh7.5-NTCP cells remained infected for a prolonged period and could potentially model chronic HBV infection, we analyzed RNA over a period of 50 days after HBV infection. HBV pgRNA increased for approximately two weeks after infection followed by a plateau and sustained pgRNA levels for the remainder of the experiment (**Figure 2.8**). The pgRNA levels were consistently higher in Huh7.5-NTCP cells cultured in the medium supplemented with HS with or without further supplementation of DMSO compared to cultures in the media supplemented with FBS in the presence or absence of DMSO. The pgRNA levels were consistently the highest in the HBV-infected cells cultured in the media supplemented with HS and DMSO throughout the 50-day post-infection period (Figure 2.8). These results suggest that the Huh7.5-NTCP cell line in the human serum culture system could potentially serve as an *in vitro* model for chronic HBV infection [38, 44].

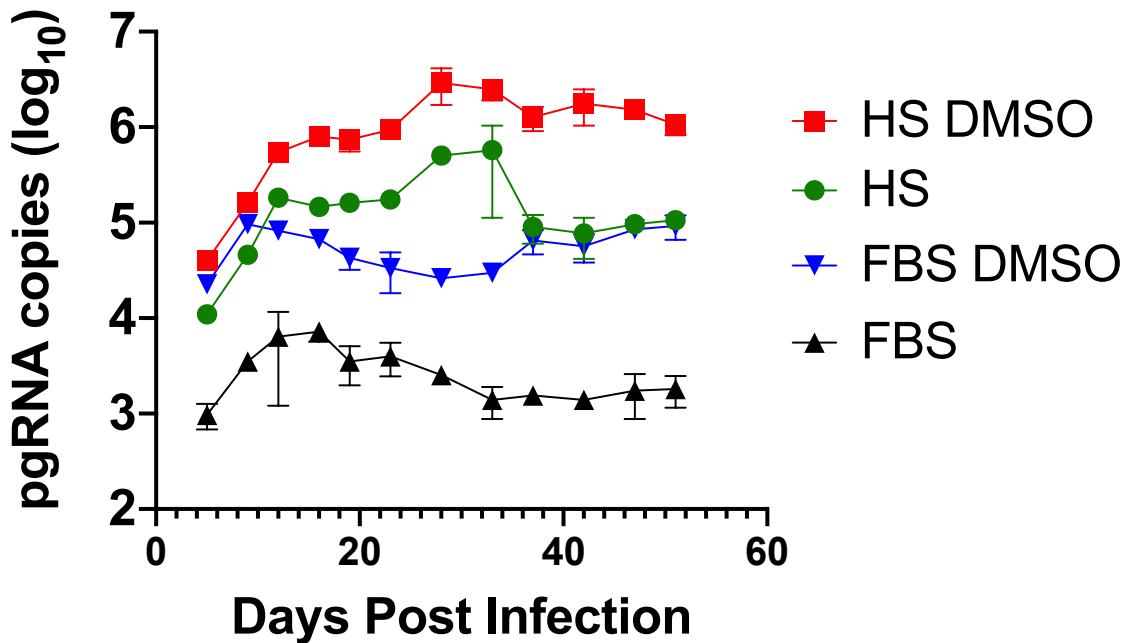


Figure 2.8. Sustained infection by HBV in Huh7.5-NTCP cells cultured in human serum. Huh7.5-NTCP cells cultured in the medium supplemented with FBS or HS were infected with 500 genome equivalents per cell with or without 2% DMSO during infection. HBV pgRNA in the cells was repeatedly measured using RT-qPCR every 4–5 days for 50 days after HBV infection. The concentration of pgRNA was expressed as pgRNA copies per 10 ng total RNA. Average values with error bars (\pm SD) derived from three experiments ($n=3$) are plotted.

2.3.4. Human Serum Alters Hepatocyte Differentiation Markers in Huh7.5-NTCP

We reasoned that enhancement of HBV infection of Huh7.5-NTCP cells in the HS-supplemented culture medium could be due to differentiation of Huh7.5-NTCP cells to become more hepatocyte-like. Previously we showed that 21 days were required to fully differentiate Huh7.5 cells in HS media [29, 30]. We therefore tested the optimum time needed for the Huh7.5-

NTCP cells to differentiate in the HS-supplemented culture medium. We cultured Huh7.5-NTCP cells in a medium containing HS for 7, 14, and 21 days prior to HBV infection of the cells. We then measured HBV pgRNA 14 days after HBV infection. The levels of HBV pgRNA increased with differentiation time prior to infection and reached a maximum between 14 and 21 days of differentiation in the HS-supplemented medium (**Figure 2.9A**).

We used the nanoluciferase recombinant virus and nanoluciferase luminescence assays as a surrogate marker for early steps in HBV infection [43]. Luminescence intensity was the highest when the cells were differentiated in the HS-supplemented medium for 21 days prior to HBV infection (**Figure 2.9B**). These results suggest that culturing in the HS-supplemented medium for 14 to 21 days prior to HBV infection is optimum for the enhanced HBV infection, which is consistent with our previous observations for the time required for HS-mediated differentiation and full restoration of hepatocyte functions [29, 30].

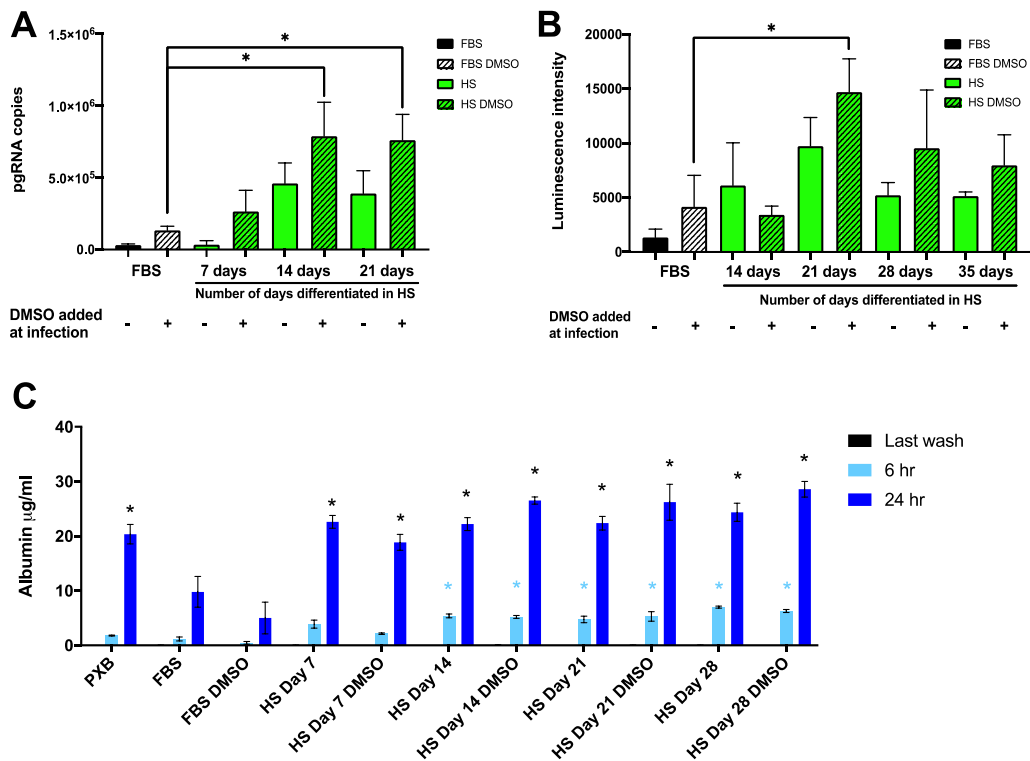


Figure 2.9. Enhancement of HBV replication and expression of hepatocyte markers in Huh7.5-NTCP cells cultured in human serum. (A–C) Huh7.5-NTCP cells were cultured for various lengths of time in a medium supplemented with FBS or HS. Cells maintained in HS-supplemented media were infected after the indicated number of days in HS-containing media. During HBV infection, DMSO was either absent (–) or present (+). Samples were collected on day 14 post-infection for (A) RT-qPCR analysis of pgRNA per 10 ng total RNA or (B) nanoluciferase reporter luminescence analysis. (A, B) One-way analysis of variance (ANOVA) was used with the Bonferroni correction for multiple comparison test. * $p < 0.05$. (C) Secreted human albumin concentration after 6 h and 24 h was determined using ELISA. Average values (\pm SD) derived from three experiments are plotted. Two-way analysis of variance (ANOVA) was used with the Bonferroni correction for multiple comparison test. Blue *, $p < 0.01$ compared to FBS albumin secretion in 6 h. Black *, $p < 0.01$ compared to FBS albumin secretion in 24 h.

Using ELISA, we assessed albumin secretion, which is a conventional marker of differentiation and viability of PHHs. Culturing Huh7.5-NTCP cells in the HS-supplemented medium increased to amounts approaching that produced by plated PHHs [45] and PXB cells (human hepatocytes isolated from chimeric humanized liver mice and then cultured in vitro) (**Figure 2.9C**). Albumin secretion increased during the initial seven days of the HS-supplemented cultures and this increased amount of albumin secretion was maintained throughout the entire 28 days of the HS-supplemented cultures (Figure 2.9C). These findings suggest that the culture in the HS-supplemented medium modified the Huh7.5-NTCP hepatoma cell line to a more hepatocyte-like phenotype similar to the effect of HS-media on Huh7.5 cells [30–32], and this correlates with the enhanced HBV infection (Figure 2.5). The increase in hepatocyte differentiation markers suggest that the cells cultured in the HS-containing medium have more differentiated characteristics than the cells cultured in the standard FBS-containing medium. The HS-induced cell differentiation may be a factor in the ability of HBV to infect the cells and maintain production of pgRNA when cultured in the HS-containing medium.

2.3.5. Involvement of NTCP and Possible Effect of Its N-Glycosylation on Viral Entry

We investigated how the human serum culture system affected expression of NTCP, the HBV entry receptor. Administration of Myreludex B (MyrB), a peptide mimic of the portion of the surface antigen that binds NTCP [46], inhibited infection of cells under all four culture conditions (**Figure 2.10**). This suggests that NTCP mediated HBV entry into these cells.

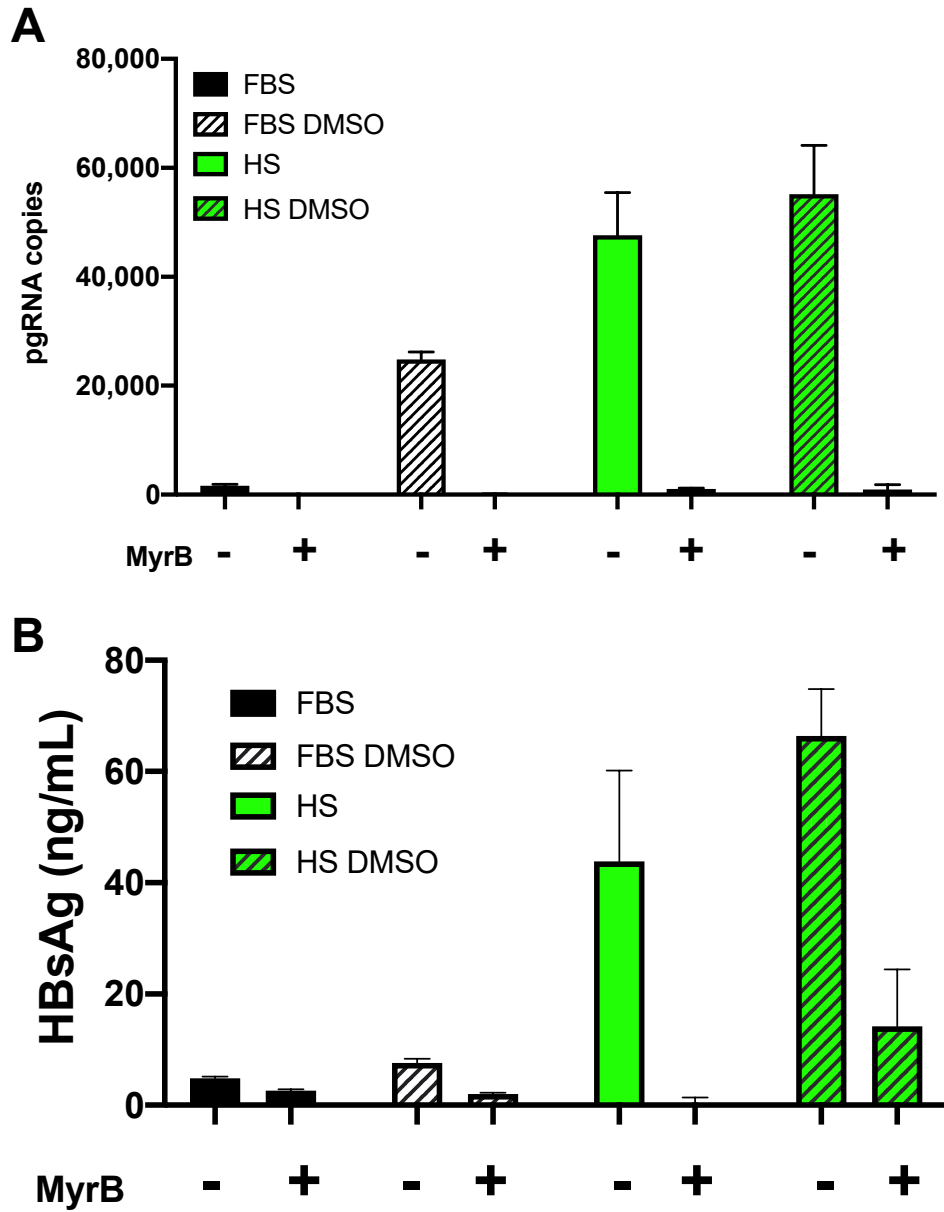


Figure 2.10. Reduction of HBV infection by MyrB, an entry inhibitor. MyrB was added to culture at 300 nM 30 min prior to infection and remained during HBV infection and one day post-infection. Cell monolayers and the culture supernatant were collected on day 7 post-infection for (A) RT-qPCR analysis of pgRNA per 10 ng total RNA and (B) ELISA of the surface antigen (HBsAg). Average values with error bars (\pm SD) derived from three experiments ($n=3$) are plotted.

DMSO has been shown to increase HBV infection in cell cultures containing FBS, and this is consistent with what we see in Huh7.5 cells where DMSO increased NTCP expression (**Figure 2.11**). However, in Huh7.5 cells overexpressing NTCP, the addition of DMSO to either the FBS-supplemented cultures or the HS-supplemented cultures decreased the expression of NTCP mRNA levels (Figure 2.11A, B). Flow cytometry analyses of Huh7.5-NTCP cells indicated that levels of NTCP on the cell surface were lower when cells were cultured in the medium supplemented with both FBS and DMSO (Figure 2.11C). The decrease in NTCP levels caused by DMSO in NTCP-overexpressing cells was counterintuitive and led us to explore other possible reasons for the enhancement of HBV infection by HS and DMSO.

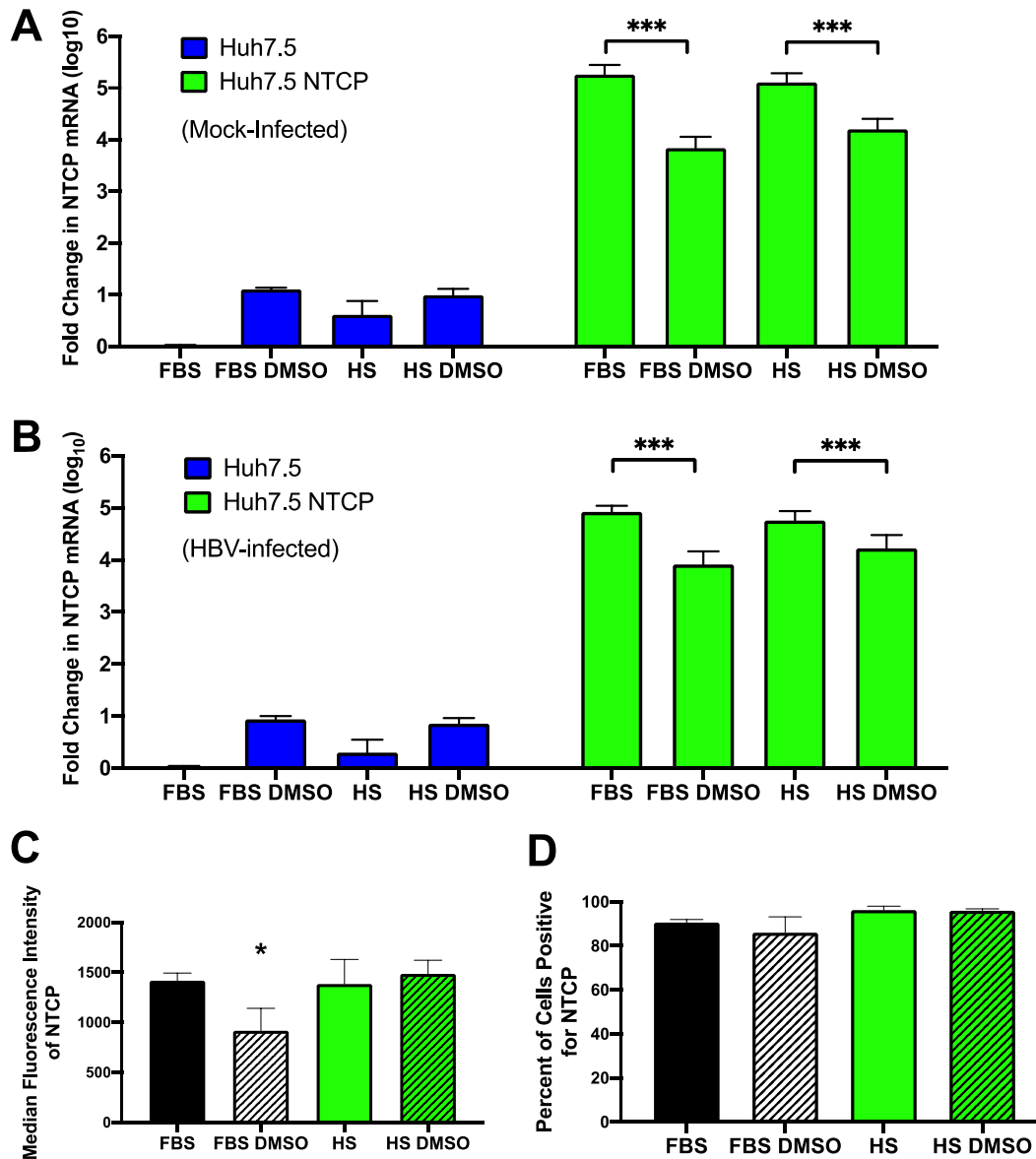


Figure 2.11. Changes in NTCP mRNA levels and surface NTCP protein expression under various culture conditions. Huh7.5 or Huh7.5-NTCP cells were (A) not infected with the virus (mock), or (B) infected with HBV. Samples were collected on day 7 post-infection for RT-qPCR analyses of NTCP mRNA and HPRT mRNA levels. $\Delta\Delta CT$ values were calculated to determine fold changes in NTCP mRNA expression normalized to that of the Huh7.5 cells cultured in the medium containing FBS. Huh7.5-NTCP cells were analyzed with flow cytometry to assess (C) cell surface expression of NTCP based on median fluorescence intensity and (D) the percentage of cells expressing NTCP. Average values with error bars (\pm SD) derived from three independent experiments are plotted. One-way analysis of variance (ANOVA) was used with the Bonferroni correction for multiple comparison test. * $p < 0.05$ compared to the FBS condition; *** $p < 0.0005$.

We examined the possible role of N-glycosylation of NTCP on viral entry. Western blots of lysates from Huh7.5-NTCP cells cultured in the absence of DMSO probed with NTCP-specific antibodies displayed two bands, one slightly above 35 kDa and one at 55 kDa (**Figure 2.12A**). Unglycosylated NTCP has a molecular weight of 37 kDa and the N-glycosylated form has a molecular weight of 55 kDa. The N-glycosylated form traffics to the cell surface and is required for HBV infection [47, 48]. Western blot analyses of the cells cultured in the FBS-supplemented medium without DMSO exhibited a smear below the 55 kDa band, suggesting incomplete glycosylation of NTCP, while the cells cultured in the medium containing both FBS and DMSO had the sharp 55 kDa band, indicating full glycosylation. Western blots of lysates from Huh7.5-NTCP cells cultured in the HS-supplemented medium with or without supplementation of DMSO consistently had a sharp band at 55 kDa. The levels and species of NTCP do not change upon HBV infection of Huh7.5-NTCP cells (**Figure 2.12A**). These results suggest both that the decrease in NTCP mRNA levels caused by DMSO (**Figure 2.11A, B**) and that enhanced HBV infection of Huh7.5-NTCP cells in HS-supplemented cultures may in part be due to increased expression of fully glycosylated NTCP on the surface of Huh7.5-NTCP cells. Similarly, DMSO improves glycosylation of NTCP in Huh7.5-NTCP cells cultured in FBS and this treatment likely increases their infectability by HBV.

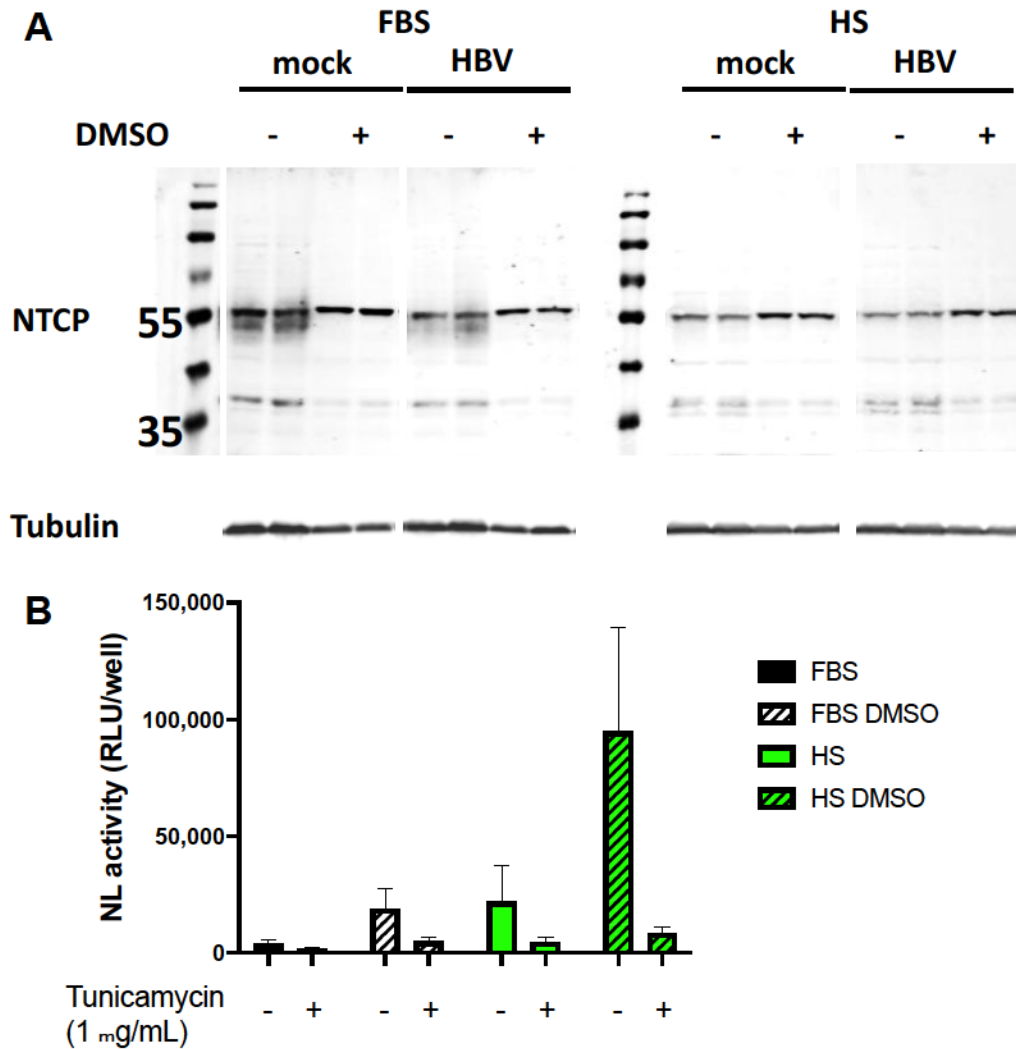


Figure 2.12. NTCP glycosylation and inhibition by tunicamycin. (A) Western blot analyses of NTCP glycosylation in Huh7.5-NTCP cells that were uninfected (mock) or infected with HBV. All combinations of HS supplement and DMSO treatment were tested. (B) Inhibition of N-glycosylation with tunicamycin suppressed HBV infection. Huh7.5-NTCP cells were incubated with 1 µg/mL tunicamycin for 2.5 h, followed by washing four times with PBS prior to infection. The cells were infected with nanoluciferase-expressing HBV (HBVNL) (MOI 500). Luminescence in relative light units (RLU) per well was measured to indicate nanoluciferase (NL) activity. Average values with error bars (\pm SD) derived from three experiments ($n=3$) are plotted.

To explore whether glycosylation of NTCP was involved, we treated Huh7.5-NTCP cells in various culture media with tunicamycin [49], an N-glycosylation inhibitor, for 2.5 h prior to infection with HBV. We used a non-replicative nanoluciferase-expressing HBV (HBV/NL) (Figure 2.3) to assess whether the tunicamycin treatment affected viral entry and early steps in HBV infection. Treatment with tunicamycin under all four culture conditions resulted in marked reductions in nanoluciferase activity (**Figure 2.12B**). Because the nanoluciferase activity of the cells infected with HBV containing the nanoluciferase reporter recapitulates only early events of infection, the suppression of infection by an inhibitor of N-glycosylation suggests N-glycosylation of NTCP is relevant to viral entry. Therefore, the full N-glycosylation of NTCP observed from Huh7.5-NTCP cells either cultured with HS- or DMSO-containing media may aid in the entry step of HBV infection.

2.4. Discussion

This chapter describes a robust hepatoma cell culture HBV infection system that does not require DMSO. The only previous example in which DMSO was not required for HBV infection used primary human hepatocytes (PHHs) [38]. Because PHHs are more difficult to acquire and maintain, our human serum culture of the Huh7.5-NTCP hepatoma cell system offers an alternative *in vitro* model for studying HBV infection.

It has been recognized that the more differentiated a liver cell culture model is, the more likely the culture system is permissive and supportive of HBV infection [10-12, 38, 47]. With actively dividing hepatoma cell lines and *ex vivo* primary hepatocyte cultures, differentiated phenotypes are conventionally established and maintained with the addition of DMSO to the culture media. The DMSO supplementation causes growth arrest and more hepatocyte-like gene expression profiles in hepatoma cell lines. However, DMSO causes cytotoxicity with its solvent

properties [33–37] and fails to restore many liver functions in hepatoma cultures [29]. In both hepatic and cardiac tissue types (3D microtissue cultures) exposed to 0.1% DMSO, “transcriptome analysis detected >2000 differentially expressed genes affecting similar biological processes, indicating consistent cross-organ actions of DMSO” [37].

Previous studies in our laboratory showed widespread changes in gene expression when Huh7.5 cells are cultured in HS, shifting toward a phenotype more resembling PHHs [29, 30]. Likewise, after transduction and overexpression of NTCP, the Huh7.5-NTCP cells exhibited contact inhibition and growth arrest when cultured in the HS-supplemented medium and retained these properties. Albumin secretion, a conventional marker of PHH function, showed that Huh7.5-NTCP cells also acquired a more differentiated phenotype in the HS-supplemented cultures.

This better differentiation induced by HS culture compared to the conventional FBS cultures may be attributed to the different growth factors, differentiation factors, and lipid composition of HS compared to FBS. Given the complex composition of human serum, empirical testing of specific differentiation factors is challenging and unlikely to reveal individual causative agents responsible for the 22–32% transcriptional changes observed with HS supplementation [30]. Although DMSO can induce growth arrest and increase transcription of some hepatocyte genes, it does not cause the comprehensive phenotypic shift towards primary liver characteristics brought about by HS-supplemented cultures. Therefore, this considerable restoration of liver function and metabolism by culture in human serum likely contributes to the observed enhancement of HBV infection and holds benefits over DMSO supplementation for physiologically relevant in vitro studies of HBV.

In Huh7.5-NTCP cells, HS differentiation promotes a more hepatocyte-like phenotype and significantly enhances HBV infection. However, the pgRNA level in HBV-infected and HS-

differentiated Huh7.5-NTCP cells (Figure 2.5A) is lower than that in HepG2-NTCP cells (**Figure 2.13**). HepG2-NTCP cells require DMSO for HBV infection and can be infected in the presence of HS and DMSO. It is not known whether HepG2-NTCP cells differentiate in HS. Figure 2.9A shows that Huh7.5-NTCP cells need to differentiate in HS for 21 days before enhanced HBV infection is achieved. The HepG2-NTCP cells were cultured in a medium with HS for 7 days. Enhanced HBV infection of HepG2-NTCP cells might not occur until these cells are more fully differentiated in HS.

We examined how culturing Huh7.5-NTCP cells with various media affected NTCP expression. Culture with DMSO supplementation resulted in reduced NTCP mRNA levels. Among the various culture media, cells cultured with FBS and DMSO supplementation displayed reduced surface protein expression of NTCP. N-glycosylation of NTCP was promoted in culture media supplemented with HS or DMSO. The inhibition of N-glycosylation suppressed HBV infection. Our results showing this potential involvement of NTCP N-glycosylation in HBV entry are consistent with those previously reported [48,49], although another study deemed this NTCP modification non-essential to HBV infection [50]. Further studies of NTCP glycosylation are needed to clarify its impact on viral entry.

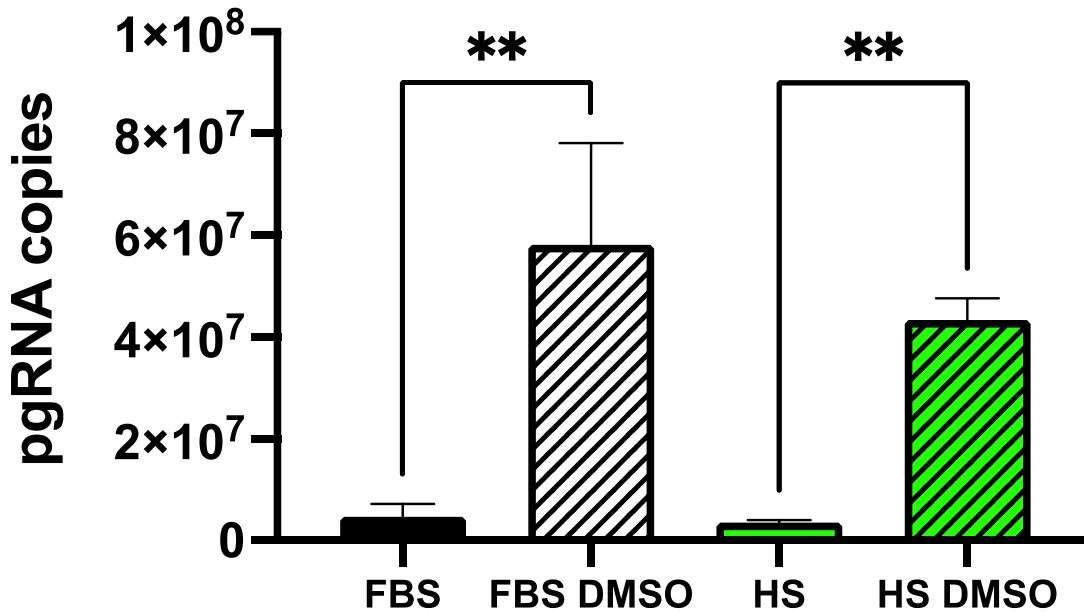


Figure 2.13. HBV pgRNA levels (per 10 ng total RNA) in infected HepG2-NTCP cells that were infected and cultured in different media. HepG2-NTCP cells were infected and cultured in DMEM medium supplemented with 10% FBS, 10% FBS and 2% DMSO, 4% HS, or 4% HS and 2% DMSO. Cells were infected with multiplicity of infections (MOI) of 1000 genome equivalents per cell. Samples were collected on day 7 post infection for RT-qPCR analysis of pgRNA from 10 ng total RNA. One-way analysis of variance (ANOVA) was used with Bonferroni's correction for multiple-comparison test. **, $p < 0.005$. The error bars indicate standard deviation from triplicate experiments (n=3).

2.5. Conclusion

Despite the high infectivity of HBV *in vivo*, the slow development of easily infectable *in vitro* culture systems delays studies of HBV. A hepatoma cell culture system that does not require DMSO for HBV infection is described in this chapter. Overexpression of NTCP bile acid transporter in hepatoma cells improved infection efficiency. We overexpressed NTCP in Huh7.5 cells and allowed these cells to differentiate in a medium supplemented with human serum (HS)

instead of fetal bovine serum (FBS). The HS culture enhanced HBV infection in Huh7.5-NTCP cells. In HS cultures, HBV pgRNA levels were increased by as much as 200-fold in comparison with FBS cultures and 19-fold in comparison with FBS+DMSO cultures. HS cultures increased levels of hepatocyte differentiation markers, such as albumin secretion, in Huh7.5-NTCP cells to similar levels found in primary human hepatocytes. N-glycosylation of NTCP induced by culture in HS may contribute to viral entry. Our study demonstrates an *in vitro* HBV infection model of Huh7.5-NTCP cells without the use of potentially toxic DMSO. The work from this chapter has been published (Le, C.; Sirajee, R.; Steenberg, R.; Joyce, M.A.; Addison, W.R.; Tyrrell, D.L. *In vitro* infection with hepatitis B virus using differentiated human serum culture of Huh7.5-NTCP cells without requiring dimethyl sulfoxide. *Viruses*, **2021**, *13*, 97). Permission for reproduction of this paper was granted under a Creative Commons Attribution 4.0 International License.

2.6. References

1. Schulze, A.; Mills, K.; Weiss, T.S.; Urban, S. Hepatocyte polarization is essential for the productive entry of the hepatitis B virus. *Hepatology* **2011**, *55*, 373–383. doi:10.1002/hep.24707.
2. Thomas, E.; Liang, T.J. Experimental models of hepatitis B and C—new insights and progress. *Nat. Rev. Gastroenterol. Hepatol.* **2016**, *13*, 362–374. doi:10.1038/nrgastro.2016.37.
3. Allweiss, L.; Dandri, M. Experimental *in vitro* and *in vivo* models for the study of human hepatitis B virus infection. *J. Hepatol.* **2016**, *64*, S17–S31, doi:10.1016/j.jhep.2016.02.012.
4. Hu, J.; Lin, Y.; Chen, P.; Watashi, K.; Wakita, T. Cell and animal models for studying hepatitis B virus infection and drug development. *Gastroenterology* **2019**, *156*, 338–354. doi:10.1053/j.gastro.2018.06.093.
5. Baumert, T.F.; Colpitts, C.C.; Schuster, C.; Zeisel, M.B.; Baumert, T.F. Cell culture models for the investigation of hepatitis B and D virus infection. *Viruses* **2016**, *8*, 261. doi:10.3390/v8090261.
6. Witt-Kehati, D.; Alaluf, M.B.; Shlomai, A. Advances and challenges in studying hepatitis B virus *in vitro*. *Viruses* **2016**, *8*, 21. doi:10.3390/v8010021.

7. Wettengel, J.; Burwitz, B.J. Innovative HBV animal models based on the entry receptor NTCP. *Viruses* **2020**, *12*, 828. doi:10.3390/v12080828.
8. Gripon, P.; Rumin, S.; Urban, S.; Le Seyec, J.; Glaise, D.; Cannie, I.; Guyomard, C.; Lucas, J.; Trepo, C.; Guguen-Guillouzo, C. Nonlinear partial differential equations and applications: Infection of a human hepatoma cell line by hepatitis B virus. *Proc. Natl. Acad. Sci. U.S.A.* **2002**, *99*, 15655–15660. doi:10.1073/pnas.232137699.
9. Hantz, O.; Parent, R.; Durantel, D.; Gripon, P.; Guguen-Guillouzo, C.; Zoulim, F. Persistence of the hepatitis B virus covalently closed circular DNA in HepaRG human hepatocyte-like cells. *J. Gen. Virol.* **2009**, *90*, 127–135. doi:10.1099/vir.0.004861-0.
10. Gripon, P.; Diot, C.; Thézé, N.; Fourel, I.; Loreal, O.; Brechot, C.; Guguen-Guillouzo, C. Hepatitis B virus infection of adult human hepatocytes cultured in the presence of dimethyl sulfoxide. *J. Virol.* **1988**, *62*, 4136–4143. doi:10.1128/jvi.62.11.4136-4143.1988.
11. Gripon, P.; Diot, C.; Guillouzo, C.G. Reproducible high level infection of cultured adult human hepatocytes by hepatitis B virus: Effect of polyethylene glycol on adsorption and penetration. *Virology* **1993**, *192*, 534–540. doi:10.1006/viro.1993.1069.
12. Hewitt, N.J.; Lechón, M.J.G.; Houston, J.B.; Hallifax, D.; Brown, H.S.; Maurel, P.; Kenna, J.G.; Gustavsson, L.; Lohmann, C.; Skonberg, C.; et al. Primary hepatocytes: Current understanding of the regulation of metabolic enzymes and transporter proteins, and pharmaceutical practice for the use of hepatocytes in metabolism, enzyme induction, transporter, clearance, and hepatotoxicity studies. *Drug Metab. Rev.* **2007**, *39*, 159–234. doi:10.1080/03602530601093489.
13. Ning, X.; Nguyen, D.; Mentzer, L.; Adams, C.; Lee, H.; Ashley, R.; Hafenstein, S.; Hu, J. Secretion of genome-free hepatitis B virus—single strand blocking model for virion morphogenesis of para-retrovirus. *PLoS Pathog.* **2011**, *7*, e1002255. doi:10.1371/journal.ppat.1002255.
14. Sureau, C.; Romet-Lemonne, J.L.; Mullins, J.I.; Essex, M. Production of hepatitis B virus by a differentiated human hepatoma cell line after transfection with cloned circular HBV DNA. *Cell* **1986**, *47*, 37–47. doi:10.1016/0092-8674(86)90364-8.
15. Sells, M.A.; Chen, M.L.; Acs, G. Production of hepatitis B virus particles in Hep G2 cells transfected with cloned hepatitis B virus DNA. *Proc. Natl. Acad. Sci. U.S.A.* **1987**, *84*, 1005–1009. doi:10.1073/pnas.84.4.1005.

16. Ladner, S.K.; Otto, M.J.; Barker, C.S.; Zaifert, K.; Wang, G.H.; Guo, J.T.; Seeger, C.; King, R.W. Inducible expression of human hepatitis B virus (HBV) in stably transfected hepatoblastoma cells: A novel system for screening potential inhibitors of HBV replication. *Antimicrob. Agents Chemother.* **1997**, *41*, 1715–1720. doi:10.1128/aac.41.8.1715.
17. Yan, H.; Zhong, G.; Xu, G.; He, W.; Jing, Z.; Gao, Z.; Huang, Y.; Qi, Y.; Peng, B.; Wang, H.; et al. Sodium taurocholate cotransporting polypeptide is a functional receptor for human hepatitis B and D virus. *eLife* **2012**, *1*, 00049, doi:10.7554/elife.00049.
18. Iwamoto, M.; Watashi, K.; Tsukuda, S.; Aly, H.H.; Fukasawa, M.; Fujimoto, A.; Suzuki, R.; Aizaki, H.; Ito, T.; Koiwai, O.; et al. Evaluation and identification of hepatitis B virus entry inhibitors using HepG2 cells overexpressing a membrane transporter NTCP. *Biochem. Biophys. Res. Commun.* **2014**, *443*, 808–813. doi:10.1016/j.bbrc.2013.12.052.
19. Seeger, C.; Sohn, J.A. Targeting hepatitis B virus with CRISPR/Cas9. *Mol. Ther.-Nucleic Acids* **2014**, *3*, e216. doi:10.1038/mtna.2014.68.
20. Yan, R.; Zhang, Y.; Cai, D.; Liu, Y.; Cuconati, A.; Guo, H. Spinoculation enhances HBV infection in NTCP-reconstituted hepatocytes. *PLoS One* **2015**, *10*, e0129889. doi:10.1371/journal.pone.0129889.
21. Li, W. The hepatitis B virus receptor. *Annu. Rev. Cell Dev. Biol.* **2015**, *31*, 125–147. doi:10.1146/annurev-cellbio-100814-125241.
22. Ni, Y.; Lempp, F.A.; Mehrle, S.; Nkongolo, S.; Kaufman, C.; Fälth, M.; Stindt, J.; Königer, C.; Nassal, M.; Kubitz, R.; et al. Hepatitis B and D viruses exploit sodium taurocholate co-transporting polypeptide for species-specific entry into hepatocytes. *Gastroenterology* **2014**, *146*, 1070–1083.e6. doi:10.1053/j.gastro.2013.12.024.
23. Lempp, F.A.; Qu, B.; Wang, Y.X.; Urban, S. Hepatitis B virus infection of a mouse hepatic cell line reconstituted with human sodium taurocholate cotransporting polypeptide. *J. Virol.* **2016**, *90*, 4827–4831, doi:10.1128/jvi.02832-15.
24. Li, J.; Zong, L.; Sureau, C.; Barker, L.; Wands, J.R.; Tong, S. Unusual features of sodium taurocholate cotransporting polypeptide as a hepatitis B virus receptor. *J. Virol.* **2016**, *90*, 8302–8313. doi:10.1128/jvi.01153-16.
25. Michailidis, E.; Pabon, J.; Xiang, K.; Park, P.; Ramanan, V.; Hoffmann, H.H.; Schneider, W.M.; Bhatia, S.N.; De Jong, Y.P.; Shlomai, A.; et al. A robust cell culture system supporting

- the complete life cycle of hepatitis B virus. *Sci. Rep.* **2017**, *7*, 16616. doi:10.1038/s41598-017-16882-5.
26. Zhou, M.; Zhao, K.; Yao, Y.; Yuan, Y.; Pei, R.; Wang, Y.; Chen, J.; Hu, X.; Zhou, Y.; Chen, X.; et al. Productive HBV infection of well-differentiated, hNTCP-expressing human hepatoma-derived (Huh7) cells. *Viol. Sin.* **2017**, *32*, 465–475. doi:10.1007/s12250-017-3983-x.
 27. Qiao, L.; Sui, J.; Luo, G. Robust human and murine hepatocyte culture models of hepatitis B virus infection and replication. *J. Virol.* **2018**, *92*, e01255–18, doi:10.1128/jvi.01255-18.
 28. Asabe, S.; Wieland, S. F.; Chattopadhyay, P.K.; Roederer, M.; Engle, R. E.; Purcell, R. H.; Chisari, F. V. The size of the viral inoculum contributes to the outcome of hepatitis B virus infection. *J. Virol.* **2009**, *83*, 9652–9662. doi:10.1128/jvi.00867-09.
 29. Steenbergen, R.H.; Joyce, M. A.; Thomas, B.; Jones, D.; Law, J.; Russell, R.; Houghton, M.; Tyrrell, D. L. Human serum leads to differentiation of human hepatoma cells, restoration of very-low-density lipoprotein secretion, and a 1000-fold increase in HCV Japanese fulminant hepatitis type 1 titers. *Hepatology* **2013**, *58*, 1907–1917. doi:10.1002/hep.26566.
 30. Steenbergen, R.; Oti, M.; ter Horst, R.; Tat, W.; Neufeldt, C.; Belovodskiy, A.; Chua, T. T.; Cho, W. J.; Joyce, M.; Dutilh, B. E.; Tyrrell, D. L. Establishing normal metabolism and differentiation in hepatocellular carcinoma cells by culturing in adult human serum. *Sci. Rep.* **2018**, *8*, 11685. doi:10.1038/s41598-018-29763-2.
 31. Hart, S.N.; Li, Y.; Nakamoto, K.; Subileau, E.-A.; Steen, D.; Zhong, X.-B. A comparison of whole genome gene expression profiles of HepaRG cells and HepG2 cells to primary human hepatocytes and human liver tissues. *Drug Metab. Dispos.* **2010**, *38*, 988–994. doi:10.1124/dmd.109.031831.
 32. Guo, L.; Dial, S.; Shi, L.; Branham, W.; Liu, J.; Fang, J. L.; Green, B.; Deng, H.; Kaput, J.; Ning, B. Similarities and differences in the expression of drug-metabolizing enzymes between human hepatic cell lines and primary human hepatocytes. *Drug Metab. Dispos.* **2011**, *39*, 528–538. doi:10.1124/dmd.110.035873.
 33. Vondráček, J.; Souček, K.; Sheard, M.A.; Chramostová, K.; Andrysík, Z.; Hofmanová, J.; Kozubík, A. Dimethyl sulfoxide potentiates death receptor-mediated apoptosis in the human myeloid leukemia U937 cell line through enhancement of mitochondrial membrane depolarization. *Leuk. Res.* **2006**, *30*, 81–89. doi:10.1016/j.leukres.2005.05.016.

34. Song, Y.M.; Song, S.O.; Jung, Y.K.; Kang, E.S.; Cha, B.S.; Lee, H.C.; Lee, B. Dimethyl sulfoxide reduces hepatocellular lipid accumulation through autophagy induction. *Autophagy* **2012**, *8*, 1085–1097. doi:10.4161/auto.20260.
35. Galvao, J.; Davis, B.; Tilley, M.; Normando, E.; Duchon, M.R.; Cordeiro, M.F. Unexpected low-dose toxicity of the universal solvent DMSO. *FASEB J.* **2014**, *28*, 1317–1330. doi:10.1096/fj.13-235440.
36. Pal, R.; Mamidi, M.K.; Das, A.; Bhonde, R. Diverse effects of dimethyl sulfoxide (DMSO) on the differentiation potential of human embryonic stem cells. *Arch. Toxicol.* **2012**, *86*, 651–661. doi:10.1007/s00204-011-0782-2.
37. Verheijen, M.; Lienhard, M.; Schrooders, Y.; Clayton, O.; Nudischer, R.; Boerno, S.; Timmermann, B.; Selevsek, N.; Schlapbach, R.; Gmuender, H.; et al. DMSO induces drastic changes in human cellular processes and epigenetic landscape in vitro. *Sci. Rep.* **2019**, *9*, 4641. doi:10.1038/s41598-019-40660-0.
38. Xiang, C.; Du, Y.; Meng, G.; Yi, L.S.; Sun, S.; Song, N.; Zhang, X.; Xiao, Y.; Wang, J.; Yi, Z.; et al. Long-term functional maintenance of primary human hepatocytes in vitro. *Science* **2019**, *364*, 399–402. doi:10.1126/science.aau7307.
39. Schoggins, J.W.; MacDuff, D.A.; Imanaka, N.; Gainey, M.D.; Shrestha, B.; Eitson, J.L.; Mar, K.B.; Richardson, R.B.; Ratushny, A.V.; Litvak, V.; et al. Pan-viral specificity of IFN-induced genes reveals new roles for cGAS in innate immunity. *Nature* **2014**, *505*, 691–695. doi:10.1038/nature12862.
40. Ishida, Y.; Yamasaki, C.; Yanagi, A.; Yoshizane, Y.; Fujikawa, K.; Watashi, K.; Abe, H.; Wakita, T.; Hayes, C.N.; Chayama, K.; et al. Novel robust in vitro hepatitis B virus infection model using fresh human hepatocytes isolated from humanized mice. *Am. J. Pathol.* **2015**, *185*, 1275–1285. doi:10.1016/j.ajpath.2015.01.028.
41. Qu, B.; Ni, Y.; Lempp, F.A.; Vondran, F.W.R.; Urban, S. T5 exonuclease hydrolysis of hepatitis B virus replicative intermediates allows reliable quantification and fast drug efficacy testing of covalently closed circular DNA by PCR. *J. Virol.* **2018**, *92*, e01117–18. doi:10.1128/jvi.01117-18.
42. Liu, Y.; Le, C.; Tyrrell, D.L.; Le, X.C.; Li, X.-F. Aptamer binding assay for the E antigen of hepatitis B using modified aptamers with G-quadruplex structures. *Anal. Chem.* **2020**, *92*, 6495–6501. doi:10.1021/acs.analchem.9b05740.

43. Nishitsuji, H.; Ujino, S.; Shimizu, Y.; Harada, K.; Zhang, J.; Sugiyama, M.; Mizokami, M.; Shimotohno, K. Novel reporter system to monitor early stages of the hepatitis B virus life cycle. *Cancer Sci.* **2015**, *106*, 1616–1624. doi:10.1111/cas.12799.
44. Shlomai, A.; Schwartz, R.E.; Ramanan, V.; Bhatta, A.; De Jong, Y.P.; Bhatia, S.N.; Rice, C.M. Modeling host interactions with hepatitis B virus using primary and induced pluripotent stem cell-derived hepatocellular systems. *Proc. Natl. Acad. Sci. U.S.A.* **2014**, *111*, 12193–12198. doi:10.1073/pnas.1412631111.
45. Kidambi, S.; Yarmush, R.S.; Novik, E.; Chao, P.; Yarmush, M.L.; Nahmias, Y. Oxygen-mediated enhancement of primary hepatocyte metabolism, functional polarization, gene expression, and drug clearance. *Proc. Natl. Acad. Sci. U.S.A.* **2009**, *106*, 15714–15719. doi:10.1073/pnas.0906820106.
46. Meier, A.; Mehrle, S.; Weiss, T.S.; Mier, W.; Urban, S. Myristoylated PreS1-domain of the hepatitis B virus L-protein mediates specific binding to differentiated hepatocytes. *Hepatology* **2013**, *58*, 31–42. doi:10.1002/hep.26181.
47. Berg, F.V.D.; Limani, S.W.; Mnyandu, N.; Maepa, M.B.; Ely, A.; Arbuthnot, P. Advances with RNAi-based therapy for hepatitis B virus infection. *Viruses* **2020**, *12*, 851. doi:10.3390/v12080851.
48. Appelman, M.D.; Chakraborty, A.; Protzer, U.; McKeating, J.A.; Van De Graaf, S.F. N-Glycosylation of the Na⁺-taurocholate cotransporting polypeptide (NTCP) determines its trafficking and stability and is required for hepatitis B virus infection. *PLoS One* **2017**, *12*, e0170419. doi:10.1371/journal.pone.0170419.
49. Sargiacomo, C.; El-Kehdy, H.; Pourcher, G.; Stieger, B.; Najimi, M.; Sokal, E. Age-dependent glycosylation of the sodium taurocholate cotransporter polypeptide: From fetal to adult human livers. *Hepatol. Commun.* **2018**, *2*, 693–702. doi:10.1002/hep4.1174.
50. Lee, J.; Zong, L.; Krotow, A.; Qin, Y.; Jia, L.; Zhang, J.; Tong, S.; Li, J. N-Linked glycosylation is not essential for sodium taurocholate cotransporting polypeptide to mediate hepatitis B virus infection in vitro. *J. Virol.* **2018**, *92*, e00732–18. doi:10.1128/jvi.00732-18.

Chapter 3

A CRISPR Technique Incorporated with Single-Cell RNA Sequencing for Studying Hepatitis B Infection

3.1. Introduction

Single-cell RNA sequencing (scRNA-seq) advances studies of transcriptomes and improves the fundamental understanding of molecular events and cell heterogeneity [1-8]. The power of the scRNA-seq transcriptomic technology has been demonstrated in recent studies examining SARS-CoV-2 infection [9-14]. scRNA-seq analyses of bronchoalveolar immune cells in patients with COVID-19 [9-13] and scRNA-seq analyses of lung cells of African green monkeys [14] revealed changes in immune cell populations in response to SARS-CoV-2 infection and demonstrated the dynamics of SARS-CoV-2 infection and host immune responses. A detailed description of the COVID-19 immune landscape by scRNA-seq analyses of 1.46 million single cells showed that SARS-CoV-2 RNA is present in diverse epithelial and immune cells and that megakaryocytes and monocyte subsets may contribute to the cytokine storms characteristic of the infection [13].

Despite highly successful applications of scRNA-seq, determining expression levels of rare or low-abundance events remains a challenge. A typical workflow of scRNA-seq includes the generation of single-cell emulsions, reverse transcription of RNA to cDNA, concurrent addition of crucial molecular barcodes and identifiers for individual cells and samples, amplification of the barcoded cDNA using polymerase chain reaction (PCR), and high-throughput sequencing of the prepared single-cell library [1-8]. The PCR step amplifies all sequences and does not

preferentially enrich the low-abundance sequence. Therefore, highly abundant sequences in the library are sequenced more frequently, and the rare transcripts could be overlooked. Selective enrichment of low-abundance transcripts is necessary for them to be sequenced. Enrichment techniques, such as hybridization pull down, could be used during library preparation. We sought to enrich low-abundance HBV transcripts in an existing single-cell library.

We aimed to develop a selective enrichment technique that takes advantage of the clustered regularly interspaced short palindromic repeats (CRISPR) technology [15-22]. In particular, we made use of the nuclease activity of CRISPR to cleave highly abundant off-target sequences amplified by PCR, permitting selective enrichment of the low-abundance sequences for the subsequent high-throughput sequencing. We demonstrated the application of such a CRISPR-mediated selective enrichment technique to single-cell RNA sequencing of hepatoma cells infected with HBV.

Previous analysis of whole lysates of hepatoma cells infected with HBV showed that HBV did not affect the overall gene expression in the host cells [23-30]. It has been proposed that HBV is a “stealth virus”, neither evading nor stimulating the host antiviral responses, resulting in minimal changes to host gene expression following infection [25-27]. It is also possible that differences among individual cells were averaged out in such experiments. The low abundance of HBV transcripts relative to the much higher amounts of the host cell RNA makes scRNA-seq studies of the HBV infection challenging. We describe here a CRISPR-Cas9 technique for the depletion of high-abundance off-target products, resulting in the preferential enrichment of HBV transcripts and enabling scRNA-seq detection of HBV in infected cells.

3.2. Materials and Methods

3.2.1. Cell Culture and HBV Infection

Huh7.5-NTCP cells were cultured in Dulbecco's modified Eagle's medium (DMEM) (Sigma Aldrich, St. Louis, MO) supplemented with 4% pooled adult human serum (HS) [31]. Huh7.5-NTCP cells cultured and differentiated in DMEM and 4% HS for 21 days were infected with HBV at a multiplicity of infection (MOI) of 500 genome equivalents per cell in the presence of 4% PEG 8000 for 18 h at 37 °C. Cells treated similarly with 4% PEG 8000 (but not with HBV) served as the mock infection control. Another set of Huh7.5-NTCP cells were also treated with 1000 international units of interferon (IFN) alpha in the DMEM medium containing 4% HS for 24 h. The cells were washed three times with the medium prior to the preparation for scRNA-seq libraries.

3.2.2. Preparation of Single-Cell RNA Sequencing Libraries (Figure 3.1 and Table 3.1)

A single-cell suspension was prepared from trypsinized Huh7.5-NTCP cell monolayers. Cell suspension was used to generate the gel bead emulsions, reverse transcription, cDNA amplification, library preparation, and sample indexing (Figure 3.1 and Table 3.1) following the latest available manufacturer's protocol (10X Genomics, Pleasanton, CA).

Libraries for single-cell RNA sequencing were prepared according to the procedures of 10X Genomics (Pleasanton, CA). A single-cell suspension was prepared from Huh7.5-NTCP cell monolayer trypsinization. After trypsin neutralization using DMEM + 10% FBS, the cells were centrifuged at 500×g for 5 min to remove supernatant. Following several washes with 1× PBS + 10% FBS, cell pellets were resuspended in 500 µL of 1× PBS + 0.1% BSA. Cell counts and viability were assessed using a Neubauer chamber and 0.4% Trypan blue solution (ThermoFisher Catalog number: 15250061). Single cell suspensions of >95% viability were selected and

resuspended with the appropriate volume of $1 \times \text{PBS} + 0.1\% \text{BSA}$ to reach a concentration of $1000 \text{ cells}/\mu\text{L}$. The cell suspension was then used to generate the gel bead emulsions, reverse transcription, cDNA amplification, library preparation, and sample indexing following the latest available manufacturer's protocol (**Figure 3.1**), using the 10X Chromium Controller (PN-1000202), the Chromium Next GEM Single Cell 3' GEM, Library & Gel Bead Kit v3 (PN-1000075), the Chromium Next GEM Chip B Single Cell Kit (PN-1000073), and the Single Index Chromium i7 Multiplex Kit (PN-120262). The transcripts in the library for sequencing were typically between 120 nucleotides (nt) and 420 nt in length.

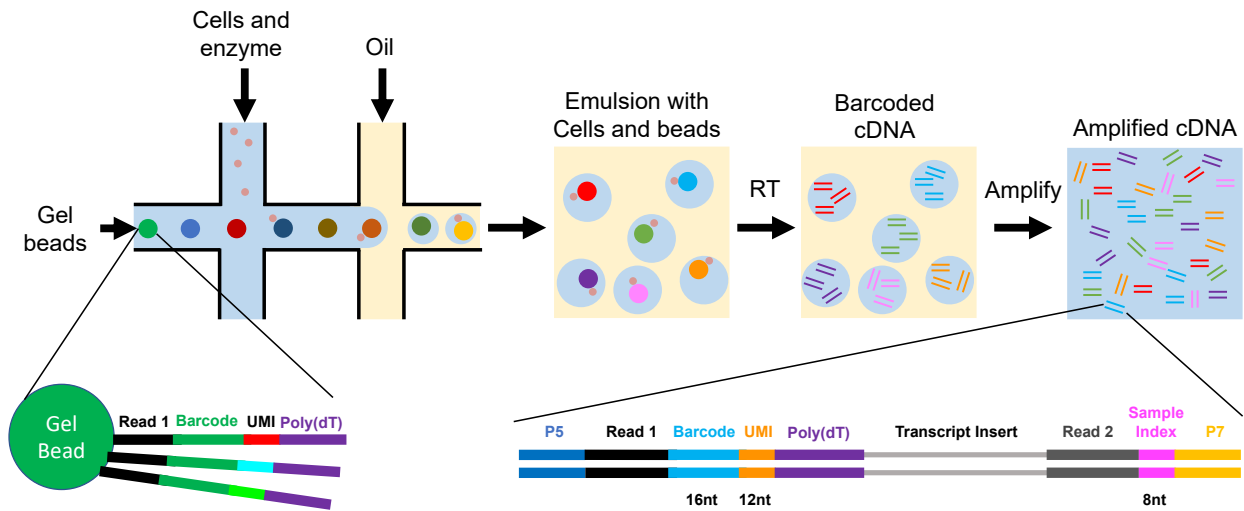


Figure 3.1. Schematic showing the processes for the preparation of a single-cell RNA sequencing (scRNA-seq) library. A 10X Genomics platform (Pleasanton, CA) was used for the preparation of the scRNA-seq library. The library was prepared for the subsequent Sequencing-by-Synthesis approach using the Illumina HiSeq technology [32].

Table 3.1. Sequences used for the preparation of 10X Genomics library.

Name	Sequence (5' to 3')
P5 (adaptor, graft-binding seq)	AATGATACGGCGACCACCGAGATCT
P7 (adaptor, graft-binding seq)	ATCTCGTATGCCGTCTTCTGCTTG
P7 reverse complement	CAAGCAGAAGACGGCATAACGAGAT
Read 1 (primer-binding seq)	ACACTCTTTCCCTACACGACGCTCTTCCGATCT
Read 2 (primer-binding seq)	AGATCGGAAGAGCACACGTCTGAACTCCAGTCAC
Read 2 reverse complement	GTGACTGGAGTTCAGACGTGTGCTCTTCCGATCT
Barcode (unique to cell/gel bead)	Random 16 nt (unique to cell/gel bead)
UMI (Unique Molecular Identifier) (unique to transcript)	Random 12 nt (unique to transcript)
Sample Index (unique to sample)	Four sequences of 8 nt each
Sample Index for HBV-treated cells	GAAACCCT ; TTTCTGTC ; CCGTGTGA ; AGCGAAAG
Sample Index for cells treated with HBV and IFN	GTCCGGTC ; AAGATCAT ; CCTGAAGG ; TGATCTCA
Transcript insert	Results obtained from Next-Generation Sequencing

3.2.3. Single-Cell RNA Sequencing

The libraries were sequenced by Novogene (Sacramento, CA) using the HiSeq PE150 sequencing-by-synthesis platform (Illumina, San Diego, CA). Samples were pooled in equimolar concentration and loaded into an Illumina HiSeq PE150. Paired-end and single-indexing parameters were used to sequence at an average depth of ~25,000 reads per cell.

3.2.4. Data Analysis

The Seurat V3 software package, developed and maintained by Dr. R. Satija and collaborators (<https://satijalab.org/seurat/>), was used for the analysis of the datasets generated from the scRNA-seq experiments. This free package was developed and is maintained by the Satija lab and released under the GNU Public License (GPL 3.0). “Seurat is an R package designed for QC, analysis, and exploration of single-cell RNA-seq data. Seurat aims to enable users to identify and interpret subpopulations of cells in the sample from single-cell transcriptomic measurements, and to integrate diverse types of single-cell data” (<https://satijalab.org/seurat/>). Uniform Manifold Approximation and Projection (UMAP) graphs were generated and gene clustering analyses were conducted using the corresponding scripts within the Seurat V3 package followed the procedures of Stuart *et al.* [1].

3.2.5. PCR Technique for the Enrichment of HBV Reads (Figure 3.2 and Table 3.2)

The libraries were PCR-amplified to enrich for sequences containing HBV transcripts (Figure 3.2 and Table 3.2). Primer sequences for the PCR are shown in Table 3.2. The first step involved an extension reaction to linearly amplify the sequences containing the last 120 nt (from the 3' end) of the HBV transcripts. Since all HBV transcripts share a common 3' end, a single primer was used to linearly amplify all HBV transcripts. The second PCR exponentially amplified the product from the extension reaction. The third step was an overlap PCR to add the sample index with an adapter to the library. The PCR products were purified using agarose gel electrophoresis and the MinElute Gel Extraction kit (Qiagen). The resulting purified product was submitted for next-generation sequencing.

The libraries were prepared from four samples of Huh7.5-NTCP cells under the following treatments: mock infection (control), HBV-infected, mock infection and interferon (IFN)

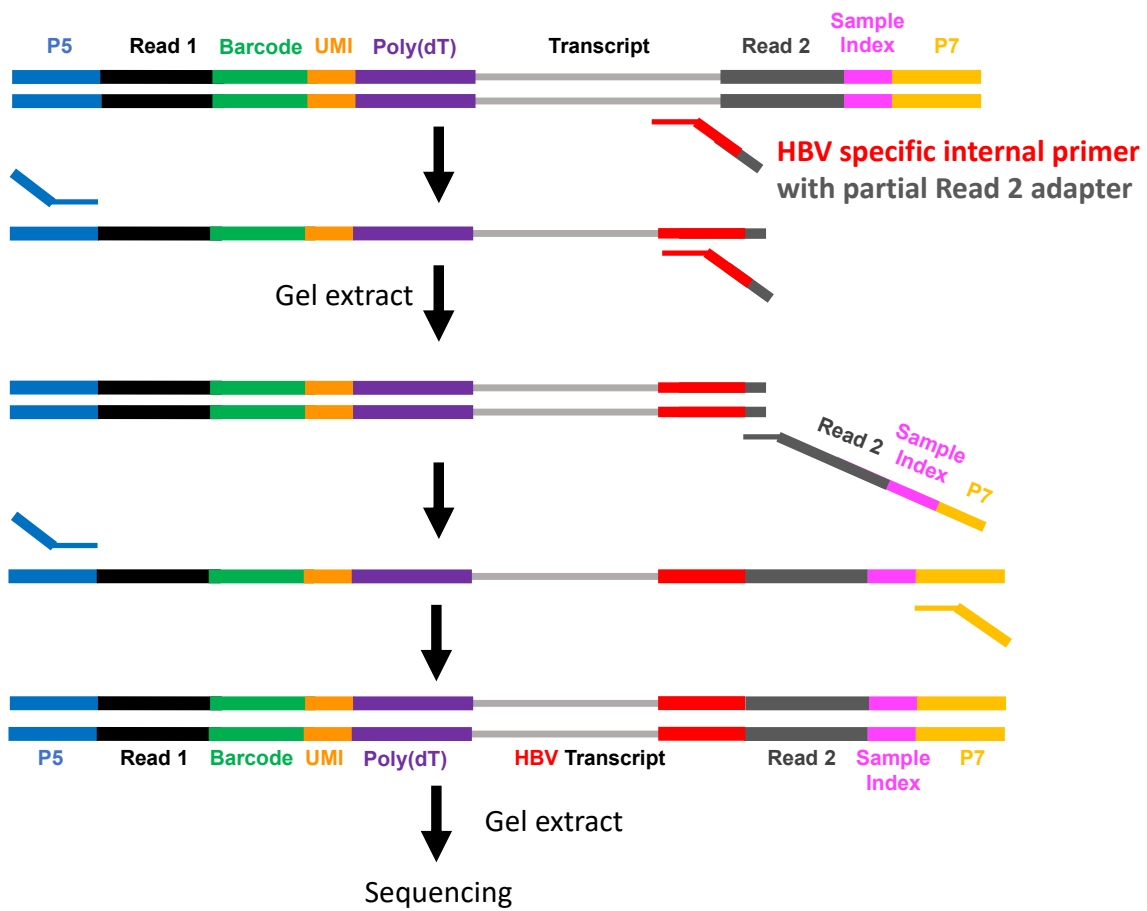
treatment, and HBV-infected and IFN treatment. An outline of the protocol is shown in **Figure 3.2**. Briefly, P5 forward primer and a nested HBV-specific internal reverse primer with partial Read 2 adaptor were used to amplify the sequences containing the last 120 nt of the HBV RNA (located at the 3' end of HBV RNA). P7-Sample index-Read 2 reverse primer was used to add the Read 2 sequence, sample index sequences, and P7 sequence onto the enriched sequences through overlap PCR. Each sample has a specific sample index composed of four sample codes in equal molecular concentration. Therefore, each sample has specific P7-Sample index-Read 2 reverse primers. Read 2, sample indices, and P7 sequences are required for sequencing. Finally, P5 forward primer and P7 reverse primer were used to further amplify the enriched sequences to generate sufficient PCR product for next-generation sequencing.

More specifically, the first step of the PCR enrichment was an extension reaction to linearly amplify the sequences containing the last 120 nt on the 3' end of the HBV transcript. Since all HBV transcripts share the same 3' sequence, a single primer can be used for this linear amplification step. A HBV-specific internal reverse primer with partial Read 2 adaptor was used. Each PCR reaction (25- μ L) included 2 μ L of pre-made library, 1 \times PCR reaction buffer, 2.0 mM MgCl₂, 0.4 μ M reverse primer, 0.2 mM dNTPs (New England Biolabs. NEB, Whitby, ON), 5% DMSO, 1 U of platinum Taq DNA polymerase (Invitrogen, Waltham, MA), and 16.55 μ L of deionized water. Thermocycling (MJ Mini Gradient Thermocycler; Bio-Rad, Hercules, CA) parameters were: denaturation at 94 °C for 10 min, followed by 35 cycles of denaturation at 94 °C for 30 s, annealing at 55 °C for 30 s, and extension at 72 °C for 30 s. After the last cycle of PCR, a final extension step was done at 72 °C for 5 min. The linear amplification with 35 cycles of the extension reaction would increase the copy numbers of the HBV transcript by 35 times.

The second step was exponential PCR amplification of the product from the first step, using P5 forward primer and the HBV-specific internal reverse primer with partial Read 2 adaptor. In this PCR reaction, a high fidelity polymerase, Platinum SuperFiDNA polymerase (Invitrogen) was used. Each PCR reaction (50- μ L) included 1 \times PCR SuperFi Buffer, 0.5 μ M forward primer, 0.5 μ M reverse primer, 0.2 mM dNTPs (NEB), 1 U of platinum SuperFi DNA polymerase (Invitrogen), 28.5 μ L of deionized water, and 5 μ L of template from extension reaction described above. PCR was conducted on the MJ Mini Gradient Thermocycler (Bio-Rad), and the conditions were: initial denaturation at 98 $^{\circ}$ C for 30 s, followed by 40 cycles of denaturation at 98 $^{\circ}$ C for 10 s, annealing at 65 $^{\circ}$ C for 10 s, and extension at 72 $^{\circ}$ C for 30 s. After the last cycle of PCR, a final extension step was done at 72 $^{\circ}$ C for 5 min.

The PCR products were separated using gel electrophoresis on a 1.5% agarose gel in 1 \times TBE buffer at 100 V. The gels were stained with ethidium bromide (Thermo Fisher Scientific, Waltham, MA) and photographed under UV light. All PCR products were purified using a MinElute Gel Extraction kit (Qiagen, Valencia, CA) according to the recommended procedures. The third step was an overlap PCR to add the sample index to the library. The products from the above second PCR were used as templates to perform the following overlap PCR. In each overlap PCR, 100 μ L mixtures included 30 nM of the above PCR products, 1 \times PCR SuperFi Buffer, 30 nM P7-Sample index-Read 2 reverse primer, 0.2 mM dNTPs (NEB), 1 U of platinum SuperFi DNA polymerase (Invitrogen), and deionized water to a final volume of 100 μ L. The overlap PCR was performed on the MJ Mini Gradient Thermocycler (Bio-Rad) using the following conditions: initial denaturation at 98 $^{\circ}$ C for 30 s, followed by 15 cycles of denaturation at 98 $^{\circ}$ C for 10 s, annealing at 57 $^{\circ}$ C for 10 s, and extension at 72 $^{\circ}$ C for 30 s. After 15 cycles, a final extension step was done at 72 $^{\circ}$ C for 5 min. After the overlap PCR, P5 forward primer and

P7 reverse primer (10 μ M) were added into each reaction to reach their final concentrations of 0.5 μ M. PCR was performed again on the MJ Mini Gradient Thermocycler with an initial denaturation at 98 °C for 30 s, followed by 30 cycles of denaturation at 98 °C for 10 s, annealing at 65 °C for 10 s, and extension at 72 °C for 30 s. After 30 cycles, a final extension step was at 72 °C for 5 min. Then, the PCR products were purified using agarose gel electrophoresis and then the MinElute Gel Extraction kit (Qiagen). The resulting purified product (enriched HBV transcripts) was submitted for next-generation sequencing.



7

Figure 3.2. Schematic showing a polymerase chain reaction (PCR) technique for the enrichment of the HBV transcripts in the scRNA-seq library. The library for sequencing was prepared from the HBV-infected Huh7.5-NTCP cells.

Table 3.2. Primers used for the PCR enrichment of the HBV transcript in the scRNA-seq library.

Steps	Primers	Sequence (5' to 3')
Extension reaction (linear amp.)	HBV-specific internal reverse primer with partial Read 2 adaptor	GTGTGCTCTTCCGATCT CTTTTTCACCTCTGCCTAATCATC (Letters highlighted in yellow are partial Read 2 adaptor sequence) (Letters highlighted in purple are sequences from the HBV transcript)
PCR exponential amp.	P5 forward primer	AATGATACGGCGACCACCGAGATCT
	HBV-specific internal reverse primer with partial Read 2 adaptor	GTGTGCTCTTCCGATCT CTTTTTCACCTCTGCCTAATCATC (Letters highlighted in yellow are partial Read 2 adaptor sequence) (Letters highlighted in purple are sequences from the HBV transcript)
Overlap PCR	P7-Sample index-Read 2 reverse primer	CAAGCAGAAGACGGCATAACGAGAT – NNNNNNNN – GTGACTGGAGTTCAGAC GTGTGCTCTTCCGATCT
	P5 forward primer	AATGATACGGCGACCACCGAGATCT
	P7 reverse primer	CAAGCAGAAGACGGCATAACGAGAT

3.2.6. CRISPR-Cas9 Technique for the Depletion of High-Abundance Transcripts and Enrichment of HBV Transcripts

In the PCR enrichment technique described in Section 3.2.5, a few nucleotides complementary at the 3' end of the “HBV-specific internal reverse primer with partial Read 2 adaptor” could potentially result in off-target (non-specific) amplification. Sequence searches identified several such targets. For example, there is complementarity between 7 nt near the 3' end of the reverse primer and the MT-ATP6 transcript at four sites, which could produce fragments from the first linear amplification step of approximately 50, 460, 540, and 545 base

pairs (bp) in length. In the case of the SLC38A7 transcript, various 7-nt stretches near the 3' end of the reverse primer were complementary to several sites at the 3' end of this transcript. There is also complementarity between a 7-nt portion of the reverse primer and the 3' ends of the MT-ATP6 and SLC38A7 transcripts, which could cause linear amplification in the 3' to 5' direction of the transcript. Depending on the length of the transcript fragment incorporated into the single cell library, short, 100-150 bp PCR products of the MT-ATP6 and SLC38A7 transcripts could be subsequently amplified exponentially with the P7 primer. Another off-target PCR product could be due to 7 nt in the reverse primer binding to the 3' end of the MT-ND2 transcript, which might produce an approximately 155-bp fragment.

To overcome this problem, a CRISPR-Cas9 technique was used to cleave the three most abundant off-target PCR products (MT-ATP6, SLC38A7 and MT-ND2) exponentially amplified by HBV enrichment PCR (**Figure 3.3** and **Table 3.3**). Three single-guide RNA (sgRNA) sequences (**Table 3.3**) were designed to target each of these three abundant products, with the objective of cleaving ~120 nt from the 3' end of these three PCR products. Each sgRNA was designed, using Alt-R[®] CRISPR-Cas9 guide RNA design tool (Integrated DNA Technologies, IDT, Coralville, IA), to contain a crRNA sequence and a tracrRNA sequence. The crRNA was a 20-nt sequence complementary to the target DNA, and the tracrRNA served as a binding scaffold for the Cas9 nuclease. Chemical modifications shown in the sgRNA sequences (**Table 3.3**) were for the purpose of improving the stability of sgRNA. All the sgRNA sequences were obtained from IDT (Coralville, IA).

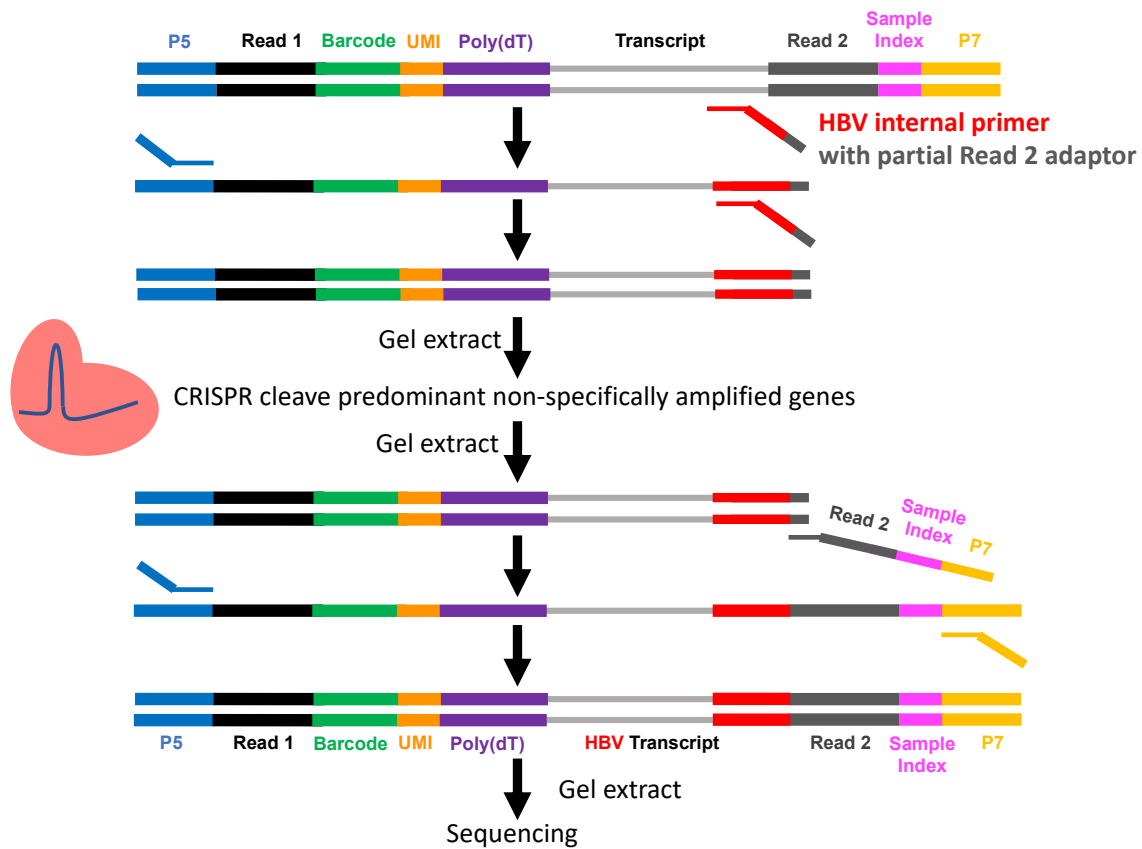


Figure 3.3. Schematic showing a CRISPR-Cas9 technique incorporated with PCR for the enrichment of HBV transcripts in the scRNA-seq library. The library for sequencing was prepared from the HBV-infected Huh7.5-NTCP cells.

Table 3.3. Single guide RNA (sgRNA) sequences used for the CRISPR-Cas9 technique to deplete three abundant sequences.

Name	Strand	DNA sequence corresponding to crRNA sequence (5' to 3')	sgRNA sequence including both crRNA and <i>tracrRNA</i> sequences (5' to 3')	PAM
MT-ATP6	-	TACTAGAAGTGTGAAAACGT	mU*mA*mC* rUrArG rArArG rUrGrU rGrArA rArArC rGrUrG rUrUrU rUrArG rArGrC rUrArG rArArA rUrArG rCrArA rGrUrU rArArA rArUrA rArGrG rCrUrA rGrUrC rCrGrU rUrArU rCrArA rCrUrU rGrArA rArArA rGrUrG rGrCrA rCrCrG rArGrU rCrGrG rUrGrC mU*mU*mU* rU	AGG
SLC38A7	+	AAGGGAAGATGGTTAATAAA	mA*mA*mG* rGrGrA rArGrA rUrGrG rUrUrA rArUrA rArArG rUrUrU rUrArG rArGrC rUrArG rArArA rUrArG rCrArA rGrUrU rArArA rArUrA rArGrG rCrUrA rGrUrC rCrGrU rUrArU rCrArA rCrUrU rGrArA rArArA rGrUrG rGrCrA rCrCrG rArGrU rCrGrG rUrGrC mU*mU*mU* rU	AGG
MT-ND2	-	ATAAGATTATTAGTATAAAA	mA*mU*mA* rArGrA rUrUrA rUrUrA rGrUrA rUrArA rArArG rUrUrU rUrArG rArGrC rUrArG rArArA rUrArG rCrArA rGrUrU rArArA rArUrA rArGrG rCrUrA rGrUrC rCrGrU rUrArU rCrArA rCrUrU rGrArA rArArA rGrUrG rGrCrA rCrCrG rArGrU rCrGrG rUrGrC mU*mU*mU* rU	GGG

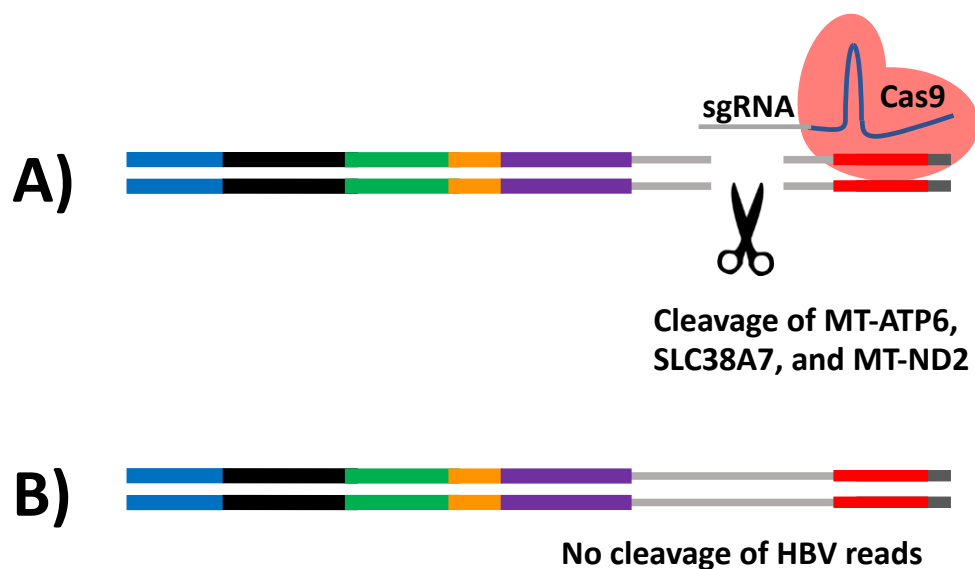


Figure 3.4. Schematic showing a CRISPR-Cas9 technique used to cut the three most abundant off-target PCR products (MT-ATP6, SLC38A7 and MT-ND2). (A) The Cas9-sgRNA ribonucleoprotein (RNP) complexes specifically cleave MT-ATP6, SLC38A7, and MT-ND2, using the specific sgRNA sequences designed to target them. (B) The sgRNA sequences do not target the HBV PCR product; and thus there is no cleavage of the HBV targets.

Prior to the CRISPR-mediated cleavage reaction, the sgRNA was refolded by first denaturing at 90 °C for 5 min and then slowly cooling to 25 °C at a rate of 0.1 °C per second. The Cas9-sgRNA ribonucleoprotein (RNP) complex was prepared by incubating 1 μM sgRNA, 0.5 μM Cas9 (NEB), and 1× NEB buffer3.1 in a 30-μL mixture at 37 °C for 30 min. The resulting RNP complex was used for the following CRISPR-mediated cleavage reactions.

The CRISPR-mediated cleavage reaction (100 μL) for each sample contained 40 nM purified PCR product from the PCR enrichment reaction described above, 25 μL each of the

Cas9-sgRNA RNP complex specifically targeting MT-ATP6, SLC38A7, and MT-ND2, and 1× NEB buffer3.1. Each reaction mixture was incubated at 37 °C for 16 h, followed by 95 °C for 10 min. The CRISPR-mediated cleavage was designed to cut MT-ATP6, SLC38A7, and MT-ND2, but keep the HBV transcript intact (**Figure 3.4**). The resulting product was separated on an agarose gel (**Figure 3.5A**). The 255-bp band of lane 6 (HBV-infected sample) and lane 8 (HBV-infected and interferon treated cell sample) on the gel, corresponding to the size of HBV transcript with markers, was extracted and purified using the MinElute Gel Extraction kit (Qiagen) according to the recommended procedures.

The products from the above CRISPR treatment (lanes 6 and 8) were used as templates to perform the following overlap PCR, which added the sample index to the sequence library. In each overlap PCR, 100 µL mixtures included 7.5 nM CRISPR-treated product, 1× PCR SuperFi Buffer, 1× PCR SuperFi GC Enhancer, 7.5 nM P7-Sample index-Read 2 reverse primer, 0.2 mM dNTPs (NEB), 2 U of platinum SuperFi DNA polymerase (Invitrogen), and deionized water to a final volume of 100 µL. The overlap PCR was performed on the MJ Mini Gradient Thermocycler (Bio-Rad) using the following conditions: initial denaturation at 98 °C for 1 min, followed by 10 cycles of denaturation at 98 °C for 10 s, annealing at 57 °C for 10 s, and extension at 72 °C for 30 s. After 10 cycles, a final extension step was at 72 °C for 5 min. After the overlap PCR, P5 forward primer and P7 reverse primer (10 µM) were added into each reaction to reach their final concentrations of 0.2 µM. The final PCR was again performed on the MJ Mini Gradient Thermocycler using the following conditions: an initial denaturation at 98 °C for 1 min, followed by 10 cycles of denaturation at 98 °C for 10 s, annealing at 65 °C for 10 s, and extension at 72 °C for 30 s. After 10 cycles, a final extension step was done at 72 °C for 5 min. The PCR products were purified using agarose gel electrophoresis (**Figure 3.5B**) and then a

MinElute Gel Extraction kit (Qiagen). The purified product (enriched HBV transcripts) was submitted for sequencing.

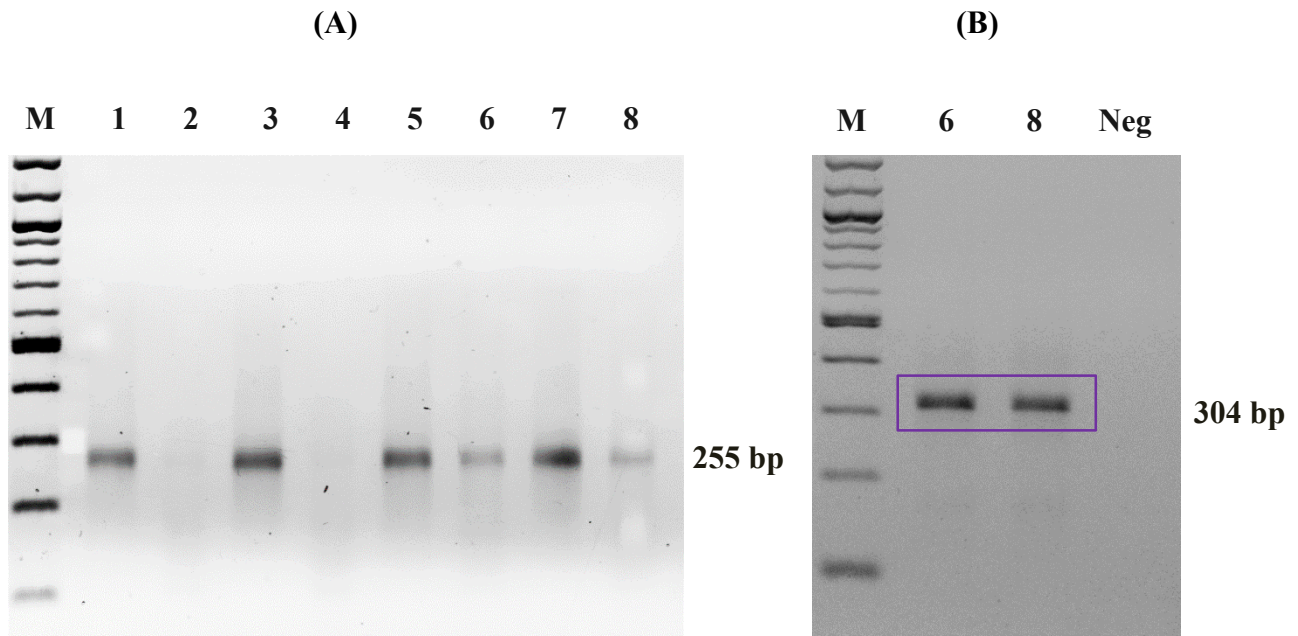


Figure 3.5. Electrophoresis gels showing (A) the 255-bp PCR products before (lanes 1, 3, 5, and 7) and after (lanes 2, 4, 6, and 8) CRISPR cleavage, and (B) final enriched 304-bp HBV transcripts. Samples were Huh7.5-NTCP cells uninfected (1 and 2), uninfected but interferon treated (3, and 4), HBV infected (5 and 6), and HBV and interferon treated (7 and 8).

3.3. Results and Discussion

Results from direct scRNA-seq analysis of two sets of Huh7.5-NTCP cells, HBV infected and the corresponding control (mock infection), are depicted in **Figure 3.6** and **Table 3.4**. These results indicate that only 0.6% of the cells in the HBV-infected population had detectable HBV transcripts (**Figure 3.6**). This was surprising because in hepatoma cell lines over-expressing NTCP, typically 50–80% of the cells were infected when the HBV inoculum was high

(500–1000 genome equivalents per cell) [31,33,34]. The scRNA-seq technique is designed to detect transcripts in proportion to their frequency in the RNA population. High-abundance sequences are detected frequently, but low-abundance sequences have lower chances of being detected. We hypothesized that the infrequent detection of HBV-infected cells could be due to the rarity of HBV transcripts in the RNA population. This rarity might be due to poor infection or a low level of HBV transcripts within infected cells or both.

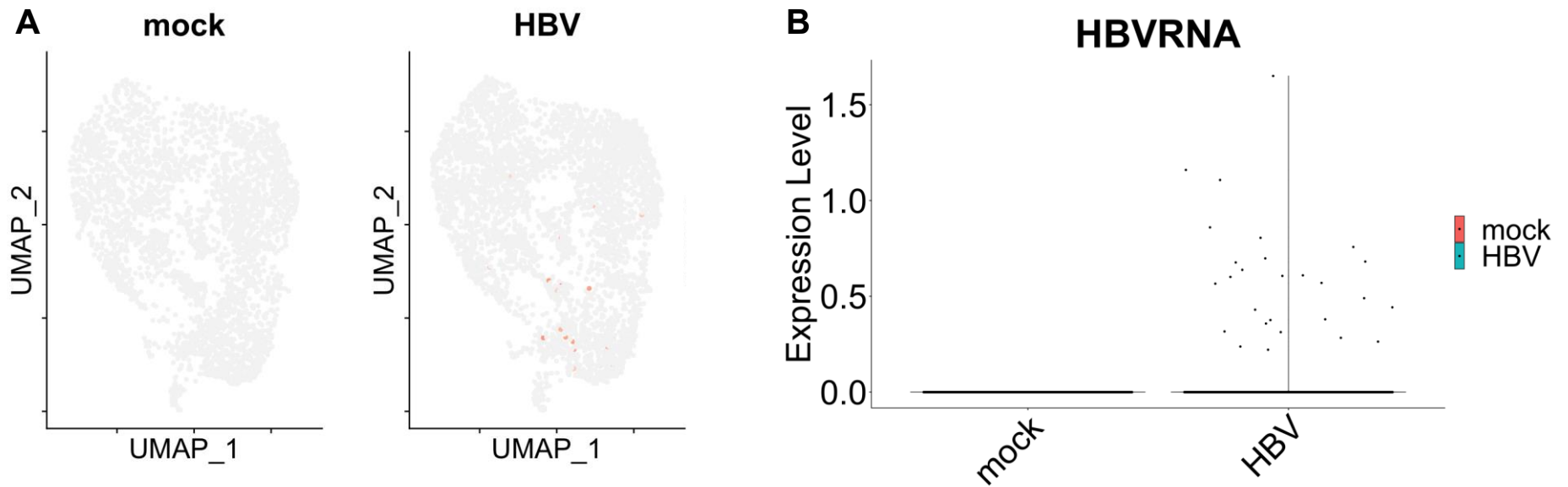


Figure 3.6. scRNA-seq analysis of Huh7.5-NTCP cells without performing genome enrichment. The Huh7.5-NTCP cells were mock-infected (control) or infected with HBV. (A) Each grey dot represents a cell and the red dots represent cells that had detectable HBV RNA. (B) Relative expression level (normalized across single cells in natural Ln scale) of HBV RNA in individual cells. UMAP denotes Uniform Manifold Approximation and Projection.

To increase the frequency of HBV RNA being detected, we amplified HBV transcripts in the scRNA-seq library using polymerase chain reaction (PCR) (**Figure 3.2**) and sequenced the enriched samples. The UMAP plots in **Figure 3.7** indicate that approximately 7% of the cells in the HBV-infected Huh7.5-NTCP cell population now had detectable HBV genes.

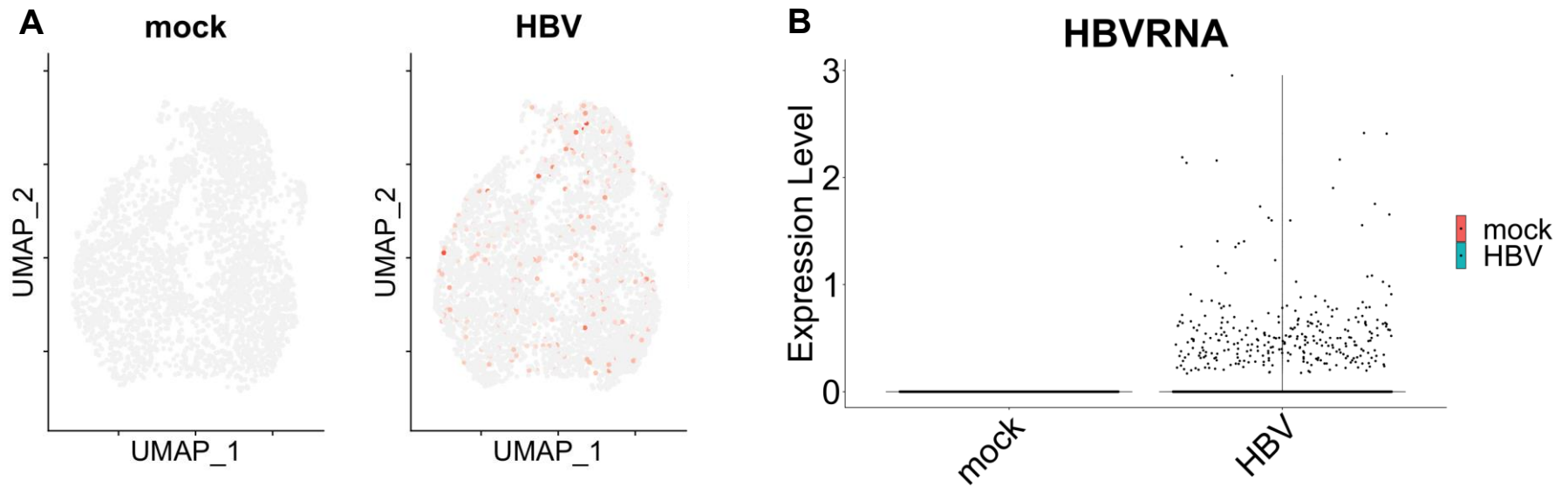


Figure 3.7. scRNA-seq analysis of Huh7.5-NTCP cells after genome enrichment using PCR. The Huh7.5-NTCP cells were mock-infected (control) or infected with HBV. (A) Each grey dot represents a cell and the red dots represent cells that had detectable HBV RNA. (B) Relative expression level (normalized across single cells in natural Ln scale) of HBV RNA in individual cells.

Sequencing analysis showed that PCR amplification enriched not only HBV transcripts but also other highly abundant human gene transcripts. This analysis showed that *MT-ATP6*, *SLC38A7*, and *MT-ND2* were the three most abundant genes sequenced after PCR enrichment for HBV sequences. They encode for mitochondrially encoded ATP synthase 6 (MT-ATP6), solute carrier family 38 member 7 (SLC38A7), and mitochondrially encoded NADH dehydrogenase 2 (MT-ND2). Their sequences are shown in **Table 3.3**. Their relative abundance was up to 310 times (for *MT-ATP6*) higher than that of the HBV transcript.

To overcome the challenge of these highly abundant transcripts, we designed a CRISPR technique (**Figure 3.3**) to deplete the three most abundant off-target transcripts after the first step of scRNA-seq library synthesis. **Figure 3.8** shows that the majority (74%) of the HBV-infected Huh7.5-NTCP cells had detectable HBV gene expression after this enrichment. It is possible that the remaining 26% of the cells are still below the levels of detection of single cell sequencing or are actually uninfected. Previous results using immunofluorescence staining of HepaRG cells indicate a variety of expression levels of HBV proteins [25-27,35]. It is also possible that expression of antigens and RNA declines as covalently closed circular DNA (cccDNA) is established, as is indicated by the lack of correlation between a specific cccDNA probe and antigen expression in biopsy samples [36]. Our results show that the technique of using CRISPR-Cas9 to deplete the abundant genes enabled successful enrichment of the HBV genes for single-cell RNA sequencing.

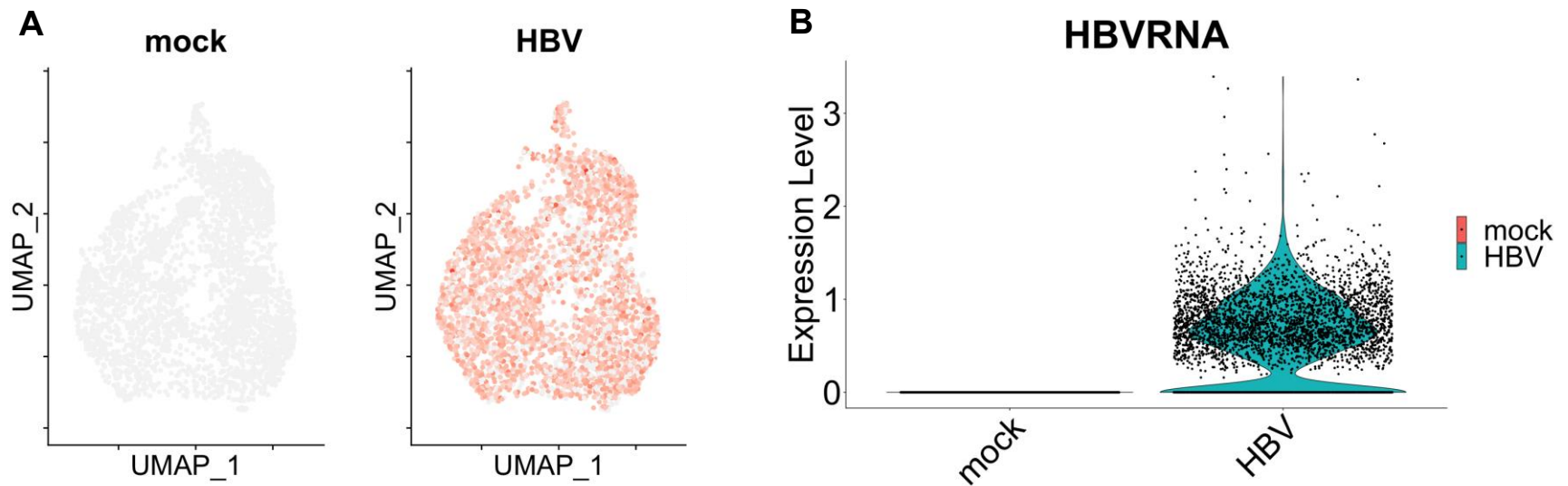


Figure 3.8. scRNA-seq analysis of Huh7.5-NTCP cells after genome enrichment using PCR amplification and CRISPR technique.

The Huh7.5-NTCP cells were mock-infected (control) or infected with HBV. (A) Each dot represents a cell, and the red dots represent cells that had detectable HBV RNA. (B) Relative expression level (normalized across single cells in natural Ln scale) of HBV RNA in individual cells. The “violin” plot on the right depicts the distribution of the expression level of the HBV RNA in the cells.

Table 3.4. Percent of Huh7.5-NTCP cells determined to contain HBV RNA

Samples	Percentage
Original sample	0.6
PCR amplified	7
CRISPR treated	74

Having succeeded in the selective enrichment of the HBV transcripts (**Table 3.4**) and obtained sequencing data from the HBV-infected Huh7.5-NTCP cells, we further analyzed the gene clusters in cell samples after four treatments of the cells: control (mock infection), HBV infection, interferon alpha (IFN) treatment, and HBV infection plus IFN treatment (**Figure 3.9**). The first pair, mock versus HBV, evaluates whether HBV influences the overall gene expression within the cells; and the second pair, which was treated with interferon, addresses whether HBV infection augments the action of interferon. In previous studies it has been suggested that HBV is a “stealth virus”, which neither induces an antiviral response, nor inhibits an externally induced interferon response; however, these studies examined bulk samples [35]. The gene clusters between the control (mock infection) and HBV-infected cells are similar, suggesting that HBV infection did not significantly alter gene expression of the host cells. In contrast, the treatment with IFN dramatically changed the gene expression pattern of Huh7.5-NTCP cells, as depicted by the gene cluster patterns (**Figure 3.9**). Again, this pattern of transcripts was not altered by HBV infection. These results from single-cell RNA sequencing are consistent with those of bulk experiments, suggesting that HBV is a “stealth virus”: it neither stimulated nor suppressed the IFN responses [23-30].

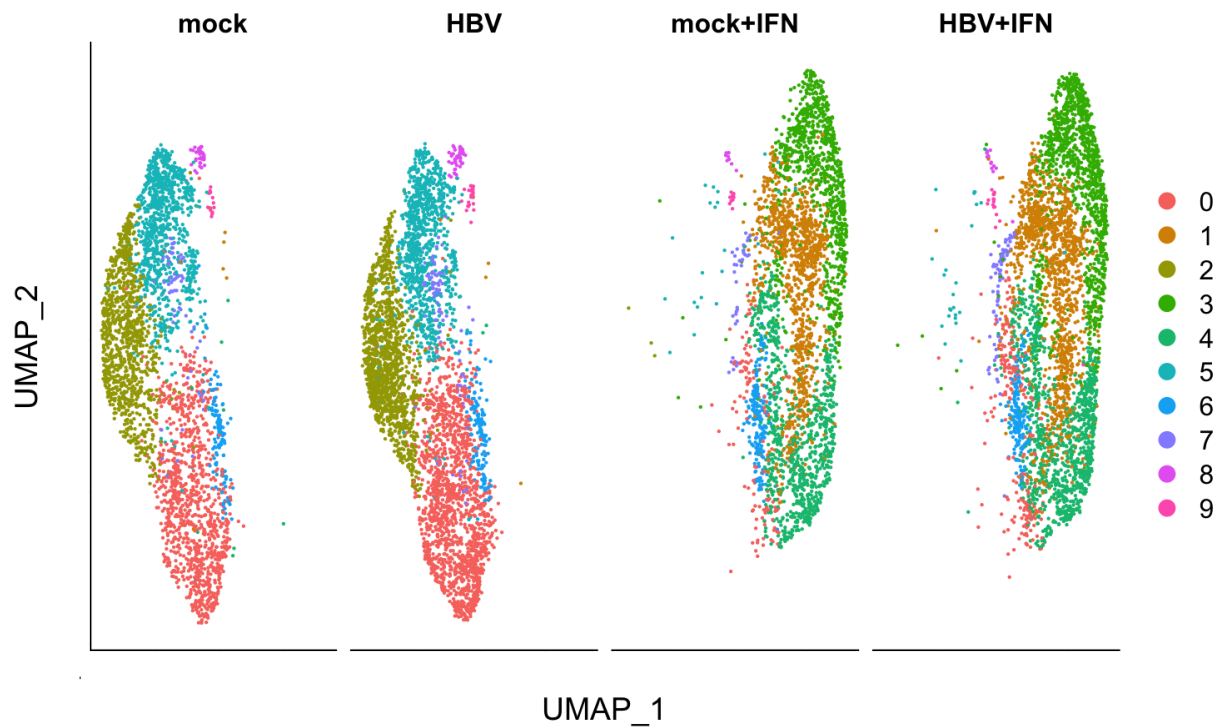


Figure 3.9. Clustering analysis of the scRNA-seq data from the Huh7.5 NTCP cells under four different treatment conditions: mock infection, infected with HBV, mock infection and IFN treatment, and infected with HBV plus treatment with IFN. Results represent the analysis of 7370 cells. The analysis has organized the cells into 10 clusters based on gene expression.

The single-cell RNA sequencing approach produced an average depth of ~25,000 reads per cell. Without any selective enrichment, the sequencing analysis detected viral RNA in 0.6% of the cells. This means that the relative viral concentration is below 1:25,000 transcripts in 99.4% of the cells. After the PCR and CRISPR-mediated selective enrichment, the sequencing analysis detected viral RNA in 74% of the cells. Selective enrichment is critical for scRNA-seq analysis of low-abundance genes.

The CRISPR technique enabled the successful enrichment of HBV transcript and played an important role in detecting HBV RNA in the cells. The ability to sequence HBV RNA occurring at a low abundance in the cells confirmed that the majority of the HBV-infected cells had HBV RNA. Thus, the observation of no significant difference between the control (mock infection) and HBV-infected Huh7.5-NTCP cells in gene expression patterns pointed to HBV being a “stealth virus”. This conclusion would not have been reached without the successful enrichment of HBV transcript for scRNA-seq in the HBV-infected cells.

3.4. Conclusions

Single-cell RNA sequencing (scRNA-seq) provides rich transcriptomic information for studying molecular events and cell heterogeneity at the single-cell level. However, it is challenging to obtain sequence information from rare or low-abundance genes in the presence of other highly abundant genes. This chapter illustrates a CRISPR-Cas9 technique for the depletion of high-abundance transcripts, resulting in preferential enrichment of rare transcripts. Direct sequencing without the CRISPR-mediated enrichment detected HBV RNA in only 0.6% of the cells. The CRISPR-mediated depletion of the three most abundant transcripts resulted in selective enrichment of the HBV transcripts and successful detection of HBV RNA in more than 74% of the cells. The improvement enabled a study of HBV infection and interferon treatment of a liver cell model. Gene clusters between the control and HBV-infected Huh7.5-NTCP cells were similar, suggesting that HBV infection did not significantly alter gene expression of the host cells. The treatment with interferon alpha dramatically changed the gene expression landscape of Huh7.5-NTCP cells. This landscape was again not altered by HBV infection. These results from the scRNA-seq analysis of 7370 cells are consistent with other studies of cell lysate

experiments, suggesting that HBV is a “stealth virus”. The contents of this chapter have been published (Le, C.; Liu, Y.; Lopez-Orozco, J.; Joyce, M.A.; Le, X.C.; Tyrrell, D.L. CRISPR technique incorporated with single-cell RNA sequencing for studying hepatitis B infection. *Analytical Chemistry*, **2021**, *93*, 10756–10761). Permission for reproduction of this published paper in this thesis was granted by the American Chemical Society (ACS) Publications Support.

3.5. References

1. Stuart, T.; Butler, A.; Hoffman, P.; Hafemeister, C.; Papalexi, E.; Mauck III, W.M.; Hao, Y.; Stoeckius, M.; Smibert, P.; Satija, R. Comprehensive integration of single-cell data. *Cell* **2019**, *177*, 1888–1902. doi: 10.1016/j.cell.2019.05.031
2. Tanay, A.; Regev, A. Scaling single-cell genomics from phenomenology to mechanism. *Nature* **2017**, *541*, 331–338. doi: 10.1038/nature21350
3. Giladi, A.; Amit, I. Single-cell genomics: a stepping stone for future immunology discoveries. *Cell* **2018**, *172*, 14–21. doi: 10.1016/j.cell.2017.11.011
4. Svensson, V.; Vento-Tormo, R.; Teichmann, S.A. Exponential scaling of single-cell RNA-seq in the past decade. *Nat. Protoc.* **2018**, *13*, 599–604. DOI: 10.1038/nprot.2017.149
5. Zheng, G.X.Y.; Terry, J.M.; Belgrader, P.; Ryvkin, P.; Bent, Z.W.; Wilson, R.; Ziraldo, S.B.; Wheeler, T.D.; McDermott, G.P.; Zhu, J.J.; Gregory, M.T.; Shuga, J. et al. Massively parallel digital transcriptional profiling of single cells. *Nat. Commun.* **2017**, *8*, 14049. doi: 10.1038/ncomms14049
6. Ramachandran, P.; Matchett, K.P.; Dobie, R.; Wilson-Kanamori, J.R.; Henderson, N.C. Single-cell technologies in hepatology: new insights into liver biology and disease pathogenesis. *Nat. Rev. Gastroenterol. Hepatol.* **2020**, *17*, 457–472. doi: 10.1038/s41575-020-0304-x
7. Fu, Y.S.; Chen, H.; Liu, L.; Huang, Y.Y. Single cell total RNA sequencing through isothermal amplification in picoliter-droplet emulsion. *Anal. Chem.* **2016**, *88*, 10795–10799. doi: 10.1021/acs.analchem.6b02581
8. Xu, X.; Zhang, Q.Q.; Song, J.; Ruan, Q.Y.; Ruan, W.D.; Chen, Y.J.; Yang, J.; Zhang, X.B.; Song, Y.L.; Zhu, Z.; Yang, C.Y. A highly sensitive, accurate, and automated single-cell

- RNA sequencing platform with digital microfluidics. *Anal. Chem.* **2020**, *92*, 8599–8606. doi: 10.1021/acs.analchem.0c01613
9. Ziegler, C.G.K.; Allon, S.J.; Nyquist, S.K.; Mbanjo, J. M.; Miao, V.N.; Tzouanas, N.; Cao, Y.M.; Yousif, A.S.; Bals, J.; Hauser, B.M.; Shalek, A.K.; Ordoñas-Montanes, J.; HCA Lung Biological Network. SARS-CoV-2 receptor ACE2 is an interferon stimulated gene in human airway epithelial cells and is detected in specific cell subsets across tissues. *Cell* **2020**, *181*, 1016–1035. doi: 10.1016/j.cell.2020.04.035
 10. Wilk, A.J.; Rustagi, A.; Zhao, N.Q.; Roque, J.; Martinez-Colon, G.J.; McKechnie, J.L.; Ivison, G.T.; Ranganath, T.; Vergara, R.; Hollis, T.; Simpson, L.J.; Grant, P.; Subramanian, A.; Rogers, A.J.; Blish, C.A. *Nat. Med.* **2020**, *26*, 1070–1076. doi: 10.1038/s41591-020-0944-y
 11. Liao, M.; Liu, Y.; Yuan, J.; Wen, Y.; Xu, G.; Zhao, J.; Cheng, L.; Li, J.; Wang, X.; Wang, F.; Liu, L.; Amit, I.; Zhang, S.; Zhang, Z. Single-cell landscape of bronchoalveolar immune cells in patients with COVID-19. *Nat. Med.* **2020**, *26*, 842–844. doi: 10.1038/s41591-020-0901-9.
 12. Wen, W.; Su, W.; Tang, H.; Le, W.; Zhang, X.; Zheng, Y.; Liu, X.; Xie, L.; Li, J.; Ye, J.; Dong, L.; Cui, X.; Miao, Y.; Wang, D.; Dong, J.; Xiao, C.; Chen, W.; Wang, H. Immune cell profiling of COVID-19 patients in the recovery stage by single-cell sequencing. *Cell Discovery* **2020**, *6*, 31. doi: 10.1038/s41421-020-0168-9
 13. Ren, X.; Wen, W.; Fan, X.; Chen, J.; Jin, R.; Zhang, Z. COVID-19 immune features revealed by a large-scale single-cell transcriptome atlas. *Cell* **2021**, *184*, 1895–1913. doi: 10.1016/j.cell.2021.01.053
 14. Speranza, E.; Williamson, B.N.; Feldmann, F.; Sturdevant, G.L.; Pérez-Pérez, L.; Meade-White, K.; Smith, B.J.; Lovaglio, J.; Martens, C.; Munster, V.J.; Okumura, A.; Shaia, C.; Feldmann, H.; Best, S.M.; de Wit, E. Single-cell RNA sequencing reveals SARS-CoV-2 infection dynamics in lungs of African green monkeys. *Sci. Transl. Med.* **2021**, *13*(578), eabe8146. doi: 10.1126/scitranslmed.abe8146
 15. Jinek, M.; Chylinski, K.; Fonfara, I.; Hauer, M.; Doudna, J. A.; Charpentier, E., A programmable dual-RNA-guided DNA endonuclease in adaptive bacterial immunity. *Science* **2012**, *337* (6096), 816–821. doi: 10.1126/science.1225829

16. Cong, L., Ran, F. A., Cox, D., Lin, S., Barretto, R., Habib, N., Hsu, P. D., Wu, X., Jiang, W.; Marraffini, L. A. Multiplex genome engineering using CRISPR/Cas systems. *Science* **2013**, *339* (6121), 819–823. doi: 10.1126/science.1231143.
17. Mali, P., Yang, L. H., Esvelt, K. M., Aach, J., Guell, M., DiCarlo, J. E., Norville, J. E.; Church, G. M. RNA-guided human genome engineering via Cas9. *Science* **2013**, *339* (6121), 823–826. doi: 10:1126/science.1232033.
18. Knott, G. J.; Doudna, J. A. CRISPR-Cas guides the future of genetic engineering. *Science* **2018**, *361* (6405), 866–869. doi:10.1126/science.aat5011
19. Gu, W.; Crawford, E. D.; O'Donovan, B. D.; Wilson, M. R.; Chow, E. D.; Retallack, H.; DeRisi, J. L., Depletion of Abundant Sequences by Hybridization (DASH): using Cas9 to remove unwanted high-abundance species in sequencing libraries and molecular counting applications. *Genome Biol.* **2016**, *17*, 41. doi: 10.1186/s13059-016-0904-5
20. Lee, S. H.; Yu, J.; Hwang, G. H.; Kim, S.; Kim, H. S.; Ye, S.; Kim, K.; Park, J.; Park, D. Y.; Cho, Y. K.; Kim, J. S.; Bae, S., CUT-PCR: CRISPR-mediated, ultrasensitive detection of target DNA using PCR. *Oncogene* **2017**, *36*, 6823–6829. doi: 10.1038/onc.2017.281
21. Quan, J.; Langelier, C.; Kuchta, A.; Batson, J.; Teyssier, N.; Lyden, A.; Caldera, S.; McGeever, A.; Dimitrov, B.; King, R.; Wilhelm, J.; Murphy, M.; Ares, L. P.; Travisano, K. A.; Sit, R.; Amato, R.; Mumbengegwi, D. R.; Smith, J. L.; Bennett, A.; Gosling, R.; Mourani, P. M.; Calfee, C. S.; Neff, N. F.; Chow, E. D.; Kim, P. S.; Greenhouse, B.; DeRisi, J. L.; Crawford, E. D., FLASH: a next-generation CRISPR diagnostic for multiplexed detection of antimicrobial resistance sequences. *Nucleic Acids Res.* **2019**, *47* (14), e83. doi: 10.1093/nar/gkz418
22. Schultzhau, Z.; Wang, Z.; Stenger, D. CRISPR-based enrichment strategies for targeted sequencing. *Biotechnol. Adv.* **2021**, *46*, 107672. doi: 10.1016/j.biotechadv.2020.107672
23. Wieland, S.; Thimme, R.; Purcell, R.H.; Chisari, F.V. Genomic analysis of the host response to hepatitis B virus infection. *Proc. Natl. Acad. Sci. U.S.A.* **2004**, *101*, 6669–6674. doi: 10.1073/pnas.0401771101
24. Cheng, X.M.; Xia, Y.C.; Serti, E.; Block, P.D.; Chung, M.; Chayama, K.; Rehmann, B.; Liang, T.J. Hepatitis B virus evades innate immunity of hepatocytes but activates cytokine production by macrophages. *Hepatology* **2017**, *66*, 1779–1793. doi: 10.1002/hep.29348

25. Ortega-Prieto, A.M.; Dorner, M. Immune evasion strategies during chronic hepatitis B and C virus infection. *Vaccines* **2017**, *5* (3), 24. doi: 10.3390/vaccines5030024
26. Suslov, A.; Boldanova, T.; Wang, X.Y.; Wieland, S.; Heim, M.H. Hepatitis B virus does not interfere with innate immune responses in the human liver. *Gastroenterology* **2018**, *154*, 1778–1790. doi: 10.1053/j.gastro.2018.01.034
27. Suslov, A.; Wieland, S.; Menne, S. Modulators of innate immunity as novel therapeutics for treatment of chronic hepatitis B. *Curr. Opin. Virol.* **2018**, *30*, 9–17. doi: 10.1016/j.coviro.2018.01.008
28. Thomas, E.; Baumert, T.F. Hepatitis B virus-hepatocyte interactions and innate immune responses: experimental models and molecular mechanisms. *Semin. Liver Dis.* **2019**, *39*, 301–314. doi: 10.1055/s-0039-1685518
29. Winer, B.Y.; Gaska, J.M.; Lipkowitz, G.; Bram, Y.; Parekh, A.; Parsons, L.; Leach, R.; Jindal, R.; Cho, C.H.; Shrirao, A.; Novik, E.; Schwartz, R.E.; Ploss, A. Analysis of host responses to hepatitis B and delta viral infections in a macro-scalable hepatic co-culture system. *Hepatology* **2020**, *71*, 14–30. doi: 10.1002/hep.30815
30. Zhang, Z.H.; Trippler, M.; Real, C.I.; Werner, M.; Luo, X.F.; Schefczyk, S.; Kemper, T.; Anastasiou, O.E.; Ladiges, Y.; Treckmann, J.; Paul, A.; Baba, H.A.; Allweiss, L.; Dandri, M.; Gerken, G.; Wedemeyer, H.; Schlaak, J.F.; Lu, M.J.; Broering, R. Hepatitis B virus particles activate Toll-Like Receptor 2 signaling initially upon infection of primary human Hepatocytes. *Hepatology* **2020**, *72*, 829–844. doi: 10.1002/hep.31112
31. Le, C.; Sirajee, R.; Steenbergen, R.; Joyce, M.A.; Addison, W.R.; Tyrrell, D.L. *In vitro* infection with hepatitis B virus using differentiated human serum culture of Huh7.5-NTCP cells without requiring dimethyl sulfoxide. *Viruses* **2021**, *13*, 97. doi: 10.3390/v13010097
32. MacParland, S. A.; Liu, J. C.; Ma, X-Z.; Innes, B. T.; Bartczak, A. M.; Gage, B. K.; Bader, G. D.; McGilvray, I. D. Single cell RNA sequencing of human liver reveals distinct intrahepatic macrophage populations. *Nat. Commun.* **2018**, *9*, 4383. doi: 10.1038/s41467-018-06318-7
33. Yan, H.; Zhong, G.; Xu, G.; He, W.; Jing, Z.; Gao, Z.; Huang, Y.; Qi, Y.; Peng, B.; Wang, H.; Fu, L.; Song, M.; Chen, P.; Gao, W.; Ren, B.; Sun, Y.; Cai, T.; Feng, X.; Sui, J.; Li, W. Sodium taurocholate cotransporting polypeptide is a functional receptor for human hepatitis B and D virus. *eLife* **2012**, *1*, e00049. doi: 10.7554/eLife.00049

34. Ni, Y.; Lempp, F.A.; Mehrle, S.; Nkongolo, S.; Kaufman, C.; Falth, M.; Stindt, J.; Koniger, C.; Nassal, M.; Kubitz, R.; Sultmann, H.; Urban, S. Hepatitis B and D viruses exploit sodium taurocholate co-transporting polypeptide for species-specific entry into hepatocytes. *Gastroenterology* **2014**, *146*, 1070–1083. doi: 10.1053/j.gastro.2013.12.024
35. Mutz, P.; Metz, P.; Lempp, F.A.; Bender, S.; Qu, B.; Schöneweis, S.; Seitz, S.; Tu, T.; Restuccia, A.; Frankish, J.; Dächert, C.; Schusser, B.; Koschny, R.; Polychronidis, G.; Schemmer, P.; Hoffmann, K.; Baumert, T.F.; Binder, M.; Urban, S.; Bartenschlager, R. HBV bypasses the innate immune response and does not protect HCV from antiviral activity of interferon. *Gastroenterology* **2018**, *154*(6), 1791–1804. doi: 10.1053/j.gastro.2018.01.044
36. Zhang, X.; Lu, W.; Zheng, Y.; Wang, W.; Bai, L.; Chen, L.; Feng, Y.; Zhang, Z.; Yuan, Z. In situ analysis of intrahepatic virological events in chronic hepatitis B virus infection. *J. Clin. Invest.* **2016**, *126*(3), 1079–1092. doi: 10.1172/JCI83339

Chapter 4

Single-Cell RNA Sequencing Reveals Heterogeneity and Cell Subtypes in Huh7.5 and Huh7.5-NTCP Cells Differentiated in Human Serum Culture

4.1. Introduction

Results in Chapter 2 show that Huh7.5-NTCP hepatoma cells in culture medium supplemented with human serum (HS) serve as a useful *in vitro* cell model system for studying HBV. Human serum culture increased levels of hepatocyte differentiation markers in Huh7.5-NTCP cells to similar levels found in primary human hepatocytes. This characterization was based on the analysis of entire population of Huh7.5-NTCP cells in the human serum culture. Previous investigations conducted by our group [1] revealed bile canalicular structures in Huh7.5 cells cultured in human serum. We hypothesize that these observed structures may be a result of Huh7.5-NTCP hepatoma cells differentiating in HS-supplemented culture medium to hepatocytes and possibly other celltypes. Single-cell RNA sequencing (scRNA-seq) technology would enable transcriptomic studies of the cell population at a single-cell resolution.

In 2018, MacParland *et al.* [2] reported a scRNA-seq study of human liver samples obtained from five healthy neurologically deceased donors. Their scRNA-seq analysis of 8444 cells established a human liver transcriptome atlas. By analyzing the expression levels of genes in various clusters, they identified discrete cell populations, including hepatocytes, endothelial cells, cholangiocytes, hepatic stellate cells, B cells, conventional and non-conventional T cells, NK-like cells, and distinct intrahepatic monocyte and macrophage populations. This transcriptomic map of the cellular landscape of the human liver at single-cell resolution provides an excellent reference for our scRNA-seq studies of hepatoma cell lines. Therefore, the primary

objective of the research in this chapter is to analyze the transcriptomic profiles of Huh7.5 and Huh7.5-NTCP cells at the single-cell level, and compare them to primary human liver. These analyses will help define the degree of differentiation of Huh7.5 and Huh7.5-NTCP cells cultured in media supplemented with human serum.

4.2. Materials and Methods

4.2.1. Huh7.5 and Huh7.5-NTCP Cells Cultured in Medium Supplemented with Human Serum

Huh7.5 and Huh7.5-NTCP cells were cultured in DMEM (Sigma Aldrich, St. Louis, MO) supplemented with 4% pooled adult human serum (HS). The same protocols and conditions as described in Chapter 2 were used for the maintenance of the Huh7.5 and Huh7.5-NTCP cell cultures. The cells were washed three times with the medium prior to the preparation of scRNA-seq libraries.

4.2.2. Single-Cell RNA Sequencing of Huh7.5 and Huh7.5-NTCP Cells Cultured in Medium Supplemented with Human Serum

Cell suspensions were prepared from the trypsinized Huh7.5 and Huh7.5-NTCP cell monolayers according to protocols provided by 10X Genomics. In brief, the cell monolayers were incubated with trypsin solution for 3 minutes at 37°C. The detached cells were then incubated with an equivalent volume of DMEM 10% FBS. The cell suspension was centrifuged at 150xg for 5 minutes at 4°C. The supernatant was removed and the cell pellet was resuspended with 4°C sterile PBS using a wide bore pipette and taking 10–15 seconds to either take up or dispense the cells from the pipette. The cell suspension was once more centrifuged at 150xg for 5 minutes at 4°C and resuspended in fresh PBS gently. The cell suspension was filtered through a

cell strainer (Bel-Art Flowmi 40µm Cell Strainer, H13680-0040). A small sample of the cell suspension was mixed with trypan blue to ensure the sample was a single cell suspension with greater than 95% viability. Libraries for single-cell RNA sequencing were prepared according to the procedures of 10X Genomics (Pleasanton, CA), and with the help of Dr. Joaquín López-Orozco, High Content Analysis Core Facility, Faculty of Medicine and Dentistry, University of Alberta. These libraries were sequenced by Novogene (Sacramento, CA) using the HiSeq PE150 sequencing-by-synthesis platform (Illumina, San Diego, CA). The same procedures as described in Figure 3.1, Section 3.2.2, and Section 3.2.3 were used.

4.2.3. Single-Cell RNA Sequencing of Human Liver Cells (MacParland et al., 2018)

The scRNA-seq data from human liver were made available by MacParland *et al.* [2] and were downloaded from <https://github.com/BaderLab/HumanLiver>. The dataset included scRNA-seq analysis of 8444 cells obtained from liver samples from five healthy neurologically deceased donors. Analyses of the human liver at single-cell resolution revealed “discrete cell populations of hepatocytes, endothelial cells, cholangiocytes, hepatic stellate cells, B cells, conventional and non-conventional T cells, NK-like cells, and distinct intrahepatic monocyte/macrophage populations” [2].

4.2.4. Data Analysis

Data from single-cell RNA sequencing of human liver [2] were integrated with the scRNA-seq data generated from the human serum cultured Huh7.5 and Huh7.5-NTCP cells. The combination of datasets followed the Seurat integration method for unsupervised analysis [3]. The Seurat V3 software package, developed and maintained by Dr. R. Satija and collaborators, enables users “to integrate diverse types of single-cell data”. (<https://satijalab.org/seurat/>)

The Seurat V3 software package was used for the analysis of the three datasets from the scRNA-seq analyses of human liver and human serum cultured Huh7.5 and Huh7.5-NTCP cells. Uniform Manifold Approximation and Projection (UMAP) graphs were generated and gene clustering analyses were conducted using the corresponding scripts within the Seurat V3 package following the procedures of Stuart *et al.* [3]. Example R scripts for data analysis are included in Appendix A.

Typical data analysis included the following components: (1) Quality control (QC) filtering of the data, (2) single cell gene expression normalization, (3) graph-based clustering and visualization by UMAP, (4) analysis of cell marker gene expression, and (5) pathway analysis on the basis of gene expression. The protocol of MacParland *et al.* [2] for quality control (QC) filtering was used for removing data of dead cells or cell doublets from the single-cell dataset.

Gene ontology (GO) enrichment analysis was performed using GOrilla (Gene Ontology enRIchment anaLysis and visuaLizAtion) by comparing differentially expressed genes from individual clusters with all of the differentially expressed genes from the other clusters. REVIGO (REduce and VISualize Gene Ontology) was used to consolidate redundant GO terms. Regulon analysis was performed with pySCENIC [6] as per authors' protocol.

4.2.5. Data Storage and Availability

Raw data is available through the Tyrrell Lab and will be uploaded to GEOBASE upon publication. Example scripts for data analysis described in this thesis are available in Appendix A. All relevant scripts for scRNA-seq data analysis are saved and available through the Tyrrell Lab.

4.3. Results and Discussion

4.3.1. Integration of three datasets from scRNA-seq analysis of human liver, Huh7.5, and Huh7.5-NTCP cells

We first integrated the data from scRNA-seq of human liver [2] with the scRNA-seq data we generated from Huh7.5 and Huh7.5-NTCP cells cultured in HS-supplemented medium. We followed the Seurat integration method [3] to combine the three datasets for unsupervised analysis.

Figure 4.1 shows a set of Uniform Manifold Approximation and Projection (UMAP) plots generated from the analysis of primary liver and Huh7.5 and Huh7.5-NTCP hepatoma cells in the integrated datasets. UMAP is a method for dimensional reduction to illustrate multi-dimensional data in a two-dimensional format for visualization. Each dot on the UMAP figure represents a single cell. The cells that share similar transcriptome profiles are clustered together. In general, cells of the same cell-type assemble in a cluster, and clusters spatially close together represent similar cell-types.

Clustering analysis of scRNA-seq data from primary liver [2] and the Huh7.5, and Huh7.5-NTCP cell samples reveals 14 distinct clusters represented by numbering and colors (Figure 4.1A). The liver tissue from five human donors contain a variety of cell types, represented in the 14 clusters. Seven of the 14 clusters also appear in the Huh7.5, and Huh7.5-NTCP hepatoma cells cultured in HS-supplemented medium. The cell clusters overlap well between the Huh7.5, and Huh7.5-NTCP cell samples (Figure 4.1 B and C), as expected.

Figure 4.2 shows the number and percentage contribution of cells to each scRNA-seq cluster shown in Figure 4.1. The integrated dataset is composed of scRNA-seq data of 8444 liver

cells, 3793 Huh7.5 cells, and 3119 Huh7.5-NTCP cells. There is a diverse distribution of cells to each cluster in human liver. Although the total numbers of Huh7.5 cells and Huh7.5-NTCP cells in the scRNA-seq dataset are lower than the primary liver cells, there are sufficient number of cells in main clusters. For example, more than 2000 single cells in Huh7.5 and Huh7.5-NTCP appear in cluster 0.

4.3.2. Expression level of NTCP transcripts in Huh7.5-NTCP cells confirmed by scRNA-seq analysis

We analyzed the scRNA-seq data for the expression level of NTCP, also known as SLC10A1 (solute carrier family 10 member 1). The NTCP mRNA levels in Huh7.5-NTCP cells are higher than in Huh7.5 and primary liver samples (**Figure 4.3**). This result from scRNA-seq analysis is consistent with that shown in Chapter 2, and this result is as expected because of the overexpression of NTCP in the Huh7.5-NTCP cell line.

4.3.3. Clustering analysis of representative genes for delineating cell types in clusters

Using the scRNA-seq information of human liver as a reference [2], we performed clustering analysis of cell marker genes to classify the cell types corresponding to each of the clusters in UMAP. As an example, **Figure 4.4A** shows expression levels of 20 representative hepatocyte genes [2]. We obtained hepatocyte scores for each cell cluster (**Figure 4.4B**) by combining the average expression levels of hepatocyte-associated genes, including ALB, AFP, APOE, ARG1, HAMP, PCK1, EPCAM, HNF4A, CYP1A1, CYP2C8, CYP2E1, CYP3A4, KRT8, SPP1, SLC22A10, FETUB, LBP, HPR, LECT2, SERPINA10, SERPINA1, ORM1, SPINK1, CYP2A7, and MLXIPL. This analysis suggests that clusters 0, 2, 3, 6, 7, and 9 are hepatocytes or hepatocyte-like cells. Clusters 3 and 6 are very rare in primary liver cells but

fairly abundant in the cultured cells. The hepatocyte score values (**Figure 4.4B**) indicate that the cells in the Huh7.5 and Huh7.5-NTCP cell lines mostly overlap with and have similar expression as the hepatocytes in the human liver sample.

We performed similar clustering analyses of cell marker genes, chosen on the basis of published marker genes [2], to classify other cell types. Expression level of liver sinusoidal endothelial cell (LSEC) genes and the LSEC score are shown in **Figure 4.5**. These results suggest that cluster 5 in primary liver represents LSECs. As expected, this cell type is not present in the hepatoma Huh7.5 and Huh7.5-NTCP cell samples (Figure 4.5B).

Expression level of monocyte and macrophage genes and the average expression of monocyte- and macrophage-associated genes are shown in **Figure 4.6**. This analysis suggests that cluster 4 in primary liver represents monocytes and macrophages. As expected, cluster 4 is not present in the hepatoma Huh7.5 and Huh7.5-NTCP cell samples (Figure 4.6B).

Expression level of lymphocyte-associated genes and lymphocyte score are shown in **Figure 4.7**. Results from this analysis show that lymphocytes contribute to clusters 1, 8, 10, and 12 in primary liver.

Figure 4.8 shows the expression level of B cell genes and B cell score, the average expression of B cell associated genes (B cell score) in various clusters. These results suggest that clusters 8 and 10 in primary liver are B cells.

Figure 4.9 shows the expression level of T cell genes and T cell score, the average expression of T and NK cell associated genes. These results suggest that clusters 1 and 12 in primary liver are T and NK cells.

Figure 4.10 shows the expression level of erythroid cell genes and erythroid score, the average expression of erythroid cell associated genes. This analysis suggests that cluster 13 in primary liver is erythroid cells.

Figure 4.11 shows the expression level of stellate cell genes and Stellate score, the average expression of stellate cell associated genes. This analysis suggests that some cells in cluster 5 are stellate cells, liver resident cells involved with collagen production and fibrosis.

The identification of monocyte, macrophage, lymphocyte, LSEC, B cell, T cell, NK cell, erythroid cell, and stellate cell in primary liver are consistent with the analysis and results of MacParland *et al.* [2]. These cell types are not present in the hepatoma Huh7.5 and Huh7.5-NTCP cell samples. These results suggest that the HS-cultured Huh7.5 and Huh7.5-NTCP hepatoma cells predominantly differentiate to cells similar to hepatocytes but not into other liver cell populations.

4.3.4. Delineation of cell types within the hepatocyte cluster

The primary liver cells used for MacParland's scRNA-seq study were originated from liver samples of five human donors. The hepatocyte population consists of cells from different regions of the liver, including pericentral (close to the central vein), midcentral, midportal, and periportal (close to the portal vein). We performed clustering analysis showing expression levels of genes associated with pericentral hepatocyte (**Figure 4.12**), midcentral hepatocyte (**Figure 4.13**), midportal hepatocyte (**Figure 4.14**), and periportal hepatocyte (**Figure 4.15**).

Genes in pericentral hepatocyte, BCHE, G6PC, GHR, ALDH6A1, RCAN1, AR, RP4-710M16.2, LINC00261, PLIN1, and RP11-390F4.3, were included in the clustering analysis. Analysis of expression levels of these pericentral hepatocyte genes in primary liver suggests that

cells in cluster 0 are pericentral hepatocytes (**Figure 4.12**). Genes in midcentral hepatocyte, HSD11B1, HAMP, APOM, G6PC, G0S2, PON3, TTC36, GOLT1A, RCAN1, AQP9, HPR, AKR1C1, NNT, APOA5, TTR, and ACADM, were analyzed. Analysis of expression levels of these midcentral hepatocyte genes in primary liver suggests that cells in cluster 2 are midcentral hepatocytes (**Figure 4.13**). Genes in midportal hepatocyte score included CYP2A7, CYP3A7, CYP2A6, TP53INP2, ATIC, SERPINH1, SAMD5, and GRB14. Analysis of expression levels of these midportal hepatocyte genes in primary liver suggests that cells in cluster 9 are midportal hepatocytes (**Figure 4.14**). Likewise, clustering analysis of periportal hepatocyte genes, including SCD, HMGCS1, ACSS2, TM7SF2, TMEM97, CP, CRP, SLPI, C2orf82, ACAT2, TM4SF5, MSMO1, and LEPR, suggests that cells in cluster 9 are periportal hepatocytes (**Figure 4.15**).

4.3.5. Clustering analysis of cell cycle related genes

Cluster 3 is present in the HS-cultured Huh7.5 and Huh7.5-NTCP cells but not in primary liver. Given that Huh7.5 and Huh7.5-NTCP are immortalized tumor cells, there are likely proliferative cells in the culture. We analyzed cell cycle gene expression in the scRNA-seq dataset, to identify cells according to their likely phase in the cell cycle. Cell-cycle phase prediction of human liver and HS-cultured Huh7.5 and Huh7.5-NTCP cells (**Figure 4.16**) shows that cells in cluster 3 are mainly in the S and G2M phase. The proliferative phenotype of these cells from the cell lines and the lymphocytes (cluster 8) likely explains their close clustering. In addition, these data show that there are a number of quiescent cells (G1 phase) in the HS-cultured cell lines. This is notable because it corresponds to the growth arrest we observed with our HS cultures.

4.3.6. Clustering analysis of cholangiocyte-associated genes suggests presence of cholangiocyte-like cells in Huh7.5 cell populations

Cluster 6 is another population present in HS-cultured Huh7.5 cells but absent in primary liver cells. Clustering analysis of the expression level of cholangiocyte-associated genes (**Figure 4.17**), including KRT19, FXRD2, CLDN4, CLDN10, MMP7, CXCL1, CFTR, and KRT7, suggests that cluster 11 are cholangiocytes in primary liver and that cluster 6 are cholangiocyte-like cells in Huh7.5 and Huh7.5-NTCP hepatoma cell lines. This finding of a subset of cholangiocyte-like cells present in the HS-cultured Huh7.5 and Huh7.5-NTCP cell lines is of particular interest. Our lab (Dr. Rineke Steenbergen) has recently observed that our HS cultures can form structures resembling bile canaliculi. If this observation proves true, this *in vitro* system would model both hepatocytes and bile canaliculi.

The identification of a hepatocyte-cholangiocyte population of cells (cluster 6) in Huh7.5 cultures with a transcriptome profile similar to liver cholangiocytes (cluster 11) is particularly novel. We undertook several analyses of the single cell transcriptome data to further characterize these cells.

4.3.7. Cell types present in human liver and HS-cultured Huh7.5 and Huh7.5-NTCP cells

Using the scRNA-seq dataset of primary liver as a reference in combination with analyses of our scRNA-seq data of Huh7.5 and Huh.5-NTCP cells, we delineated the cell types in primary liver and the HS-cultured Huh7.5 and Huh.5-NTCP hepatoma cells (**Figure 4.18**). The cell types include hepatocytes, hepatocyte-like cells, hepatocyte-cholangiocyte-like cells, cholangiocytes, liver sinusoidal endothelial cells (LSECs), monocytes and macrophages, T cells, B cells, and erythroid cells. The analysis of the combined dataset also allowed different classes of

hepatocytes to be distinguished: pericentral, midcentral, midportal, and periportal, based on location relative to the central vein or portal triad in the liver lobule.

4.3.8. Hepatocyte and cholangiocyte cell types present in human liver and HS-cultured Huh7.5, and Huh7.5-NTCP cells

The expression level of hepatocyte-associated genes and hepatocyte score shown in Figure 4.4 suggest that clusters 0, 2, 3, 6, 7, and 9 are hepatocytes or hepatocyte-like cells. The expression level of cholangiocyte-associated genes and cholangiocyte score shown in Figure 4.17 suggest that cells in cluster 11 are cholangiocytes in primary liver and cluster 6 are cholangiocyte-like cells in Huh7.5 and Huh7.5-NTCP hepatoma cell lines. For simplicity of visualizing hepatocyte and cholangiocyte cell types, UMAP plots of only the clusters relevant to hepatocyte and cholangiocyte are shown in **Figure 4.19**. As expected, all hepatocyte and cholangiocyte cell types are present in the human liver sample. The predominant cell types in the HS-cultured Huh7.5 and Huh7.5-NTCP hepatoma cell lines appear to be pericentral hepatocyte, hepatocyte-like, and cholangiocyte-like cells.

4.3.9. Analysis of differential gene expression

Heat maps (**Figure 4.20** and **Figure 4.21**) show differentially expressed genes among the different clusters within integrated dataset of primary liver and HS-cultured Huh7.5 and Huh7.5-NTCP hepatoma cell lines. **Figure 4.20** includes all 14 clusters and all three samples, primary liver, HS-cultured Huh7.5 and Huh7.5-NTCP hepatoma cells. **Figure 4.21** shows that the cholangiocyte-associated genes are differentially upregulated (represented by yellow color in the heat map) in the cholangiocyte cluster of cells (cluster 11). The dot plot (**Figure 4.22**) also shows differentially expressed genes representative of cholangiocyte cell type. These results of

upregulation of cholangiocyte-associated genes further support our finding of cholangiocyte-like cells in the HS-cultured Huh7.5 and Huh7.5-NTCP hepatoma cell lines.

4.3.10. Analysis of gene ontology term enrichment

Differentially upregulated genes from different cell types were analyzed for gene ontology (GO) term enrichment (**Figure 4.23**). The color of bars represents different cell types, the length of the bars represent GO term enrichment score, and the white circles indicate p values. Cholangiocytes are involved with fluid and ion transport. In cholangiocytes (dark green bars) and hepatocyte-cholangiocyte-like cells (green bars), the gene ontology term enrichment are as expected, such as transepithelia transport, ion transport, regulation of morphogenesis of a branching structure, epithelial structure maintenance, and regulation of microvillus organization. Enrichment scores of gene ontology terms are significant ($p < 0.001$) for all hepatocyte and cholangiocyte cell types.

4.3.11. Regulon analysis of cell clusters

Regulons are units of gene expression defined by a particular transcription factor and all of the downstream genes it regulates. The SCENIC analysis [6] looks at whether a transcription factor is upregulated and whether the downstream genes it regulates are in turn either upregulated or downregulated. If a transcription factor and its downstream effects are more 'active', the regulon is shown to be stronger, representing more activity of that regulatory network. **Figure 4.24** shows regulon specificity scores illustrating the most active regulons in each cluster.

Figure 4.25 shows active regulons in hepatocyte-cholangiocyte-like cells and cholangiocytes. Figure 4.25A shows that regulons ELF3, KLF5, EHF, TFF3, and ARNTL2 are

active in hepatocyte-cholangiocyte-like cells (cluster 6) and cholangiocytes (cluster 11). Figure 4.25B shows that regulons SOX9, ETV4, and GLIS2 are more active in cholangiocytes (cluster 11) than in hepatocyte-cholangiocyte-like cells (cluster 6). Figure 4.25C shows that regulon SP6 is active in hepatocyte-cholangiocyte-like cells (cluster 6) but not in cholangiocytes.

The regulon analysis supports that the hepatocyte-cholangiocyte-like cells in the HS-cultured Huh7.5 and Huh7.5-NTCP hepatoma cells lines have similar regulons/regulation as the cholangiocytes from the primary liver tissue. This further supports the similarity of these cell types and illustrates the regulatory pathways that are active in both. These pathways may be involved in the development of the unique hepatocyte-cholangiocyte-like cell type.

Analysis of the regulons is more meaningful than only analyzing the expression level of transcription factors because regulons represent regulatory networks (**Figure 4.26**). For example, analysis of regulons of ELF3 and KLF5 (Figure 4.26, graphs on the left) shows that these regulons are active (yellow to green color) in cholangiocytes (cluster 11). Analysis of expression levels of ELF3 and KLF5 (graphs on the right) cannot conclude upregulation of these transcription factors.

4.4. Conclusions

scRNA-seq analysis of 3793 Huh7.5 cells and 3119 Huh7.5-NTCP cells at the single cell resolution revealed heterogeneity within the cell culture. With the scRNA-seq data of cells of human liver tissue as a reference, analysis of transcriptomic profiles in the integrated dataset showed that most cells in the human serum culture of Huh7.5 and Huh7.5-NTCP had similar gene expression profiles to those of primary hepatocytes from human liver. These results confirm

that our HS-supplemented cell culture model is a useful alternative to primary human hepatocytes.

scRNA-seq analysis also revealed the presence of cholangiocyte-like cells in addition to hepatocyte-like cells in the human serum cultured Huh7.5 and Huh7.5-NTCP cell lines. The cholangiocyte-like cells in these hepatoma cell population had similar regulatory pathways to cholangiocytes from human liver tissue. This finding suggests that the new HS-supplemented cell culture model may be forming more complex cell types and organization (**Figure 4.27**) than what might be expected for an immortalized cell line.

4.5. References

1. Steenbergen, R.; Oti, M.; ter Horst, R.; Tat, W.; Neufeldt, C.; Belovodskiy, A.; Chua, T. T.; Cho, W. J.; Joyce, M.; Dutilh, B. E.; Tyrrell, D. L. Establishing normal metabolism and differentiation in hepatocellular carcinoma cells by culturing in adult human serum. *Sci. Rep.* **2018**, *8*, 11685. doi:10.1038/s41598-018-29763-2.
2. MacParland, S. A.; Liu, J. C.; Ma, X-Z.; Innes, B. T.; Bartczak, A. M.; Gage, B. K.; Bader, G. D.; McGilvray, I. D. Single cell RNA sequencing of human liver reveals distinct intrahepatic macrophage populations. *Nat. Commun.* **2018**, *9*, 4383. doi:10.1038/s41467-018-06318-7
3. Stuart, T.; Butler, A.; Hoffman, P.; Hafemeister, C.; Papalexi, E.; Mauck III, W.M.; Hao, Y.; Stoeckius, M.; Smibert, P.; Satija, R. Comprehensive integration of single-cell data. *Cell* **2019**, *177*, 1888–1902. doi:10.1016/j.cell.2019.05.031
4. Le, C.; Sirajee, R.; Steenbergen, R.; Joyce, M.A.; Addison, W.R.; Tyrrell, D.L. *In vitro* infection with hepatitis B virus using differentiated human serum culture of Huh7.5-NTCP cells without requiring dimethyl sulfoxide. *Viruses* **2021**, *13*, 97. doi:10.3390/v13010097

5. Su, X.; Shi, Y.; Zou, X.; Lu, Z.-N.; Xie, G.; Yang, J. Y. H.; Wu, C.-C.; Cui, X.-F.; He, K.-Y.; Luo, Q.; Qu, Y.-L.; Wang, N.; Wang, L.; Han, Z-G. Single-cell RNA-Seq analysis reveals dynamic trajectories during mouse liver development. *BMC Genomics* **2017**, *18*, 946. doi:10.1186/s12864-017-4342-x
6. Aibar, S.; González-Blas, C.B.; Moerman, T.; Huynh-Thu, V.A.; Imrichova, H.; Hulselmans, G.; Rambow, F.; Marine, J.-C.; Geurts, P.; Aerts, J.; van den Oord, J.; Atak, Z.K.; Wouters, J.; Stein Aerts, S. SCENIC: Single-cell regulatory network inference and clustering, *Nat. Methods* **2017**, *14*(11), 1083–1086. doi:10.1038/nmeth.4463.

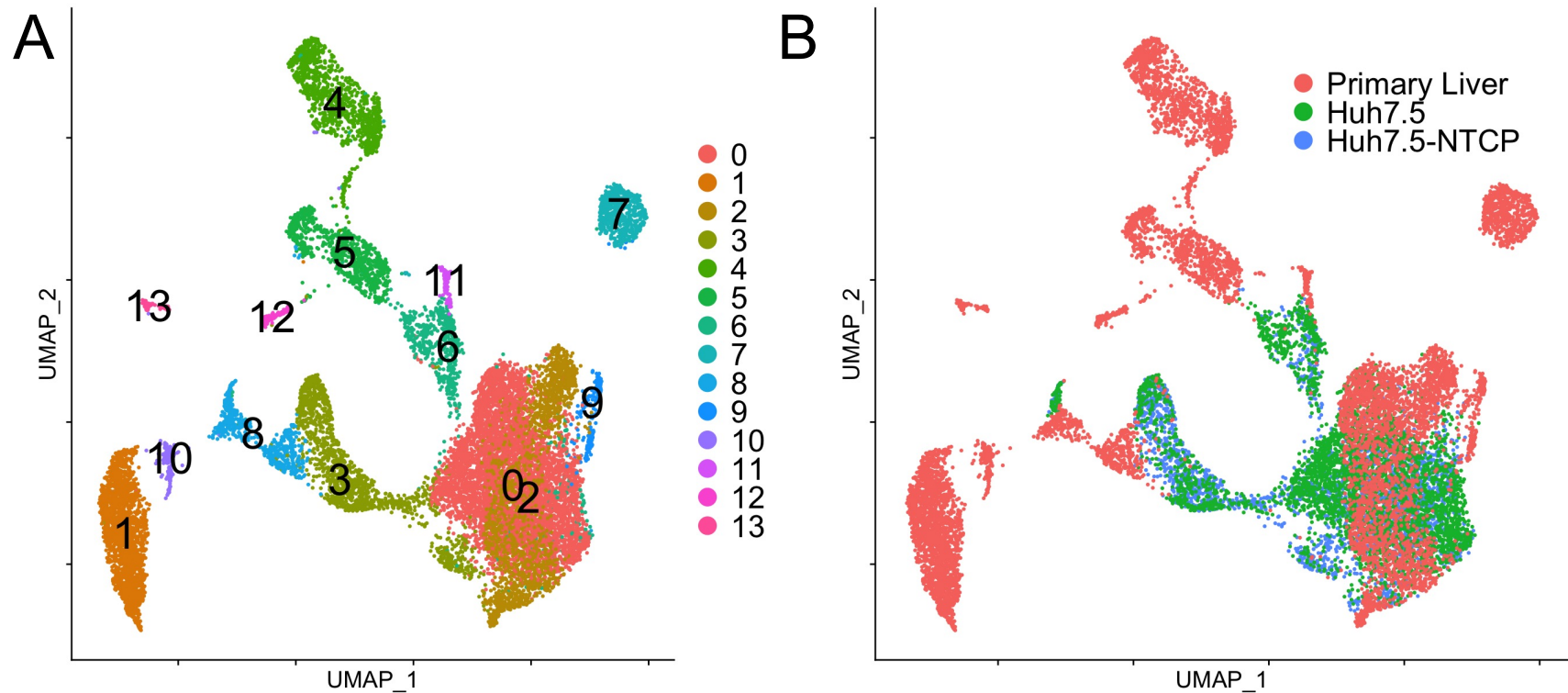


Figure 4.1 A and B. UMAP visualization of scRNA-seq data obtained from primary liver, Huh7.5, and Huh7.5-NTCP cells.

Cells that share similar transcriptome profiles are grouped by colors and numbers representing clusters.

(A) Results of unsupervised clustering analysis of the integrated scRNA-seq datasets of primary liver, Huh7.5, and Huh7.5-NTCP cells, showing all 14 clusters (0-13).

(B) UMAP organized by input sample: primary liver cells (red), Huh7.5 (green), and Huh7.5-NTCP (blue).

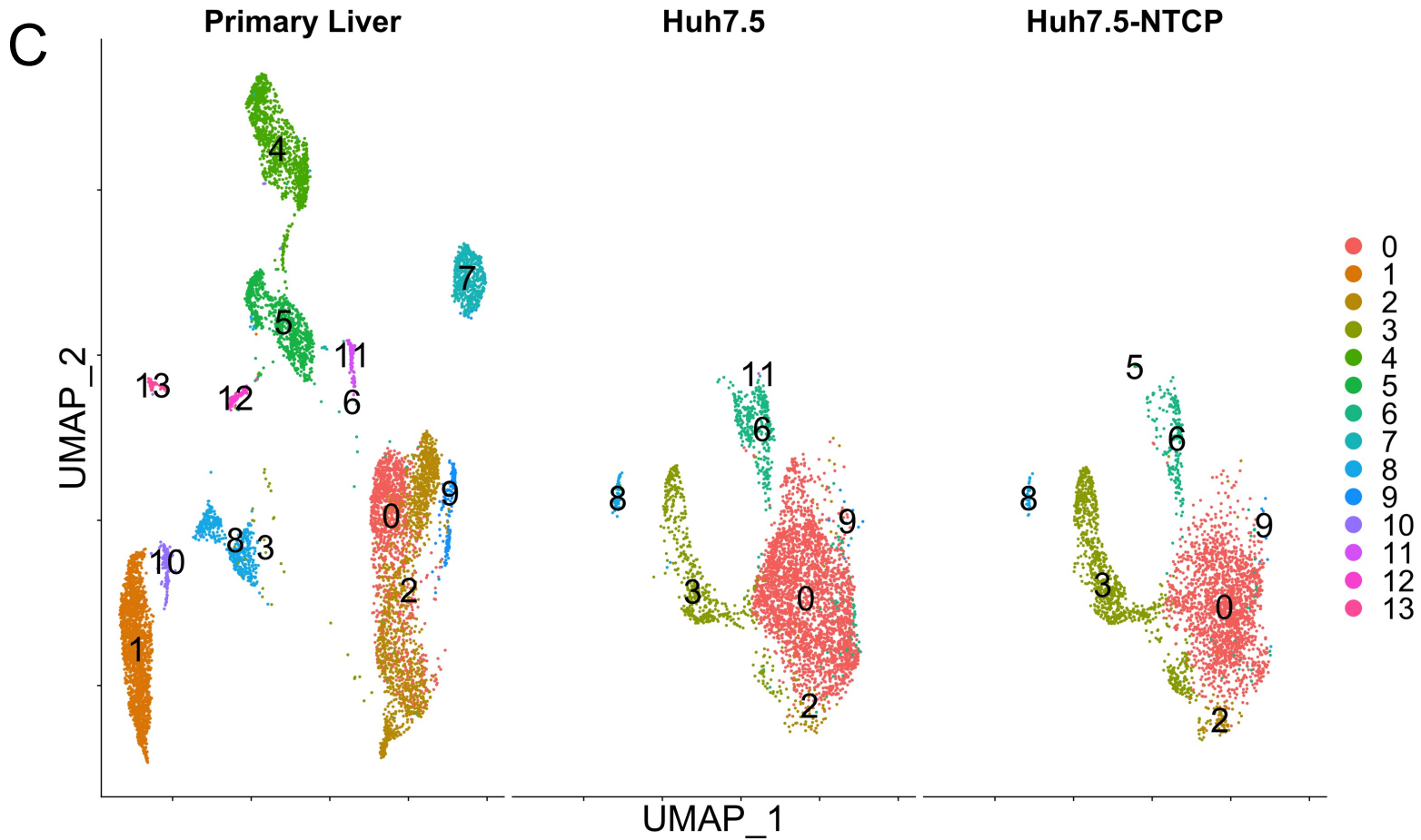


Figure 4.1 C. UMAP visualization of scRNA-seq data obtained from primary liver, Huh7.5, and Huh7.5-NTCP cells. (C) UMAP showing 14 clusters (from cluster 0 to 13) in each of the three samples. Cells that share similar transcriptome profiles are grouped to clusters by colors and numbers.

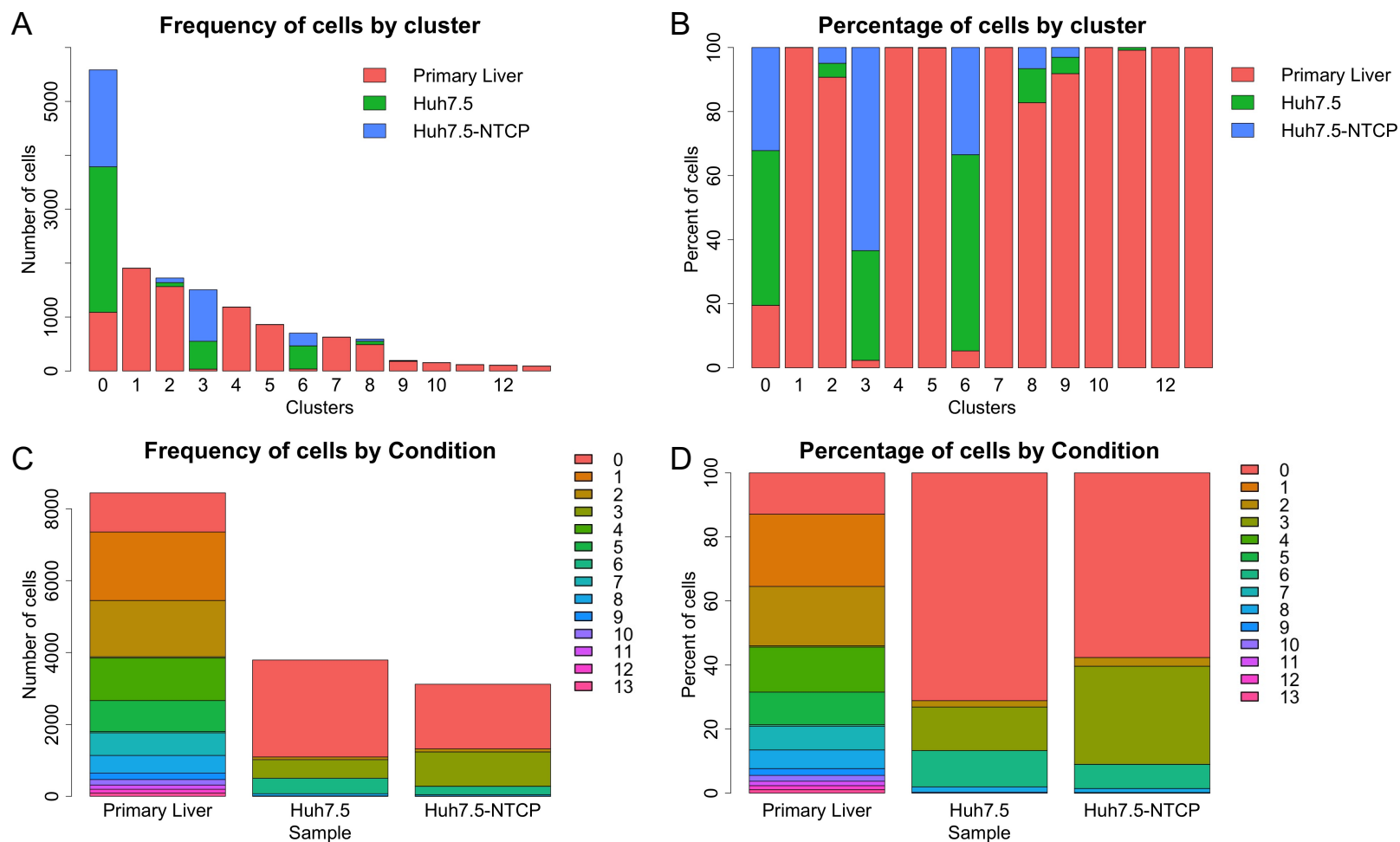


Figure 4.2. Number of cells and contribution of cells to each scRNA-seq cluster by sample. (A) Number of cells contributed to each cluster by the three input samples. (B) Percentage of cells contributed to each cluster by the three input samples: primary liver cells (red), Huh7.5 (green), and Huh7.5-NTCP (blue). (C) Number of cells contributed to each cluster by each of the three input samples. (D) Percentage of cells contributed to each cluster by each of the three input samples.

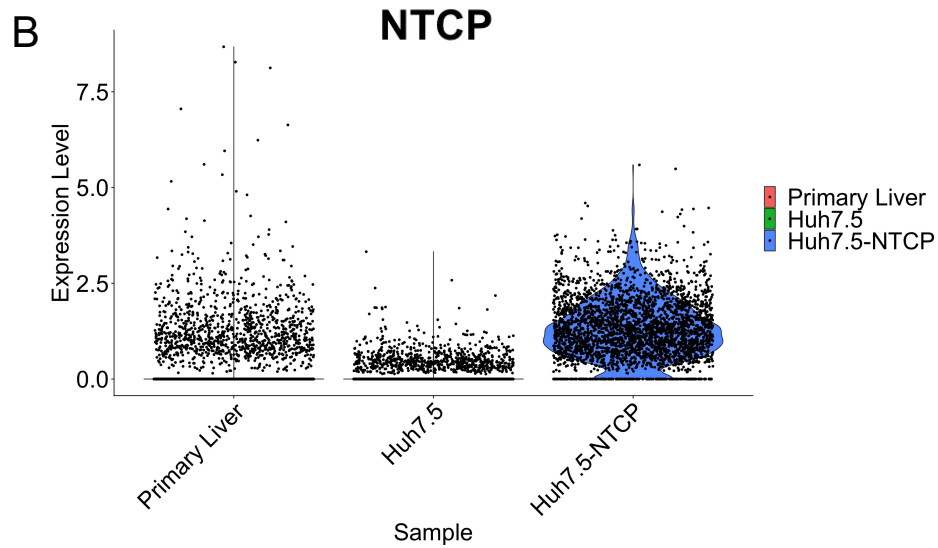
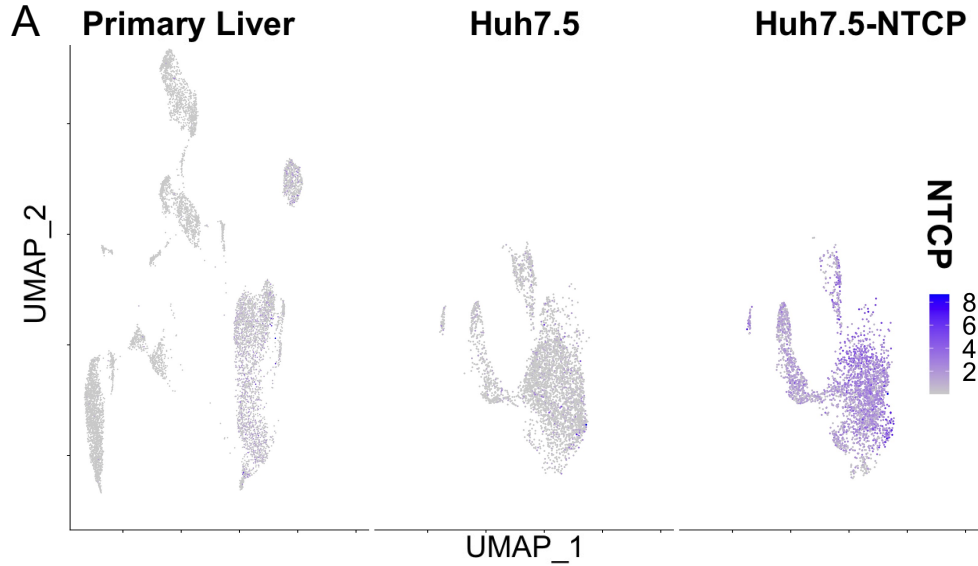


Figure 4.3. Expression level of SLC10A1 (NTCP) in primary liver, Huh7.5, and Huh.5-NTCP samples. (A) UMAP and (B) violin plot illustrating expression level of SLC10A1 (NTCP) in the three sample datasets.

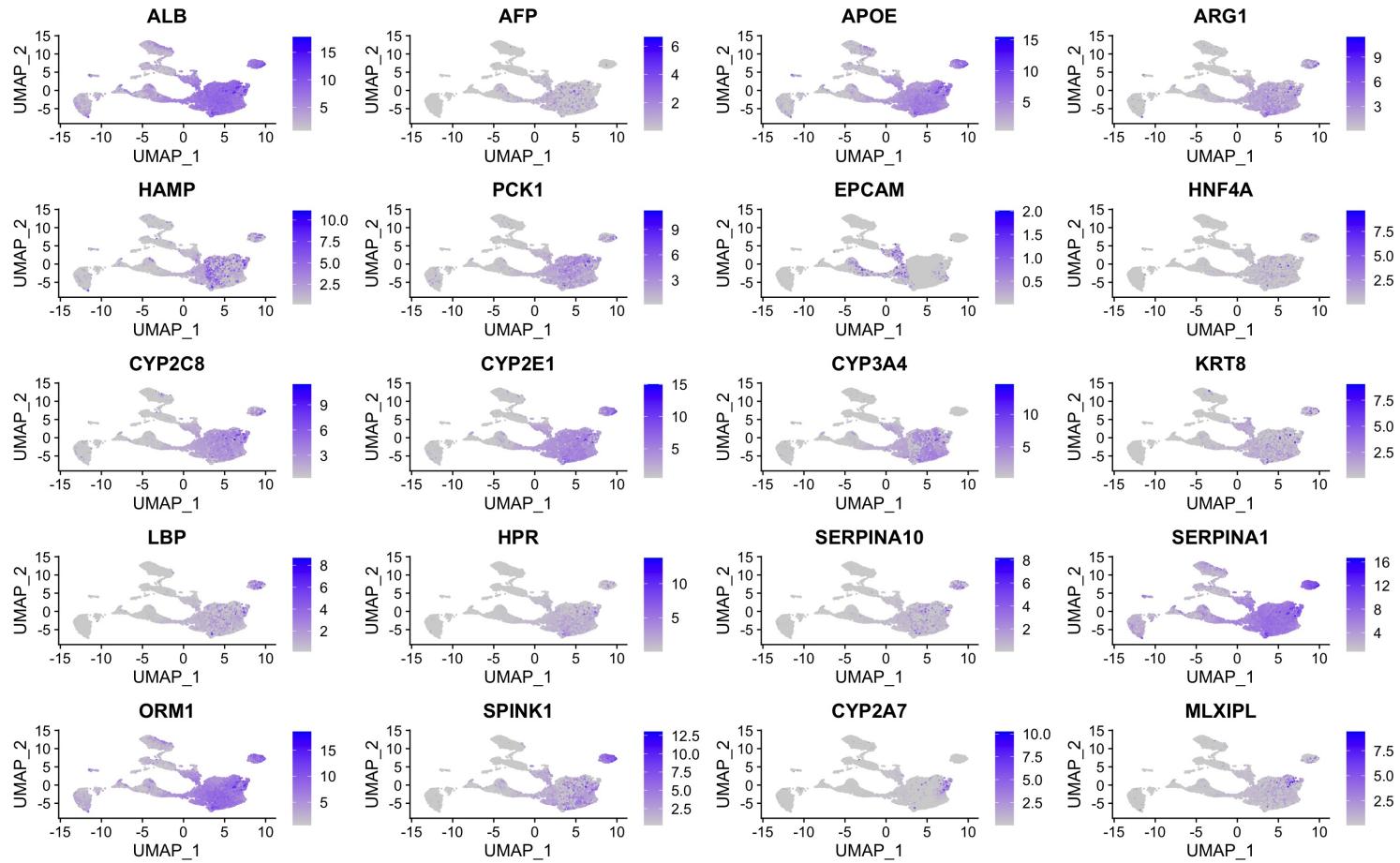
A

Figure 4.4 A. UMAPs showing the expression level of 20 representative hepatocyte-associated genes.

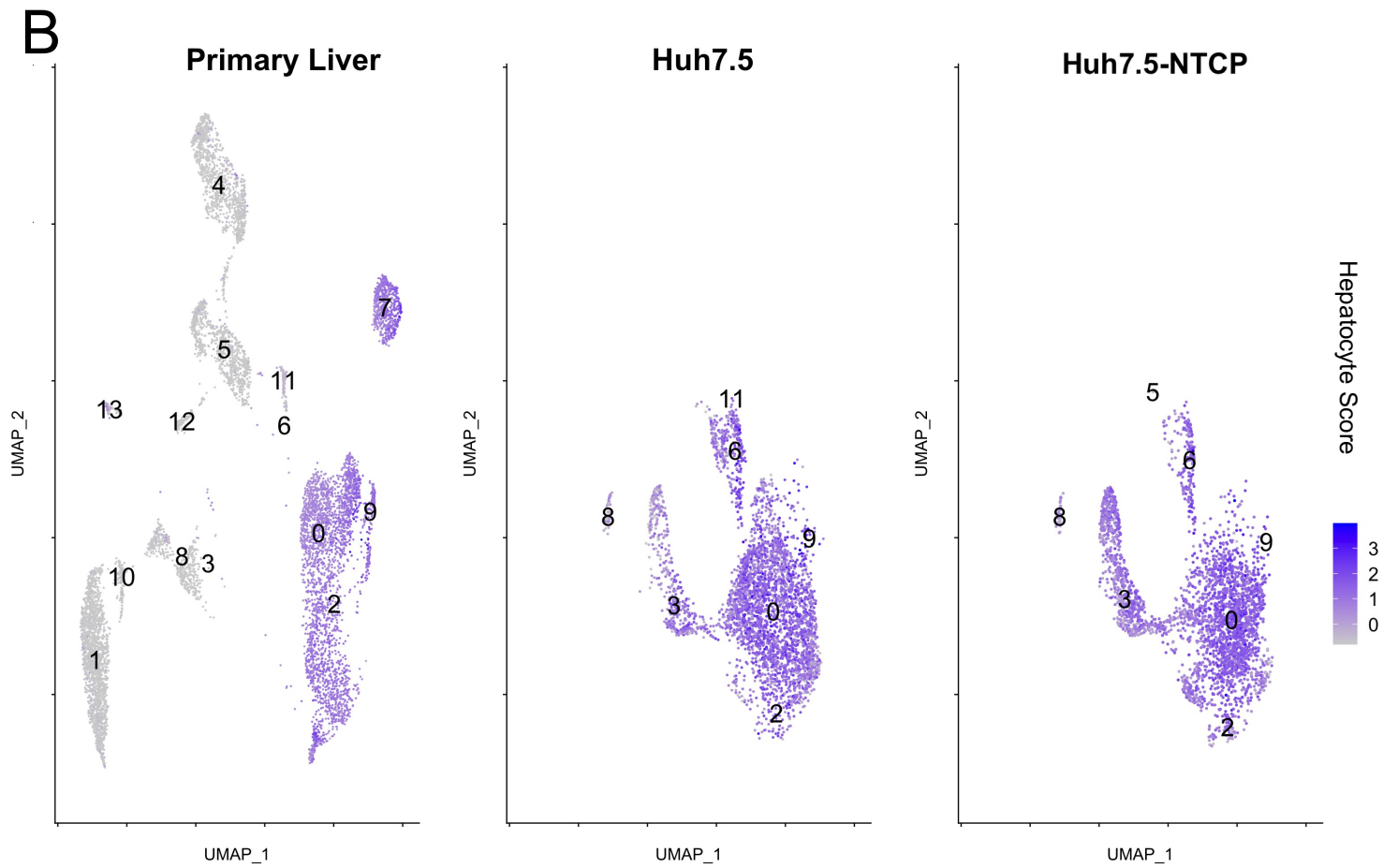


Figure 4.4 B. UMAPs of primary liver, Huh7.5, and Huh7.5-NTCP cells illustrating hepatocyte score, the average expression of hepatocyte-associated genes.

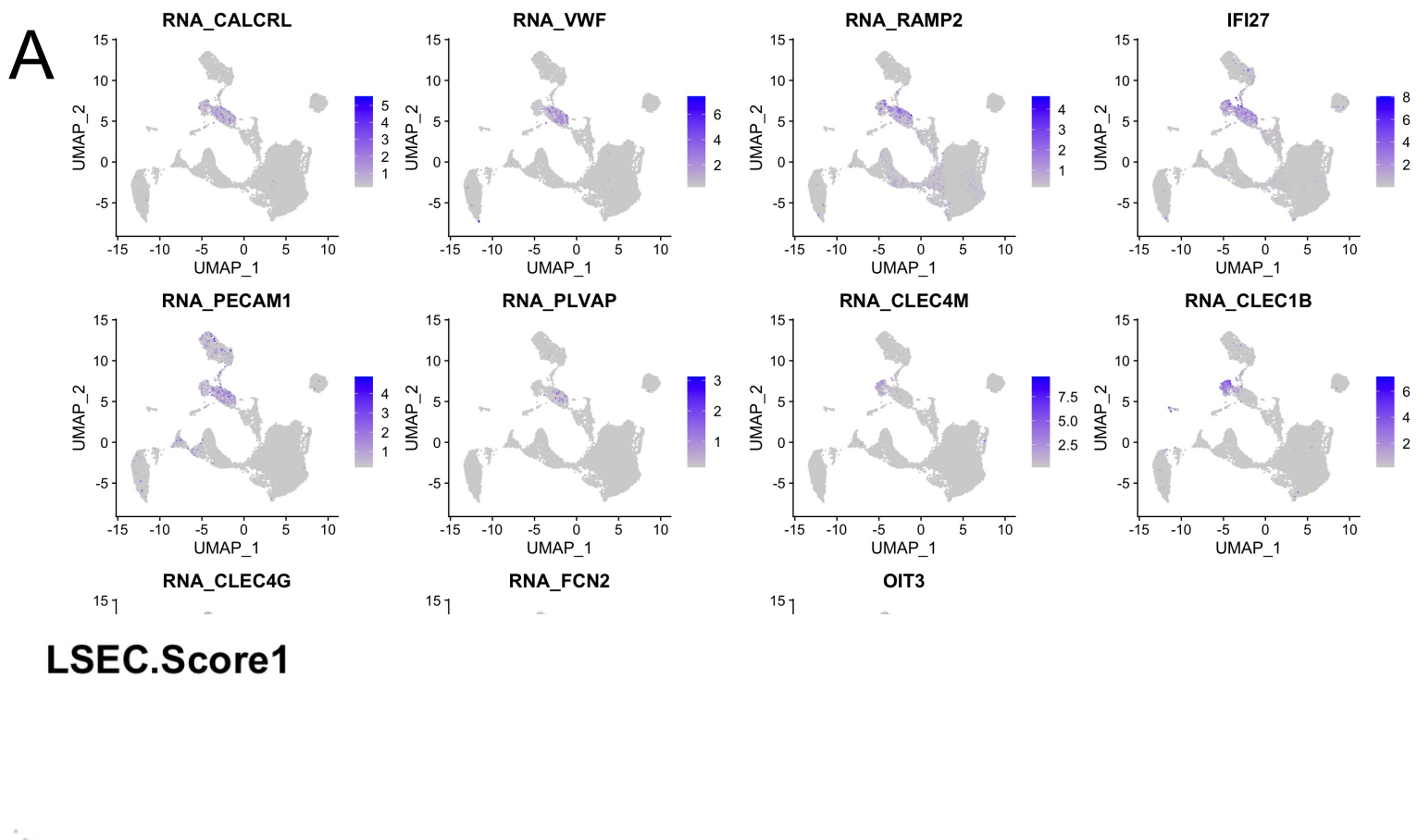


Figure 4.5 A. UMAPs showing the expression level of 11 LSEC-associated genes.

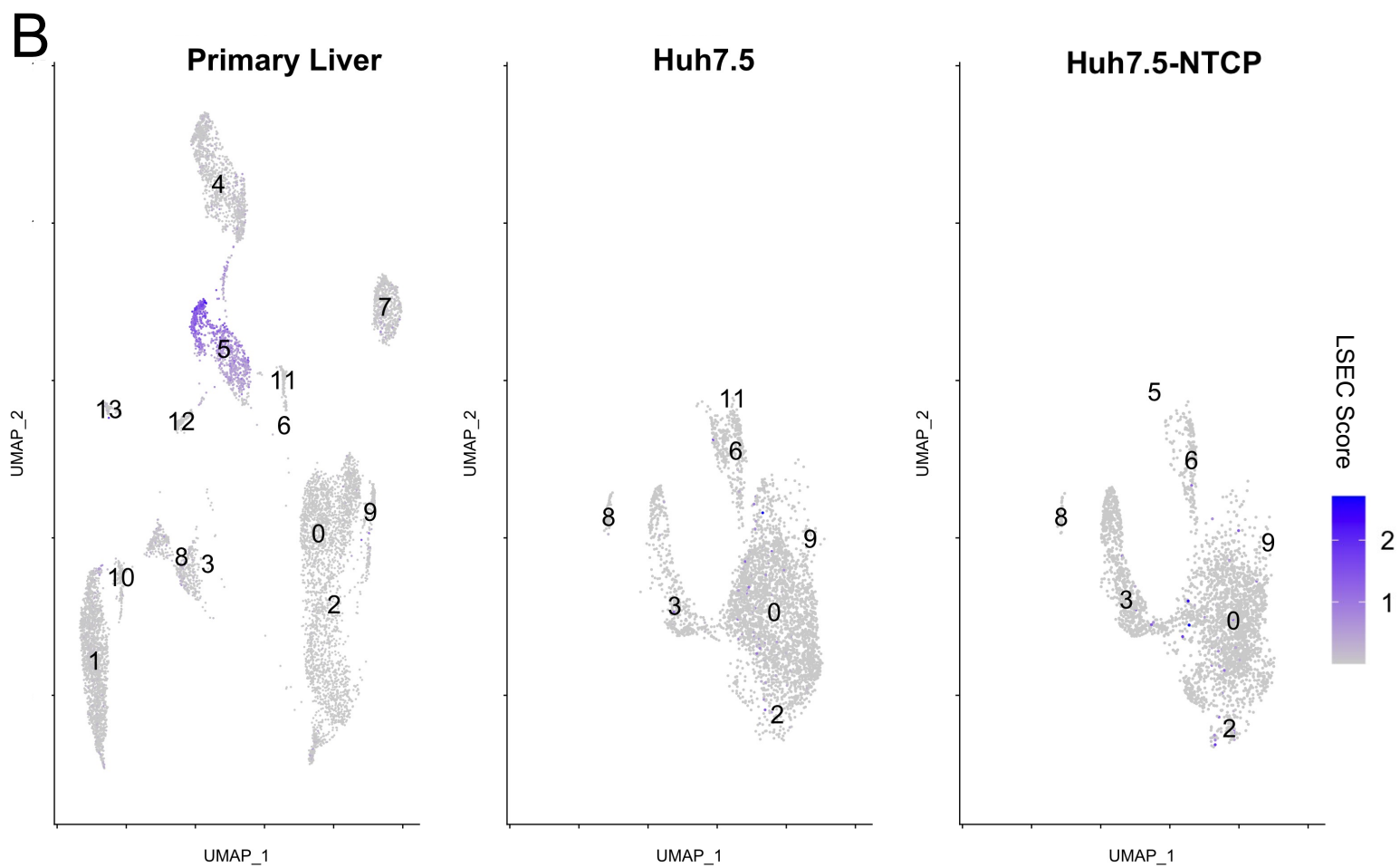


Figure 4.5 B. UMAPs illustrating LSEC score, the average expression of LSEC-associated genes.

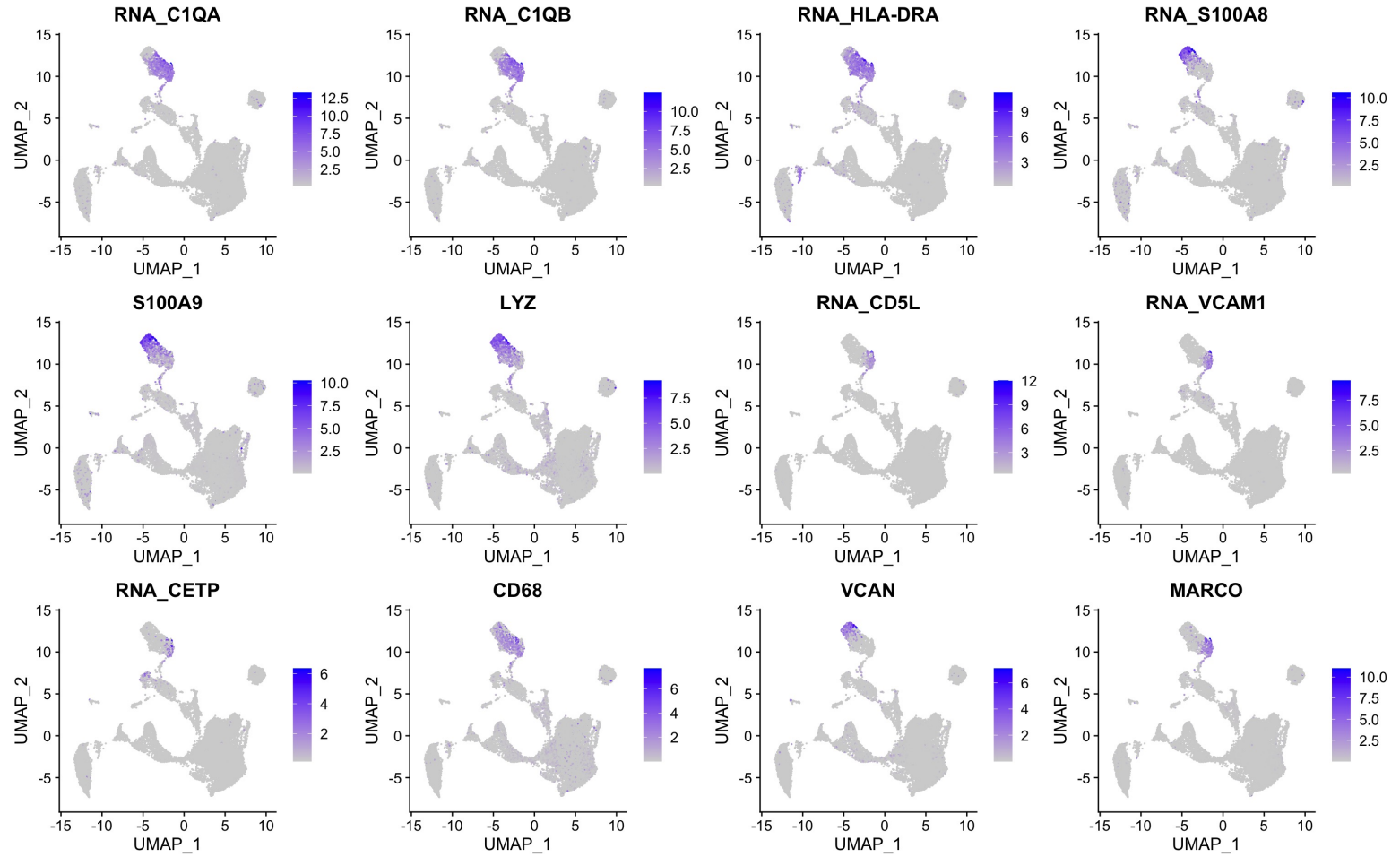
A

Figure 4.6 A. UMAPs showing the expression level of 12 monocyte- and macrophage-associated genes.

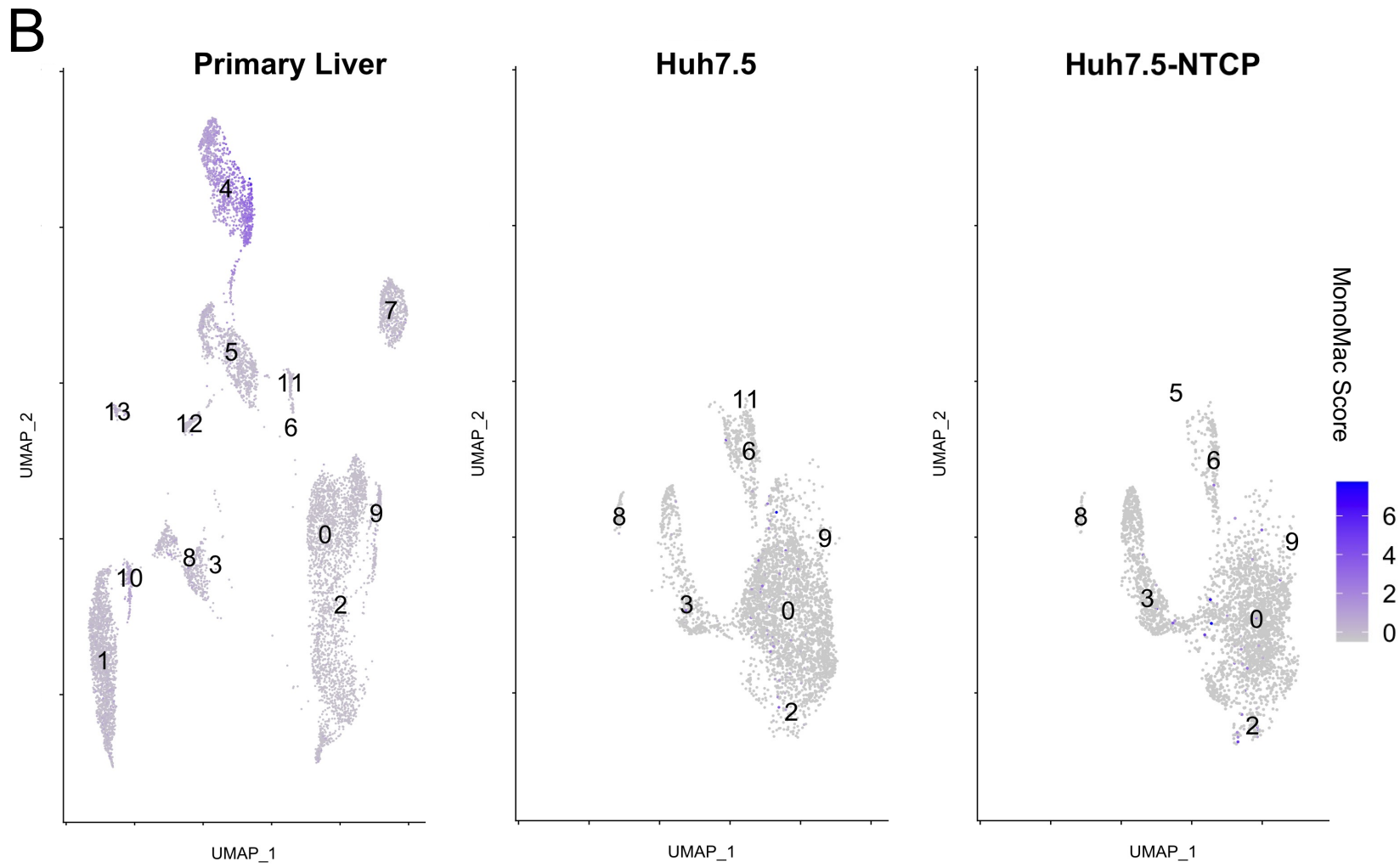


Figure 4.6 B. UMAPs illustrating MonoMac score, the average expression of monocyte- and macrophage-associated genes.

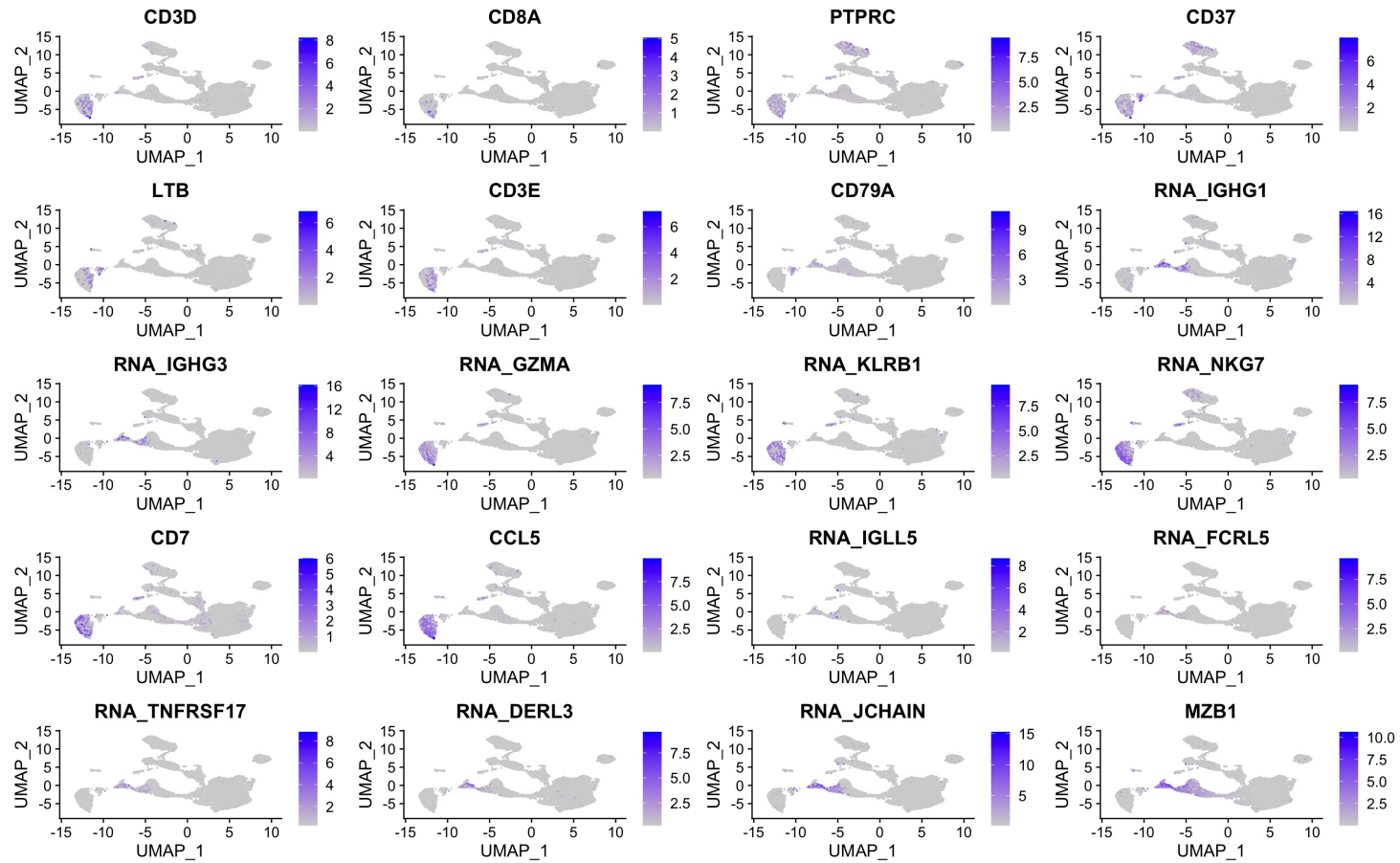
A

Figure 4.7 A. UMAPs showing the expression level of 20 lymphocyte-associated genes.

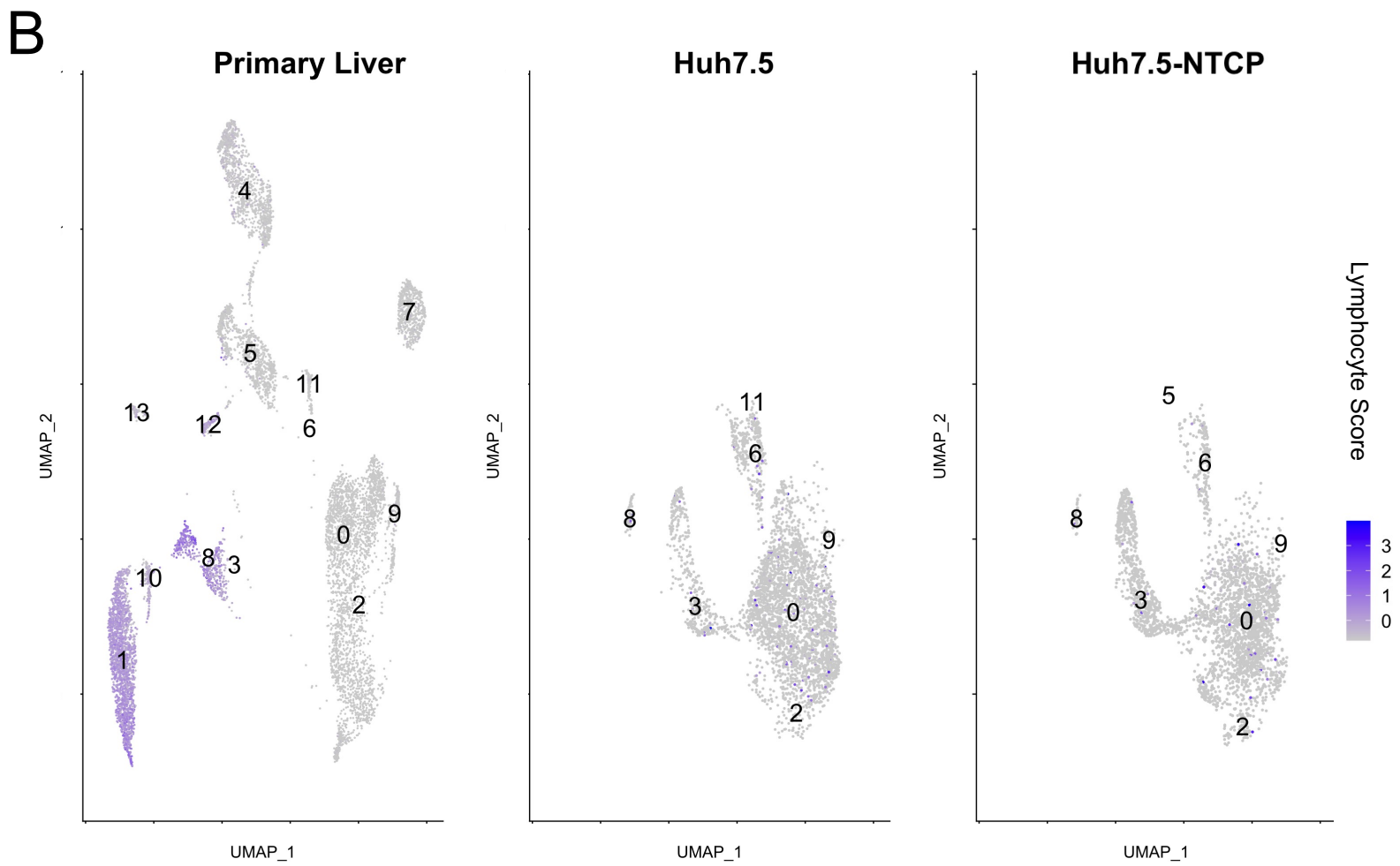


Figure 4.7 B. UMAPs illustrating lymphocyte score, the average expression of lymphocyte-associated genes.

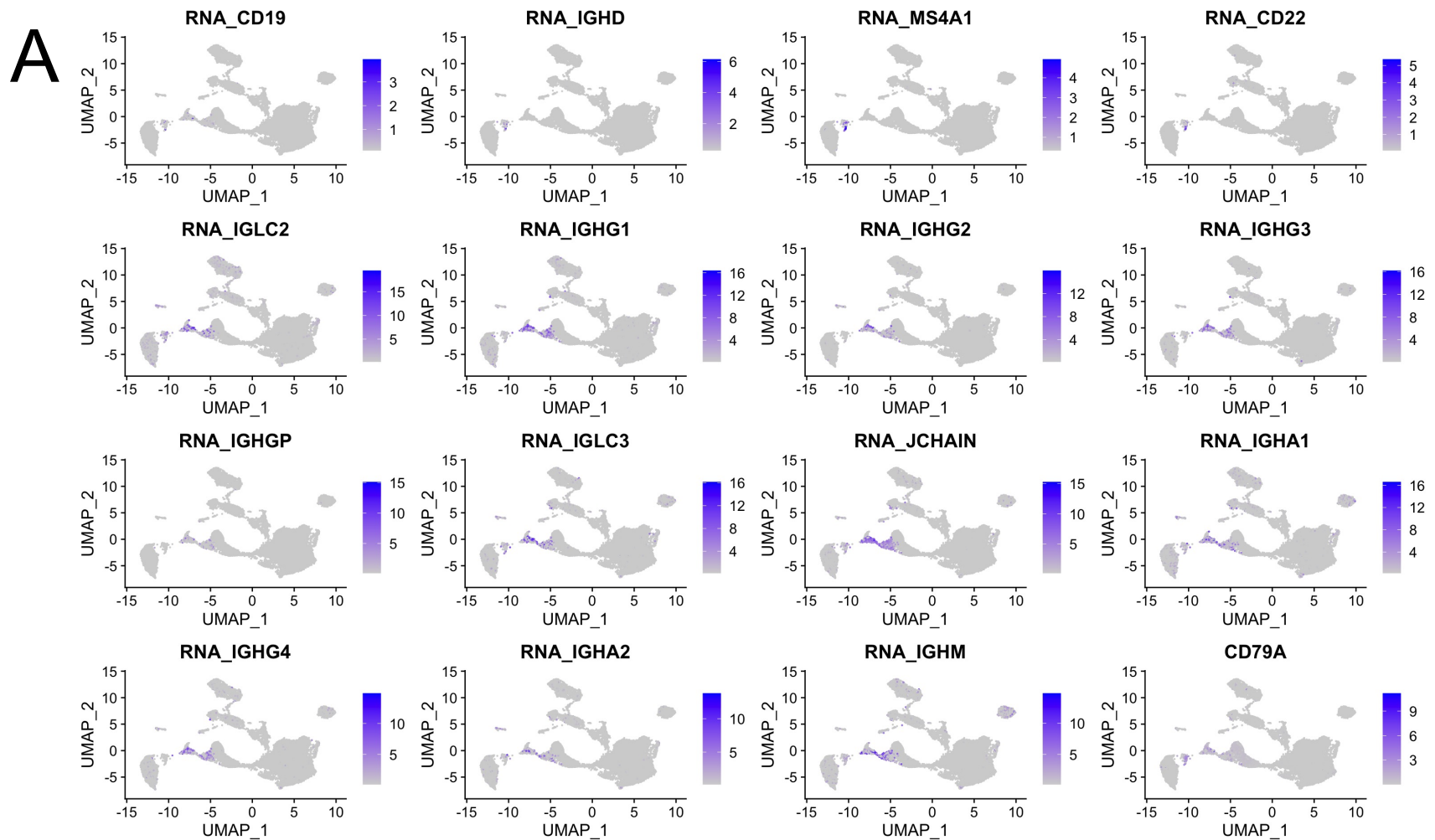


Figure 4.8 A. UMAPs showing the expression level of 16 B cell-associated genes.

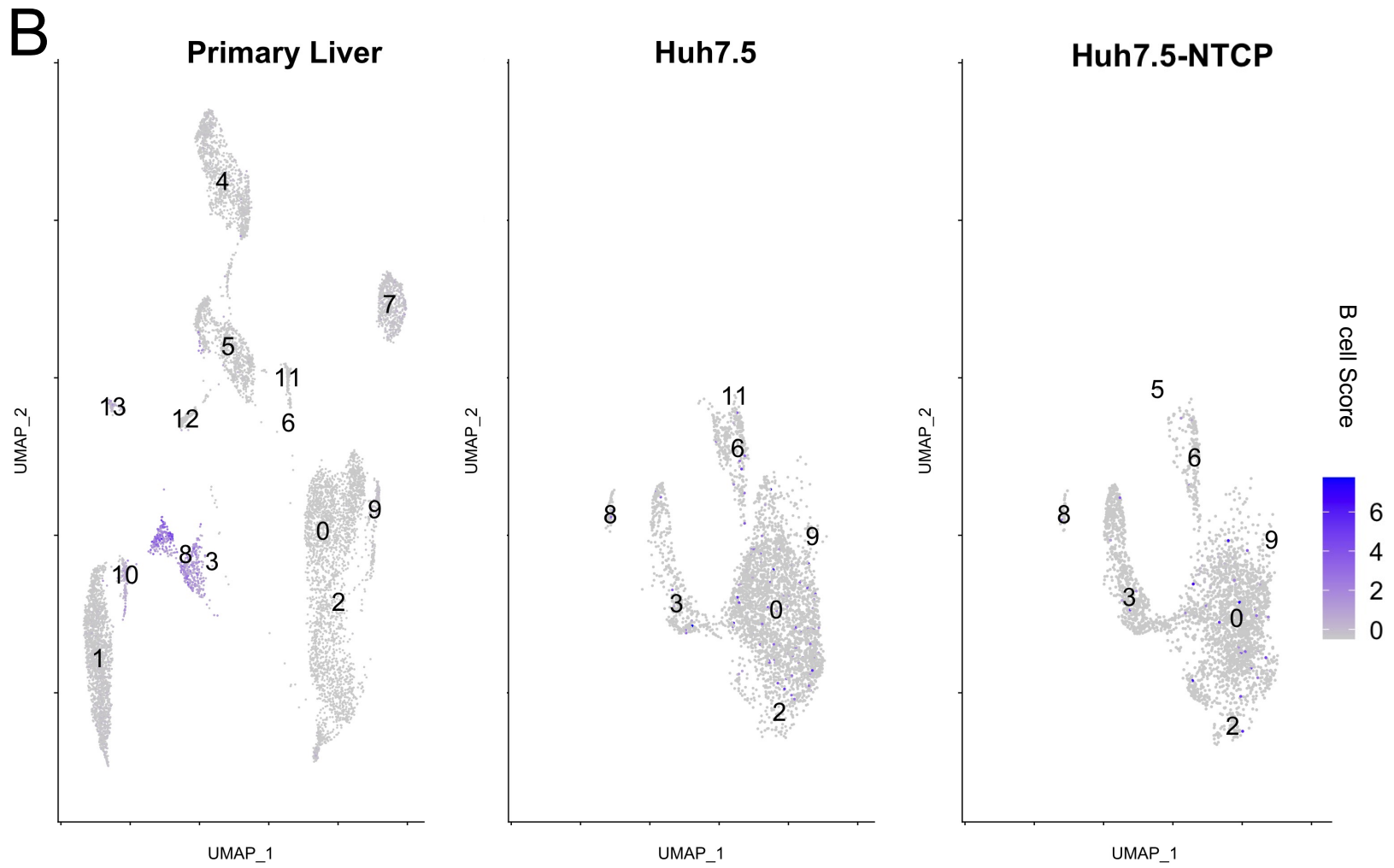


Figure 4.8 B. UMAPs illustrating B cell score, the average expression of B cell-associated genes.

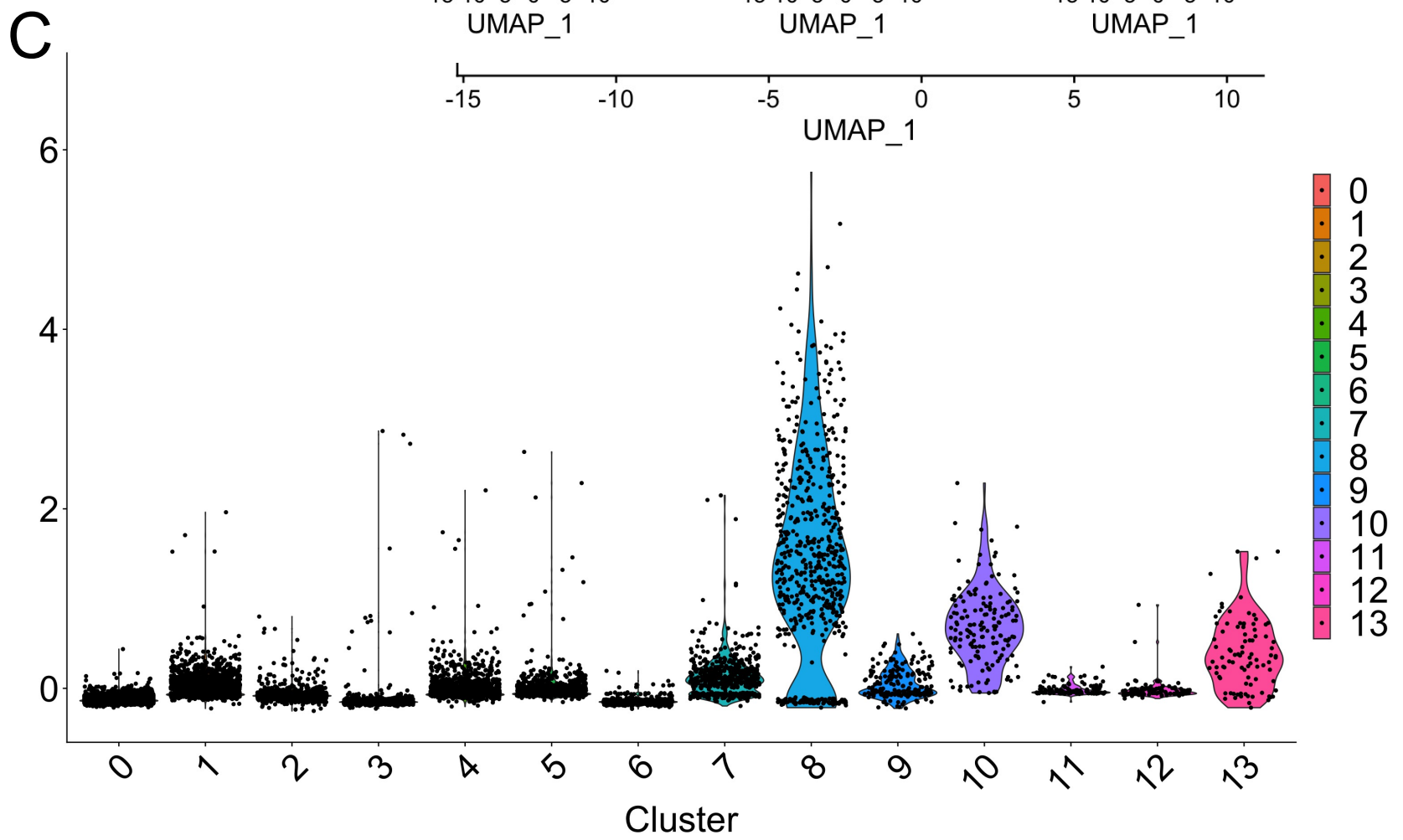


Figure 4.8 C. Violin plot illustrating B cell score in various clusters.

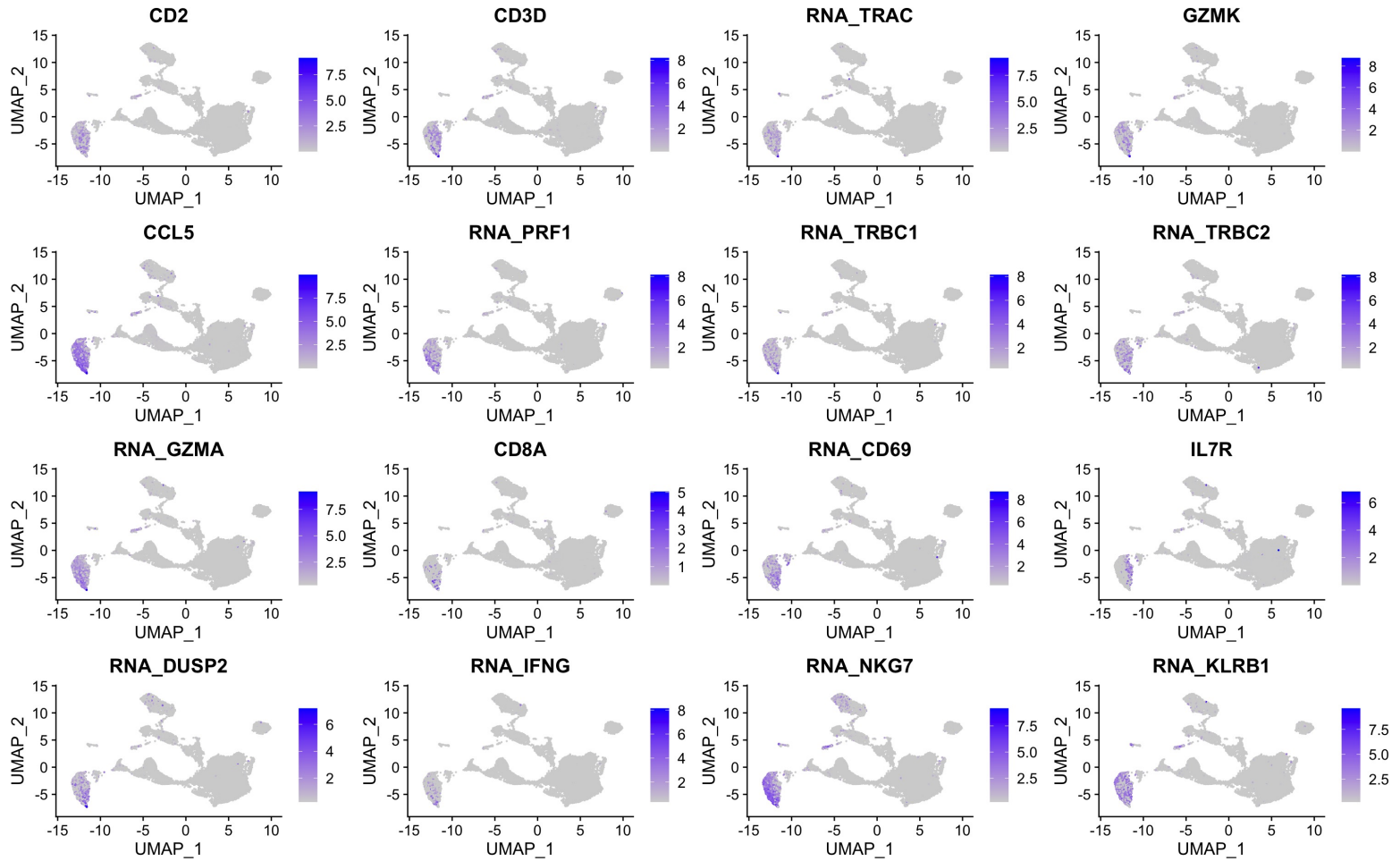
A

Figure 4.9 A. UMAPs showing the expression level of 16 T cell- and NK cell-associated genes.

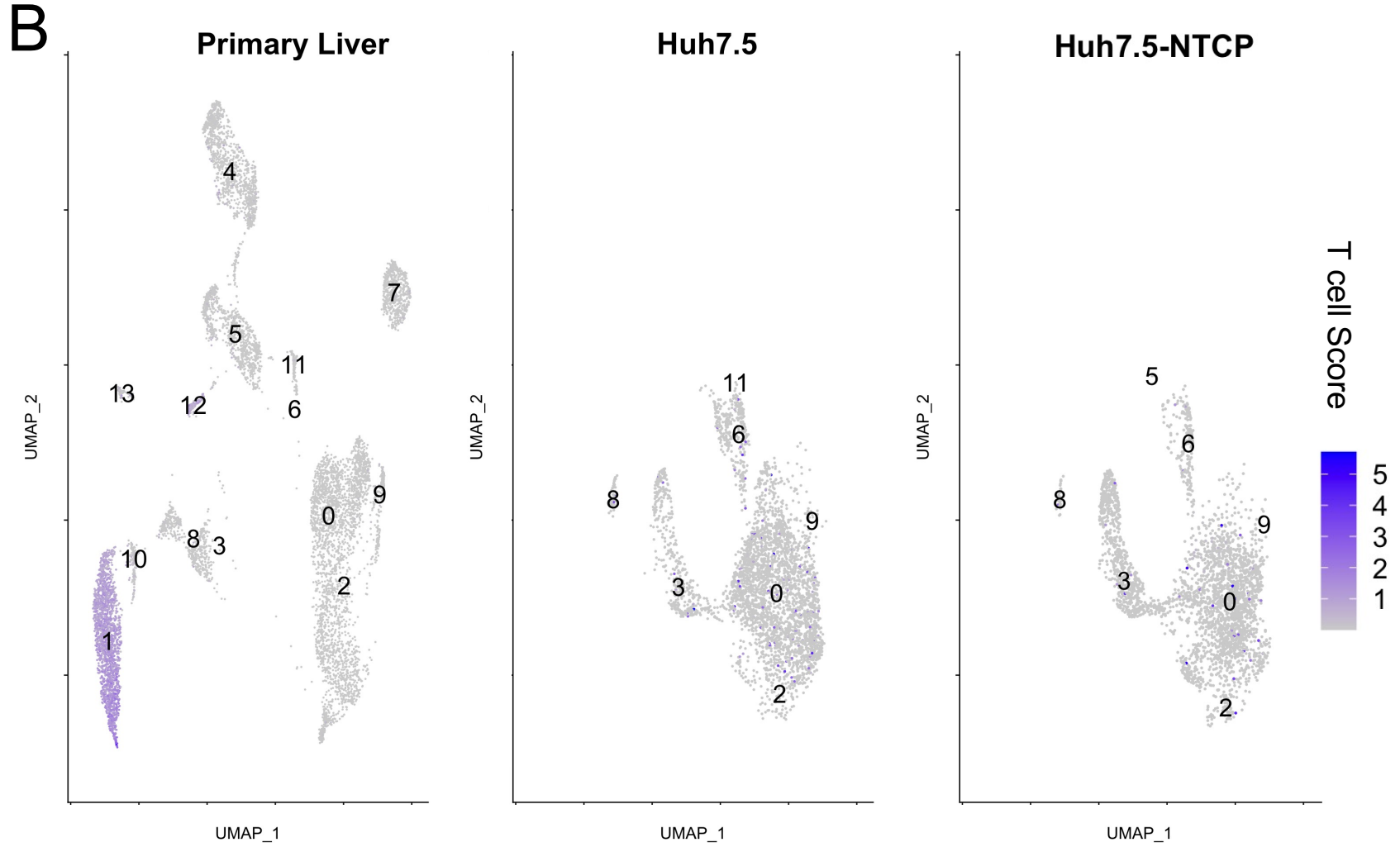


Figure 4.9 B. UMAPs illustrating T cell score, the average expression of T cell- and NK cell-associated genes.

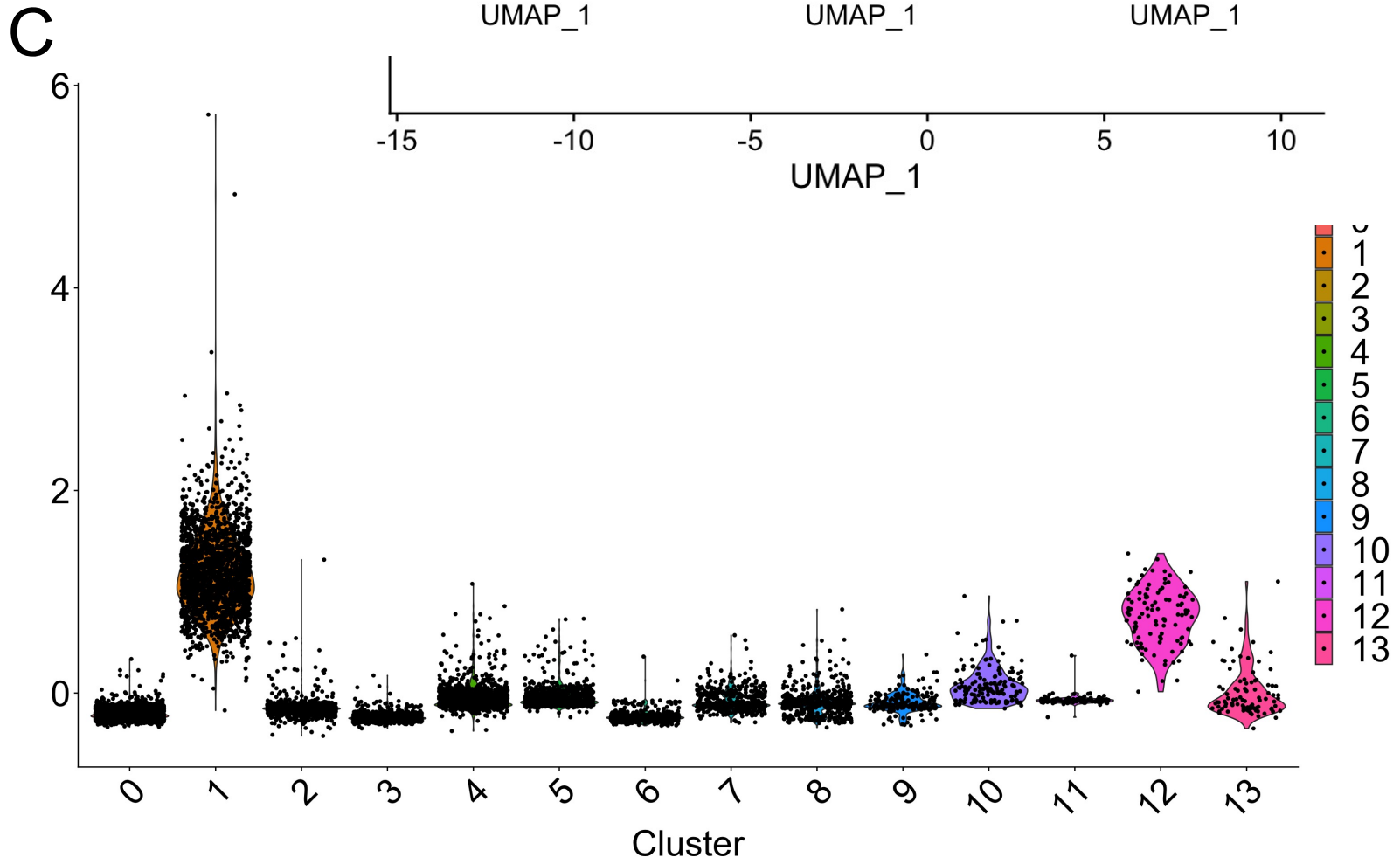


Figure 4.9 C. Violin plot illustrating T cell score in various clusters.

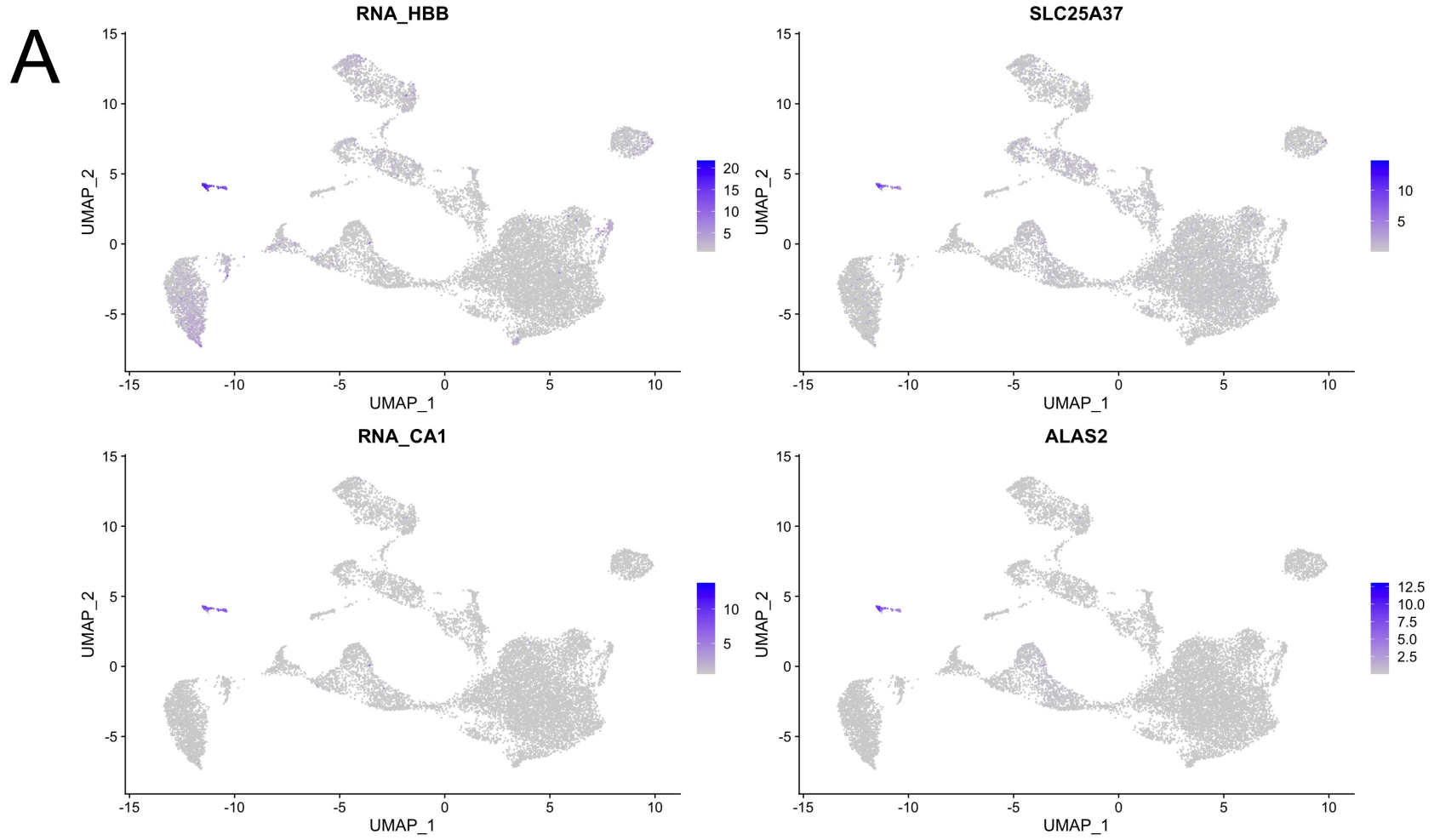


Figure 4.10 A. UMAPs showing the expression level of four erythroid cell-associated genes.

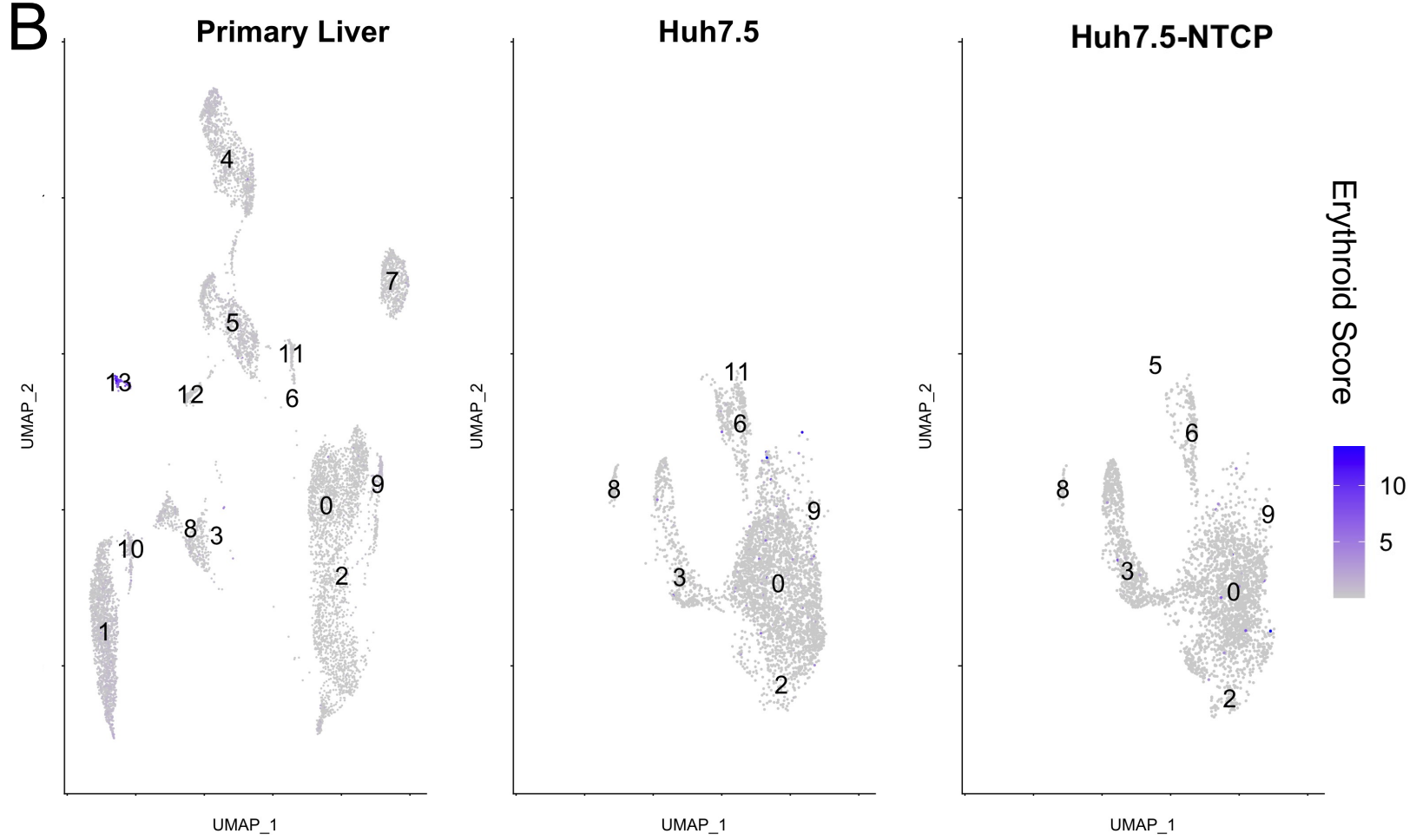


Figure 4.10 B. UMAPs illustrating erythroid score, the average expression of erythroid cell-associated genes.

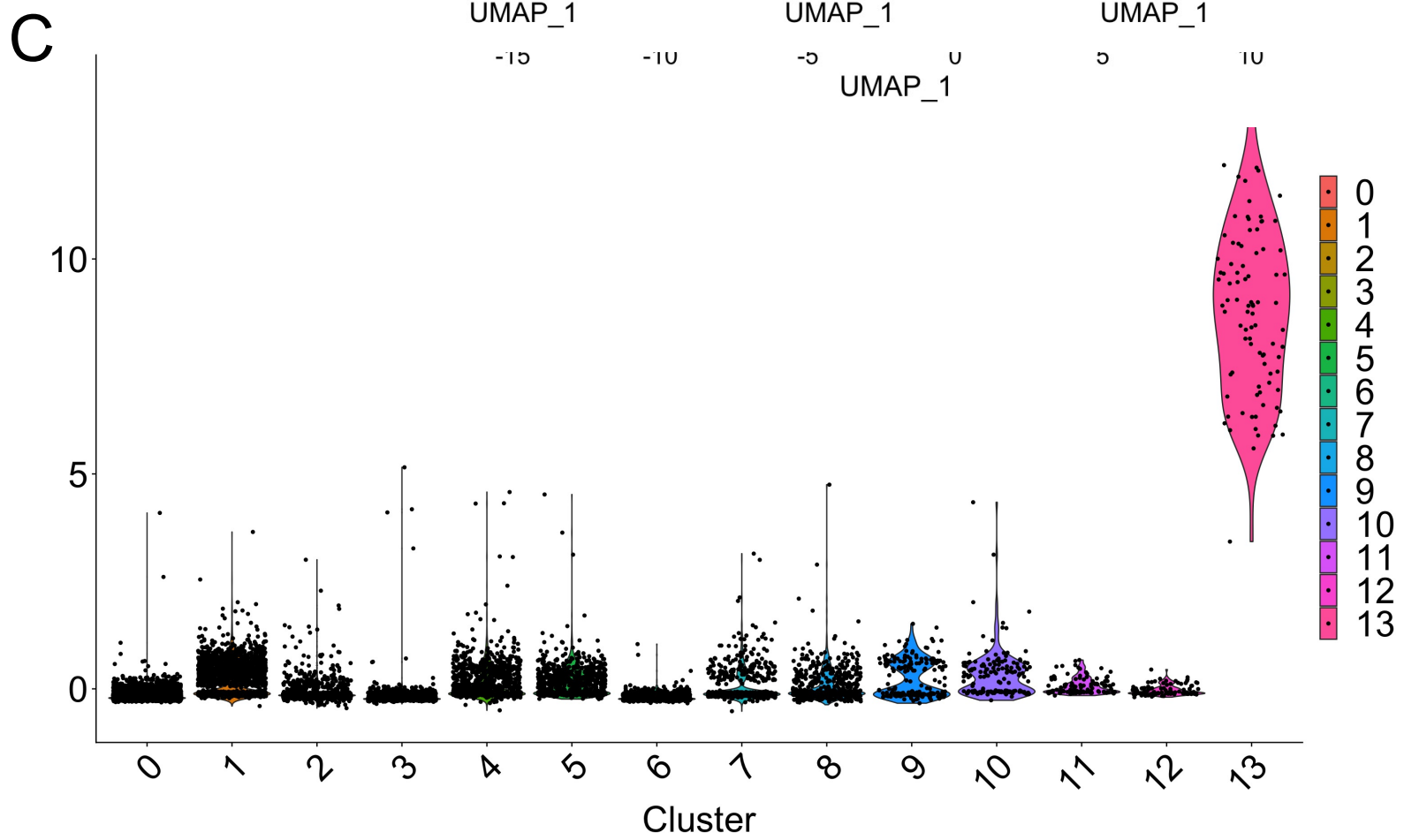


Figure 4.10 C. Violin plot illustrating erythroid score in different clusters.

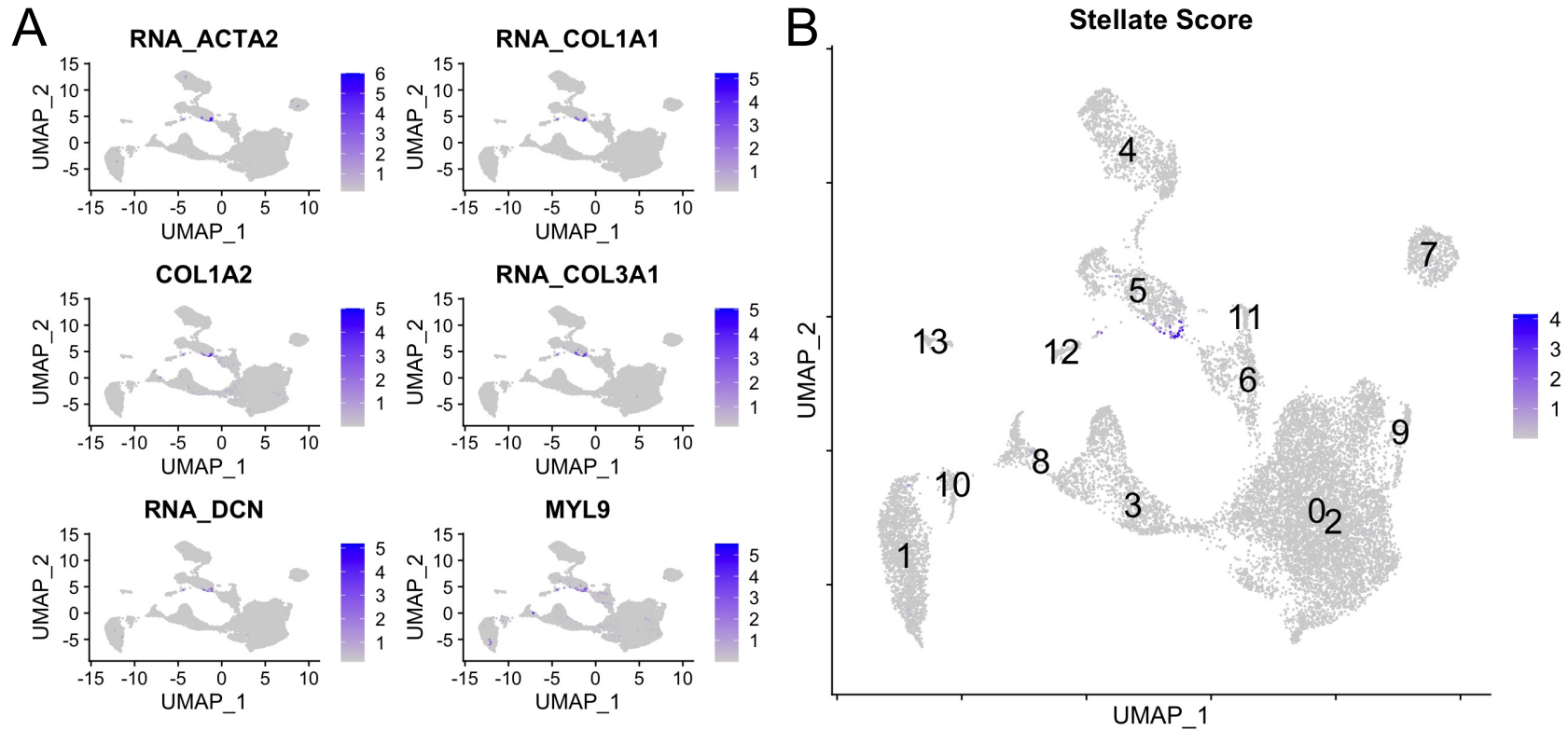


Figure 4.11. (A) UMAPs showing the expression level of six stellate cell genes. (B) UMAPs of integrated primary liver and two hepatoma cell line datasets illustrating stellate score, the average expression of stellate cell-associated genes, in different clusters.

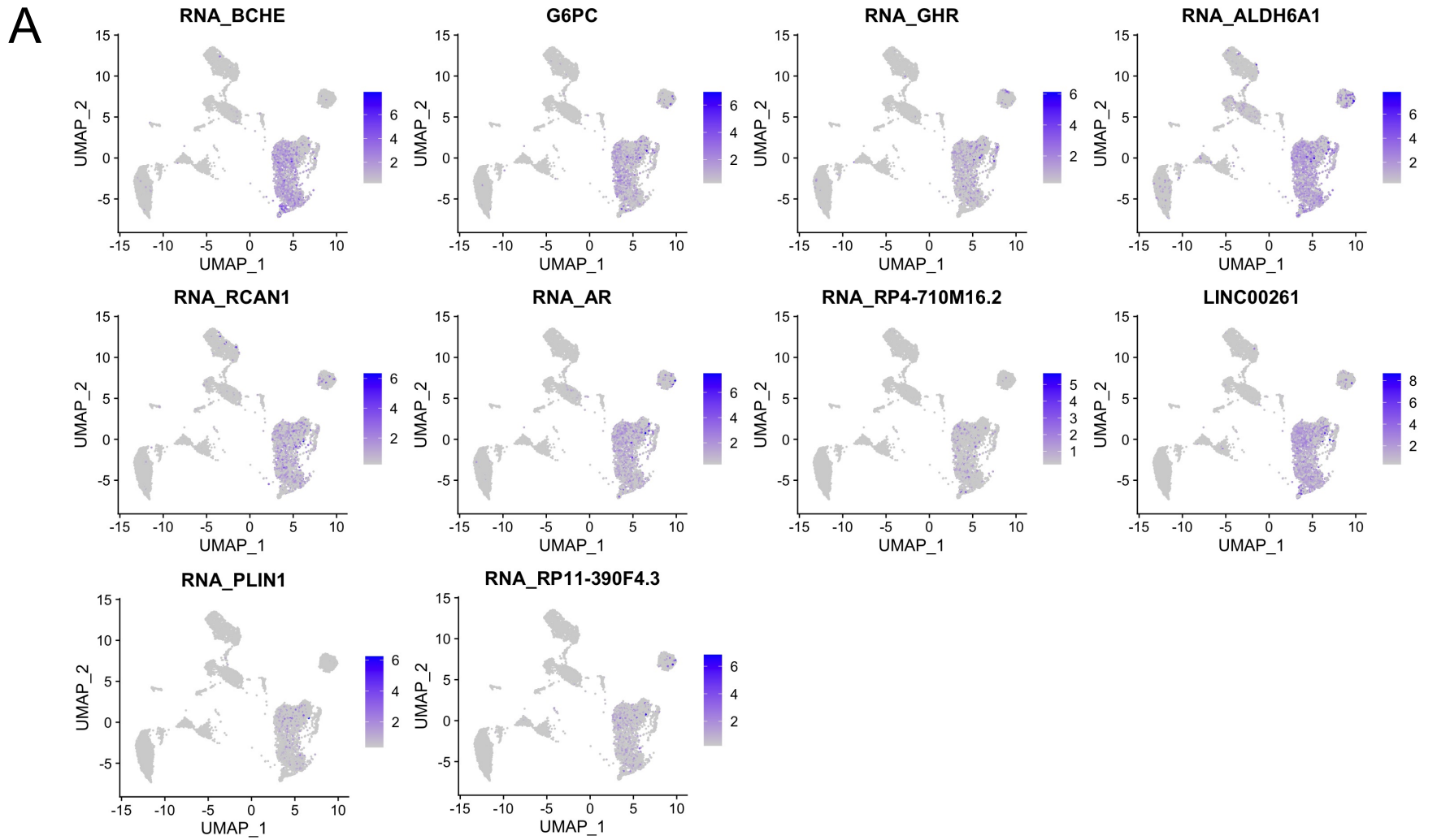


Figure 4.12 A. UMAPs showing the expression level of ten pericentral hepatocyte genes in primary liver (MacParland *et al.* 2018).

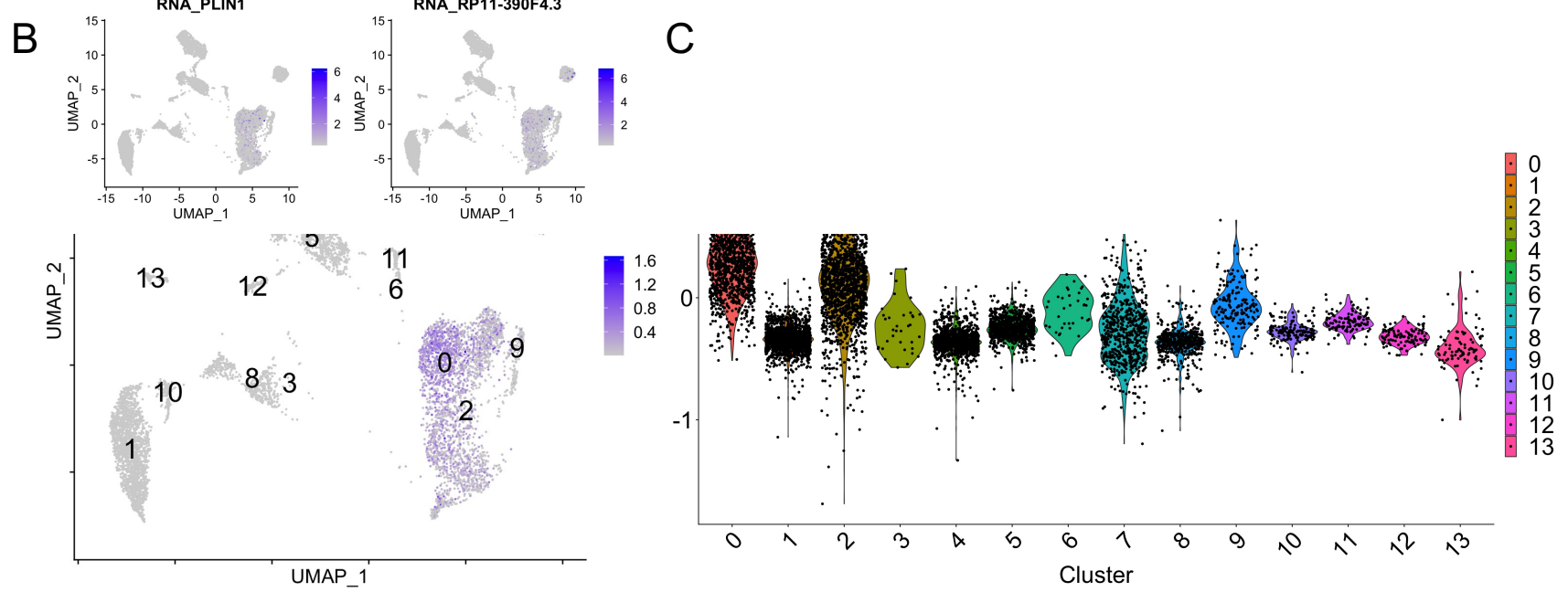


Figure 4.12. (B) UMAP and (C) violin plot of primary liver dataset illustrating pericentral hepatocyte score, the average expression of pericentral hepatocyte associated genes, in different clusters.

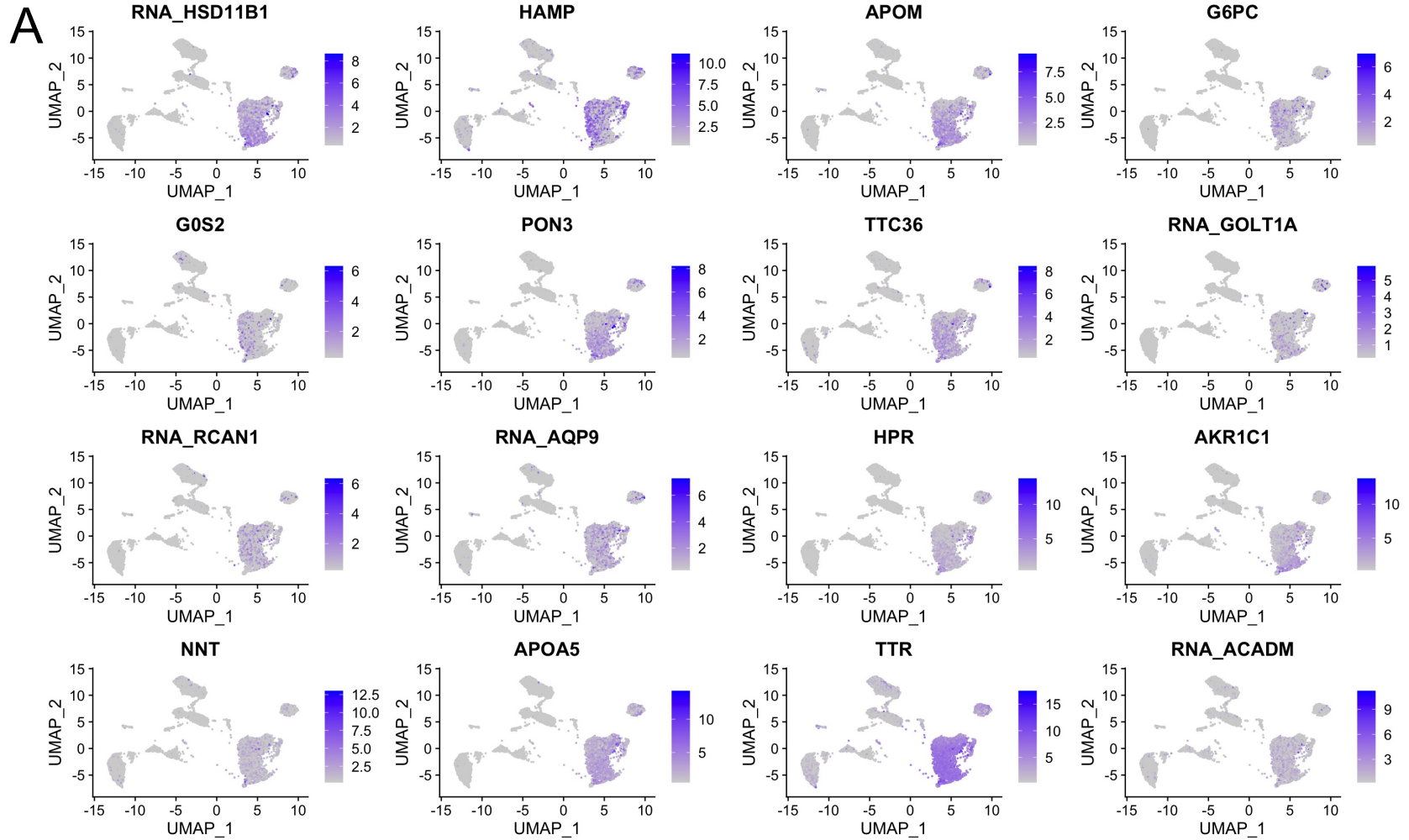


Figure 4.13 A. UMAPs showing the expression level of 16 midcentral hepatocyte genes in primary liver (MacParland *et al.* 2018).

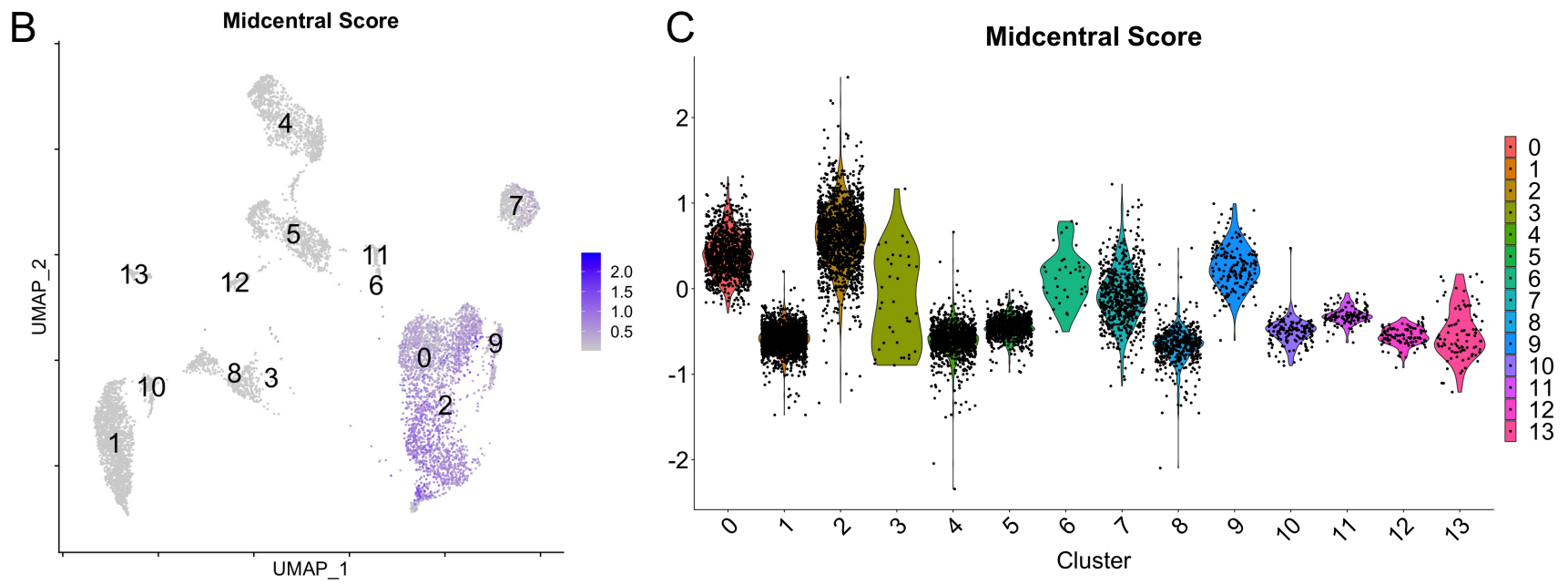


Figure 4.13. (B) UMAP and (C) violin plot of primary liver dataset illustrating midcentral hepatocyte score, the average expression of midcentral hepatocyte associated genes, in different clusters.

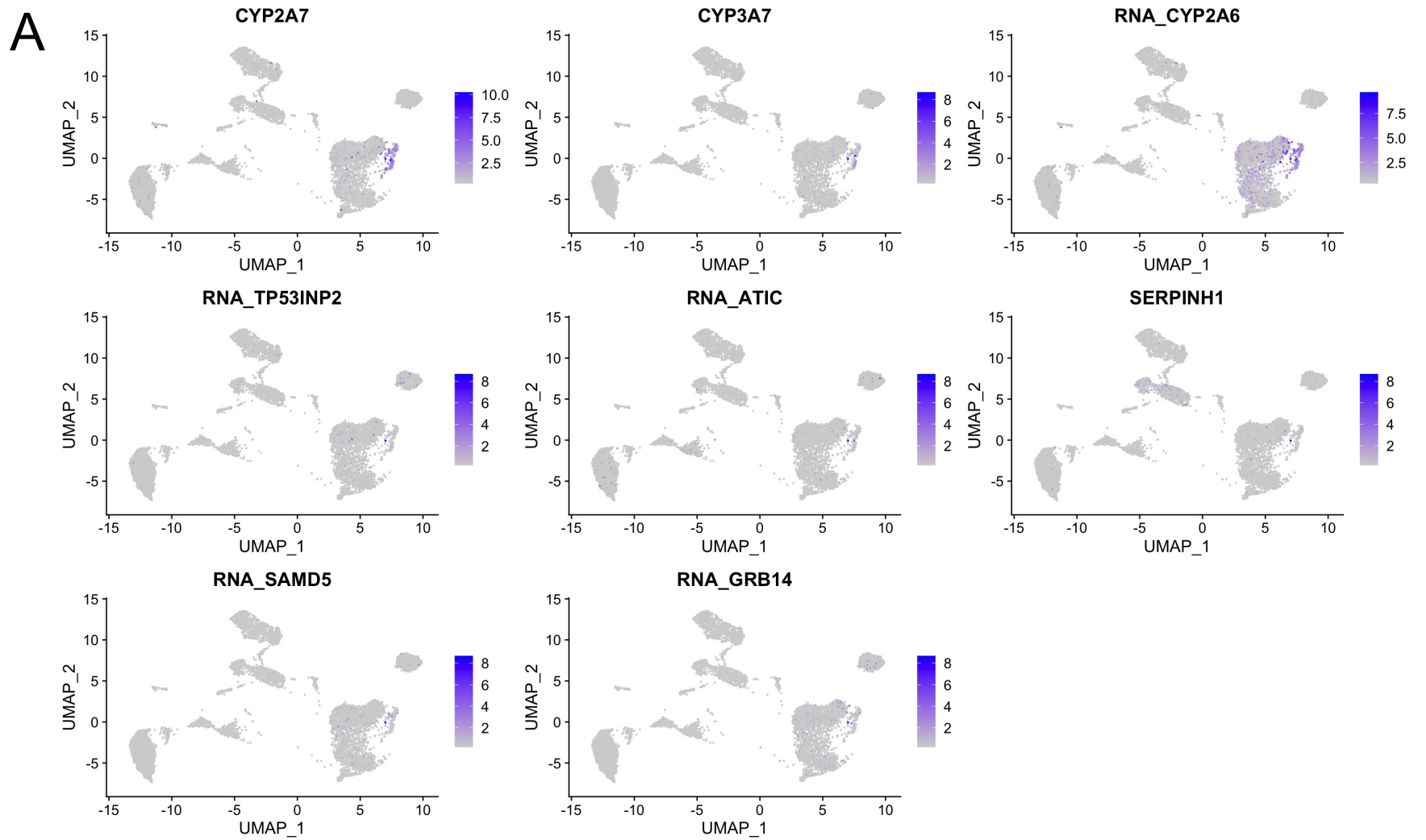


Figure 4.14 A. UMAPs showing the expression level of eight midportal hepatocyte genes in primary liver (MacParland *et al.* 2018).

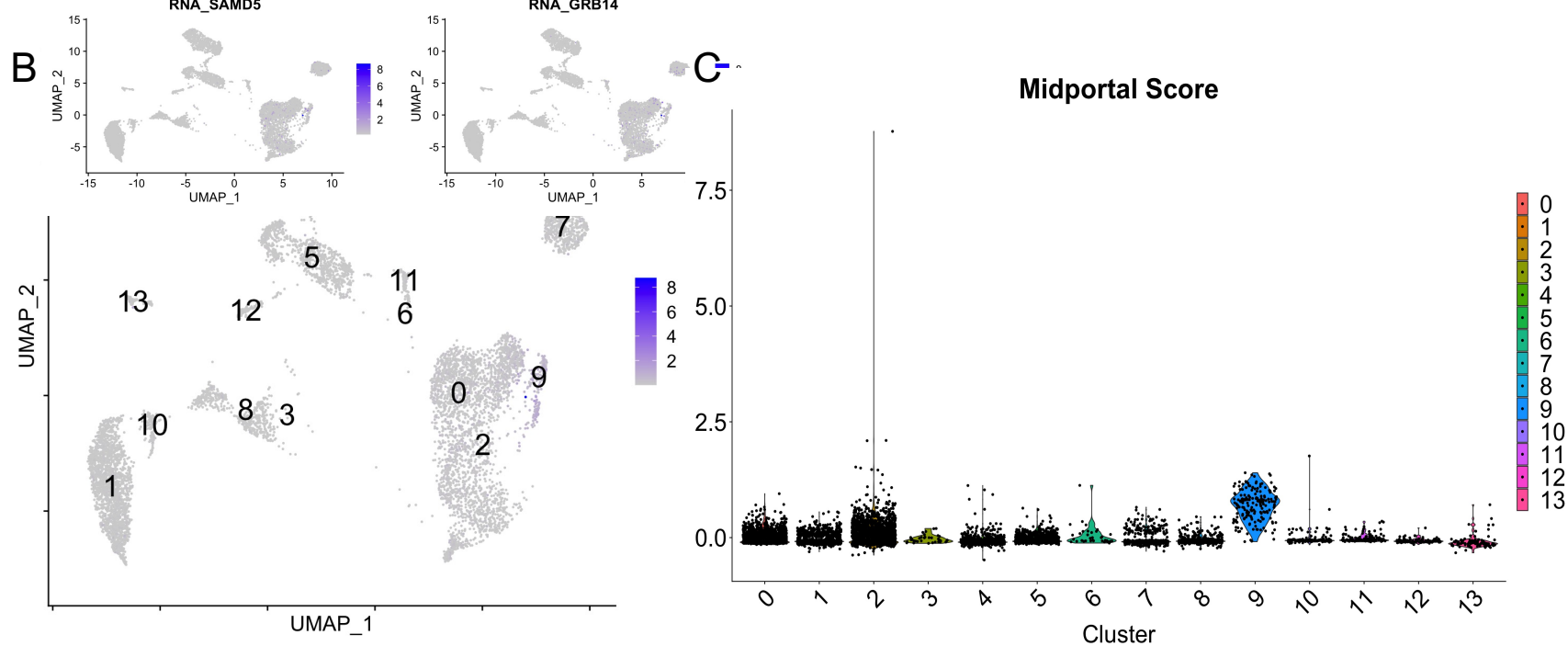


Figure 4.14. (B) UMAP and (C) violin plot of primary liver dataset illustrating midportal hepatocyte score, the average expression of midportal hepatocyte associated genes, in different clusters.

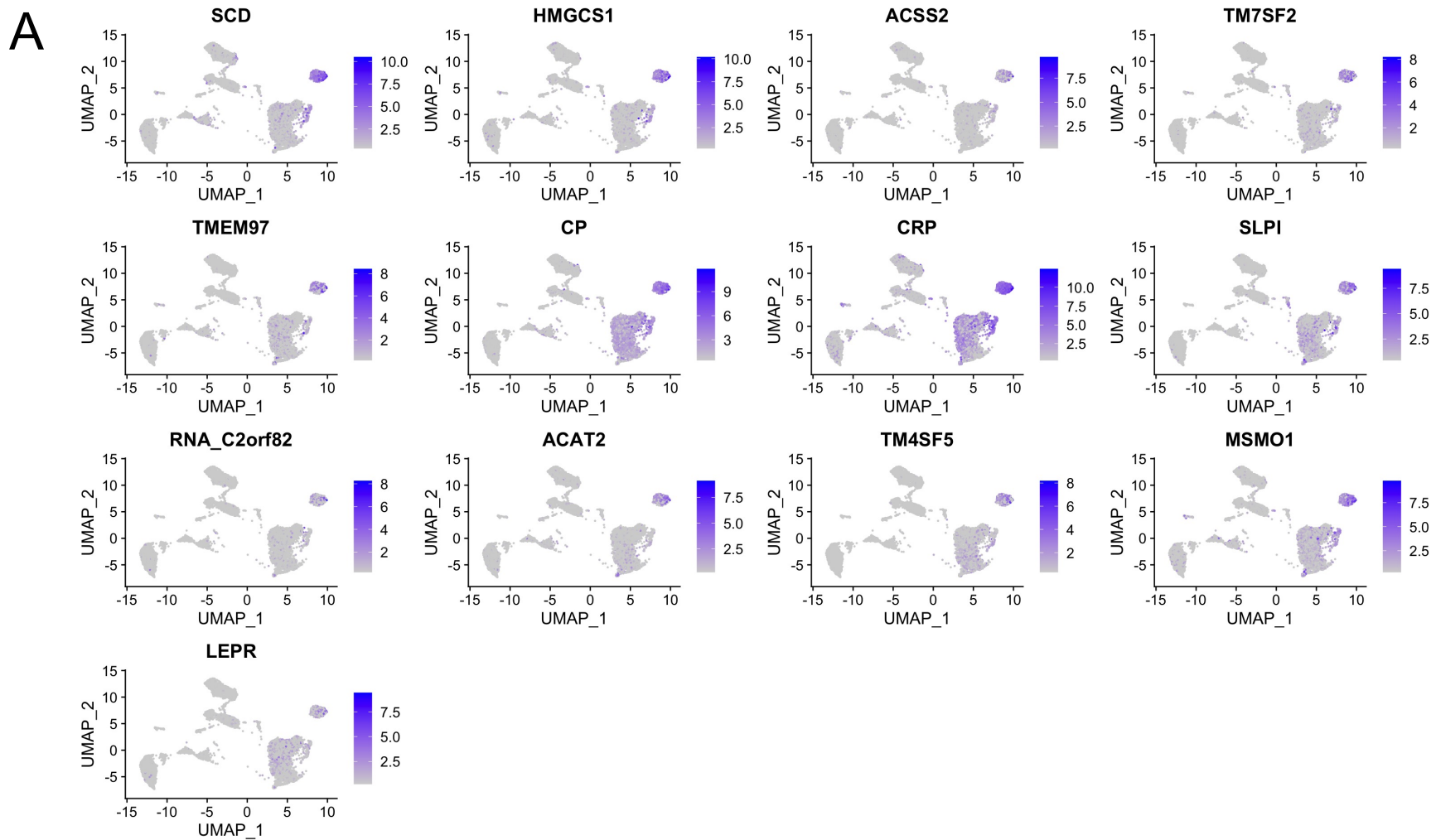


Figure 4.15 A. UMAPs showing the expression level of 13 periportal hepatocyte genes in primary liver (MacParland *et al.* 2018).

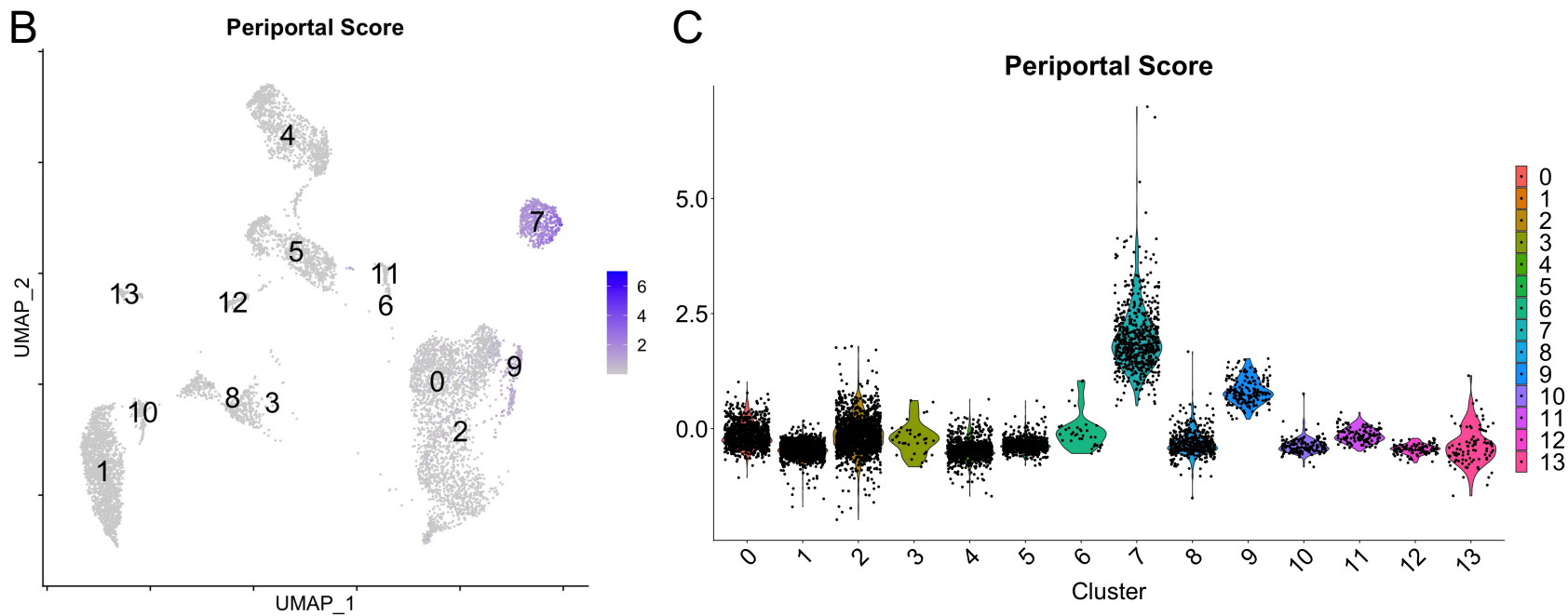


Figure 4.15. (B) UMAP and (C) violin plot of primary liver dataset illustrating periportal hepatocyte score, the average expression of periportal hepatocyte associated genes, in different clusters.

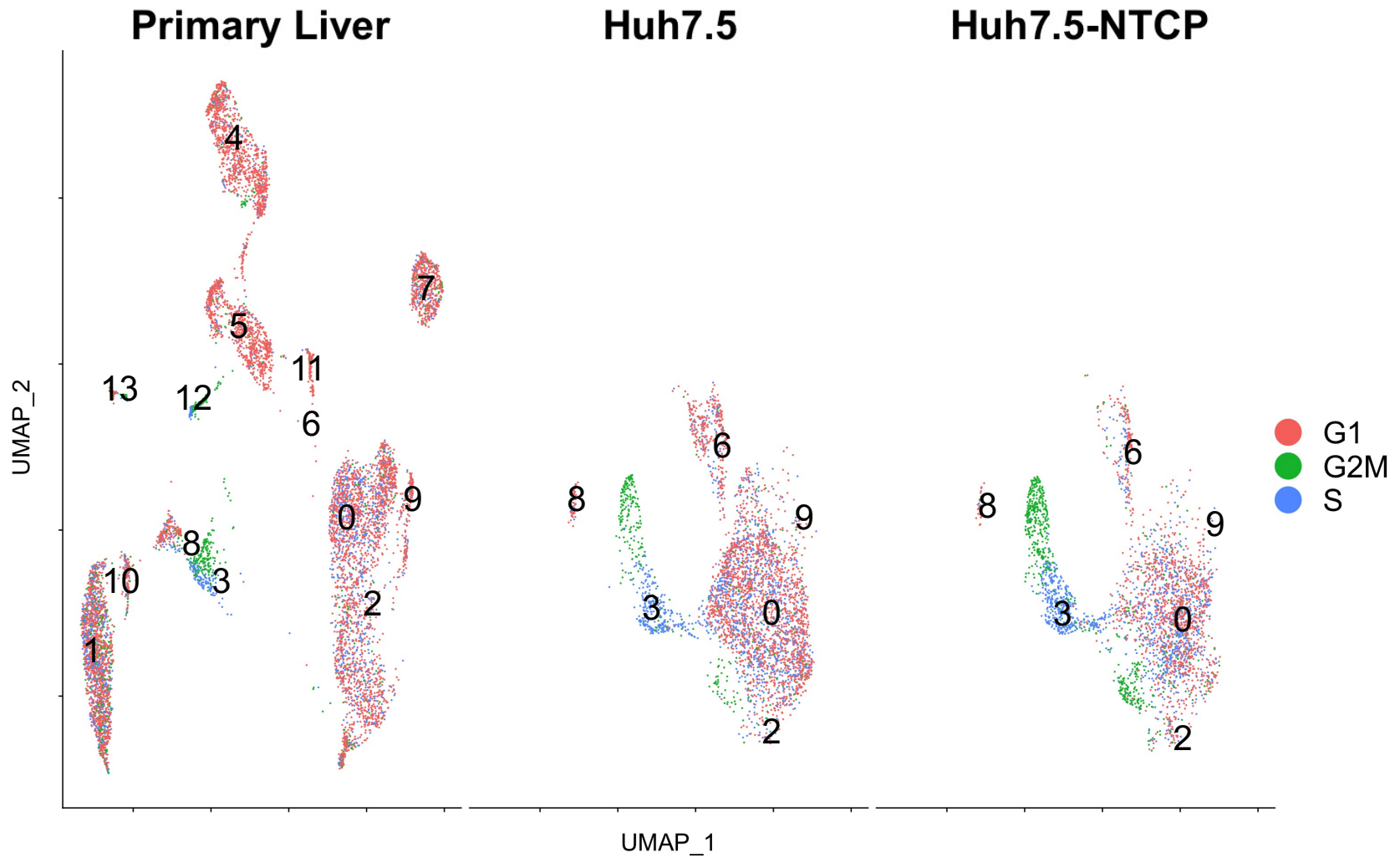


Figure 4.16. Cell-cycle phase prediction of human liver, and HS-differentiated Huh7.5 and Huh7.5-NTCP cells. Red represents G1 quiescent cells. Green (G2 and M phase) and blue (S phase) represents proliferative and dividing cells.

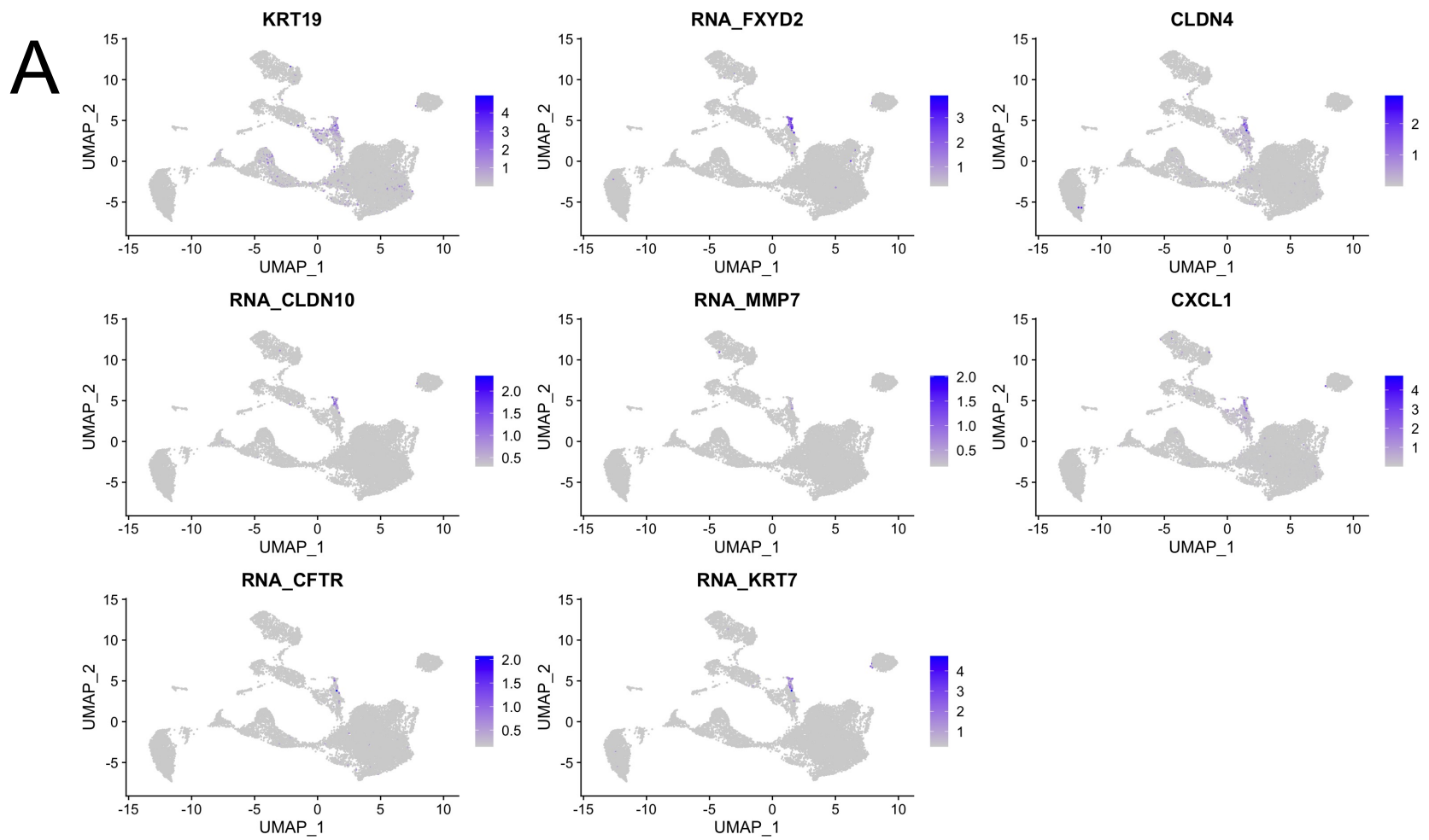


Figure 4.17 A. UMAPs showing the expression level of eight cholangiocyte-associated genes.

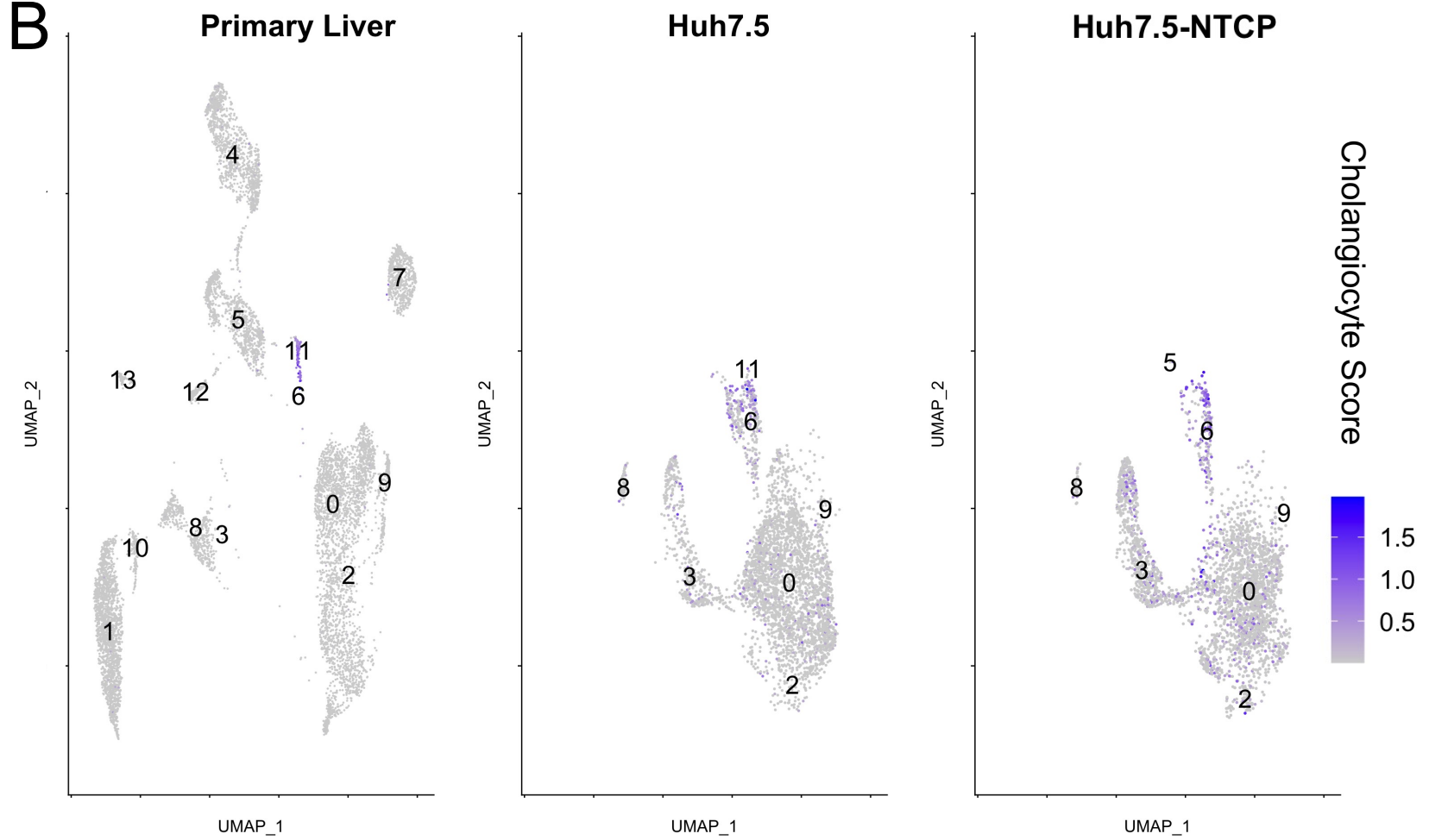


Figure 4.17 B. UMAPs illustrating cholangiocyte score, the average expression of cholangiocyte-associated genes, in primary liver and hepatoma cell lines.

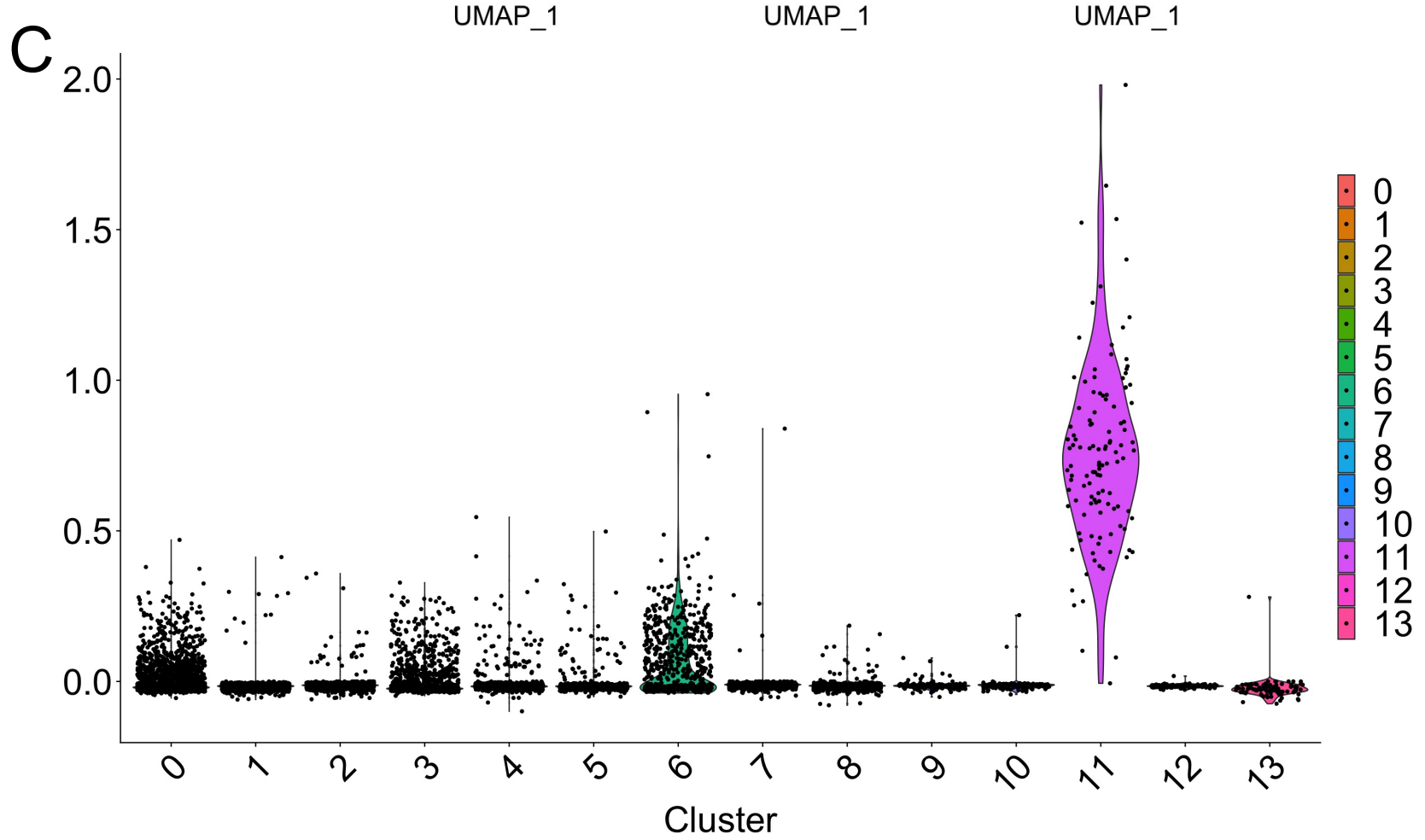


Figure 4.17 C. Violin plot illustrating cholangiocyte score in various clusters of in primary liver and hepatoma cell samples.

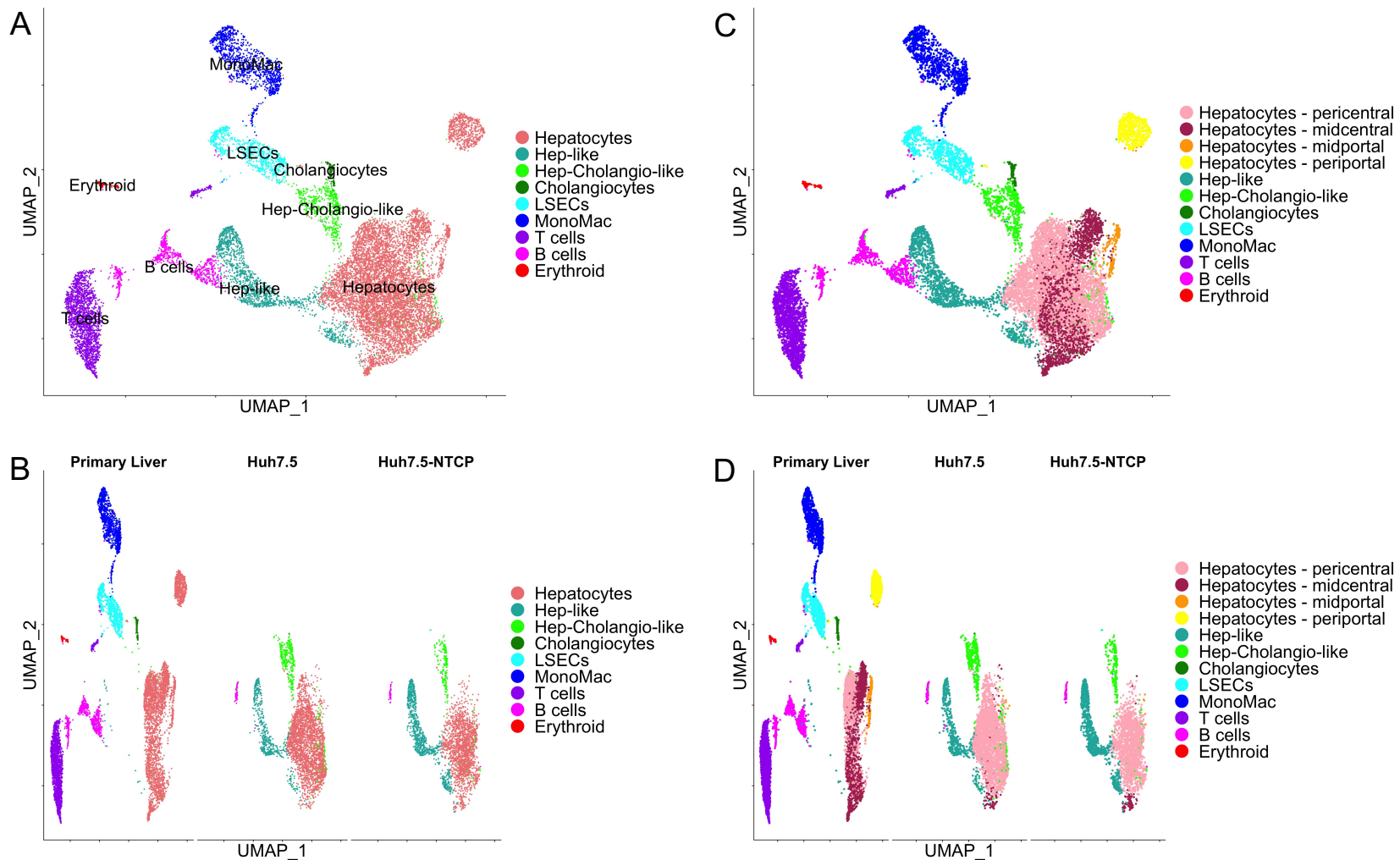


Figure 4.18. Cell types present in analysis of primary liver and human serum cultured Huh7.5 and Huh7.5-NTCP hepatoma cell lines. (A, C) UMAPs of cell types identified in the integrated datasets or (B, D) divided into the original samples. The cell types include hepatocytes (based on location relative to the central vein or portal triad in the liver lobule: pericentral, midcentral, midportal, or periportal), hepatocyte-like cells, hepatocyte-cholangiocyte-like cells, cholangiocytes, liver sinusoidal endothelial cells (LSECs), monocytes and macrophages, T cells, B cells, and erythroid cells.

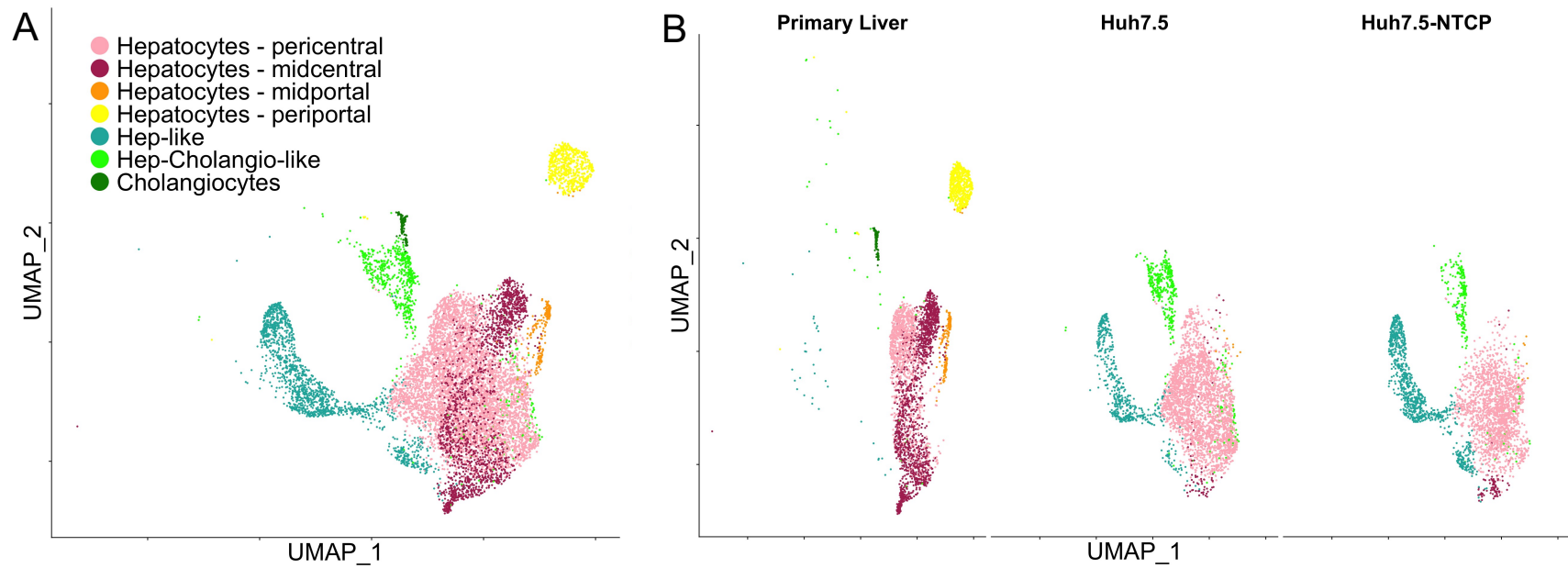


Figure 4.19. Hepatocyte and cholangiocyte celltypes present in analysis of primary liver and human serum cultured Huh7.5 and Huh7.5-NTCP hepatoma cell lines. (A) UMAP of hepatocyte and cholangiocyte cell types identified in the integrated datasets and (B) divided into the original samples.

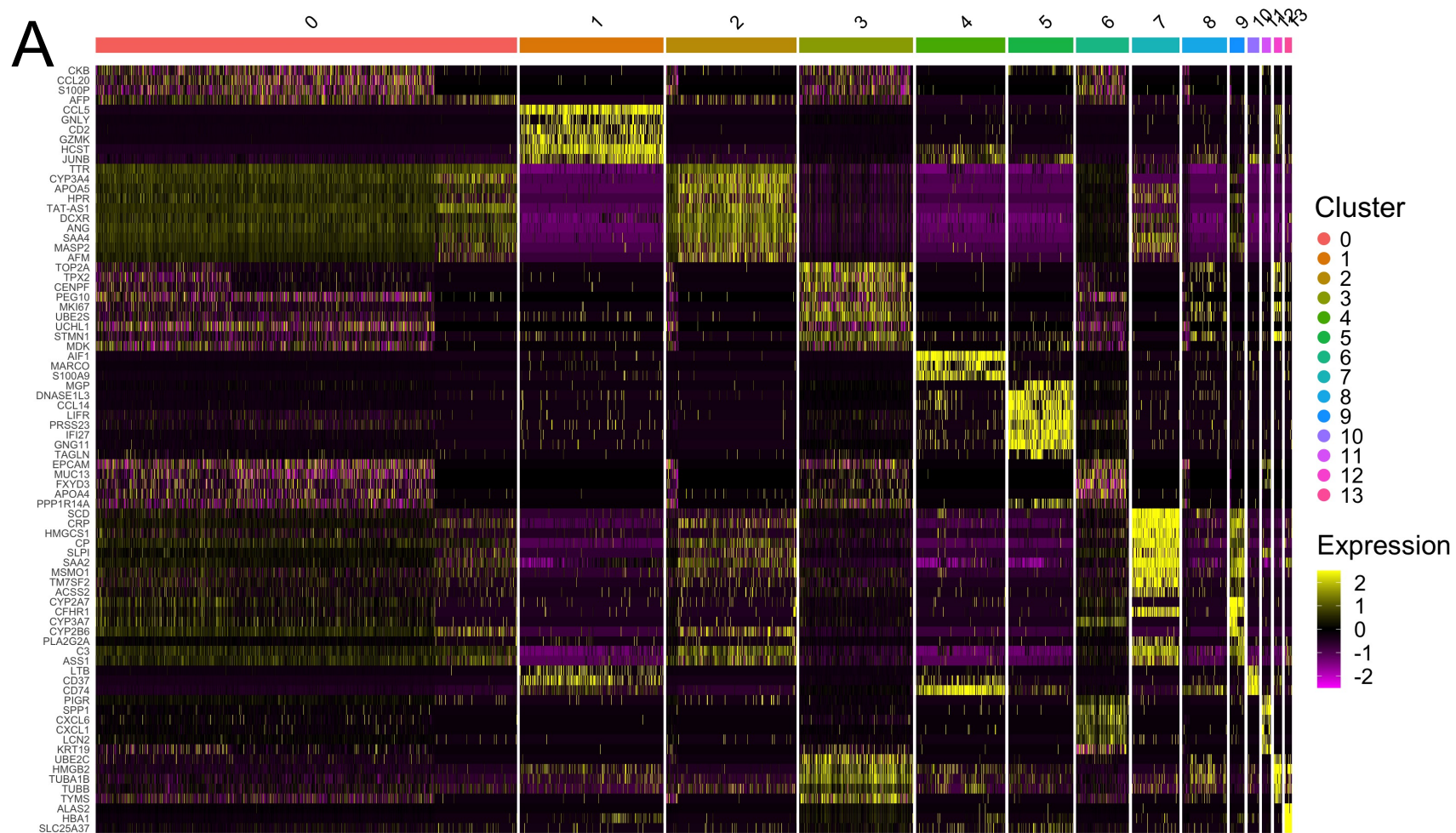


Figure 4.20 A. Differentially expressed genes among the different clusters within integrated primary liver and hepatoma cell line datasets. Heat maps of highly upregulated genes organized by cell cluster.

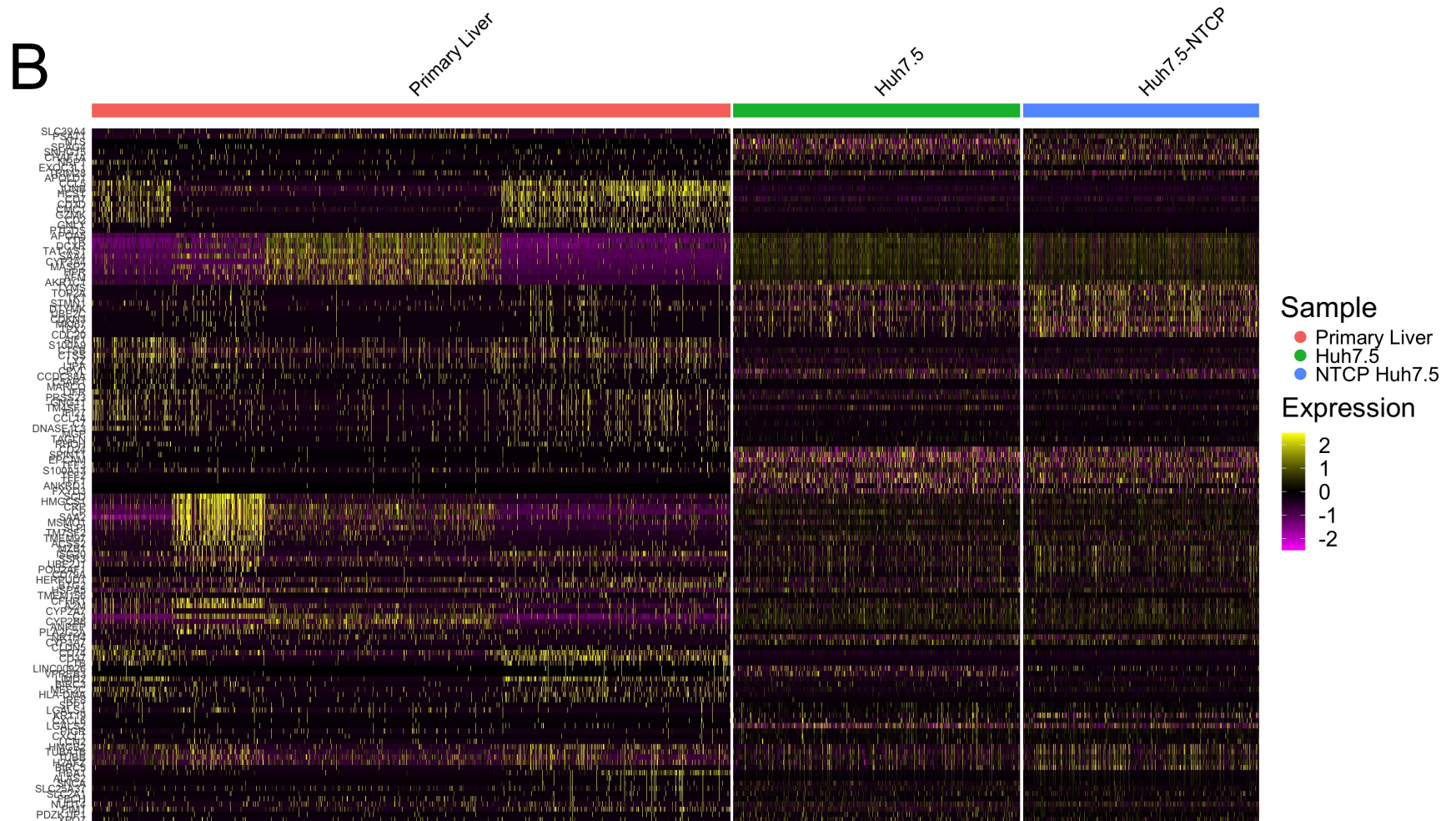


Figure 4.20 B. Differentially expressed genes among the different clusters within integrated primary liver and hepatoma cell line datasets. Heatmaps of highly upregulated genes organized by samples.

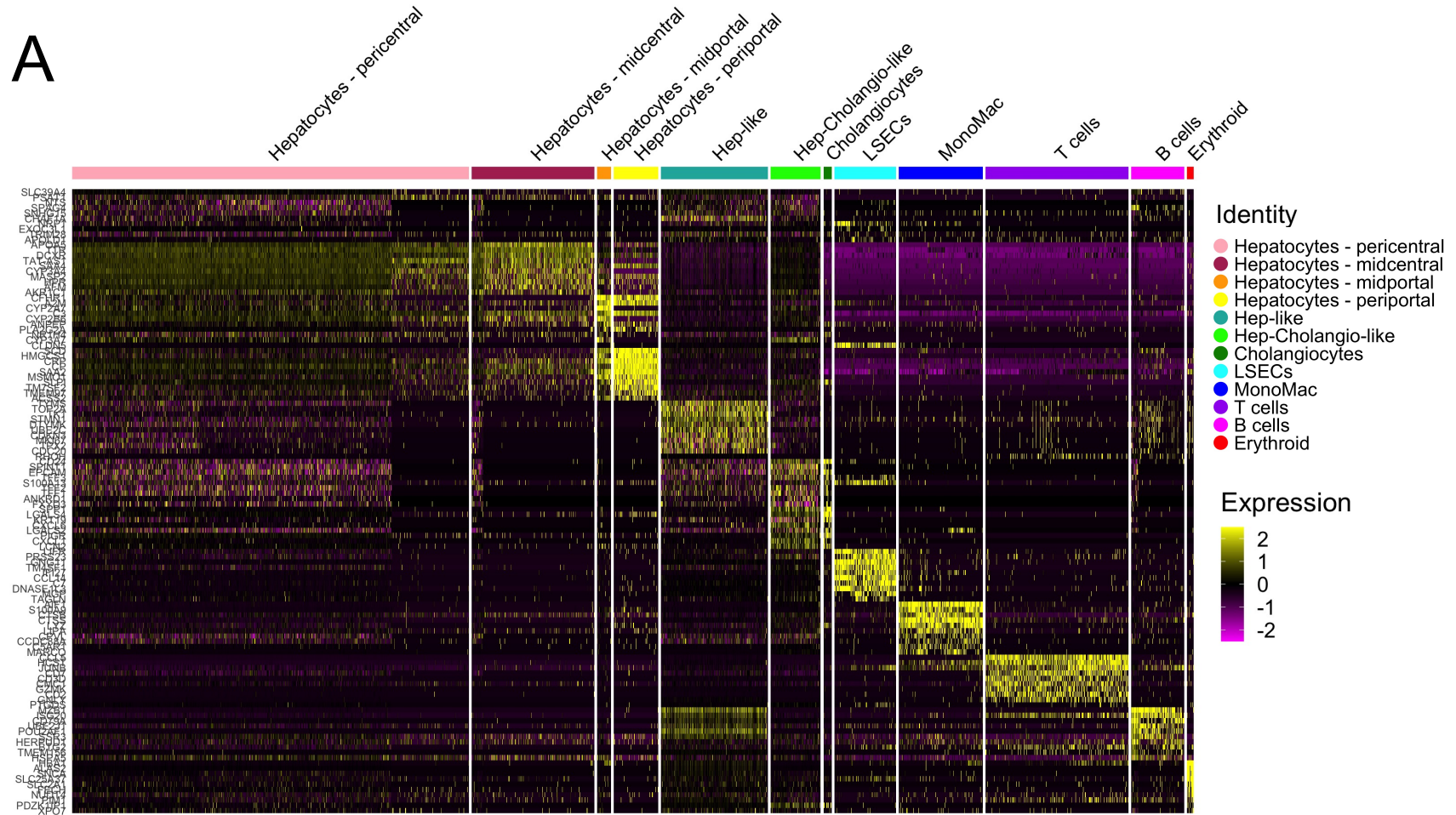


Figure 4.21 A. Differentially expressed genes among the different clusters within integrated primary liver and hepatoma cell line datasets, showing 12 celltypes. Heatmaps of highly upregulated differentially expressed genes organized by cell cluster.

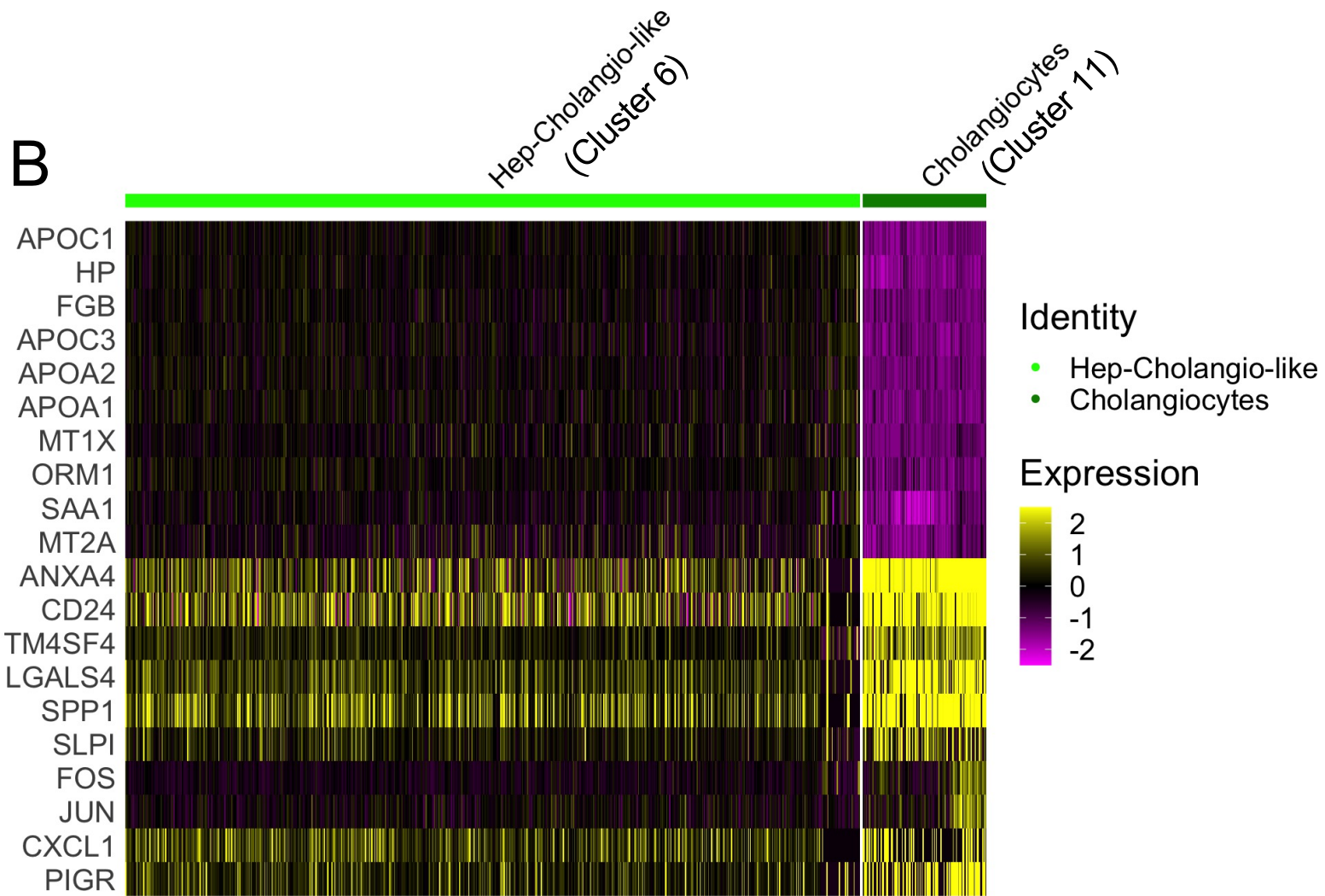


Figure 4.21 B. Differentially expressed genes in clusters 6 and 11 within integrated primary liver and hepatoma cell line datasets. Heatmap of the differentially expressed genes in the hepatocyte-cholangiocyte-like (cluster 6) and cholangiocyte (11) cell types.

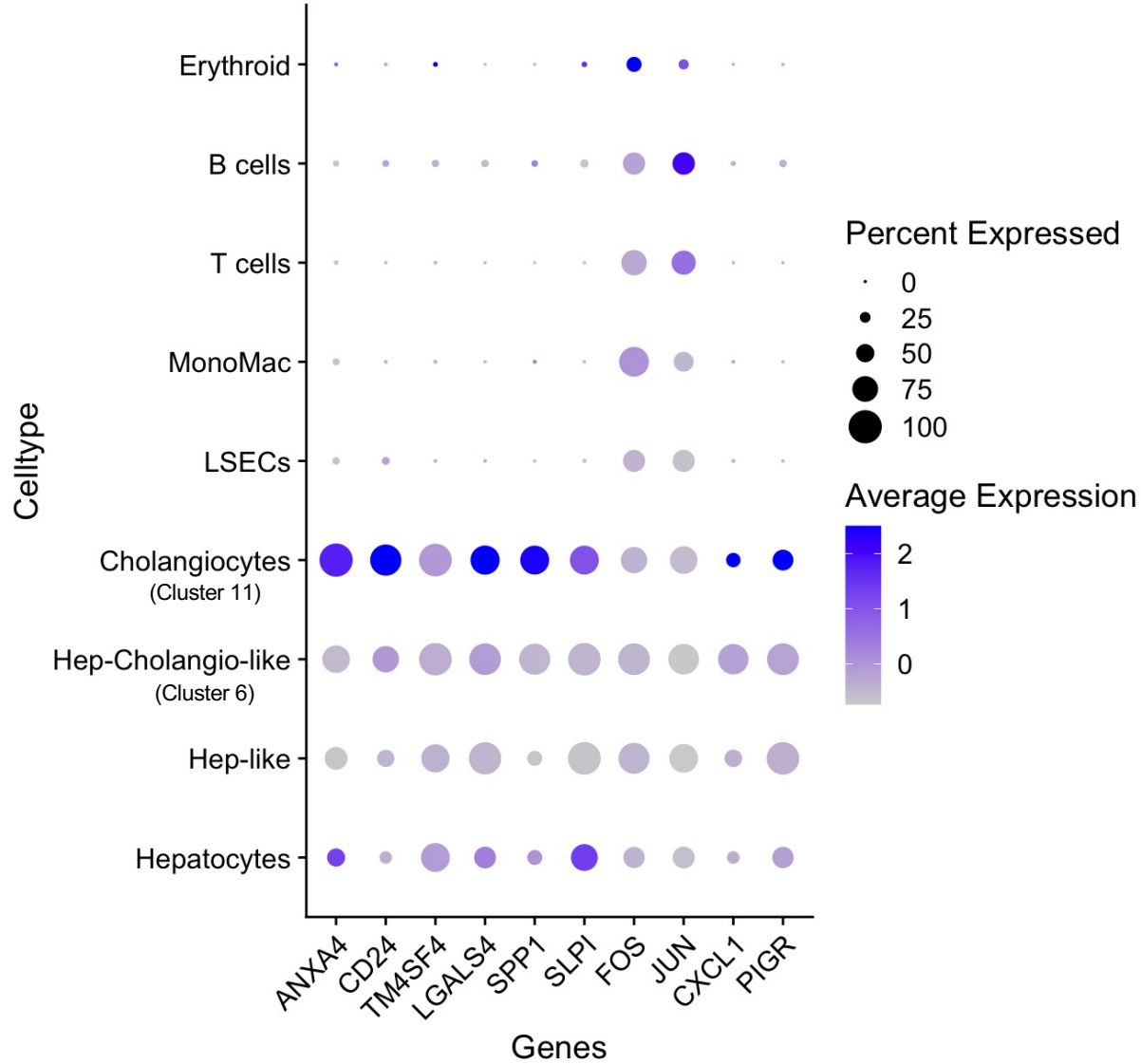


Figure 4.22. Dot plot illustrating differential expression of cholangiocyte-associated genes across nine cell types.

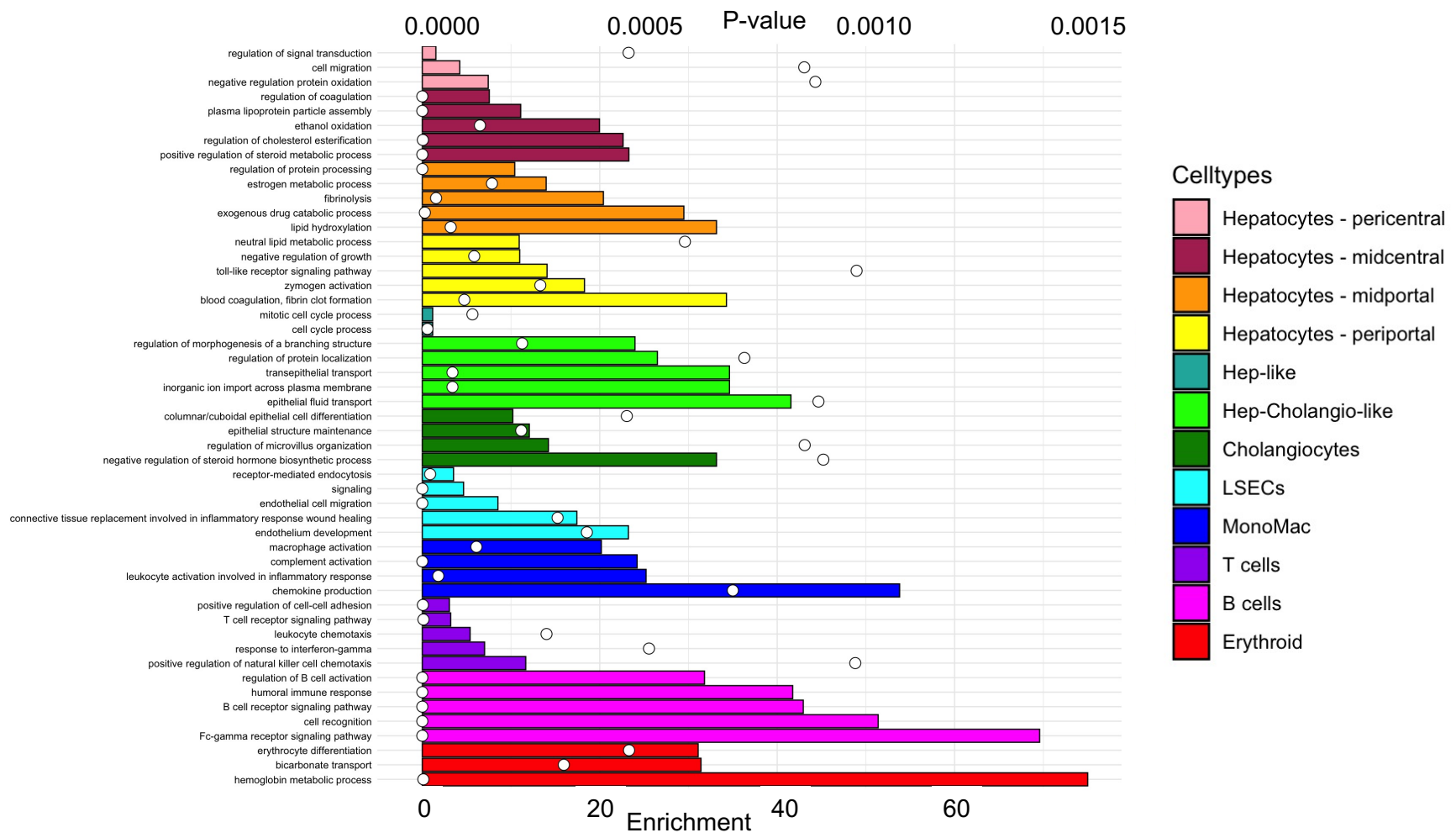


Figure 4.23 A. Gene ontology (GO) term enrichment in the various cell types. Differentially upregulated genes from different cell types were analyzed for gene ontology term enrichment. Enrichment score is indicated by bar length and p-value is depicted with white circles.

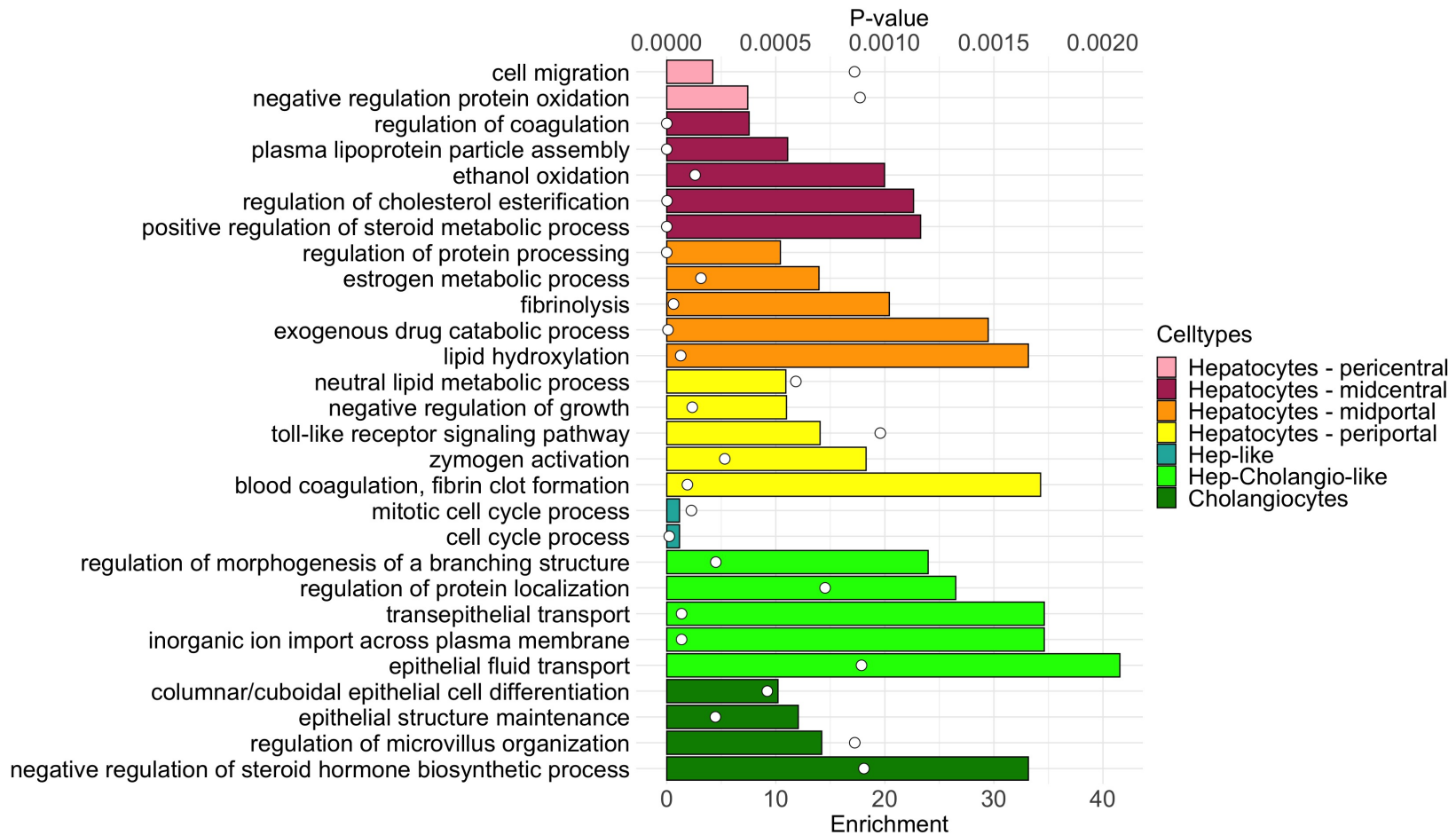
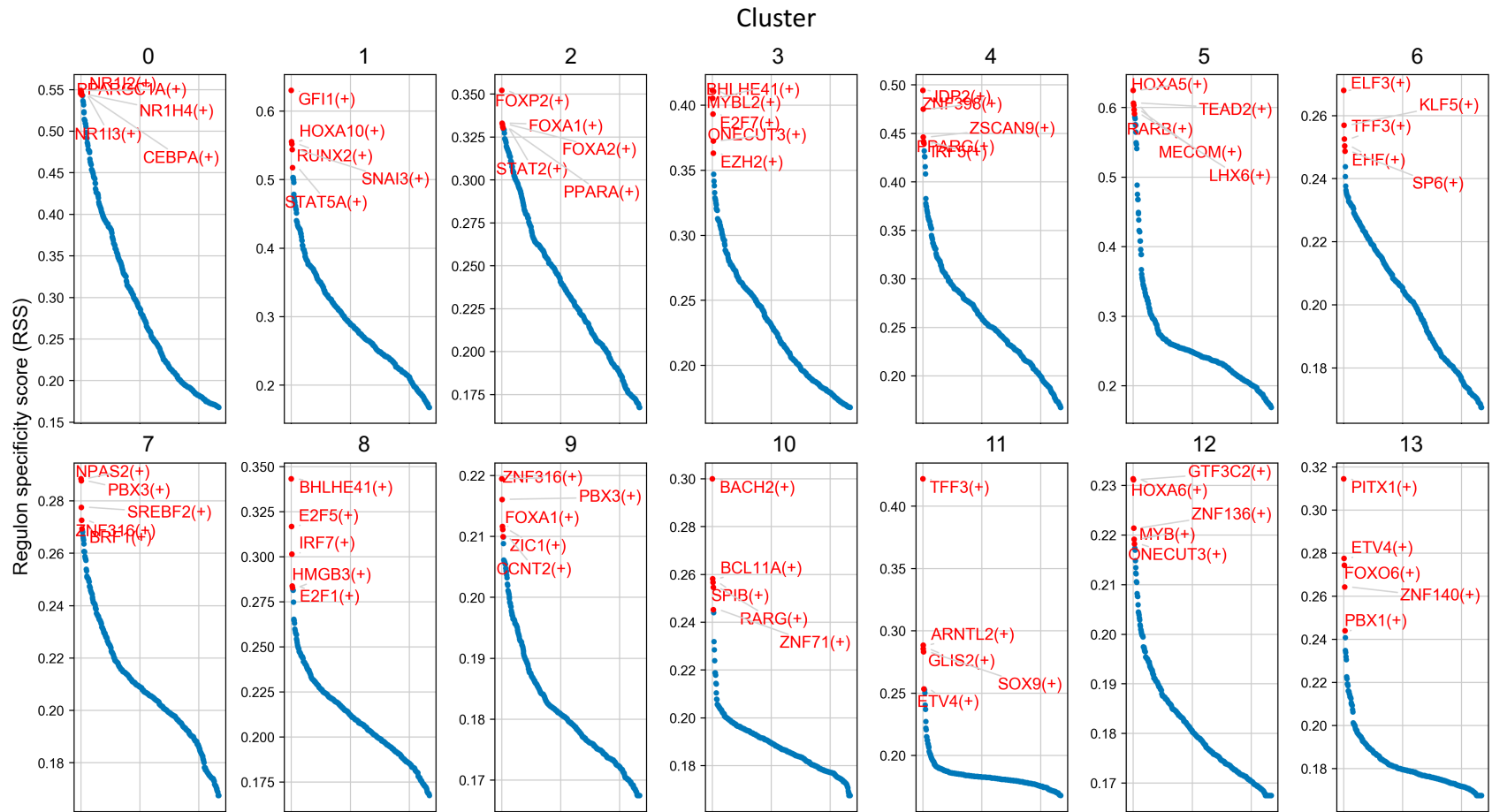


Figure 4.23 B. Gene ontology (GO) term enrichment in the hepatocytes, cholangiocytes, hepatocyte-like, and hepatocyte-cholangiocyte-like cells. Differentially upregulated genes from different cell types were analyzed for gene ontology term enrichment. Enrichment score is indicated by bar length and p-value is depicted with white circles.



Regulon with highest Specificity Scores	Cluster													
	0	1	2	3	4	5	6	7	8	9	10	11	12	13
	NR12	GFI1	FOXP2	BHLHE41	IDP2	HOXA5	ELF3	NPAS2	BHLHE41	ZNF316	BACH2	TFF3	GTF3C2	PITX1
	PPARCC1A	HOXA10	FOXA1	MYBL2	ZNP398	TEAD2	KLF5	PBS3	E2F5	PBX3	BCL11A	ARNTL2	HOXA6	ETV4
	NR1H4	RUNX2	FOXA2	E2F7	ZSCAN9	RARB	TFF3	SREBF2	IRF7	FOXA1	SPIB	GLIS2	ZNF136	FOXO6
	CEBPA	SNAI3	PPARA	ONECUT3	PPARG	MECOM	EHF	ZNF316	HMGB3	ZIC1	RARG	SOX9	MYB	ZNF140
	NR1I3	STAT5A	STAT2	EZH2	IRF5	LHX6	SP6	BRF1	E2F1	CCNT2	ZNF71	ETV4	ONECUT3	PBX1

Figure 4.24. pySCENIC regulon analysis of cell clusters. Regulon specificity score plots illustrated most active regulons in the cell clusters 0 to 13. Table lists the five most active regulons in each cluster.

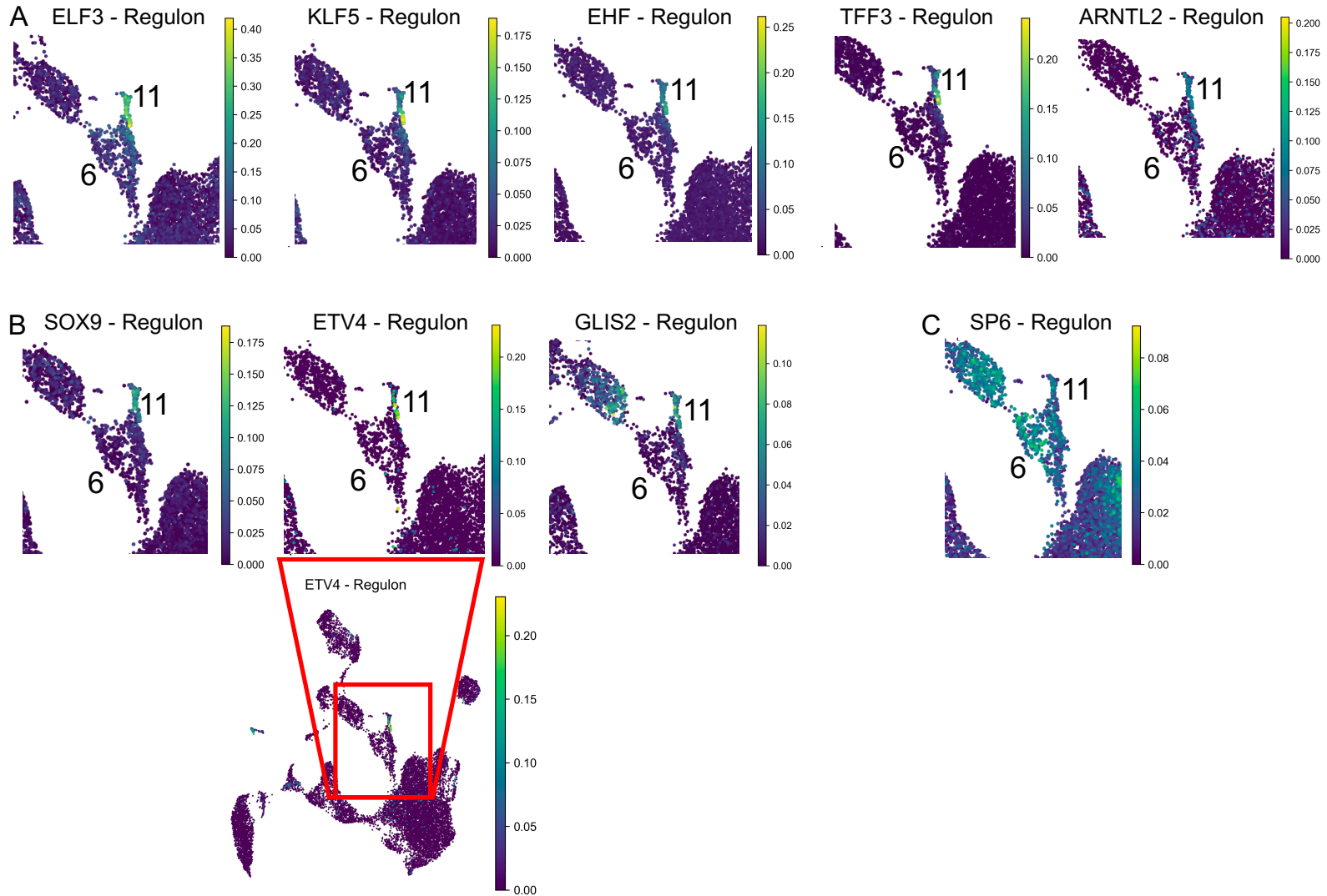


Figure 4.25. Enlarged area of UMAPs illustrating active regulons. (A) Active regulons in hepatocyte-cholangiocyte-like cells and cholangiocytes (cluster 6 and cluster 11, respectively). (B) Active regulons in cholangiocytes (cluster 11) and less so in hepatocyte-cholangiocyte-like cells (cluster 6). (C) SP6, a regulon active in hepatocyte-cholangiocyte-like cells but less active in cholangiocytes.

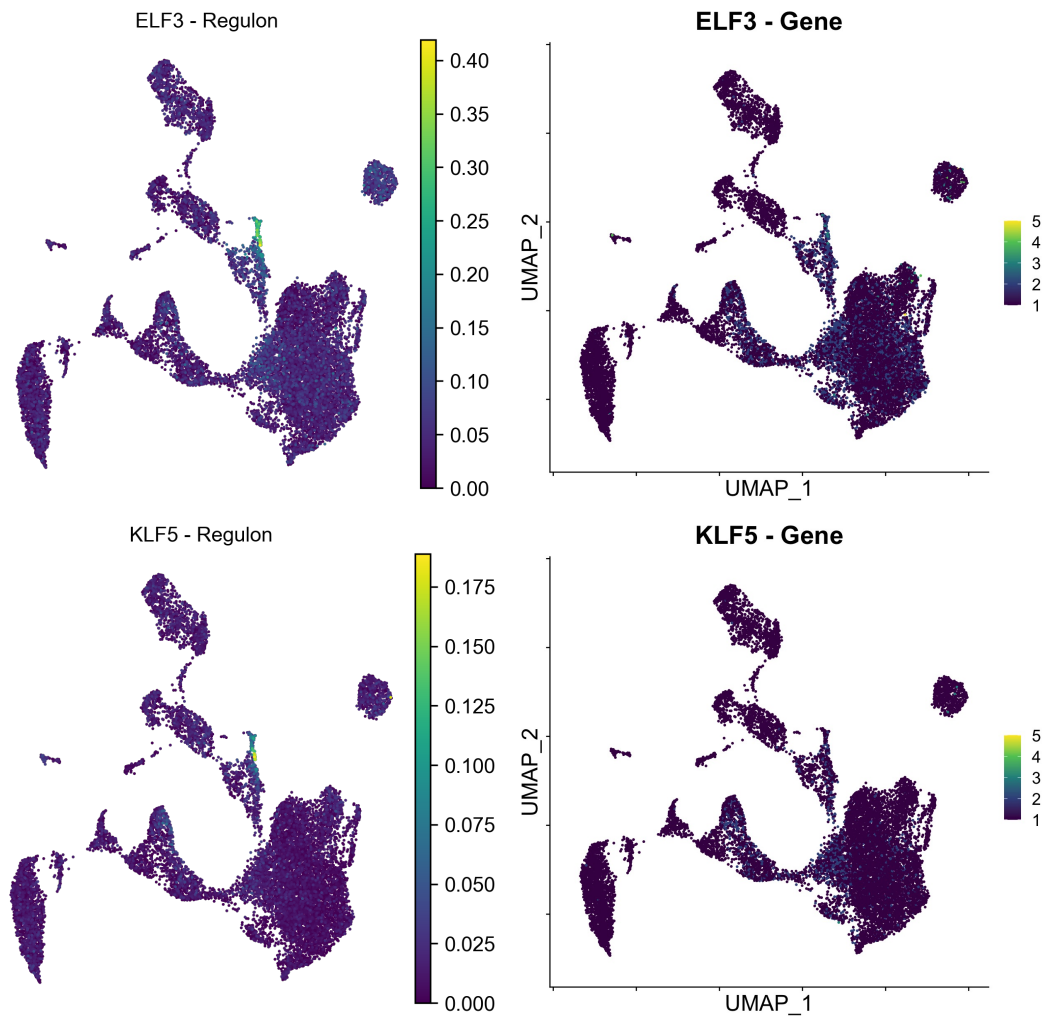


Figure 4.26. A comparison representing the analysis of regulon (left) and gene expression levels (right) of transcription factors.

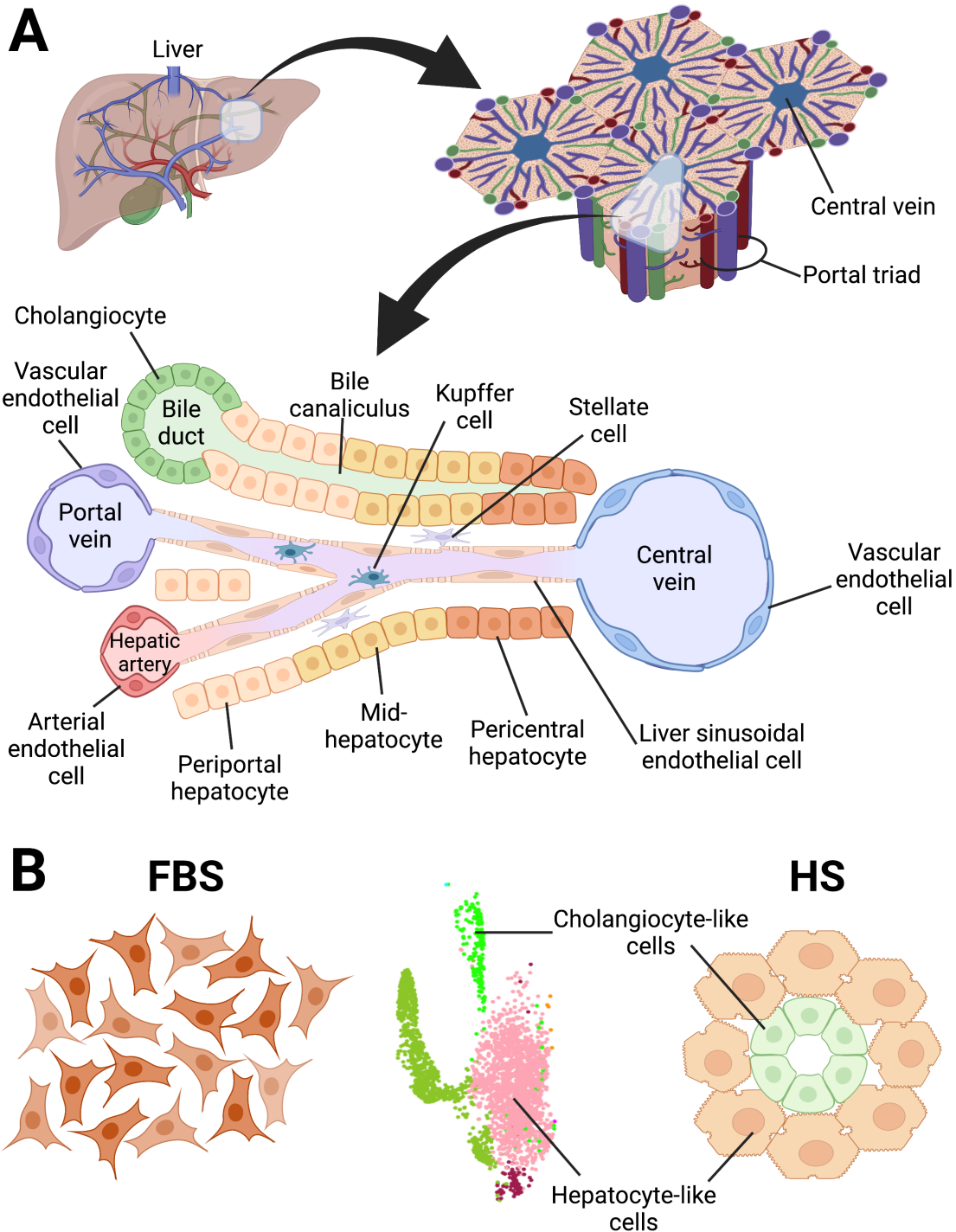


Figure 4.27. Resident liver cell types (A) and Huh7.5 cells cultured in FBS or HS (B). (A) Schematic of the liver, liver lobules, and liver sinusoids, illustrating the organization of cell types in the liver. (B) Representation of morphology of Huh7.5 cells cultured in FBS or HS. A UMAP of Huh7.5-NTCP cells depicts the identified cell clusters, including cholangiocyte-like and hepatocyte-like cells. Adapted from [2] with permission under a Creative Commons Attribution 4.0 International License and created using tools from BioRender.com.

Chapter 5

Single-Cell RNA Sequencing of Huh7.5-NTCP Cells Infected with Hepatitis B Virus and Huh7.5 Cells Infected with Hepatitis C Virus

5.1. Introduction

Previous studies have shown that HBV replication in various infection models can be reduced, but not eliminated, by interferon (IFN) treatment [1]. This is consistent with clinical observations: only a minor proportion of patients with chronic hepatitis B can eliminate the virus by pegylated IFN treatment [2]. HBV does not induce an IFN response as observed in chimpanzees [3], acutely infected patients [4, 5], and some *in vitro* infection experiments [6, 7]. HBV has been regarded as “stealth” virus, that is, HBV neither activates nor inhibits the IFN response [7-14].

However, Luangsay *et al.* [15] have reported an inhibition of IFN induction by unknown factor(s) present in their HBV inoculum. Lebossé *et al.* [16] reported a down-regulation of selected innate immune genes in the liver of patients with chronic hepatitis B (CHB), although it was not correlated with HBV replication. Shlomain *et al.* [17] reported an IFN- λ response to HBV infection of induced hepatocyte-like cells derived from pluripotent stem cells. Giersch *et al.* [18] reported a moderate up-regulation of IFN and IFN-stimulated genes (ISGs) in HBV-infected uPA/SCID mice repopulated with primary human hepatocytes (PHH). How HBV interacts with the IFN system is not fully understood [19, 20].

The primary objective of this chapter is to conduct a single-cell RNA sequencing (scRNA-seq) study of Huh7.5-NTCP hepatoma cells differentiated in human serum culture and infected

with HBV alone or in combination with IFN treatment. A comparison of gene expression profiles in the control (mock infection) and HBV-infected Huh7.5-NTCP cells will determine whether HBV infection activates an IFN response. HBV infection of IFN-treated cells, compared to IFN treatment alone, will reveal whether HBV alters expression of IFN-stimulated genes and whether IFN reduces HBV RNA levels. With the benefit of single-cell resolution, this scRNA-seq study is feasible because of two advances described in Chapters 2 and 3: Huh7.5-NTCP cells differentiated in human serum supplemented cultures are permissive to HBV infection (Chapter 2), and enrichment of HBV transcripts enables their detection in the cells (Chapter 3).

Hepatitis C virus (HCV) is highly sensitive to IFN- α treatment both *in vitro* [21] and in infected patients [22]. HCV induces a strong interferon response in primary human hepatocytes (PHH) [23], chimpanzees [24], and acutely infected patients [25]. These previous studies were conducted using cell lysates, which reflect the average state of the cell population. Results of scRNA-seq described in Chapter 4 revealed heterogeneity of cells in culture samples. Therefore, a scRNA-seq study of HCV-infected and IFN-treated cells will be useful for assessing the effect of HCV on IFN-stimulated transcriptome. Results from scRNA-seq studies of HCV-infected and HBV-infected cells will also help test and validate that HBV is a “stealth virus”.

5.2. Materials and Methods

5.2.1. Huh7.5-NTCP Cells Cultured in Medium Supplemented with Human Serum

Huh7.5-NTCP cells were cultured in DMEM (Sigma Aldrich, St. Louis, MO) supplemented with 4% pooled adult human serum (HS). The same protocols and conditions as described in Chapter 2 were used for the maintenance of the Huh7.5-NTCP cell cultures [26]. The cells were washed three times with the medium prior to the preparation for scRNA-seq libraries. The same

procedures as described in Chapter 3 (Section 3.2.2) were used for the preparation of scRNA-seq libraries [27].

5.2.2. Infection of Huh7.5-NTCP Cells with HBV and Treatment with Interferon (IFN)

Huh7.5-NTCP cells cultured and differentiated in DMEM and 4% HS for 21 days were infected with HBV at a multiplicity of infection (MOI) of 500 genome equivalents per cell in the presence of 4% PEG 8000 for 18 h at 37 °C. Cells treated similarly with 4% PEG 8000 (but not with HBV) served as the mock infection control. Another set of Huh7.5-NTCP cells were infected with HBV and also treated with 1000 international units of interferon alpha (IFN α) in the DMEM medium containing 4% HS for 24 h prior to sample collection. This treatment condition is denoted as (HBV+IFN). Cells treated similarly with 1000 international units of IFN α and 4% PEG 8000 (but not with HBV) are denoted as the (mock+IFN) group. No DMSO was used in these cultures. The cells were washed three times with the medium prior to the preparation for scRNA-seq libraries.

5.2.3. scRNA-seq of Huh7.5-NTCP Cells Infected with HBV and Treated with IFN

scRNA-seq analyses were performed on Huh7.5-NTCP cells cultured and differentiated in HS-supplemented medium under four different treatment conditions: control (mock infection), HBV infection, IFN treatment, and HBV infection plus IFN treatment. The first pair, mock infection versus HBV infection, was used to evaluate whether HBV influences the overall gene expression within the cells. The second pair, IFN treatment and HBV+IFN treatment, was used to study whether HBV alters the action of interferon. The same procedures as described in Chapter 3 were used for PCR enrichment of HBV transcripts. Sequences of the P5 forward primer, P7 forward primer, P7 reverse primer, and P7-Sample index-Read 2 reverse primer were listed in Table 3.2 (Chapter 3). The sequence of the “HBV-specific internal reverse primer with

partial Read 2 adaptor” was 5’-

GTGTGCTCTTCCGATCTCTCTGCCTAATCATCTCTTGTTTC-3’.

The same procedures as described in Chapter 3 (Figure 3.1, Section 3.2.2, and Section 3.2.3) were used for the preparation and sequencing of scRNA-seq libraries. Briefly, scRNA-seq libraries were prepared according to the procedures of 10X Genomics (Pleasanton, CA), and with the help of Dr. Joaquín López-Orozco, High Content Analysis Core Facility, Faculty of Medicine and Dentistry, University of Alberta. The scRNA-seq libraries were sequenced by Novogene (Sacramento, CA) using the HiSeq PE150 sequencing-by-synthesis platform (Illumina, San Diego, CA).

5.2.4. scRNA-seq of Huh7.5 Cells Infected with Hepatitis C Virus and Treated with IFN

This set of scRNA-seq data were obtained by Dr. Michael Joyce, Karyn Berry-Wynne, and Theodore Dos Santos (Li Ka Shing Institute of Virology, University of Alberta). scRNA-seq analyses were performed on human serum cultured Huh7.5 cells under four different treatment conditions: control (mock infection), HCV infection, IFN treatment, and HCV infection plus IFN treatment. The Huh7.5 cells were differentiated in human serum and infected with HCV as per previously described protocols [28, 29]. For the IFN treated samples, 1000 international units of IFN α was added to the culture 24 h prior to sample collection. The data from these samples were compared with those of HBV infection and IFN treatment of Huh7.5-NTCP cells.

5.2.5. Data Analysis

Data from single-cell RNA sequencing of Huh7.5-NTCP cells under four treatment conditions including HBV infection were integrated with the scRNA-seq data of Huh7.5 cells under four treatment conditions including HCV infection. The combination of datasets followed

the Seurat integration method for unsupervised analysis [30]. The Seurat V3 software package, developed and maintained by Dr. R. Satija and collaborators, enables users “to integrate diverse types of single-cell data”. (<https://satijalab.org/seurat/>)

Similar to the data analysis described in Chapter 4, the Seurat V3 software package was used for the analysis of the both datasets from the scRNA-seq analyses of HBV-infected Huh7.5-NTCP cells and HCV-infected Huh7.5 cells. Uniform Manifold Approximation and Projection (UMAP) graphs were generated and gene clustering analyses were conducted using the corresponding scripts within the Seurat V3 package followed the procedures of Stuart *et al.* [30].

5.3. Results and Discussion

5.3.1. scRNA-seq Analysis of Huh7.5-NTCP Cells with or without HBV Infection and IFN Treatment

scRNA-seq data can be visualized with Uniform Manifold Approximation and Projection (UMAP) plots, with each dot representing a single cell. The cells that share similar transcriptome profiles are spatially clustered together. Results in **Figure 5.1** are generated from scRNA-seq analysis of four samples, of Huh7.5-NTCP cells differentiated in human serum culture under the following four treatment conditions: mock infection control, HBV infection, mock infection but treatment with IFN, and HBV infection plus IFN treatment.

Figure 5.1A shows that the scRNA-seq data from all four Huh7.5-NTCP samples are grouped in nine clusters (from 0 to 8). **Figure 5.1B** shows two distinct groups. Cells after IFN treatment, with or without HBV infection, exhibit a cluster profile different from that of the cells without IFN treatment. Cells treated with IFN (represented by blue dots) have the same cluster

similarly to the cells infected with HBV and treated with IFN (purple dots). Cells from the mock infection control (represented by red dots) have a cluster profile overlapping with that of cells after HBV infection (green dots). **Figure 5.1C** shows the clusters in each of the four samples. The clusters are very similar between the mock infection control and the HBV-infected cell sample. These results indicate that HBV infection of Huh7.5-NTCP cells does not change the overall transcriptome profile of the host cells. Treatment of Huh7.5-NTCP cells with IFN results in a distinct transcriptome profile different from that of the control. However, HBV infection of IFN-treated cells does not further alter the overall transcriptome profile. These results suggest that HBV infection does not change the overall transcriptome profile of the Huh7.5-NTCP cells already treated with IFN. These results would be those of expected if the stealth virus hypothesis is true.

Results shown in Figure 5.1 are from scRNA-seq analyses of 3000–4000 Huh7.5-NTCP cells in each sample. **Figure 5.2A** shows the number of cells analyzed in the four samples: mock infection, HBV infection, mock infection but IFN treatment, and HBV infection plus IFN treatment. In the samples of mock infection and HBV infection, majority of the cells are in clusters 0, 2, and 5. In the samples of IFN treatment and HBV infection plus IFN treatment, majority of the cells are in clusters 1, 3, and 4. **Figure 5.2B** shows percentages of total number of cells in each sample contributing to each of the nine clusters. Between the samples of mock infection and HBV infection, similar percentage of cells are in three main clusters (0, 2, and 5). Between the samples of IFN treatment and HBV infection plus IFN treatment, percentage of cells in three main clusters (1, 3, and 4) are similar.

5.3.2. HBV Transcripts in Huh7.5-NTCP Cells after HBV Infection and IFN Treatment

As discussed in Chapter 3, HBV transcripts were not detectable in majority of HBV-infected cells in the original sequenced libraries. Enrichment of HBV transcripts in the HBV-infected samples using the PCR and CRISPR technique described in Chapter 3 enabled the detection of HBV transcripts. **Figure 5.3** shows the levels of HBV transcripts detected in Huh7.5-NTCP cells. When the cell culture is not infected with HBV, there are no detectable HBV transcripts in the cells of control (mock infection) and mock infection plus IFN treatment (Figure 5.3A and C). HBV transcripts are detected in Huh7.5-NTCP cells only after HBV infection and HBV infection in combination with IFN treatment. All nine clusters of cells have detectable levels of HBV transcripts (Figure 5.3B). Consistent with the results in Figure 5.2 showing that majority of HBV-infected cells are in clusters 0, 2, and 5, these clusters have higher levels of HBV transcripts (Figure 5.3B).

Nearly all of the HBV-infected cells contain HBV RNA, a unique finding compared to most literature using NTCP-overexpressing cell lines where approximately 30-80% of cells stain positive for core protein post-infection [31,32]. As the first group so far to perform HBV RNA analysis at a single cell resolution, we demonstrate that likely all of the cells are infected *in vitro*.

IFN treatment of the HBV-infected cell culture reduces the levels of HBV transcripts in the cell population, as shown in a comparison between the samples of HBV infection and HBV+IFN treatment (Figure 5.3C). Majority of cells in the HBV+IFN treatment samples are in clusters 1, 3, and 4 (Figure 5.2). The lower levels of HBV transcripts in clusters 1, 3, and 4 (Figure 5.3B) probably reflect the overall decrease of HBV transcripts in the HBV+IFN treatment samples seen in Figure 5.3C.

5.3.3. Differentially Expressed Genes in Huh7.5-NTCP Cells with or without HBV Infection and IFN Treatment

Differentially expressed genes in Huh7.5-NTCP cells of four culture samples are shown in **Figure 5.4**, as heat maps. A brighter yellow color indicates higher level of differential gene expression. Cells in the mock infection and HBV infection samples have similar differential expression heat maps. Cells in the IFN-treated samples have differential gene expression heat maps different from that of no IFN treatment. HBV infection of IFN-treated cell culture does not change the differential gene expression heat maps.

5.3.4. Interferon-Stimulated Gene Expression in Huh7.5-NTCP Cells after IFN Treatment and HBV Infection

The expression levels of 44 interferon-regulated genes in Huh7.5-NTCP cells of the four culture samples are summarized in **Figure 5.5**. The IFN-stimulated gene transcripts analyzed include ADAR, BST2, CD74, DDIT4, DDX58, DDX60, EIF2AK2, GBP1, GBP2, HPSE, IFI44L, IFI6, IFIH1, IFIT1, IFIT2, IFIT3, IFIT5, IFITM1, IFITM2, IFITM3, IRF1, IRF7, ISG15, ISG20, MAP3K14, MOV10, MX1, MX2, NAMPT, OAS1, OAS2, OAS3, OASL, P2RY6, PML, RSAD2, RTP4, SLC15A3, SLC25A28, SSBP3, SUN2, TRIM5, TRIM25, and ZC3HAV1. Average levels of these IFN-stimulated genes are presented as interferon scores, shown in Figure 5.5B and 5.5C. Higher interferon scores are primarily in clusters 1, 3, and 5, and to a lesser extent in clusters 6 and 8 (bottom graph in Figure 5.5C), consistent with the results of clustering analysis shown in Figures 5.1 and 5.2. Cells in both the mock infection and HBV infection samples have a negligible interferon score. Cells in both IFN treatment and HBV+IFN samples have a higher, but similar interferon score (Figure 5.5B and 5.5C). These results indicate that HBV infection does not upregulate IFN-related genes and does not downregulate IFN-stimulated

genes in the IFN-treated cells. These results at the single-cell resolution support the idea that HBV is a “stealth virus”, which is neither immunostimulatory nor immunomodulatory.

5.3.5. scRNA-seq Analysis of Huh7.5 Cells with or without HCV Infection and IFN

Treatment

To compare the “stealth” response of HBV infection in hepatoma cells to the vigorous response of these cells to HCV infection, we conducted scRNA-seq analyses of human serum cultured Huh7.5 hepatoma cells infected with HCV. NTCP is not involved in HCV infection, hence Huh7.5 cells without NTCP overexpression were used. Previous experiments demonstrate 100% infection with HCV in the human serum cultured Huh7.5 model [28, 29], which was also confirmed from qPCR analysis of replicate samples. **Figure 5.6** shows UMAP plots generated from the data of scRNA-seq analysis of four Huh7.5 cell culture samples. These Huh7.5 cell cultures include uninfected control, HCV infection, IFN treatment, and HCV infection plus IFN treatment. **Figure 5.6A** shows that the scRNA-seq data from all four Huh7.5 samples are grouped in nine clusters (from cluster 0 to cluster 8). **Figure 5.6B** shows there is not much overlap of transcriptome profiles among the cells in the four samples. Clustering of cells is different among the four culture samples (**Figure 5.6C**). For example, the majority of cells in the control sample (mock infection) are in cluster 1, whereas most of the cells in the HCV-infected sample are in cluster 4. The IFN-treated cell samples, with or without HCV infection, have very few cells in cluster 1 and cluster 4. Cells in the IFN-treated sample are mostly in cluster 0, whereas cells in the HCV+IFN treated sample are mostly in clusters 5 and 3. These results are in contrast to those shown in Figure 5.1, reflecting differences between HBV and HCV infections.

Data in Figure 5.6 originated from scRNA-seq analyses of 3700–4500 Huh7.5 cells in each sample. **Figure 5.7A** shows the number of cells analyzed in the four samples: control (mock

infection), HCV infection, IFN treatment, and HCV infection combined with IFN treatment. The number of cells in each cluster are very different among the four samples. **Figure 5.7B** shows percentages of total number of cells in each sample contributing to each of the nine clusters. These percentages also differ among the four samples. For example, majority of the Huh7.5 cells in the control sample are in cluster 1. Most of the cells in the HCV-infected sample are in clusters 3 and 4. Most of the cells in the IFN-treated sample are in cluster 0. Cells in the HCV+IFN sample are mainly in clusters 3 and 5. These results from HCV-infected cells (Figures 5.6 and 5.7) are different from those of the HBV-infected cells (Figures 5.1 and 5.2). These results suggest that unlike HBV, HCV alters transcriptome profiles of the host cells.

5.3.6. Interferon-Stimulated Gene Expression in Huh7.5 Cells after IFN Treatment and HCV Infection

Figure 5.8. shows the expression levels of 44 interferon-regulated gene transcripts in Huh7.5 cells of the four culture samples. These 44 transcripts include ADAR, BST2, CD74, DDIT4, DDX58, DDX60, EIF2AK2, GBP1, GBP2, HPSE, IFI44L, IFI6, IFIH1, IFIT1, IFIT2, IFIT3, IFIT5, IFITM1, IFITM2, IFITM3, IRF1, IRF7, ISG15, ISG20, MAP3K14, MOV10, MX1, MX2, NAMPT, OAS1, OAS2, OAS3, OASL, P2RY6, PML, RSAD2, RTP4, SLC15A3, SLC25A28, SSBP3, TRIM5, TRIM25, SUN2, and ZC3HAV1. Figure 5.8B and 5.8C show interferon scores, which are average levels of these IFN-stimulated gene transcripts detected. As expected, higher interferon scores are detected in the cells treated with IFN. In addition, HCV infection of the cells also results in a slightly higher interferon score than the control.

Figure 5.9 shows a comparison of interferon scores of Huh7.5 cells treated with IFN alone or with both IFN and HCV. Although the overall interferon scores are similar between the two samples, there are differences in interferon scores among clusters between the IFN and

IFN+HCV samples. For example, cluster 3 in the IFN+HCV sample has a higher interferon score than cluster 3 from the IFN sample. In addition, cluster 0 is predominant in the IFN-treated sample, whereas clusters 3 and 5 are in the IFN+HCV sample. These results suggest that there is a heterogeneous response to HCV, with some cells having increased interferon scores (cluster 3) while some other cells having decreased interferon scores (cluster 2).

Figure 5.10. shows examples of interferon-stimulated gene expression in the control, HCV, IFN, and HCV+IFN treated Huh7.5 cell culture samples. Comparing the control (far left column for each gene) with HCV-infected (the second column from the left) (Figure 4.10A), one can see that more cells have higher expression levels in the HCV-infected samples than in the control (mock infection). For example, higher expression levels of DDX6, IFIT3, and OASL in the HCV-infected cells as compared to the control are visible from Figure 5.10A. Other interferon-stimulated genes that are upregulated by HCV infection include BST2, IFIH1, IFIT1, IFIT2, ISG20, MX1, OAS2, PML, SLC15A3, and SLC25A28. Upregulation of these genes suggests immunostimulatory effects of HCV infection.

Figure 5.10B shows examples of antiviral genes, DDIT4, GBP2, and IFITM2, which are downregulated by HCV infection. Comparing the control (far left columns) with HCV-infected (second columns from left), expression levels of DDIT4, GBP2, and IFITM2 are consistently lower in the HCV-infected cell samples. Comparing the IFN-treated (second columns from the right) with the combined HCV+IFN treatment (columns on the far right), the expression levels of DDIT4, GBP2, and IFITM2 are also lower in the HCV+IFN treatment samples. These results suggest HCV infection repress these IFN-stimulated genes.

Fig 5.10C shows that IFI6 and ISG15 are stimulated by HCV infection as compared to the control. But IFI6, ISG15, and OAS1 are downregulated when the cells are HCV-infected and

IFN-treated, as compared to the IFN treatment alone (comparing the two violin plots on the right of each panel). These results suggest that HCV both stimulates and downregulates these genes.

5.3.7. Comparison of Interferon-Stimulated Gene Expression in HBV-infected Huh7.5-NTCP Cells and HCV-infected Huh7.5 Cells

Figure 5.11 shows a comparison of interferon-stimulated gene expression in cell samples infected with either HBV or HCV. Four genes, DDX60, OASL, IFITM2, and ISG15, are included in this analysis. Results on the left-hand side graphs show that HBV does not change expression levels of these interferon-stimulated genes compared to the mock or IFN-treated conditions. In contrast, HCV infection stimulates DDX60 and OASL, but downregulates IFITM2 and ISG15. These results support the paradigm that HBV is a stealth virus [7-14], whereas HCV is an immunostimulatory and immunomodulatory virus [21-25].

5.4. Conclusion

Transcriptome profiles were obtained from scRNA-seq analyses of more than 3000 Huh7.5-NTCP cells in each of the culture samples: mock infection, HBV infection, IFN treatment, and combined HBV infection IFN treatment. Cells in the mock infection and HBV infection samples have the same transcriptome profiles, indicating that HBV does not affect gene expression patterns in Huh7.5-NTCP hepatoma cells differentiated in human serum cultures. IFN treatment of Huh7.5-NTCP cells results in increased levels of IFN-stimulated genes. But HBV infection of the IFN-treated Huh7.5-NTCP cells does not alter the pattern or expression level of IFN-stimulated genes. Results of scRNA-seq analyses of more than 3000 cells with single-cell resolution confirms that HBV neither increases nor inhibits IFN-stimulated genes; HBV does not change transcriptome profiles of the host cells.

In contrast, HCV infection significantly changes transcriptome profiles of the host cells as seen from scRNA-seq analyses of HCV-infected Huh7.5 hepatoma cells. HCV infection also modulates IFN-stimulated genes, with upregulation of most and downregulation of a few IFN-stimulated genes.

The scRNA-seq study of HBV- and HCV-infected hepatoma cells is useful for understanding IFN response of viral infection. Although both viruses share hepatotropism, their effect on IFN response differ profoundly. While HCV induces and modulates IFN response, HBV does not induce IFN and has no effect on IFN-stimulated gene expression.

5.5. References

1. Lucifora, J.; Xia, Y.; Reisinger, F.; Zhang, K.; Stadler, D.; Cheng, X.; Sprinzl, M.F.; Koppensteiner, H.; Makowska, Z.; Volz, T.; Remouchamps, C.; Chou, W.M.; Thasler, W.E.; Huser, N.; Durantel, D.; Liang, T.J.; Munk, C.; Heim, M.H.; Browning, J.L.; Dejardin, E.; Dandri, M.; Schindler, M.; Heikenwalder, M.; Protzer, U. Specific and nonhepatotoxic degradation of nuclear hepatitis B virus cccDNA. *Science* **2014**, *343*, 1221-1228. doi:10.1126/science.1243462.
2. Trepo, C.; Chan, H.L.; Lok, A. Hepatitis B virus infection. *Lancet* **2014**, *384*, 2053-2063. doi: 10.1016/S0140-6736(14)60220-8
3. Wieland, S.; Thimme, R.; Purcell, R.H.; Chisari, F.V. Genomic analysis of the host response to hepatitis B virus infection. *Proc. Natl. Acad. Sci. U.S.A.* **2004**, *101*, 6669–6674. doi: 10.1073/pnas.0401771101
4. Stacey, A.R.; Norris, P.J.; Qin, L. *et al.* Induction of a striking systemic cytokine cascade prior to peak viremia in acute human immunodeficiency virus type 1 infection, in contrast to more modest and delayed responses in acute hepatitis B and C virus infections. *J. Virol.* **2009**, *83*, 3719-3733.
5. Dunn, C.; Peppas, D.; Khanna, P.; Nebbia, G.; Jones, M.; Brendish, N.; Lascar, R.M.; Brown, D.; Gilson, R.J.; Tedder, R.J.; Dusheiko, G.M.; Jacobs, M.; Klenerman, P., Maini, M.K.

- Temporal analysis of early immune responses in patients with acute hepatitis B virus infection. *Gastroenterology* **2009**, *137*, 1289-1300.
6. Niu, C.; Livingston, C.M.; Li, L.; Beran, R.K.; Daffis, S.; Ramakrishnan, D.; Burdette, D.; Peiser, L.; Salas, E.; Ramos, H.; Yu, M.; Cheng, G.; Strubin, M.; Delaney IV, W.E.; Fletcher, S.P. The Smc5/6 complex restricts HBV when localized to ND10 without inducing an innate immune response and is counteracted by the HBV X protein shortly after infection. *PLoS One* **2017**, *12*, e0169648. doi: 10.1371/journal.pone.0169648
 7. Cheng, X.M.; Xia, Y.C.; Serti, E.; Block, P.D.; Chung, M.; Chayama, K.; Rehmann, B.; Liang, T.J. Hepatitis B virus evades innate immunity of hepatocytes but activates cytokine production by macrophages. *Hepatology* **2017**, *66*, 1779–1793. doi: 10.1002/hep.29348
 8. Ortega-Prieto, A.M.; Dorner, M. Immune evasion strategies during chronic hepatitis B and C virus infection. *Vaccines* **2017**, *5* (3), 24. doi: 10.3390/vaccines5030024
 9. Suslov, A.; Boldanova, T.; Wang, X.Y.; Wieland, S.; Heim, M.H. Hepatitis B virus does not interfere with innate immune responses in the human liver. *Gastroenterology* **2018**, *154*, 1778–1790. doi: 10.1053/j.gastro.2018.01.034
 10. Suslov, A.; Wieland, S.; Menne, S. Modulators of innate immunity as novel therapeutics for treatment of chronic hepatitis B. *Curr. Opin. Virol.* **2018**, *30*, 9–17. doi: 10.1016/j.coviro.2018.01.008
 11. Thomas, E.; Baumert, T.F. Hepatitis B virus-hepatocyte interactions and innate immune responses: experimental models and molecular mechanisms. *Semin. Liver Dis.* **2019**, *39*, 301–314. doi: 10.1055/s-0039-1685518
 12. Winer, B.Y.; Gaska, J.M.; Lipkowitz, G.; Bram, Y.; Parekh, A.; Parsons, L.; Leach, R.; Jindal, R.; Cho, C.H.; Shrirao, A.; Novik, E.; Schwartz, R.E.; Ploss, A. Analysis of host responses to hepatitis B and delta viral infections in a macro-scalable hepatic co-culture system. *Hepatology* **2020**, *71*, 14–30. doi: 10.1002/hep.30815
 13. Mutz, P.; Metz, P.; Lempp, F.A.; Bender, S.; Qu, B.; Schöneweis, S.; Seitz, S.; Tu, T.; Restuccia, A.; Frankish, J.; Dächert, C.; Schusser, B.; Koschny, R.; Polychronidis, G.; Schemmer, P.; Hoffmann, K.; Baumert, T.F.; Binder, M.; Urban, S.; Bartenschlager, R. HBV bypasses the innate immune response and does not protect HCV from antiviral activity of interferon. *Gastroenterology* **2018**, *154*(6), 1791–1804. doi: 10.1053/j.gastro.2018.01.044

14. Zhang, Z.H.; Trippler, M.; Real, C.I.; Werner, M.; Luo, X.F.; Schefczyk, S.; Kemper, T.; Anastasiou, O.E.; Ladiges, Y.; Treckmann, J.; Paul, A.; Baba, H.A.; Allweiss, L.; Dandri, M.; Gerken, G.; Wedemeyer, H.; Schlaak, J.F.; Lu, M.J.; Broering, R. Hepatitis B virus particles activate Toll-Like Receptor 2 signaling initially upon infection of primary human Hepatocytes. *Hepatology* **2020**, *72*, 829–844. doi: 10.1002/hep.31112
15. Luangsay, S.; Gruffaz, M.; Isorce, N.; Testoni, B.; Michelet, M.; Faure-Dupuy, S.; Maadadi, S.; Ait-Goughoulte, M.; Parent, R.; Rivoire, M.; Javanbakht, H.; Lucifora, J.; Durantel, D.; Zoulim, F. Early inhibition of hepatocyte innate responses by hepatitis B virus. *J. Hepatol.* **2015**, *63*, 1314–1322.
16. Lebosse, F.; Testoni, B.; Fresquet, J. *et al.* Intrahepatic innate immune response pathways are downregulated in untreated chronic hepatitis B. *J. Hepatol.* **2017**, *66*, 897-909.
17. Shlomai, A.; Schwartz, R.E.; Ramanan, V.; Bhatta, A.; de Jong, Y.P.; Bhatia, S.N.; Rice, C.M. Modeling host interactions with hepatitis B virus using primary and induced pluripotent stem cell-derived hepatocellular systems. *Proc. Natl. Acad. Sci. U. S. A.* **2014**, *111*, 12193–12198.
18. Giersch, K.; Allweiss, L.; Volz, T. *et al.* Hepatitis Delta co-infection in humanized mice leads to pronounced induction of innate immune responses in comparison to HBV mono-infection. *J. Hepatol.* **2015**, *63*, 346-353.
19. Faure-Dupuy, S.; Lucifora, J.; Durantel, D. Interplay between the Hepatitis B Virus and Innate Immunity: From an Understanding to the Development of Therapeutic Concepts. *Viruses* **2017**, *9*, 95. doi: 10.3390/v9050095
20. Golsaz-Shirazi, F.; Shokri, F. Cross talk between hepatitis B virus and innate immunity of hepatocytes. *Rev. Med. Virol.* **2022**, *32(1)*, e2256. doi: 10.1002/rmv.2256
21. Metz, P.; Reuter, A.; Bender, S. *et al.* Interferon-stimulated genes and their role in controlling hepatitis C virus. *J. Hepatol.* **2013**, *59*, 1331-1341.
22. Carreno, V. Present treatment expectations and risks of chronic hepatitis C. *Clin. Microbiol. Infect.* **2002**, *8*, 74-79.
23. Hiet, M.S.; Bauhofer, O.; Zayas, M. *et al.* Control of temporal activation of hepatitis C virus-induced interferon response by domain 2 of nonstructural protein 5A. *J. Hepatol.* **2015**, *63*, 829-837.

24. Su, A.I.; Pezacki, J.P.; Wodicka, L. *et al.* Genomic analysis of the host response to hepatitis C virus infection. *Proc. Natl. Acad. Sci. U. S. A.* **2002**, *99*, 15669-15674.
25. Heim, M.H.; Thimme, R. Innate and adaptive immune responses in HCV infections. *J. Hepatol.* **2014**, *61*, S14-S25. doi: 10.1016/j.jhep.2014.06.035
26. Le, C.; Sirajee, R.; Steenbergen, R.; Joyce, M.A.; Addison, W.R.; Tyrrell, D.L. *In vitro* infection with hepatitis B virus using differentiated human serum culture of Huh7.5-NTCP cells without requiring dimethyl sulfoxide. *Viruses* **2021**, *13*, 97. doi: 10.3390/v13010097
27. Le, C.; Liu, Y.; Lopez-Orozco, J.; Joyce, M.A.; Le, X.C.; Tyrrell, D.L. CRISPR technique incorporated with single-cell RNA sequencing for studying hepatitis B infection. *Anal. Chem.* **2021**, *93*, 10756-10761. doi:10.1021/acs.analchem.1c02227.
28. Steenbergen, R.H.; Joyce, M. A.; Thomas, B.; Jones, D.; Law, J.; Russell, R.; Houghton, M.; Tyrrell, D. L. Human serum leads to differentiation of human hepatoma cells, restoration of very-low-density lipoprotein secretion, and a 1000-fold increase in HCV Japanese fulminant hepatitis type 1 titers. *Hepatology* **2013**, *58*, 1907–1917, doi:10.1002/hep.26566.
29. Steenbergen, R.; Oti, M.; Ter Horst, R.; Tat, W.; Neufeldt, C.; Belovodskiy, A.; Chua, T.T.; Cho, W.J.; Joyce, M.; Dutilh, B.E.; et al. Establishing normal metabolism and differentiation in hepatocellular carcinoma cells by culturing in adult human serum. *Sci. Rep.* **2018**, *8*, 11685. doi:10.1038/s41598-018-29763-2.
30. Stuart, T.; Butler, A.; Hoffman, P.; Hafemeister, C.; Papalexi, E.; Mauck III, W.M.; Hao, Y.; Stoeckius, M.; Smibert, P.; Satija, R. Comprehensive integration of single-cell data. *Cell* **2019**, *177*, 1888–1902. doi: 10.1016/j.cell. 2019.05.031
31. Yan, H.; Zhong, G.; Xu, G.; He, W.; Jing, Z.; Gao, Z.; Huang, Y.; Qi, Y.; Peng, B.; Wang, H.; Fu, L.; Song, M.; Chen, P.; Gao, W.; Ren, B.; Sun, Y.; Cai, T.; Feng, X.; Sui, J.; Li, W. Sodium taurocholate cotransporting polypeptide is a functional receptor for human hepatitis B and D virus. *Elife* **2012**, *1*, e00049. doi:10.7554/eLife.00049.
32. Konig, A.; Yang, J.; Jo, E.; Park, K.H.P.; Kim, H.; Than, T.T.; Song, X.; Qi, X.; Dai, X.; Park, S.; Shum, D.; Ryu, W.S.; Kim, J.H.; Yoon, S.K.; Park, J.Y.; Ahn, S.H.; Han, K.H.; Gerlich, W.H.; Windisch, M.P. Efficient long-term amplification of hepatitis B virus isolates after infection of slow proliferating HepG2-NTCP cells. *J. Hepatol.* **2019**, *71*, 289-300. doi:10.1016/j.jhep.2019.04.010.

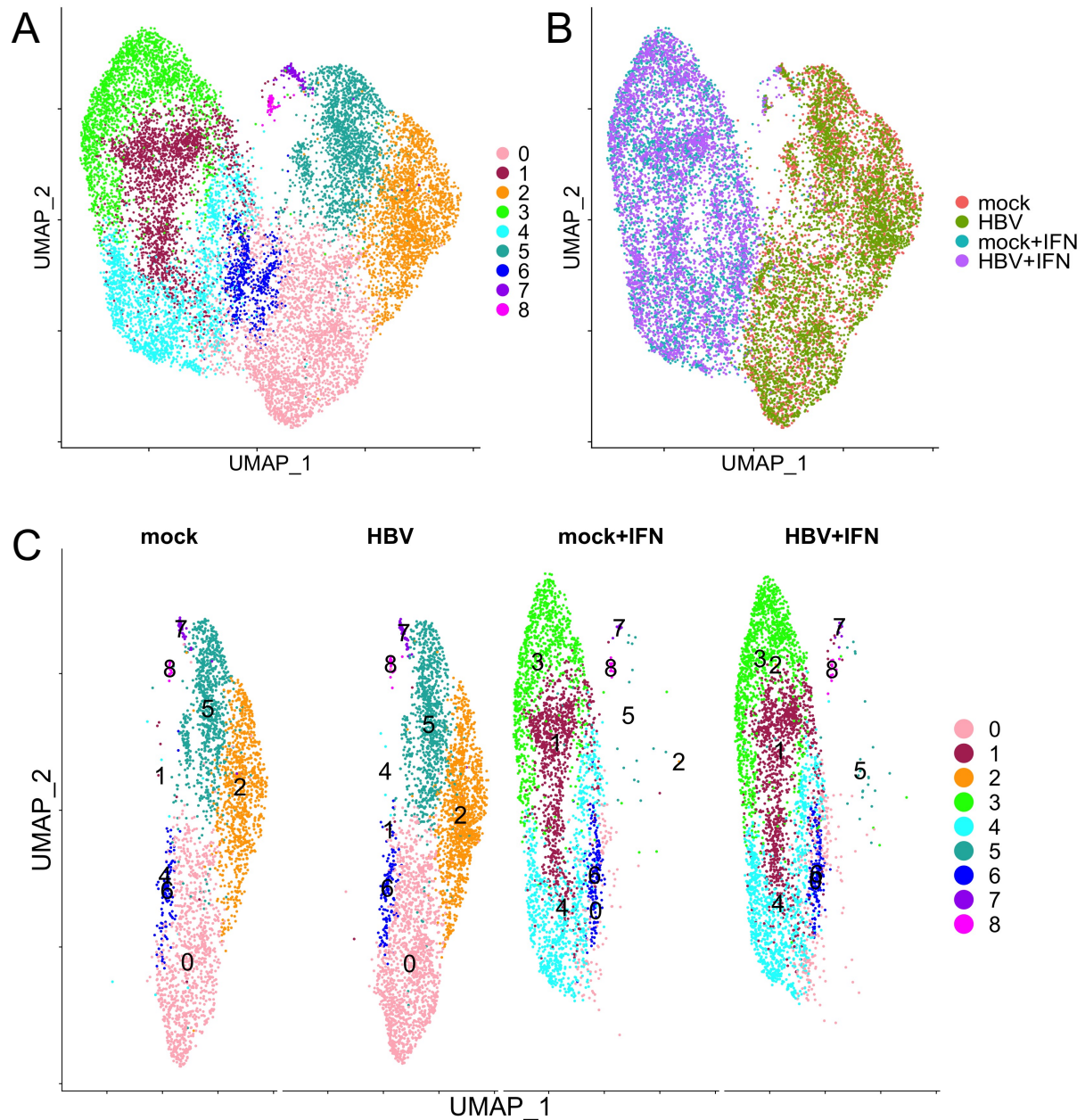


Figure 5.1. UMAP visualization of scRNA-seq data generated from four culture samples of Huh7.5-NTCP cells. These four samples represent Huh7.5-NTCP cells differentiated in human serum culture and treated under four conditions: mock infection control, HBV infection, mock infection and treatment with IFN, and HBV infection plus IFN treatment. Cells that share similar transcriptome profiles are grouped by clusters. (A) UMAP showing nine clusters (from 0 to 8) of scRNA-seq data from all four samples. (B) UMAP organized by input sample: mock infection control (red), HBV infection (green), IFN treatment (blue), and HBV infection plus IFN treatment (purple). (C) UMAP showing the clusters in each of the four samples. Different colors and numbers (0-8) represent nine clusters.

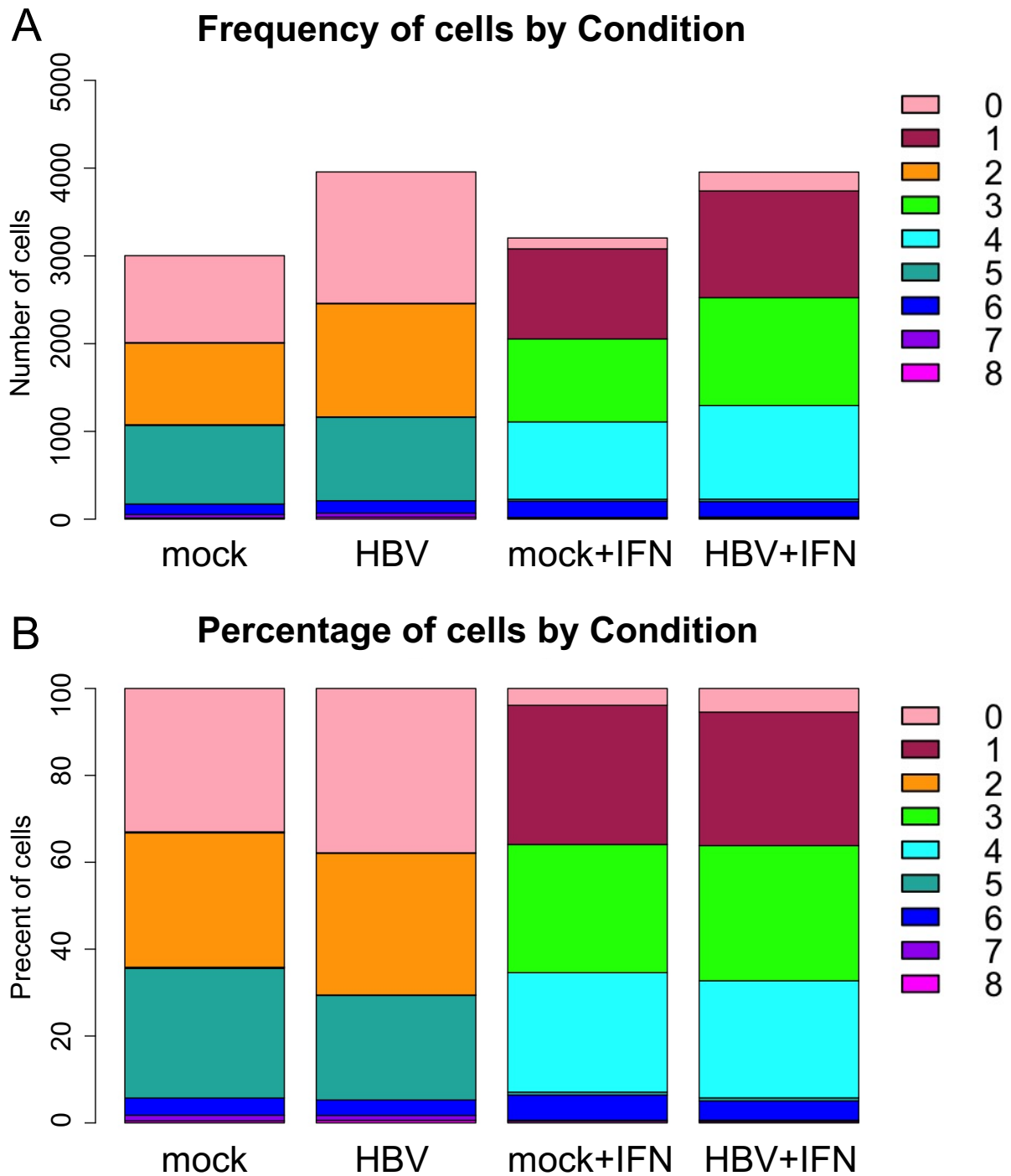


Figure 5.2. Number of cells contributing to each cluster of the four Huh7.5-NTCP cell culture samples. (A) Number of cells analyzed in the four samples: mock infection, HBV infection, mock infection but IFN treatment, and HBV infection plus IFN treatment. (B) Percentage of total number of cells in each sample contributed to each of the nine clusters (from cluster 0 to cluster 8).

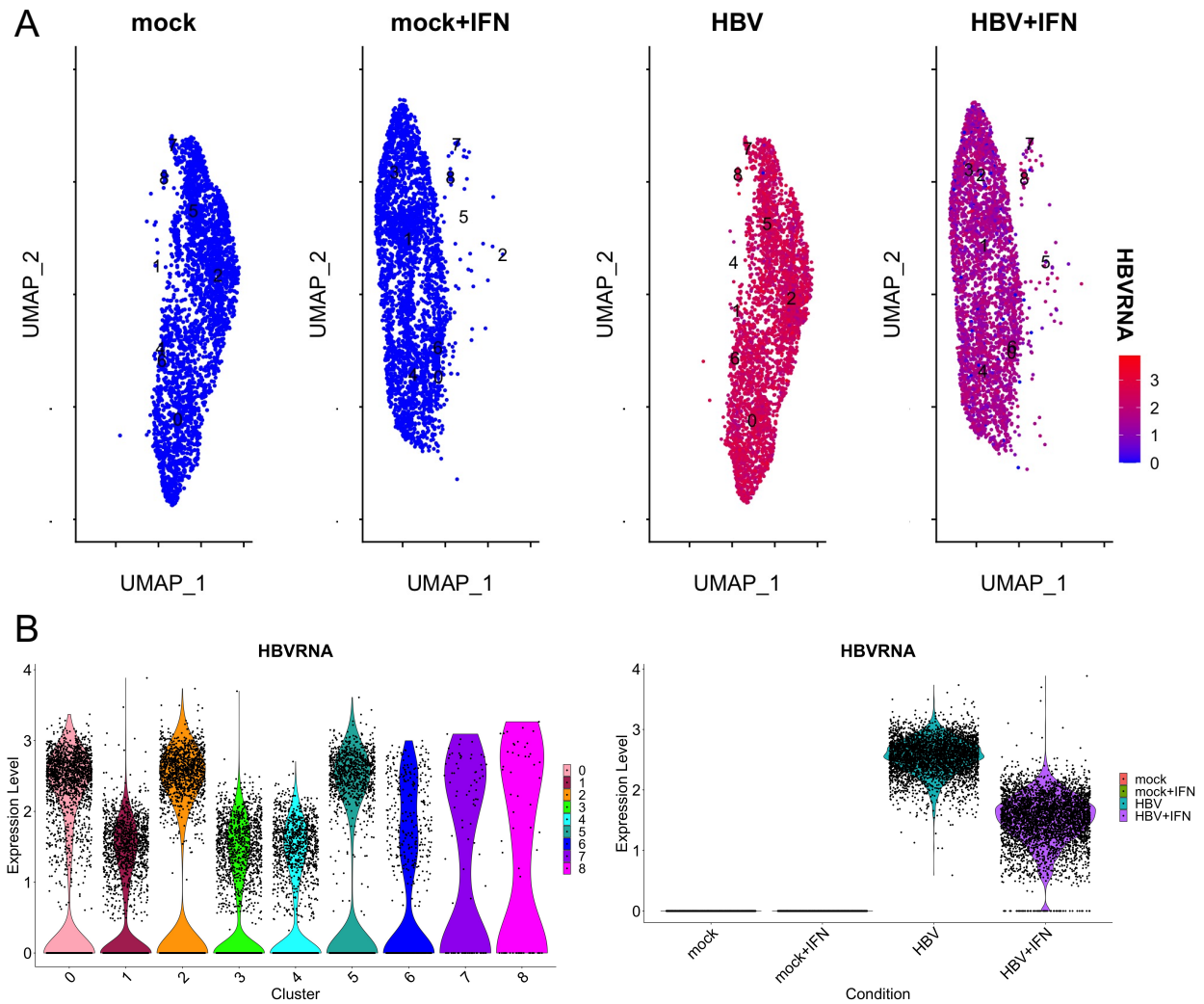


Figure 5.3. HBV transcripts detected in Huh7.5-NTCP cells after HBV infection and IFN treatment. (A) UMAP illustrating the levels of HBV transcripts detected in cells of four culture samples: mock infection, IFN treatment, HBV infection, and HBV infection plus IFN treatment. Dark red color indicates high level, and blue color indicates undetectable level of HBV transcripts. (B) Violin plots showing the levels of HBV transcripts in the nine clusters of cells. (C) Levels of HBV transcripts in cells of the four culture samples.

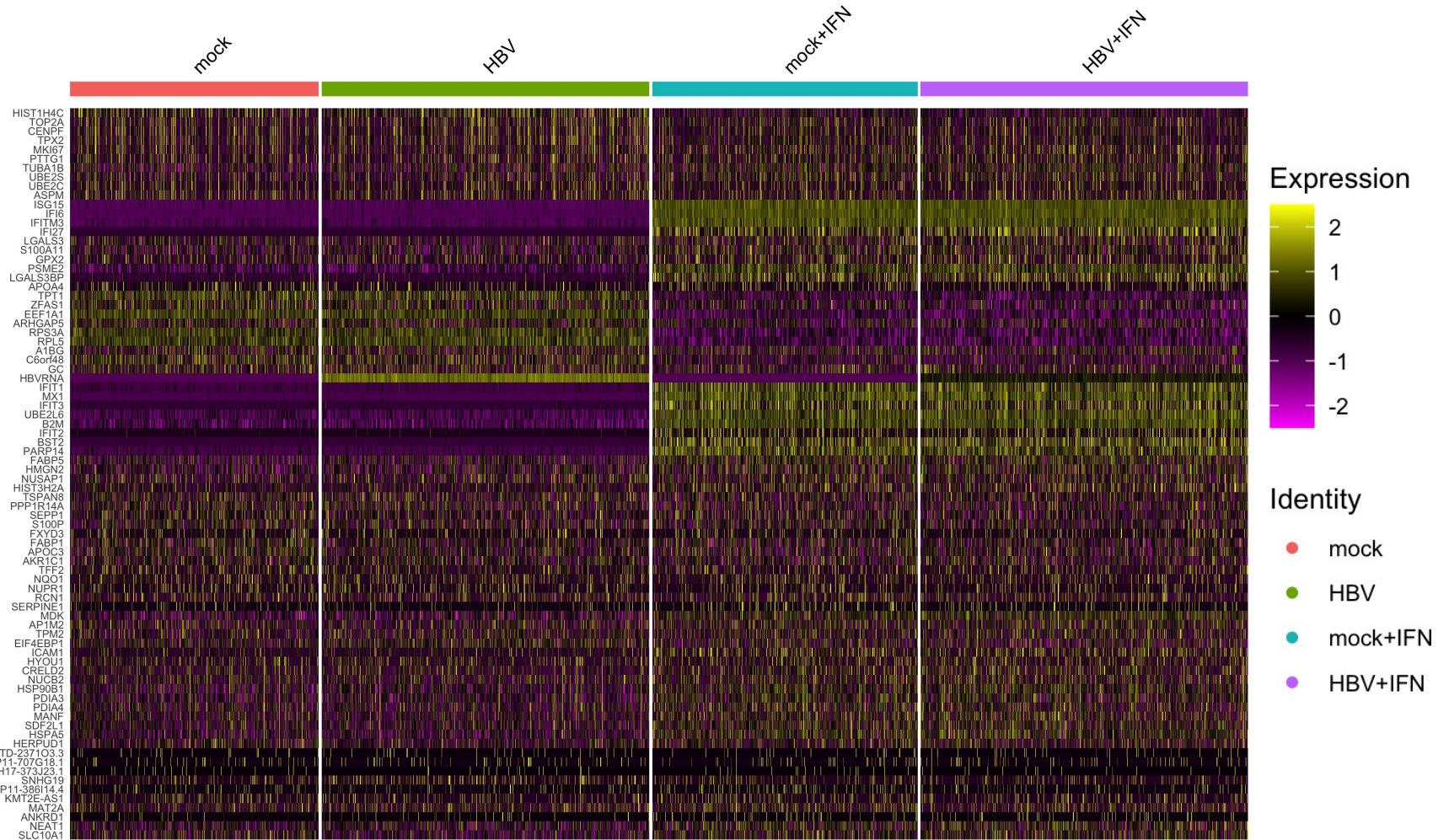


Figure 5.4. Heat maps illustrating differentially expressed genes in Huh7.5-NTCP cells of four culture samples. The yellow color indicates high levels of upregulation of genes whereas a purple color indicates down regulation of genes. Four cell culture samples are mock infection (control), HBV infection, IFN treatment, and HBV infection plus IFN treatment.

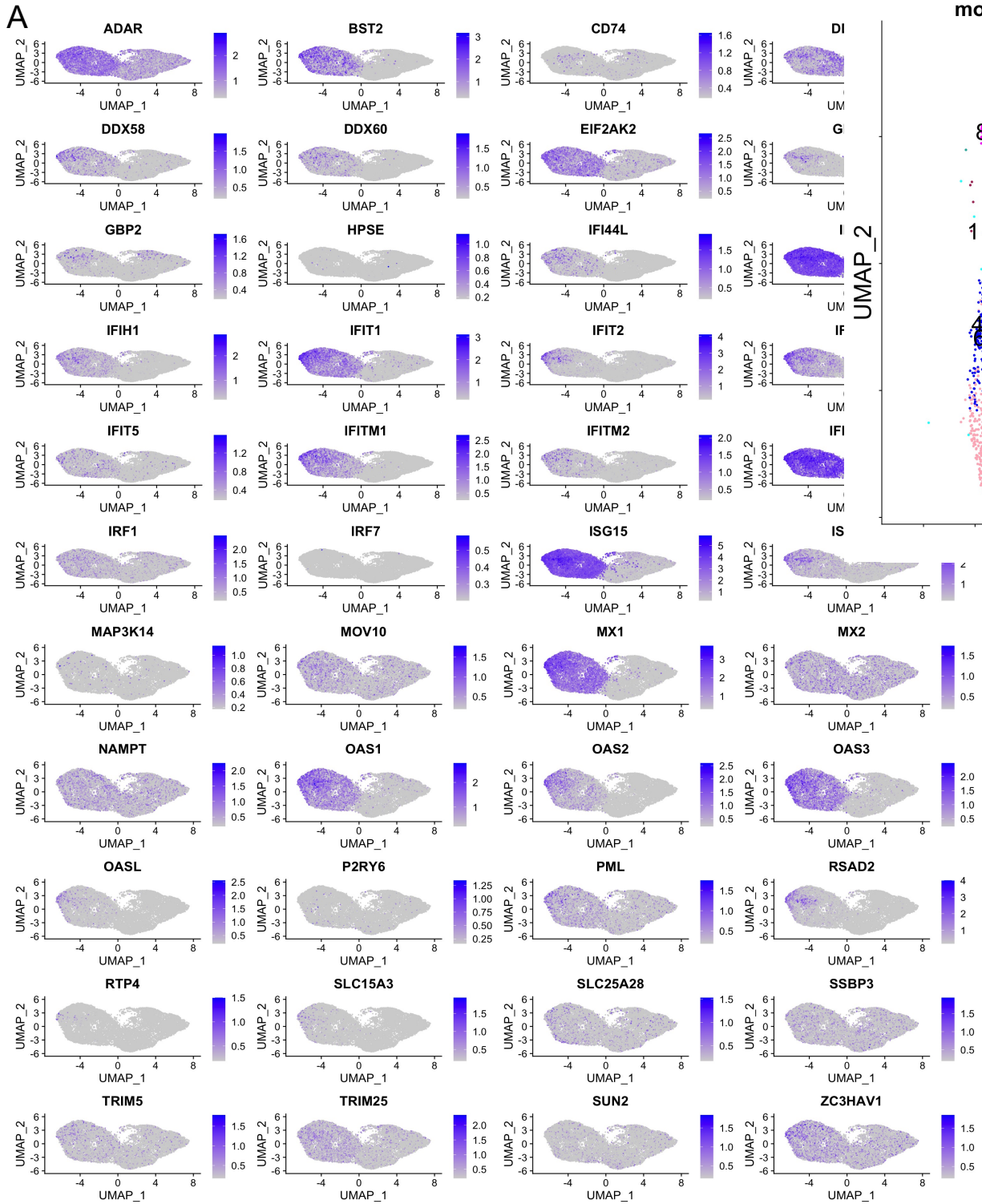


Figure 5.5 A. UMAPs illustrating expression levels of 44 interferon-stimulating genes in Huh7.5-NTCP cells of four culture samples. Darker blue colors indicate higher levels of gene expression.

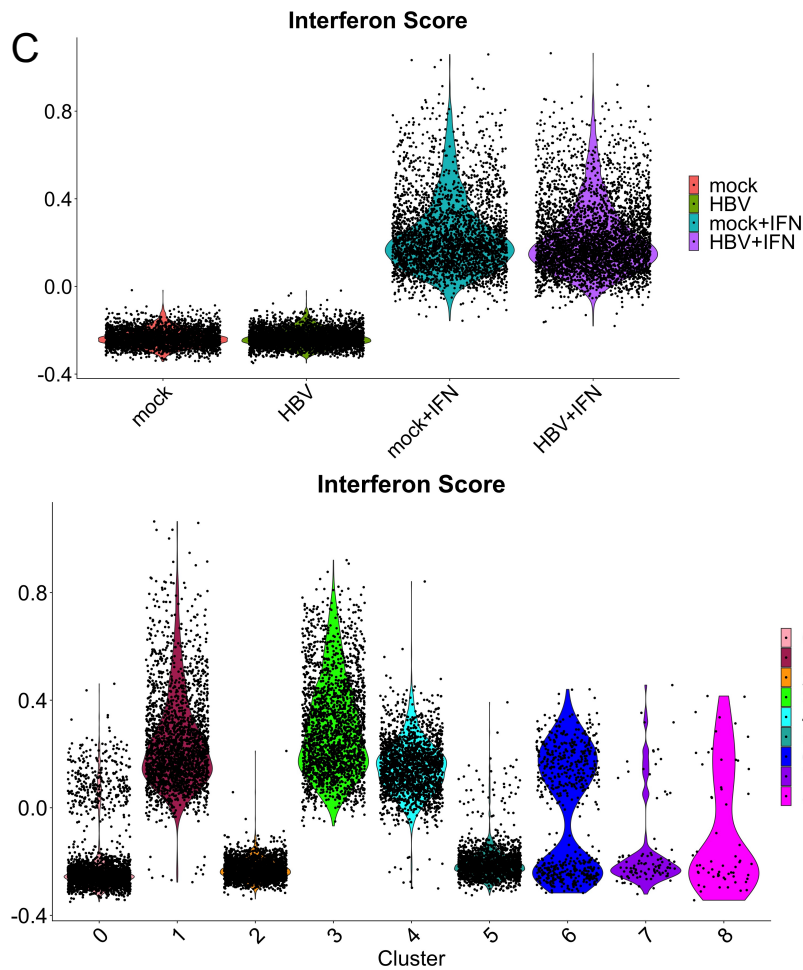
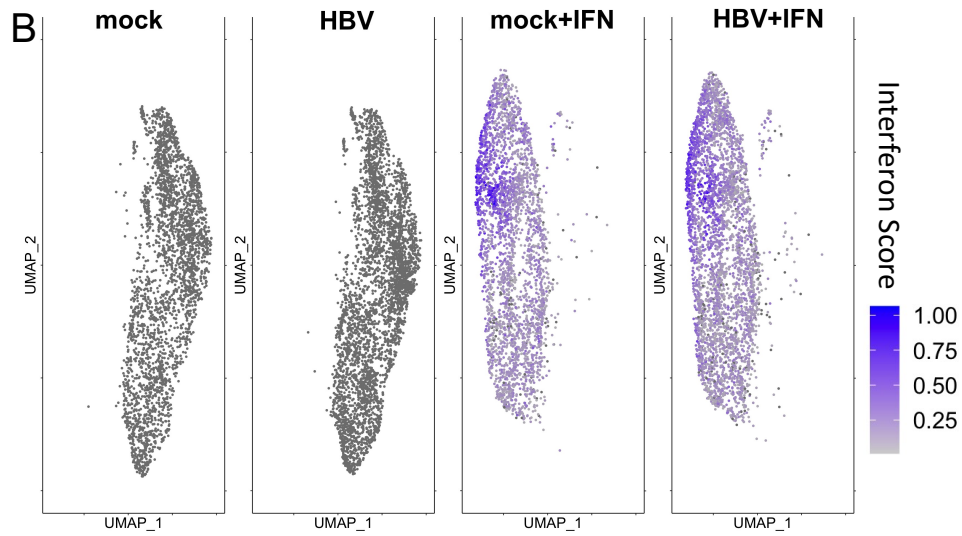


Figure 5.5 B and C. Expression of interferon-related genes in Huh7.5-NTCP cells under the four culture conditions. (B) UMAPs illustrating interferon scores, representing the average expression of the interferon-stimulated genes. A darker blue color indicates a higher interferon score. (C) Violin plots showing the interferon scores among the four samples and nine clusters.

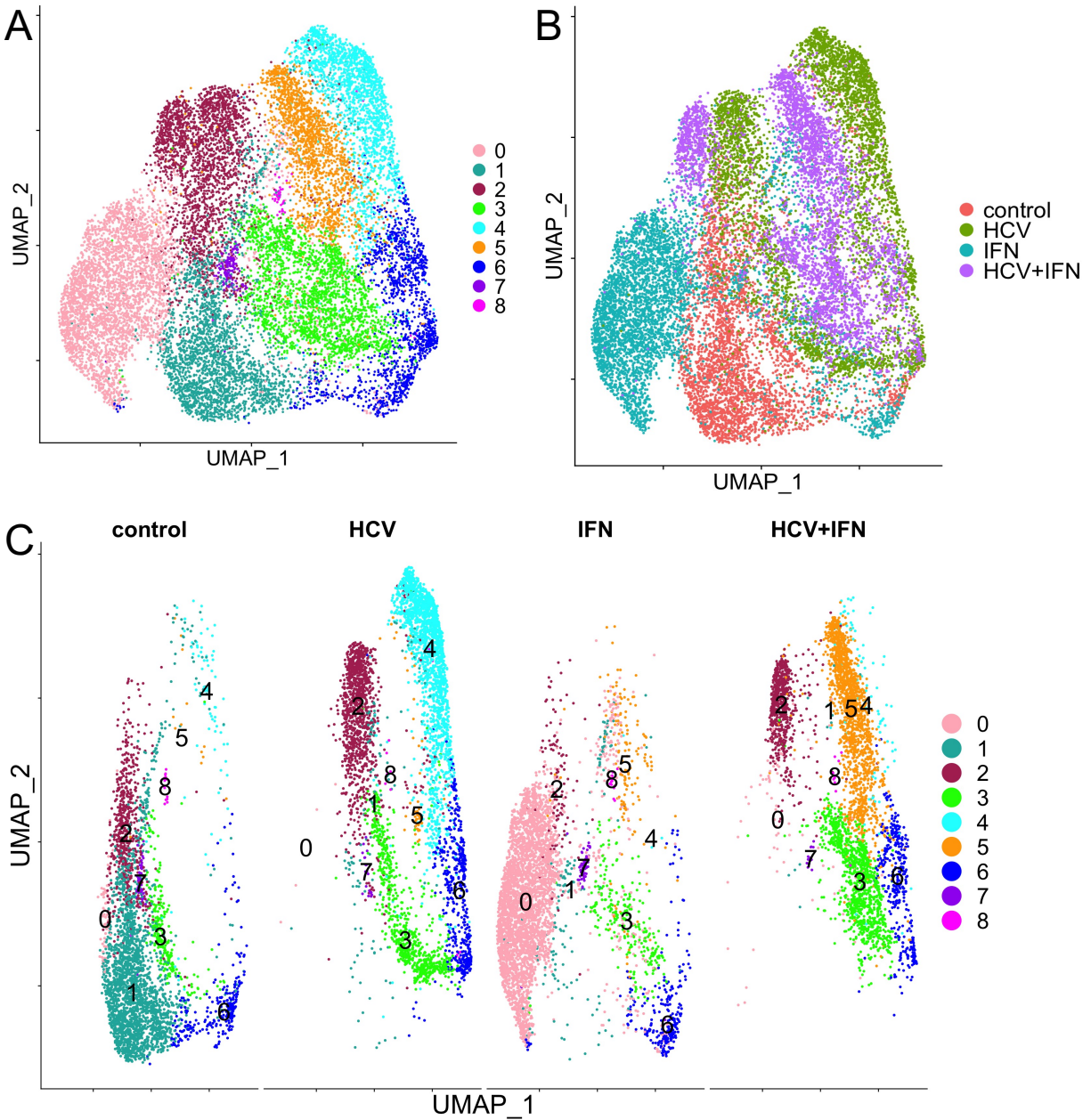


Figure 5.6. UMAP visualization of scRNA-seq data generated from four culture samples of Huh7.5 cells. These four samples represent Huh7.5 cells treated under four conditions: mock infection control, HCV infection, mock infection and treatment with IFN, and HCV infection plus IFN treatment. Cells that share similar transcriptome profiles are grouped by clusters. (A) UMAP showing nine clusters (from 0 to 8) of scRNA-seq data from all four samples. (B) UMAP organized by input sample: mock infection control (red), HCV infection (green), IFN treatment (blue), and HCV infection plus IFN treatment (purple). (C) UMAP showing the clusters in each of the four samples. Different colors and numbers (0-8) represent nine clusters.

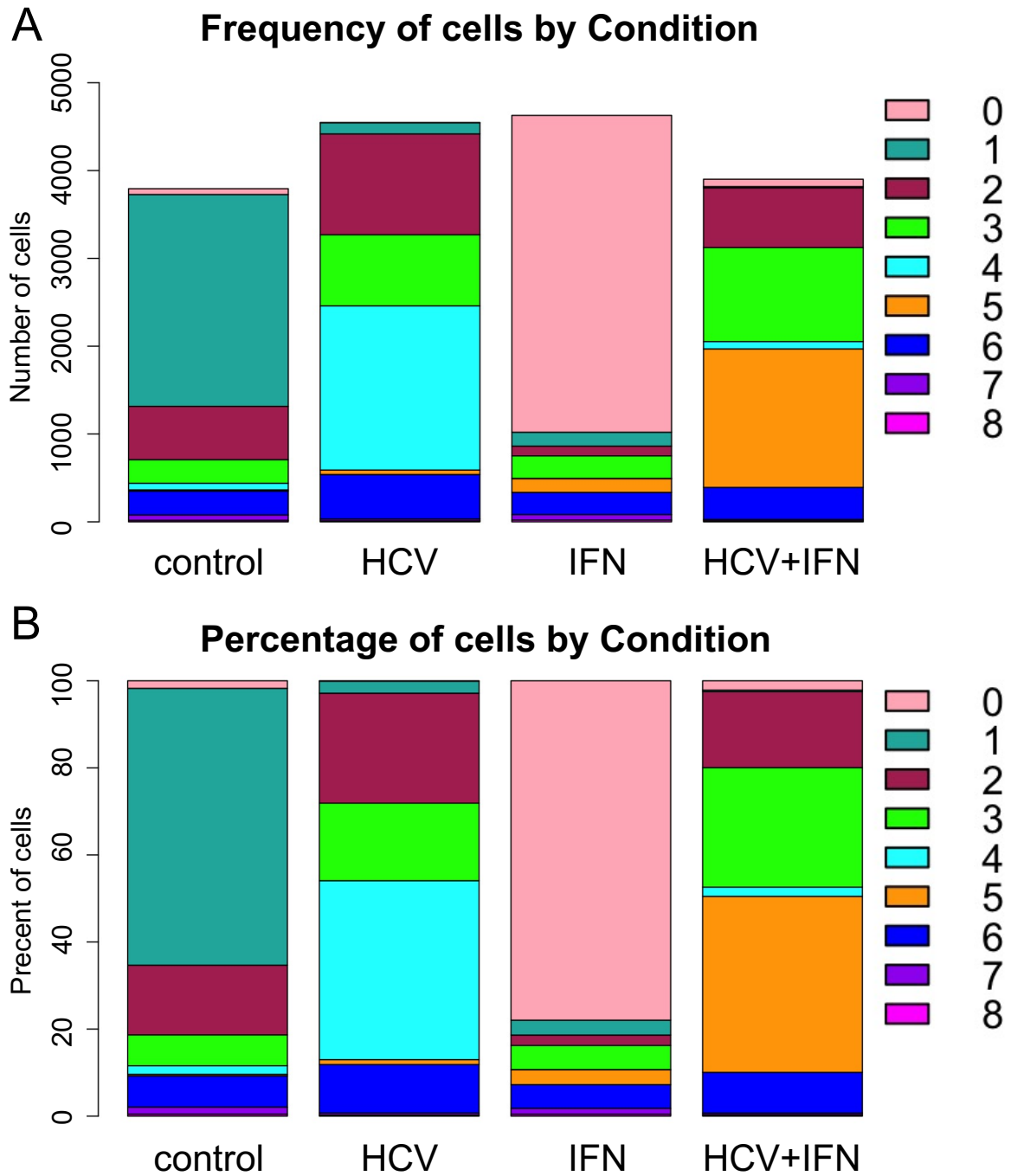


Figure 5.7. Number of cells contributing to each cluster of the four Huh7.5 cell culture samples. (A) Number of cells analyzed in the four samples: mock infection, HBV infection, mock infection but IFN treatment, and HBV infection plus IFN treatment. (B) Percentage of total number of cells in each sample contributed to each of the nine clusters (from cluster 0 to cluster 8).

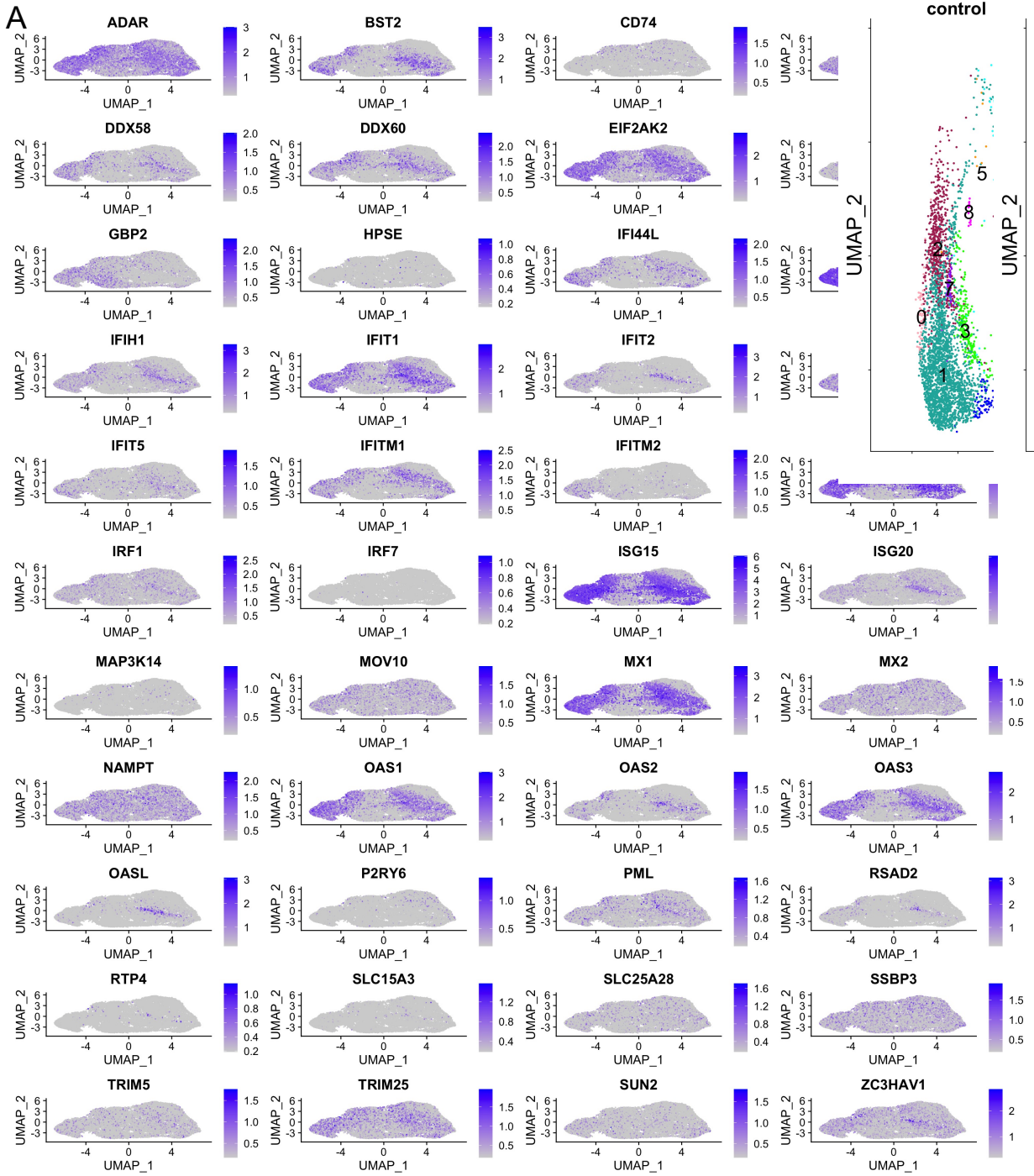


Figure 5.8 A. UMAPs illustrating expression level of 44 interferon-stimulating genes in Huh7.5 cells of four culture samples. Darker blue colors indicate higher levels of gene expression.

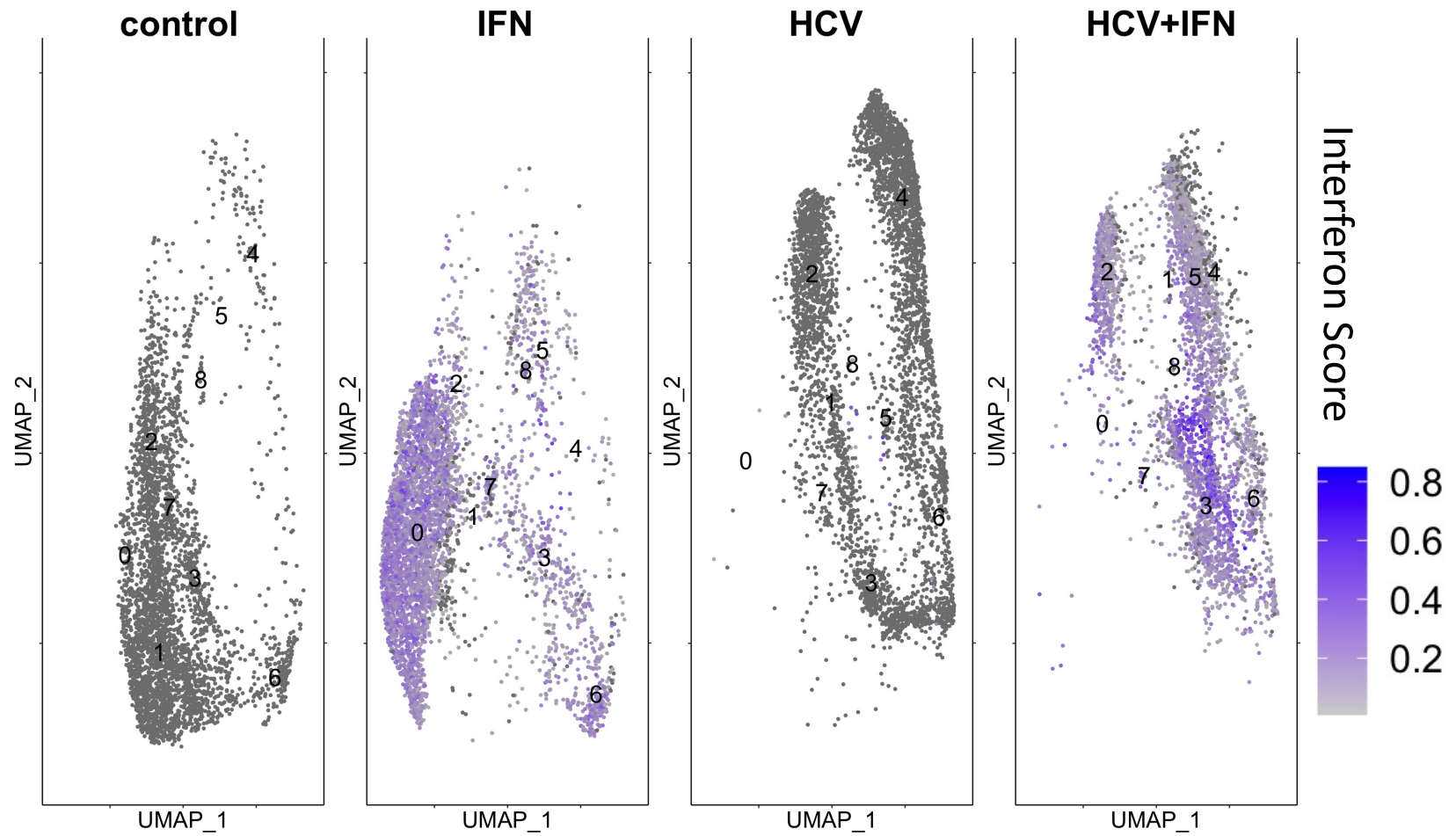


Figure 5.8 B. UMAPs illustrating interferon scores, representing the average expression of the interferon-stimulated genes in Huh7.5 cells of four culture samples. A darker blue color indicates a higher interferon score.

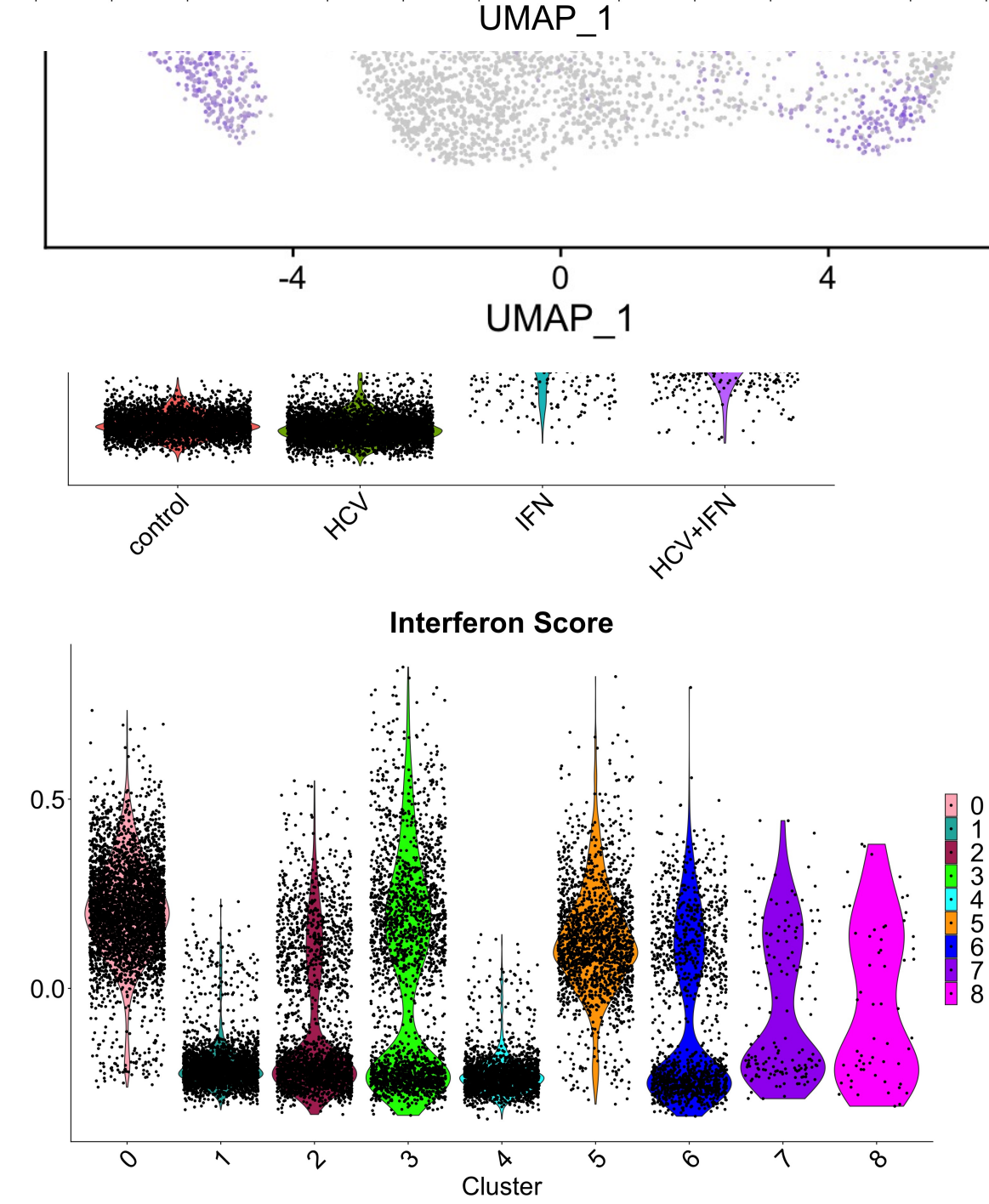


Figure 5.8 C. Violin plots showing the interferon scores of interferon-stimulated genes in Huh7.5 cells, presented as in four culture samples and nine clusters.

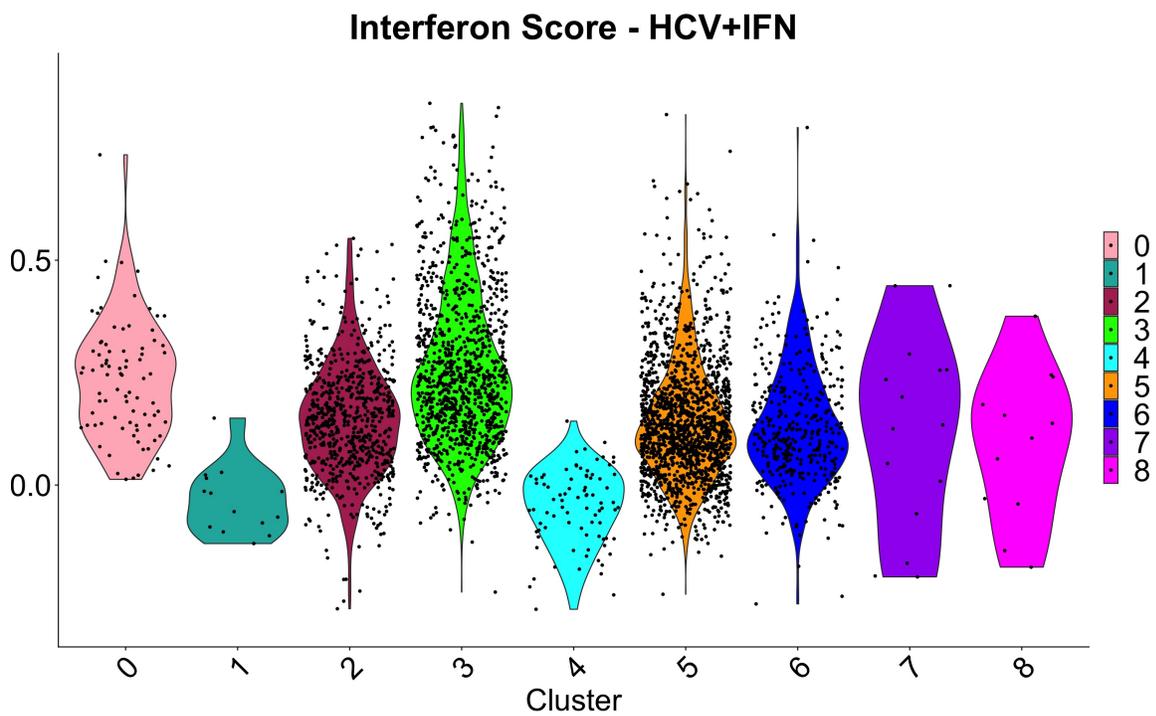
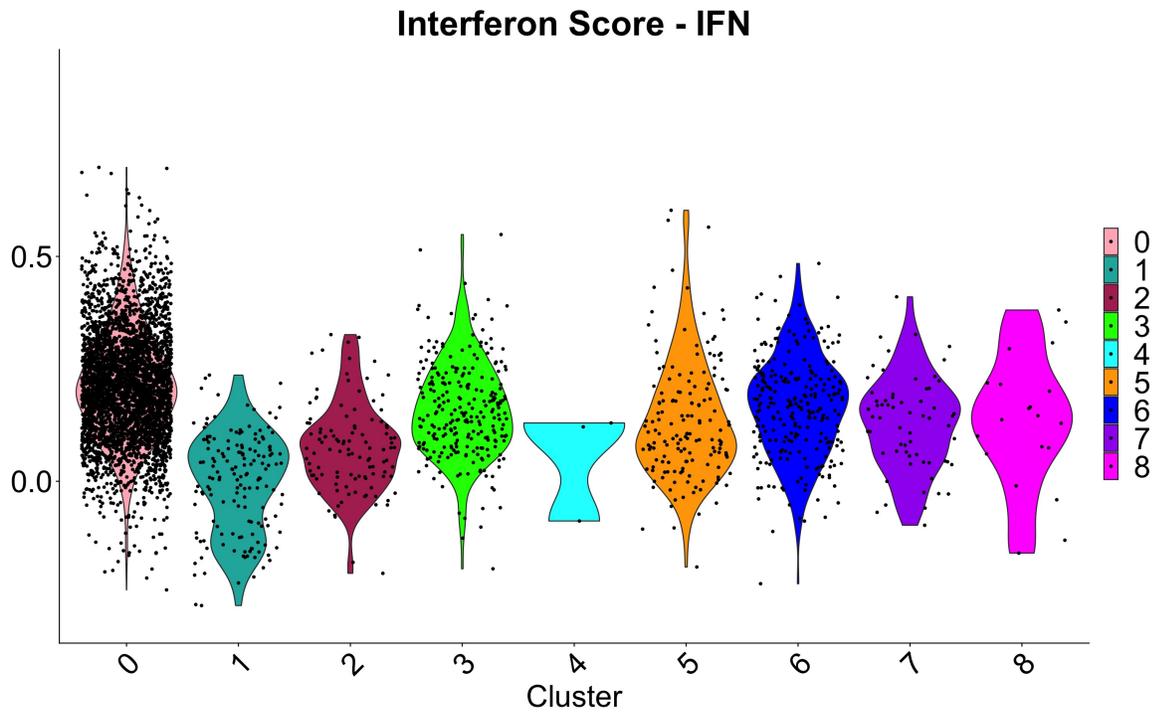


Figure 5.9. Violin plots showing the interferon scores of Huh7.5 cells treated with IFN alone or in combination with HCV infection.

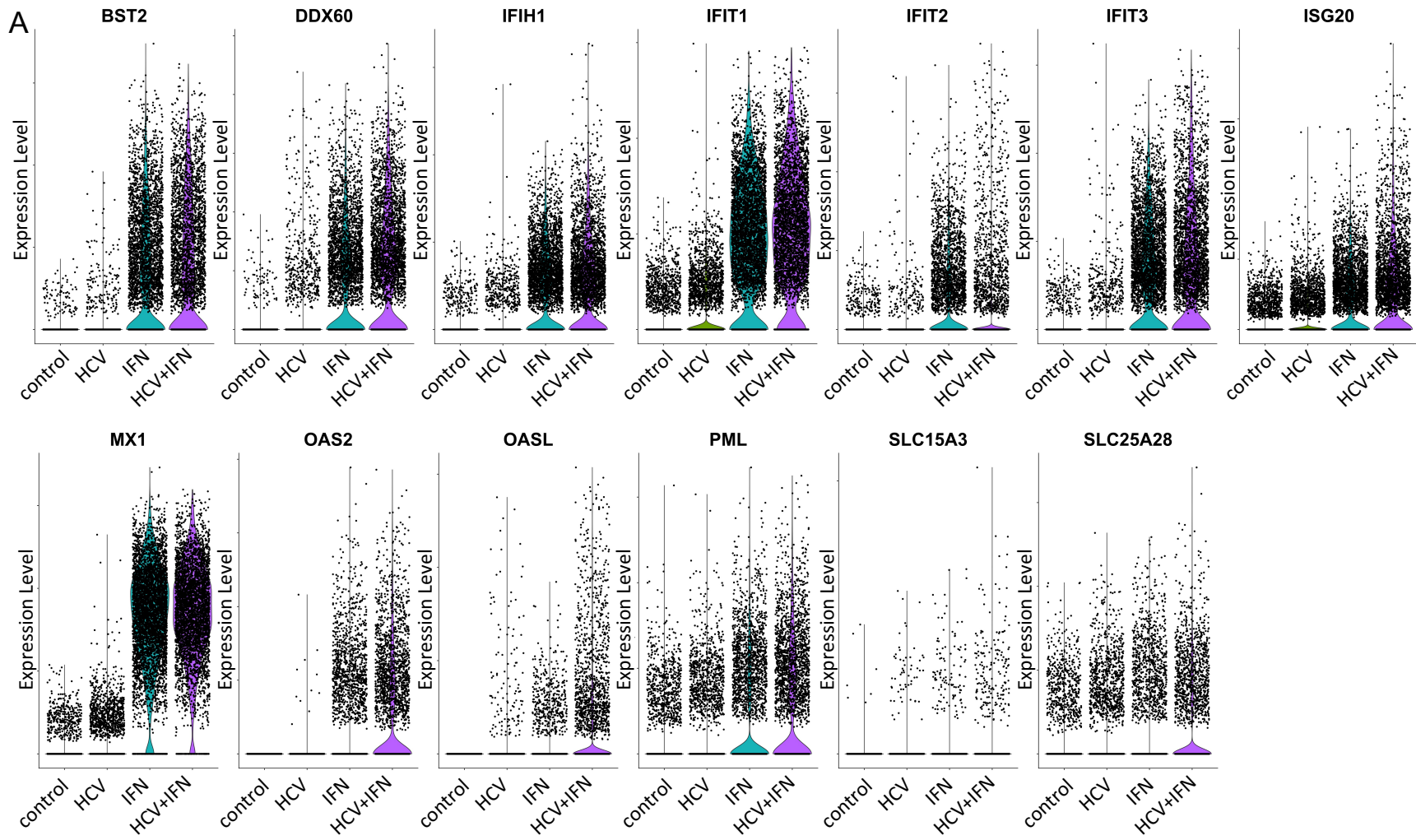


Figure 5.10 A. Interferon-stimulated gene expression in control, HCV, IFN, and HCV+IFN treated Huh7.5 cell culture samples. Examples of interferon genes that are upregulated in HCV-infected samples.

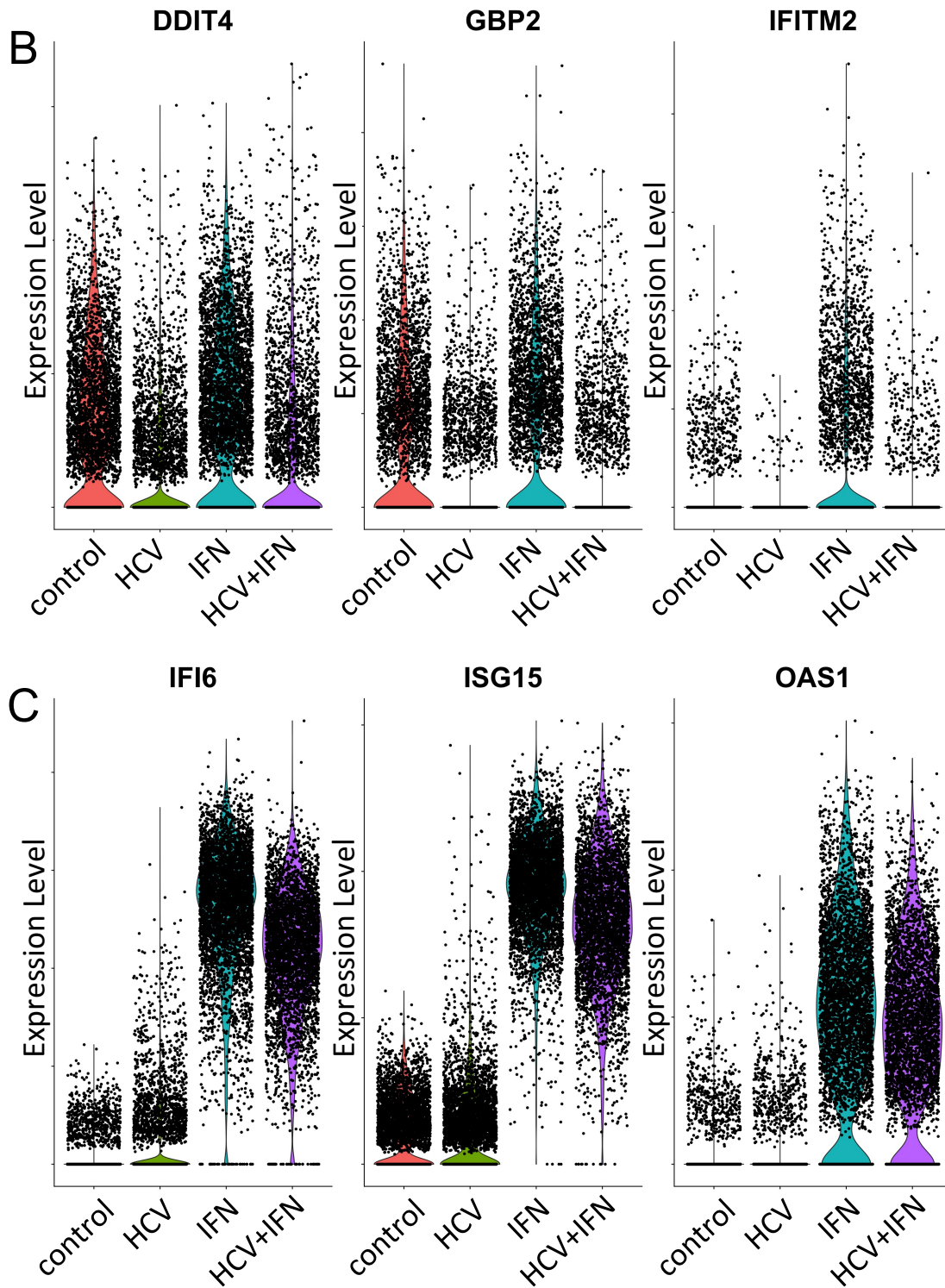


Figure 5.10 B and C. Interferon-stimulated gene expression in control, HCV, IFN, and HCV+IFN treated Huh7.5 cell culture samples. (A) Examples of interferon-stimulated genes that are upregulated in HCV-infected samples. (B) Examples of genes that are downregulated in HCV-infected samples. (C) Examples of genes that are upregulated in HCV over control samples but downregulated in HCV+IFN compared to IFN samples.

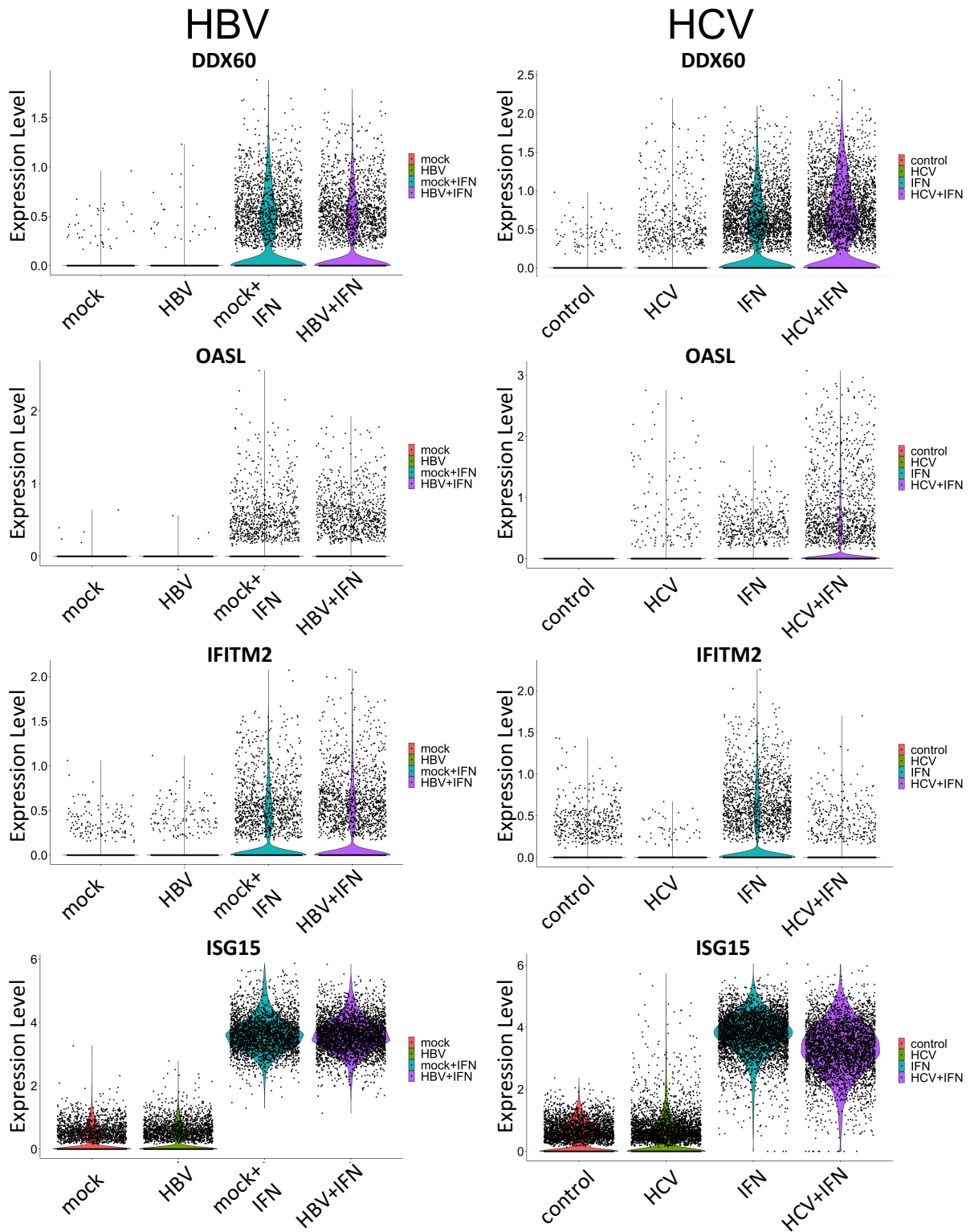


Figure 5.11. Comparison of interferon-stimulated gene expression in cell samples infected with HBV or HCV.

Chapter 6

Conclusions and Perspectives on Further Research

6.1. Conclusions

The slow development of biologically representative and feasible *in vitro* cell models for HBV infection has been a major challenge in the pursuit of understanding HBV virology. Immortalized cell lines have low HBV infection efficiency, while primary human hepatocytes are difficult to acquire and maintain in culture. Previous studies by others showed that overexpression of sodium taurocholate co-transporting polypeptide (NTCP) bile acid transporter in hepatoma cells moderately improved infection efficiency. Following HBV infection, these cultures must be maintained in high concentrations (2–2.5%) of DMSO for infection [1-11]. However, DMSO is known to cause a variety of adverse effects on cells, such as significant alterations in viability and protein expression [12-16]. Therefore, an HBV infection model that eliminates the requirement of DMSO treatment would be desirable to more closely mimic physiological conditions [17].

In studies of hepatitis C virus (HCV) infection, our group found that culturing the human hepatoma cell line Huh7 or Huh7.5 in a medium supplemented with human serum (HS) increased production of HCV [18]. Hepatoma cells cultured in an HS-supplemented medium underwent growth arrest and developed characteristics similar to primary human hepatocytes [19-21]. This method of producing hepatocyte-like cells enhanced production of HCV 1000-fold and resulted in a virus that more closely resembled the HCV present in the serum of infected patients.

Building on the findings of NTCP as the receptor for HBV viral entry and cell cultures in HS-supplemented media, this thesis research established a Huh7.5-NTCP cell culture system for studying HBV infection. NTCP was overexpressed in the Huh7.5 human hepatoma cell line. The resulting Huh7.5-NTCP hepatoma cells were differentiated in DMEM medium supplemented with

4% human serum (HS) instead of the conventional fetal bovine serum (FBS). This culture system produced robust HBV infection in Huh7.5-NTCP hepatoma cells in the absence of DMSO. In HS-supplemented cultures, HBV pgRNA levels were increased by as much as 200-fold in comparison with FBS-supplemented cultures and 19-fold in comparison with FBS+DMSO cultures. Human serum culture increased levels of hepatocyte differentiation markers, such as albumin secretion, in Huh7.5-NTCP cells to similar levels found in primary human hepatocytes. N-glycosylation of NTCP induced by culture in human serum may contribute to viral entry. This study demonstrates an *in vitro* HBV infection model of Huh7.5-NTCP cells without the use of potentially toxic DMSO.

To further characterize Huh7.5-NTCP cells differentiated in HS-supplemented cultures, we conducted single-cell RNA sequencing (scRNA-seq) analyses of these cells with or without HBV infection. However, high abundance of the host cell RNA relative to the much lower abundance of HBV transcripts presented a challenge in scRNA-seq studies of HBV infection. In the presence of a large excess of host cell RNA, low levels of HBV transcripts were often undetectable. To overcome this problem, we developed a CRISPR-Cas9 technique for the depletion of highly abundant transcripts, resulting in preferential enrichment of the low-abundance HBV transcripts. The CRISPR-mediated depletion of the three most abundant transcripts (MT-ATP6, SLC38A7 and MT-ND2) resulted in selective enrichment and successful scRNA-seq detection of HBV transcripts in more than 74% of the cells. This is compared to only 0.6% of the cells having detectable HBV transcripts when they were not enriched using the CRISPR-mediated technique. The improved detection of HBV transcripts facilitated our subsequent scRNA-seq studies of HBV infection and interferon treatment of hepatoma cells.

Our scRNA-seq analyses of Huh7.5 and Huh7.5-NTCP cells differentiated in HS-supplemented cultures provided rich gene expression data for characterizing their transcriptomes

and cell heterogeneity. Other than a difference in gene expression of NTCP, the Huh7.5 and Huh7.5-NTCP hepatoma cells share a similar gene expression landscape. Compared with the scRNA-seq data obtained from human liver [22], most of the cells in Huh7.5 and Huh7.5-NTCP cultures had transcriptome profiles overlapping with those of primary hepatocytes in the human liver. These scRNA-seq results support that the hepatoma cells differentiated in HS cultures serve as a useful alternative to primary human hepatocytes.

scRNA-seq analysis also revealed the presence of cholangiocyte-like cells in the HS-cultured Huh7.5 and Huh7.5-NTCP cell populations. The cholangiocyte-like cells in these hepatoma cell population had similar regulatory pathways to cholangiocytes from human liver tissue. The discovery of cholangiocyte-like cells in the HS-cultured Huh7.5 and Huh7.5-NTCP cell lines is exciting because our group has observed that the HS cultures of hepatoma cell lines formed structures resembling bile canaliculi.

The predominant cell types in the HS-cultured Huh7.5 and Huh7.5-NTCP hepatoma cell lines had transcriptome profiles similar to pericentral hepatocyte, hepatocyte-like, and hepatocyte-cholangiocyte-like cells. As expected, other cell types identified in primary liver, including monocyte, macrophage, lymphocyte, LSEC, B cell, T cell, NK cell, erythroid cell, and stellate cell, were not present in the hepatoma Huh7.5 and Huh7.5-NTCP cell culture.

scRNA-seq analyses were conducted to determine whether HBV infection alters interferon (IFN)-stimulated gene expression. Cells in the mock infection and HBV infection samples had the same transcriptome profiles. HBV did not affect gene expression patterns or levels in Huh7.5-NTCP hepatoma cells differentiated in HS cultures. IFN treatment of Huh7.5-NTCP cells resulted in increased levels of IFN-stimulated genes. But HBV infection of the IFN-treated Huh7.5-NTCP cells did not alter the patterns or expression levels of IFN-stimulated genes. These

results at the single-cell resolution support the idea that HBV is a “stealth virus”, which neither activates nor inhibits IFN-stimulated genes.

In contrast, scRNA-seq analyses of HCV-infected Huh7.5 hepatoma cells showed that HCV infection significantly changed expression levels of IFN-stimulated genes in the host cells. HCV infection of Huh7.5 hepatoma cells increased their expression levels of DDX6, IFIT3, and OASL, and to a lesser extent BST2, IFIH1, IFIT1, IFIT2, ISG20, MX1, OAS2, PML, SLC15A3, and SLC25A28, example IFN-stimulated genes. On the other hand, HCV infection downregulated a few other IFN-stimulated genes, such as DDIT4, GBP2, and IFITM2. Unlike HBV, HCV infection changed transcriptome profiles of the host cells, with upregulation and downregulation of IFN-stimulated genes. These results demonstrate the immunostimulatory and immunomodulatory nature of HCV, in contrast to the “stealth” nature of HBV, highlighting differences between these hepatotropic viruses.

6.2. Perspectives and future research

Cell culture models are invaluable to HBV research. Future research underway in our group will assess whether human serum culture can enhance HBV infection of other cells, e.g., HepG2-NTCP or PHH. The HepG2-NTCP hepatoma cell line is commonly used for *in vitro* HBV studies because it is more susceptible to HBV infection than Huh7 or Huh7.5 cells [23]. Huh7.5-NTCP cells differentiated in HS culture had a hepatocyte-like phenotype and significantly enhanced HBV infection. However, the pgRNA level in HBV-infected and HS-differentiated Huh7.5-NTCP cells (Figure 2.5A) was lower than that in HepG2-NTCP cells (Figure 2.13). HepG2-NTCP cells require DMSO for HBV infection and can be infected in the presence of HS and DMSO (Figure 2.13). It would be useful to test whether HepG2-NTCP cells differentiate or whether PHH remain

differentiated in human serum. Figure 2.9A shows that Huh7.5-NTCP cells need to differentiate in human serum for 21 days before enhanced HBV infection is achieved. Likely because the HepG2-NTCP cells were only cultured short-term (7 days) in a medium with human serum, there was no enhancement of HBV infection. Enhanced infection of HepG2-NTCP cells might not occur until these cells are cultured for longer periods in human serum. It would be necessary to optimize the protocol for HS-culture of HepG2-NTCP and PHH.

N-glycosylation of NTCP was promoted in culture media supplemented with HS. The inhibition of N-glycosylation suppressed HBV infection (Figure 2.12). Our results suggest potential involvement of NTCP N-glycosylation in HBV entry. Our results are consistent with those of Appelman *et al.* [24] and Sargiacomo *et al.* [25] who found that N-glycosylation of NTCP was required for HBV infection. However, Lee *et al.* [26] reported that N-glycosylation of NTCP was not essential to mediate HBV infection. Future work may extend to studies of NTCP glycosylation and its impact on viral entry. To evaluate the contribution of NTCP glycosylation to the HS phenotype, future experiments could include mutating NTCP glycosylation sites (e.g., N5Q and N11Q) [24, 26], transducing Huh7.5 cells with the NTCP mutants, and evaluating whether culture in HS leads to an increase in HBV replication.

scRNA-seq analysis identified a hepatocyte-cholangiocyte-like cluster of cells in the HS-supplemented Huh7.5 and Huh7.5-NTCP cultures with a transcriptome profile similar to cholangiocytes. The regulon analysis supports that the hepatocyte-cholangiocyte-like cells in the HS-cultured Huh7.5 and Huh7.5-NTCP cell lines have similar regulons/active regulatory networks as the cholangiocytes from the human liver tissue. There has been much interest in the *in vitro* culture of cholangiocytes, mostly focusing on primary cholangiocytes or cholangiocytes derived from stem cells [27-28]. Our group has observed bile canalicular-like structure in the HS

cultures of Huh7.5 cells [20]. Further research could include additional morphological, biochemical, and scRNA-seq studies of other hepatoma cell lines differentiated in HS-supplemented cultures to examine the formation of cholangiocytes and bile canaliculi structures. Further research will potentially lead to a useful *in vitro* culture model for both hepatocytes and cholangiocytes.

Several challenges and questions remain in the development of a representative *in vitro* HBV infection model. Although the advent of NTCP-overexpressing cell lines has resulted in numerous novel infectable culture systems, high multiplicity of infection (MOI) of 100 to 1000 as well as DMSO and PEG are necessary [1, 29]. This is in stark contrast to *in vivo* systems where it is estimated a single virion is sufficient to establish infection in chimpanzees and humans [30]. Even PHH cultures, considered to be the *in vitro* ideal and gold standard for HBV experiments, require an MOI of at least 10 for infection and DMSO or small molecules to maintain PHH differentiation [17]. The only *in vitro* system to date that has demonstrated infection with a single HBV virion has been PHHs cultured in a microfluidic chip [31]. This unique scaffold circulated medium, thereby imitating the physiologic conditions and structural organization of hepatocytes in the liver. Therefore, the intricacies of three-dimensional organ architecture appear to drastically influence hepatocyte function, metabolism, survival, and susceptibility to HBV. Given the highly ordered configuration in which PHHs exist within the liver and how these purposeful designs permit optimal function, it is understandable that the closer an *in vitro* system resembles liver structure, the better that model confers native liver function.

Future research may continue to develop novel three-dimensional platforms for organizing *in vitro* cultures that may potentially enhance HBV infection. The differences between three-

dimensional or *in vivo* systems compared to two-dimensional cultures can be further elucidated to identify additional factors involved in HBV infection. *In vitro* systems can subsequently be modified and improved by identifying these factors that result in improved infection *in vivo*.

6.3. References

1. Yan, H.; Zhong, G.; Xu, G.; He, W.; Jing, Z.; Gao, Z.; Huang, Y.; Qi, Y.; Peng, B.; Wang, H.; Fu, L.; Song, M.; Chen, P.; Gao, W.; Ren, B.; Sun, Y.; Cai, T.; Feng, X.; Sui, J.; Li, W. Sodium taurocholate cotransporting polypeptide is a functional receptor for human hepatitis B and D virus. *Elife* **2012**, *1*, e00049. doi:10.7554/eLife.00049.
2. Ni, Y.; Lempp, F.A.; Mehrle, S.; Nkongolo, S.; Kaufman, C.; Falth, M.; Stindt, J.; Koniger, C.; Nassal, M.; Kubitz, R.; Sultmann, H.; Urban, S. Hepatitis B and D viruses exploit sodium taurocholate co-transporting polypeptide for species-specific entry into hepatocytes. *Gastroenterology* **2014**, *146*, 1070–1083. doi:10.1053/j.gastro.2013.12.024.
3. Iwamoto, M.; Watashi, K.; Tsukuda, S.; Aly, H.H.; Fukasawa, M.; Fujimoto, A.; Suzuki, R.; Aizaki, H.; Ito, T.; Koiwai, O.; et al. Evaluation and identification of hepatitis B virus entry inhibitors using HepG2 cells overexpressing a membrane transporter NTCP. *Biochem. Biophys. Res. Commun.* **2014**, *443*, 808–813. doi:10.1016/j.bbrc.2013.12.052.
4. Seeger, C.; Sohn, J.A. Targeting hepatitis B virus with CRISPR/Cas9. *Mol. Ther. Nucleic Acids* **2014**, *3*, e216. doi:10.1038/mtna.2014.68.
5. Yan, R.; Zhang, Y.; Cai, D.; Liu, Y.; Cuconati, A.; Guo, H. Spinoculation enhances HBV infection in NTCP-reconstituted hepatocytes. *PLoS ONE* **2015**, *10*, e0129889. doi:10.1371/journal.pone.0129889.
6. Li, W. The hepatitis B virus receptor. *Annu. Rev. Cell Dev. Biol.* **2015**, *31*, 125–147. doi:10.1146/annurev-cellbio-100814-125241.
7. Lempp, F.A.; Qu, B.; Wang, Y.X.; Urban, S. Hepatitis B virus infection of a mouse hepatic cell line reconstituted with human sodium taurocholate cotransporting polypeptide. *J. Virol.* **2016**, *90*, 4827–4831 doi:10.1128/jvi.02832-15.

8. Li, J.; Zong, L.; Sureau, C.; Barker, L.; Wands, J.R.; Tong, S. Unusual features of sodium taurocholate cotransporting polypeptide as a hepatitis B virus receptor. *J. Virol.* **2016**, *90*, 8302–8313, doi:10.1128/jvi.01153-16.
9. Michailidis, E.; Pabon, J.; Xiang, K.; Park, P.; Ramanan, V.; Hoffmann, H.H.; Schneider, W.M.; Bhatia, S.N.; De Jong, Y.P.; Shlomai, A.; et al. A robust cell culture system supporting the complete life cycle of hepatitis B virus. *Sci. Rep.* **2017**, *7*, 16616. doi:10.1038/s41598-017-16882-5.
10. Zhou, M.; Zhao, K.; Yao, Y.; Yuan, Y.; Pei, R.; Wang, Y.; Chen, J.; Hu, X.; Zhou, Y.; Chen, X.; et al. Productive HBV infection of well-differentiated, hNTCP-expressing human hepatoma-derived (Huh7) cells. *Virol. Sin.* **2017**, *32*, 465–475. doi:10.1007/s12250-017-3983-x.
11. Qiao, L.; Sui, J.; Luo, G. Robust human and murine hepatocyte culture models of hepatitis B virus infection and replication. *J. Virol.* **2018**, *92*, e01255–18. doi:10.1128/jvi.01255-18.
12. Vondráček, J.; Souček, K.; Sheard, M.A.; Chramostová, K.; Andryšik, Z.; Hofmanová, J.; Kozubík, A. Dimethyl sulfoxide potentiates death receptor-mediated apoptosis in the human myeloid leukemia U937 cell line through enhancement of mitochondrial membrane depolarization. *Leuk. Res.* **2006**, *30*, 81–89. doi:10.1016/j.leukres.2005.05.016.
13. Song, Y.M.; Song, S.O.; Jung, Y.K.; Kang, E.S.; Cha, B.S.; Lee, H.C.; Lee, B. Dimethyl sulfoxide reduces hepatocellular lipid accumulation through autophagy induction. *Autophagy* **2012**, *8*, 1085–1097. doi:10.4161/auto.20260.
14. Galvao, J.; Davis, B.; Tilley, M.; Normando, E.; Duchon, M.R.; Cordeiro, M.F. Unexpected low-dose toxicity of the universal solvent DMSO. *FASEB J.* **2014**, *28*, 1317–1330. doi:10.1096/fj.13-235440.
15. Pal, R.; Mamidi, M.K.; Das, A.; Bhonde, R. Diverse effects of dimethyl sulfoxide (DMSO) on the differentiation potential of human embryonic stem cells. *Arch. Toxicol.* **2012**, *86*, 651–661. doi:10.1007/s00204-011-0782-2.
16. Verheijen, M.; Lienhard, M.; Schrooders, Y.; Clayton, O.; Nudischer, R.; Boerno, S.; Timmermann, B.; Selevsek, N.; Schlapbach, R.; Gmuender, H.; et al. DMSO induces drastic changes in human cellular processes and epigenetic landscape in vitro. *Sci. Rep.* **2019**, *9*, 4641. doi:10.1038/s41598-019-40660-0.
17. Xiang, C.; Du, Y.; Meng, G.; Yi, L.S.; Sun, S.; Song, N.; Zhang, X.; Xiao, Y.; Wang, J.; Yi, Z.; Liu, Y.; Xie, B.; Wu, M.; Shu, J.; Sun, D.; Jia, J.; Liang, Z.; Sun, D.; Huang, Y.; Shi, Y.;

- Xu, J.; Lu, F.; Li, C.; Xiang, K.; Yuan, Z.; Lu, S.; Deng, H. Long-term functional maintenance of primary human hepatocytes *in vitro*. *Science* **2019**, *364*, 399–402. doi:10.1126/science.aau7307.
18. Steenbergen, R.H.; Joyce, M. A.; Thomas, B.; Jones, D.; Law, J.; Russell, R.; Houghton, M.; Tyrrell, D. L. Human serum leads to differentiation of human hepatoma cells, restoration of very-low-density lipoprotein secretion, and a 1000-fold increase in HCV Japanese fulminant hepatitis type 1 titers. *Hepatology* **2013**, *58*, 1907–1917. doi:10.1002/hep.26566.
 19. Guo, L.; Dial, S.; Shi, L.; Branham, W.; Liu, J.; Fang, J.L.; Green, B.; Deng, H.; Kaput, J.; Ning, B. Similarities and differences in the expression of drug-metabolizing enzymes between human hepatic cell lines and primary human hepatocytes. *Drug Metab. Dispos.* **2011**, *39*, 528–538. doi:10.1124/dmd.110.035873.
 20. Steenbergen, R.; Oti, M.; ter Horst, R.; Tat, W.; Neufeldt, C.; Belovodskiy, A.; Chua, T. T.; Cho, W. J.; Joyce, M.; Dutilh, B. E.; Tyrrell, D. L. Establishing normal metabolism and differentiation in hepatocellular carcinoma cells by culturing in adult human serum. *Sci. Rep.* **2018**, *8*, 11685. doi:10.1038/s41598-018-29763-2.
 21. Hart, S.N.; Li, Y.; Nakamoto, K.; Subileau, E.-A.; Steen, D.; Zhong, X.-B. A comparison of whole genome gene expression profiles of HepaRG cells and HepG2 cells to primary human hepatocytes and human liver tissues. *Drug Metab. Dispos.* **2010**, *38*, 988–994. doi:10.1124/dmd.109.031831.
 22. MacParland, S. A.; Liu, J. C.; Ma, X-Z.; Innes, B. T.; Bartczak, A. M.; Gage, B. K.; Bader, G. D.; McGilvray, I. D. Single cell RNA sequencing of human liver reveals distinct intrahepatic macrophage populations. *Nat. Commun.* **2018**, *9*, 4383. doi:10.1038/s41467-018-06318-7
 23. Ni, Y.; Lempp, F.A.; Mehrle, S.; Nkongolo, S.; Kaufman, C.; Fälth, M.; Stindt, J.; Königer, C.; Nassal, M.; Kubitz, R.; et al. Hepatitis B and D viruses exploit sodium taurocholate co-transporting polypeptide for species-specific entry into hepatocytes. *Gastroenterology* **2014**, *146*, 1070–1083.e6. doi:10.1053/j.gastro.2013.12.024.
 24. Appelman, M.D.; Chakraborty, A.; Protzer, U.; McKeating, J.A.; Van De Graaf, S.F. N-Glycosylation of the Na⁺-taurocholate cotransporting polypeptide (NTCP) determines its trafficking and stability and is required for hepatitis B virus infection. *PLoS ONE* **2017**, *12*, e0170419. doi:10.1371/journal.pone.0170419.

25. Sargiacomo, C.; El-Kehdy, H.; Pourcher, G.; Stieger, B.; Najimi, M.; Sokal, E. Age-dependent glycosylation of the sodium taurocholate cotransporter polypeptide: From fetal to adult human livers. *Hepatol. Commun.* **2018**, *2*, 693–702. doi:10.1002/hep4.1174.
26. Lee, J.; Zong, L.; Krotow, A.; Qin, Y.; Jia, L.; Zhang, J.; Tong, S.; Li, J. N-Linked glycosylation is not essential for sodium taurocholate cotransporting polypeptide to mediate hepatitis B virus infection in vitro. *J. Virol.* **2018**, *92*, e00732–18. doi:10.1128/jvi.00732-18.
27. Dianat, N.; Dubois-Pot-Schneider, H.; Steichen, C.; Desterke, C.; Leclerc, P.; Raveux, A.; Combettes, L.; Weber, A.; Corlu, A.; Dubart-Kupperschmit, A. Generation of functional cholangiocyte-like cells from human pluripotent stem cells and HepaRG cells. *Hepatology* **2014**, *60*, 700–714. doi:10.1002/hep.27165
28. Wang, Z.; Faria, J.; Penning, L.C.; Masereeuw, R.; Spee, B. Tissue-engineered bile ducts for disease modeling and therapy. *Tissue Engineer. Part C* **2021**, *27*(2), 59–76. doi: 10.1089/ten.tec.2020.0283
29. Konig, A.; Yang, J.; Jo, E.; Park, K.H.P.; Kim, H.; Than, T.T.; Song, X.; Qi, X.; Dai, X.; Park, S.; Shum, D.; Ryu, W.S.; Kim, J.H.; Yoon, S.K.; Park, J.Y.; Ahn, S.H.; Han, K.H.; Gerlich, W.H.; Windisch, M.P. Efficient long-term amplification of hepatitis B virus isolates after infection of slow proliferating HepG2-NTCP cells. *J. Hepatol.* **2019**, *71*, 289–300. doi:10.1016/j.jhep.2019.04.010.
30. Shikata, T.; Karasawa, T. Abe, K. Two distinct types of hepatitis in experimental hepatitis B virus infection. *Am. J. Pathol.* **1980**, *99*, 353–368.
31. Ortega-Prieto, A.M.; Skelton, J.K.; Wai, S.N.; Large, E.; Lussignol, M.; Vizcay-Barrena, G.; Hughes, D.; Fleck, R.A.; Thursz, M.; Catanese, M.T.; Dorner, M. 3D microfluidic liver cultures as a physiological preclinical tool for hepatitis B virus infection. *Nat. Commun.* **2018**, *9*, 682. doi:10.1038/s41467-018-02969-8.

Bibliography

- Addison, W.R.; Walters, K.A.; Wong, W.W.; Wilson, J.S.; Madej, D.; Jewell, L.D.; Tyrrell, D.L. Half-life of the duck hepatitis B virus covalently closed circular DNA pool *in vivo* following inhibition of viral replication. *J. Virol.* **2002**, *76*, 6356-6363. doi:10.1128/jvi.76.12.6356-6363.2002.
- Aden, D.P.; Fogel, A.; Plotkin, S.; Damjanov, I.; Knowles, B.B. Controlled synthesis of HBsAg in a differentiated human liver carcinoma-derived cell line. *Nature* **1979**, *282*, 615-616. doi:10.1038/282615a0.
- Aevermann, B.D.; Shannon, C.P.; Novotny, M.; Ben-Othman, R.; Cai, B.; Zhang, Y.; Ye, J.C.; Kobor, M.S.; Gladish, N.; Lee, A.H.; Blimkie, T.M.; Hancock, R.E.; Llibre, A.; Duffy, D.; Koff, W.C.; Sadarangani, M.; Tebbutt, S.J.; Kollmann, T.R.; Scheuermann, R.H. Machine learning-based single cell and integrative analysis reveals that baseline mDC predisposition correlates with hepatitis B vaccine antibody response. *Front. Immunol.* **2021**, *12*, 690470. doi:10.3389/fimmu.2021.690470.
- Aibar, S.; González-Blas, C.B.; Moerman, T.; Huynh-Thu, V.A.; Imrichova, H.; Hulselmans, G.; Rambow, F.; Marine, J.-C.; Geurts, P.; Aerts, J.; van den Oord, J.; Atak, Z.K.; Wouters, J.; Stein Aerts, S. SCENIC: Single-cell regulatory network inference and clustering, *Nat. Methods* **2017**, *14*(11), 1083–1086. doi:10.1038/nmeth.4463.
- Aizarani, N.; Saviano, A.; Sagar, M.; Maily, L.; Durand, S.; Herman, J.S.; Pessaux, P.; Baumert, T.F.; Grun, D. A human liver cell atlas reveals heterogeneity and epithelial progenitors. *Nature* **2019**, *572*, 199-204. doi:10.1038/s41586-019-1373-2.
- Allweiss, L.; Dandri, M. Experimental *in vitro* and *in vivo* models for the study of human hepatitis B virus infection. *J. Hepatol.* **2016**, *64*, S17–S31, doi:10.1016/j.jhep.2016.02.012.
- Alter, H.; Block, T.; Brown, N.; Brownstein, A.; Brosgart, C.; Chang, K.M.; Chen, P.J.; Chisari, F.V.; Cohen, C.; El-Serag, H.; Feld, J.; Gish, R.; Glenn, J.; Greten, T.; Guo, H.; Guo, J.T.; Hoshida, Y.; Hu, J.; Kowdley, K.V.; Li, W.; Liang, J.; Locarnini, S.; Lok, A.S.; Mason, W.; McMahon, B.; Mehta, A.; Perrillo, R.; Revill, P.; Rice, C.M.; Rinaudo, J.; Schinazi, R.; Seeger, C.; Shetty, K.; Tavis, J.; Zoulim, F. A research agenda for curing chronic hepatitis B virus infection. *Hepatology* **2018**, *67*, 1127-1131. doi:10.1002/hep.29509.

- Altmae, S.; Molina, N.M.; Sola-Leyva, A. Omission of non-poly(A) viral transcripts from the tissue level atlas of the healthy human virome. *BMC Biol.* **2020**, *18*, 179. doi:10.1186/s12915-020-00907-z
- Alvarez, E.G.; Demeulemeester, J.; Otero, P.; Jolly, C.; Garcia-Souto, D.; Pequeno-Valtierra, A.; Zamora, J.; Tojo, M.; Temes, J.; Baez-Ortega, A.; Rodriguez-Martin, B.; Oitaben, A.; Bruzos, A.L.; Martinez-Fernandez, M.; Haase, K.; Zumalave, S.; Abal, R.; Rodriguez-Castro, J.; Rodriguez-Casanova, A.; Diaz-Lagares, A.; Li, Y.; Raine, K.M.; Butler, A.P.; Otero, I.; Ono, A.; Aikata, H.; Chayama, K.; Ueno, M.; Hayami, S.; Yamaue, H.; Maejima, K.; Blanco, M.G.; Forns, X.; Rivas, C.; Ruiz-Banobre, J.; Perez-Del-Pulgar, S.; Torres-Ruiz, R.; Rodriguez-Perales, S.; Garaigorta, U.; Campbell, P.J.; Nakagawa, H.; Van Loo, P.; Tubio, J.M.C. Aberrant integration of Hepatitis B virus DNA promotes major restructuring of human hepatocellular carcinoma genome architecture. *Nat. Commun.* **2021**, *12*, 6910. doi:10.1038/s41467-021-26805-8.
- Alzarani, N.; Saviano, A.; Sagar, M.; Mailly, L.; Durand, S.; Herman, J.S.; Pessaux, P.; Baumert, T.F.; Grün, D. A human liver cell atlas reveals heterogeneity and epithelial progenitors. *Nature* **2019**, *572*, 199-204. doi:10.1038/s41586-019-1373-2
- Andrews, T.S.; Atif, J.; Liu, J.C.; Perciani, C.; Ma, X.-Z.; Thoeni, C.; Slyper, M.; Eraslan, G.; Segersrolpe, A.; Manuel, J.; Chung, S.; Winter, E.; Cirlan, J.; Kkun, N.; Fischer, S.; Rozenblatt-Rosen, O.; Regev, A.; McGilvray, I.D.; Bader, G.D.; MacParland, S.A. Single-cell, single-nucleus, and spatial RNA sequencing of the human liver identifies cholangiocyte and mesenchymal heterogeneity. *Hepatology Commun.* **2022**, *6*, 821-840. doi:10.1002/hep4.1854
- Appelman, M.D.; Chakraborty, A.; Protzer, U.; McKeating, J.A.; Van De Graaf, S.F. N-Glycosylation of the Na⁺-taurocholate cotransporting polypeptide (NTCP) determines its trafficking and stability and is required for hepatitis B virus infection. *PLoS One* **2017**, *12*, e0170419. doi:10.1371/journal.pone.0170419.
- Argelaguet, R.; Cuomo, A.S.E.; Stegle, O.; Marioni, J.C. Computational principles and challenges in single-cell data integration. *Nat. Biotechnol.* **2021**, *39*, 1202-1215. doi:10.1038/s41587-021-00895-7

- Asabe, S.; Wieland, S.F.; Chattopadhyay, P.K.; Roederer, M.; Engle, R.E.; Purcell, R.H.; Chisari, F.V. The size of the viral inoculum contributes to the outcome of hepatitis B virus infection. *J. Virol.* **2009**, *83*, 9652-9662. doi:10.1128/JVI.00867-09.
- Asabe, S.; Wieland, S.F.; Chattopadhyay, P.K.; Roederer, M.; Engle, R.E.; Purcell, R.H.; Chisari, F.V. The size of the viral inoculum contributes to the outcome of hepatitis B virus infection. *J. Virol.* **2009**, *83*, 9652-9662. doi:10.1128/JVI.00867-09.
- Balagopal, A.; Grudde, T.; Ribeiro, R.M.; Saad, Y.S.; Hwang, H.S.; Quinn, J.; Murphy, M.; Ward, K.; Sterling, R.K.; Zhang, Y.; Perelson, A.S.; Sulkowski, M.S.; Osburn, W.O.; Thio, C.L. Single hepatocytes show persistence and transcriptional inactivity of hepatitis B. *JCI Insight* **2020**, *5*. doi:10.1172/jci.insight.140584.
- Balagopal, A.; Hwang, H.S.; Grudde, T.; Quinn, J.; Sterling, R.K.; Sulkowski, M.S., Thio, C.L. Single hepatocyte hepatitis B virus transcriptional landscape in HIV coinfection. *J. Infect. Dis.* **2020**, *221*, 1462-1469. doi:10.1093/infdis/jiz607.
- Bartenschlager, R.; Junker-Niepmann, M.; Schaller, H. The P gene product of hepatitis B virus is required as a structural component for genomic RNA encapsidation. *J. Virol.* **1990**, *64*, 5324-5332.
- Bartenschlager, R.; Schaller, H. Hepadnaviral assembly is initiated by polymerase binding to the encapsidation signal in the viral RNA genome. *EMBO J.* **1992**, *11*, 3413-3420.
- Baumert, T.F.; Colpitts, C.C.; Schuster, C.; Zeisel, M.B.; Baumert, T.F. Cell culture models for the investigation of hepatitis B and D virus infection. *Viruses* **2016**, *8*, 261. doi:10.3390/v8090261.
- Becht, E.; McInnes, L.; Healy, J.; Dutertre, C.A.; Kwok, I.W.H.; Ng, L.G.; Ginhoux, F.; Newell, E.W. Dimensionality reduction for visualizing single-cell data using UMAP. *Nat. Biotechnol.* **2018**, doi:10.1038/nbt.4314.
- Belloni, L.; Pollicino, T.; De Nicola, F.; Guerrieri, F.; Raffa, G.; Fanciulli, M.; Raimondo, G.; Levrero, M. Nuclear HBx binds the HBV minichromosome and modifies the epigenetic regulation of cccDNA function. *Proc. Natl. Acad. Sci. U. S. A.* **2009**, *106*, 19975-19979. doi:10.1073/pnas.0908365106.
- Berg, F.V.D.; Limani, S.W.; Mnyandu, N.; Maepa, M.B.; Ely, A.; Arbuthnot, P. Advances with RNAi-based therapy for hepatitis B virus infection. *Viruses* **2020**, *12*, 851. doi:10.3390/v12080851.

- Bertoletti, A.; Sette, A.; Chisari, F.V.; Penna, A.; Levrero, M.; De Carli, M.; Fiaccadori, F.; Ferrari, C. Natural variants of cytotoxic epitopes are T-cell receptor antagonists for antiviral cytotoxic T cells. *Nature* **1994**, *369*, 407-410. doi:10.1038/369407a0.
- Bill, C.A.; Summers, J. Genomic DNA double-strand breaks are targets for hepadnaviral DNA integration. *Proc. Natl. Acad. Sci. U. S. A.* **2004**, *101*, 11135-11140. doi:10.1073/pnas.0403925101.
- Birnbaum, F.; Nassal, M. Hepatitis B virus nucleocapsid assembly: primary structure requirements in the core protein. *J. Virol.* **1990**, *64*, 3319-30.
- Blumberg, B.S.; Alter, H.J.; Visnich, S. A "new" antigen in leukemia sera. *JAMA*, **1965**, *191*, 541-546. doi:10.1001/jama.1965.03080070025007.
- Bock, C.T.; Schranz, P.; Schroder, C.H.; Zentgraf, H. Hepatitis B virus genome is organized into nucleosomes in the nucleus of the infected cell. *Virus Genes* **1994**, *8*, 215-29. doi:10.1007/BF01703079.
- Bock, C.T.; Schwinn, S.; Locarnini, S.; Fyfe, J.; Manns, M.P.; Trautwein, C.; Zentgraf, H. Structural organization of the hepatitis B virus minichromosome. *J. Mol. Biol.* **2001**, *307*, 183-96. doi:10.1006/jmbi.2000.4481.
- Bost, P.; Giladi, A.; Liu, Y.; Bendjelal, Y.; Xu, G.; David, E.; Blecher-Gonen, R.; Cohen, M.; Medaglia, C.; Li, H.; Deczkowska, A.; Zhang, S.; Schwikowski, B.; Zhang, Z.; Amit, I. Host-viral infection maps reveal signatures of severe COVID-19 patients. *Cell* **2020**, *181*, 1475-1488 e12. doi:10.1016/j.cell.2020.05.006.
- Brancale, J.; Vilarinho, S. A single cell gene expression atlas of 28 human livers. *J. Hepatol.* **2001**, *75*, 219-220. doi:10.1016/j.jhep.2021.03.005.
- Brechot, C.; Gozuacik, D.; Murakami, Y.; Paterlini-Brechot, P. Molecular bases for the development of hepatitis B virus (HBV)-related hepatocellular carcinoma (HCC). *Semin. Cancer Biol.* **2000**, *10*, 211-231. doi:10.1006/scbi.2000.0321.
- Brechot, C.; Pourcel, C.; Louise, A.; Rain, B.; Tiollais, P. Presence of integrated hepatitis B virus DNA sequences in cellular DNA of human hepatocellular carcinoma. *Nature* **1980**, *286*, 533-535. doi:10.1038/286533a0.
- Bruss, V. A short linear sequence in the pre-S domain of the large hepatitis B virus envelope protein required for virion formation. *J. Virol.* **1997**, *71*, 9350-9357.

- Bruss, V. Hepatitis B virus morphogenesis. *World J. Gastroenterol.* **2007**, *13*, 65-73.
doi:10.3748/wjg.v13.i1.65.
- Bruss, V.; Ganem, D. The role of envelope proteins in hepatitis B virus assembly. *Proc. Natl. Acad. Sci. U. S. A.* **1991**, *88*, 1059-1063. doi:10.1073/pnas.88.3.1059.
- Bruss, V.; Thomssen, R. Mapping a region of the large envelope protein required for hepatitis B virion maturation. *J. Virol.* **1994**, *68*, 1643-1650.
- Butler, A.; Hoffman, P.; Smibert, P.; Papalex, E.; Satija, R. Integrating single-cell transcriptomic data across different conditions, technologies, and species. *Nat. Biotechnol.* **2018**, *36*, 411-420. doi:10.1038/nbt.4096.
- Carreno, V. Present treatment expectations and risks of chronic hepatitis C. *Clin. Microbiol. Infect.* **2002**, *8*, 74-79.
- Cavanaugh, V.J.; Guidotti, L.G.; Chisari, F.V. Inhibition of hepatitis B virus replication during adenovirus and cytomegalovirus infections in transgenic mice. *J. Virol.* **1998**, *72*, 2630-2637. doi:10.1128/JVI.72.4.2630-2637.1998.
- Chai, N.; Chang, H.E.; Nicolas, E.; Han, Z.; Jarnik, M.; Taylor, J. Properties of subviral particles of hepatitis B virus. *J. Virol.* **2008**, *82*, 7812-7817. doi:10.1128/JVI.00561-08.
- Chakraborty, P.R.; Ruiz-Opazo, N.; Shouval, D.; Shafritz, D.A. Identification of integrated hepatitis B virus DNA and expression of viral RNA in an HBsAg-producing human hepatocellular carcinoma cell line. *Nature* **1980**, *286*, 531-533. doi:10.1038/286531a0.
- Chen, C.J.; Yang, H.I.; Su, J.; Jen, C.L.; You, S.L.; Lu, S.N.; Huang, G.T.; Iloeje, U.H.; Group, R.-H.S. Risk of hepatocellular carcinoma across a biological gradient of serum hepatitis B virus DNA level. *JAMA* **2006**, *295*, 65-73. doi:10.1001/jama.295.1.65.
- Chen, G.; Ning, B.; Shi, T. Single-cell RNA-seq technologies and related computational data analysis. *Front. Genet.* **2019**, *10*, 317. doi:10.3389/fgene.2019.00317
- Chen, M.T.; Billaud, J.N.; Sallberg, M.; Guidotti, L.G.; Chisari, F.V.; Jones, J.; Hughes, J.; Milich, D.R. A function of the hepatitis B virus precore protein is to regulate the immune response to the core antigen. *Proc. Natl. Acad. Sci. U. S. A.* **2004**, *101*, 14913-14918. doi:10.1073/pnas.0406282101.
- Chen, R.; Kobewka, M.; Addison, W.; Lachance, G.; Tyrrell, D.L. Intrinsic viral factors are the dominant determinants of the hepatitis C virus response to interferon alpha treatment in chimeric mice. *PLoS ONE* **2016**, *11*(1), e0147007. doi:10.1371/journal.pone.0147007

- Cheng, X.M.; Xia, Y.C.; Serti, E.; Block, P.D.; Chung, M.; Chayama, K.; Rehermann, B.; Liang, T.J. Hepatitis B virus evades innate immunity of hepatocytes but activates cytokine production by macrophages. *Hepatology* **2017**, *66*, 1779–1793. DOI: 10.1002/hep.29348
- Chu, C.M.; Liaw, Y.F. Chronic hepatitis B virus infection acquired in childhood: special emphasis on prognostic and therapeutic implication of delayed HBeAg seroconversion. *J. Viral. Hepat.* **2007**, *14*, 147-52. doi:10.1111/j.1365-2893.2006.00810.x.
- Clark, D.N.; Hu, J. Unveiling the roles of HBV polymerase for new antiviral strategies. *Future Virol.* **2015**, *10*, 283-295. doi:10.2217/fvl.14.113.
- Clark, Z.A.; Andres, T.S.; Atif, J.; Pouyabahr, D.; Innes, B.T.; MacParland, S.A.; Bader, G.D. Tutorial: guidelines for annotating single-cell transcriptomic maps using automated and manual methods. *Nat. Protoc.* **2021**, *16*, 2749-2764. doi:10.1038/s41596-021-00534-0
- Clement, B.; Guguen-Guillouzo, C.; Campion, J.P.; Glaise, D.; Bourel, M.; Guillouzo, A. Long-term co-cultures of adult human hepatocytes with rat liver epithelial cells: modulation of albumin secretion and accumulation of extracellular material. *Hepatology* **1984**, *4*, 373-380. doi:10.1002/hep.1840040305.
- Cong, L., Ran, F. A., Cox, D., Lin, S., Barretto, R., Habib, N., Hsu, P. D., Wu, X., Jiang, W.; Marraffini, L. A. Multiplex genome engineering using CRISPR/Cas systems. *Science* **2013**, *339* (6121), 819–823. DOI: 10.1126/science.1231143.
- Crowther, R.A.; Kiselev, N.A.; Bottcher, B.; Berriman, J.A.; Borisova, G.P.; Ose, V.; Pumpens, P. Three-dimensional structure of hepatitis B virus core particles determined by electron cryomicroscopy. *Cell* **1994**, *77*, 943-50. doi:10.1016/0092-8674(94)90142-2.
- Cui, X.; McAllister, R.; Boregowda, R.; Sohn, J.A.; Cortes Ledesma, F.; Caldecott, K.W.; Seeger, C.; Hu, J. Does Tyrosyl DNA Phosphodiesterase-2 Play a Role in Hepatitis B Virus Genome Repair? *PLoS One* **2015**, *10*, e0128401. doi:10.1371/journal.pone.0128401.
- Dane, D.S.; Cameron, C.H.; Briggs, M. Virus-like particles in serum of patients with Australia-antigen-associated hepatitis. *Lancet* **1970**, *1*, 695-698. doi:10.1016/s0140-6736(70)90926-8.
- Dansako, H.; Ueda, Y.; Okumura, N.; Satoh, S.; Sugiyama, M.; Mizokami, M.; Ikeda, M.; Kato, N. The cyclic GMP-AMP synthetase-STING signaling pathway is required for both the innate immune response against HBV and the suppression of HBV assembly. *FEBS J.* **2016**, *283*, 144-156. doi:10.1111/febs.13563.

- Das, K.; Xiong, X.; Yang, H.; Westland, C.E.; Gibbs, C.S.; Sarafianos, S.G.; Arnold, E. Molecular modeling and biochemical characterization reveal the mechanism of hepatitis B virus polymerase resistance to lamivudine (3TC) and emtricitabine (FTC). *J. Virol.* **2001**, *75*, 4771-4779. doi:10.1128/JVI.75.10.4771-4779.2001.
- Decorsiere, A.; Mueller, H.; van Breugel, P.C.; Abdul, F.; Gerossier, L.; Beran, R.K.; Livingston, C.M.; Niu, C.; Fletcher, S.P.; Hantz, O.; Strubin, M. Hepatitis B virus X protein identifies the Smc5/6 complex as a host restriction factor. *Nature* **2016**, *531*, 386-389. doi:10.1038/nature17170.
- Deng, F.; Xu, G.; Cheng, Z.; Huang, Y.; Ma, C.; Luo, C.; Yu, C.; Wang, J.; Xu, X.; Liu, S.; Zhu, Y. Hepatitis B surface antigen suppresses the activation of nuclear factor Kappa B pathway via interaction with the TAK1-TAB2 complex. *Front. Immunol.* **2021**, *12*, 618196. doi:10.3389/fimmu.2021.618196.
- Dill, J.A.; Camus, A.C.; Leary, J.H.; Di Giallonardo, F.; Holmes, E.C.; Ng, T.F. Distinct viral lineages from fish and amphibians reveal the complex evolutionary history of hepadnaviruses. *J. Virol.* **2016**, *90*, 7920-7933. doi:10.1128/JVI.00832-16.
- Ding, D.; Lou, X.; Hua, D.; Yu, W.; Li, L.; Wang, J.; Gao, F.; Zhao, N.; Ren, G.; Li, L.; Lin, B. Recurrent targeted genes of hepatitis B virus in the liver cancer genomes identified by a next-generation sequencing-based approach. *PLoS Genet.* **2012**, *8*, e1003065. doi:10.1371/journal.pgen.1003065.
- Drayman, N.; Patel, P.; Vistain, L.; Tay, S. HSV-1 single-cell analysis reveals the activation of anti-viral and developmental programs in distinct sub-populations. *Elife* **2019**, *8*. doi:10.7554/eLife.46339.
- Duan, M.; Hao, J.; Cui, S.; Worthley, D.L.; Zhang, S.; Wang, Z.; Shi, J.; Liu, L.; Wang, X.; Ke, A.; Cao, Y.; Xi, R.; Zhang, X.; Zhou, J.; Fan, J.; Li, C.; Gao, Q. Diverse modes of clonal evolution in HBV-related hepatocellular carcinoma revealed by single-cell genome sequencing. *Cell Res.* **2018**, *28*, 359-373. doi:10.1038/cr.2018.11.
- Dunn, C.; Peppas, D.; Khanna, P.; Nebbia, G.; Jones, M.; Brendish, N.; Lascar, R.M.; Brown, D.; Gilson, R.J.; Tedder, R.J.; Dusheiko, G.M.; Jacobs, M.; Klenerman, P.; Maini, M.K. Temporal analysis of early immune responses in patients with acute hepatitis B virus infection. *Gastroenterology* **2009**, *137*, 1289-1300. doi:10.1053/j.gastro.2009.06.054.

- Dusheiko, G. Treatment of HBeAg positive chronic hepatitis B: interferon or nucleoside analogues. *Liver Int.* **2013**, *33 Suppl 1*, 137-150. doi:10.1111/liv.12078.
- Eble, B.E.; Lingappa, V.R.; Ganem, D. The N-terminal (pre-S2) domain of a hepatitis B virus surface glycoprotein is translocated across membranes by downstream signal sequences. *J. Virol.* **1990**, *64*, 1414-1419.
- Eble, B.E.; MacRae, D.R.; Lingappa, V.R.; Ganem, D. Multiple topogenic sequences determine the transmembrane orientation of the hepatitis B surface antigen. *Mol. Cell Biol.* **1987**, *7*, 3591-3601. doi:10.1128/mcb.7.10.3591.
- Eckhardt, S. G., Milich, D. R.; McLachlan, A. Hepatitis B virus core antigen has two nuclear localization sequences in the arginine-rich carboxyl terminus. *J. Virol.* **1991**, *65*, 575–582.
- Fabregat, I. Dysregulation of apoptosis in hepatocellular carcinoma cells. *World J. Gastroenterol.* **2009**, *15*, 513-520. doi:10.3748/wjg.15.513.
- Fan, H.C.; Fu, G.K.; Fodor, S.P. Expression profiling. Combinatorial labeling of single cells for gene expression cytometry. *Science* **2015**, *347*, 1258367. doi:10.1126/science.1258367.
- Fanning, G.C.; Zoulim, F.; Hou, J.; Bertoletti, A. Therapeutic strategies for hepatitis B virus infection: towards a cure. *Nat. Rev. Drug Discov.* **2019**, *18*, 827-844. doi:10.1038/s41573-019-0037-0.
- Faure-Dupuy, S.; Lucifora, J.; Durantel, D. Interplay between the Hepatitis B Virus and Innate Immunity: From an Understanding to the Development of Therapeutic Concepts. *Viruses* **2017**, *9*, 95. DOI: 10.3390/v9050095
- Ferlay, J.; Shin, H.R.; Bray, F.; Forman, D.; Mathers, C.; Parkin, D.M. Estimates of worldwide burden of cancer in 2008: GLOBOCAN 2008. *Int. J. Cancer* **2010**, *127*, 2893-2917. doi:10.1002/ijc.25516.
- Ferreira, A.R.; Ramos, B.; Nunes, A.; Ribeiro, D. Hepatitis C virus: Evading the intracellular innate immunity. *J. Clin. Med.* **2020**, *9*, 790. doi:10.3390/jcm9030790
- Fisicaro, P.; Barili, V.; Montanini, B.; Acerbi, G.; Ferracin, M.; Guerrieri, F.; Salerno, D.; Boni, C.; Massari, M.; Cavallo, M.C.; Grossi, G.; Giuberti, T.; Lampertico, P.; Missale, G.; Levrero, M.; Ottonello, S. Ferrari, C. Targeting mitochondrial dysfunction can restore antiviral activity of exhausted HBV-specific CD8 T cells in chronic hepatitis B. *Nat. Med.* **2017**, *23*, 327-336. doi:10.1038/nm.4275.

- Franco, A.; Guidotti, L.G.; Hobbs, M.V.; Pasquetto, V.; Chisari, F.V. Pathogenetic effector function of CD4-positive T helper 1 cells in hepatitis B virus transgenic mice. *J. Immunol.* **1997**, *159*, 2001-2008.
- Fu, Y.S.; Chen, H.; Liu, L.; Huang, Y.Y. Single cell total RNA sequencing through isothermal amplification in picoliter-droplet emulsion. *Anal. Chem.* **2016**, *88*, 10795–10799. DOI: 10.1021/acs.analchem.6b02581
- Gage, B.K.; Liu, J.C.; Innes, B.T.; MacParland, S.A.; McGilvray, I.D.; Bader, G.D.; Keller, G.M. Generation of functional liver sinusoidal endothelial cells from human pluripotent stem-cell-derived venous angioblasts. *Cell Stem Cell* **2020**, *27*, 254-269. doi:10.1016/j.stem.2020.06.007
- Galvao, J.; Davis, B.; Tilley, M.; Normando, E.; Duchon, M.R.; Cordeiro, M.F. Unexpected low-dose toxicity of the universal solvent DMSO. *FASEB J.* **2014**, *28*, 1317–1330. doi:10.1096/fj.13-235440.
- Ganem, D. Assembly of hepadnaviral virions and subviral particles. *Curr. Top. Microbiol. Immunol.* **1991**, *168*, 61-83. doi:10.1007/978-3-642-76015-0_4.
- Gao, W.; Hu, J. Formation of hepatitis B virus covalently closed circular DNA: removal of genome-linked protein. *J. Virol.* **2007**, *81*, 6164-6174. doi:10.1128/JVI.02721-06.
- Garcia, T.; Li, J.; Sureau, C.; Ito, K.; Qin, Y.; Wands, J.; Tong, S. Drastic reduction in the production of subviral particles does not impair hepatitis B virus virion secretion. *J. Virol.* **2009**, *83*, 11152-11165. doi:10.1128/JVI.00905-09.
- Gavilanes, F.; Gonzalez-Ros, J.M.; Peterson, D.L. Structure of hepatitis B surface antigen. Characterization of the lipid components and their association with the viral proteins. *J. Biol. Chem.* **1982**, *257*, 7770-7777.
- GBD 2017 Causes of Death Collaborators (Roth, G.A. *et al.*). Global, regional, and national age-sex-specific mortality for 282 causes of death in 195 countries and territories, 1980-2017: A systematic analysis for the Global Burden of Disease Study 2017. *Lancet* **2018**, *392*, 1736-1788. doi:10.1016/S0140-6736(18)32203-7.
- GBD 2017 Disease Injury and Prevalence Collaborators (James, S.L. *et al.*). Global, regional, and national incidence, prevalence, and years lived with disability for 354 diseases and injuries for 195 countries and territories, 1990-2017: a systematic analysis for the Global

- Burden of Disease Study 2017. *Lancet* **2018**, *392*, 1789-1858. doi:10.1016/S0140-6736(18)32279-7.
- Geng, M.; Xin, X.; Bi, L.Q.; Zhou, L.T.; Liu, X.H. Molecular mechanism of hepatitis B virus X protein function in hepatocarcinogenesis. *World J. Gastroenterol.* **2015**, *21*, 10732-10738. doi:10.3748/wjg.v21.i38.10732.
- Gerelsaikhan, T.; Tavis, J.E.; Bruss, V. Hepatitis B virus nucleocapsid envelopment does not occur without genomic DNA synthesis. *J. Virol.* **1996**, *70*, 4269-4274.
- Gerets, H.H.; Tilmant, K.; Gerin, B.; Chanteux, H.; Depelchin, B.O.; Dhalluin, S.; Atienzar, F.A. Characterization of primary human hepatocytes, HepG2 cells, and HepaRG cells at the mRNA level and CYP activity in response to inducers and their predictivity for the detection of human hepatotoxins. *Cell Biol. Toxicol.* **2012**, *28*, 69-87. doi:10.1007/s10565-011-9208-4.
- Gerlich, W.H.; Robinson, W.S. Hepatitis B virus contains protein attached to the 5' terminus of its complete DNA strand. *Cell* **1980**, *21*, 801-809. doi:10.1016/0092-8674(80)90443-2.
- Giersch, K.; Allweiss, L.; Volz, T.; Helbig, M.; Bierwolf, J.; Lohse, A.W.; Pollok, J.M.; Petersen, J.; Dandri, M.; Lutgehetmann, M. Hepatitis Delta co-infection in humanized mice leads to pronounced induction of innate immune responses in comparison to HBV mono-infection. *J. Hepatol.* **2015**, *63*, 346-353. doi: 10.1016/j.jhep.2015.03.011
- Giladi, A.; Amit, I. Single-cell genomics: a stepping stone for future immunology discoveries. *Cell* **2018**, *172*, 14–21. doi: 10.1016/j.cell.2017.11.011
- Golsaz-Shirazi, F.; Shokri, F. Cross talk between hepatitis B virus and innate immunity of hepatocytes. *Rev. Med. Virol.* **2022**, *32(1)*, e2256. DOI: 10.1002/rmv.2256
- Gripon, P.; Cannie, I.; Urban, S. Efficient inhibition of hepatitis B virus infection by acylated peptides derived from the large viral surface protein. *J. Virol.* **2005**, *79*, 1613-1622. doi:10.1128/JVI.79.3.1613-1622.2005.
- Gripon, P.; Diot, C.; Corlu, A.; Guguen-Guillouzo, C. Regulation by dimethylsulfoxide, insulin, and corticosteroids of hepatitis B virus replication in a transfected human hepatoma cell line. *J. Med. Virol.* **1989**, *28*, 193-199. doi:10.1002/jmv.1890280316.
- Gripon, P.; Diot, C.; Guguen-Guillouzo, C. Reproducible high level infection of cultured adult human hepatocytes by hepatitis B virus: effect of polyethylene glycol on adsorption and penetration. *Virology* **1993**, *192*, 534–540. doi:10.1006/viro.1993.1069.

- Gripon, P.; Diot, C.; Thézé, N.; Fourel, I.; Loreal, O.; Brechot, C.; Guguen-Guillouzo, C. Hepatitis B virus infection of adult human hepatocytes cultured in the presence of dimethyl sulfoxide. *J. Virol.* **1988**, *62*, 4136–4143. doi:10.1128/jvi.62.11.4136-4143.1988.
- Gripon, P.; Le Seyec, J.; Rumin, S. Guguen-Guillouzo, C. Myristylation of the hepatitis B virus large surface protein is essential for viral infectivity. *Virology* **1995**, *213*, 292-299. doi:10.1006/viro.1995.0002.
- Gripon, P.; Rumin, S.; Urban, S.; Le Seyec, J.; Glaise, D.; Cannie, I.; Guyomard, C.; Lucas, J.; Trepo, C.; Guguen-Guillouzo, C. Infection of a human hepatoma cell line by hepatitis B virus. *Proc. Natl. Acad. Sci. U. S. A.* **2002**, *99*, 15655-15660. doi:10.1073/pnas.232137699.
- Gu, W.; Crawford, E. D.; O'Donovan, B. D.; Wilson, M. R.; Chow, E. D.; Retallack, H.; DeRisi, J. L., Depletion of Abundant Sequences by Hybridization (DASH): using Cas9 to remove unwanted high-abundance species in sequencing libraries and molecular counting applications. *Genome Biol.* **2016**, *17*, 41. DOI: 10.1186/s13059-016-0904-5
- Guidotti, L.G.; Ishikawa, T.; Hobbs, M.V.; Matzke, B.; Schreiber, R., Chisari, F.V. Intracellular inactivation of the hepatitis B virus by cytotoxic T lymphocytes. *Immunity* **1996**, *4*, 25-36. doi:10.1016/s1074-7613(00)80295-2.
- Guidotti, L.G.; Rochford, R.; Chung, J.; Shapiro, M.; Purcell, R., Chisari, F.V. Viral clearance without destruction of infected cells during acute HBV infection. *Science* **1999**, *284*, 825-829. doi:10.1126/science.284.5415.825.
- Guo, H.; Jiang, D.; Zhou, T.; Cuconati, A.; Block, T.M.; Guo, J.T. Characterization of the intracellular deproteinized relaxed circular DNA of hepatitis B virus: an intermediate of covalently closed circular DNA formation. *J. Virol.* **2007**, *81*, 12472-12484. doi:10.1128/JVI.01123-07.
- Guo, H.; Xu, C.; Zhou, T.; Block, T.M.; Guo, J.T. Characterization of the host factors required for hepadnavirus covalently closed circular (ccc) DNA formation. *PLoS One* **2012**, *7*, e43270. doi:10.1371/journal.pone.0043270.
- Guo, L.; Dial, S.; Shi, L.; Branham, W.; Liu, J.; Fang, J. L.; Green, B.; Deng, H.; Kaput, J.; Ning, B. Similarities and differences in the expression of drug-metabolizing enzymes between human hepatic cell lines and primary human hepatocytes. *Drug Metab. Dispos.* **2011**, *39*, 528–538. doi:10.1124/dmd.110.035873.

- Hahn, C.M.; Iwanowicz, L.R.; Cornman, R.S.; Conway, C.M.; Winton, J.R.; Blazer, V.S. Characterization of a novel hepadnavirus in the White Sucker (*Catostomus commersonii*) from the Great Lakes region of the United States. *J. Virol.* **2015**, *89*, 11801-11811. doi:10.1128/JVI.01278-15.
- Hai, H.; Tamori, A.; Kawada, N. Role of hepatitis B virus DNA integration in human hepatocarcinogenesis. *World J Gastroenterol*, **2014**, *20*, 6236-43. doi:10.3748/wjg.v20.i20.6236.
- Haines, K.M.; Loeb, D.D. The sequence of the RNA primer and the DNA template influence the initiation of plus-strand DNA synthesis in hepatitis B virus. *J. Mol. Biol.* **2007**, *370*, 471-480. doi:10.1016/j.jmb.2007.04.057.
- Hantz, O.; Parent, R.; Durantel, D.; Gripon, P.; Guguen-Guillouzo, C.; Zoulim, F. Persistence of the hepatitis B virus covalently closed circular DNA in HepaRG human hepatocyte-like cells. *J. Gen. Virol.* **2009**, *90*, 127–135. doi:10.1099/vir.0.004861-0.
- Harrison, S.P.; Baumgarten, S.F.; Verma, R.; Lunov, O.; Dejneka, A.; Sullivan, G.J. Liver organoids: Recent developments, limitations and potential. *Front. Med.* **2021**, *8*, 574047. doi:10.3389/fmed.2021.574047.
- Hart, S.N.; Li, Y.; Nakamoto, K.; Subileau, E.-A.; Steen, D.; Zhong, X.-B. A comparison of whole genome gene expression profiles of HepaRG cells and HepG2 cells to primary human hepatocytes and human liver tissues. *Drug Metab. Dispos.* **2010**, *38*, 988–994. doi:10.1124/dmd.109.031831.
- Hashimshony, T.; Senderovich, N.; Avital, G.; Klochendler, A.; de Leeuw, Y.; Anavy, L.; Gennert, D.; Li, S.; Livak, K.J.; Rozenblatt-Rosen, O.; Dor, Y.; Regev, A.; Yanai, I. CEL-Seq2: sensitive highly-multiplexed single-cell RNA-Seq. *Genome Biol.* **2016**, *17*, 77. doi:10.1186/s13059-016-0938-8.
- Hashimshony, T.; Wagner, F.; Sher, N.; Yanai, I. CEL-Seq: single-cell RNA-Seq by multiplexed linear amplification. *Cell Rep.* **2012**, *2*, 666-673. doi:10.1016/j.celrep.2012.08.003.
- Hatton, T.; Zhou, S.; Standring, D.N. RNA- and DNA-binding activities in hepatitis B virus capsid protein: a model for their roles in viral replication. *J. Virol.* **1992**, *66*, 5232-5241.
- Heim, M.H.; Thimme, R. Innate and adaptive immune responses in HCV infections. *J. Hepatol.* **2014**, *61*, S14-S25.

- Hewitt, N.J.; Lechón, M.J.G.; Houston, J.B.; Hallifax, D.; Brown, H.S.; Maurel, P.; Kenna, J.G.; Gustavsson, L.; Lohmann, C.; Skonberg, C.; et al. Primary hepatocytes: Current understanding of the regulation of metabolic enzymes and transporter proteins, and pharmaceutical practice for the use of hepatocytes in metabolism, enzyme induction, transporter, clearance, and hepatotoxicity studies. *Drug Metab. Rev.* **2007**, *39*, 159–234. doi:10.1080/03602530601093489.
- Hiet, M.S.; Bauhofer, O.; Zayas, M. *et al.* Control of temporal activation of hepatitis C virus-induced interferon response by domain 2 of nonstructural protein 5A. *J. Hepatol.* **2015**, *63*, 829-837.
- Hirsch, R.C.; Lavine, J.E.; Chang, L.J.; Varmus, H.E.; Ganem, D. Polymerase gene products of hepatitis B viruses are required for genomic RNA packaging as well as for reverse transcription. *Nature* **1990**, *344*, 552-555. doi:10.1038/344552a0.
- Hirschman, S.Z.; Gerber, M.; Garfinkel, E. Purification of naked intranuclear particles from human liver infected by hepatitis B virus. *Proc. Natl. Acad. Sci. U. S. A.* **1974**, *71*, 3345-3349. doi:10.1073/pnas.71.9.3345.
- Ho, D.W.-H.; Tsui, Y.M.; Chan, L.K.; Sze, K.M.; Zhang, X.; Cheu, J.W.; Chiu, Y.T.; Lee, J.M.; Chan, A.C.; Cheung, E.T.; Yau, D.T.; Chia, N.H.; Lo, I.L.; Sham, P.C.; Cheung, T.T.; Wong, C.C.; Ng, I.O. Single-cell RNA sequencing shows the immunosuppressive landscape and tumor heterogeneity of HBV-associated hepatocellular carcinoma. *Nat. Commun.* **2021**, *12*, 3684. doi:10.1038/s41467-021-24010-1.
- Horner, S.M.; Gale Jr, M. Regulation of hepatic innate immunity by hepatitis C virus. *Nat. Med.* **2013**, *19*(7), 879-888. doi:10.1038/nm.3253
- Hsu, Y.S.; Chien, R.N.; Yeh, C.T.; Sheen, I.S.; Chiou, H.Y.; Chu, C.M.; Liaw, Y.F. Long-term outcome after spontaneous HBeAg seroconversion in patients with chronic hepatitis B. *Hepatology* **2002**, *35*, 1522-1527. doi:10.1053/jhep.2002.33638.
- Hu, J.; Boyer, M. Hepatitis B virus reverse transcriptase and epsilon RNA sequences required for specific interaction in vitro. *J. Virol.* **2006**, *80*, 2141-2150. doi:10.1128/JVI.80.5.2141-2150.2006.
- Hu, J.; Flores, D.; Toft, D.; Wang, X.; Nguyen, D. Requirement of heat shock protein 90 for human hepatitis B virus reverse transcriptase function. *J. Virol.* **2004**, *78*, 13122-31. doi:10.1128/JVI.78.23.13122-13131.2004.

- Hu, J.; Lin, Y.; Chen, P.; Watashi, K.; Wakita, T. Cell and animal models for studying hepatitis B virus infection and drug development. *Gastroenterology* **2019**, *156*, 338–354. doi:10.1053/j.gastro.2018.06.093.
- Huch, M.; Gehart, H.; Van Boxtel, R.; Hamer, K.; Blokzijl, F.; Verstegen, M.M.A.; Ellis, E.; van Wenum, M.; Fuchs, S.A.; Clevers, H. et al. Long-term culture of genome-stable bipotent stem cells from adult human liver. *Cell* **2015**, *160*, 299-312. doi:10.1016/j.cell.2014.11.050
- Ichai, P.; Samuel, D. Management of Fulminant Hepatitis B. *Curr. Infect. Dis. Rep.* **2019**, *21*, 25. doi:10.1007/s11908-019-0682-9.
- Iloeje, U.H.; Yang, H.I.; Su, J.; Jen, C.L.; You, S.L.; Chen, C.J.; Risk Evaluation of Viral Load, E., Associated Liver Disease/Cancer-In, H.B.V.S.G. Predicting cirrhosis risk based on the level of circulating hepatitis B viral load. *Gastroenterology* **2006**, *130*, 678-686. doi:10.1053/j.gastro.2005.11.016.
- Ishida, Y.; Yamasaki, C.; Yanagi, A.; Yoshizane, Y.; Fujikawa, K.; Watashi, K.; Abe, H.; Wakita, T.; Hayes, C.N.; Chayama, K.; et al. Novel robust in vitro hepatitis B virus infection model using fresh human hepatocytes isolated from humanized mice. *Am. J. Pathol.* **2015**, *185*, 1275–1285. doi:10.1016/j.ajpath.2015.01.028.
- Islam, S.; Kjallquist, U.; Moliner, A.; Zajac, P.; Fan, J.B.; Lonnerberg, P.; Linnarsson, S. Characterization of the single-cell transcriptional landscape by highly multiplex RNA-seq. *Genome Res.* **2011**, *21*, 1160-1167. doi:10.1101/gr.110882.110.
- Islam, S.; Zeisel, A.; Joost, S.; La Manno, G.; Zajac, P.; Kasper, M.; Lonnerberg, P.; Linnarsson, S. Quantitative single-cell RNA-seq with unique molecular identifiers. *Nat. Methods* **2014**, *11*, 163-166. doi:10.1038/nmeth.2772.
- Isogawa, M.; Robek, M.D.; Furuichi, Y.; Chisari, F.V. Toll-like receptor signaling inhibits hepatitis B virus replication in vivo. *J. Virol.* **2005**, *79*, 7269-7272. doi:10.1128/JVI.79.11.7269-7272.2005.
- Iwamoto, M.; Saso, W.; Nishioka, K.; Ohashi, H.; Sugiyama, R.; Ryo, A.; Ohki, M.; Yun, J.H.; Park, S.Y.; Ohshima, T.; Suzuki, R.; Aizaki, H.; Muramatsu, M.; Matano, T.; Iwami, S.; Sureau, C.; Wakita, T.; Watashi, K. The machinery for endocytosis of epidermal growth factor receptor coordinates the transport of incoming hepatitis B virus to the endosomal network. *J. Biol. Chem.* **2020**, *295*, 800-807. doi:10.1074/jbc.AC119.010366.

- Iwamoto, M.; Saso, W.; Sugiyama, R.; Ishii, K.; Ohki, M.; Nagamori, S.; Suzuki, R.; Aizaki, H.; Ryo, A.; Yun, J.H.; Park, S.Y.; Ohtani, N.; Muramatsu, M.; Iwami, S.; Tanaka, Y.; Sureau, C.; Wakita, T.; Watashi, K. Epidermal growth factor receptor is a host-entry cofactor triggering hepatitis B virus internalization. *Proc. Natl. Acad. Sci. U. S. A.* **2019**, *116*, 8487-8492. doi:10.1073/pnas.1811064116.
- Iwamoto, M.; Watashi, K.; Tsukuda, S.; Aly, H.H.; Fukasawa, M.; Fujimoto, A.; Suzuki, R.; Aizaki, H.; Ito, T.; Koiwai, O.; et al. Evaluation and identification of hepatitis B virus entry inhibitors using HepG2 cells overexpressing a membrane transporter NTCP. *Biochem. Biophys. Res. Commun.* **2014**, *443*, 808–813. doi:10.1016/j.bbrc.2013.12.052.
- Jiang, T.; Liu, M.; Wu, J.; Shi, Y. Structural and biochemical analysis of Bcl-2 interaction with the hepatitis B virus protein HBx. *Proc. Natl. Acad. Sci. U. S. A.* **2016**, *113*, 2074-2079. doi:10.1073/pnas.1525616113.
- Jiao, X-Y.; Steenbergen, R.H.G.; Tyrrell, D.L. The use of human umbilical cord blood serum is beneficial for the continuous production of hepatitis C virus. *J. Gen. Virol.* **2016**, *97*, 3248-3252. doi:10.1099/jgv.0.000636
- Jinek, M.; Chylinski, K.; Fonfara, I.; Hauer, M.; Doudna, J. A.; Charpentier, E., A programmable dual-RNA-guided DNA endonuclease in adaptive bacterial immunity. *Science* **2012**, *337* (6096), 816–821. DOI: 10.1126/science.1225829
- Jones, S.A.; Clark, D.N.; Cao, F.; Tavis, J.E.; Hu, J. Comparative analysis of hepatitis B virus polymerase sequences required for viral RNA binding, RNA packaging, and protein priming. *J. Virol.* **2014**, *88*, 1564-1572. doi:10.1128/JVI.02852-13.
- Juhling, F.; Saviano, A.; Ponsolles, C.; Heydmann, L.; Crouchet, E.; Durand, S.C.; El Saghire, H.; Felli, E.; Lindner, V.; Pessaux, P.; Pochet, N.; Schuster, C.; Verrier, E.R.; Baumert, T.F. Hepatitis B virus compartmentalization and single-cell differentiation in hepatocellular carcinoma. *Life Sci. Alliance* **2021**, *4*, e202101036. doi:10.26508/lsa.202101036.
- Junker-Niepmann, M.; Bartenschlager, R.; Schaller, H. A short cis-acting sequence is required for hepatitis B virus pregenome encapsidation and sufficient for packaging of foreign RNA. *EMBO J.* **1990**, *9*, 3389-96.
- Kakimi, K.; Guidotti, L.G.; Koezuka, Y.; Chisari, F.V. Natural killer T cell activation inhibits hepatitis B virus replication *in vivo*. *J. Exp. Med.* **2000**, *192*, 921-930. doi:10.1084/jem.192.7.921.

- Karayiannis, P. Hepatitis B virus: virology, molecular biology, life cycle and intrahepatic spread. *Hepatol. Int.* **2017**, *11*, 500-508. doi:10.1007/s12072-017-9829-7.
- Keren-Shaul, H.; Kenigsberg, E.; Jaitin, D.A.; David, E.; Paul, F.; Tanay, A.; Amit, I. MARS-seq2.0: an experimental and analytical pipeline for indexed sorting combined with single-cell RNA sequencing. *Nat. Protoc.* **2019**, *14*, 1841-1862. doi:10.1038/s41596-019-0164-4.
- Khan, M.; Syed, G.H.; Kim, S.J.; Siddiqui, A. Hepatitis B Virus-Induced Parkin-Dependent recruitment of Linear Ubiquitin Assembly Complex (LUBAC) to mitochondria and attenuation of innate immunity. *PLoS Pathog.* **2016**, *12*, e1005693. doi:10.1371/journal.ppat.1005693.
- Kidambi, S.; Yarmush, R.S.; Novik, E.; Chao, P.; Yarmush, M.L.; Nahmias, Y. Oxygen-mediated enhancement of primary hepatocyte metabolism, functional polarization, gene expression, and drug clearance. *Proc. Natl. Acad. Sci. U.S.A.* **2009**, *106*, 15714–15719. doi:10.1073/pnas.0906820106.
- Kitamura, K.; Que, L.; Shimadu, M.; Koura, M.; Ishihara, Y.; Wakae, K.; Nakamura, T.; Watashi, K.; Wakita, T.; Muramatsu, M. Flap endonuclease 1 is involved in cccDNA formation in the hepatitis B virus. *PLoS Pathog.* **2018**, *14*, e1007124. doi:10.1371/journal.ppat.1007124.
- Klein, A.M.; Mazutis, L.; Akartuna, I.; Tallapragada, N.; Veres, A.; Li, V.; Peshkin, L.; Weitz, D.A.; Kirschner, M.W. Droplet barcoding for single-cell transcriptomics applied to embryonic stem cells. *Cell* **2015**, *161*, 1187-1201. doi:10.1016/j.cell.2015.04.044.
- Knaus, T.; Nassal, M. The encapsidation signal on the hepatitis B virus RNA pregenome forms a stem-loop structure that is critical for its function. *Nucleic Acids Res.* **1993**, *21*, 3967-3975. doi:10.1093/nar/21.17.3967.
- Knockenauer, K. E.; Schwartz, T. U. The Nuclear Pore Complex as a Flexible and Dynamic Gate. *Cell* **2016**, *164*, 1162–1171.
- Knott, G. J.; Doudna, J. A. CRISPR-Cas guides the future of genetic engineering. *Science* **2018**, *361* (6405), 866–869. DOI: 10.1126/science.aat5011
- Ko, S.; Russell, J.O.; Molina, L.M.; Monga, S.P. Liver progenitors and adult cell plasticity in hepatic injury and repair: Knowns and unknowns. *Annu. Rev. Pathol. Mech. Dis.* **2020**, *15*, 23-50. doi:10.1146/annurev-pathmechdis-012419-032824

- Ko, C.; Chakraborty, A.; Chou, W.M.; Hasreiter, J.; Wettengel, J.M.; Stadler, D.; Bester, R.; Asen, T.; Zhang, K.; Wisskirchen, K.; McKeating, J.A.; Ryu, W.S.; Protzer, U. Hepatitis B virus genome recycling and de novo secondary infection events maintain stable cccDNA levels. *J. Hepatol.* **2018**, *69*, 1231-1241. doi:10.1016/j.jhep.2018.08.012.
- Kock, J.; Nassal, M.; MacNelly, S.; Baumert, T.F.; Blum, H.E.; von Weizsacker, F. Efficient infection of primary tupaia hepatocytes with purified human and woolly monkey hepatitis B virus. *J. Virol.* **2001**, *75*, 5084-5089. doi:10.1128/JVI.75.11.5084-5089.2001.
- Kock, J.; Schlicht, H.J. Analysis of the earliest steps of hepadnavirus replication: genome repair after infectious entry into hepatocytes does not depend on viral polymerase activity. *J. Virol.* **1993**, *67*, 4867-4874. doi:10.1128/JVI.67.8.4867-4874.1993.
- Konig, A.; Yang, J.; Jo, E.; Park, K.H.P.; Kim, H.; Than, T.T.; Song, X.; Qi, X.; Dai, X.; Park, S.; Shum, D.; Ryu, W.S.; Kim, J.H.; Yoon, S.K.; Park, J.Y.; Ahn, S.H.; Han, K.H.; Gerlich, W.H.; Windisch, M.P. Efficient long-term amplification of hepatitis B virus isolates after infection of slow proliferating HepG2-NTCP cells. *J. Hepatol.* **2019**, *71*, 289-300. doi:10.1016/j.jhep.2019.04.010.
- Koniger, C.; Wingert, I.; Marsmann, M.; Rosler, C.; Beck, J.; Nassal, M. Involvement of the host DNA-repair enzyme TDP2 in formation of the covalently closed circular DNA persistence reservoir of hepatitis B viruses. *Proc. Natl. Acad. Sci. U. S. A.* **2014**, *111*, E4244-53. doi:10.1073/pnas.1409986111.
- Kumar, M.; Jung, S.Y.; Hodgson, A.J.; Madden, C.R.; Qin, J.; Slagle, B.L. Hepatitis B virus regulatory HBx protein binds to adaptor protein IPS-1 and inhibits the activation of beta interferon. *J. Virol.* **2011**, *85*, 987-995. doi:10.1128/JVI.01825-10.
- La Manno, G.; Soldatov, R.; Zeisel, A.; Braun, E.; Hochgerner, H.; Petukhov, V.; Lidschreiber, K.; Kastrioti, M.E.; Lonnerberg, P.; Furlan, A.; Fan, J.; Borm, L.E.; Liu, Z.; van Bruggen, D.; Guo, J.; He, X.; Barker, R.; Sundstrom, E.; Castelo-Branco, G.; Cramer, P.; Adameyko, I.; Linnarsson, S.; Kharchenko, P.V. RNA velocity of single cells. *Nature* **2018**, *560*, 494-498. doi:10.1038/s41586-018-0414-6.
- Ladner, S.K.; Otto, M.J.; Barker, C.S.; Zaifert, K.; Wang, G.H.; Guo, J.T.; Seeger, C.; King, R.W. Inducible expression of human hepatitis B virus (HBV) in stably transfected hepatoblastoma cells: A novel system for screening potential inhibitors of HBV replication. *Antimicrob. Agents Chemother.* **1997**, *41*, 1715-1720. doi:10.1128/aac.41.8.1715.

- Ladner, S.K.; Otto, M.J.; Barker, C.S.; Zaifert, K.; Wang, G.H.; Guo, J.T.; Seeger, C.; King, R.W. Inducible expression of human hepatitis B virus (HBV) in stably transfected hepatoblastoma cells: A novel system for screening potential inhibitors of HBV replication. *Antimicrob. Agents Chemother.* **1997**, *41*, 1715–1720, doi:10.1128/aac.41.8.1715
- Lam, D.T.U.H.; Dan, Y.Y.; Chan, Y-S.; Ng, H-H. Emerging liver organoid platforms and technologies. *Cell Regeneration* **2021**, *10*, 27. doi:10.1186/s13619-021-00089-1
- Lambert, C.; Doring, T. Prange, R. Hepatitis B virus maturation is sensitive to functional inhibition of ESCRT-III, Vps4, and gamma 2-adaptin. *J. Virol.* **2007**, *81*, 9050-9060. doi:10.1128/JVI.00479-07.
- Le, C.; Liu, Y.; Lopez-Orozco, J.; Joyce, M.A.; Le, X.C.; Tyrrell, D.L. CRISPR technique incorporated with single-cell RNA sequencing for studying hepatitis B infection. *Anal. Chem.* **2021**, *93*, 10756-10761. doi:10.1021/acs.analchem.1c02227.
- Le, C.; Sirajee, R.; Steenbergen, R.; Joyce, M.A.; Addison, W.R.; Tyrrell, D.L. *In vitro* infection with hepatitis B virus using differentiated human serum culture of Huh7.5-NTCP cells without requiring dimethyl sulfoxide. *Viruses* **2021**, *13*, 97. doi:10.3390/v13010097
- Lebosse, F.; Testoni, B.; Fresquet, J. *et al.* Intrahepatic innate immune response pathways are downregulated in untreated chronic hepatitis B. *J. Hepatol.* **2017**, *66*, 897-909.
- Lee, J.; Zong, L.; Krotow, A.; Qin, Y.; Jia, L.; Zhang, J.; Tong, S.; Li, J. N-Linked glycosylation is not essential for sodium taurocholate cotransporting polypeptide to mediate hepatitis B virus infection in vitro. *J. Virol.* **2018**, *92*, e00732–18. doi:10.1128/jvi.00732-18.
- Lee, S. H.; Yu, J.; Hwang, G. H.; Kim, S.; Kim, H. S.; Ye, S.; Kim, K.; Park, J.; Park, D. Y.; Cho, Y. K.; Kim, J. S.; Bae, S., CUT-PCR: CRISPR-mediated, ultrasensitive detection of target DNA using PCR. *Oncogene* **2017**, *36*, 6823-6829. DOI: 10.1038/onc.2017.281
- Lempp, F.A.; Qu, B.; Wang, Y.X.; Urban, S. Hepatitis B virus infection of a mouse hepatic cell line reconstituted with human sodium taurocholate cotransporting polypeptide. *J. Virol.* **2016**, *90*, 4827–4831. doi:10.1128/jvi.02832-15.
- Lentz, T.B.; Loeb, D.D. Roles of the envelope proteins in the amplification of covalently closed circular DNA and completion of synthesis of the plus-strand DNA in hepatitis B virus. *J. Virol.* **2011**, *85*, 11916-11927. doi:10.1128/JVI.05373-11.
- Levin, A.; Neufeldt, C. J.; Pang, D.; Wilson, K.; Loewen-Dobler, D.; Joyce, M. A.; Wozniak, R. W.; Tyrrell, D. L. J. Functional Characterization of Nuclear Localization and Export Signals

- in Hepatitis C Virus Proteins and Their Role in the Membranous Web. *PLoS ONE* **2014**, *9(12)*: e114629. doi:10.1371/journal.pone.0114629
- Lewellyn, E.B.; Loeb, D.D. Base pairing between cis-acting sequences contributes to template switching during plus-strand DNA synthesis in human hepatitis B virus. *J. Virol.* **2007**, *81*, 6207-6215. doi:10.1128/JVI.00210-07.
- Li, J.; Zong, L.; Sureau, C.; Barker, L.; Wands, J.R.; Tong, S. Unusual features of sodium taurocholate cotransporting polypeptide as a hepatitis B virus receptor. *J. Virol.* **2016**, *90*, 8302–8313. doi:10.1128/jvi.01153-16.
- Li, W. The hepatitis B virus receptor. *Annu. Rev. Cell Dev. Biol.* **2015**, *31*, 125–147. doi:10.1146/annurev-cellbio-100814-125241.
- Li, Y.; Zhu, Y.; Feng, S.; Ishida, Y.; Chiu, T-P.; Saito, T. Wang, S.; Ann, D.K.; Ou, J-h. J. Macrophages activated by hepatitis B virus have distinct metabolic profiles and suppress the virus via IL-1 β to downregulate PPAR α and FOXO3. *Cell Rep.* **2022**, *36*, 110284. doi:10.1016/j.celrep.2021.110284.
- Liao, M.; Liu, Y.; Yuan, J.; Wen, Y.; Xu, G.; Zhao, J.; Cheng, L.; Li, J.; Wang, X.; Wang, F.; Liu, L.; Amit, I.; Zhang, S.; Zhang, Z. Single-cell landscape of bronchoalveolar immune cells in patients with COVID-19. *Nat. Med.* **2020**, *26*, 842–844. doi:10.1038/s41591-020-0901-9.
- Liaw, Y.F.; Chu, C.M. Hepatitis B virus infection. *Lancet* **2009**, *373*, 582-592. doi:10.1016/S0140-6736(09)60207-5.
- Lichter, E.A. Chimpanzee antibodies to Australia antigen. *Nature* **1969**, *224*, 810-811. doi:10.1038/224810a0.
- Lin, Y.; Nomura, T.; Cheong, J.; Dorjsuren, D.; Iida, K.; Murakami, S. Hepatitis B virus X protein is a transcriptional modulator that communicates with transcription factor IIB and the RNA polymerase II subunit 5. *J. Biol. Chem.* **1997**, *272*, 7132-7139. doi:10.1074/jbc.272.11.7132.
- Ling, R.; Harrison, T.J. Production of hepatitis B virus covalently closed circular DNA in transfected cells is independent of surface antigen synthesis. *J. Gen. Virol.* **1997**, *78 (Pt 6)*, 1463-1467. doi:10.1099/0022-1317-78-6-1463.
- Liu, Y.; Le, C.; Tyrrell, D.L.; Le, X.C.; Li, X.-F. Aptamer binding assay for the E antigen of hepatitis B using modified aptamers with G-quadruplex structures. *Anal. Chem.* **2020**, *92*, 6495–6501. doi:10.1021/acs.analchem.9b05740.

- Liu, Y.; Li, J.; Chen, J.; Li, Y.; Wang, W.; Du, X.; Song, W.; Zhang, W.; Lin, L.; Yuan, Z. Hepatitis B virus polymerase disrupts K63-linked ubiquitination of STING to block innate cytosolic DNA-sensing pathways. *J. Virol.* **2015**, *89*, 2287-2300. doi:10.1128/JVI.02760-14.
- Loeb, D.D.; Hirsch, R.C.; Ganem, D. Sequence-independent RNA cleavages generate the primers for plus strand DNA synthesis in hepatitis B viruses: implications for other reverse transcribing elements. *EMBO J.* **1991**, *10*, 3533-3540.
- Loffler-Mary, H.; Dumortier, J.; Klentsch-Zimmer, C.; Prange, R. Hepatitis B virus assembly is sensitive to changes in the cytosolic S loop of the envelope proteins. *Virology*, **2000**, *270*, 358-67. doi:10.1006/viro.2000.0268.
- Long, Q.; Yan, R.; Hu, J.; Cai, D.; Mitra, B.; Kim, E.S.; Marchetti, A.; Zhang, H.; Wang, S.; Liu, Y.; Huang, A.; Guo, H. The role of host DNA ligases in hepadnavirus covalently closed circular DNA formation. *PLoS Pathog.* **2017**, *13*, e1006784. doi:10.1371/journal.ppat.1006784.
- Lopez-Terrada, D.; Cheung, S.W.; Finegold, M.J.; Knowles, B.B. Hep G2 is a hepatoblastoma-derived cell line. *Hum. Pathol.* **2009**, *40*, 1512-1515. doi:10.1016/j.humpath.2009.07.003.
- Losic, B.; Craig, A.J.; Villacorta-Martin, C.; Martins-Filho, S.N.; Akers, N.; Chen, X.; Ahsen, M.E.; von Felden, J.; Labгаа, I.; D'Avola, D.; Allette, K.; Lira, S.A.; Furtado, G.C.; Garcia-Lezana, T.; Restrepo, P.; Stueck, A.; Ward, S.C.; Fiel, M.I.; Hiotis, S.P.; Gunasekaran, G.; Sia, D.; Schadt, E.E.; Sebra, R.; Schwartz, M.; Llovet, J.M.; Thung, S.; Stolovitzky, G.; Villanueva, A. Intratumoral heterogeneity and clonal evolution in liver cancer. *Nat. Commun.* **2020**, *11*, 291. doi:10.1038/s41467-019-14050-z.
- Lott, L.; Beames, B.; Notvall, L.; Lanford, R.E. Interaction between hepatitis B virus core protein and reverse transcriptase. *J. Virol.* **2000**, *74*, 11479-11489. doi:10.1128/jvi.74.24.11479-11489.2000.
- Lu, H.L. Liao, F. Melanoma differentiation-associated gene 5 senses hepatitis B virus and activates innate immune signaling to suppress virus replication. *J. Immunol.* **2013**, *191*, 3264-3276. doi:10.4049/jimmunol.1300512.
- Luangsay, S.; Gruffaz, M.; Isorce, N.; Testoni, B.; Michelet, M.; Faure-Dupuy, S.; Maadadi, S.; Ait-Goughoulte, M.; Parent, R.; Rivoire, M.; Javanbakht, H.; Lucifora, J.; Durantel, D.; Zoulim, F. Early inhibition of hepatocyte innate responses by hepatitis B virus. *J. Hepatol.* **2015**, *63*, 1314-1322. doi:10.1016/j.jhep.2015.07.014.

- Lucifora, J.; Durantel, D.; Testoni, B.; Hantz, O.; Levrero, M.; Zoulim, F. Control of hepatitis B virus replication by innate response of HepaRG cells. *Hepatology* **2010**, *51*, 63-72.
doi:10.1002/hep.23230.
- Lucifora, J.; Xia, Y.; Reisinger, F.; Zhang, K.; Stadler, D.; Cheng, X.; Sprinzl, M.F.; Koppensteiner, H.; Makowska, Z.; Volz, T.; Remouchamps, C.; Chou, W.M.; Thasler, W.E.; Huser, N.; Durantel, D.; Liang, T.J.; Munk, C.; Heim, M.H.; Browning, J.L.; Dejardin, E.; Dandri, M.; Schindler, M.; Heikenwalder, M.; Protzer, U. Specific and nonhepatotoxic degradation of nuclear hepatitis B virus cccDNA. *Science* **2014**, *343*, 1221-1228.
doi:10.1126/science.1243462.
- Lythgoe, K.A.; Lumley, S.F.; Pellis, L.; McKeating, J.A.; Matthews, P.C. Estimating hepatitis B virus cccDNA persistence in chronic infection. *Virus Evol.* **2021**, *7*, veaa063.
doi:10.1093/ve/veaa063.
- Ma, L.; Wang, L.; Khatib, S.A.; Chang, C.W.; Heinrich, S.; Dominguez, D.A.; Forgues, M.; Candia, J.; Hernandez, M.O.; Kelly, M.; Zhao, Y.; Tran, B.; Hernandez, J.M.; Davis, J.L.; Kleiner, D.E.; Wood, B.J.; Greten, T.F.; Wang, X.W. Single-cell atlas of tumor cell evolution in response to therapy in hepatocellular carcinoma and intrahepatic cholangiocarcinoma. *J. Hepatol.* **2021**, *75*, 1397-1408. doi:10.1016/j.jhep.2021.06.028.
- Macosko, E.Z.; Basu, A.; Satija, R.; Nemesh, J.; Shekhar, K.; Goldman, M.; Tirosh, I.; Bialas, A.R.; Kamitaki, N.; Martersteck, E.M.; Trombetta, J.J.; Weitz, D.A.; Sanes, J.R.; Shalek, A.K.; Regev, A.; McCarroll, S.A. Highly parallel genome-wide expression profiling of individual cells using nanoliter droplets. *Cell* **2015**, *161*, 1202-1214.
doi:10.1016/j.cell.2015.05.002.
- MacParland, S.A.; Liu, J.C.; Ma, X.Z.; Innes, B.T.; Bartczak, A.M.; Gage, B.K.; Manuel, J.; Khuu, N.; Echeverri, J.; Linares, I.; Gupta, R.; Cheng, M.L.; Liu, L.Y.; Camat, D.; Chung, S.W.; Seliga, R.K.; Shao, Z.; Lee, E.; Ogawa, S.; Ogawa, M.; Wilson, M.D.; Fish, J.E.; Selzner, M.; Ghanekar, A.; Grant, D.; Greig, P.; Sapisochin, G.; Selzner, N.; Winegarden, N.; Adeyi, O.; Keller, G.; Bader, G.D.; McGilvray, I.D. Single cell RNA sequencing of human liver reveals distinct intrahepatic macrophage populations. *Nat. Commun.* **2018**, *9*, 4383.
doi:10.1038/s41467-018-06318-7.
- Maini, M.K.; Boni, C.; Ogg, G.S.; King, A.S.; Reignat, S.; Lee, C.K.; Larrubia, J.R.; Webster, G.J.; McMichael, A.J.; Ferrari, C.; Williams, R.; Vergani, D., Bertoletti, A. Direct ex vivo

- analysis of hepatitis B virus-specific CD8(+) T cells associated with the control of infection. *Gastroenterology* **1999**, *117*, 1386-1396. doi:10.1016/s0016-5085(99)70289-1.
- Mali, P., Yang, L. H., Esvelt, K. M., Aach, J., Guell, M., DiCarlo, J. E., Norville, J. E.; Church, G. M. RNA-guided human genome engineering via Cas9. *Science* **2013**, *339* (6121), 823–826. DOI: 10.1126/science.1232033.
- Mason, W.S.; Gill, U.S.; Litwin, S.; Zhou, Y.; Peri, S.; Pop, O.; Hong, M.L.; Naik, S.; Quaglia, A.; Bertolotti, A.; Kennedy, P.T. HBV DNA Integration and Clonal Hepatocyte Expansion in Chronic Hepatitis B Patients Considered Immune Tolerant. *Gastroenterology* **2016**, *151*, 986-998 e4. doi:10.1053/j.gastro.2016.07.012.
- Massalha, H.; Bahar Halpern, K.; Abu-Gazala, S.; Jana, T.; Massasa, E.E.; Moor, A.E.; Buchauer, L.; Rozenberg, M.; Pikarsky, E.; Amit, I.; Zamir, G.; Itzkovitz, S. A single cell atlas of the human liver tumor microenvironment. *Mol. Syst. Biol.* **2020**, *16*, e9682. doi:10.15252/msb.20209682.
- McClary, H.; Koch, R.; Chisari, F.V.; Guidotti, L.G. Inhibition of hepatitis B virus replication during schistosoma mansoni infection in transgenic mice. *J. Exp. Med.* **2000**, *192*, 289-294. doi:10.1084/jem.192.2.289.
- Megahed, F.A.K.; Zhou, X.; Sun, P. The interactions between HBV and the innate immunity of hepatocytes. *Viruses* **2020**, *12*, 285. doi:10.3390/v12030285
- Meier, A.; Mehrle, S.; Weiss, T.S.; Mier, W.; Urban, S. Myristoylated PreS1-domain of the hepatitis B virus L-protein mediates specific binding to differentiated hepatocytes. *Hepatology* **2013**, *58*, 31–42. doi:10.1002/hep.26181.
- Messageot, F.; Salhi, S.; Eon, P.; Rossignol, J.M. Proteolytic processing of the hepatitis B virus e antigen precursor. Cleavage at two furin consensus sequences. *J. Biol. Chem.* **2003**, *278*, 891-895. doi:10.1074/jbc.M207634200.
- Metz, P.; Reuter, A.; Bender, S. *et al.* Interferon-stimulated genes and their role in controlling hepatitis C virus. *J. Hepatol.* **2013**, *59*, 1331-1341.
- Michailidis, E.; Pabon, J.; Xiang, K.; Park, P.; Ramanan, V.; Hoffmann, H.H.; Schneider, W.M.; Bhatia, S.N.; De Jong, Y.P.; Shlomai, A.; et al. A robust cell culture system supporting the complete life cycle of hepatitis B virus. *Sci. Rep.* **2017**, *7*, 16616. doi:10.1038/s41598-017-16882-5.

- Milich, D.; Liang, T.J. Exploring the biological basis of hepatitis B e antigen in hepatitis B virus infection. *Hepatology* **2003**, *38*, 1075-1086. doi:10.1053/jhep.2003.50453.
- Milich, D.R.; Jones, J.E.; Hughes, J.L.; Price, J.; Raney, A.K.; McLachlan, A. Is a function of the secreted hepatitis B e antigen to induce immunologic tolerance in utero? *Proc. Natl. Acad. Sci. U. S. A.* **1990**, *87*, 6599-6603. doi:10.1073/pnas.87.17.6599.
- Moolla, N.; Kew, M.; Arbuthnot, P. Regulatory elements of hepatitis B virus transcription. *J. Viral. Hepat.* **2002**, *9*, 323-331. doi:10.1046/j.1365-2893.2002.00381.x.
- Mutz, P.; Metz, P.; Lempp, F.A.; Bender, S.; Qu, B.; Schöneweis, S.; Seitz, S.; Tu, T.; Restuccia, A.; Frankish, J.; Dächert, C.; Schusser, B.; Koschny, R.; Polychronidis, G.; Schemmer, P.; Hoffmann, K.; Baumert, T.F.; Binder, M.; Urban, S.; Bartenschlager, R. HBV bypasses the innate immune response and does not protect HCV from antiviral activity of interferon. *Gastroenterology* **2018**, *154*(6),1791-1804. doi:10.1053/j.gastro.2018.01.044
- Mylka, V.; Matetovici, I.; Poovathingal, S.; Aerts, J.; Vandamme, N.; Seurinck, R.; Verstaen, K.; Hulselmans, G.; Van den Hoecke, S.; Scheyltjens, I.; Movahedi, K.; Wils, H.; Reumers, J.; van Houdt, J.; Aerts, S.; Saeys, Y. Comparative analysis of antibody- and lipid- based multiplexing methods for single-cell RNA-seq. *Genome Biol.* **2022**, *23*, 55. doi:10.1186/s13059-022-02628-8
- Nassal, M. Hepatitis B viruses: reverse transcription a different way. *Virus Res*, **2008**. *134*, 235-249. doi:10.1016/j.virusres.2007.12.024.
- Nassal, M. The arginine-rich domain of the hepatitis B virus core protein is required for pregenome encapsidation and productive viral positive-strand DNA synthesis but not for virus assembly. *J. Virol.* **1992**, *66*, 4107–4116.
- Nassal, M.; Rieger, A. A bulged region of the hepatitis B virus RNA encapsidation signal contains the replication origin for discontinuous first-strand DNA synthesis. *J. Virol.* **1996**, *70*, 2764-2773.
- Nayagam, S.; Thursz, M.; Sicuri, E.; Conteh, L.; Wiktor, S.; Low-Ber, D.; Hallett, T.B. Requirements for global elimination of hepatitis B: a modelling study. *Lancet Infect. Dis.* **2016**, *16*, 1399-1408. doi:10.1016/S1473-3099(16)30204-3.
- Ni, Y.; Lempp, F.A.; Mehrle, S.; Nkongolo, S.; Kaufman, C.; Falth, M.; Stindt, J.; Koniger, C.; Nassal, M.; Kubitz, R.; Sultmann, H.; Urban, S. Hepatitis B and D viruses exploit sodium

- taurocholate co-transporting polypeptide for species-specific entry into hepatocytes. *Gastroenterology* **2014**, *146*, 1070–1083. doi:10.1053/j.gastro.2013.12.024.
- Niklasch, M.; Zimmermann, P.; Nassal, M. The hepatitis B virus nucleocapsid-dynamic compartment for infectious virus production and new antiviral target. *Biomedicines* **2021**, *9*. doi:10.3390/biomedicines9111577.
- Ning, X.; Basagoudanavar, S.H.; Liu, K.; Luckenbaugh, L.; Wei, D.; Wang, C.; Wei, B.; Zhao, Y.; Yan, T.; Delaney, W.; Hu, J. Capsid Phosphorylation State and Hepadnavirus Virion Secretion. *J. Virol.* **2017**, *91*. doi:10.1128/JVI.00092-17.
- Ning, X.; Luckenbaugh, L.; Liu, K.; Bruss, V.; Sureau, C.; Hu, J. Common and Distinct Capsid and Surface Protein Requirements for Secretion of Complete and Genome-Free Hepatitis B Virions. *J. Virol.* **2018**, *92*. doi:10.1128/JVI.00272-18.
- Ning, X.; Nguyen, D.; Mentzer, L.; Adams, C.; Lee, H.; Ashley, R.; Hafenstein, S.; Hu, J. Secretion of genome-free hepatitis B virus--single strand blocking model for virion morphogenesis of para-retrovirus. *PLoS Pathog.* **2011**, *7*, e1002255. doi:10.1371/journal.ppat.1002255.
- Nishitsuji, H.; Ujino, S.; Shimizu, Y.; Harada, K.; Zhang, J.; Sugiyama, M.; Mizokami, M.; Shimotohno, K. Novel reporter system to monitor early stages of the hepatitis B virus life cycle. *Cancer Sci.* **2015**, *106*, 1616–1624, doi:10.1111/cas.12799
- Niu, C.; Livingston, C.M.; Li, L. *et al.* The Smc5/6 complex restricts HBV when localized to ND10 without inducing an innate immune response and is counteracted by the HBV X protein shortly after infection. *PLoS One* **2017**, *12*, e0169648
- O'Neal, J.T.; Upadhyay, A.A.; Wolabaugh, A.; Patel, N.B.; Bosinger, S.E.; Suthar, M.S. West Nile virus-inclusive single-cell RNA sequencing reveals heterogeneity in the type I interferon response within single cells. *J. Virol.* **2019**, *93*. doi:10.1128/JVI.01778-18.
- O'Neill, M.B.; Quach, H.; Pothlichet, J.; Aquino, Y.; Bisiaux, A.; Zidane, N.; Deschamps, M.; Libri, V.; Hasan, M.; Zhang, S.Y.; Zhang, Q.; Matuozzo, D.; Cobat, A.; Abel, L.; Casanova, J.L.; Naffakh, N.; Rotival, M.; Quintana-Murci, L. Single-cell and bulk RNA-sequencing reveal differences in monocyte susceptibility to influenza A virus infection between Africans and Europeans. *Front. Immunol.* **2021**, *12*, 768189. doi:10.3389/fimmu.2021.768189.
- Ortega-Prieto, A.M.; Dorner, M. Immune evasion strategies during chronic hepatitis B and C virus infection. *Vaccines* **2017**, *5* (3), 24. DOI: 10.3390/vaccines5030024

- Ortega-Prieto, A.M.; Skelton, J.K.; Wai, S.N.; Large, E.; Lussignol, M.; Vizcay-Barrena, G.; Hughes, D.; Fleck, R.A.; Thursz, M.; Catanese, M.T.; Dorner, M. 3D microfluidic liver cultures as a physiological preclinical tool for hepatitis B virus infection. *Nat. Commun.* **2018**, *9*, 682. doi:10.1038/s41467-018-02969-8.
- Ott, J.J.; Stevens, G.A.; Groeger, J.; Wiersma, S.T. Global epidemiology of hepatitis B virus infection: new estimates of age-specific HBsAg seroprevalence and endemicity. *Vaccine* **2012**, *30*, 2212-2219. doi:10.1016/j.vaccine.2011.12.116.
- Pal, R.; Mamidi, M.K.; Das, A.; Bhonde, R. Diverse effects of dimethyl sulfoxide (DMSO) on the differentiation potential of human embryonic stem cells. *Arch. Toxicol.* **2012**, *86*, 651–661. doi:10.1007/s00204-011-0782-2.
- Papalex, E.; Satija, R. Single-cell RNA sequencing to explore immune cell heterogeneity. *Nat. Rev. Immunol.* **2018**, *18*, 35-45. doi:10.1038/nri.2017.76.
- Parekh, S.; Zoulim, F.; Ahn, S.H.; Tsai, A.; Li, J.; Kawai, S.; Khan, N.; Trepo, C.; Wands, J.; Tong, S. Genome replication, virion secretion, and e antigen expression of naturally occurring hepatitis B virus core promoter mutants. *J. Virol.* **2003**, *77*, 6601-12. doi:10.1128/jvi.77.12.6601-6612.2003.
- Pasquetto, V.; Guidotti, L.G.; Kakimi, K.; Tsuji, M.; Chisari, F.V. Host-virus interactions during malaria infection in hepatitis B virus transgenic mice. *J. Exp. Med.* **2000**, *192*, 529-536. doi:10.1084/jem.192.4.529.
- Pastor, F.; Herrscher, C.; Patient, R.; Eymieux, S.; Moreau, A.; Burlaud-Gaillard, J.; Seigneuret, F.; de Rocquigny, H.; Roingeard, P.; Hourieux, C. Direct interaction between the hepatitis B virus core and envelope proteins analyzed in a cellular context. *Sci. Rep.* **2019**, *9*, 16178. doi:10.1038/s41598-019-52824-z.
- Paterlini-Brechot, P.; Saigo, K.; Murakami, Y.; Chami, M.; Gozuacik, D.; Mugnier, C.; Lagorce, D.; Brechot, C. Hepatitis B virus-related insertional mutagenesis occurs frequently in human liver cancers and recurrently targets human telomerase gene. *Oncogene* **2003**, *22*, 3911-3916. doi:10.1038/sj.onc.1206492.
- Patient, R.; Hourieux, C.; Sizaret, P.Y.; Trassard, S.; Sureau, C.; Roingeard, P. Hepatitis B virus subviral envelope particle morphogenesis and intracellular trafficking. *J. Virol.* **2007**, *81*, 3842-3851. doi:10.1128/JVI.02741-06.

- Peneau, C.; Imbeaud, S.; La Bella, T.; Hirsch, T.Z.; Caruso, S.; Calderaro, J.; Paradis, V.; Blanc, J.F.; Letouze, E.; Nault, J.C.; Amaddeo, G.; Zucman-Rossi, J. Hepatitis B virus integrations promote local and distant oncogenic driver alterations in hepatocellular carcinoma. *Gut* **2022**, *71*, 616-626. doi:10.1136/gutjnl-2020-323153.
- Peng, Z.; Zhang, Y.; Gu, W.; Wang, Z.; Li, D.; Zhang, F.; Qiu, G.; Xie, K. Integration of the hepatitis B virus X fragment in hepatocellular carcinoma and its effects on the expression of multiple molecules: a key to the cell cycle and apoptosis. *Int. J. Oncol.* **2005**, *26*, 467-473.
- Polaris Observatory Collaborators (Razavi-Shearer, D. et al.). Global prevalence, treatment, and prevention of hepatitis B virus infection in 2016: a modelling study. *Lancet Gastroenterol. Hepatol.* **2018**, *3*, 383-403. doi:10.1016/S2468-1253(18)30056-6.
- Pollack, J.R.; Ganem, D. An RNA stem-loop structure directs hepatitis B virus genomic RNA encapsidation. *J. Virol.* **1993**, *67*, 3254-3263.
- Pollack, J.R.; Ganem, D. Site-specific RNA binding by a hepatitis B virus reverse transcriptase initiates two distinct reactions: RNA packaging and DNA synthesis. *J. Virol.* **1994**, *68*, 5579-5587.
- Porterfield, J.Z.; Dhasan, M.S.; Loeb, D.D.; Nassal, M.; Stray, S.J.; Zlotnick, A. Full-length hepatitis B virus core protein packages viral and heterologous RNA with similarly high levels of cooperativity. *J. Virol.* **2010**, *84*, 7174-84. doi:10.1128/JVI.00586-10.
- Prakash, K.; Larsson, S.B.; Rydell, G.E.; Andersson, M.E.; Ringlander, J.; Norkrans, G.; Norder, H.; Lindh, M. Hepatitis B Virus RNA Profiles in Liver Biopsies by Digital Polymerase Chain Reaction. *Hepatol. Commun.* **2020**, *4*, 973-982. doi:10.1002/hep4.1507.
- Prince, A.M.; Brotman, B.; Purcell, R.H.; Gerin, J.L. A final report on safety and immunogenicity of a bivalent aqueous subunit HBV vaccine. *J. Med. Virol.* **1985**, *15*, 399-419. doi:10.1002/jmv.1890150410.
- Qi, Y.; Gao, Z.; Xu, G.; Peng, B.; Liu, C.; Yan, H.; Yao, Q.; Sun, G.; Liu, Y.; Tang, D.; Song, Z.; He, W.; Sun, Y.; Guo, J.T.; Li, W. DNA Polymerase kappa Is a Key Cellular Factor for the Formation of Covalently Closed Circular DNA of Hepatitis B Virus. *PLoS Pathog.* **2016**, *12*, e1005893. doi:10.1371/journal.ppat.1005893.
- Qiao, L.; Sui, J.; Luo, G. Robust human and murine hepatocyte culture models of hepatitis B virus infection and replication. *J. Virol.* **2018**, *92*, e01255-18. doi:10.1128/jvi.01255-18.

- Qu, B.; Ni, Y.; Lempp, F.A.; Vondran, F.W.R.; Urban, S. T5 exonuclease hydrolysis of hepatitis B virus replicative intermediates allows reliable quantification and fast drug efficacy testing of covalently closed circular DNA by PCR. *J. Virol.* **2018**, *92*, e01117–18, doi:10.1128/jvi.01117-18
- Quan, J.; Langelier, C.; Kuchta, A.; Batson, J.; Teyssier, N.; Lyden, A.; Caldera, S.; McGeever, A.; Dimitrov, B.; King, R.; Wilhelm, J.; Murphy, M.; Ares, L. P.; Travisano, K. A.; Sit, R.; Amato, R.; Mumbengegwi, D. R.; Smith, J. L.; Bennett, A.; Gosling, R.; Mourani, P. M.; Calfee, C. S.; Neff, N. F.; Chow, E. D.; Kim, P. S.; Greenhouse, B.; DeRisi, J. L.; Crawford, E. D., FLASH: a next-generation CRISPR diagnostic for multiplexed detection of antimicrobial resistance sequences. *Nucleic Acids Res.* **2019**, *47* (14), e83. DOI: 10.1093/nar/gkz418
- Quasdorff, M.; Hosel, M.; Odenthal, M.; Zedler, U.; Bohne, F.; Gripon, P.; Dienes, H.P.; Drebber, U.; Stippel, D.; Goeser, T.; Protzer, U. A concerted action of HNF4alpha and HNF1alpha links hepatitis B virus replication to hepatocyte differentiation. *Cell Microbiol.* **2008**, *10*, 1478-1490. doi:10.1111/j.1462-5822.2008.01141.x.
- Rabe, B., Glebe, D.; Kann, M. Lipid-mediated introduction of hepatitis B virus capsids into nonsusceptible cells allows highly efficient replication and facilitates the study of early infection events. *J. Virol.* **2006**, *80*, 5465–5473.
- Rabe, B.; Delaleau, M.; Bischof, A.; Foss, M.; Sominskaya, I.; Pumpens, P.; Cazenave, C.; Castroviejo, M.; Kann, M. Nuclear entry of hepatitis B virus capsids involves disintegration to protein dimers followed by nuclear reassociation to capsids. *PLoS Pathog.* **2009**, *5*, e1000563. doi:10.1371/journal.ppat.1000563.
- Rabe, B.; Vlachou, A.; Pante, N.; Helenius, A.; Kann, M. Nuclear import of hepatitis B virus capsids and release of the viral genome. *Proc. Natl. Acad. Sci. U. S. A.* **2003**, *100*, 9849-9854. doi:10.1073/pnas.1730940100.
- Raimondo, G.; Locarnini, S.; Pollicino, T.; Levrero, M.; Zoulim, F.; Lok, A.S., Taormina Workshop on Occult HBV Infection Faculty Members. Update of the statements on biology and clinical impact of occult hepatitis B virus infection. *J. Hepatol.* **2019**, *71*, 397-408. doi:10.1016/j.jhep.2019.03.034.
- Rall, L.B.; Standring, D.N.; Laub, O.; Rutter, W.J. Transcription of hepatitis B virus by RNA polymerase II. *Mol. Cell Biol.* **1983**, *3*, 1766-1773. doi:10.1128/mcb.3.10.1766.

- Ramachandran, P.; Matchett, K.P.; Dobie, R.; Wilson-Kanamori, J.R.; Henderson, N.C. Single-cell technologies in hepatology: new insights into liver biology and disease pathogenesis. *Nat. Rev. Gastroenterol. Hepatol.* **2020**, *17*, 457–472. DOI: 10.1038/s41575-020-0304-x
- Regev, A.; Teichmann, S.A.; Lander, E.S.; Amit, I.; Benoist, C.; Birney, E.; Bodenmiller, B.; Campbell, P.; Carninci, P.; Clatworthy, M.; Clevers, H.; Deplancke, B.; Dunham, I.; Eberwine, J.; Eils, R.; Enard, W.; Farmer, A.; Fugger, L.; Gottgens, B.; Hacohen, N.; Haniffa, M.; Hemberg, M.; Kim, S.; Klenerman, P.; Kriegstein, A.; Lein, E.; Linnarsson, S.; Lundberg, E.; Lundberg, J.; Majumder, P.; Marioni, J.C.; Merad, M.; Mhlanga, M.; Nawijn, M.; Netea, M.; Nolan, G.; Pe'er, D.; Phillipakis, A.; Ponting, C.P.; Quake, S.; Reik, W.; Rozenblatt-Rosen, O.; Sanes, J.; Satija, R.; Schumacher, T.N.; Shalek, A.; Shapiro, E.; Sharma, P.; Shin, J.W.; Stegle, O.; Stratton, M.; Stubbington, M.J.T.; Theis, F.J.; Uhlen, M.; van Oudenaarden, A.; Wagner, A.; Watt, F.; Weissman, J.; Wold, B.; Xavier, R.; Yosef, N., Human Cell Atlas Meeting Participants. The human cell atlas. *Elife* **2017**, *6*. doi:10.7554/eLife.27041.
- Rehermann, B. Intrahepatic T cells in hepatitis B: viral control versus liver cell injury. *J. Exp. Med.* **2000**, *191*, 1263-1268. doi:10.1084/jem.191.8.1263.
- Rehermann, B.; Fowler, P.; Sidney, J.; Person, J.; Redeker, A.; Brown, M.; Moss, B.; Sette, A.; Chisari, F.V. The cytotoxic T lymphocyte response to multiple hepatitis B virus polymerase epitopes during and after acute viral hepatitis. *J. Exp. Med.* **1995**, *181*, 1047-1058. doi:10.1084/jem.181.3.1047.
- Reignat, S.; Webster, G.J.; Brown, D.; Ogg, G.S.; King, A.; Seneviratne, S.L.; Dusheiko, G.; Williams, R.; Maini, M.K.; Bertolotti, A. Escaping high viral load exhaustion: CD8 cells with altered tetramer binding in chronic hepatitis B virus infection. *J. Exp. Med.* **2002**, *195*, 1089-1101. doi:10.1084/jem.20011723.
- Ren, X.; Wen, W.; Fan, X.; Chen, J.; Jin, R.; Zhang, Z. COVID-19 immune features revealed by a large-scale single-cell transcriptome atlas. *Cell* **2021**, *184*, 1895–1913. DOI: 10.1016/j.cell.2021.01.053
- Revill, P.; Testoni, B.; Locarnini, S.; Zoulim, F. Global strategies are required to cure and eliminate HBV infection. *Nat. Rev. Gastroenterol. Hepatol.* **2016**, *13*, 239-248. doi:10.1038/nrgastro.2016.7.
- Rieger, A.; Nassal, M. Specific hepatitis B virus minus-strand DNA synthesis requires only the 5' encapsidation signal and the 3'-proximal direct repeat DR1. *J. Virol.* **1996**, *70*, 585-589.

- Robinson, W.S. Greenman, R.L. DNA polymerase in the core of the human hepatitis B virus candidate. *J. Virol.* **1974**, *14*, 1231-1236.
- Robinson, W.S.; Clayton, D.A.; Greenman, R.L. DNA of a human hepatitis B virus candidate. *J. Virol.* **1974**, *14*, 384-91.
- Rost, M.; Mann, S.; Lambert, C.; Doring, T.; Thome, N.; Prange, R. Gamma-adaptin, a novel ubiquitin-interacting adaptor, and Nedd4 ubiquitin ligase control hepatitis B virus maturation. *J. Biol. Chem.* **2006**, *281*, 29297-29308. doi:10.1074/jbc.M603517200.
- Sanada, T.; Tsukiyama-Kohara, K.; Shin, I.T.; Yamamoto, N.; Kayesh, M.E.H.; Yamane, D.; Takano, J.I.; Shiogama, Y.; Yasutomi, Y.; Ikeo, K.; Gojobori, T.; Mizokami, M. Kohara, M. Construction of complete Tupaia belangeri transcriptome database by whole-genome and comprehensive RNA sequencing. *Sci. Rep.* **2019**, *9*, 12372. doi:10.1038/s41598-019-48867-x.
- Sargiacomo, C.; El-Kehdy, H.; Pourcher, G.; Stieger, B.; Najimi, M.; Sokal, E. Age-dependent glycosylation of the sodium taurocholate cotransporter polypeptide: From fetal to adult human livers. *Hepatol. Commun.* **2018**, *2*, 693–702. doi:10.1002/hep4.1174.
- Satija, R.; Farrell, J.A.; Gennert, D.; Schier, A.F.; Regev, A. Spatial reconstruction of single-cell gene expression data. *Nat. Biotechnol.* **2015**, *33*, 495-502. doi:10.1038/nbt.3192.
- Sato, S.; Li, K.; Kameyama, T.; Hayashi, T.; Ishida, Y.; Murakami, S.; Watanabe, T.; Iijima, S.; Sakurai, Y.; Watashi, K.; Tsutsumi, S.; Sato, Y.; Akita, H.; Wakita, T.; Rice, C.M.; Harashima, H.; Kohara, M.; Tanaka, Y., Takaoka, A. The RNA sensor RIG-I dually functions as an innate sensor and direct antiviral factor for hepatitis B virus. *Immunity* **2015**, *42*, 123-132. doi:10.1016/j.immuni.2014.12.016.
- Sattler, F.; Robinson, W.S. Hepatitis B viral DNA molecules have cohesive ends. *J. Virol.* **1979**, *32*, 226-233.
- Schmitz, A.; Schwarz, A.; Foss, M.; Zhou, L.; Rabe, B.; Hoellenriegel, J.; Stoeber, M.; Pante, N.; Kann, M. Nucleoporin 153 arrests the nuclear import of hepatitis B virus capsids in the nuclear basket. *PLoS Pathog.* **2010**, *6*, e1000741. doi:10.1371/journal.ppat.1000741.
- Schneeberger, K.; Sanchez-Romero, N.; Ye, S.; van Steenbeek, F.G.; Oosterhoff, L.A.; Palacin, I.P.; Chen, C.; Spee, B. et al. Large-scale production of LGR5-positive bipotential human liver stem cells. *Hepatology* **2020**, *72*, 257-270. doi:10.1002/hep.31037.
- Schoggins, J.W.; Rice, C.M. Interferon-stimulated genes and their antiviral effector functions. *Current Opinion Virol.* **2011**, *1*, 519–525. doi:10.1016/j.coviro.2011.10.008.

- Schoggins, J.W.; MacDuff, D.A.; Imanaka, N.; Gainey, M.D.; Shrestha, B.; Eitson, J.L.; Mar, K.B.; Richardson, R.B.; Ratushny, A.V.; Litvak, V.; Rice, C.M. Pan-viral specificity of IFN-induced genes reveals new roles for cGAS in innate immunity. *Nature* **2014**, *505*, 691–695. doi:10.1038/nature12862.
- Schultzhaus, Z.; Wang, Z.; Stenger, D. CRISPR-based enrichment strategies for targeted sequencing. *Biotechnol. Adv.* **2021**, *46*, 107672. DOI: 10.1016/j.biotechadv.2020.107672
- Schulze, A.; Gripon, P.; Urban, S. Hepatitis B virus infection initiates with a large surface protein-dependent binding to heparan sulfate proteoglycans. *Hepatology* **2007**, *46*, 1759-1768. doi:10.1002/hep.21896.
- Schulze, A.; Mills, K.; Weiss, T.S.; Urban, S. Hepatocyte polarization is essential for the productive entry of the hepatitis B virus. *Hepatology* **2011**, *55*, 373–383. doi:10.1002/hep.24707.
- Scotto, J.; Hadchouel, M.; Wain-Hobson, S.; Sonigo, P.; Courouce, A.M.; Tiollais, P.; Brechot, C. Hepatitis B virus DNA in Dane particles: evidence for the presence of replicative intermediates. *J. Infect. Dis.* **1985**, *151*, 610-617. doi:10.1093/infdis/151.4.610.
- Seeger, C.; Sohn, J.A. Targeting hepatitis B virus with CRISPR/Cas9. *Mol. Ther.-Nucleic Acids* **2014**, *3*, e216. doi:10.1038/mtna.2014.68.
- Segal, J.M.; Kent, D.; Wesche, D.J.; Ng, S.S.; Serra, M.; Oules, B.; Kar, G.; Emerton, G.; Blackford, S.J.I.; Darmanis, S.; Miquel, R.; Luong, T.V.; Yamamoto, R.; Bonham, A.; Jassem, W.; Heaton, N.; Vigilante, A.; King, A.; Sancho, R.; Teichmann, S.; Quake, S.R.; Nakauchi, H.; Rashid, S.T. Single cell analysis of human foetal liver captures the transcriptional profile of hepatobiliary hybrid progenitors. *Nat. Commun.* **2019**, *10*, 3350. doi:10.1038/s41467-019-11266-x.
- Sells, M.A.; Chen, M.L.; Acs, G. Production of hepatitis B virus particles in Hep G2 cells transfected with cloned hepatitis B virus DNA. *Proc. Natl. Acad. Sci. U.S.A.* **1987**, *84*, 1005–1009. doi:10.1073/pnas.84.4.1005.
- Seto, W.K.; Lo, Y.R.; Pawlotsky, J.M.; Yuen, M.F. Chronic hepatitis B virus infection. *Lancet* **2018**, *392*, 2313-2324. doi:10.1016/S0140-6736(18)31865-8.
- Sharma, A.; Seow, J.J.W.; Dutertre, C.A.; Pai, R.; Bleriot, C.; Mishra, A.; Wong, R.M.M.; Singh, G.S.N.; Sudhagar, S.; Khalilnezhad, S.; Erdal, S.; Teo, H.M.; Khalilnezhad, A.; Chakarov, S.; Lim, T.K.H.; Fui, A.C.Y.; Chieh, A.K.W.; Chung, C.P.; Bonney, G.K.; Goh,

- B.K.; Chan, J.K.Y.; Chow, P.K.H.; Ginhoux, F.; DasGupta, R. Onco-fetal Reprogramming of Endothelial Cells Drives Immunosuppressive Macrophages in Hepatocellular Carcinoma. *Cell* **2020**, *183*, 377-394 e21. doi:10.1016/j.cell.2020.08.040.
- Shen, F.; Li, Y.; Wang, Y.; Sozzi, V.; Revill, P.A.; Liu, J.; Gao, L.; Yang, G.; Lu, M.; Sutter, K.; Dittmer, U.; Chen, J.; Yuan, Z. Hepatitis B virus sensitivity to interferon-alpha in hepatocytes is more associated with cellular interferon response than with viral genotype. *Hepatology* **2018**, *67*, 1237-1252. doi:10.1002/hep.29609.
- Sheraz, M.; Cheng, J.; Tang, L.; Chang, J.; Guo, J.T. Cellular DNA Topoisomerases Are Required for the Synthesis of Hepatitis B Virus Covalently Closed Circular DNA. *J. Virol.* **2019**, *93*. doi:10.1128/JVI.02230-18.
- Shih, J.W.; Gerin, J.L. Immunochemistry of hepatitis B surface antigen (HBsAg): preparation and characterization of antibodies to the constituent polypeptides. *J. Immunol.* **1975**, *115*, 634-639.
- Shikata, T.; Karasawa, T. Abe, K. Two distinct types of hepatitis in experimental hepatitis B virus infection. *Am. J. Pathol.* **1980**, *99*, 353-368.
- Shlomai, A.; Schwartz, R.E.; Ramanan, V.; Bhatta, A.; De Jong, Y.P.; Bhatia, S.N.; Rice, C.M. Modeling host interactions with hepatitis B virus using primary and induced pluripotent stem cell-derived hepatocellular systems. *Proc. Natl. Acad. Sci. U.S.A.* **2014**, *111*, 12193–12198. doi:10.1073/pnas.1412631111.
- Shnyder, M.; Nachshon, A.; Rozman, B.; Bernshtein, B.; Lavi, M.; Fein, N.; Poole, E.; Avdic, S.; Blyth, E.; Gottlieb, D.; Abendroth, A.; Slobedman, B.; Sinclair, J.; Stern-Ginossar, N.; Schwartz, M. Single cell analysis reveals human cytomegalovirus drives latently infected cells towards an anergic-like monocyte state. *Elife* **2020**, *9*. doi:10.7554/eLife.52168.
- Sivaraman, A.; Leach, J.K.; Townsend, S.; Iida, T.; Hogan, B.J.; Stolz, D.B.; Fry, R.; Samson, L.D.; Tannenbaum, S.R.; Griffith, L.G. A microscale in vitro physiological model of the liver: predictive screens for drug metabolism and enzyme induction. *Curr. Drug Metab.* **2005**, *6*, 569-591. doi:10.2174/138920005774832632.
- Song, Y.M.; Song, S.O.; Jung, Y.K.; Kang, E.S.; Cha, B.S.; Lee, H.C.; Lee, B. Dimethyl sulfoxide reduces hepatocellular lipid accumulation through autophagy induction. *Autophagy* **2012**, *8*, 1085–1097. doi:10.4161/auto.20260.

- Speranza, E.; Williamson, B.N. Feldmann, F.; Sturdevant, G.L.; Pérez-Pérez, L.; Meade-White, K.; Smith, B.J.; Lovaglio, J.; Martens, C.; Munster, V.J.; Okumura, A.; Shaia, C.; Feldmann, H.; Best, S.M.; de Wit, E. Single-cell RNA sequencing reveals SARS-CoV-2 infection dynamics in lungs of African green monkeys. *Sci. Transl. Med.* **2021**, *13*(578), eabe8146. doi: 10.1126/scitranslmed.abe8146
- Sprinzi, M.F.; Oberwinkler, H.; Schaller, H.; Protzer, U. Transfer of hepatitis B virus genome by adenovirus vectors into cultured cells and mice: crossing the species barrier. *J. Virol.* **2001**, *75*, 5108-5118. doi:10.1128/JVI.75.11.5108-5118.2001.
- Stacey, A.R.; Norris, P.J.; Qin, L. *et al.* Induction of a striking systemic cytokine cascade prior to peak viremia in acute human immunodeficiency virus type 1 infection, in contrast to more modest and delayed responses in acute hepatitis B and C virus infections. *J. Virol.* **2009**, *83*, 3719-3733.
- Staprans, S.; Loeb, D.D.; Ganem, D. Mutations affecting hepadnavirus plus-strand DNA synthesis dissociate primer cleavage from translocation and reveal the origin of linear viral DNA. *J. Virol.* **1991**, *65*, 1255-1262.
- Steenbergen, R.; Oti, M.; ter Horst, R.; Tat, W.; Neufeldt, C.; Belovodskiy, A.; Chua, T. T.; Cho, W. J.; Joyce, M.; Dutilh, B. E.; Tyrrell, D. L. Establishing normal metabolism and differentiation in hepatocellular carcinoma cells by culturing in adult human serum. *Sci. Rep.* **2018**, *8*, 11685, doi:10.1038/s41598-018-29763-2.
- Steenbergen, R.; Oti, M.; ter Horst, R.; Tat, W.; Neufeldt, C.; Belovodskiy, A.; Chua, T. T.; Cho, W. J.; Joyce, M.; Dutilh, B. E.; Tyrrell, D. L. Establishing normal metabolism and differentiation in hepatocellular carcinoma cells by culturing in adult human serum. *Sci. Rep.* **2018**, *8*, 11685. doi:10.1038/s41598-018-29763-2.
- Steenbergen, R.H.; Joyce, M. A.; Thomas, B.; Jones, D.; Law, J.; Russell, R.; Houghton, M.; Tyrrell, D. L. Human serum leads to differentiation of human hepatoma cells, restoration of very-low-density lipoprotein secretion, and a 1000-fold increase in HCV Japanese fulminant hepatitis type 1 titers. *Hepatology* **2013**, *58*, 1907–1917. doi:10.1002/hep.26566.
- Steuerman, Y.; Cohen, M.; Peshes-Yaloz, N.; Valadarsky, L.; Cohn, O.; David, E.; Frishberg, A.; Mayo, L.; Bacharach, E.; Amit, I.; Gat-Viks, I. Dissection of influenza infection *in vivo* by single-cell RNA sequencing. *Cell Syst.* **2018**, *6*, 679-691 e4. doi:10.1016/j.cels.2018.05.008.

- Stibbe, W.; Gerlich, W.H. Structural relationships between minor and major proteins of hepatitis B surface antigen. *J. Virol.* **1983**, *46*, 626-628.
- Street, K.; Risso, D.; Fletcher, R.B.; Das, D.; Ngai, J.; Yosef, N.; Purdom, E.; Dudoit, S. Slingshot: cell lineage and pseudotime inference for single-cell transcriptomics. *BMC Genomics* **2018**, *19*, 477. doi:10.1186/s12864-018-4772-0.
- Stuart, T.; Butler, A.; Hoffman, P.; Hafemeister, C.; Papalexi, E.; Mauck, W.M., 3rd; Hao, Y.; Stoeckius, M.; Smibert, P.; Satija, R. Comprehensive integration of single-cell data. *Cell* **2019**, *177*, 1888-1902. doi:10.1016/j.cell.2019.05.031.
- Su, X.; Shi, Y.; Zou, X.; Lu, Z.-N.; Xie, G.; Yang, J. Y. H.; Wu, C.-C.; Cui, X.-F.; He, K.-Y.; Luo, Q.; Qu, Y.-L.; Wang, N.; Wang, L.; Han, Z.-G. Single-cell RNA-Seq analysis reveals dynamic trajectories during mouse liver development. *BMC Genomics* **2017**, *18*, 946. doi:10.1186/s12864-017-4342-x
- Su, A.I.; Pezacki, J.P.; Wodicka, L. *et al.* Genomic analysis of the host response to hepatitis C virus infection. *Proc. Natl. Acad. Sci. U. S. A.* **2002**, *99*, 15669-15674.
- Summers, J.; O'Connell, A.; Millman, I. Genome of hepatitis B virus: restriction enzyme cleavage and structure of DNA extracted from Dane particles. *Proc. Natl. Acad. Sci. U. S. A.* **1975**, *72*, 4597-4601. doi:10.1073/pnas.72.11.4597.
- Summers, J.; Smith, P.M.; Horwich, A.L. Hepadnavirus envelope proteins regulate covalently closed circular DNA amplification. *J. Virol.* **1990**, *64*, 2819-2824. doi:10.1128/JVI.64.6.2819-2824.1990.
- Sung, W.K.; Zheng, H.; Li, S.; Chen, R.; Liu, X.; Li, Y.; Lee, N.P.; Lee, W.H.; Ariyaratne, P.N.; Tennakoon, C.; Mulawadi, F.H.; Wong, K.F.; Liu, A.M.; Poon, R.T.; Fan, S.T.; Chan, K.L.; Gong, Z.; Hu, Y.; Lin, Z.; Wang, G.; Zhang, Q.; Barber, T.D.; Chou, W.C.; Aggarwal, A.; Hao, K.; Zhou, W.; Zhang, C.; Hardwick, J.; Buser, C.; Xu, J.; Kan, Z.; Dai, H.; Mao, M.; Reinhard, C.; Wang, J.; Luk, J.M. Genome-wide survey of recurrent HBV integration in hepatocellular carcinoma. *Nat. Genet.* **2012**, *44*, 765-769. doi:10.1038/ng.2295.
- Sureau, C.; Romet-Lemonne, J.L.; Mullins, J.I.; Essex, M. Production of hepatitis B virus by a differentiated human hepatoma cell line after transfection with cloned circular HBV DNA. *Cell* **1986**, *47*, 37-47. doi:10.1016/0092-8674(86)90364-8.
- Suresh, M.; Czerwinski, S.; Murreddu, M.G.; Kallakury, B.V.; Ramesh, A.; Gudima, S.O.; Menne, S. *PLoS Pathog.* **2019**, *15*, e1008248. doi:10.1371/journal.ppat.1008248

- Suslov, A.; Boldanova, T.; Wang, X.; Wieland, S.; Heim, M.H. Hepatitis B virus does not interfere with innate immune responses in the human liver. *Gastroenterology* **2018**, *154*, 1778-1790. doi:10.1053/j.gastro.2018.01.034.
- Suslov, A.; Boldanova, T.; Wang, X.Y.; Wieland, S.; Heim, M.H. Hepatitis B virus does not interfere with innate immune responses in the human liver. *Gastroenterology* **2018**, *154*, 1778–1790. doi: 10.1053/j.gastro.2018.01.034
- Suslov, A.; Wieland, S.; Menne, S. Modulators of innate immunity as novel therapeutics for treatment of chronic hepatitis B. *Curr. Opin. Virol.* **2018**, *30*, 9–17.
doi:10.1016/j.coviro.2018.01.008
- Svensson, V.; Vento-Tormo, R.; Teichmann, S.A. Exponential scaling of single-cell RNA-seq in the past decade. *Nat. Protoc.* **2018**, *13*, 599–604. doi: 10.1038/nprot.2017.149
- Takahashi, K.; Yamanaka, S. Induction of pluripotent stem cells from mouse embryonic and adult fibroblast cultures by defined factors. *Cell* **2006**, *126*, 663-676.
doi:10.1016/j.cell.2006.07.024.
- Tanay, A.; Regev, A. Scaling single-cell genomics from phenomenology to mechanism. *Nature* **2017**, *541*, 331-338. doi: 10.1038/nature21350
- Tang, F.; Barbacioru, C.; Wang, Y.; Nordman, E.; Lee, C.; Xu, N.; Wang, X.; Bodeau, J.; Tuch, B.B.; Siddiqui, A.; Lao, K.; Surani, M.A. mRNA-Seq whole-transcriptome analysis of a single cell. *Nat. Methods* **2009**, *6*, 377-382. doi:10.1038/nmeth.1315.
- Tang, J.; Wu, Z-Y.; Dai, R-J.; Ma, J.; Gong, G-Z. Hepatitis B virus-persistent infection and innate immunity defect: Cell-related or virus-related? *World J. Clin. Cases* **2018**, *6*, 233-241.
doi:10.12998/wjcc.v6.i9.233
- Tang, L.; Sheraz, M.; McGrane, M.; Chang, J.; Guo, J.T. DNA Polymerase alpha is essential for intracellular amplification of hepatitis B virus covalently closed circular DNA. *PLoS Pathog.* **2019**, *15*, e1007742. doi:10.1371/journal.ppat.1007742.
- Tavis, J.E.; Cheng, X.; Hu, Y.; Totten, M.; Cao, F.; Michailidis, E.; Aurora, R.; Meyers, M.J.; Jacobsen, E.J.; Parniak, M.A.; Sarafianos, S.G. The hepatitis B virus ribonuclease H is sensitive to inhibitors of the human immunodeficiency virus ribonuclease H and integrase enzymes. *PLoS Pathog.* **2013**, *9*, e1003125. doi:10.1371/journal.ppat.1003125.
- Te, H.S.; Jensen, D.M. Epidemiology of hepatitis B and C viruses: a global overview. *Clin. Liver Dis.* **2010**, *14*, 1-21, vii. doi:10.1016/j.cld.2009.11.009.

- Terrault, N.A.; Lok, A.S.F.; McMahon, B.J.; Chang, K.M.; Hwang, J.P.; Jonas, M.M.; Brown, R.S., Jr.; Bzowej, N.H.; Wong, J.B. Update on prevention, diagnosis, and treatment of chronic hepatitis B: AASLD 2018 hepatitis B guidance. *Hepatology* **2018**, *67*, 1560-1599. doi:10.1002/hep.29800.
- Thimme, R.; Wieland, S.; Steiger, C.; Ghayeb, J.; Reimann, K.A.; Purcell, R.H., Chisari, F.V. CD8(+) T cells mediate viral clearance and disease pathogenesis during acute hepatitis B virus infection. *J. Virol.* **2003**, *77*, 68-76. doi:10.1128/jvi.77.1.68-76.2003.
- Thomas, E.; Baumert, T.F. Hepatitis B virus-hepatocyte interactions and innate immune responses: experimental models and molecular mechanisms. *Semin. Liver Dis.* **2019**, *39*, 301–314. doi: 10.1055/s-0039-1685518
- Thomas, E.; Liang, T.J. Experimental models of hepatitis B and C—new insights and progress. *Nat. Rev. Gastroenterol. Hepatol.* **2016**, *13*, 362–374. doi:10.1038/nrgastro.2016.37.
- Thomson, J.A.; Itskovitz-Eldor, J.; Shapiro, S.S.; Waknitz, M.A.; Swiergiel, J.J.; Marshall, V.S.; Jones, J.M. Embryonic stem cell lines derived from human blastocysts. *Science* **1998**, *282*, 1145-1147. doi:10.1126/science.282.5391.1145.
- Tian, Q.; Jia, J. Hepatitis B virus genotypes: epidemiological and clinical relevance in Asia. *Hepatol. Int.* **2016**, *10*, 854-860. doi:10.1007/s12072-016-9745-2.
- Trapnell, C.; Cacchiarelli, D.; Grimsby, J.; Pokharel, P.; Li, S.; Morse, M.; Lennon, N.J.; Livak, K.J.; Mikkelsen, T.S.; Rinn, J.L. The dynamics and regulators of cell fate decisions are revealed by pseudotemporal ordering of single cells. *Nat Biotechnol*, **2014**. *32*, 381-386. doi:10.1038/nbt.2859.
- Trepo, C.; Chan, H.L.; Lok, A. Hepatitis B virus infection. *Lancet* **2014**, *384*, 2053-2063. doi: 10.1016/S0140-6736(14)60220-8
- Tropberger, P.; Mercier, A.; Robinson, M.; Zhong, W.; Ganem, D.E.; Holdorf, M. Mapping of histone modifications in episomal HBV cccDNA uncovers an unusual chromatin organization amenable to epigenetic manipulation. *Proc. Natl. Acad. Sci. U. S. A.* **2015**, *112*, E5715-24. doi:10.1073/pnas.1518090112.
- Tu, T.; Budzinska, M.A.; Vondran, F.W.R.; Shackel, N.A.; Urban, S. Hepatitis B Virus DNA Integration Occurs Early in the Viral Life Cycle in an In Vitro Infection Model via Sodium Taurocholate Cotransporting Polypeptide-Dependent Uptake of Enveloped Virus Particles. *J. Virol.* **2018**, *92*. doi:10.1128/JVI.02007-17.

- Tu, T.; Mason, W.S.; Clouston, A.D.; Shackel, N.A.; McCaughan, G.W.; Yeh, M.M.; Schiff, E.R.; Ruszkiewicz, A.R.; Chen, J.W.; Harley, H.A.; Stroehrer, U.H.; Jilbert, A.R. Clonal expansion of hepatocytes with a selective advantage occurs during all stages of chronic hepatitis B virus infection. *J. Viral. Hepat.* **2015**, *22*, 737-753. doi:10.1111/jvh.12380.
- Tu, T.; Zehnder, B.; Qu, B.; Urban, S. De novo synthesis of hepatitis B virus nucleocapsids is dispensable for the maintenance and transcriptional regulation of cccDNA. *JHEP Rep.* **2021**, *3*, 100195. doi:10.1016/j.jhepr.2020.100195.
- Tuttleman, J.S.; Pourcel, C.; Summers, J. Formation of the pool of covalently closed circular viral DNA in hepadnavirus-infected cells. *Cell* **1986**, *47*, 451-460. doi:10.1016/0092-8674(86)90602-1.
- Ueda, K.; Tsurimoto, T.; Matsubara, K. Three envelope proteins of hepatitis B virus: large S, middle S, and major S proteins needed for the formation of Dane particles. *J. Virol.* **1991**, *65*, 3521-3529.
- Urban, S.; Schulze, A.; Dandri, M.; Petersen, J. The replication cycle of hepatitis B virus. *J. Hepatol.* **2010**, *52*, 282-284. doi:10.1016/j.jhep.2009.10.031.
- Urban, S.; Urban, S.; Fischer, K.P.; Tyrrell, D.L. Efficient pyrophosphorolysis by a hepatitis B virus polymerase may be a primer-unblocking mechanism. *Proc. Natl. Acad. Sci. U. S. A.* **2001**, *98*, 4984-4989. doi:10.1073/pnas.091324398.
- Van de Sande, B.; Flerin, C.; Davie, K.; De Waegeneer, M.; Hulselmans, G.; Aibar, S.; Seurinck, R.; Saelens, W.; Cannoodt, R.; Rouchon, Q.; Verbeiren, T.; De Maeyer, D.; Reumers J.; Saeys, Y.; Aerts, S. A scalable SCENIC workflow for single-cell gene regulatory network analysis. *Nat. Protoc.* **2020**, *15*, 2247-2276. doi:10.1038/s41596-020-0336-2
- Van den Berge, K.; Roux de Bezieux, H.; Street, K.; Saelens, W.; Cannoodt, R.; Saeys, Y.; Dudoit, S.; Clement, L. Trajectory-based differential expression analysis for single-cell sequencing data. *Nat. Commun.* **2020**, *11*, 1201. doi:10.1038/s41467-020-14766-3.
- Venook, A.P.; Papandreou, C.; Furuse, J.; de Guevara, L.L. The incidence and epidemiology of hepatocellular carcinoma: a global and regional perspective. *Oncologist* **2010**, *15 Suppl 4*, 5-13. doi:10.1634/theoncologist.2010-S4-05.
- Verheijen, M.; Lienhard, M.; Schrooders, Y.; Clayton, O.; Nudischer, R.; Boerno, S.; Timmermann, B.; Selevsek, N.; Schlapbach, R.; Gmuender, H.; et al. DMSO induces drastic

- changes in human cellular processes and epigenetic landscape *in vitro*. *Sci. Rep.* **2019**, *9*, 4641. doi:10.1038/s41598-019-40660-0.
- Verrier, E.R.; Colpitts, C.C.; Schuster, C.; Zeisel, M.B.; Baumert, T.F. Cell Culture Models for the Investigation of Hepatitis B and D Virus Infection. *Viruses* **2016**, *8*. doi:10.3390/v8090261.
- Volz, T.; Allweiss, L.; Ben, M.M.; Warlich, M.; Lohse, A.W.; Pollok, J.M.; Alexandrov, A.; Urban, S.; Petersen, J.; Lutgehetmann, M. Dandri, M. The entry inhibitor Myrcludex-B efficiently blocks intrahepatic virus spreading in humanized mice previously infected with hepatitis B virus. *J. Hepatol.* **2013**, *58*, 861-867. doi:10.1016/j.jhep.2012.12.008.
- Vondráček, J.; Souček, K.; Sheard, M.A.; Chramostová, K.; Andrysík, Z.; Hofmanová, J.; Kozubík, A. Dimethyl sulfoxide potentiates death receptor-mediated apoptosis in the human myeloid leukemia U937 cell line through enhancement of mitochondrial membrane depolarization. *Leuk. Res.* **2006**, *30*, 81–89. doi:10.1016/j.leukres.2005.05.016.
- Vong, J.S.L.; Ji, L.; Heung, M.M.S.; Cheng, S.H.; Wong, J.; Lai, P.B.S.; Wong, V.W.S.; Chan, S.L.; Chan, H.L.Y.; Jiang, P.; Chan, K.C.A.; Chiu, R.W.K.; Lo, Y.M.D. Single cell and plasma RNA sequencing for RNA liquid biopsy for hepatocellular carcinoma. *Clin. Chem.* **2021**, *67*, 1492-1502. doi:10.1093/clinchem/hvab116.
- Walter, E.; Keist, R.; Niederost, B.; Pult, I.; Blum, H.E. Hepatitis B virus infection of tupaia hepatocytes in vitro and in vivo. *Hepatology* **1996**, *24*, 1-5. doi:10.1002/hep.510240101.
- Walters, K.A.; Joyce, M.A.; Addison, W.R.; Fischer, K.P.; Tyrrell, D.L. Superinfection exclusion in duck hepatitis B virus infection is mediated by the large surface antigen. *J. Virol.* **2004**, *78*, 7925-7937. doi:10.1128/JVI.78.15.7925-7937.2004.
- Wang, H.; Ryu, W.S. Hepatitis B virus polymerase blocks pattern recognition receptor signaling via interaction with DDX3: implications for immune evasion. *PLoS Pathog.* **2010**, *6*, e1000986. doi:10.1371/journal.ppat.1000986.
- Wang, H.C.; Huang, W.; Lai, M.D.; Su, I.J. Hepatitis B virus pre-S mutants, endoplasmic reticulum stress and hepatocarcinogenesis. *Cancer Sci.* **2006**, *97*, 683-688. doi:10.1111/j.1349-7006.2006.00235.x.
- Wang, X.; Li, Y.; Mao, A.; Li, C.; Li, Y.; Tien, P. Hepatitis B virus X protein suppresses virus-triggered IRF3 activation and IFN-beta induction by disrupting the VISA-associated complex. *Cell Mol. Immunol.* **2010**, *7*, 341-348. doi:10.1038/cmi.2010.36.

- Wei, L.; Ploss, A. Hepatitis B virus cccDNA is formed through distinct repair processes of each strand. *Nat. Commun.* **2021**, *12*, 1591. doi:10.1038/s41467-021-21850-9.
- Wei, L.; Ploss, A. Mechanism of Hepatitis B Virus cccDNA Formation. *Viruses* **2021**, *13*. doi:10.3390/v13081463.
- Wei, L.; Ploss, A. Core components of DNA lagging strand synthesis machinery are essential for hepatitis B virus cccDNA formation. *Nat. Microbiol.* **2020**, doi:10.1038/s41564-020-0678-0.
- Wei, X.; Xiang, T.; Ren, G.; Tan, C.; Liu, R.; Xu, X.; Wu, Z. miR-101 is down-regulated by the hepatitis B virus x protein and induces aberrant DNA methylation by targeting DNA methyltransferase 3A. *Cell Signal* **2013**, *25*, 439-446. doi:10.1016/j.cellsig.2012.10.013.
- Wei, Y.; Tavis, J.E.; Ganem, D. Relationship between viral DNA synthesis and virion envelopment in hepatitis B viruses. *J. Virol.* **1996**, *70*, 6455-6458.
- Wen, W.; Su, W.; Tang, H.; Le, W.; Zhang, X.; Zheng, Y.; Liu, X.; Xie, L.; Li, J.; Ye, J.; Dong, L.; Cui, X.; Miao, Y.; Wang, D.; Dong, J.; Xiao, C.; Chen, W.; Wang, H. Immune cell profiling of COVID-19 patients in the recovery stage by single-cell sequencing. *Cell Discovery* **2020**, *6*, 31. DOI: 10.1038/s41421-020-0168-9
- Wettengel, J.; Burwitz, B.J. Innovative HBV animal models based on the entry receptor NTCP. *Viruses* **2020**, *12*, 828. doi:10.3390/v12080828.
- Wieland, S.; Thimme, R.; Purcell, R.H.; Chisari, F.V. Genomic analysis of the host response to hepatitis B virus infection. *Proc. Natl. Acad. Sci. U. S. A.* **2004**, *101*, 6669-6674. doi:10.1073/pnas.0401771101.
- Wilk, A.J.; Rustagi, A.; Zhao, N.Q.; Roque, J.; Martinez-Colon, G.J.; McKechnie, J.L.; Ivison, G.T.; Ranganath, T.; Vergara, R.; Hollis, T.; Simpson, L.J.; Grant, P.; Subramanian, A.; Rogers, A.J.; Blish, C.A. *Nat. Med.* **2020**, *26*, 1070–1076. doi: 10.1038/s41591-020-0944-y
- Winer, B.Y.; Gaska, J.M.; Lipkowitz, G.; Bram, Y.; Parekh, A.; Parsons, L.; Leach, R.; Jindal, R.; Cho, C.H.; Shrirao, A.; Novik, E.; Schwartz, R.E.; Ploss, A. Analysis of host responses to hepatitis B and Delta viral infections in a micro-scalable hepatic co-culture system. *Hepatology* **2020**, *71*, 14–30. doi:10.1002/hep.30815.
- Winer, B.Y.; Huang, T.S.; Pludwinski, E.; Heller, B.; Wojcik, F.; Lipkowitz, G.E.; Parekh, A.; Cho, C.; Shrirao, A.; Muir, T.W.; Novik, E.; Ploss, A. Long-term hepatitis B infection in a scalable hepatic co-culture system. *Nat. Commun.* **2017**, *8*, 125. doi:10.1038/s41467-017-00200-8.

- Witt-Kehati, D.; Alaluf, M.B.; Shlomai, A. Advances and challenges in studying hepatitis B virus in vitro. *Viruses* **2016**, *8*, 21. doi:10.3390/v8010021.
- Wittkop, L.; Schwarz, A.; Cassany, A.; Grun-Bernhard, S.; Delaleau, M.; Rabe, B.; Cazenave, C.; Gerlich, W.; Glebe, D.; Kann, M. Inhibition of protein kinase C phosphorylation of hepatitis B virus capsids inhibits virion formation and causes intracellular capsid accumulation. *Cell Microbiol.* **2010**, *12*, 962-975. doi:10.1111/j.1462-5822.2010.01444.x.
- Wooddell, C.I.; Yuen, M.F.; Chan, H.L.; Gish, R.G.; Locarnini, S.A.; Chavez, D.; Ferrari, C.; Given, B.D.; Hamilton, J.; Kanner, S.B.; Lai, C.L.; Lau, J.Y.N.; Schlupe, T.; Xu, Z.; Lanford, R.E.; Lewis, D.L. RNAi-based treatment of chronically infected patients and chimpanzees reveals that integrated hepatitis B virus DNA is a source of HBsAg. *Sci. Transl. Med.* **2017**, *9*. doi:10.1126/scitranslmed.aan0241.
- World Health Organization (WHO). *Combating Hepatitis B and C to reach elimination by 2030: Advocacy brief.* **2016**. <https://apps.who.int/iris/handle/10665/206453>
- World Health Organization (WHO). Global Health Sector Strategy on Viral Hepatitis 2016-2021, Towards ending viral hepatitis. **2016**. <https://apps.who.int/iris/handle/10665/246177>
- World Health Organization (WHO). *Hepatitis B Fact Sheets*. July 27, **2021**. [https://www.who.int/news-room/fact-sheets/detail/hepatitis-b#:~:text=WHO%20estimates%20that%20296%20million,carcinoma%20\(primary%20live](https://www.who.int/news-room/fact-sheets/detail/hepatitis-b#:~:text=WHO%20estimates%20that%20296%20million,carcinoma%20(primary%20live)
- World Health Organization (WHO). *HIV/AIDS Fact Sheets*. November 30, **2021**. <https://www.who.int/news-room/fact-sheets/detail/hiv-aids> (Accessed February 10, 2022).
- Wu, J.; Meng, Z.; Jiang, M.; Pei, R.; Trippler, M.; Broering, R.; Bucchi, A.; Sowa, J.P.; Dittmer, U.; Yang, D.; Roggendorf, M.; Gerken, G.; Lu, M.; Schlaak, J.F. Hepatitis B virus suppresses toll-like receptor-mediated innate immune responses in murine parenchymal and nonparenchymal liver cells. *Hepatology* **2009**, *49*, 1132-1140. doi:10.1002/hep.22751.
- Wu, S.; Kanda, T.; Nakamoto, S.; Jiang, X.; Nakamura, M.; Sasaki, R.; Haga, Y.; Shirasawa, H.; Yokosuka, O. Cooperative effects of hepatitis B virus and TNF may play important roles in the activation of metabolic pathways through the activation of NF-kappaB. *Int. J. Mol. Med.* **2016**, *38*, 475-481. doi:10.3892/ijmm.2016.2643.
- Wu, Z.J.; Zhu, Y.; Huang, D.R.; Wang, Z.Q. Constructing the HBV-human protein interaction network to understand the relationship between HBV and hepatocellular carcinoma. *J. Exp. Clin. Cancer Res.* **2010**, *29*, 146. doi:10.1186/1756-9966-29-146.

- Wynne, S.A.; Crowther, R.A.; Leslie, A.G. The crystal structure of the human hepatitis B virus capsid. *Mol. Cell* **1999**, *3*, 771-780. doi:10.1016/s1097-2765(01)80009-5.
- Xia, Y.; Carpentier, A.; Cheng, X.; Block, P.D.; Zhao, Y.; Zhang, Z.; Protzer, U.; Liang, T.J. Human stem cell-derived hepatocytes as a model for hepatitis B virus infection, spreading and virus-host interactions. *J. Hepatol.* **2017**, *66*, 494-503. doi:10.1016/j.jhep.2016.10.009.
- Xiang, C.; Du, Y.; Meng, G.; Yi, L.S.; Sun, S.; Song, N.; Zhang, X.; Xiao, Y.; Wang, J.; Yi, Z.; Liu, Y.; Xie, B.; Wu, M.; Shu, J.; Sun, D.; Jia, J.; Liang, Z.; Sun, D.; Huang, Y.; Shi, Y.; Xu, J.; Lu, F.; Li, C.; Xiang, K.; Yuan, Z.; Lu, S.; Deng, H. Long-term functional maintenance of primary human hepatocytes in vitro. *Science* **2019**, *364*, 399–402. doi:10.1126/science.aau7307.
- Xu, C.; Chen, J.; Chen, X. Host innate immunity against hepatitis viruses and viral immune evasion. *Front. Microbiol.* **2021**, *12*, 740464. doi:10.3389/fmicb.2021.740464
- Xu, X.; Zhang, Q.Q.; Song, J.; Ruan, Q.Y.; Ruan, W.D.; Chen, Y.J.; Yang, J.; Zhang, X.B.; Song, Y.L.; Zhu, Z.; Yang, C.Y. A highly sensitive, accurate, and automated single-cell RNA sequencing platform with digital microfluidics. *Anal. Chem.* **2020**, *92*, 8599–8606. doi:10.1021/acs.analchem.0c01613
- Xu, Y.; Qi, Y.; Luo, J.; Yang, J.; Xie, Q.; Deng, C.; Su, N.; Wei, W.; Shi, D.; Xu, F.; Li, X.; Xu, P. Hepatitis B virus X protein stimulates proliferation, wound closure and inhibits apoptosis of Huh-7 cells via CDC42. *Int. J. Mol. Sci.* **2017**, *18*. doi:10.3390/ijms18030586.
- Yan, H.; Yang, Y.; Zhang, L.; Tang, G.; Wang, Y.; Xue, G.; Zhou, W.; Sun, S. Characterization of the genotype and integration patterns of hepatitis B virus in early- and late-onset hepatocellular carcinoma. *Hepatology* **2015**, *61*, 1821-1831. doi:10.1002/hep.27722.
- Yan, H.; Zhong, G.; Xu, G.; He, W.; Jing, Z.; Gao, Z.; Huang, Y.; Qi, Y.; Peng, B.; Wang, H.; Fu, L.; Song, M.; Chen, P.; Gao, W.; Ren, B.; Sun, Y.; Cai, T.; Feng, X.; Sui, J.; Li, W. Sodium taurocholate cotransporting polypeptide is a functional receptor for human hepatitis B and D virus. *eLife* **2012**, *1*, e00049. doi: 10.7554/eLife.00049
- Yan, R.; Zhang, Y.; Cai, D.; Liu, Y.; Cuconati, A.; Guo, H. Spinoculation enhances HBV infection in NTCP-reconstituted hepatocytes. *PLoS One* **2015**, *10*, e0129889. doi:10.1371/journal.pone.0129889.

- Yang, C.; Ruan, P.; Ou, C.; Su, J.; Cao, J.; Luo, C.; Tang, Y.; Wang, Q.; Qin, H.; Sun, W.; Li, Y. Chronic hepatitis B virus infection and occurrence of hepatocellular carcinoma in tree shrews (*Tupaia belangeri chinensis*). *Viol. J.* **2015**, *12*, 26. doi:10.1186/s12985-015-0256-x.
- Yang, W.; Summers, J. Integration of hepadnavirus DNA in infected liver: evidence for a linear precursor. *J. Virol.* **1999**, *73*, 9710-9717. doi:10.1128/JVI.73.12.9710-9717.1999.
- Yeh, C. T., Liaw, Y. F.; Ou, J. H. The arginine-rich domain of hepatitis B virus precore and core proteins contains a signal for nuclear transport. *J. Virol.* **1990**, *64*, 6141–6147.
- Yue, L.; Li, C.; Xu, M.; Wu, M.; Ding, J.; Liu, J.; Zhang, X.; Yuan, Z. probing the spatiotemporal patterns of HBV multiplication reveals novel features of its subcellular processes. *PLoS Pathog.* **2021**, *17*, e1009838. doi:10.1371/journal.ppat.1009838
- Zanini, F.; Pu, S.Y.; Bekerman, E.; Einav, S.; Quake, S.R. Single-cell transcriptional dynamics of flavivirus infection. *Elife* **2018**, *7*. doi:10.7554/eLife.32942.
- Zhang, C.; Li, J.; Cheng, Y.; Meng, F.; Song, J-W.; Fan, X.; Fan, H.; Li, J.; Fu, Y-L.; Zhou, M-J.; Hu, W.; Wang, S-Y.; Fu, Y-J.; Zhang, J-Y.; Xu, R-N.; Shi, M.; Hu, X.; Zhang, Z.; Ren, X.; Wang, F-S. Single-cell RNA sequencing reveals intrahepatic and peripheral immune characteristics related to disease phases in HBV-infected patients. *Gut* **2022**, *0*, 1-15. doi:10.1136/gutjnl-2021-325915.
- Zhang, S.; Liu, Z.; Wu, D.; Chen, L.; Xie, L. Single-Cell RNA-Seq Analysis Reveals Microenvironmental Infiltration of Plasma Cells and Hepatocytic Prognostic Markers in HCC With Cirrhosis. *Front. Oncol.* **2020**, *10*, 596318. doi:10.3389/fonc.2020.596318.
- Zhang, Z.; Trippler, M.; Real, C.I.; Werner, M.; Luo, X.; Schefczyk, S.; Kemper, T.; Anastasiou, O.E.; Ladiges, Y.; Treckmann, J.; Paul, A.; Baba, H.A.; Allweiss, L.; Dandri, M.; Gerken, G.; Wedemeyer, H.; Schlaak, J.F.; Lu, M.; Broering, R. Hepatitis B virus particles activate toll-like receptor 2 signaling initial upon infection of primary human hepatocytes. *Hepatology* **2020**, *72* (3), 829-244. doi:10.1002/hep.31112.
- Zhang, Z.H.; Trippler, M.; Real, C.I.; Werner, M.; Luo, X.F.; Schefczyk, S.; Kemper, T.; Anastasiou, O.E.; Ladiges, Y.; Treckmann, J.; Paul, A.; Baba, H.A.; Allweiss, L.; Dandri, M.; Gerken, G.; Wedemeyer, H.; Schlaak, J.F.; Lu, M.J.; Broering, R. Hepatitis B virus particles activate Toll-Like Receptor 2 signaling initially upon infection of primary human Hepatocytes. *Hepatology* **2020**, *72*, 829–844. doi: 10.1002/hep.31112

- Zhang, X.; Lu, W.; Zheng, Y.; Wang, W.; Bai, L.; Chen, L.; Feng, Y.; Zhang, Z.; Yuan, Z. In situ analysis of intrahepatic virological events in chronic hepatitis B virus infection. *J. Clin. Invest.* **2016**, *126*(3), 1079-1092. doi: 10.1172/JCI83339
- Zhao, L.H.; Liu, X.; Yan, H.X.; Li, W.Y.; Zeng, X.; Yang, Y.; Zhao, J.; Liu, S.P.; Zhuang, X.H.; Lin, C.; Qin, C.J.; Zhao, Y.; Pan, Z.Y.; Huang, G.; Liu, H.; Zhang, J.; Wang, R.Y.; Yang, Y.; Wen, W.; Lv, G.S.; Zhang, H.L.; Wu, H.; Huang, S.; Wang, M.D.; Tang, L.; Cao, H.Z.; Wang, L.; Lee, T.L.; Jiang, H.; Tan, Y.X.; Yuan, S.X.; Hou, G.J.; Tao, Q.F.; Xu, Q.G.; Zhang, X.Q.; Wu, M.C.; Xu, X.; Wang, J.; Yang, H.M.; Zhou, W.P.; Wang, H.Y. Genomic and oncogenic preference of HBV integration in hepatocellular carcinoma. *Nat. Commun.* **2016**, *7*, 12992. doi:10.1038/ncomms12992.
- Zheng, G.X.; Terry, J.M.; Belgrader, P.; Ryvkin, P.; Bent, Z.W.; Wilson, R.; Ziraldo, S.B.; Wheeler, T.D.; McDermott, G.P.; Zhu, J.; Gregory, M.T.; Shuga, J.; Montesclaros, L.; Underwood, J.G.; Masquelier, D.A.; Nishimura, S.Y.; Schnall-Levin, M.; Wyatt, P.W.; Hindson, C.M.; Bharadwaj, R.; Wong, A.; Ness, K.D.; Beppu, L.W.; Deeg, H.J.; McFarland, C.; Loeb, K.R.; Valente, W.J.; Ericson, N.G.; Stevens, E.A.; Radich, J.P.; Mikkelsen, T.S.; Hindson, B.J.; Bielas, J.H. Massively parallel digital transcriptional profiling of single cells. *Nat. Commun.* **2017** *8*, 14049. doi:10.1038/ncomms14049.
- Zhou, L.; He, R.; Fang, P.; Li, M.; Yu, H.; Wang, Q.; Yu, Y.; Wang, F.; Zhang, Y.; Chen, A.; Peng, N.; Lin, Y.; Zhang, R.; Trilling, M.; Broering, R.; Lu, M.; Zhu, Y.; Liu, S. Hepatitis B virus rigs the cellular metabolome to avoid innate immune recognition. *Nat. Commun.* **2021**, *12*, 98. doi:10.1038/s41467-020-20316-8.
- Zhou, M.; Zhao, K.; Yao, Y.; Yuan, Y.; Pei, R.; Wang, Y.; Chen, J.; Hu, X.; Zhou, Y.; Chen, X.; et al. Productive HBV infection of well-differentiated, hNTCP-expressing human hepatoma-derived (Huh7) cells. *Viol. Sin.* **2017**, *32*, 465–475. doi:10.1007/s12250-017-3983-x.
- Zhou, S.; Standring, D.N. Hepatitis B virus capsid particles are assembled from core-protein dimer precursors. *Proc. Natl. Acad. Sci. U. S. A.* **1992**, *89*, 10046-10050. doi:10.1073/pnas.89.21.10046.
- Ziegler, C.G.K.; Allon, S.J.; Nyquist, S.K.; Mbanjo, J. M.; Miao, V.N.; Tzouanas, N.; Cao, Y.M.; Yousif, A.S.; Bals, J.; Hauser, B.M.; Shalek, A.K.; Ordovas-Montanes, J.; HCA Lung Biological Network. SARS-CoV-2 receptor ACE2 is an interferon stimulated gene in human

airway epithelial cells and is detected in specific cell subsets across tissues. *Cell* **2020**, *181*, 1016–1035. DOI: 10.1016/j.cell.2020.04.035

Zlotnick, A.; Cheng, N.; Stahl, S.J.; Conway, J.F.; Steven, A.C.; Wingfield, P.T. Localization of the C terminus of the assembly domain of hepatitis B virus capsid protein: Implications for morphogenesis and organization of encapsidated RNA. *Proc. Natl. Acad. Sci. U. S. A.* **1997**, *94*, 9556–9561. doi: 10.1073/pnas.94.18.9556

Zoulim, F.; Seeger, C. Reverse transcription in hepatitis B viruses is primed by a tyrosine residue of the polymerase. *J. Virol.* **1994**, *68*, 6-13. doi: 10.1128/JVI.68.1.6-13.1994

Appendix A. Example script (Seurat code) used for scRNA-seq data analysis

```
library(Seurat)
library(cowplot)
library(ggplot2)
library(dplyr)

# Read datasets for own data
H75HS_data <- Read10X(data.dir = "/H75HS_filepath")
NTCP75HS_data <- Read10X(data.dir = "/NTCP75HS_filepath")
MacParland_data <- load("filepath/HumanLiver.rdata")

HumanLiverSeurat_cellnames <- HumanLiverSeurat
names(cluster.ids) <- levels(HumanLiverSeurat_cellnames)
HumanLiverSeurat_cellnames <- RenameIdents(HumanLiverSeurat_cellnames, cluster.ids)
HumanLiverSeurat$celltype <- "Primary Liver"

# Set up Huh7.5 NTCP HS object
cell_line <- CreateSeuratObject(counts = H75HS_data, project = "cell_line", min.cells = 3,
min.features = 200)
cell_line$celltype <- "Huh7.5"
cell_line[["percent.KCNQ1OT1"]] <- PercentageFeatureSet(cell_line, pattern = "KCNQ1OT1")
cell_line[["percent.MT"]] <- PercentageFeatureSet(cell_line, pattern = "^MT-")
cell_line <- subset(cell_line, nFeature_RNA > 200 & percent.KCNQ1OT1 < 2 & nFeature_RNA <
7000 & nCount_RNA > 5000 & percent.MT < 25 & percent.MT > 1)
cell_line <- NormalizeData(cell_line, normalization.method = "LogNormalize", scale.factor = 10000)
cell_line <- FindVariableFeatures(cell_line, selection.method = "vst", nfeatures = 2000)

# Set up Huh7.5 NTCP HS object
ntcp_cell_line <- CreateSeuratObject(counts = NTCP75HS_data, project = "ntcp_cell_line", min.cells
= 3, min.features = 200)
ntcp_cell_line$celltype <- "Huh7.5-NTCP"
ntcp_cell_line[["percent.KCNQ1OT1"]] <- PercentageFeatureSet(ntcp_cell_line, pattern =
"KCNQ1OT1")
ntcp_cell_line[["percent.MT"]] <- PercentageFeatureSet(ntcp_cell_line, pattern = "^MT-")
ntcp_cell_line <- subset(ntcp_cell_line, nFeature_RNA > 200 & percent.KCNQ1OT1 < 2 &
nFeature_RNA < 7000 & nCount_RNA > 5000 & percent.MT < 25 & percent.MT > 1)
ntcp_cell_line <- NormalizeData(ntcp_cell_line, normalization.method = "LogNormalize", scale.factor
= 10000)
ntcp_cell_line <- FindVariableFeatures(ntcp_cell_line, selection.method = "vst", nfeatures = 2000)

# Integration
Liver_anchors <- FindIntegrationAnchors(object.list = list(ntcp_cell_line, cell_line,
HumanLiverSeurat), dims = 1:15)
Liver_combined <- IntegrateData(anchorset = Liver_anchors, dims = 1:15)

# Integrated or RNA analysis
DefaultAssay(Liver_combined) <- "integrated"
```

```

DefaultAssay(Liver_combined) <- "RNA"

# Run the standard workflow for visualization and clustering
Liver_combined <- ScaleData(Liver_combined, verbose = FALSE)
Liver_combined <- RunPCA(Liver_combined, npcs = 30, verbose = FALSE)

# Dimensional reductionality Clustering
Liver_combined <- FindNeighbors(Liver_combined, reduction = "pca", dims = 1:15)
Liver_combined <- FindClusters(Liver_combined, resolution = 0.3)
Liver_combined <- RunUMAP(Liver_combined, dims = 1:15)

Liver_combined$celltype <- factor(x = Liver_combined$celltype, levels = c("Primary
Liver", "Huh7.5", "Huh7.5-NTCP"))

DimPlot(Liver_combined, reduction = "umap", label.size = 7.5, cols =
c("lightpink", "maroon", "orange", "yellow", "yellowgreen", "green", "green4", "cyan", "blue", "purple", "ma
genta", "red", "gold", "midnightblue")) +
  theme(text = element_text(size = 20), axis.text = element_blank())

DimPlot(Liver_combined, reduction = "umap", label.size = 10, label = T, pt.size = 0.5) +
  theme(text = element_text(size=15), legend.text = element_text(size=20), axis.text =
element_blank())+
  guides(colour = guide_legend(override.aes = list(size=5)))

DimPlot(Liver_combined, reduction = "umap", label.size = 7.5, pt.size = 0.5, group.by = "celltype") +
  theme(text = element_text(size = 15), axis.text = element_blank(), legend.text =
element_text(size=20), legend.position = c(.6,.85))+
  guides(colour = guide_legend(override.aes = list(size=5)))

# Macparland zonation markers
#Cluster 3 (innermost, pericentral)
FeaturePlot(Liv_combined_Hep, features = c("BCHE", "G6PC", "GHR",
"ALDH6A1", "RCAN1", "AR", "RP4-710M16.2", "LINC00261", "PLIN1", "RP11-390F4.3"), min.cutoff
= "q1")
Hepato.3.gene.set <- list(c("BCHE", "G6PC", "GHR", "ALDH6A1", "RCAN1", "AR", "RP4-
710M16.2", "LINC00261", "PLIN1", "RP11-390F4.3"))
Liv_combined_Hep <- AddModuleScore(object = Liv_combined_Hep, features =
Hepato.3.gene.set, assay = 'RNA', name = 'Pericentral.Score')
FeaturePlot(Liv_combined_Hep, features = c("Pericentral.Score1"), min.cutoff = "q1", label = T,
label.size = 7.5)+
  theme(text = element_text(size=15), axis.text = element_blank())+ labs(title = "Pericentral Score")
VlnPlot(Liv_combined_Hep, features = "Pericentral.Score1")+ labs(title = "Pericentral Score", x=
"Cluster")+
  theme(legend.text = element_text(size=30), title = (element_text(size=30)), axis.text =
(element_text(size=30)))+
  guides(colour = guide_legend(override.aes = list(size=10)))

```

```

#Cluster 1, 6, and 15 midcentral genes combined
FeaturePlot(Liv_combined_Hep, features = c("HSD11B1", "HAMP",
"APOM", "G6PC", "G0S2", "PON3", "TTC36", "GOLT1A", "RCAN1", "AQP9", "HPR", "AKR1C1", "NNT",
", "APOA5", "TTR", "ACADM"), min.cutoff = "q1")
Hepato.midcentral.gene.set <- list(c("HSD11B1", "HAMP",
"APOM", "G6PC", "G0S2", "PON3", "TTC36", "GOLT1A", "RCAN1", "AQP9", "HPR", "AKR1C1", "NNT",
", "APOA5", "TTR", "ACADM"))
Liv_combined_Hep <- AddModuleScore(object = Liv_combined_Hep, features =
Hepato.midcentral.gene.set, assay = 'RNA', name = 'Midcentral.Score')
FeaturePlot(Liv_combined_Hep, features = c("Midcentral.Score1"), min.cutoff = "q1", label = T,
label.size = 7.5)+
  theme(text = element_text(size=15), axis.text = element_blank()+ labs(title = "Midcentral Score"))
VlnPlot(Liv_combined_Hep, features = "Midcentral.Score1")+ labs(title = "Midcentral Score", x=
"Cluster")+
  theme(legend.text = element_text(size=30), title = (element_text(size=30)), axis.text =
(element_text(size=30)))+
  guides(colour = guide_legend(override.aes = list(size=10)))

#Cluster 14
# In the integrated data, most similar to cluster 9 (midportal)
FeaturePlot(Liv_combined_Hep, features = c("CYP2A7",
"CYP3A7", "CYP2A6", "TP53INP2", "ATIC", "SERPINH1", "SAM5D5", "GRB14"), min.cutoff = "q1")
Hepato.14.gene.set <- list(c("CYP2A7",
"CYP3A7", "CYP2A6", "TP53INP2", "ATIC", "SERPINH1", "SAM5D5", "GRB14"))
Liv_combined_Hep <- AddModuleScore(object = Liv_combined_Hep, features =
Hepato.14.gene.set, assay = 'RNA', name = 'Clus14.Score')
FeaturePlot(Liv_combined_Hep, features = c("Clus14.Score1"), min.cutoff = "q1", label = T, label.size
= 7.5)+
  theme(text = element_text(size=15), axis.text = element_blank()+ labs(title = "Midportal Score"))
VlnPlot(Liv_combined_Hep, features = "Clus14.Score1")+ labs(title = "Midportal Score", x=
"Cluster")+
  theme(legend.text = element_text(size=30), title = (element_text(size=30)), axis.text =
(element_text(size=30)))+
  guides(colour = guide_legend(override.aes = list(size=10)))

#Cluster 5 (outermost, periportal)
# In the integrated data, most similar to cluster 7 (periportal)
FeaturePlot(Liv_combined_Hep, features = c("SCD", "HMGCS1",
"ACSS2", "TM7SF2", "TMEM97", "CP", "CRP", "SLPI", "C2orf82", "ACAT2", "TM4SF5", "MSMO1", "L
EPR"), min.cutoff = "q1")
Hepato.5.gene.set <- list(c("SCD", "HMGCS1",
"ACSS2", "TM7SF2", "TMEM97", "CP", "CRP", "SLPI", "C2orf82", "ACAT2", "TM4SF5", "MSMO1", "L
EPR"))
Liv_combined_Hep <- AddModuleScore(object = Liv_combined_Hep, features =
Hepato.5.gene.set, assay = 'RNA', name = 'Periportal.Score')
FeaturePlot(Liv_combined_Hep, features = c("Periportal.Score1"), min.cutoff = "q1", label = T,
label.size = 7.5)+
  theme(text = element_text(size=15), axis.text = element_blank()+ labs(title = "Periportal Score"))

```

```

VlnPlot(Liv_combined_Hep, features = "Periportal.Score1")+ labs(title = "Periportal Score", x =
"Cluster")+
  theme(legend.text = element_text(size=30), title = (element_text(size=30)), axis.text =
(element_text(size=30)))+
  guides(colour = guide_legend(override.aes = list(size=10)))

Liver_combined_cellnames <- Liver_combined
cluster.ids <- c("Hepatocytes", "T cells", "Hepatocytes", "Hep-like", "MonoMac", "LSECs",
  "Hep-Cholangio-like", "Hepatocytes", "B cells", "Hepatocytes", "B cells",
  "Cholangiocytes", "T cells", "Erythroid")
names(cluster.ids) <- levels(Liver_combined_cellnames)
Liver_combined_cellnames <- RenameIdents(Liver_combined_cellnames, cluster.ids)
my_levels2 <- c("Hepatocytes", "Hep-like", "Hep-Cholangio-like", "Cholangiocytes", "LSECs",
  "MonoMac", "T cells", "B cells", "Erythroid")
Liver_combined_cellnames@active.ident <- factor(x=Liver_combined_cellnames@active.ident, levels
= my_levels2)
Liver_combined_cellnames[["orig.ident"]] <- Liver_combined_cellnames@active.ident
DimPlot(Liver_combined_cellnames, reduction = "umap", label = T, pt.size = 0.5, label.size = 10,
cols=c("lightcoral", "lightseagreen", "green", "green4", "cyan", "blue", "purple", "magenta", "red", "gold", "m
idnightblue")) +
  theme(legend.text = element_text(size=30), axis.title = (element_text(size=30)), axis.text =
(element_blank()))+
  guides(colour = guide_legend(override.aes = list(size=10)))
DimPlot(Liver_combined_cellnames, reduction = "umap", pt.size = 0.5, split.by = "celltype", cols =
c("lightcoral", "lightseagreen", "green", "green4", "cyan", "blue", "purple", "magenta", "red", "gold", "midnig
htblue")) +
  theme(text = element_text(size=30), legend.text = element_text(size=30), axis.title =
(element_text(size=30)), axis.text = (element_blank()))+
  guides(colour = guide_legend(override.aes = list(size=10)))

#All hepatocyte markers
FeaturePlot(Liver_combined, features = c("ALB", "AFP", "APOE", "ARG1", "HAMP",
"PCK1", "EPCAM", "HNF4A", "CYP2C8", "CYP2E1", "CYP3A4", "KRT8", "LBP",
"HPR", "SERPINA10", "SERPINA1", "ORM1", "SPINK1", "CYP2A7", "MLXIPL"), min.cutoff = "q1")
Hepatocyte.gene.set <- list(c("ALB", "AFP", "APOE", "ARG1", "HAMP", "PCK1", "EPCAM",
"HNF4A", "CYP1A1", "CYP2C8", "CYP2E1", "CYP3A4", "KRT8", "SPP1", "SLC22A10", "FETUB",
"LBP", "HPR", "LECT2", "SERPINA10", "SERPINA1", "ORM1", "SPINK1", "CYP2A7", "MLXIPL"))
Liver_combined <- AddModuleScore(object = Liver_combined, features = Hepatocyte.gene.set, assay =
'RNA', name = 'Hepatocyte.Score')
FeaturePlot(Liver_combined, features = c("Hepatocyte.Score1"), split.by = "celltype", min.cutoff =
"q1", label = T, label.size = 7.5)
FeaturePlot(Liver_combined, features = c("Hepatocyte.Score1"), split.by = "celltype", min.cutoff =
"q1", cols = vir)
FeaturePlot(Liver_combined, features = c("Hepatocyte.Score1"))
FeaturePlot(Liver_combined, features = c("Hepatocyte.Score1"), cols = vir)
FeaturePlot(Liver_combined, features = c("ALB"), split.by = "celltype", min.cutoff = "q5")
VlnPlot(Liver_combined, features = "Hepatocyte.Score1")

```

```

FeaturePlot(Liver_combined, features = c("SLC10A1"),min.cutoff = "q1", pt.size = 0.5, label =
T,label.size = 7.5, split.by = "celltype")
VlnPlot(Liver_combined, features = "SLC10A1", group.by = "celltype")+ labs(x = "Sample")+
  theme(legend.text = element_text(size=30), title = (element_text(size=30)), axis.text =
(element_text(size=30)))+
  guides(colour = guide_legend(override.aes = list(size=10)))

#LSEC FEATURES Macparland
FeaturePlot(Liver_combined, features = c("CALCRL",
"VWF","RAMP2","IFI27","PECAM1","PLVAP","CLEC4M","CLEC1B","CLEC4G","FCN2","OIT3"
), min.cutoff = "q1")
LSEC.gene.set <- list(c("CALCRL",
"VWF","RAMP2","IFI27","PECAM1","PLVAP","CLEC4M","CLEC1B","CLEC4G","FCN2","OIT3"
))
Liver_combined <- AddModuleScore(object = Liver_combined,features = LSEC.gene.set,assay =
'RNA',name = 'LSEC.Score')
FeaturePlot(Liver_combined, features = c("LSEC.Score1"), split.by = "celltype", min.cutoff = "q1",
label = T, label.size = 7.5)
FeaturePlot(Liver_combined, features = c("LSEC.Score1"), min.cutoff = "q1")
FeaturePlot(Liver_combined, features = c("RAMP2"), split.by = "celltype", min.cutoff = "q1")
patchwork::wrap_plots(FeaturePlot(Liver_combined, features="LSEC.Score1", split.by = "celltype",
label = T, label.size = 7.5, combine=FALSE), ncol = 3) &
  theme_classic()+theme(axis.title = element_text(size = 20), plot.title = element_blank(),axis.text =
element_blank(),axis.title.y.right = element_blank(),legend.position = "none") &
scale_color_gradient(low = "gray", high = "blue", limits = c(0,3))

#Kupffer cell features Macparland
FeaturePlot(Liver_combined, features = c("CD68", "VCAN","CXCL8","MARCO"), min.cutoff =
"q9")
FeaturePlot(Liver_combined, features = c("C1QA","C1QB","HLA-
DRA","S100A8","CD5L","VCAM1","CETP"), min.cutoff = "q1")
MoMac.gene.set <- list(c("C1QA","C1QB","HLA-DRA","S100A8","CD5L","VCAM1","CETP"))
Liver_combined <- AddModuleScore(object = Liver_combined,features = MoMac.gene.set,assay =
'RNA',name = 'MoMac.Score')
patchwork::wrap_plots(FeaturePlot(Liver_combined, features="MoMac.Score1", split.by = "celltype",
label = T, label.size = 7.5, combine=FALSE), ncol = 3) &
  theme_classic()+theme(axis.title = element_text(size = 20), plot.title = element_blank(),axis.text =
element_blank(),axis.title.y.right = element_blank(),legend.position = "none") &
scale_color_gradient(low = "gray", high = "blue", limits = c(0,3))

#Lymphocyte features Macparland
FeaturePlot(Liver_combined, features = c("CD3D", "CD8A", "PTPRC",
"CD37","LTB","CD3E","CD79A","IGHG1","IGHG3","GZMA","KLRB1","NKG7","CD7","CCL5","I
GLL5","FCRL5","TNFRSF17","DERL3","JCHAIN","MZB1"),min.cutoff = "q1")
FeaturePlot(Liver_combined, features = c("CD79A", "CD79B", "MS4A1",
"LTB","CD52","IGHD","JCHAIN","MZB1"),min.cutoff = "q1")

```

```

Lymphocyte.gene.set <- list(c("CD3D", "CD8A", "PTPRC",
"CD37", "LTB", "CD3E", "CD79A", "IGHG1", "IGHG3", "GZMA", "KLRB1", "NKG7", "CD7", "CCL5", "IGLL5", "FCRL5", "TNFRSF17", "DERL3", "JCHAIN", "MZB1"))
Liver_combined <- AddModuleScore(object = Liver_combined, features = Lymphocyte.gene.set, assay = 'RNA', name = 'Lymphocyte.Score')
VlnPlot(Liver_combined, features = "Lymphocyte.Score1")
patchwork::wrap_plots(FeaturePlot(Liver_combined, features="Lymphocyte.Score1", split.by = "celltype", label = T, label.size = 7.5, combine=FALSE), ncol = 3) &
  theme_classic()+theme(axis.title = element_text(size = 20), plot.title = element_blank(), axis.text = element_blank(), axis.title.y.right = element_blank(), legend.position = "none") &
  scale_color_gradient(low = "gray", high = "blue", limits = c(0,3))

#Bcell markers
FeaturePlot(Liver_combined, features = c("CD19", "IGHD", "MS4A1", "CD22", "IGLC2", "IGHG1", "IGHG2", "IGHG3", "IGHGP", "IGLC3", "JCHAIN", "IGHA1", "IGHG4", "IGHA2", "IGHM", "CD79A"), min.cutoff = "q1")
Bcell.gene.set <- list(c("CD19", "IGHD", "MS4A1", "CD22", "IGLC2", "IGHG1", "IGHG2", "IGHG3", "IGHGP", "IGLC3", "JCHAIN", "IGHA1", "IGHG4", "IGHA2", "IGHM", "CD79A"))
Liver_combined <- AddModuleScore(object = Liver_combined, features = Bcell.gene.set, assay = 'RNA', name = 'Bcell.Score')
FeaturePlot(Liver_combined, features = c("Bcell.Score1"), split.by = "celltype", min.cutoff = "q1", label = T, label.size = 7.5)
VlnPlot(Liver_combined, features = "Bcell.Score1")+ labs(title = "B cell Score", x = "Cluster") +
  theme(legend.text = element_text(size=30), title = (element_text(size=30)), axis.text = (element_text(size=30)))+
  guides(colour = guide_legend(override.aes = list(size=10)))
patchwork::wrap_plots(FeaturePlot(Liver_combined, features="Bcell.Score1", split.by = "celltype", label = T, label.size = 7.5, combine=FALSE), ncol = 3) &
  theme_classic()+theme(axis.title = element_text(size = 20), plot.title = element_blank(), axis.text = element_blank(), axis.title.y.right = element_blank(), legend.position = "none") &
  scale_color_gradient(low = "gray", high = "blue", limits = c(0,6))

#Tcell markers
FeaturePlot(Liver_combined, features = c('CD2', 'CD3D', 'TRAC', 'GZMK', 'CCL5', 'PRF1', 'TRBC1', 'TRBC2', 'GZMA', 'CD8A', 'CD69', 'IL7R', 'DUSP2', 'IFNG', 'NKG7', 'KLRB1'), min.cutoff = "q1")
Tcell.gene.set <- list(c('CD2', 'CD3D', 'TRAC', 'GZMK', 'CCL5', 'PRF1', 'TRBC1', 'TRBC2', 'GZMA', 'CD3E', 'CD69', 'IL7R', 'DUSP2', 'IFNG', 'NKG7', 'KLRB1', 'CD8A', 'CD4'))
Liver_combined <- AddModuleScore(object = Liver_combined, features = Tcell.gene.set, assay = 'RNA', name = 'Tcell.Score')
FeaturePlot(Liver_combined, features = c("Tcell.Score1"), min.cutoff = "q1", label = T, label.size = 7.5)
VlnPlot(Liver_combined, features = "Tcell.Score1")+ labs(title = "T cell Score", x = "Cluster") +
  theme(legend.text = element_text(size=30), title = (element_text(size=30)), axis.text = (element_text(size=30)))+
  guides(colour = guide_legend(override.aes = list(size=10)))
patchwork::wrap_plots(FeaturePlot(Liver_combined, features="Tcell.Score1", split.by = "celltype", label = T, label.size = 7.5, combine=FALSE), ncol = 3) &

```

```

theme_classic()+theme(axis.title = element_text(size = 20), plot.title = element_blank(),axis.text =
element_blank(),axis.title.y.right = element_blank(),legend.position = "none") &
scale_color_gradient(low = "gray", high = "blue", limits = c(0,5))

```

```

#Cholangiocyte markers

```

```

FeaturePlot(Liver_combined, features = c("KRT19", "FXYD2", "CLDN4",
"CLDN10","MMP7","CXCL1","CFTR","KRT7"),min.cutoff = "q1")
Cholangiocyte.gene.set <- list(c("KRT19", "FXYD2", "CLDN4",
"CLDN10","MMP7","CXCL1","CFTR","KRT7"))
Liver_combined <- AddModuleScore(object = Liver_combined,features =
Cholangiocyte.gene.set,assay = 'RNA',name = 'Cholangiocyte.Score')
VlnPlot(Liver_combined, features ="Cholangiocyte.Score1") + labs(title = "Cholangiocyte Score", x =
"Cluster") +
  theme(legend.text = element_text(size=30), title = (element_text(size=30)), axis.text =
(element_text(size=30)))+
  guides(colour = guide_legend(override.aes = list(size=10)))
patchwork::wrap_plots(FeaturePlot(Liver_combined, features="Cholangiocyte.Score1", split.by =
"celltype", label = T, label.size = 7.5, combine=FALSE), ncol = 3) &
  theme_classic()+theme(axis.title = element_text(size = 20), plot.title = element_blank(),axis.text =
element_blank(),axis.title.y.right = element_blank(),legend.position = "none") &
  scale_color_gradient(low = "gray", high = "blue", limits = c(0,1))

```

```

#Stellate markers

```

```

FeaturePlot(Liver_combined, features = c("ACTA2", "COL1A1", "COL1A2",
"COL3A1","DCN","MYL9"),min.cutoff = "q1")
Stellate.gene.set <- list(c("ACTA2", "COL1A1", "COL1A2", "COL3A1","DCN","MYL9"))
Liver_combined <- AddModuleScore(object = Liver_combined,features = Stellate.gene.set,assay =
'RNA',name = 'Stellate.Score')
FeaturePlot(Liver_combined, features = c("Stellate.Score1"), min.cutoff = "q1", label = T, label.size =
7.5)+
  theme(text = element_text(size=15), axis.text = element_blank())+ labs(title = "Stellate Score")
VlnPlot(Liver_combined, features ="Stellate.Score1") + labs(title = "Stellate Score", x = "Cluster")+
  theme(legend.text = element_text(size=30), title = (element_text(size=30)), axis.text =
(element_text(size=30)))+
  guides(colour = guide_legend(override.aes = list(size=10)))

```

```

#Erythroid features Macparland

```

```

FeaturePlot(Liver_combined, features = c("HBB", "SLC25A37", "CA1", "ALAS2"), min.cutoff =
"q9")
Erythroid.gene.set <- list(c("HBB", "SLC25A37", "CA1", "ALAS2"))
Liver_combined <- AddModuleScore(object = Liver_combined,features = Erythroid.gene.set,assay =
'RNA',name = 'Erythroid.Score')
VlnPlot(Liver_combined, features ="Erythroid.Score1")+ labs(title = "Erythroid Score", x = "Cluster")
+
  theme(legend.text = element_text(size=30), title = (element_text(size=30)), axis.text =
(element_text(size=30)))+
  guides(colour = guide_legend(override.aes = list(size=10)))

```

```

patchwork::wrap_plots(FeaturePlot(Liver_combined, features="Erythroid.Score1", split.by =
"celltype", label = T, label.size = 7.5, combine=FALSE), ncol = 3) &
  theme_classic()+theme(axis.title = element_text(size = 20), plot.title = element_blank(),axis.text =
element_blank(),axis.title.y.right = element_blank(),legend.position = "none") &
  scale_color_gradient(low = "gray", high = "blue", limits = c(0,15))

#Cell cycle
s.genes <- cc.genes$s.genes
g2m.genes <- cc.genes$g2m.genes
Liver_combined_cellcycle <- CellCycleScoring(Liver_combined, s.features = s.genes, g2m.features =
g2m.genes, set.ident = TRUE)
Liver_combined_cellcycle <- RunPCA(Liver_combined_cellcycle, features = c(s.genes, g2m.genes))
DimPlot(Liver_combined_cellcycle, split.by = "celltype") + theme(text = element_text(size = 20))
DimPlot(Liver_combined_cellcycle) + theme(text = element_text(size = 20))

#DEG analysis
Liver_combined.markers <- FindAllMarkers(Liver_combined, min.pct = 0.25, logfc.threshold = 0.25)
Top_ten_Liver_combined <- Liver_combined.markers %>% group_by(cluster) %>% top_n(n = 10, wt
= avg_logFC)
View(Top_ten_Liver_combined)

#saveRDS(Liver_combined, file="/ Liver_combined.Rds")
#Liver_combined <- readRDS("/Liver_combined.Rds")
write.xlsx(Liver_combined.markers, "Liver_Huh.w.wo.NTCP.DEGs.xlsx")

DoHeatmap(Liver_combined, features = Top_ten_Liver_combined$gene)
DoHeatmap(Liver_combined, features = Top_ten_Liver_combined$gene, group.by = "celltype")

Liver_combined_Hepnames.markers <- FindAllMarkers(Liver_combined_Hepnames, min.pct = 0.25,
logfc.threshold = 0.25)
write.xlsx(Liver_combined_Hepnames.markers,
"Liver_Huh.w.wo.NTCP.DEGs.all.celltype.diff.hepatocytes.xlsx")
Top_ten_Liver_combined_Hepnames <- Liver_combined_Hepnames.markers %>% group_by(cluster)
%>% top_n(n = 10, wt = avg_logFC)
DoHeatmap(Liver_combined_Hepnames, features = Top_ten_Liver_combined_Hepnames$gene,
  group.colors =
c("lightpink", "maroon", "orange", "yellow", "lightseagreen", "green", "green4", "cyan", "blue", "purple", "m
agenta", "red"))

Liver_combined_cellnames.markers <- FindAllMarkers(Liver_combined_cellnames, min.pct = 0.25,
logfc.threshold = 0.25)
write.xlsx(Liver_combined_Hepnames.markers, "Liver_Huh.w.wo.NTCP.DEGs.all.celltype.xlsx")
Top_ten_Liver_combined_cellnames <- Liver_combined_cellnames.markers %>% group_by(cluster)
%>% top_n(n = 10, wt = avg_logFC)
DoHeatmap(Liver_combined_cellnames, features = Top_ten_Liver_combined_cellnames$gene,
  group.colors =
c("lightcoral", "lightseagreen", "green", "green4", "cyan", "blue", "purple", "magenta", "red"))

```

```

Liver_6_11 <- subset(Liver_combined_Hepnames, idents = c("Hep-Cholangio-
like","Cholangiocytes"))
Liver_6_11$seurat_clusters <- factor(x = Liver_6_11$seurat_clusters, levels = c("6","11"))
Liver_6_11.markers <- FindAllMarkers(Liver_6_11, min.pct = 0.25, logfc.threshold = 0.25)
Top_ten_Liver_6_11 <- Liver_6_11.markers %>% group_by(cluster) %>% top_n(n = 10, wt =
avg_logFC)
View(Top_ten_Liver_6_11)
DoHeatmap(Liver_6_11, features = Top_ten_Liver_6_11$gene, group.colors = c("#00C094",
"#DF70F8"))+
  theme(text = element_text(size=20))
DoHeatmap(Liver_6_11, features = Top_ten_Liver_6_11$gene, group.colors = c("green","green4"))+
  theme(text = element_text(size=20))
DotPlot(Liver_combined_cellnames, features =
c("ANXA4","CD24","TM4SF4","LGALS4","SPP1","SLPI","FOS","JUN","CXCL1","PIGR")) +
RotatedAxis()+
  ylab("Celltype") + xlab("Genes")
DotPlot(Liver_combined_cellnames, features =
c("APOC1","HP","FGB","APOC3","APOA2","APOA1","MT1X","ORM","SAA1","MT2A")) +
RotatedAxis()

#Proportions of groups within clusters
Liver_combined[["clusters_Liver_combined"]] <- Liver_combined@active.ident
Cluster_diff_freq_Liver_combined <- table(Liver_combined$celltype,
Liver_combined$clusters_Liver_combined)
Cluster_diff_prop_Liver_combined <- prop.table(Cluster_diff_freq_Liver_combined, margin=2)
Cluster_diff_percent_Liver_combined <- prop.table(Cluster_diff_freq_Liver_combined,
margin=2)*100

Liver_combined$clusters_Liver_combined <- factor(x = Liver_combined$clusters_Liver_combined,
levels = c("13","12","11","10","9","8","7","6","5","4","3","2","1","0"))
Cluster_diff_freq_ident <- table(Liver_combined$clusters_Liver_combined,Liver_combined$celltype)
Cluster_diff_prop_ident <- prop.table(Cluster_diff_freq_ident, margin=2)
Cluster_diff_percent_ident <- prop.table(Cluster_diff_freq_ident, margin=2)*100

Liver_combined$clusters_Liver_combined <- factor(x = Liver_combined$clusters_Liver_combined,
levels = c("0","1","2","3","4","5","6","7","8","9","10","11","12","13"))

library(scales)
par(mfrow=c(1,1))
show_col(hue_pal()(3)) #change number based on number of orig.ident you have
show_col(hue_pal()(14)) #change number based on number of clusters you have

par(mar = c(5, 4, 4, 7),          # Specify par parameters
  xpd = TRUE)
par(mar=c(5,6,4,1)+.1)
barplot(Cluster_diff_freq_Liver_combined, main="Frequency of cells by cluster",
  xlab="Clusters", ylab="Number of cells",ylim = c(0,6000)), #change y limit based on how many
cells you have

```

```

col=c("#F8766D", "#00BA38", "#619CFF"), cex.lab=2, cex.axis = 2, cex.names = 2,
cex.main=2.5)) #change colors based on how many orig.ident you have, you find these colors from
show_col(hue_pal()(#))
legend("topright", bty="n", legend = c("Primary Liver", "Huh7.5", "Huh7.5-NTCP"), inset = c(-0.3, 0),
fill=(col=(hue_pal()(3)))) #change number based on how many orig.ident you have

```

```

barplot(Cluster_diff_percent_Liver_combined,
main="Percentage of cells by cluster",
xlab="Clusters", ylab="Percent of cells",
col=c("#F8766D", "#00BA38", "#619CFF"),
cex.lab=2, cex.axis = 2, cex.names = 2, cex.main=2.5)

```

```
#####
```

```

barplot(Cluster_diff_freq_ident, main="Frequency of cells by Condition",
xlab="Sample", ylab="Number of cells", ylim = c(0,9000),
col=c("#FF66A8", "#FB61D7", "#DF70F8", "#A58AFF", "#06A4FF", "#00B6EB", "#00BFC4", "#00C094",
"#00BC56", "#53B400", "#99A800", "#C49A00", "#E38900", "#F8766D"), #change colors based on
how many clusters you have
cex.lab=2, cex.axis = 2, cex.names = 2, cex.main=2.5)
legend("topright", bty="n", inset = c(-0.125, 0),
legend = c("0", "1", "2", "3", "4", "5", "6", "7", "8", "9", "10", "11", "12", "13"),
fill=(col=(hue_pal()(14))))

```

```

barplot(Cluster_diff_percent_ident,
main="Percentage of cells by Condition",
xlab="Sample", ylab="Percent of cells",
col=c("#FF66A8", "#FB61D7", "#DF70F8", "#A58AFF", "#06A4FF", "#00B6EB", "#00BFC4", "#00C094",
"#00BC56", "#53B400", "#99A800", "#C49A00", "#E38900", "#F8766D"),
cex.lab=2, cex.axis = 2, cex.names = 2, cex.main=2.5)
par(mar=c(5, 4, 4, 2) + 0.1) #Change back to default par parameters

```

Appendix B

Peptide Array Enabling Studies of Nuclear Localization and Export Signals of Hepatitis B Virus

1. Introduction

After HBV crosses the cell membrane and enters the cytoplasm, the virus (capsid) must traffic to the nucleus to release its genome (**Figure 1.2**). The nuclear envelope is fenestrated with nuclear pore complexes (NPCs), which control the selective permeability of this organelle membrane and regulate nuclear transport of particles larger than 60 kDa [1]. These large specialized channels are composed of an octagonal arrangement of approximately 30 distinct proteins known as nucleoporins (nups). These transport processes also rely on nuclear transport factors (NTFs), which are not attached to the NPC network but rather function as cytoplasmic or nucleoplasmic chaperones to shuttle particles through the nuclear pores. NTFs include importins and exportins involved in nuclear import and export of cargos, respectively. These chaperone proteins recognize cargo by binding to special peptide sequences called nuclear localization signals (NLSs) or nuclear export signals (NESs). Controlled nucleo-cytoplasmic transport is paramount for rapid exchange of proteins and transcripts.

The 3.2 kb HBV genome expresses five major proteins from overlapping open reading frames. Thus, the few proteins expressed by HBV must perform several functions including nuclear localization and export of viral components, host-viral interactions, organization of cccDNA processing, and more. For instance, the HBV core protein, which multimerizes to form the capsid, has an arginine rich domain (ARD) that contains 4 nuclear localization signals and resembles importin beta binding domains. However, prior literature describes inconsistent

nuclear transport functions to this HBV ARD [2-5]. Furthermore, association of core proteins with immature or mature viral DNA genomes appears to direct conformational changes and steric accessibility of the ARD [6]. Studies using microinjection, lipofection, or permeabilized cells demonstrate capsids migrating to the nucleus and subsequent nuclear release of the viral genome [5,7,8].

Because NPCs are the gateway and NTFs provide the mechanism for the nucleocytoplasmic transportation, viruses that have a nuclear phase of infection often have NLSs or NESs to mediate nuclear import and export, respectively. We hypothesize that HBV has NLSs and NESs that interact with NTFs to direct nuclear transport. The primary objective of this work is to identify putative NLS and NES sequences in all five HBV proteins. Previous work conducted in our group was successful in identifying novel functional NLS and NES sequences in hepatitis C virus (HCV) proteins and demonstrated activity at various steps in the HCV lifecycle [9]. Modelled after Dr. Levin's work [9], we describe here the design and application of a 384-spot peptide array enabling the identification of nuclear localization signal (NLS) and nuclear export signal (NES) relevant to HBV infection.

2. Materials and Methods

2.1. Peptide Arrays

Peptide sequences, selected by Dr. Levin, were spotted on peptide arrays [9] custom-made by Intavis Bioanalytical Instruments (Koeln, Germany). The configuration of a 384-spot (16×24) array and the peptide sequences on each spot are shown in **Table 1**. Each acetylated peptide (at the N-terminus) was conjugated on a specified spot of a microscope slide using a CelluSpots peptide array technology (Koeln).

Peptide arrays were incubated in Tris-buffered saline (TBS) supplemented with 0.05% Tween 20 (v/v) and 10% skim milk (g/v) overnight at 4 °C on a gentle shaker. The peptide arrays were then washed three times with TBS supplemented with 0.05% Tween 20 (v/v) for 5 min at room temperature on a gentle shaker. Duplicate peptide arrays were incubated for 4 h with either cell lysates or lysis buffer (control) at room temperature on a gentle shaker. The lysis buffer contained 10 mM Tris-HCl (pH 7.5), 150 mM NaCl, 2 mM EDTA, 0.1% Triton-X100, 1 mM phenylmethylsulfonyl fluoride (PMSF) (a protease inhibitor), 2 mg/ml aprotinin, 2 mg/ml leupeptin, and 0.1 units/ml RNasin. Following this incubation, peptide arrays were rinsed with washing buffer (TBS containing 0.05% Tween 20) for 30 s and then washed five times for 5 min in washing buffer on a gentle shaker. Following washing, the peptide arrays were incubated with the primary antibodies for 4 h at room temperature on a gentle shaker. Arrays were then rinsed, washed as described above, and incubated for 2 h at room temperature with a secondary antibody that was conjugated to horse radish peroxidase (HRP). The peptide arrays were rinsed and washed again as described above, followed by incubation with Luminol to initiate the HRP-catalyzed chemiluminescence detection (GE Healthcare, RPN2106). The peptide array was imaged using Fuji RX film (Fujifilm, 47410 08399).

2.2. Antibodies and Synthetic Peptides

Antibodies binding to importin alpha 1 (IPOA5) (Thermo Fisher PA5-21034), importin beta 1 (IPO1) (Thermo Fisher PA5-18450), importin 5 (IPO5) (Thermo Fisher PA5-30076), exportin 1 (XPO1) (Thermo Fisher PA1-083), and exportin 6 (Thermo Fisher PA5-31813) were originally available from Santa Cruz Biotechnology.

Peptides corresponding to the identified putative NLS or NES sequences (**Table 2**) were synthesized with fusions to penetratin (RQIKIWFQNRRMKWKK), a peptide that facilitates cell

uptake. These peptide sequences are listed in **Table 3**. The peptides were synthesized by GL Biochem Ltd (Shanghai, China).

2.3. HBV, Mutant HBV, and HBV Viruses Containing the Nanoluciferase (NL) Reporter

HBV inoculum was prepared using HepAD38 cells, a hepatoma cell line with a greater than genome length HBV integrand [10]. PEG 8000 was mixed with medium from HepAD38 cell cultures to a final concentration of 40% and then centrifuged at 20,000xg for 1 h at 4°C. The resulting precipitated pellet was resuspended in approximately 1/100 volume PBS and stored at -80°C until use.

Mutations were introduced into HBV expression plasmids (Addgene, Watertown, MA. <https://www.addgene.org/65459/>), creating three mutant HBV viruses. In the first mutant HBV, the entire putative NES peptide sequence (aa37-57: VAEDLN~~LG~~NLNVSIPWTHKVG) was deleted from the terminal protein region of the HBV polymerase. In the second mutant HBV, eight amino acids (aa50-57: **IPWTHKVG**) were deleted from the putative NES sequence (VAEDLN~~LG~~NLNVS**IPWTHKVG**) of the HBV polymerase. In the third mutant HBV, two leucine (L) residues in the putative NES sequence (VAED**LN**LG~~LN~~NLNVSIPWTHKVG) of the HBV polymerase were mutated to alanine (A) and glutamine (Q) (VAED**AN**Q~~GN~~NLNVSIPWTHKVG).

The nanoluciferase (NL) reporter was introduced into both the wild-type and mutant HBV viruses. Constructs for producing HBV virus containing the nanoluciferase (NL) reporter were a kind gift from Dr. K. Shimotohno (Research Center for Hepatitis and Immunology, National Center for Global Health and Medicine, Tokyo, Japan). [11] The HBV/NL plasmid encodes the HBV genome with the nanoluciferase gene in frame with the viral pre-core/core open reading frame. The HBV/NL viruses and the viruses with wild-type and mutant HBV polymerases, were used to infect HepG2-NTCP cells. Luminescence was monitored for studying early steps in HBV infection, from entry to transcription.

2.4. Cell Cultures

The Huh7.5 cells, a kind gift from Dr. Charles Rice (Rockefeller University, New York, NY, USA), were cultured in DMEM supplemented with 4% (v/v) pooled adult human serum (HS), as described in Chapter 2 [12]. The HepG2-NTCP cells were cultured in DMEM (D5796, Sigma–Aldrich) supplemented with 10% (v/v) fetal bovine serum (FBS) (Sigma–Aldrich) and $1 \times$ penicillin/streptomycin (Sigma–Aldrich). Cells were incubated at 37 °C in a 5% CO₂ incubator.

2.5. Infection of Cells with HBV

Huh7.5 and HepG2-NTCP cells were infected with HBV or its mutants at a multiplicity of infection (MOI) of 500 genome equivalents, unless otherwise stated, in the presence of 4% PEG 8000 for 18 h at 37 °C.

2.6. Assay for pgRNA, cccDNA, HBsAg, HBeAg

Methods for the analysis of pgRNA, cccDNA, HBsAg, and HBeAg were described in Chapter 2 [12, 14].

2.7. Nanoluciferase Reporter Luminescence Assay

HepG2-NTCP cells were infected with HBV/NL in the same manner as described for HBV infection. The Nano-Glo Luciferase Assay System (Promega, Madison, WI) was used according to the manufacturer's protocol to assess intra cellular nanoluciferase reporter activity. Briefly, for a 96-well plate with 100 μ L medium per well, 50 μ L of the medium were removed, leaving 50 μ L in each well. Subsequently, 50 μ L of the Nano-Glo reagent (a 1:50 solution of substrate/buffer) was added to each well and incubated for 2 min at room temperature. The contents of the wells were thoroughly mixed to lyse the cell monolayers and then the luminescence of 50 μ L of the mixture was measured on a Perkin Elmer Enspire 2300 plate reader.

3. Results and Discussion

3.1. Design of a peptide array for studying nuclear localization signal (NLS) and nuclear export signal (NES) of HBV

Our goal was to (1) determine nuclear transport signals potentially responsible for HBV infection and (2) identify inhibitory peptides as potential therapeutics. On the basis of HBV proteins and previous studies showing that nuclear transport signals are linear peptide motifs of approximately 15 amino acids (aa) in length [9], we designed our peptide arrays by conjugating 15-aa peptides on the array. The HBV peptide array that we designed displays peptides that are 15 aa in length and 9 aa overlaps with the preceding and following peptide sequences (**Figure 1**). These peptides (sequences shown in **Table 1**) encompass the complete HBV proteome, including the surface antigens (PreS1, PreS2, S), nucleocapsid core protein (Pre-core, Core), polymerase, and the X protein (**Figure 2**). Each spot on a 384-spot array (16×24) contains a peptide sequence (**Table 1**). Each peptide was acetylated at its N-terminus to allow its conjugation to the three-dimensional cellulose spots on the surface of microscope slides [9].

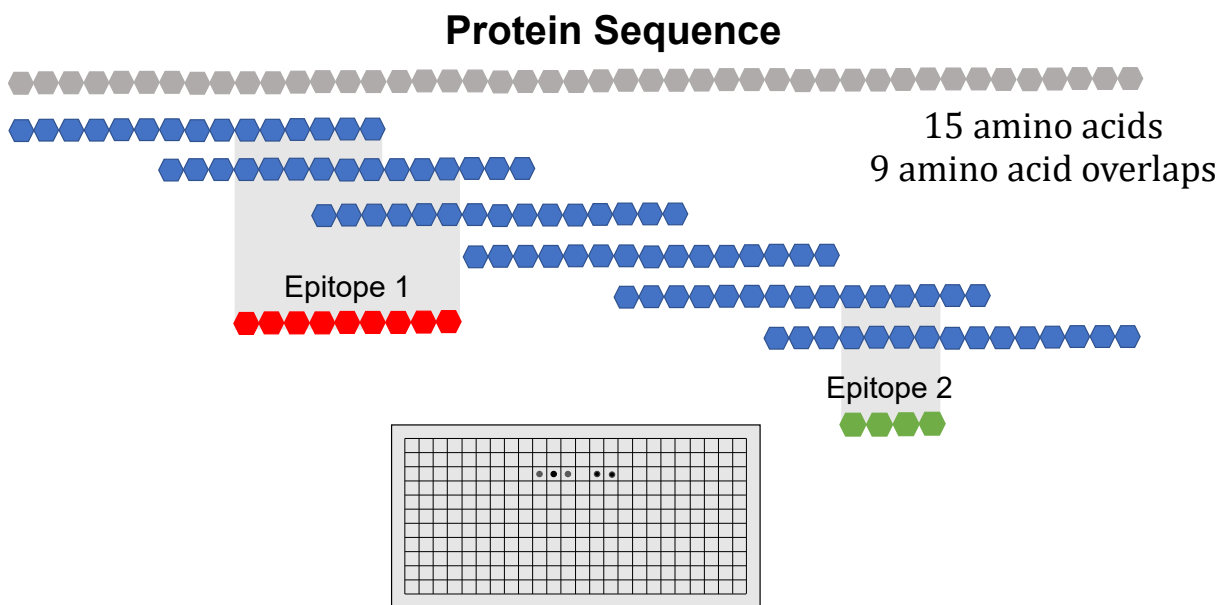


Figure 1. Schematic displaying peptides of 15 amino acid residues in length and 9 amino acid overlaps. Hypothetical positive signals on the array result from binding of epitope 1 to three peptides and binding of epitope 2 to two peptides.

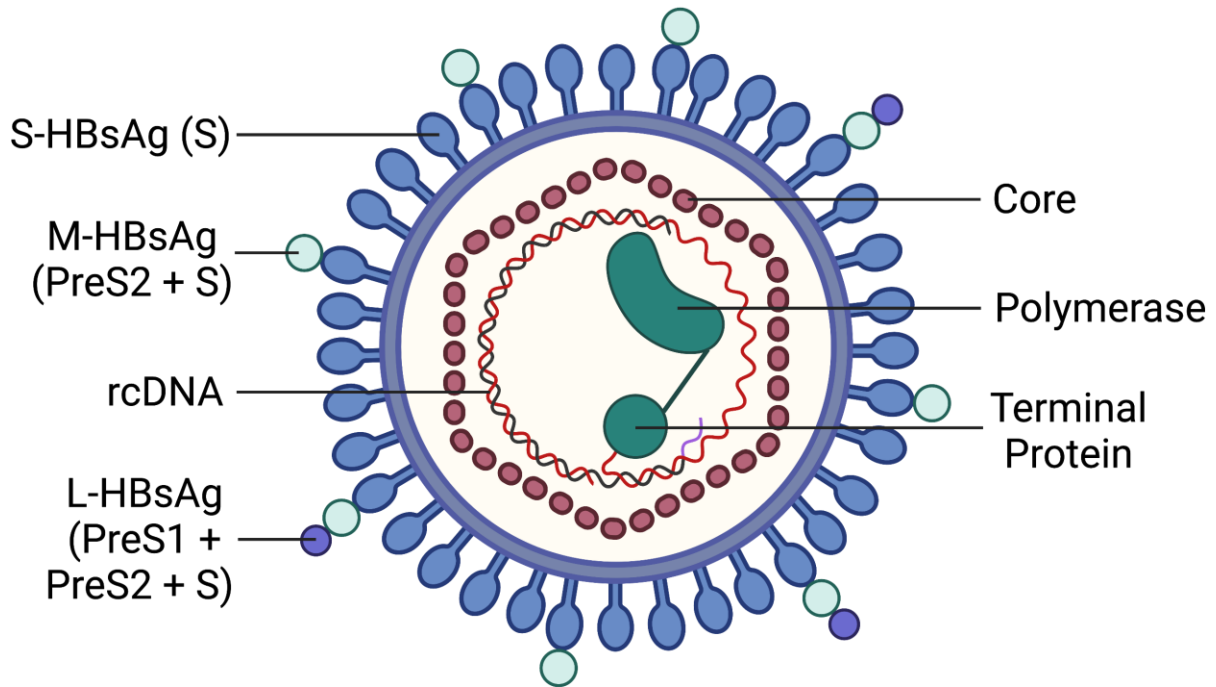


Figure 2. Schematic showing main proteins of HBV. Created using tools from BioRender.com.

3.2. Identification of putative nuclear localization signal (NLS) and nuclear export signal (NES) peptide sequences using HBV peptide arrays

Incubation of Huh7.5 cell lysates with peptide arrays allows for binding of cellular proteins to HBV peptides on the array. Probing the bound proteins using specific antibodies for importins and exportins reveals the HBV peptide spots on the array that bind to these nuclear transport proteins. Results in **Figure 3** and **Table 2** show that the Huh7.5 cellular proteins bind to at least five nuclear localization signal (NLS) peptide sequences and six nuclear export signal (NES) peptide sequences. One peptide sequence binds to both an importin and an exportin (**Table 2**).

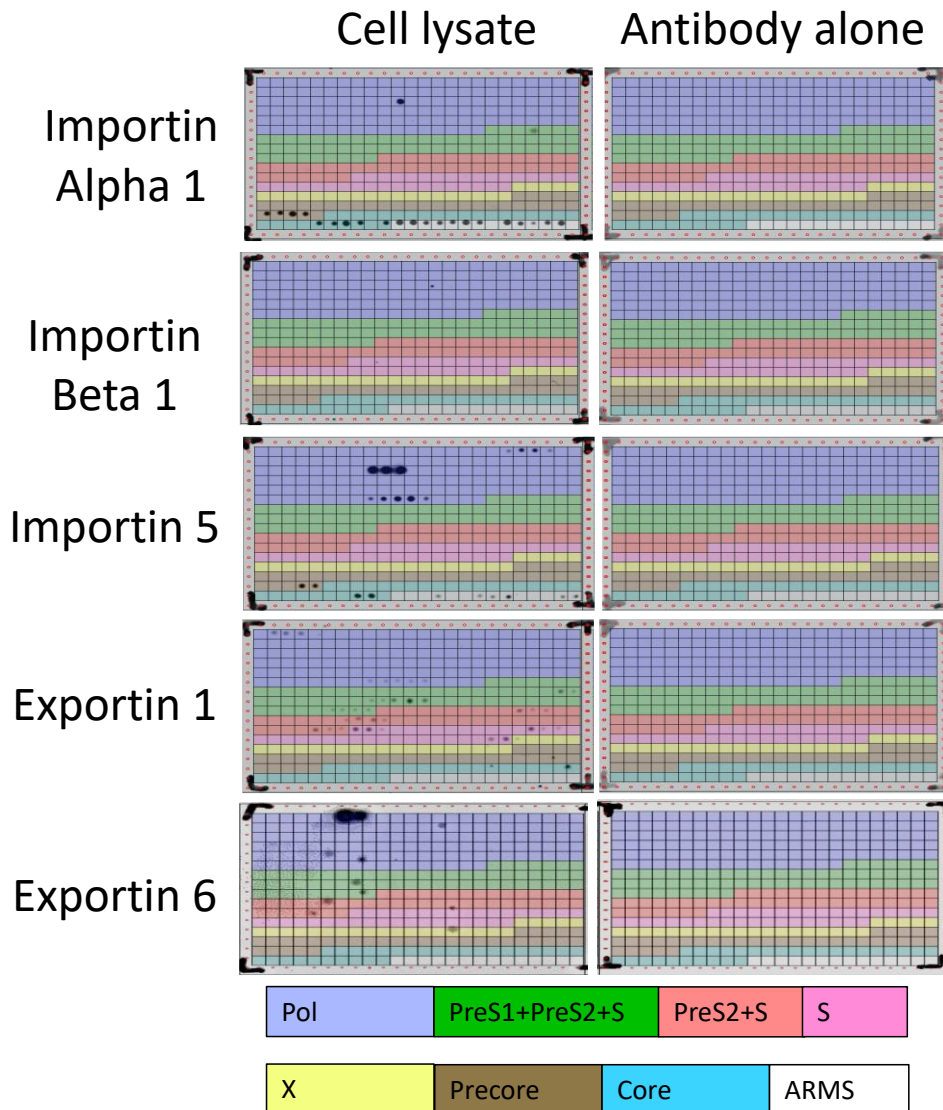


Figure 3. Identification of peptide sequences within the HBV proteome that bind nuclear import proteins (importins) and nuclear export proteins (exportins). The arrays shown on the left were incubated with Huh7.5 cell lysates. The bound proteins were probed with antibodies specific for importins and exportins. Shown here are arrays probed with antibodies for importin alpha 1, importin beta 1, importin 5, exportin 1, and exportin 6. Control peptide arrays shown on the right were not incubated with the cell lysates but were probed with the same antibodies; no signals were detected. Regions with different colors represent peptides derived from specific HBV proteins, including polymerase (pol), surface protein (PreS1, PreS2, S), Core protein (Precore and Core), and X protein. The C-terminus of the core protein contains 16 arginine residues making up four arginine-rich motifs (ARMS). The peptide sequences that bound to the importins and exportins are summarized in Table 2.

3.3. Inhibition of HBV Infection Using Synthetic Peptides of Identified Sequence

We tested whether the identified putative NLS and NES peptide sequences could inhibit HBV infection by competing with HBV proteins for importins or exportins. We incubated synthetic peptides (coupled to penetratin peptide) during HBV infection of HepG2-NTCP cells and measured pregenomic RNA (pgRNA) as well as the E antigen (HBeAg) and surface antigen (HBsAg) levels (**Figures 4, 5, and 6**). Indeed, several of the tested peptides suppressed HBV infection, the most effective of which was the synthetic peptide derived from the putative NES sequence (VAEDLNLGNLNVSIPWTHKVG) present in polymerase. The putative NES bound exportin 6 (**Figure 3**). The synthetic peptide derived from this NES sequence suppressed HBV infection of HepG2 cells, measured by reductions of pgRNA as well as the E antigen (HBeAg) and S antigen (HBsAg) levels by more than 50% (**Figures 4**).

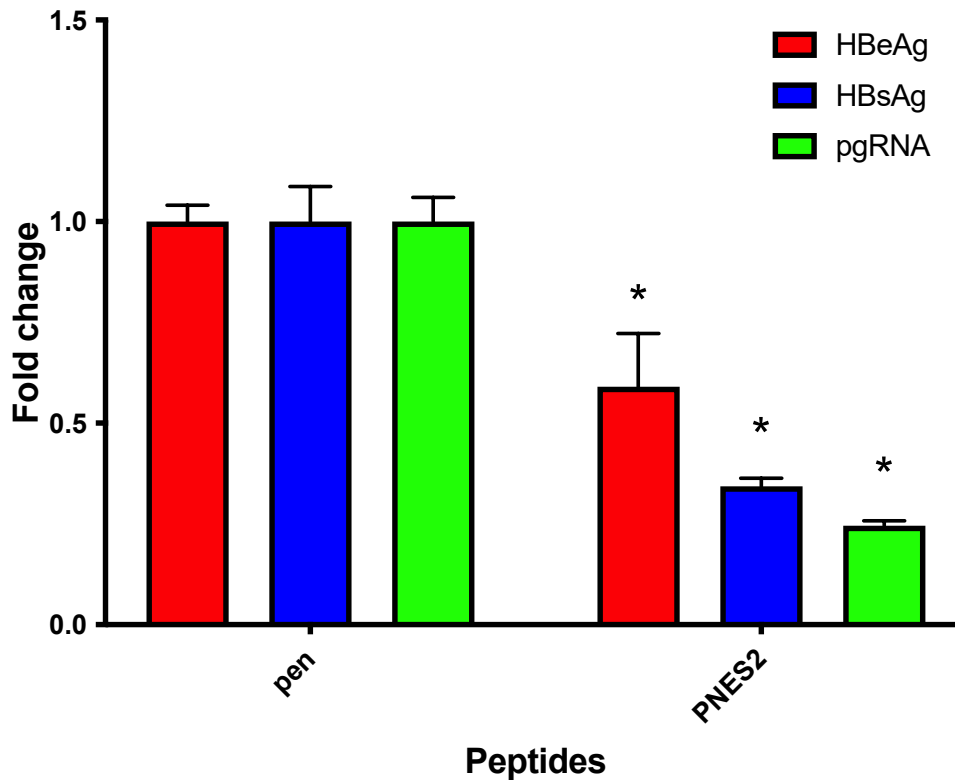


Figure 4. A synthetic peptide derived from a putative NES sequence present in polymerase protein reduced HBV infection of HepG2-NTCP cells. Normalized expression levels of the HBV E antigen (HBeAg), surface antigen (HBsAg), and pregenomic RNA (pgRNA) in HBV-infected HepG2-NTCP cells. The cells were incubated with either penetratin (RQIKIWFQNRRMKWKK) or penetratin fused to a synthetic peptide sequence (VAEDLN LGNLNVSIPWTHKVG) corresponding to the putative NES located in the HBV polymerase (PNES2). Penetratin (PEN) was used to facilitate cell uptake of the peptide. RT-qPCR was used to measure pgRNA, which was expressed as per 10 ng total RNA. The levels of HBeAg, HBsAg, and pgRNA in HepG2-NTCP cells incubated with the PNES2 synthetic peptide were each normalized against the respective levels in HepG2-NTCP cells incubated with the penetratin (PEN). One-way ANOVA was used with Bonferroni's correction for multiple-comparison test. *, $P < 0.05$. The error bars indicate standard deviation from triplicate experiments ($n=3$).

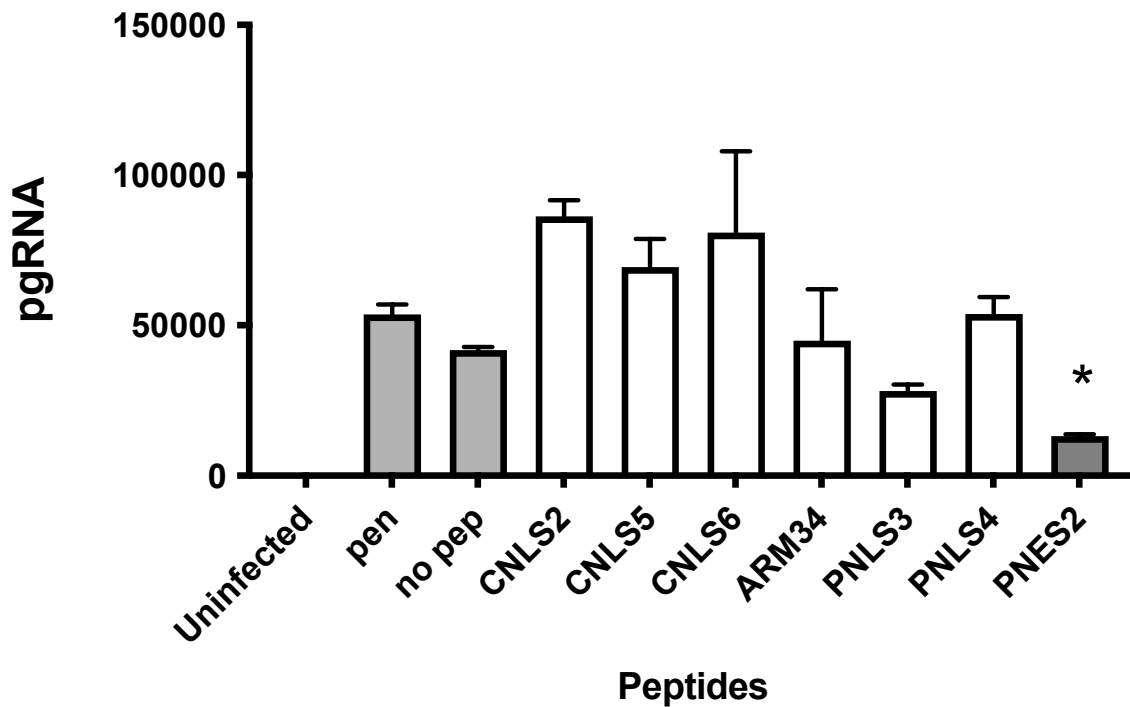


Figure 5. Changes in pregenomic RNA (pgRNA) in HBV-infected HepG2-NTCP cells after co-incubation with synthetic NLS or NES peptides from HBV core or polymerase proteins. pgRNA levels were measured using RT-qPCR, and the results were expressed as pgRNA gene equivalents per 10 ng of total RNA. The peptides identified from the array experiments were synthesized with fusions to penetratin (RQIKIWFQNRRMKWKK). Penetratin allows for cell uptake. Cells not incubated with any synthetic peptide (no pep) served as a control. One-way ANOVA was used with Bonferroni's correction for multiple-comparison test. *, $P < 0.05$. The error bars indicate standard deviation from triplicate experiments ($n=3$).

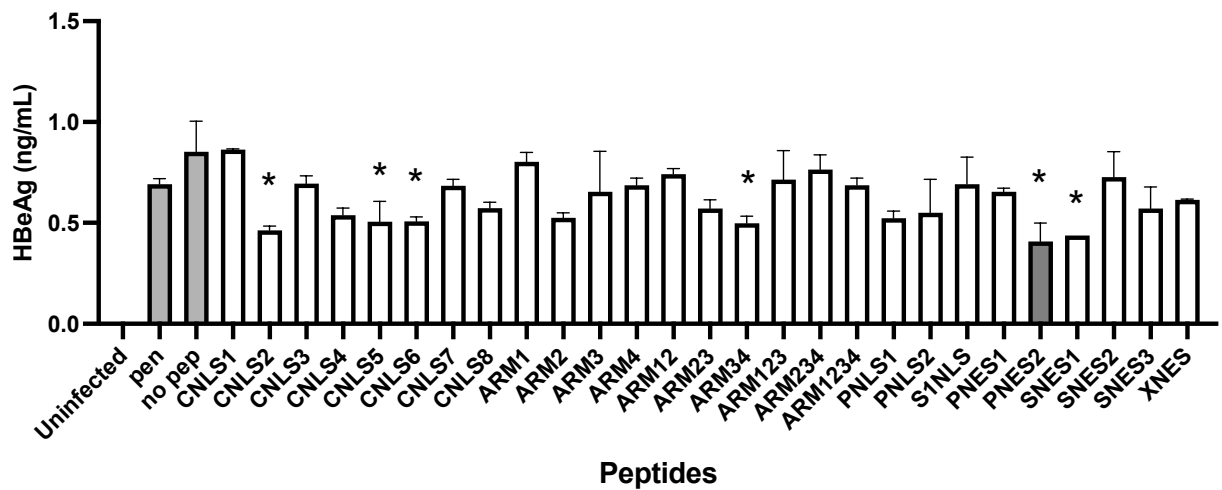
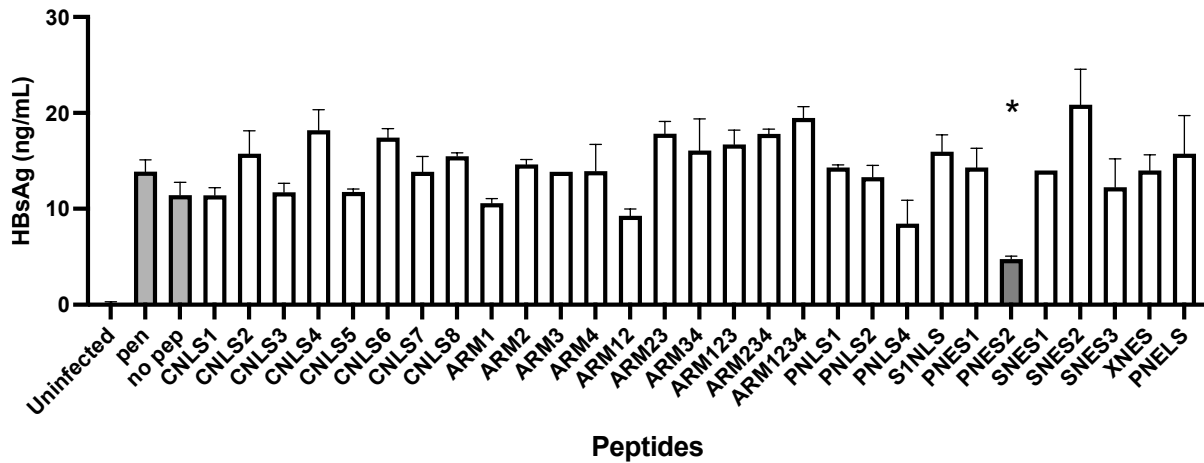


Figure 6. Changes in the E antigen (HBeAg) and surface antigen (HBsAg) levels in the medium of HBV-infected HepG2-NTCP cells after the cells were co-incubated with the synthetic peptides. ELISA was used to measure HBeAg and HBsAg levels. The peptides identified from the array experiments were synthesized with fusions to penetratin (RQIKIWFQNRRMKWKK). Penetratin allows for cell uptake. Cells not incubated with any synthetic peptide (no pep) served as a control. One-way ANOVA was used with Bonferroni's correction for multiple-comparison test. *, $P < 0.05$. The error bars indicate standard deviation from triplicate experiments ($n=3$).

3.4. Mutations to the NES sequence in the HBV polymerase attenuates HBV infection

To test the function of the putative PNES2 in the context of the whole virus, we deleted 8 amino acids from PNES2 in an HBV expression plasmid. We found that the amounts of secreted virus (3.2×10^8 genome equivalents /mL) from Huh7.5 cells transfected with the mutant HBV plasmids were lower than the amount of virus secreted (1.0×10^9 genome equivalents /mL) from Huh7.5 cells transfected with the wild-type HBV plasmid ($p=0.0038$). Thus, the partial deletion of the PNES2 sequence $\Delta(50-57\text{aa})$ (VAEDLN~~LG~~NLNVSI~~PWTHK~~VG) from the HBV polymerase attenuates the amount of viruses secreted from the HBV-infected HepG2-NTCP cells.

We used wild type and PNES2 deletion secreted viruses as infectious inocula at the same genome equivalents per cell to infect HepG2-NTCP cells. The cells infected with the PNES2 mutant HBV produced 20-fold lower levels of cccDNA and about 2/3 the level of pgRNA (Figure 7).

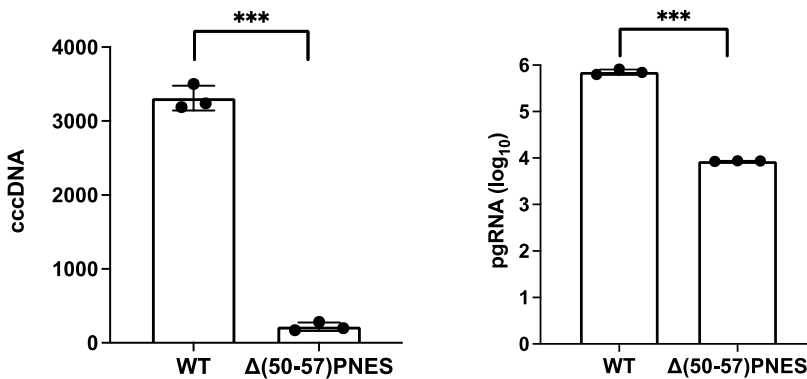


Figure 7. Partial deletion of the PNES2 sequence $\Delta(50-57\text{aa})$ (VAEDLN~~LG~~NLNVSI~~PWTHK~~VG) from the HBV polymerase attenuates HBV infection. Covalently closed circular DNA (cccDNA) levels were measured using PCR, and were expressed as cccDNA copies per 10 ng total genomic DNA (gDNA). pgRNA levels were measured using RT-qPCR, and the results (logarithmic scale) were expressed as pgRNA gene equivalents per 10 ng of total RNA. HepG2-NTCP cells were infected with wildtype (WT) or mutant HBV. The error bars indicate standard deviation, and the differences are statistically significant (two-tailed unpaired t test, $n=3$, $p<0.001$)

The cells infected with the NES mutant HBV/NL virus generated significantly lower luminescence than the cells infected with the wild-type HBV/NL virus (**Figure 8**).

Complementing the measures of cccDNA and pgRNA (**Figure 7**), the luciferase assay using the HBV/NL virus (**Figure 7**) gauges the early steps in HBV infection, from entry to transcription. These results consistently show that mutations of the NES sequence in the HBV polymerase attenuate the resulting HBV infection.

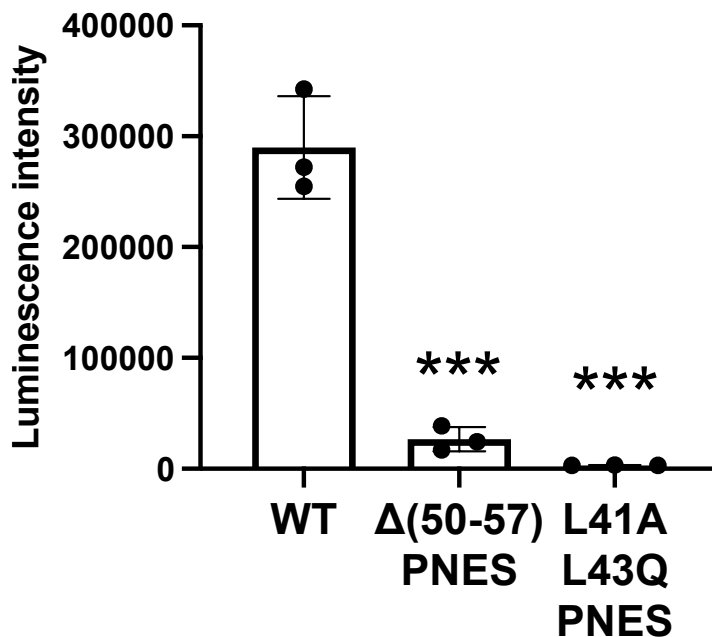


Figure 8. Partial deletion $\Delta(50-57\text{aa})$ or mutation to leucine L41A and L43Q of the PNES2 sequence (VAEDLNLGNLNVSIPWTHKVG) from the HBV polymerase attenuates HBV infection. HepG2-NTCP cells were infected with wildtype (WT) or mutant HBV/NL viruses. The mutant virus, with either partial deletion of PNES2 sequence (VAEDLNLGNLNVS) or leucine mutation to alanine and glutamine (VAEDANQGNLNVSIPWTHKVG), resulted in much lower luminescence, indicative of much lower infection, than HepG2-NTCP cells infected with the wildtype virus. Two-tailed unpaired t test. ***, $p < 0.001$. The error bars indicate standard deviation from the triplicate experiments ($n=3$), and the differences are statistically significant (two-tailed unpaired t test, $p < 0.001$).

3.5. Experiments to assess whether the putative NLS and NES are functional

To assess the function of the identified putative HBV NLS sequences, we cloned these sequences into a double GFP vector (**Figure 9**) and imaged the localization of fluorescence in transfected Huh7.5 cells (**Figure 10**) as per methods previously developed in our group [9]. As a positive control, we cloned the well characterized SV40 NLS into the double GFP vector. As expected, the double GFP (56 kDa) is large enough that it remains in the cytoplasm and cannot diffuse through nuclear pores, as indicated by little overlap between the green fluorescence and the Hoechst stain fluorescence labeling of the nucleus. Fusion of the SV40 NLS with double GFP results in more localization of green fluorescence in the nucleus (**Figure 10A**). Quantitation of this colocalization by its Pearson Correlation Coefficient (**Figure 10B**), confirms that SV40 NLS are functional in Huh7.5 cells. Plasmids containing double GFP fused to the putative NLS sequences, S1NLS, PNLS1-3, and PNLS4, do not show significant colocalization of the blue (Hoechst) and green fluorescence. These results suggest that these sequences may not be functional NLSs despite binding importins in peptide array experiments.

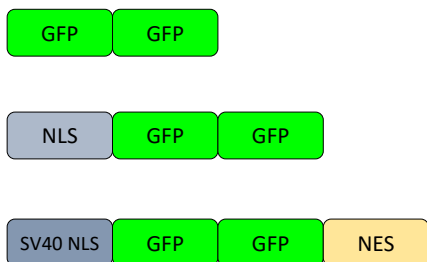
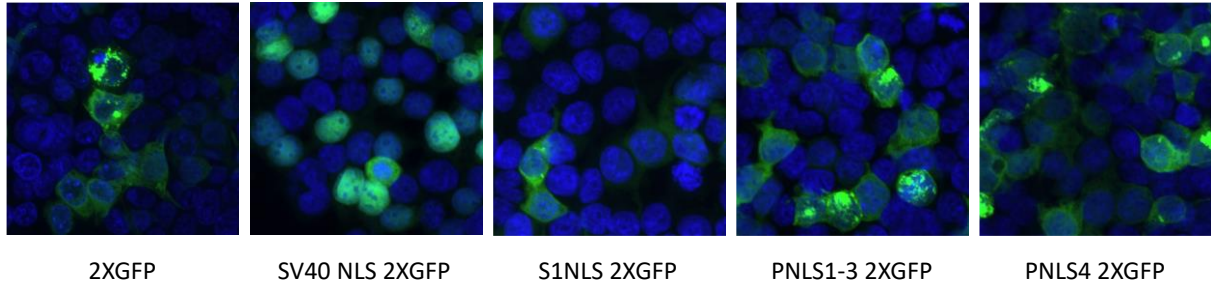


Figure 9. Schematic showing cloning of putative NLS or NES sequences to fuse with the double green fluorescence protein (GFP) motif.

(A)



(B)

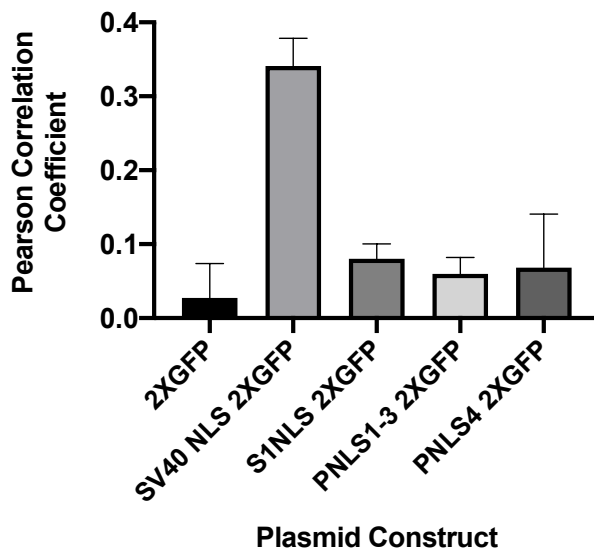


Figure 10. (A) Image of cells showing fluorescence from GFP and labeling of cell nuclei with Hoechst stain (blue). (B) Pearson correlation coefficient between the green and blue fluorescence, indicating the extent of co-localization. 2×GFP denotes the cells were transfected with the double GFP construct. SV40 NLS 2×GFP denotes the cells were transfected with the plasmid containing double GFP and SV40 NLS, which serves as a positive control. S1NLS 2×GFP, PNLS1-3 2×GFP, and PNLS4 2×GFP denote the cells were transfected with the plasmid containing double GFP and one of the putative NLS sequences.

To assess whether the PNES2 sequence functions as a NES, we cloned this sequence into the double GFP vector, fusing PNES2 to its N-terminus of the double GFP and fusing the SV40 NLS to its C-terminus (**Figure 9, schematic at the bottom**). We detected the green GFP

fluorescence (**Figure 11, left panel**) and blue (nuclear) fluorescence (**Figure 11, middle panel**) in the transfected Huh7.5 cells. The merged image (**Figure 11, right panel**) does not show significant migration of GFP into the cytoplasm by the NES. These results are not sufficient to determine whether the identified PNES2 is functional. The putative PNES2 may not be able to counteract the powerful SV40 NLS present in this construct.

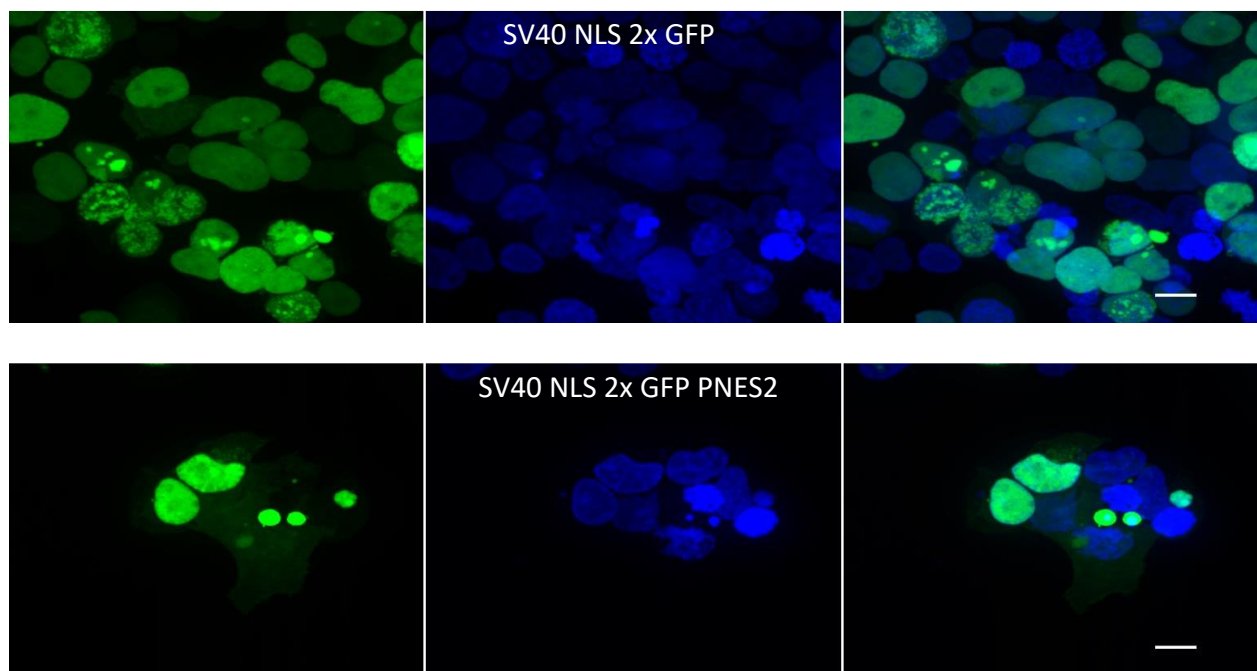


Figure 11. Image of cells showing fluorescence from GFP (green) and Hoechst (blue). SV40 NLS 2×GFP denotes the cells were transfected with the plasmid containing double GFP and SV40 NLS. SV40 NLS 2×GFP PNES2 denotes fusion of SV40 NLS to the N-terminus of the double GFP and fusion of PNES2 to the C-terminus of the double GFP. The left panels show green fluorescence; the middle panels show blue fluorescence from Hoechst stain, and the right panels show the merged images of both green and blue fluorescence.

We further investigated the function of PNES2 by fusing a single GFP to the whole polymerase protein (**Figure 12**). We introduced three mutations to the PNES2 sequence in this construct: partial deletion of the C-terminus of PNES2 (Δ aa50-57), full deletion of PNES2

(Δ aa37-57), and mutation of two lysine residues to alanine and glutamine as well as D40E and V48A in polymerase ORF but which cause silent mutations in the overlapping core protein ORF thereby ensuring that core amino acids are unaltered. We used flow cytometry to measure the fluorescence intensity of these GFP-pol constructs in transfected Huh7.5 cells. The results show that all three mutations to the PNES2 sequence result in significant reductions in the median fluorescence intensity of the cells (**Figure 13A**).

To test whether the decrease of median fluorescence intensity in the cells could be due to a faster degradation of the mutant construct, we measured fluorescence intensity in cells treated with a proteosomal degradation inhibitor, MG132. If the decreased fluorescence in cells transfected with the mutants was a result of faster degradation, one would expect all four of the MG132-treated samples to have a similar fluorescence intensity. However, fluorescence intensity differences remain in the cells transfected with the wild-type and the mutants and follow the same trend seen in the previous experiment (**Figure 13B**). Therefore, the decrease of median fluorescence intensity in the cells observed in **Figure 13A** is unlikely to be due to a faster proteosomal degradation of the mutant constructs.

Although PNES2 has not been demonstrated as a functional NES, mutations to PNES2 sequence in the HBV polymerase attenuated HBV infection (**Figures 7 and 8**). PNES2 binds Exportin 6 which is so named because silencing of Exportin 6 results in accumulation of actin in the nucleus [15]. It is unclear whether Exportin 6 is a transport factor for any other proteins. Some evidence shows that Exportin 6 acts to regulate nuclear actin function rather than causes its nuclear export. Hence, it is possible that the putative NES identified by our peptide screen may be interacting with Exportin 6 without being involved with nuclear transport. This may be why we see PNES2 suppress viral infection despite not showing evidence of being a functional NES.

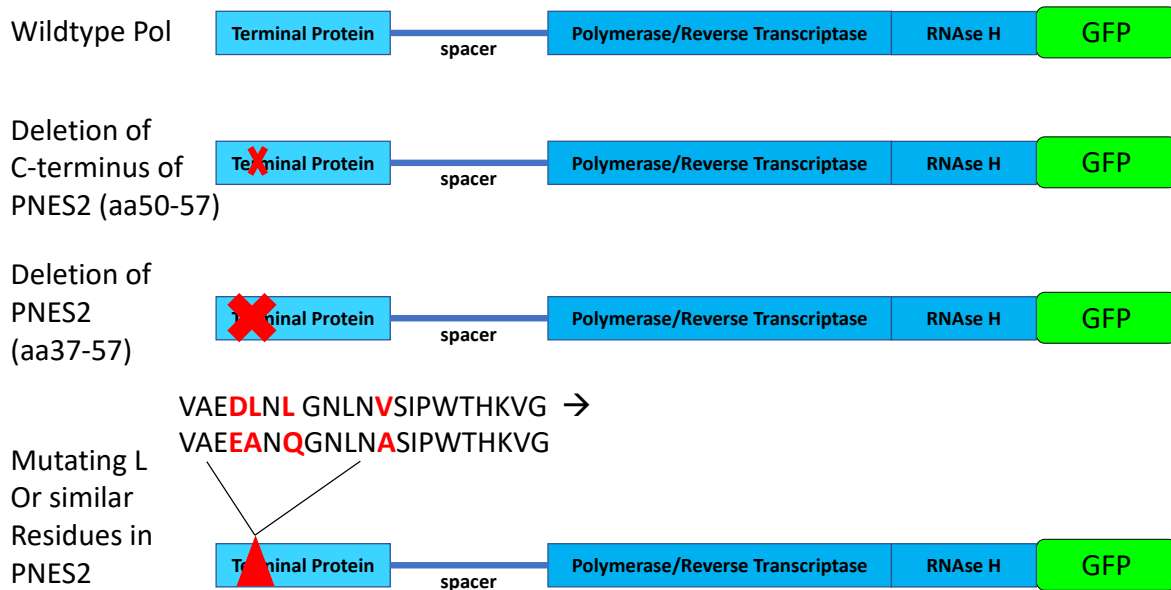


Figure 12. Schematic showing HBV polymerase fused with a green fluorescence protein (GFP) marker. Three constructs with mutations to the PNES2 region were also made. The first two mutants contain a partial deletion (Δ aa50-57) or full deletion (Δ aa37-57) of the PNES2 sequence. The third mutant replaced two leucine residues (L41 and L43) with alanine (A) and glutamine (Q), replacing D40 (aspartic acid) with E (glutamic acid), and replacing V48 (valine) with A (alanine).

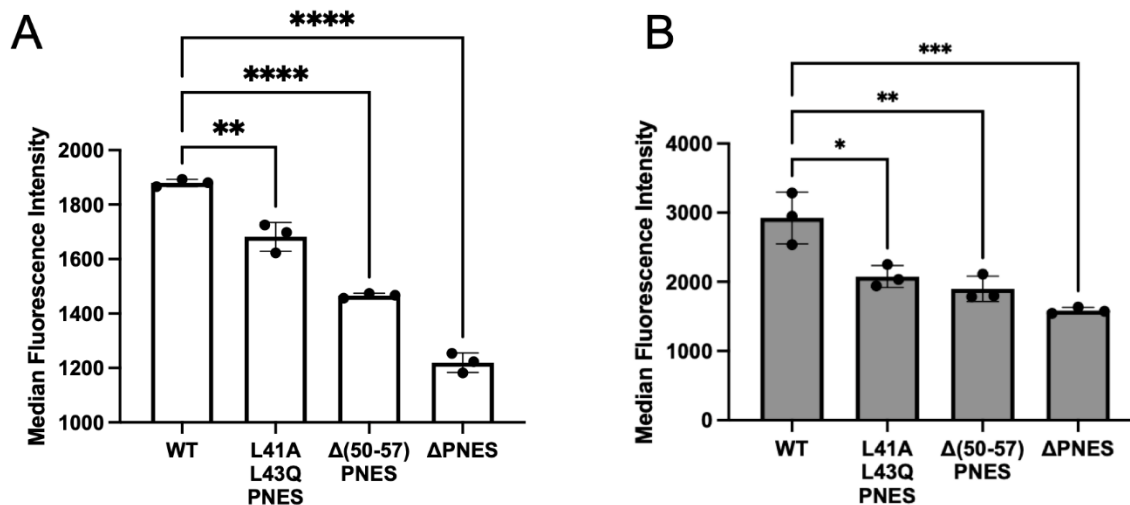


Figure 13. Median fluorescence intensity of Huh7.5 cells transfected with wild-type and mutant HBV polymerase-GFP fusions. (A) Flow cytometry analysis of the transfected Huh7.5 cells. (B) Flow cytometry analysis of the transfected Huh7.5 cells treated with MG132, a proteasomal degradation inhibitor. WT denotes the wild-type HBV polymerase fused to GFP. L41A L43Q PNES denote mutations to the PNES2 sequence by replacing leucine residues 41 and 43 with alanine and glutamate. $\Delta(50-57)$ PNES denotes partial deletion (aa50-57) of the C-terminus of PNES2 sequence. Δ PNES denotes full deletion (aa37-57) of the PNES2 sequence. The error bars indicate standard deviation from the triplicate experiments (n=3), and the differences are statistically significant (ANOVA analysis, * p= 0.01, ** p<0.005, *** p<0.001, **** p<0.0001)

4. Conclusion

Current evidence suggests that the persistence and accumulation of HBV cccDNA is established through trafficking of intracellular capsids back into the nucleus, rather than towards encapsidation and secretion. Furthermore, nuclear transport immediately following viral entry remains poorly understood. HBV is a compact virus, with its genome consisting of only 3kb of DNA. The few proteins expressed by HBV perform several functions, which likely include nuclear localization and export of viral components. Therefore, identification of linear peptide

motifs that may act as nuclear localization signals (NLSs) or nuclear export signals (NESs) can elucidate steps in the HBV lifecycle and potentially reveal novel therapeutic targets.

We report on the design and application of a 384-spot peptide array enabling the identification of nuclear localization signals (NLS) and nuclear export signals (NES) relevant to the hepatitis B virus (HBV) infection. The 384 overlapping peptide sequences conjugated on the array encompassed the full sequence of the HBV proteome. Using cell lysates to interrogate this peptide array and using specific antibodies directed against nuclear import proteins (importins) and nuclear export proteins (exportins) to detect the bound proteins, we revealed the domains on the HBV proteins that may bind to these nuclear transport proteins. An application of this peptide array to a study of HBV infection identified six putative NLS and five NES peptides, as well as a sequence with potential NLS and NES function (Table 6.3). These include a novel putative NES peptide sequence, PNES2 (VAEDLN LGNLNVSIPWTHKVG), located in the N-terminus region of the HBV polymerase. Mutations to this NES sequence in the HBV polymerase resulted in significant attenuation of HBV infection in HepG2 cells. Compared to the wild-type HBV, the HBV with the NES mutation produced ~100-fold lower amount of pregenomic RNA and 20-fold lower amount of covalently closed circular DNA (cccDNA) in HepG2 cells. These results were consistent with the observation of more than 10-fold lower luminescence in HepG2 cells infected with the PNES2 mutant HBV than with the wild-type HBV, containing a nanoluciferase marker. To inhibit HBV infection, we used synthetic peptides to compete with the interaction between the viral NES and the host cells. The synthetic peptide derived from the PNES2 sequence suppressed HBV infection of HepG2 cells, measured by reductions of both the E antigen (HBeAg) and S antigen (HBsAg) levels by more than 50%.

References

1. Knockenhauer, K. E.; Schwartz, T. U. The nuclear pore complex as a flexible and dynamic gate. *Cell* **2016**, *164*, 1162–1171.
2. Eckhardt, S. G., Milich, D. R.; McLachlan, A. Hepatitis B virus core antigen has two nuclear localization sequences in the arginine-rich carboxyl terminus. *J. Virol.* **1991**, *65*, 575–582.
3. Nassal, M. The arginine-rich domain of the hepatitis B virus core protein is required for pregenome encapsidation and productive viral positive-strand DNA synthesis but not for virus assembly. *J. Virol.* **1992**, *66*, 4107–4116.
4. Yeh, C. T., Liaw, Y. F.; Ou, J. H. The arginine-rich domain of hepatitis B virus precore and core proteins contains a signal for nuclear transport. *J. Virol.* **1990**, *64*, 6141–6147.
5. Rabe, B., Vlachou, A., Panté, N., Helenius, A.; Kann, M. Nuclear import of hepatitis B virus capsids and release of the viral genome. *Proc. Natl. Acad. Sci. U. S. A.* **2003**, *100*, 9849–9854.
6. Zlotnick, A.; Cheng, N.; Stahl, S.J.; Conway, J.F.; Steven, A.C.; Wingfield, P.T. Localization of the C terminus of the assembly domain of hepatitis B virus capsid protein: Implications for morphogenesis and organization of encapsidated RNA. *Proc. Natl. Acad. Sci. U. S. A.* **1997**, *94*, 9556–9561. doi: 10.1073/pnas.94.18.9556
7. Rabe, B., Glebe, D.; Kann, M. Lipid-mediated introduction of hepatitis B virus capsids into nonsusceptible cells allows highly efficient replication and facilitates the study of early infection events. *J. Virol.* **2006**, *80*, 5465–5473.
8. Schmitz, A.; Foss, M.; Zhou, L.; Rabe, B.; Hoellenriegel, J.; Stoeber, M.; Pante, N.; Kann, M. Nucleoporin 153 arrests the nuclear import of hepatitis B virus capsids in the nuclear basket. *PLoS Pathog.* **2010**, *6*, e1000741. doi:10.1371/journal.ppat.1000741.
9. Levin, A.; Neufeldt, C. J.; Pang, D.; Wilson, K.; Loewen-Dobler, D.; Joyce, M. A.; Wozniak, R. W.; Tyrrell, D. L. J. Functional characterization of nuclear localization and export signals in hepatitis C virus proteins and their role in the membranous web. *PLoS ONE* **2014**, *9*(12), e114629. doi:10.1371/journal.pone.0114629
10. Ladner, S.K.; Otto, M.J.; Barker, C.S.; Zaifert, K.; Wang, G.H.; Guo, J.T.; Seeger, C.; King, R.W. Inducible expression of human hepatitis B virus (HBV) in stably transfected

- hepatoblastoma cells: A novel system for screening potential inhibitors of HBV replication. *Antimicrob. Agents Chemother.* **1997**, *41*, 1715–1720, doi:10.1128/aac.41.8.1715
11. Nishitsuji, H.; Ujino, S.; Shimizu, Y.; Harada, K.; Zhang, J.; Sugiyama, M.; Mizokami, M.; Shimotohno, K. Novel reporter system to monitor early stages of the hepatitis B virus life cycle. *Cancer Sci.* **2015**, *106*, 1616–1624, doi:10.1111/cas.12799
 12. Le, C.; Sirajee, R.; Steenbergen, R.; Joyce, M.A.; Addison, W.R.; Tyrrell, D.L. *In vitro* infection with hepatitis B virus using differentiated human serum culture of Huh7.5-NTCP cells without requiring dimethyl sulfoxide. *Viruses* **2021**, *13*, 97. doi: 10.3390/v13010097
 13. Qu, B.; Ni, Y.; Lempp, F.A.; Vondran, F.W.R.; Urban, S. T5 exonuclease hydrolysis of hepatitis B virus replicative intermediates allows reliable quantification and fast drug efficacy testing of covalently closed circular DNA by PCR. *J. Virol.* **2018**, *92*, e01117–18, doi:10.1128/jvi.01117-18
 14. Liu, Y.; Le, C.; Tyrrell, D.L.; Le, X.C.; Li, X.-F. Aptamer binding assay for the E antigen of hepatitis B using modified aptamers with G-quadruplex structures. *Anal. Chem.* **2020**, *92*, 6495–6501, doi:10.1021/acs.analchem.9b05740
 15. Stüven, T.; Hartmann, E.; Görlich, D. Exportin 6: a novel nuclear export receptor that is specific for profilin-actin complexes. *EMBO J.* **2003**, *21*, 5928-5940. doi:10.1093/emboj/cdg565

Table 1B. Sequences of peptides conjugated on the 384-spot (16×24) peptide array.

Peptide no	Location on array	Peptide sequence
1	A 1	MPLSYQHFRLLLLLD
2	A 2	HFRLLLLLDDEAGPL
3	A 3	LLDDEAGPLEEELPR
4	A 4	GPLEEELPRLADEGL
5	A 5	LPRLADEGLNRRVAE
6	A 6	EGLNRRVAEDLNLGN
7	A 7	VAEDLNLGNLNSIP
8	A 8	LGNLNSIPWTHKVG
9	A 9	SIPWTHKVGNFTGLY
10	A10	KVGNFTGLYSSTVPV
11	A11	GLYSSTVPVFNPHWK
12	A12	VPVFNPHWKTPSFPN
13	A13	HWKTPSFPNIHLHQD
14	A14	FPNIHLHQDIKKCE
15	A15	HQDIKKCEQFVGPL
16	A16	KCEQFVGPLTVNEKR
17	A17	GPLTVNEKRRLQLIM
18	A18	EKRRLQLIMPARFYP
19	A19	LIMPARFYPKVTKYL
20	A20	FYPKVTKYLPLDKGI
21	A21	KYLPLDKGIKPYYPE
22	A22	KGIKPYYPEHLVNHY
23	A23	YPEHLVNHYFQTRHY
24	A24	NHYFQTRHYLHTLWK
25	B 1	RHYLHTLWKAGILYK
26	B 2	LWKAGILYKRETTHS
27	B 3	LYKRETTHSASFCGS
28	B 4	THSASFCGSPYSWEQ
29	B 5	CGSPYSWEQDLQHGA
30	B 6	WEQDLQHGAESFHQQ
31	B 7	HGAESFHQQSSGILS
32	B 8	HQQSSGILSRPPVGS
33	B 9	ILSRPPVGSSLQSKH
34	B10	VGSSLQSKHRKSRLG
35	B11	SKHRKSRLGLQSQQG
36	B12	RLGLQSQQGHLARRQ
37	B13	QQGHLARRQQGRSWS
38	B14	RRQQGRSWSIRAGFH
39	B15	SWSIRAGFHPTARRP
40	B16	GFHPTARRPFGVEPS
41	B17	RRPFGVEPSGSGHTT
42	B18	EPSPSGHTTNFASKS

43	B19	HTTNFASKSASCLHQ
44	B20	SKSASCLHQSPVRKA
45	B21	LHQSPVRKAAYPAVS
46	B22	RKAAYPAVSTFEKHS
47	B23	AVSTFEKHSSSGHAV
48	B24	KHSSSGHAVEFHNL
49	C 1	HAVEFHNLPPNSARS
50	C 2	NLPPNSARSQSERP
51	C 3	ARSQSERPVFPCWWL
52	C 4	RPVFPCWWLQFRNSK
53	C 5	WWLQFRNSKPCSDYC
54	C 6	NSKPCSDYCLSLIVN
55	C 7	DYCLSLIVNLLEDWG
56	C 8	IVNLLEDWGPCAHEG
57	C 9	DWGPCAHEGHEHIRI
58	C10	EHGHEHIRIPRTPSR
59	C11	IRIPRTPSRVTGGVF
60	C12	PSRVTGGVFLVDKNP
61	C13	GVFLVDKNPHNTAES
62	C14	KNPHNTAESRLVDF
63	C15	AESRLVDFSQFSRG
64	C16	VDFSQFSRGNRVSW
65	C17	SRGNRVSWPKFAVP
66	C18	VSWPKFAVPNLQSLT
67	C19	AVPNLQSLTNLLSSN
68	C20	SLTNLLSSNLSWLSL
69	C21	SSNLSWLSLDVSAAF
70	C22	LSDVSAAFYHLPLH
71	C23	AAFYHLPLHPAAMPH
72	C24	PLHPAAMPHLLVGSS
73	D 1	MPHLLVGSSGLSRYV
74	D 2	GSSGLSRYVARLSSN
75	D 3	RYVARLSSNSRILNN
76	D 4	SSNSRILNNQHGTMP
77	D 5	LNNQHGTMPDLHDYC
78	D 6	TMPDLHDYCSRNLVY
79	D 7	DYCSRNLVSLLLLY
80	D 8	LYVSLLLLYQTFGRK
81	D 9	LLYQTFGRKLHLYSH
82	D10	GRKLHLYSHPIILGF
83	D11	YSHPIILGFRKIPMG
84	D12	LGFRKIPMGVGLSPF
85	D13	PMGVGLSPFLLAQFT
86	D14	SPFLLAQFTSAICSV
87	D15	QFTSAICSVVRRAFP

88	D16	CSVVRRAFPCLAFS
89	D17	AFPHCLAFSYMDDVV
90	D18	AFSYMDDVVLGAKSV
91	D19	DVVLGAKSVQHLESL
92	D20	KSVQHLESLFTAVTN
93	D21	ESLFTAVTNFLLSLG
94	D22	VTNFLLSLGIHLNPN
95	D23	SLGIHLNPNKTKRWG
96	D24	NPNKTKRWGYSLNFM
97	E 1	RWGYSLNFMGYVIGC
98	E 2	NFMGYVIGCYGSLPQ
99	E 3	IGCYGSLPQEHIQK
100	E 4	LPQEHIQKIKECFR
101	E 5	IQKIKECFRKLPINR
102	E 6	CFRKLPINRPIDWKV
103	E 7	INRPIDWKVCQRIVG
104	E 8	WKVCQRIVGLLGFAA
105	E 9	IVGLLGFAAPFTQCG
106	E10	FAAPFTQCGYPALMP
107	E11	QCGYPALMPYACIQ
108	E12	LMPLYACIQSKQAFT
109	E13	CIQSKQAFTFSPTYK
110	E14	AFTFSPTYKAFLCKQ
111	E15	TYKAFLCKQYLNLYP
112	E16	CKQYLNLYPVARQRP
113	E17	LYPVARQRPGLCQVF
114	E18	QRPGLCQVFADATPT
115	E19	QVFADATPTGWGLVM
116	E20	TPTGWGLVMGHQMR
117	E21	LVMGHQMRGTFMSAP
118	E22	RMRGTFMSAPLPIHTA
119	E23	SAPLPIHTAELLAAC
120	E24	HTAELLAACFARSRS
121	F 1	AACFARSRSGANIIG
122	F 2	SRSGANIIGTDNSV
123	F 3	IIGTDNSVLSRKYT
124	F 4	SVVLSRKYTSFPWLL
125	F 5	KYTSFPWLLGCAANW
126	F 6	WLLGCAANWILRGTS
127	F 7	ANWILRGTSFVYVPS
128	F 8	GTSFVYVPSALNPAD
129	F 9	VPSALNPADDPGR
130	F10	PADDPGRGLGLSRP
131	F11	RGRLGLSRPLLRPF
132	F12	SRPLLRPFRRPTTGR

133	F13	LPFRPTTGRTSLYAD
134	F14	TGRTSLYADSPSVPS
135	F15	YADSPSVPSHLPDRV
136	F16	VPSHLPDRVHFASPL
137	F17	DRVHFASPLHVAWRP
138	F18	MGQNLSTSNPLGFFP
139	F19	TSNPLGFFPDHQLDP
140	F20	FFPDHQLDPAFRANT
141	F21	LDPAFRANTANPDWD
142	F22	ANTANPDWDFNPNKD
143	F23	DWDFNPNKDTWPDAN
144	F24	NKDTWPDANKVGAGA
145	G 1	DANKVGAGAFGLGFT
146	G 2	AGAFGLGFTPPHGGL
147	G 3	GFTPPHGGLLGWSPQ
148	G 4	GGLLGWSPQAQGILQ
149	G 5	SPQAQGILQTLPANP
150	G 6	ILQTLPANPPPASTN
151	G 7	ANPPPASTNRQSGRQ
152	G 8	STNRQSGRQPTPLSP
153	G 9	GRQPTPLSPPLRNTH
154	G10	LSPPLRNTHPQAMQW
155	G11	NTHPQAMQWNSTTFH
156	G12	MQWNSTTFHQTLQDP
157	G13	TFHQTLQDPRVRGLY
158	G14	QDPRVRGLYFPAGGS
159	G15	GLYFPAGGSSSGTVN
160	G16	GGSSSGTVNPVLTTA
161	G17	TVNPVLTASPLSSI
162	G18	TTASPLSSIFSRIGD
163	G19	SSIFSRIGDPALNME
164	G20	IGDPALNMENITSGF
165	G21	NMENITSGFLGPLLV
166	G22	SGFLGPLLVLQAGFF
167	G23	LLVLQAGFFLLTRIL
168	G24	GFFLLTRILTIPQSL
169	H 1	RILTIPQSLDSWWTS
170	H 2	QSLDSWWTSLNFLGG
171	H 3	WTSLNFLGGTTVCLG
172	H 4	LGTTVCLGQNSQSP
173	H 5	CLGQNSQSPTS NHSP
174	H 6	QSPTS NHSP TSCPPT
175	H 7	HSPTSCPPTCPGYRW
176	H 8	PPTCPGYRWMCLRRF
177	H 9	YRWMCLRRFIIFLFI

178	H10	RRFIIFLIFLLLCI
179	H11	LFILLCLIFLLVLL
180	H12	CLIFLLVLLDYQGML
181	H13	VLLDYQGMLPVCPLI
182	H14	GMLPVCPLIPGSSTT
183	H15	PLIPGSSTTSTGPCR
184	H16	STTSTGPCRTCMTTA
185	H17	PCRTCMTTAQGTSMY
186	H18	TTAQGTSMYPSCCCT
187	H19	SMYPSCCCTKPSDGN
188	H20	CCTKPSDGNCTCIPI
189	H21	DGNCTCIPISSWAF
190	H22	IPISSWAFGKFLWE
191	H23	WAFGKFLWEWASARF
192	H24	LWEWASARFSWLSLL
193	I 1	ARFSWLSLLVPFVQW
194	I 2	SLLVPFVQWFVGLSP
195	I 3	VQWFVGLSPTVWLSV
196	I 4	LSPTVWLSVIWMMWY
197	I 5	LSVIWMMWYWGPSLY
198	I 6	MWYWGPSLYSILSPF
199	I 7	SLYSILSPFLPLLPI
200	I 8	SPFLPLLPIFFCLWV
201	I 9	LPIFFCLWVYI
202	I10	MQWNSTTFHQTLQDP
203	I11	TFHQTLQDPRVRGLY
204	I12	QDPRVRGLYFPAGGS
205	I13	GLYFPAGGSSSGTVN
206	I14	GGSSSGTVNPVLTTA
207	I15	TVNPVLTASPLSSI
208	I16	TTASPLSIFSRIGD
209	I17	SSIFSRIGDPALNME
210	I18	IGDPALNMENITSGF
211	I19	NMENITSGFLGPLLV
212	I20	SGFLGPLLVLQAGFF
213	I21	LLVLQAGFFLLTRIL
214	I22	GFFLLTRILTIPQSL
215	I23	RILTIPQSLDSWWTS
216	I24	QSLDSWWTSLNFLGG
217	J 1	WTSNFLGGTTVCLG
218	J 2	LGTTVCLGQNSQSP
219	J 3	CLGQNSQSPTS NHSP
220	J 4	QSPTS NHSP TSCPPT
221	J 5	HSPTSCPPTCPGYRW
222	J 6	PPTCPGYRWMCLRRF

223	J 7	YRWMCLRRFIIFLFI
224	J 8	RRFIIFLIFILLLCLI
225	J 9	LFILLLCLIFLLVLL
226	J10	CLIFLLVLLDYQGML
227	J11	VLLDYQGMLPVCPLI
228	J12	GMLPVCPLIPGSSTT
229	J13	PLIPGSSTTSTGPCR
230	J14	STTSTGPCRTCMTTA
231	J15	PCRTCMTTAQGTSMY
232	J16	TTAQGTSMYPSCCCT
233	J17	SMYPSCCCTKPSDGN
234	J18	CCTKPSDGNCTCIPI
235	J19	DGNCTCIPISSWAF
236	J20	IPISSWAFGKFLWE
237	J21	WAFGKFLWEWASARF
238	J22	LWEWASARFSWLSLL
239	J23	ARFSWLSLLVPFVQW
240	J24	SLLVPFVQWFVGLSP
241	K 1	VQWFVGLSPTVWLSV
242	K 2	LSPTVWLSVIWMMWY
243	K 3	LSVIWMMWYWGPSLY
244	K 4	MWYWGPSLYSILSPF
245	K 5	SLYSILSPFLPLLPI
246	K 6	SPFLPLLPIFFCLWV
247	K 7	LPIFFCLWVYI
248	K 8	MENITSGFLGPLLVL
249	K 9	GFLGPLLVLQAGFFL
250	K10	LVLQAGFFLLTRILT
251	K11	FFLLTRILTIPQSLD
252	K12	ILTIPQSLDSWWTSL
253	K13	SLDSWWTSLNFLGGT
254	K14	TSLNFLGGTTVCLGQ
255	K15	GGTTVCLGQNSQSPT
256	K16	LGQNSQSPTSNHSPT
257	K17	SPTSNHSPTSCPPTC
258	K18	SPTSCPPTCPGYRWM
259	K19	PTCPGYRWMCLRRFI
260	K20	RWMCLRRFIIFLFI
261	K21	RFIIFLIFILLLCLIF
262	K22	FILLLCLIFLLVLLD
263	K23	LIFLLVLLDYQGMLP
264	K24	LLDYQGMLPVCPLIP
265	L 1	MLPVCPLIPGSSTTS
266	L 2	LIPGSSTTSTGPCRT
267	L 3	TTSTGPCRTCMTTAQ

268	L 4	CRTCMTTAQGTSMYP
269	L 5	TAQGTSMYPSCCCTK
270	L 6	MYPSCCCTKPSDGNC
271	L 7	CTKPSDGNCTCIPIP
272	L 8	GNCTCIPIPSSWAFG
273	L 9	PIPSSWAFGKFLWEW
274	L10	AFGKFLWEWASARFS
275	L11	WEWASARFSWLSLLV
276	L12	RFSWLSLLVPFVQWF
277	L13	LLVPFVQWFVGLSPT
278	L14	QWFVGLSPTVWLSVI
279	L15	SPTVWLSVIWMMWYW
280	L16	SVIWMMWYWGPSLYS
281	L17	WYWGPSLYSILSPFL
282	L18	LYSILSPFLPLLPIF
283	L19	PFLPLLPIFFCLWVY
284	L20	MAARLCCQLDPARDV
285	L21	CQLDPARDVLCCLRPV
286	L22	RDVLCCLRPVGAESCG
287	L23	RPVGAESCGRPFSGS
288	L24	SCGRPFSGSLGTLSS
289	M 1	SGSLGTLSSPSPSAV
290	M 2	LSSPSPSAVPTDHGA
291	M 3	SAVPTDHGAHLSLRG
292	M 4	HGAHLSLRGLPVCAF
293	M 5	LRGLPVCAFSSAGPC
294	M 6	CAFSSAGPCALRFTS
295	M 7	GPCALRFTSARRMET
296	M 8	FTSARRMETTVNAHQ
297	M 9	METTVNAHQILPKVL
298	M10	AHQILPKVLHKRTLK
299	M11	KVLHKRTLGLSAMST
300	M12	TLGLSAMSTTDLEAY
301	M13	MSTTDLEAYFKDCLF
302	M14	EAYFKDCLFKDWEEL
303	M15	CLFKDWEELGEEIRL
304	M16	EELGEEIRLKVFVLG
305	M17	IRLKVFVLGGCRHKL
306	M18	VLGGCRHKLVCAPAP
307	M19	HKLVCAPAPCNFFTS
308	M20	MQLFHLCLIISCSCP
309	M21	CLIISCSCPTVQASK
310	M22	SCPTVQASKLCLGWL
311	M23	ASKLCLGWLWGMDID
312	M24	GWLWGMDIDPYKEFG

313	N 1	DIDPYKEFGATVELL
314	N 2	EFGATVELLSFLPSD
315	N 3	ELLSFLPSDFFPSVR
316	N 4	PSDFFPSVRDLLDTA
317	N 5	SVRDLLDTASALYRE
318	N 6	DTASALYREALESPE
319	N 7	YREALESPEHCSPHH
320	N 8	SPEHCSPHHTALRQA
321	N 9	PHHTALRQAILCWGE
322	N10	RQAILCWGELMTLAT
323	N11	WGELMTLATWVGVNL
324	N12	LATWVGVNLEDPASR
325	N13	VNLEDPASRDLVVS
326	N14	ASRDLVVS YVNTNMG
327	N15	VSYVNTNMGLKFRQL
328	N16	NMGLKFRQLLWFHIS
329	N17	RQLLWFHISCLTFGR
330	N18	HISCLTFGRETVIEW
331	N19	FGRETVIEWLVSFGV
332	N20	IEYLVSFGWWIRTPP
333	N21	FGWWIRTPPAYRPPN
334	N22	TPPAYRPPNAPILST
335	N23	PPNAPILSTLPETTV
336	N24	LSTLPETTVVRRRGR
337	O 1	TTVRRRGRSPRRRT
338	O 2	RGRSPRRRTPSPRRR
339	O 3	RRTSPRRRRRSQSPR
340	O 4	RRRRSQSPRRRRSQS
341	O 5	SPRRRRSQSRESQC
342	O 6	MDIDPYKEFGATVEL
343	O 7	KEFGATVELLSFLPS
344	O 8	VELLSFLPSDFFPSV
345	O 9	LPSDFFPSVRDLLDT
346	O10	PSVRDLLDTASALYR
347	O11	LDTASALYREALESPE
348	O12	LYREALESPEHCSPH
349	O13	ESPEHCSPHHTALRQ
350	O14	SPHHTALRQAILCWG
351	O15	LRQAILCWGELMTLA
352	O16	CWGELMTLATWVGVN
353	O17	TLATWVGVNLEDPAS
354	O18	GVNLEDPASRDLVVS
355	O19	PASRDLVVS YVNTNM
356	O20	VVS YVNTNMGLKFRQ
357	O21	TNMGLKFRQLLWFHI

358	O22	FRQLLWFHISCLTFG
359	O23	FHISCLTFGRETVIE
360	O24	TFGRETVIEYLVSFG
361	P 1	VIEYLVSFGWIRTP
362	P 2	SFGVWIRTPPAYRPP
363	P 3	RTPPAYRPPNAPILS
364	P 4	RPPNAPILSTLPETT
365	P 5	ILSTLPETT VRRRG
366	P 6	ETTVRRRGRSPRRR
367	P 7	RRGRSPRRRTPSPRR
368	P 8	RRRTPSPRRRRSQSP
369	P 9	PRRRRSQSPRRRRSQ
370	P10	QSPRRRRSQSRESQC
371	P11	TLPETTVRRRDRG
372	P12	PRRRTPSPRRR
373	P13	PRRRRSQSPRR
374	P14	PRRRRSQSRES
375	P15	RSPRRRTPS
376	P16	PSPRRRRSQS
377	P17	QSPRRRRSQS
378	P18	VRRRGRSPRRRTPS
379	P19	RSPRRRTPSPRRRRS
380	P20	ETTVRRRGRSP
381	P21	RRRRSQSRESQC
382	P22	RQRERWRRRRNRRART
383	P23	VKRKKKP
384	P24	RQIKIWFQNRMMKWKK

Table 2. Summary of probing antibodies used to detect import proteins (importins) and nuclear export proteins (exportins), peptide sequence on the array where the protein was detected, the interacting domains on the HBV proteins, and the name of synthetic peptides.

Probing antibody	Peptide sequence	HBV protein of peptide sequence	Synthetic Peptide(s)
Importin alpha 1	IRIPRTPSRVTGGVF	Polymerase	PNLS4
	LDPAFRANTANPDWD	PreS1	S1NLS
	TTVVRRRGRSPRRRT	Core	CNLS2, ARM12
	RGRSPRRRTSPRRR	Core	ARM123
	RRTSPRRRRSQSPR	Core	CNLS4, ARM34
	RRRRSQSPRRRRSQS	Core	CNLS6, ARM34
	ILSTLPETTIVRRRG	Core	CNLS1
	ETTVVRRRGRSPRRR	Core	CNLS2, ARM1
	RRGRSPRRRTSPRRR	Core	ARM23
	RRRTSPRRRRSQSP	Core	CNLS4
	QSPRRRRSQSRESQC	Core	CNLS8, ARM4
	TLPETTVVRRRDRG	Core	CNLS1
	PRRRTSPRRR	Core	CNLS3
	PRRRRSQSPRR	Core	CNLS5
	PRRRRSQSRES	Core	CNLS7
	RSPRRRTPS	Core	ARM2
	PSPRRRRSQS	Core	ARM3
	QSPRRRRSQS	Core	ARM4
	RSPRRRTSPRRRRS	Core	CNLS3, ARM23
	ETTVVRRRGRSP	Core	CNLS2
RRRRRSQSRESQC	Core	CNLS8	
RQRERWRRRRNRRAQRT	Core		
VKRKKKP	Core		
Importin 5	LIMPARFYPKVTKYL	Polymerase	PNLS3
	FYPKVTKYLPDKGI	Polymerase	PNLS1, PNLS3
	KYLPLDKGIKPYYPE	Polymerase	PNLS1, PNLS3
	KGIKPYYPEHLVNHY	Polymerase	PNLS1, PNLS3

	DWGPCAEGEHHIRI	Polymerase	PNLS4
	EHGEHHIRIPRTPSR	Polymerase	PNLS4
	IRIPRTPSRVTTGGVF	Polymerase	PNLS4
	VPSALNPADDPSRGR	Polymerase	PNELS1
	PADDPSRGRLGLSRP	Polymerase	PNELS1
	RGRLGLSRPLLRLPF	Polymerase	PNELS1
	SRPLLRLPFRPTTGR	Polymerase	PNELS1
	LPFRPTTGRTSLYAD	Polymerase	PNELS1
	RRRRSQSPRRRRSQS	Core	CNLS6, ARM34
	SPRRRRSQSRESQC	Core	CNLS8
	RRRTPSRRRRSQSP	Core	CNLS4
	PRRRRSQSPRRRRSQ	Core	CNLS6, ARM34
	PRRRRSQSRES	Core	CNLS7
	QSPRRRRSQS	Core	ARM4
	VVRRRGRSPRRRTPS	Core	ARM12
	RSPRRRTPSRRRRS	Core	ARM23
	VKRKKKP	Core	
	RQIKIWFQNRRMKWKK	Core	
Exportin 1	HFRRLLLLDDEAGPL	Polymerase	PNES1
	LLDDEAGPLEEELPR	Polymerase	PNES1
	GPLEEELPRLADEGL	Polymerase	PNES1
	VPSALNPADDPSRGR	Polymerase	PNELS1
	PADDPSRGRLGLSRP	Polymerase	PNELS1
	RGRLGLSRPLLRLPF	Polymerase	PNELS1
	SRPLLRLPFRPTTGR	Polymerase	PNELS1
	LPFRPTTGRTSLYAD	Polymerase	PNELS1
	LLVLQAGFFLLTRIL	Surface	SNES1
	GFFLLTRILTIPQSL	Surface	SNES1
	YRWMCLRRFIIFLFI	Surface	SNES2
	RRFIIFLIFILLCLI	Surface	SNES2
	LFILLCLIFLLVLL	Surface	SNES2
	CLIFLLVLLDYQGML	Surface	SNES2
	VLLDYQGMLPVCPLI	Surface	SNES2
	MWYWGPSLYSILSPF	Surface	SNES3
	SLYSILSPFLPLLPI	Surface	SNES3
	SPFLPLLPIFFCLWV	Surface	SNES3
	LPIFFCLWVYI	Surface	SNES3
	SGFLGPLLVLQAGFF	Surface	SNES1
	LLVLQAGFFLLTRIL	Surface	SNES1
	GFFLLTRILTIPQSL	Surface	SNES1

	YRWMCLRRFIIFLFI	Surface	SNES2
	RRFIIFLIFILLCLI	Surface	SNES2
	LFILLCLIIFLLVLL	Surface	SNES2
	CLIFLLVLLDYQGML	Surface	SNES2
	SLYSILSPFLPLLPI	Surface	SNES3
	SPFLPLLPIFFCLWV	Surface	SNES3
	LPIFFCLWVYI	Surface	SNES3
	MENITSGFLGPLLVL	Surface	SNES1
	GFLGPLLVLQAGFFL	Surface	SNES1
	LVLQAGFFLLTRILT	Surface	SNES1
	RFIIFLIFILLCLIF	Surface	SNES2
	FILLCLIIFLLVLLD	Surface	SNES2
	LIFLLVLLDYQGMLP	Surface	SNES2
	LYSILSPFLPLLPIF	Surface	SNES3
	PFLPLLPIFFCLWVY	Surface	SNES3
	MAARLCCQLDPARDV	X	
Exportin 6	VAEDNLGNLNVSIP	Polymerase	PNES2
	LGNLNVSIPWTHKVG	Polymerase	PNES2
	RRQQGRSWSIRAGFH	Polymerase	
	CFRKLPINRPIDWKV	Polymerase	
	WKVCQRIVGLLGFAA	Polymerase	
	PPTCPGYRWMCLRRF	PreS1	
	CLFKDWEELGEEIRL	X	XNES

Table 3. Synthetic peptides containing the identified putative NLS or NES sequences and the penetratin sequence (RQIKIWFQNRRMKWKK). Bolded peptides are novel putative NLS or NES sequences.

Peptide Name	Peptide Sequence
CNLS1	TLPETTVVRRRDRG-RQIKIWFQNRRMKWKK
CNLS2	ETTVVRRRGRSP-RQIKIWFQNRRMKWKK
CNLS3	PRRRTSPRRR-RQIKIWFQNRRMKWKK
CNLS4	RRRTSPRRRRSQSPRRR-RQIKIWFQNRRMKWKK
CNLS5	PRRRRSQSPRR-RQIKIWFQNRRMKWKK
CNLS6	PRRRRSQSPRRRRSQSR-RQIKIWFQNRRMKWKK
CNLS7	PRRRRSQSRES-RQIKIWFQNRRMKWKK
CNLS8	RRRRRSQSRESQC-RQIKIWFQNRRMKWKK
ARM1	TVVRRRGRS-RQIKIWFQNRRMKWKK
ARM2	RSPRRRTPS-RQIKIWFQNRRMKWKK
ARM3	PSPRRRSQS-RQIKIWFQNRRMKWKK
ARM4	QSPRRRSQS-RQIKIWFQNRRMKWKK
ARM12	TVVRRRGRSPRRRTPS-RQIKIWFQNRRMKWKK
ARM23	RSPRRRTSPRRRRSQS-RQIKIWFQNRRMKWKK
ARM34	PSPRRRSQSPRRRRSQS-RQIKIWFQNRRMKWKK
ARM123	TVVRRRGRSPRRRTPSRRRRSQS-RQIKIWFQNRRMKWKK
ARM234	RSPRRRTSPRRRRSQSPRRRRSQS-RQIKIWFQNRRMKWKK
ARM1234	TVVRRRGRSPRRRTPSRRRRSQSPRRRRSQS-RQIKIWFQNRRMKWKK
PNLS1	FYPKVTKYLPDKGKIPYPE-RQIKIWFQNRRMKWKK
PNLS2	GPLTVNEKRRLQLIMPARFYP-RQIKIWFQNRRMKWKK
PNLS3	LIMPARFYPKVTKYLPDKGKIPYPE-RQIKIWFQNRRMKWKK
PNLS4	DWGPCAEGEHHIRIPRTPSRVTTGGVF-RQIKIWFQNRRMKWKK
S1NLS	LDPAFRANTANPDWD-RQIKIWFQNRRMKWKK
PNES1	HFRLLLLDDEAGPLEEELPRLADEGL-RQIKIWFQNRRMKWKK
PNES2	VAEDLNLGNLNVSIPWTHKVG-RQIKIWFQNRRMKWKK
SNES1	LLVLQAGFFLLTRILTIPQSL-RQIKIWFQNRRMKWKK
SNES2	YRWMCLRRFIIFLFILLCLIFLLVLLDYQGMLPVCPLI-RQIKIWFQNRRMKWKK
SNES3	MWYWGPSLYSILSPFLPLPIFFCLWVYI-RQIKIWFQNRRMKWKK
XNES	EAYFKDCLFKDWEELGEEIRL-RQIKIWFQNRRMKWKK
PNELS	VPSALNPADDPSRGLGLSRPLLRPFRTTGRSLYAD-RQIKIWFQNRRMKWKK